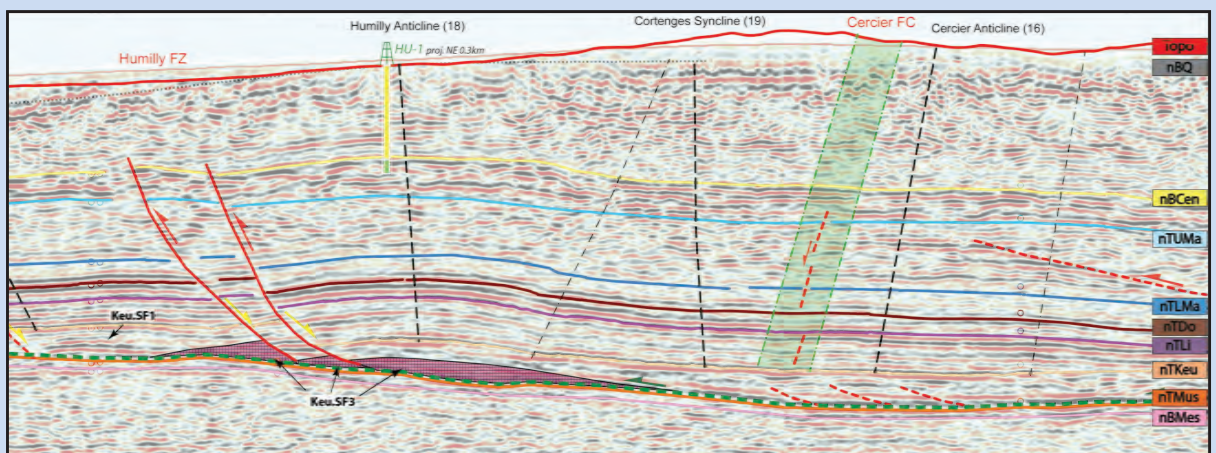
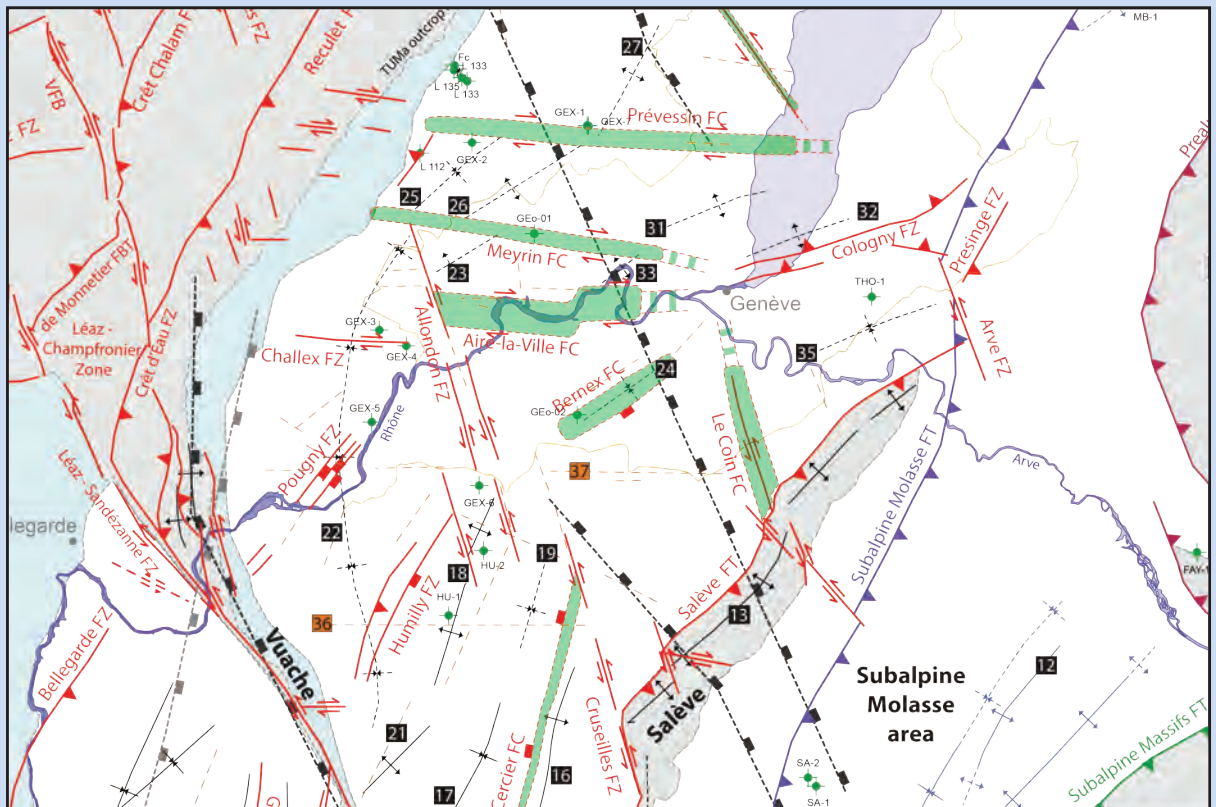


Louis HAUVETTE

Tectonics of the Western North Alpine Foreland based on Seismic interpretation of the Greater Geneva Basin



<https://doi.org/10.51363/unifr.sth.2024.009>

© Louis Hauvette, 2024



This work is published under a Creative Commons Attribution 4.0 International (CC BY 4.0) license: <https://creativecommons.org/licenses/by/4.0>

DEPARTMENT OF GEOSCIENCES – EARTH SCIENCES

UNIVERSITY OF FRIBOURG (SWITZERLAND)

Tectonics of the Western North Alpine Foreland

Based on

Seismic interpretation of the Greater Geneva Basin

Thesis

Presented to the Faculty of Science and Medicine of the University of Fribourg
(Switzerland)

In consideration for the award of the academic grade of

Doctor of Philosophy in Earth Sciences

By

Louis Hauvette

From France

Thesis No: 4721

Media f sa, March 2024

Accepted by the Faculty of Science and Medicine of the University of Fribourg (Switzerland) upon the recommendation of:

Prof. Jon MOSAR	University of Fribourg (CH)	Thesis supervisor
PD. Dr. Anna SOMMARUGA	University of Fribourg (CH)	Thesis co-supervisor
Prof. Dr. Juan Soto	Bureau of Economic Geology (USA)	Expert
Dr. Bernd Fiebig	Ad Terra Energy SA (CH)	Expert
Dr. Michel Meyer	Services Industriels de Genève SIG (CH)	Expert
Prof. Anneleen Foubert	University of Fribourg (CH)	President of the Jury

Fribourg, March 25, 2024

Thesis supervisor:



Prof. Jon Mosar

Dean:



Prof. Ulrich Ultes-Nitsche

*L'interprétation n'a pas plus à être vraie que fausse ;
Elle a à être juste*

Jacques Lacan

TABLE OF CONTENTS

List of Appendices and Enclosures	i
Nomenclature.....	v
Résumé.....	vii
Abstract	xi
Acknowledgments.....	xiii
1. Introduction.....	1
1.1 Motivation, rationale.....	1
1.2 Study area, hypothesis and scientific key questions.....	1
1.3 Methodology and structuring of manuscript.....	3
2. Geological context.....	5
2.1 Tectonic.....	5
2.1.1 Regional tectonic overview	5
2.1.2 Thin-skinned and thick-skinned tectonics.....	7
2.2 Stratigraphy.....	9
2.2.1 The pre-Mesozoic rock units	11
2.2.2 The Mesozoic and Cenozoic sedimentary cover	11
2.3 Geodynamics and tectonic evolution.....	20
2.3.1 The Late Paleozoic evolution.....	21
2.3.2 The Mesozoic evolution	21
2.3.3 The Cenozoic evolution	24
2.3.4 Recent tectonic activity and present-day stress	26
3. Data inventory – seismic and well Data	27
3.1 Historical context from oil and gas to geothermal exploration data.....	28
3.2 2D Seismic reflection profiles.....	29
3.2.1 Principles of seismic reflection (onshore acquisition).....	29
3.2.2 Seismic data resolution and quality types.....	31
3.2.3 Seismic profiles from Canton Geneva	37
3.2.4 Seismic profiles from France and from Canton Vaud.....	44
3.2.5 Seismic Profiles Depth Converted (SPDC)	44
3.2.6 Datum plane and misfit correction	46
3.2.7 Seismic data processing.....	51

3.2.8	Post-processing filtered seismic data and data nomenclature.....	56
3.2.9	Incoming 3D seismic (2022).....	59
3.3	Well data	60
3.3.1	Well log data.....	62
3.3.2	Image well log data	64
3.4	Surface data.....	66
3.4.1	Previous work.....	66
3.4.2	New surface tectonic map.....	66
4.	Seismic interpretation: methodology.....	69
4.1	Calibration of seismic profiles	69
4.1.1	Seismic to well tie.....	69
4.1.2	Seismic horizon definition	76
4.2	Interpretation of seismic profiles.....	78
4.1.3	Stratigraphic interpretation: methodology.....	78
4.1.4	Paleozoic interval	86
4.1.5	Triassic interval.....	87
4.1.6	Liassic interval	89
4.1.7	Dogger interval.....	91
4.1.8	Lower Malm interval	91
4.1.9	Upper Malm interval	92
4.1.10	Cretaceous and Eocene interval.....	94
4.1.11	Cenozoic and post- Eocene intervals.....	99
4.1.12	Quaternary interval	100
4.1.13	Structural interpretation	101
4.3	Horizon mistie correction.....	104
4.4	Uncertainty of the seismic interpretation in the Geneva Basin.....	105
5.	Modelling and 3D geological model.....	113
5.1	Time to depth conversion	113
5.1.1	Methodology	113
5.1.2	Regional velocity model 1	115
5.1.3	Geneva Basin velocity model 2.....	120
5.1.4	Velocity model 3 test.....	126
5.1.5	Discussion about the velocity models and uncertainties.....	127
5.2	Gridding methods.....	132

5.2.1	TWT grids.....	132
5.2.2	Depth grids	134
5.2.3	Interval thickness grids.....	135
5.2.4	Uncertainty of gridding.....	136
6.	Seismic interpretation results	137
6.1	Structural styles.....	137
6.2	The Triassic, basal décollement zone and mechanical basement.....	142
6.3	Tectonic interpretation	150
6.3.1	Geneva – Nyon area / North part of GVA Molasse Basin.....	152
6.3.2	Humilly – Vuache area / Southern part of the Geneva Molasse Basin	172
6.3.3	Salève and Subalpine Molasse area	186
6.3.4	Rumilly Molasse Basin area	198
6.3.5	The Jura area	209
6.4	Main Stratigraphical observations	224
6.4.1	The Liassic and Dogger intervals	224
6.4.2	The Malm reef complex.....	227
6.4.3	The Mesozoic-Cenozoic boundary and the Siderolithic deposits.....	232
7.	Geological history	237
7.1	Late Paleozoic.....	237
7.2	Triassic.....	238
7.3	Jurassic.....	239
7.4	Cretaceous to Eocene.....	241
7.5	Late Eocene to Oligocene.....	241
7.6	Eo-Oligocene rifting of ECRIS.....	242
7.7	From Middle Miocene to the present day	243
8.	Conclusions.....	247
	References.....	253
	Curriculum Vitae - Louis Hauvette	269

LIST OF APPENDICES AND ENCLOSURES

Appendices:

App_01_Seismic_Listing.xls
App_02_Seismic_Listing_and_PDF_Catalog_Numbering.xls
App_03_wells_listing.xls
App_04_Synthetic_Humilly-2_with_Line_88SVO07.pdf
App_05_Synthetic_Faucigny-1_with_Line_83BV10.pdf
App_06_Synthetic_Chapery-1_with_Line_NS04_part1.pdf
App_07_Synthetic_La-Chandelière-1D_with_Line_EW03_part2.pdf

Enclosures:

Maps:

Encl_M00_Seismic_Basemap.pdf
Encl_M01_Structural_Sketch_Map.pdf
Encl_M02_Surface_Geological_Map.pdf
Encl_M03_Kinematic_Sketch_Map.pdf
See chap 5 for Velocity Model definition:
Encl_M05 to Encl_M11 = Depth maps from GVA Velocity Model 2
Encl_M12 to Encl_M15 = Depth maps from Regional Velocity Model 1
Encl_M16 to Encl_M19 = Depth maps from Merged Regional Velocity Model 1 & GVA Vel Model 2
Encl_M20 to Encl_M27 = TWT maps from GVA Velocity Model 2
Encl_M28 to Encl_M31 = TWT maps from Regional Velocity Model 1
Encl_M32 to Encl_M35 = TWT maps from Merged Regional Velocity Model 1 & GVA Vel Model 2
Encl_M36 to Encl_M44 = Thickness maps from GVA Velocity Model 2
Encl_M45 to Encl_M48 = Thickness maps from Regional Velocity Model 1
Encl_M49 to Encl_M52 = Thickness maps from Merged Regional Velocity Model 1 & GVA Vel Model 2
Encl_M53 to Encl_M59 = Interval velocity maps from GVA Velocity Model 2

Seismic line catalog:

Encl_01 to Encl_85 = 117 interpreted seismic sections with:

- Depth converted section with “D” extension at naming Encl_XXD
- Velocity model sections with “V” extension at naming Encl_XXV
- See App_02_Seismic_Listing_and_PDF_Catalog_Numbering.xls for listing of these enclosures

See Table 0-1 for further details about these enclosures.

List of Appendices and Enclosures

Country	Line name	Arbitrary Line name	Fig number in text	Tab number in text	Chap 6 Area (Fig)	Encl Num (TWT) Encl Num D (Depth) Encl Num V (Velocity Models)	Projected wells
CH	9001		Fig 3-20; 3-21; 4-23, 6-17	Tab 4-9	GVA	Encl 01	
CH	9002			Tab 4-6		Encl 02	
CH	9003					Encl 03	Geo-02
CH	9004					Encl 04	
CH	9005		Fig 3-20			Encl 05	
CH	9006	A_GVA_2	Fig 4-15; 6-19		GVA	Encl 06	GEo-02
CH	20UNIGE_001	A_GVA_2	Fig 6-19		GVA	Encl 06	
FR	82GEX06	A_GVA_2	Fig 6-19		GVA	Encl 06	L112
CH	15SIG_002					Encl 07	
CH	15SIG_003					Encl 08	
CH	15SIG_004					Encl 09	
CH	15SIG_005					Encl 10	
CH	15SIG_006					Encl 11	
CH	15SIG_007		Fig 3-8			Encl 12	
CH	15SIG_008		Fig 3-22	Tab 4-9		Encl 13	GEo-01
CH	15SIG_010			Tab 4-12		Encl 14	
CH	15SIG_013		Fig 6-64; 6-65			Encl 15	L410E
CH	15SIG_016		Fig 3-5			Encl 16	
CH	15SIG_019					Encl 17	367
CH	15SIG_101					Encl 18	
CH	18SIG_001_with_15SIG_001_Merged		Fig 6-8	Tab 4-2	GVA	Encl 19	
CH	18SIG_002		Fig 6-16	Tab 4-3; 4-4	GVA	Encl 20	
CH & FR	18SIG_003		Fig 3-7; 3-8; 3-16; 4-8; 4-11; 4-12; 5-6; 6-18; 6-60	Tab 4-4; 4-7; 4-8		Encl 21	GEX-2
FR	18SIG_004		Fig 3-5; 3-19; 6-8		GVA	Encl 22	
CH & FR	18SIG_005					Encl 23	
FR	18SIG_006					Encl 24	
FR	18SIG_007		Fig 6-59			Encl 25	
CH	18SIG_008					Encl 26	
CH	18SIG_009					Encl 27	
CH	18SIG_010		Fig 3-18			Encl 28	
CH	18SIG_011		Fig 3-23; 4-16; 6-64; 6-65	Tab 4-10; 4-12		Encl 29	GEo-02
CH	18SIG_012					Encl 30	
CH	18SIG_014		Fig 3-6	Tab 4-13		Encl 31	
CH	18SIG_015					Encl 32	
FR	18CPG_001		Fig 3-7			Encl 33	GEX-1, GEX-7
CH	20SIG_001					Encl 34	
CH	20SIG_002					Encl 35	
FR	20SIG_003					Encl 36	
FR	80-JU-01	A-JURA	Fig 3-16; 4-8; 6-46; 6-47		JURA	Encl 37 & 37D & 37V	
FR	81-JU-06	A-JURA	Fig 5-4; 5-10; 6-46; 6-47		JURA	Encl 37 & 37D & 37V	
FR	82GEX01	A-HUM-1	Fig 6-25		HUM	Encl 38	HU-2
FR	88SVO07	A-HUM-1 & A-SAM-2	Fig 4-5; 4-22; 6-25	Tab 4-4; 4-5	HUM	Encl 38 & 85	HU-2
FR	82GEX02		Fig 4-13			Encl 39	GEX-3, (GEX-4), GEX-5
FR	82GEX03					Encl 40	GEX-3, GEX-4
FR	82GEX04					Encl 41	
FR	82GEX07		Fig 6-13		VAUD	Encl 42	
FR	82GEX08					Encl 43	
FR	82GEX09					Encl 44	
FR	82GEX10					Encl 45	
FR	83BV09		Fig 6-35		SAM	Encl 46 & 46D & 46V	
FR	83BV10	A-SAM-1	Fig 6-33; 6-34		SAM	Encl 47 & 47D & 47V	FAY-1
FR	HR535	A-SAM-2			SAM	Encl 85 & 85D & 85V	SA-1, SA-2
FR	HR536	A-SAM-1	Fig 6-33; 6-34		SAM	Encl 47 & 47D & 47V	
FR	HR545	A-SAM-1	Fig 6-33; 6-34		SAM	Encl 47 & 47D & 47V	
FR	88SVO02	A-RUM			RUM	Encl 48 & 48D & 48V	SV-107
FR	HR528	A-RUM			RUM	Encl 48 & 48D & 48V	SV-101, CHY-1
FR	88SVO03		Fig 6-36; 6-39		SAM / RUM	Encl 49 & 49D & 49V	SV-106, SV-108
FR	88SVO04		Fig 6-40		RUM	Encl 50 & 50D & 50V	
FR	88SVO06					Encl 51	
FR	88SVO08		Fig 3-24; 6-26; 6-64; 6-65		HUM	Encl 52 & 52D & 52V	
FR	88SVO09					Encl 53	
FR	90SVO02				RUM	Encl 54 & 54D & 54V	
FR	90SVO05		Fig 6-41		RUM	Encl 55 & 55D & 55V	
FR	01AC1					Encl 56	GEX-6

List of Appendices and Enclosures

FR	O2AC1					Encl 57	
FR	16AC1					Encl 58	
FR	2CC1		Fig 3-8; 6-14		VAUD	Encl 59	MEY-1
FR	EW02		Fig 6-9; 6-24		HUM	Encl 60	HU-1
FR	EW02_W_SAM		Fig 5-12; 6-32		SAM	Encl 61 & 61D & 61V	
FR	EW02_W_JUR		Fig 6-48; 6-49; 6-50; 6-51		JURA	Encl 62 & 62D & 62V	CHT-1
FR	EW03_part2		Fig 6-52; 6-53		JURA	Encl 63 & 63D & 63V	CYT-1, CTL-1, LCD-1
FR	EW03_part3		Fig 6-29		HUM	Encl 64	
CH	GG87-01		Fig 3-26			Encl 65	
CH	GG87-02	A-GVA-1	Fig 3-25; 4-24; 4-25; 6-18		GVA	Encl 66	GEo-01
CH	GG87-04	A-GVA-1	Fig 6-18		GVA	Encl 66	
CH	GG87-05	A-GVA-1			GVA	Encl 66	
CH	GG87-03		Fig 3-18			Encl 67	
CH	GG87-06					Encl 68	
CH	GG87-07		Fig 6-17		GVA	Encl 69	
FR	HR530			Tab 4-2	SAM	Encl 70 & 70D & 70V	
FR	NS03_part3		Fig 6-42; 6-43		RUM	Encl 71 & 71D & 71V	SV-107
FR	NS03_part4					Encl 72	L112
FR	NS04_part1		Fig 6-27; 6-28		HUM	Encl 73 & 73D & 73V	CHY-1
FR	SJ1U2					Encl 74	GEX-1, GEX-7
FR	SJ1U3					Encl 75	GEX-2
FR	SJ1U4		Fig 3-5; 3-19			Encl 76	
FR	SJ1U6		Fig 6-16		GVA	Encl 77	
FR	SJ1U7					Encl 78	
FR	SJ1V2		Fig 6-13		VAUD	Encl 79	
FR	SJ1V3					Encl 80	
CH	THO1					Encl 81	THO-1
CH	THO2		Fig 6-17		GVA	Encl 82	THO-1
CH	VD-P730016		Fig 6-13		VAUD	Encl 83	313_G
CH	XI-74VD52-74SADH6		Fig 6-14		VAUD	Encl 84	

CH = Switzerland FR = France	A-Line = Arbitrary line made of a combination of several seismic sections	GVA: Geneva area, text part 6.3.1 VAUD: Nyon area, text part 6.3.1 HUM: Humilly area, text part 6.3.2 RUM: Rumilly area, text part 6.3.4 SAM: Subalpine Molasse and Salève areas, text part 6.3.3 JURA: Jura area, text part 6.3.5
---------------------------------	---	---

Table 0-1: Listing of seismic lines and their related figures & tables & enclosures presented in this study. The areas where these seismic lines are located and the wells projected into them are informed in this table. This information is also sum up in App_02 file in the attached files of this work.

NOMENCLATURE

AFBD	Alpine Foreland Basal Décollement
App	Appendix
BF	Black Forest
BG	Bresse Graben
BRGM	Bureau de Recherches Géologiques et Minières (French geological survey)
BSJA	Burgundy-Swabian Jura Anticline
Celtique	Celtique Energies Petroleum Ltd (Celtique)
Cen	Cenozoic
CMP	Common Mid Point
CRS	Common Reflection Surface Processing
CS	Coordinate System
DEM	Digital Elevation Model
Do	Dogger
ECM	External Crystalline Massifs
ECRIS	European Cenozoic Rift System
Encl	Enclosure
FBT	Frontal Back Thrust
FTB	Fold Thrust Belt
FC	Fault corridor
FT	Frontal Thrust
FZ	Fault zone
GEOMOL	International project for 3D geological modeling (BRGM, Swisstopo)
GGB	Greater Geneva Basin
GGE	Geneva Geo Energy SA, renamed Ad Terra Energy SA in 2021
GIS	Geographic Information System
GL	Ground level
GMB	Geneva Molasse Basin
GVA	Geneva
GVAB	Geneva Basin
HARMOS	Swiss project (Swisstopo) for harmonizing geological data in Switzerland
HGE	HydroGeo Environment
IJ	Internal Jura
InPal	Intra Paleozoic
Int Vel	Interval Velocity
JFTB	Jura Fault-and-Thrust Belt

Nomenclature

JUR	Jura
KB	Kelly Bushing
Keu	Keuper
MB	Molasse Basin
Mes	Mesozoic
NAF	North Alpine Foreland
NAFB	North Alpine Foreland Basin
NAGRA	National Cooperative for the Storage of Radioactive Waste
nB	near Base
nT	near Top
OMM	Obere Meeresmolasse (= Upper Marine Molasse in English)
OSM	Obere Süsswassermolasse (= Upper Freshwater Molasse in English)
PostSTM	Post Stack Time Migration
PreSTM	Pre Stack Time Migration
proj.	Projected
Q	Quaternary
RTS	Real Time Seismic
RUM	Rumilly area
s	Seconds
SAM	Subalpine Molasse area
SIG	Services industriels de Genève
SPDC	Seismic Profile Depth Converted
SRD	Seismic Reference Datum
Swisstopo	Swiss federal office for topography
TD	Total Depth
Trace	Seismic trace
TWT	Two Way Traveltime
UMM	Untere Meeresmolasse (= Lower Marine Molasse in English)
UNIFR	Université de Fribourg
UNIGE	Université de Genève
URG	Upper Rhine Graben
USM	Untere Süsswassermolasse (= Lower Freshwater Molasse in English)
Vibro	Vibrator truck
Vrepl	Replacement Velocity
VSP	Vertical seismic profile
WD	Weight Drop
WMB	Western Molasse Basin
WNAFB	Western North Alpine Foreland Basin

RÉSUMÉ

L'Avant-Pays Nord-Alpin (NAF) est divisé en deux domaines : le Bassin Molassique (MB) et la Ceinture de Plissement et de Chevauchement du Jura (FTB). Ces domaines sont détachés du socle mécanique au-dessus d'un décollement dans les évaporites du Trias. Les chevauchements, les plis et les failles décrochantes sont les principales structures qui se développent dans la couverture sédimentaire détachée du Mésozoïque et du Cénozoïque de la région. Ces structures sont principalement liées à l'orogénèse alpine du Cénozoïque et certaines d'entre elles sont héritées de la période d'extension du Jurassique (réactivation). Des failles préexistantes dans le socle peuvent également influencer le développement de ces structures dans le cadre de déformations épidermiques minces (« thin-skinned ») et épaisses (« thick-skinned »). Le Bassin Genevois, en Suisse occidentale, fait partie du Plateau Molassique au sein du Bassin Molassique et est limité au nord-ouest par la Ceinture de Plissement et de Chevauchement du Jura (JFTB) et au sud-est par la Molasse Subalpine (SAM).

Le projet "GEothermies" du Canton de Genève a permis de réévaluer le cadre structural et la cinématique de la partie la plus occidentale de l'Avant-Pays Nord-Alpin, y compris les domaines de la Haute Chaîne de la Ceinture de Plissement et de Chevauchement du Jura. L'analyse s'étend donc du Bassin Genevois aux régions voisines du Salève vers le sud-est, au système de failles du Vuache et du Bassin de Rumilly au sud, ainsi qu'aux montagnes du Jura à l'ouest. L'interprétation sismique est basée sur des données sismiques 2D datant dès années 1960 jusqu'à des lignes récemment acquises en 2018 (plus de 150 profils sismiques 2D). Elle a été combinée avec des données de surface, e.g. des pendages stratigraphiques, des cartes géologiques, des Modèles Altimétriques Numériques (DEM), et surtout avec 66 puits (dans la base de données) et diverses cartes géoréférencées provenant de la littérature. Cette étude s'est appuyée sur cet ensemble complet de données pour créer les nouveaux résultats géologiques et géophysiques suivants :

- Un nouveau positionnement **régional** affiné de la **surface approchée du socle pré-Mésozoïque** (nBMes), pour toute la région voisine du Bassin de Genève. Cette carte comprend le Bassin de Rumilly, la région de la Molasse Subalpine et, plus important encore, une partie du Jura Interne. Ce résultat a été obtenu grâce à une nouvelle méthodologie sophistiquée de modélisation des vitesses et de conversion des profondeurs à l'aide des quatre horizons sismiques interprétés à l'échelle régionale : Base approchée du Cénozoïque (nBCen), Toît approché du Dogger (nTDo), Toît approché du Keuper (nTKeu), Base approchée du Mésozoïque (nBMes).
- Un nouveau **modèle de profondeur affiné et à haute résolution du Bassin de Genève**. Nous nous sommes spécifiquement concentrés sur cette zone, puisqu'elle constitue l'intérêt principal du projet "GEothermies" mené par SIG dans le Canton de Genève. Il est basé sur les huit horizons sismiques interprétés suivants : Base approchée du Cénozoïque (nBCen), Toît approché du Malm supérieur (nTUMa), Toît approché du Malm inférieur (nTLMa), Toît approché du Dogger supérieur (nTDo), Toît approché du Lias supérieur (nTLi), Toît approché du Keuper supérieur (nTKeu), Toît approché du Muschelkalk supérieur (nTMu), Base approchée du Mésozoïque de base (nBMes). Par la suite, nous avons mis en œuvre une **méthode de conversion temps-profondeur plus détaillée et plus avancée** par rapport au modèle de vitesse régional. Elle consiste en une loi de vitesse polynomiale complexe pour la

couche Cénozoïque et en des grilles de vitesses d'intervalles interpolées pour les autres couches Mésozoïques.

- Un **catalogue de lignes sismiques** (fichiers PDF, voir Annexes) montrant les données brutes, l'interprétation et le modèle géologique. En outre, une vingtaine de lignes sont également présentées dans un format converti en profondeur.
- Un nouveau **modèle cinématique** ainsi qu'un nouveau modèle structurel illustré dans la nouvelle **carte tectonique de la région**. Ensuite, les structures identifiées ont été analysées en relation avec l'épaisseur principale (**cartes d'épaisseur**) et les variations latérales de faciès sismique. En effet, la signature sismique de dépôt de chaque sous-unité a également été étudiée et compilée dans un catalogue de faciès sismiques.

Les principaux résultats structuraux et géologiques de notre interprétation sismique concernent les zones de failles spécifiques ou les distributions de faciès sismiques suivantes:

- Nous avons identifié des **Couloirs de Failles (FC)** qui agissent comme **des systèmes de failles décrochantes conjuguées** prolongeant les systèmes de failles connus dans le FTB du Jura qui s'étendent donc dans le bassin molassique. Ces couloirs mesurent dans le Bassin Molassique Genevois jusqu'à 15 km de long et environ 500 m de large, et sont constitués de multiples segments de faille de plus petite échelle non corrélés et d'extension verticale d'environ 100-300 ms.
- Deux configurations principales de failles décrochantes conjuguées peuvent être identifiées à l'est et à l'ouest de la Zone de Faille (FZ) du Vuache :
 - A l'est de la FZ du Vuache, nous observons des failles décrochantes dextres orientées E-O (par exemple les FC de Saint-Cergue, Divonne, Prévessin, Meyrin ou Aire-la-Ville) conjuguées à des failles décrochantes sénèstres NNW-SSE (par exemple la FC du Coin ou la FC de Mourex). Ce contexte conjugué correspond à une direction de raccourcissement orientée NW-SE.
 - A l'ouest de la FZ du Vuache, des failles décrochantes dextres orientées ENE-WSW se conjuguent avec des failles décrochantes sénèstre orientées NW-SE, ce qui suggère une direction de raccourcissement WNW-ESE.
- Des failles normales listriques d'extension syn-sédimentaires ont été clairement identifiées et interprétées, avec une activité et une croissance principales pendant la période du Jurassique Inférieur à Moyen (en particulier pendant le Lias). Ces failles ont ensuite été légèrement inversées au cours de la compression alpine. Elles forment une zone d'extension en éventail imbriqué qui s'est développée le long et à l'est de la zone de faille décrochante NW-SE du Vuache. Elle englobe la FZ d'Humilly, de direction NE-SW et de vergence SE, qui est reliée comme une branche à la faille principale du Vuache. Ce système de failles héritées pourrait également inclure la ceinture de failles du Salève qui a été interprétée avec la même activité syn-sédimentaire d'extension du Jurassique. La FZ NE-SW de Pougny et le FC de Cercier sont rattachées au même système d'extension mais peuvent être datées de la période d'extension Eo-Oligocène. D'autres branches de failles NE-SW peuvent également être associées à la FZ du

Vuache-Humilly-Salève. Ceci concerne les zones de failles à l'ouest de la FZ du Vuache telles que la FZ de Musiège ou la FZ du Gros Foug.

- Les tendances des faciès sismiques ont également été étudiées, en particulier en relation avec les faciès de l'Eocène (Sidérolithique) et du Malm Supérieur (complexe récifal). Les origines sédimentaires ont été analysées en relation avec la configuration structurale à l'époque du dépôt (rôle important des sommets paléo-topographiques).

En conclusion, l'Avant-Pays Nord-Alpin occidental entourant Genève est maintenant mieux contraint structurellement et sédimentairement avec des concepts nouveaux ou plus développés qu'auparavant.

ABSTRACT

The North Alpine Foreland (NAF) is divided into two domains: the Molasse Basin (MB) and the Jura fold-and-thrust belt (FTB). These domains are detached from the mechanical basement above a *décollement* in the Triassic evaporites. Thrusts, folds and strike-slip faults are the major structures developing in the detached Mesozoic and Cenozoic sedimentary cover of the area. These structures are mainly related to the Cenozoic Alpine orogeny and part of them are inherited from the Jurassic extensional period (reactivation). Pre-existing faults in the basement may also influence the development of these structures in the frame of the thin-skinned or thick-skinned deformations. The Geneva Basin, in western Switzerland, is part of the Plateau Molasse within the Molasse Basin and is limited to the NW by the JJFTB and to the SE by the Subalpine Molasse (SAM).

The “GEothermies” project of the Canton Geneva has provided an incentive to re-assess the structural setting and kinematics of the westernmost portion of the North Alpine Foreland, including the Haute Chaîne domains of the Jura Fold-and-Thrust Belt. Therefore, the analysis extends from the Geneva Basin to the neighboring regions of the Salève to the Southeast, the Vuache fault system and the Rumilly Basin to the South, as well as the Jura Mountains to the West. The seismic interpretation is based on vintage surveys since 1960’ and recently acquired 2D seismic data in 2018 (more than 150 seismic 2D profiles). It was combined with surface data e.g. bedding dips, geological maps, DEM, and especially with 66 wells (in the database) and various georeferenced maps from the literature. This study relied on this comprehensive dataset to create the following new geological and geophysical outputs:

- A new **regional** refined positioning of the **near pre-Mesozoic basement surface** (nBMes), for all the neighboring area of the Geneva Basin. It includes the Rumilly Basin, the Subalpine Molasse area and more importantly a part of the Internal Jura. This was achieved using a new sophisticated **regional velocity modelling** and depth conversion methodology using the four regionally interpreted seismic horizons, near Base Cenozoic (nBCen), near Top Dogger (nTDo), near Top Keuper (nTKeu), near Base Mesozoic (nBMes).
- A new refined and **high-resolution depth model of the Geneva Basin**. We specifically focused on this area, since it is the main interest of the “GEothermies” project run by SIG in the Canton of Geneva. It is based on the following eight interpreted seismic horizons; near Base Cenozoic (nBCen), near Top Upper Malm (nTUMa), near Top Lower Malm (nTLMa), near Top Dogger (nTDo), near Top Lias (nTLi), near Top Keuper (nTKeu), near Top Muschelkalk (nTMu), near Base Mesozoic (nBMes). Subsequently we implemented a more **refined and advanced time-to-depth conversion** method in comparison to the regional velocity model. It consists of a complex polynomial velocity law for the Cenozoic layer and of advanced interpolated interval velocity grids for the other Mesozoic layers.
- A **seismic line catalogue** (PDF files, see Enclosures) showing the raw data, the interpretation and the geological model. In addition, some 20 lines are also presented in depth converted format.

Abstract

- A new **kinematic model** together with a new structural model shown in the new **tectonic map** of the area. Then, the structures identified were analyzed in relation with the main thickness (**thickness maps**) and seismic facies lateral variations. Indeed, the depositional seismic signature of each sub-unit has also been investigated and compiled in a **seismic facies catalog**.

The main structural and geological findings of our seismic interpretation concerns the following specific fault zones or seismic facies distribution:

- We have identified **fault corridors** that act as **conjugate strike-slip fault** systems that are an extension of the fault systems known from the Jura FTB and which thus extend into the Molasse Basin. These corridors measure in the Geneva Molasse Basin, up to 15km length and around 500 m wide, and are made of multiple non-correlated near vertical small-scale fault segments of vertical extent around 100-300ms.
- Two main different conjugate strike-slip fault settings can be identified east and west of the Vuache Fault Zone:
 - East of the Vuache FZ, we observe E-W striking dextral strike-slip faults (e.g Saint-Cergue FC, Divonne FC, Prévessin FC, Meyrin FC, or Aire-la-Ville FC) conjugated with NNW-SSE sinistral strike-slip faults (e.g Le Coin FC, or Mourex FC). This conjugate setting corresponds to a NW-SE oriented shortening direction.
 - West of the Vuache FZ, ENE-WSW oriented dextral strike-slip faults conjugated with NW-SE sinistral strike-slip faults, suggesting a WNW-ESE shortening direction.
- **Syn-sedimentary extensional listric normal faults** have been clearly identified and interpreted, with a main activity and **growth during the Early to Middle Jurassic** period (especially during the Lias). These faults have been subsequently modestly inverted during alpine compression. They form an extensional imbricated fan zone developed along, and east of the leading NW-SE strike-slip Vuache fault zone. It encompasses the NE-SW striking SE-vergent Humilly FZ linked as a branch to the Vuache leading fault. These inherited fault system, may also include the Salève FZ belt that was interpreted with the same extensional Jurassic syn-sedimentary activity. The NE-SW Pougny FZ and the Cercier FC are attached to the same extensional system but possibly dated from the **Eo-Oligocene extensional period**. Other NE-SW fault branches may also be associated to the Vuache-Humilly-Salève FZ. This concerns fault zones west of the Vuache FZ such as the Musiège FZ or the Gros Foug FBT.
- **Seismic facies trends** have also been investigated especially in relation to the **Eocene (Siderolithic)** and **Upper Malm facies (recifal complex)**. The sedimentary origins were analyzed in relation to the structural configuration at the depositional time (important role of the paleo-topographical highs).

This study has made it possible to better constrain the alpine and synsedimentary structural setting of the western Alpine foreland surrounding Geneva and develop a new tectonic and kinematic understanding.

ACKNOWLEDGMENTS

I feel like I am not exactly the same person than when I began this project beginning of 2019. I have not only gathered scientific knowledge, I think the personal outcome of this adventure is way more larger. I have been extremely lucky to get the possibility to work on this project, and it happened thanks to amazing support from many persons and entities. I would like to share my immense and sincere gratefulness to all the contributors, who gave me unforgettable moments and who changed forever my way of thinking.

This project would never have seen the light without Dr. Bernd Fiebig from Ad Terra Company, where I used to work at the beginning of the study. Bernd initiated the project from scratch for several reasons. I think he kindly wanted me to evolve in my technical abilities, but also saw the common benefit that it could provide to all the different stakeholders. The idea was to provide an academic-level geophysical study of the great Geneva Basin, for a direct industrial application (geothermal energy exploration). Thank you Bernd!

I want to sincerely thank the company Ad Terra (previously named Geneva GeoEnergy or GGE before 2021), which gave me the framework to achieve this study (access to data, working space, IT, HR, and coverage of additional costs).

The second part of the puzzle that allowed launching the project is inevitably the Services Industriels de Genève (SIG). This amazing company with great geothermal ambitions accepted to support almost all the costs of the project. SIG not only took care of the financing of the project but gave me a continuous technical and human support particularly from the head of the geothermal department of the company, Dr. Michel Meyer. Thank you so much Michel for believing in this project! Thank you also Carole, François and Frédéric from the SIG.

I gratefully acknowledge SIG for giving the access to the entire well and seismic data that are the raw materials of this study.

The last crucial part of the puzzle comes from the Geosciences Department of the University of Fribourg (UNIFR, Switzerland) who accepted to accompany me throughout the project (including additional financial contribution). I was so lucky to have incredible two thesis supervisors. My study was so much well guided by Prof. Jon Mosar, who has always kindly shared with me his immense knowledge in structural geology, which gave me the right distance to look at the tectonic of the region. Working with Jon was moreover always achieved in a very friendly atmosphere that made me so happy all the days spent at the UNIFR office. Jon was also a great coach to help me keeping my motivations, and dealing the project in relation to personal matters. Thank you so much Jon!

I had the great privilege to have PD Dr. Anna Sommaruga as co-supervisor. Anna helped me a lot to achieve seismic interpretation in a rigorous and academic manner. I have learnt so much at her side, and especially concerning the link between geology and geophysics, but also concerning the scientific methodology and approaches. Her teaching has definitely changed my way of working forever. Anna has played a very important role in helping me organizing the project, and in structuring my work. Moreover, I enjoyed so much spending times with Anna during all the coffee and lunch breaks, discussing about everything. I spent very great times in Fribourg thanks to Anna. Thank you so much Anna!

Acknowledgments

My work has been reviewed, commented and finally accepted by the members of the jury who spent a lot of time on it. Therefore, I warmly thank Prof. Dr. Juan Soto, Prof. Anneleen Foubert and Prof. Vincent Serneels for their time and passion for Science.

I am very appreciative to the different companies that provided me with their software licenses:

- IHS Markit company, for the Kingdom software to run the seismic interpretation;
- Petrosys company, for the best subsurface mapping and gridding software, Petrosys;
- ESRI company, for the ArcMap software for complementary mapping.

I would like to express my gratitude to University of Geneva which shared with me some knowledges about the structural geology of the Geneva region (including the GEOMOL project). In this context, I personally thank the following persons of the University of Geneva for their kind help and very interesting discussions we had together: Prof. Georges Gorin, PD Dr. Mario Sartori, Prof. Andrea Moscariello, Dr. Nicolas Clerc, PD. Dr. Joël Ruch, David Polasek and Dr. Elme Rusillon.

I am also thankful to the following institutions who provided me with additional data:

- the Canton Vaud and its “Musée cantonal de géologie” who shared the last GEOMOL seismic interpretation results of the Canton de Vaud (from Dr. Robin Marchant);
- The Celtique Energie company;
- The Federal Office of Topography Swisstopo.

I am grateful to all my former colleagues from Ad Terra company where I used to work. Their technical and friendly support contributed greatly to this work, Benjamin, Korina, Adeline, Mikhail, Antoine, Rodolphe, Simon, Gilles, Vincent, Jeremy, Pablo, Bastien, Serge, Olivier and Vincent V.

I moved in 2022 to another company HydroGeo Environment (HGE) in Geneva. It was very pleasant to spend the last months of this study in very nice conditions with the support of the company and of all my new colleagues, Jérôme, Ludovic, Marius, Elme, Maud, Antoine, David, Pierre, and Florian.

All the team members of the Geosciences Department of the UNIFR have certainly played a very important role in either helping me keeping faith in the achievement of this work or in having a good time outside of work. I particularly think of the great talks and laughs exchanged with Dr. Omar Radaideh, but I also think of Dr. Sandra Borderie, Dr. Marc Schori and Adeline Marro with many shared projects always done in an amazing, nice atmosphere. I also enjoyed a lot discussing with Valentin, Nicole, Janine, Anina and Jürgen von Raumer. The Geosciences Department of the UNIFR would not work so well without the great IT job of Alex Vaira who was always available and kind to manage all sort of issues or installations.

I could always rely on all my dear friends to give me fresh air when I needed it. Thank you to all my friends of Annecy, all the poets and friends from Géol Nancy and all the Dagoveranians.

I am eternally thankful to my parents Anne and Jacques Hauvette who always helped me a lot and took care to put me in good conditions in my studies. Your support was very important to me and surely gave me the strength to complete this work. I would like to also thank my brothers and sisters for always giving me good vibrations each time we meet. Thanks Ségo, Djé, Gabi and Clairette. Same feeling with my family in law, thank you.

I will finish these acknowledgments with the most important persons of my life, my dear wife Marine Cazy and my lovely son Célestin. You are an infinite source of inspiration and happiness. Thank you so much for supporting me during this long project.

I dedicate this work to Marine and Célestin.

1. INTRODUCTION

1.1 Motivation, rationale

Switzerland has the great ambition to reach carbon neutrality in the next 30 years. Moreover, the current global geopolitical situation is pushing countries to seek for energy self-sufficiency. These are major arguments in favor of geothermal exploration. Switzerland is betting on this energy of the future, which is local, continuous, and without CO₂ emissions. Switzerland is already the world champion in geothermal probe for individuals (highest probe density on the planet), and several very promising projects for deep geothermal energy raised these last years in several cantons. In Canton Geneva, the “GEothermies” project is led by the “Services Industriels de Geneve” (SIG) targets to obtain 20% of its needs in heating with geothermal energy.

For this purpose, it is crucial to improve the knowledge of the underground. Indeed, there are several known levels of aquifer reservoir in the sedimentary cover in the Geneva area, but more exploration studies are still needed for a proper exploitation. All this research may benefit from the numerous data acquired during decades (increase after World War II) for the unsuccessful oil&gas exploration. There are also tremendous public Swiss geological/geophysical studies achieved in relation to the nuclear waste repository project (NAGRA, National Cooperative for the Storage of Radioactive Waste), or to international academic project such as the GeoMol project (Allenbach et al., 2017) or the Seismic Atlas of the Swiss Molasse Basin (Sommaruga et al., 2012).

The present project (2019-2022) is placed in this frame of improving our knowledge of the subsurface as part of the geothermal project. The study area (Figure 1-1) extend outside the Canton Geneva (GVA) to the southern part of the Canton Vaud (North of GVA), and to the French departments of the Jura (west of GVA), l’Ain (West of GVA), and to the Haute-Savoie and Savoie (South of GVA). It is particularly focused on the tectonic setting of the subsurface, since fault and fracture systems (natural) represent major permeability vectors (water flow potentials). It was financed by the Services Industriels de Genève (SIG) and supported by Ad Terra Energy SA (Geneva) which gave the opportunity and the availability to its employee (until April 2022, myself-Louis Hauvette) to achieve this study at the University of Fribourg in Switzerland (Department of Geosciences, Earth Science unit). To be noted that Ad Terra Energy SA was named Geneva Geoenergy SA before 2021, and both names are used in this document depending on the year the mentioned studies were achieved (before or after 2021). This work was supervised and co-supervised by respectively Prof. Jon Mosar and Dr. Anna Sommaruga.

1.2 Study area, hypothesis and scientific key questions

The studied area focusses on the Geneva Basin but includes the Salève thrust anticline and the Subalpine Molasse area to the SE, the Vuache Mountain and the adjacent Rumilly Basin to the S, as well as the meridional parts of the JFTB to the West (Figure 1-1).

The main working hypothesis considers that the Alpine foreland, including the Molasse Basin and the Jura Mountains, are part of a detached foreland fold-and-thrust-belt. This foreland forms a mechanical

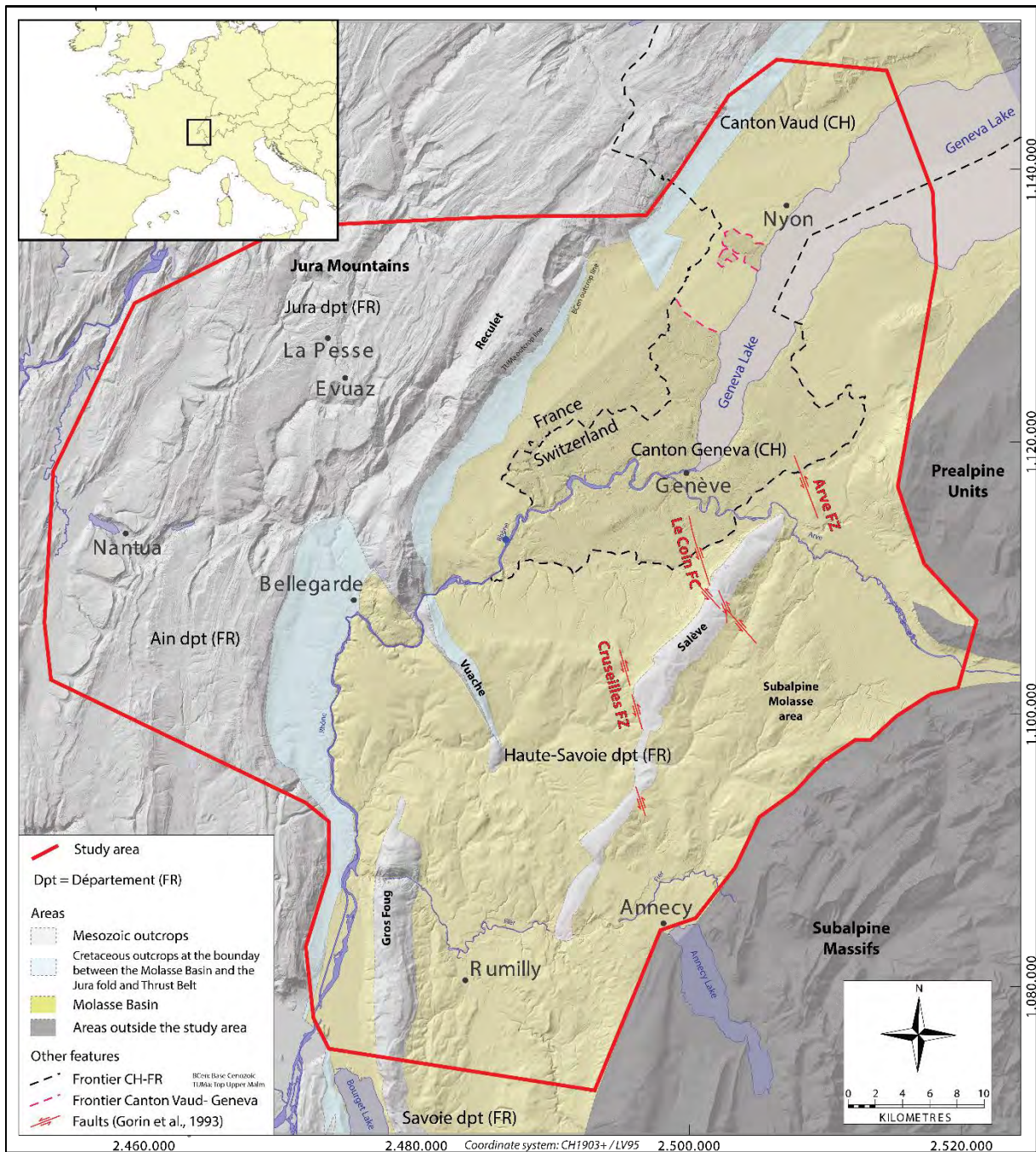


Figure 1-1 : Localisation of the area of investigation, extended around Canton Geneva to the Canton Vaud to the North, to the French departments (dpt) of the Jura (W), Ain (SW), and Haute-Savoie and Savoie (S). (coordinate system: CH1303+/LV95)

wedge which is detached above Upper Triassic salt-rich evaporites and deformation inside the wedge is mainly accommodated by thrust-related folding and strike-slip faults.

The overall foreland-directed transport direction of the wedge is towards the N-NW and the wedge-internal, oscillating and repetitive thrust sequence is driven by wedge mechanical process linked to erosion, friction along the décollement zone, and topography of the basal décollement.

The objectives of this work are to constrain the thrust and fold geometry as well as define near top basement surface in order to gain a better understanding of the thrust and fold development. Using seismic data (Gorin et al., well data, combined with surface geological data, we will devise a new kinematic

model. This model will rely on the interpretation of the structural geology ranging from inherited faults to recent tectonics. Main issues relevant to achieve this goal can be formulated as follows:

- Do the main transpressional NW-SE faults supposed for the last decades, and formerly named as Cruseilles/ Le Coin/ Arve faults from SW to NE (Gorin et al., 1993), exist and cross-cut the whole Geneva Basin from the Salève area to the Jura Mountains?
- Are strike-slip faults from the Jura Mountains and seen in the Haute-Chaine (mainly sinistral NW-SE and dextral WNW-ESE), extending southward into the Geneva Basin and are they forming one similar fault system?
- How are, the seismically interpretable faults, vertically partitioned and developed in the Mesozoic cover? Can secondary décollement levels be determined in addition to the main Triassic décollement level?
- To what extent is the rheology and thickness distribution in Triassic units influencing main folds in the Basin (halokinetic movements, lateral migration of anhydrites, thrusting and duplexing in the Keuper)? Can surface geology help constrain the deeper structures, orientations and geometries?
- Can we identify extensional faults associated with the opening of the Alpine Tethys during the Jurassic period? Could syn-sedimentary faults have occurred during this period and be interpreted on the seismic images by lateral seismic facies or thickness variations?
- Does the Molasse unit give indications on the kinematics of the different tectonic events (onlapping of the Molasse reflector on top of the Top Cretaceous reflectors).

This study thus makes it possible constrain the alpine and synsedimentary structural settings in the detached foreland fold-and-thrust belt in the Geneva are. The novelty of this work is the integrated approach combining surface and subsurface data across the Mollasse basin into the Jura Mountains. This makes it possible to have a more comprehensive understanding of the fault/thrust and fold processes inside the mechanical foreland wedge. Refined seismic processing and interpretation have yielded a more precise image of the structural setting and in finито made it possible to develop a new tectonic and kinematic understanding.

1.3 Methodology and structuring of manuscript

The investigation is mainly based on the re-interpretation of existing seismic surveys (191 seismic profiles in the database acquired from 1950 to 2022) and well data (66 wells). Surface data and other geological information have been implemented in the interpretation and have made it possible to propose a new tectonic and kinematic understanding of this part of the detached alpine foreland.

The seismic interpretation was achieved using the Kingdom software from IHS Markit, allowing to draw all seismic horizons and fault sticks along seismic sections (seismic Basemap on Encl_M00). The seismic horizon data were then gridded (to obtain 3D surfaces) and mapped using the Petrosys software and part of these results were transferred or exported in ArcGis (ESRI) format. Several maps were also exported into pdf format with layering of the displayed data. The main results concerns the final structural map (Encl_M01), the surface geological map (Encl_M02), and the grid maps of the eight

Chapter 1

following horizons (Encl M05 to Encl_M59), near Base Cenozoic (nBCen), near Top Upper Malm (nTUMa), near Top Lower Malm (nTLMa), near Top Dogger (nTDo), near Top Lias (nTLi), near Top Keuper (nTKeu), near Top Muschelkalk (nTMu), near Base Mesozoic (nBMes).

This manuscript begins with an overview of the geological context of the area in terms of tectonic and sedimentary history (chapter 2). It is followed by a description of the seismic and well data in the inventory (chapter 3). The methodology of seismic interpretation (stratigraphical and structural) is presented in the chapter 4. Examples of fault picking and a seismic facies catalog is then detailed. The interpretation is achieved in the time domain of the seismic sections (twt) and need therefore a time-to-depth conversion process to obtain the final depth maps. The velocity models calculated for such tasks are then described in chapter 5. All results are detailed in the chapter 6, divided by several structural areas, and many seismic sections are displayed. Chapter 7 summarizes the geological history of the area (per geological units) that comes out of our interpretation. The conclusions are finally presented in chapter 8.

2. GEOLOGICAL CONTEXT

In this chapter, we propose an overview of the tectonic (chapter 2.1), the stratigraphic (chapter 2.2) and the geodynamic (chapter 2.3) setting of the region of investigation.

2.1 Tectonic

2.1.1 Regional tectonic overview

The area of investigation is located in the detached North Alpine Foreland Basin (NAFB, (Laubscher, 1961)), which refers to the detached Molasse Basin including, the Plateau Molasse, the Subalpine Molasse, and the Jura Molasse in France and Switzerland. The study area, within a radius of 40km around the city of Geneva (Switzerland) is located in the Western North Alpine Foreland (WNAF) (Figure 2-1). It includes in its eastern part, the Western Molasse Basin (WMB), also sometimes presented as the Geneva Basin, and in its western and northern part, the Jura Fold-and-Thrust Belt (JFTB). In both parts, the Mesozoic and Cenozoic cover is detached from the underlying lower Mesozoic series (middle and lower Triassic) and the pre-Mesozoic basement units, since Mio-Pliocene alpine compression and forms the detached NAF. Since Serravallian times thin-skinned tectonic was enabled along the basal décollement zone located at the base of the Triassic salt-rich evaporite of the Keuper Group. The initiation of the main décollement concurs with the transition of the Western North Alpine Foreland Basin (WNAFB) from a classical flexural foreland basin (asymmetrical geometry) to a wedge-top basin (Bonnet et al., 2007; DeCelles & Giles, 1996; Willett & Schlunegger, 2010). It also marks the start of the formation of the JFTB. The existence of the décollement level has been well documented since the works of Buxtorf (1907, 1916), and displacement has been shown to reach 30km (Affolter & Gratier, 2004; Guellec et al., 1990; Laubscher, 1965).

The Plateau Molasse is characterized by gentle Mesozoic-Cenozoic folding limited in amplitude by the load of the overlying Cenozoic sediments (Burkhard & Sommaruga, 1998). The anticlines of the Plateau Molasse are frequently developed over evaporites-cored features (with possible presence of salt), with typical elongated geometries (Sommaruga, 1995). To the NW, the Plateau Molasse is outcropping against the Haute Chaine Jura relief along an erosive boundary. Several distinct fault systems can be recognized in this area, such as tear faults, strike-slips, reverse and inherited normal faults. Important ramps, frontal and lateral, are known along the Salève Thrust (Fault Zone, FZ), the Gros Foug Thrust or the Vuache Fault Zone (FZ). The attribution of these latter fault systems to the Plateau Molasse will be discussed in this study. These fault systems may have been active at various times, from their time of triggering possibly during the Jurassic to more recent tectonically active periods. In addition to the basal décollement zone, other, secondary, décollement levels exist within the Mesozoic-Cenozoic cover (Figure 2-2)(Clerc & Moscariello, 2020). The southeastern part of the Plateau Molasse is bordered by the frontal Subalpine Molasse Thrust, north-east of the Vuache Fault Zone, whereas it is overlain by the Bauges Front Thrust (Subalpine Massifs) south-west of the Vuache FZ. The Subalpine Molasse is formed by a series of thrust sheets, probably rooted in the basal Molasse layers (clay-rich Lower Marine Molasse UMM, (Gorin et al., 1993), see chap 2.2.2 for further stratigraphical details). It is distributed along a narrow band (average of around 10km wide) and is located in our area of investigation in the trailing domain, to the SE of the Salève structure. These allochthonous

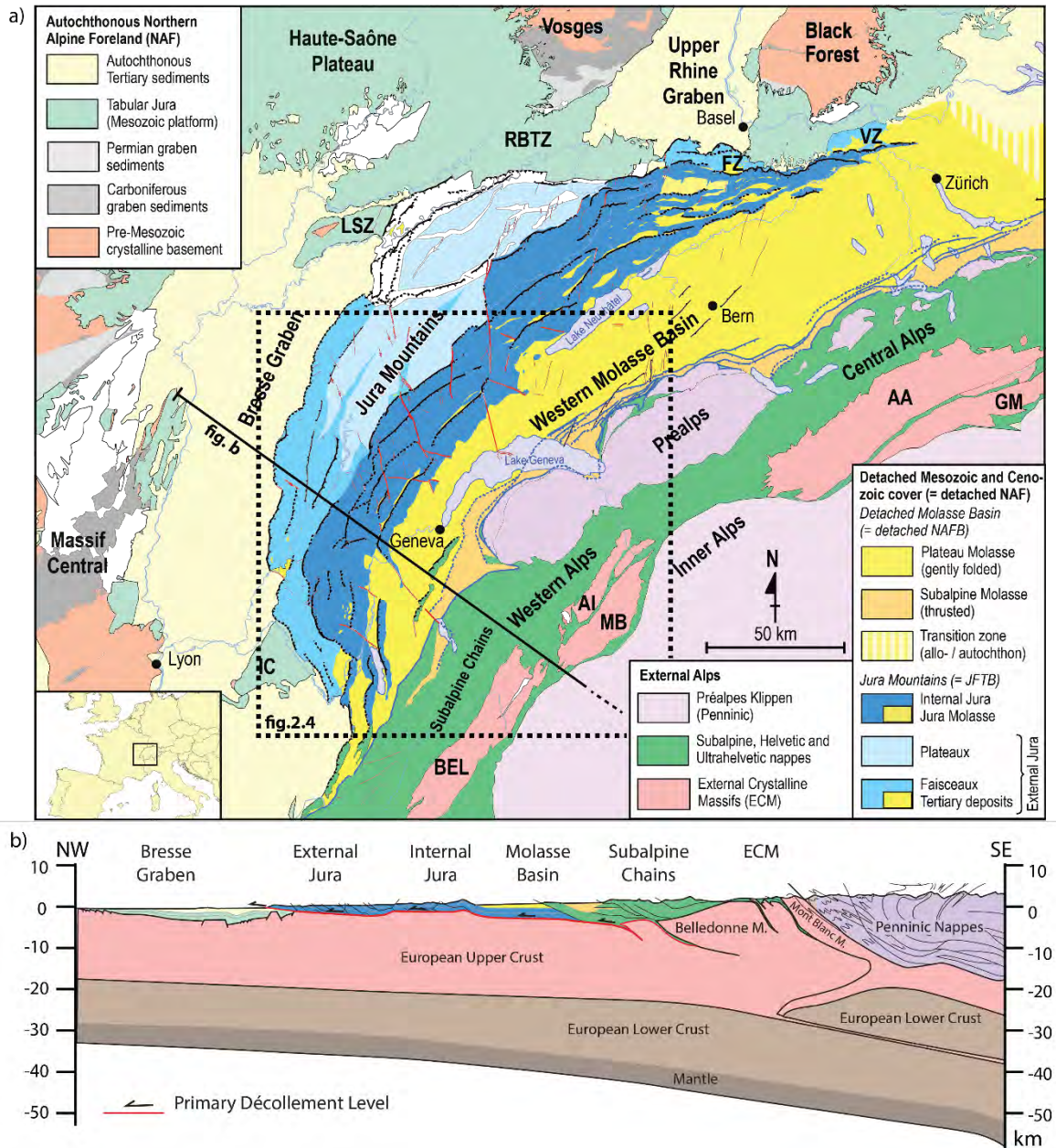


Figure 2-1 : a) Tectonic overview map of the Northern Alpine Foreland Basin (NAF), modified after Marro (2021), Schori (2021); Sommaruga et al (2017). b) Regional cross section of the Western Alpine foreland through the GVA Basin. The dashed black square highlights the study area, which focuses particularly on the Molasse Basin and Internal areas. AA: Aar Massif, AI: Aiguilles Rouges Massif, BEL: Belledonne Massif, FZ: Ferrette Zone, GM: Gotthard Massif, IC: Île Crémieu, LSZ: La Serre Zone, MB: Mont Blanc Massif, NAF: Northern Alpine Foreland, NAFB: Northern Alpine Foreland Basin, RBTZ: Rhine Bresse Transfer Zone, VZ: Vorfaltenzone.

thrust imbricates are dipping southeastward and pinch out underneath the Alpine nappes. Complex folding associated with these tectonic imbricates can be observed at the surface. In the northeastern part of the study area, northeast of the Arve valley, the Subalpine Molasse is overthrust by the French Préalpes Klippen (Penninic nappes), whereas to the SW, the Subalpine Molasse is bordered by the thrust Subalpine Massifs. Molasse type sediments can also be found inside synclines of the Haute Chaîne Jura proving that the Molasse Basin extended into the Jura FTB prior to folding and thrusting, (Charollais et al., 2006), and are subsequently passively involved in the deformation of the Jura FTB.

The Jura Fold-and-Thrust belt is divided into two main parts, with different tectonic characteristics: the Internal and the External Jura (Chauve et al., 1980; Sommaruga, 1997). The Internal Jura is the southeastern and most deformed part of the JFTB. It is also called the High Jura or Haute-Chaîne, because the highest topographic elevations are found in this domain. Indeed, the first chain (premier chaînon) in the SE is composed of the Crêt de la Neige summit culminating at 1720m.a.s.l and the Reculet summit at 1718 m.a.s.l. The Internal Jura consists of a series of high amplitude thrust-related folds often associated with complex strike-slip fault systems acting locally as lateral ramps. The important thrusts may lead to the duplication of the Mesozoic sedimentary rock cover. The morphology of the Jura FTB is actually closely related to the thickness (tectonic and stratigraphic) of the Triassic evaporites layers (Sommaruga et al., 2017). The displacement of the Jura FTB northwestward triggered NW-vergent ramps but also SE-vergent back-thrusts. Few oblique ramps are also present within the Internal Jura. These latter faults may be kinematically linked to pre-existing basement faults and thus influence the displacement path of the detached sedimentary cover (Schori, 2021). Note that tectonic structures, mostly tear faults or strike-slip faults similar to the Vuache FZ, extend from the Molasse Basin into the Internal Jura. We have dedicated special attention to the nature and distribution of these fault systems in this study.

To the NW, the Plateaux and Faisceaux units form External Jura part. The Plateaux area is relatively undeformed and appears flat with subhorizontal bedding, whereas the Faisceaux are highly deformed narrow stripes made of imbricated thrust systems, often offset laterally by strike-slip faults. The Jura FTB terminates northwestward by overthrusting the autochthonous Tabular Jura (Ile Crémieu), which is associated to the eastern rift shoulder of the Bresse Graben. The latter resulted from the European Cenozoic Rift System (ECRIS, (Chauve & Perriaux, 1974; Philippe et al., 1996)). The Avant Monts (Schori, 2021) form the outermost northwestern part of the External Jura, and are highly folded and thrust, and their relationship with the mechanical basement is still debated (thin-skinned or thick-skinned tectonic, Madritsch et al., 2008).

Deep basement grabens, filled with Permo-Carboniferous continental sediments are scattered through the WNAF and some of them are documented in deep well drillings (Schori 2021). The faults associated with these graben systems have different directions and are responsible for creating topographic irregularities and offsets at the top of the mechanical basement. As such, they are important inherited structures that have been shown to preferentially induce the formation of thrusts in the detached cover series during the formation of the Alpine foreland. This type of structures has not been further addressed in the PhD thesis because of the great uncertainties involved in their interpretation on a 2D seismic dataset.

2.1.2 *Thin-skinned and thick-skinned tectonics*

The thin-skinned tectonics are conceptionally opposed to the thick-skinned theory (Figure 2-2). As previously mentioned, the thin-skinned concept considers a main décollement level that allows the detachment and displacement of the above sedimentary cover and the development of structures in the cover decoupled from the basement. The thick-skinned tectonics lead to uplifted structures in the cover triggered by an inversion of an underneath pre-existing basement fault. The involvement of the basement in the thrusting and folding (Sommaruga, 1995) is possible, but seismic interpretation of the western alpine foreland has not shown clear evidence of inverted Permo-Carboniferous grabens or

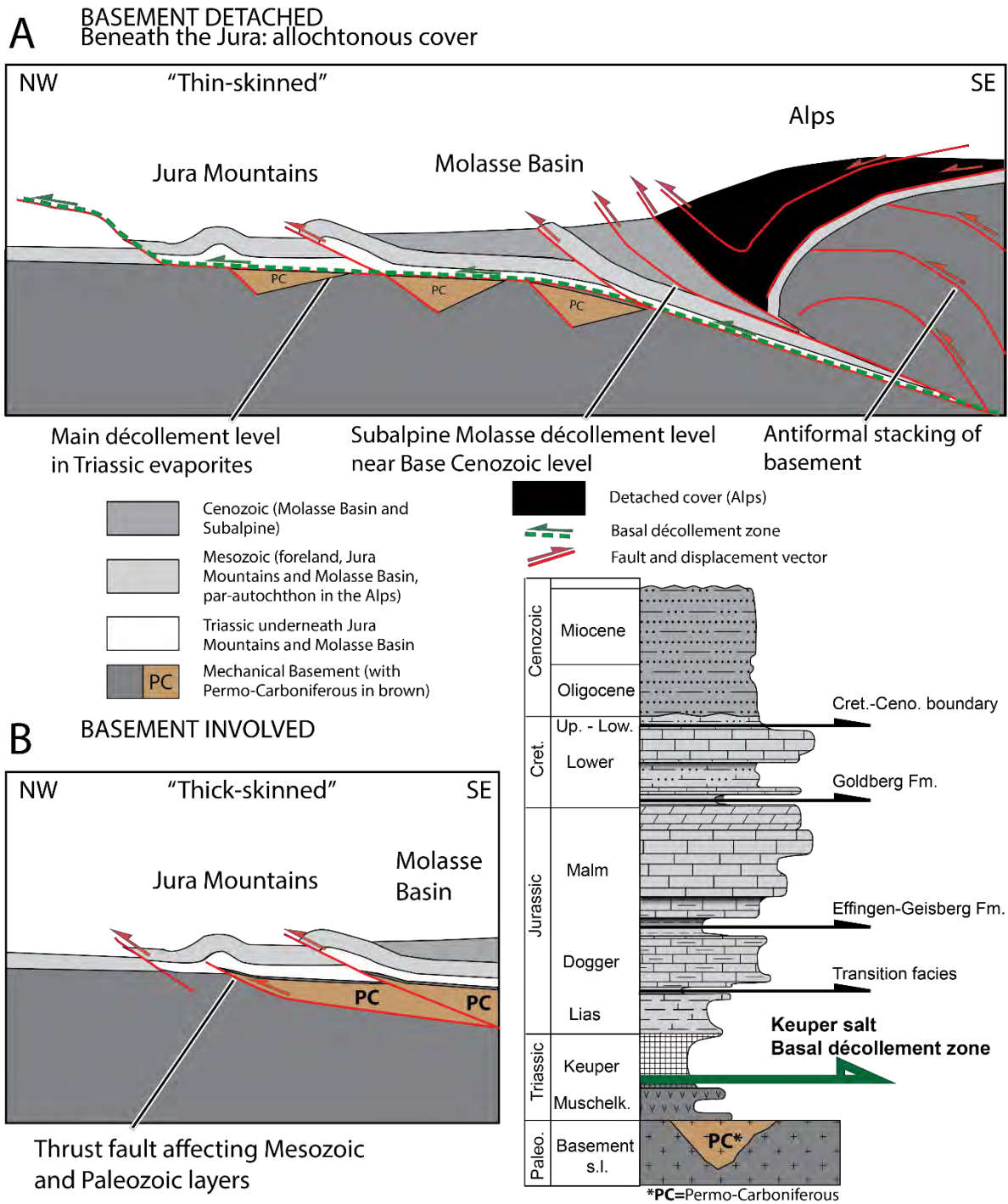


Figure 2-2 : Scheme highlighting the two opposing tectonic concepts of thin-skinned (A) and thick-skinned (B) tectonics applied at a regional scale. Localisation of these theoretical sections (A and B) approximately along the same path of cross section b) of Figure 2-1. The two concepts entails different hypothesis about the involvement of basement faults and dating of the geodynamic process. The stratigraphical section on the right bottom of the figure is modified from Marro (2021) and is based mainly on Humilly-2 well data (see location on Figure 2-4).

thrusts faults linked to underlying Paleozoic-early Triassic basement (Sommaruga, 1997). The moderate resolution of the seismic images due mainly to the relatively important depth of Pre-Mesozoic basement (approximately around 2-5 km depth below topography) is complicating this kind of analysis. Only latest technologies of 3D seismic volumes may help clarify the potential tectonic basement involvement. It was the case, in Heuberger et al., (2016), who were able to interpret on a 3D seismic data, basements normal faults extending upward on the overlying Mesozoic sedimentary

cover. However, the investigation area of this study is located in the Saint-Gallen fault zone (Eastern Swiss Molasse Basin, ESMB) which is outside the range of the supposed “Fernshub” (“distant-push” or thin skinned tectonic) hypothesis (Buxtorf, 1916). A recent study (Schori, 2021) has shown the importance of inherited basement topography in the kinematic development of the the detached thin-skinned Jura FTB, as also discussed in Burkhard and Sommaruga (1998).

2.2 Stratigraphy

The regional stratigraphical knowledge was built since decades on the combined analysis of the numerous deep wells drilled in France and Switzerland, and the outcrops of the sedimentary cover (mainly in the Jura Mountains). The surface stratigraphy is documented via the French and Swiss geological maps (Swiss Geological Atlas 1:25000, GA25, and the French BRGM geological surveys 1:50000). BRGM implemented a harmonization of the maps by department, which is available in a vectorized format on their website (BRGM, 2020). However, some discrepancies between different maps remain on this new version. Moreover, it is not in line with the recent work on the stratigraphy of the Geneva Basin of Brentini (2018) and Rusillon (2017), who integrated their work along with the Swiss HARMOS stratigraphy (Swiss Committee on Stratigraphy, 2017). The stratigraphy used in this project benefited from the collaboration with Marro (2021), who harmonized the BRGM maps of the French departments of Ain and Jura (Egal, 2007; Nagel, 2007) with the HARMOS stratigraphy. Therefore, several French maps from other departments (Savoie and Haute-Savoie) were homogenized using the same methodology than Marro (Marro, 2021). The harmonized legend is displayed on Figure 2-3, showing also the groupings of geological formation that were necessary for compiling the stratigraphical information of the BRGM maps.

In addition to surface data, well data were interpreted by Brentini (2018) and Rusillon (2017) on all main wellbores of the Greater Geneva Basin, in accordance with the HARMOS stratigraphy. This work has been revised and detailed using petrophysical interpretation from log data by the consultancy company Geneva Geo Energy, GGE (2018) on behalf of the Services Industriels de Genève SIG (see more details on chapter 3.3). With additional wells from the Vaud Canton, retrieved from the study of Gruber (2017), we compiled a total of 54 homogenized well data sets in the region of investigation. Moreover, the recent study from Schori (2021) gives a very exhaustive compilation of all wells of the Western North Alpine Foreland, with updated interpretation of the main Mesozoic boundaries. In this work, we used a combination of all these stratigraphical results with a particular focus on the work from Brentini (2018) and Rusillon, (2017), and its updates from Marro (2021) for the Geneva Basin area. Additionally, we used mainly the well lithologs from Schori (2021), in order to propose three regional lithostratigraphic well correlations (see Figure 2-4, Figure 2-5, Figure 2-6). It consists of NE-SW correlations, one through the Internal Jura (Figure 2-6, wells from SW to NE; La Chandelière-1d, Châtillon-1d, Chaleyriat-1, Charmont-1, Bonlieu-1, Toilon-1, Essavilly-101), one through the central part of the Molasse Basin (Figure 2-5, wells from NW to SE; La Tailla-1, Savoie-107, Savoie-106, Musiège-1, Humilly-2, Eclepens-1, Essertines-1, Treycovagnes-1), and another one through the eastern part of Molasse Basin (Figure 2-4, wells from NW to SE; Chapery-1, Faucigny-1, Romanens-1). This gives an overview of the thickening or thinning of the main Mesozoic units across the three different domains. Applying a single harmonized stratigraphy to all regional wells may, however, minimize regional lateral changes in stratigraphy from the Jura part to the Geneva Basin. Thus, Rusillon (2017) was able to depict this evolution through the Geneva Basin, with a chronostratigraphy highlighting

Chapter 2

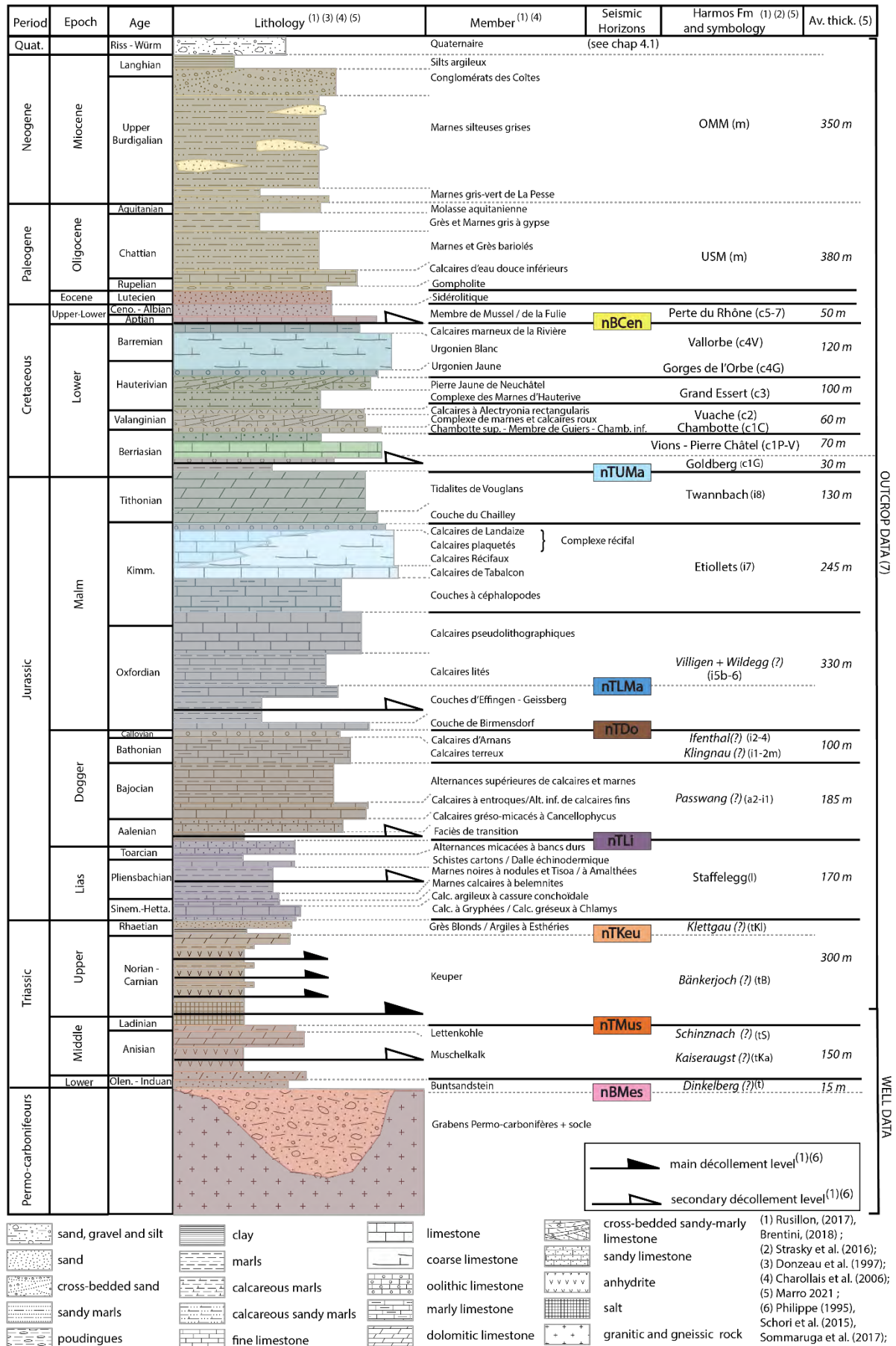


Figure 2-3 : Stratigraphic log (modified from Marro (2021)) and harmonization summary of the map legend with few grouping units (see Encl_M02 for surface map). This stratigraphical column is mainly based on Humilly-2 well and Haute-Chaîne outcrops (Marro, 2021)

diachronism from NW to SE in several layers. In that sense, a more detailed chronostratigraphy would perhaps be needed for a truly accurate large-scale stratigraphy. However, in our study, the vertical resolution inherent of seismic data compensates this possible limitation related to the regional stratigraphy.

2.2.1 The pre-Mesozoic rock units

The pre-Mesozoic basement is made of a variety of rocks, including sedimentary series, some of which are highly metamorphosed (Siletto et al., 1993; von Raumer & Neubauer, 1993). Parts of the Pre-Mesozoic crystalline basement can be linked to the Variscan orogeny, which is the latest Paleozoic deformation phase that ended during the Stephanien (Stampfli et al., 2001; von Raumer, 1998). The closest wells of our study area (Bonlieu-1, Essavilly-101 and La Chandelière-1D, see Figure 2-4 for localisation) reached this unit and showed a main composition of biotite-rich gneiss, and few green schists, as well as intrusive granite (Rusillon, 2017).

During the post-Variscan orogenic collapse and extension, Permo-Carboniferous (P-C) clastic sediments infilled basement grabens or half grabens developing in an extensional setting. Several wells in the region were drilled into this kind of structure such as, Chaleyriat-1, Charmont-1 (more than 500m of P-C sediments drilled), Chatelblanc-1, Chatillon-1d, Faucigny-1, Chapery-1, La Tailla-1, Essavilly-1, and Treycovagnes-1 (see Figure 2-4 for localisation). The origins of these sediments are continental to possibly deltaic. They are composed mainly of brownish conglomerates in combination with fine grained sandy to argillaceous deposits, as well as coal beds. The infilled grabens are scattered irregularly through the NAF. Several other grabens are well known and their geometry clearly identified, such as the Constance-Frick Trough located in northern part of Switzerland (Naef & Madritsch, 2014). In this well-known example, the authors supposed several depositional sequences in relation to syn-sedimentary activity of the basement faults (laterally variable subsidence). The pre-Alpine (Variscan) tectonics and their inheritance are key for understanding the origins and locations of these grabens (Ballèvre et al., 2018; Capuzzo & Wetzel, 2004). The boundary of this layer with the overlying Mesozoic sediments is considered as an erosive surface – the post Hercynian erosional peneplain. From the lithological point of view, the Permian sandstones may be difficult to differentiate from the Triassic Buntsandstein sandstones. However, the depositional geometries associated with this major unconformity may usually help identifying this boundary.

2.2.2 The Mesozoic and Cenozoic sedimentary cover

The following description of the Mesozoic and Cenozoic cover is based on the main regional well analysis such as Humilly-2 (Rusillon, 2017) or Charmont-1 (Raynaud & Marmion, 1992)(see Figure 2-4 for well localization), as well as on the major outcrops of the Internal Jura of our area that were summarized recently by Marro (2021).

Triassic

Above the Paleozoic angular unconformity, the Germanic Basin developed in the Triassic between the Vindelician Land to the south east, with the Massif Central to the west (Figure 2-10, (Ziegler, 1990)).

For the purpose of our study, the Triassic is divided into two main groups: The Muschelkalk Group and the Keuper Group. The first series of the Mesozoic unit are the relatively uniform and thin layers of the Buntsandstein (around 15m thickness in the GVA Basin, also called “grès Bigarrés”). This thickness of this layer (Lower Triassic) is supposed to increase towards the Jura Mountains (Sommaruga et al., 2017). It is mainly composed of coarse sandstones and conglomerates. Then the epicontinental basin went through clear shallow marine incursions. Therefore, the Muschelkalk and Lettenkohle (Middle

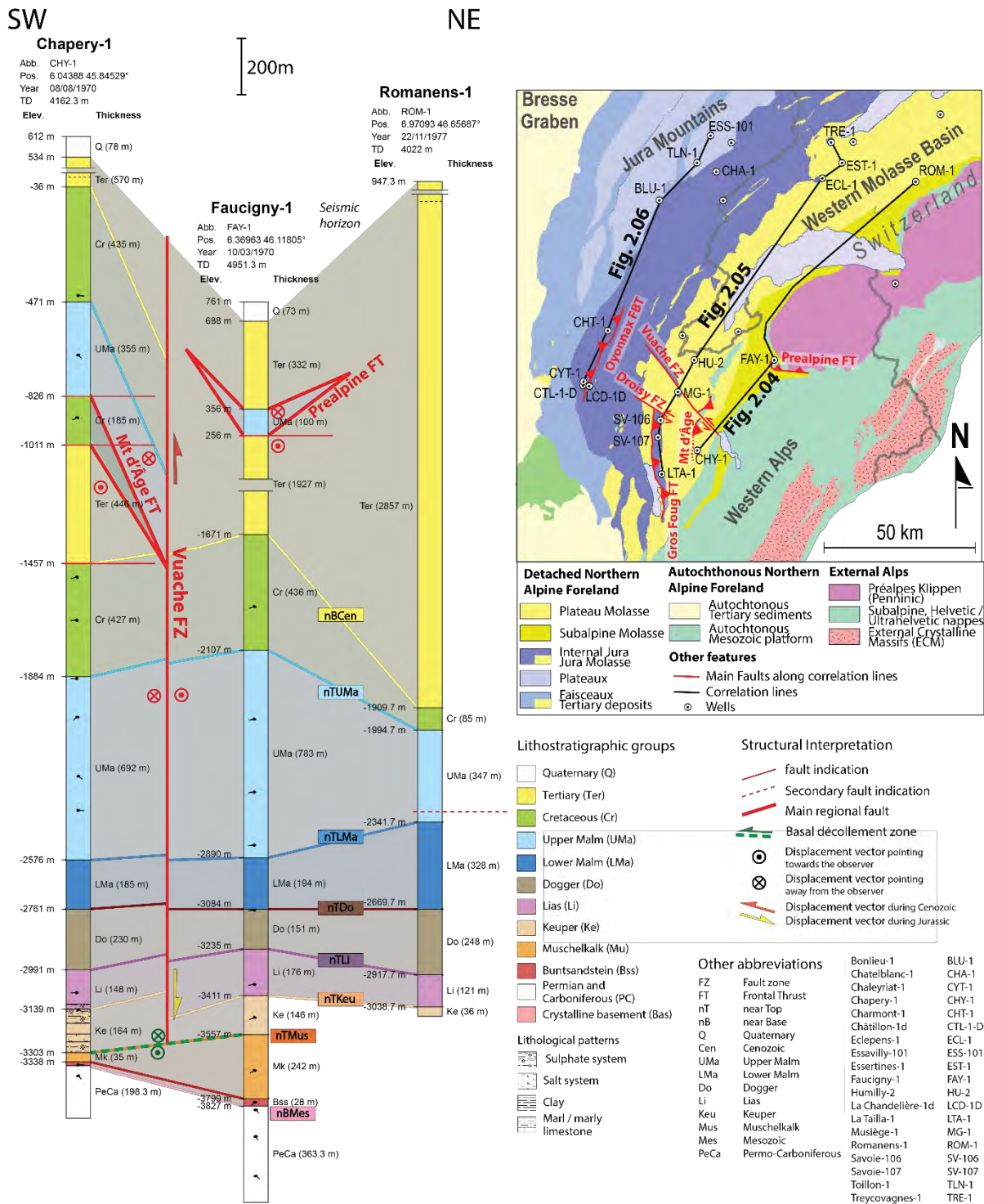


Figure 2-4 : Well correlation in NE-SW direction in the Subalpine Molasse area in front of the Penninic and Helvetic nappes. The wells are vertically positioned with nTDo as a flat reference (flattening). See the map on the right of the figure for localization. The main fault zones and thrusts are represented along the correlation. The well data come from Schori (2021).

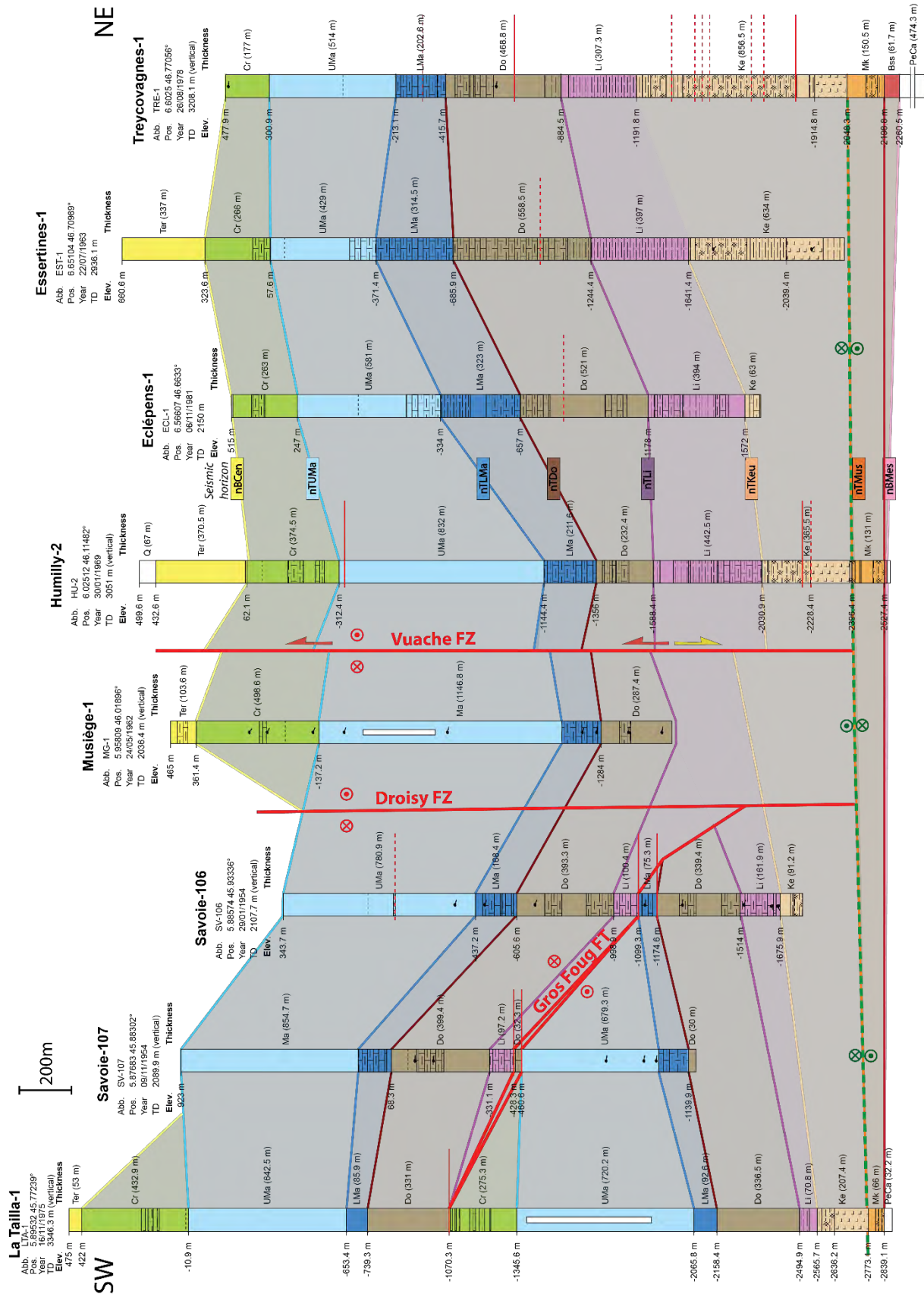


Figure 2-5 Well correlation in NE-SW direction located in the center of the Molasse Basin (Figure 2-4 for localisation and legend). The correlation is flattened along Top Buntsandstein marker (Bss), and the main fault zones and thrusts are represented along the correlation. Core-loss are displayed by white bars. The well data come from Schori (2021).

NE

SW

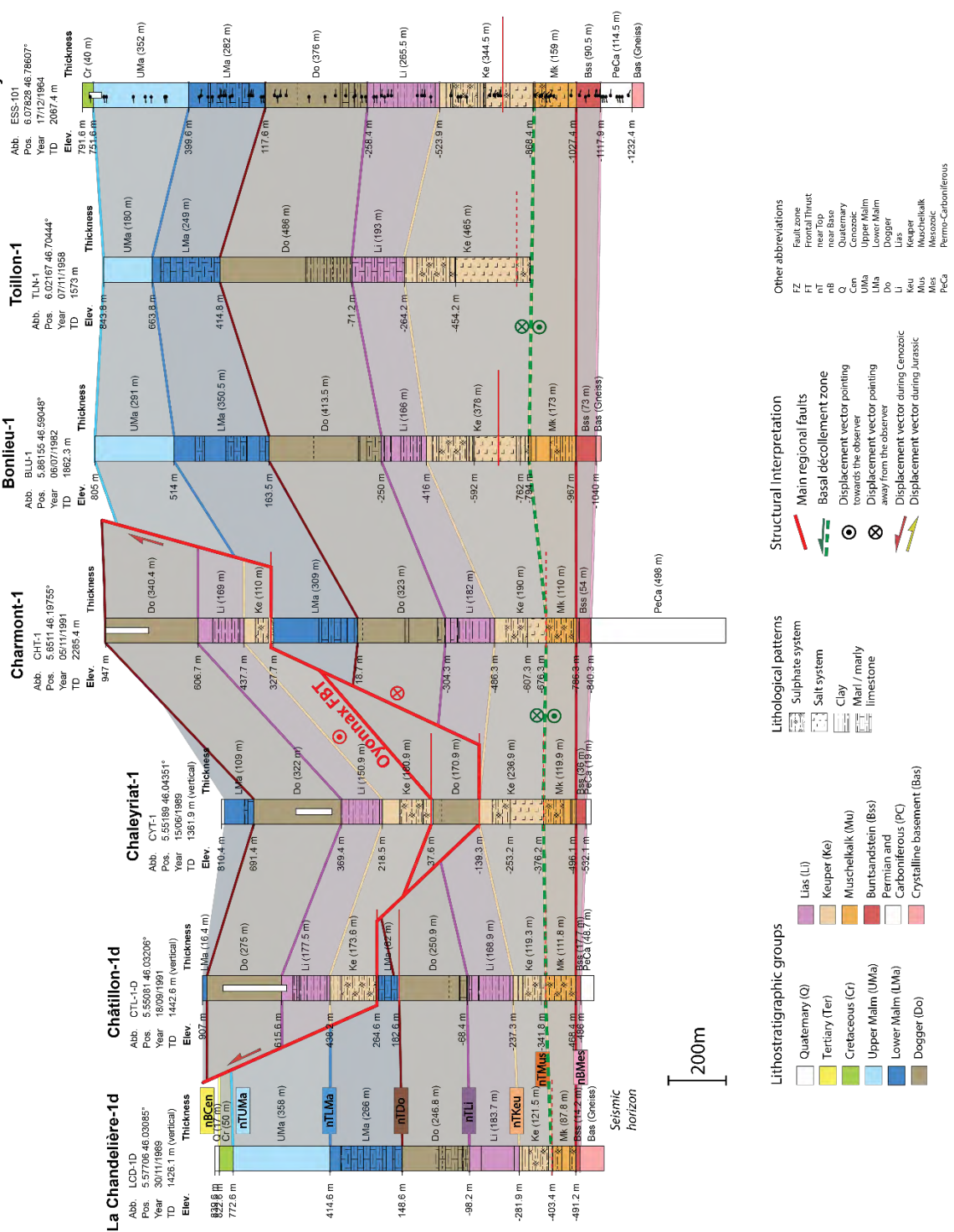


Figure 2-6 : Well correlation in NE-SW direction located in the Internal Jura (Figure 2-4 for localisation and legend). The correlation is flattened along Top Buntsandstein marker (Bss), and the main fault zones and thrusts are represented along the correlation. Note that the Cenozoic unit is barely present. The well data come from Schori (2021). Core-loss are displayed by white bars.

Triassic) are made of alternating anhydrites and dolomites with few shales. These two formations are thickening northeastward from an average thickness around 150m in our area to 450m of thickness in between the cities of Fribourg and Biel (Schori, 2021). The lithology is also changing northeastward, with the presence of salt-rich layers (Pfaffnu-1 see Gruber, (2017)). Considering the thickness of these formations in relation to the resolution of the seismic, the Buntsandstein, the Muschelkalk and the

Lettenkhole are merged into the Muschelkalk s.l. of this study. The overlying Upper Triassic is formed by the Keuper Group. Two evaporitic units in the Keuper Group can be distinguished in the studied

wells. First, the basal unit is mainly made of massive halite, with intercalated gypsum/anhydrites layers. Note that the basal décollement zone of the detached foreland is placed at the base of the salt-rich layer in our area, whereas it is located in the salt-rich layer of the Muschelkalk s.l. (mentioned above) northeastward of our area (Philippe, 1995; Sommaruga et al., 2017). The upper part of the Keuper Group is characterized by a succession of dolomite and anhydrite layers, along which secondary décollement zones may be present. The upper limit of the Keuper Group is composed of sandstones (“grès blonds”). The thickness range of this group is evaluated between 100m up to 600m thickness (Schori, 2021) in the studied area. Note that the amplitude of the thickness is related to tectonic processes (duplication), therefore it does not reflect the depositional energy. The halite content of the lower part of the Keuper Group seems to diminish southwestward, as indicated in Faucigny-1 well (Rusillon, 2017). This fact has an impact on the role of the basal décollement layer since less salt will change overall basal friction, which in turn changes the shape and deformation of the foreland mechanical wedge (Deville, 2021).

Jurassic - Cretaceous

Three main depositional periods are recognized in the Jurassic times: the Lias, the Dogger and the Malm from the older to the youngest.

The Triassic-Jurassic transition is marked by the onset of a transgression phase during the Lias. The bioclastic formation of “Calcaires gréseux à Chlamys” (Hettangian) characterize this evolution from continental (“grès blond” of the Rhaetien) to shallow environment (early Lias). This sedimentary sequence was triggered by the connection of the Germanic Basin with the Tethys Basin (Lemoine et al., 1986), initiated by a major rifting phase (opening of Central Atlantic and Alpine Tethys, (Stampfli, 2000)). The Liassic is then subdivided into two subunits, with an older limestone dominated layer deposited during transgression phase (with the main formation of the “Calcaires à Gryphées”), and followed by a shales-dominated layer corresponding to deep marine setting (with the main formation of “Marnes noires à nodules”). The Liassic unit ends with white limestones of the “Alternances micacées à banc durs” overlain by the marly limestone “facies de transition” representing the transition toward the Dogger. Note that this argillaceous layer is considered as a potential secondary décollement level (Philippe, 1995), similarly to what was proposed in the central Jura by Rime et al., (2019) and Schori et al., (2015). An average thickness of the Liassic series over the area is around 170m, and an overall thinning southwestwards is observed.

The Dogger unit is characterized by a shallower depositional environment, represented by alternating bioclastic limestones and marly layers. The Bajocian formations of the “alternance inférieure de calcaires fins”, the “Calcaires à entroques” and “alternances supérieures de calcaires et marnes” are perfect examples of this alternations. The Klingnau and Ifenthal formations are also following the same lithological trend and testify again the fast fluctuations between shallow to more distal position in relation to the continental platform to the North (Figure 2-10). The average thickness of the Dogger in the GGB is closed to 250m. The depositional evolution during the Lias and the Dogger, suggests an implication of NW-SE trending fault in the subsidence inversion of the area (Rusillon, 2017). Northeastward of our area in the Vaud Canton, the wells Treyconvagnes-1 and Essertines-1 (Figure 2-5) show the highest thickness of cumulated Lias-Dogger layers of the western Molasse Basin. Several

authors proposed to explain this thicknesses by a combination of differential subsidence and normal faulting during this times (R Marchant et al., 2005; Schori, 2021; Wetzel et al., 2003).

The Upper Jurassic unit (Malm) is divided into the Upper and Lower Malm. During this entire period, an overall regression of sea level occurred and modified the depositional environment from a deep marine setting into a carbonate platform configuration. When present, the formation of the “pseudo brèche de Saint Claude” (Haute Chaîne, (Rusillon, 2017)) defines the Dogger-Malm transition. Then, the Lower Malm period begins with the stratified limestone of the “Couche de Birmensdorf” (Donzeau et al., 1997). This is marked by the formation of a topographical depression during the Oxfordian (Rusillon, 2017). It is followed by the Villigen formation composed of marly limestones of the “Couches d’Effingen-Geissberg” and the overlying “Calcaires lités” and “Calcaires pseudolithostratigraphique”. The “Couches d’Effingen-Geissberg” represent a possible secondary décollement zone thanks to its marly stratification (Clerc & Moscariello, 2020; Philippe, 1995). The first unit of the Upper Malm layers are formed by the “Couches à Céphalopodes”, which are marly limestones similar to the Oxfordian layers. The so-called “reef complex” corresponds to prograding patch reefs from NW to SE. It is divided into three sub-units “Calcaires récifaux” (1), “Calcaires plaquetés” (2) and the “Calcaires de Landaize” (3). They are interpreted to represent reef and peri-reefal deposits (1), back reef (2), and more lagoonal (3) environments respectively. The diachronous reefal system is overlain and is completed by the “Calcaire de Tabalcon” corresponding to a shallow marine dolomitic limestone (front reef environment, Meyer, 2000; OCEN, 1994; Rusillon, 2017). The last formations of the Malm (“Couches de Challey” and “Tidatiltés de Vouglans”) are part of the “Twannbach Formation” and are characterized by bioclastic limestones pointing to a calm, subtidal and lagoonal environment. The thickness of the entire Malm unit can reach values up to 1000m in the GVA Molasse Basin.

The Malm-Cretaceous transition is clearly defined by the “Goldberg Formation” (previously called “Purbeckian”). This marly limestone layer often found in topographical depression marks the beginning of the Cretaceous unit (Donzeau et al., 1997; Strasser et al., 2016). As in other marly layers, this formation may host a secondary detachment (Philippe, 1995). The Cretaceous unit is very well defined and described, due to numerous outcrops and well analysis (references therein). Certain Cretaceous formations are more massive limestones (sometimes bioclastic), such as the “Pierre Châtel”, “Chambotte” and “Vallorbe” and are witnesses of shallow marine (sometimes high energy), or lagoon environment. On the other hand, the formations of “Vions”, “Vuache”, “Grand Essert”, “Gorges de l’Orbe”, and “Perte du Rhône” are less competent marly limestones formed possibly in a shallow marine to more open depositional environment. Philippe, (1995) proposed a possible décollement zone in the “Perte du Rhône” formation, but we could also suppose another intra-Cretaceous décollement zones in marly layers such as the “Marnes d’Hauterive”. The cyclic and stacked lithologies of the Cretaceous unit are linked to quick depositional environment changes. In fact, the still ongoing N-S opening of the Alpine Tethys has most likely influenced the rapid lateral variations of the different facies (Figure 2-9, (Strasser et al., 2016; Wildi et al., 1989).

Upper Cretaceous is not outcropping in the Geneva Basin or in the neighboring Jura Haute-Chaîne, and that is why it is not represented in the main stratigraphical column of Figure 2-3. However, several outcrops reveal Upper Cretaceous deposits in the Valserine Valley, near the city of Bellegarde, in the Rumilly Basin, and also in oil drillings of Mont-de-Boisy-1 and Messery-1 described in Charollais et al. (2007) (see localization in Figure 2-8). The related formation is called “Calcaires crayeux à Silex” (Donzeau et al., 1997), and is made up of biomicrites creamy-white to yellowish chalk, dated from the

Turonian age. Fragments of this formation of the “Calcaires crayeux à Silex” have been witnessed in many areas of the Geneva Basin (Charollais et al., 2007), as pebbles in the Tertiary “Gompholites” at the base of the Molasse interval, proving the early presence of Upper Cretaceous deposits before the main later erosion during Cenozoic times (Alpine orogeny).

Cenozoic

The Cretaceous-Tertiary boundary marks the end of the Mesozoic cover and the beginning of the Cenozoic period. It is characterized by an important hiatus from the end of the Lower Cretaceous until the Eocene times, which is thought to be due to a major erosional period, with an estimated eroded thickness of more than 500m (Mazurek et al., 2006). During the Eocene, the WNAFB experienced a down-bending flexure of the lithosphere leading to the establishment of a flexural foreland basin, subsequently followed by a transition to a “wedge-top” configuration during the Miocene with the initiation of the main décollement level and the formation of the Jura FTB (Bonnet et al., 2007; Sinclair et al., 1991; Willett & Schlunegger, 2010). Therefore, the Tertiary sediments deposited on top of the strongly eroded Mesozoic cover, logically form an angular unconformity with its substratum (Homewood et al., 1986). The Siderolithic sediments (clastic sediments from Eocene, see Figure 2-7) are the first deposits of the Cenozoic cover. These iron-rich continental sandstones have a scattered presence in the WNAFB, and can be observed in several wells in the basin and outcrops such as in the Vuache (Blondel et al., 1988; Bordon & Charollais, 2009; Charollais et al., 2013; Schardt, 1891) or Salève (Conrad & Ducloz, 1977; Joukowsky & Favre, 1913; Mastrangelo et al., 2013)). They are locally infilling karstic features or found along fault planes of the uppermost parts of the Mesozoic cover. They may also have a fluvial or aeolian origin and form stratified deposits in topographic depressions (Chablais & Savoy, 2021). The thickness of siderolithic deposits is highly variable, but it can reach at least 140m, such as in the recent well GGeo-02 (2020 (highest thickness of this formation found in the WNAFB, Chablais & Savoy, (2021).

Starting at the Priabonian-Rupelian times, a succession of marine transgression and regression inside the WNAFB led to the deposits of the four formations of the Molasse sediments (Figure 2-7 and Figure 2-8); from the oldest to the youngest, the Lower Marine Molasse (UMM), the Lower Fresh-water Molasse (USM), the Upper Marine Molasse (OMM), and the Upper Fresh-water Molasse (OSM). The OSM was not deposited in our area of study, whereas the three others are present but with a lateral variability. The UMM marks the onset of the filled stage of the WNAFB, mainly during the Rupelian times. Therefore, it is present mostly in the South-East of the basin, corresponding to the highest subsidence zone after the flexural stage of the lithosphere (starting in Eocene). In our area, it was found in wells southeastward of the Salève and its northwestern delimitation seems to coincide with the frontal thrust of the allochthonous Subalpine Molasse (Deville et al., 1994; Gorin et al., 1993). In that sense, its southwestern termination is likely situated along the Vuache FZ. It is composed of sandstones and conglomerates (“Doriaz”) in its lower part, overlain by a marly layer (“Meletta”) and of a sandstone-dominated succession in its upper part (“Dessert-Bonneville”) (Deville et al., 1994; Diem, 1986). The softer intermediate part is likely playing the role of a décollement of the allochthonous Subalpine Molasse (Gorin et al., 1993). Above the UMM layer, the USM is deposited throughout the WNAFB with relatively high thicknesses (more than 900m in the GVA Basin). A regression of sea level led first to the development of a fluvial environment in the WNAFB, the early Burdigalian times. This formation is observed only in the Rumilly Molasse Basin area, west of the Vuache Mountain ridge, and in certain synclinal valleys of the Jura FTB (for instance in La Pesse valleys,

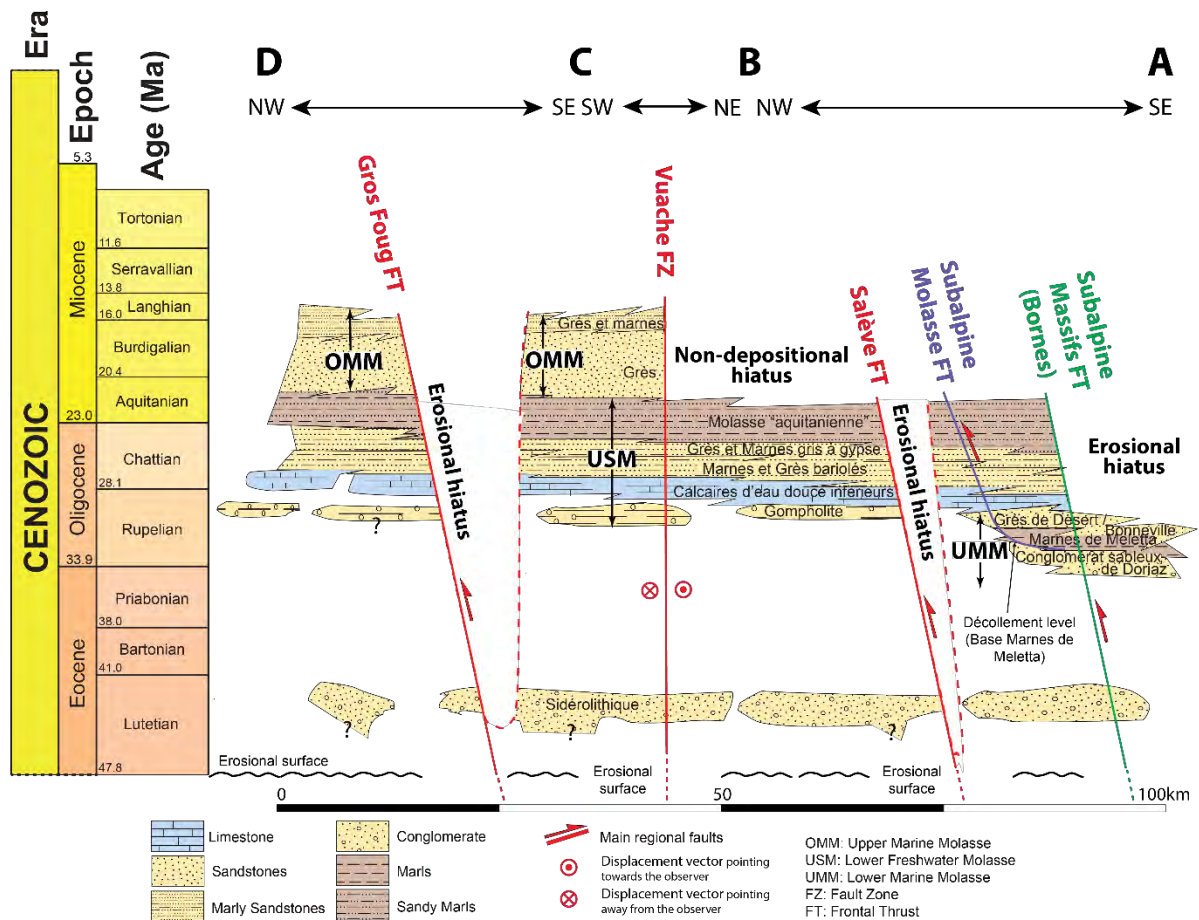


Figure 2-7 : Molasse vertical and lateral distribution through the Western Molasse Basin in relation to the main fault zones and thrusts. See Figure 2-8 for localization of the section. This figure is based on Brentini (2018), Rusillon (2017) and Deville et al. (1994).

J. Charollais et al., (2006) of the Internal Jura, see Figure 2-8). In these Jura valleys, Charollais et al., (2006) divide the OMM into four units. The two first are the “Marnes gris-vert de La Pesse” and the “Marnes silteuses grises” showing a fining up sequence, with conglomerates at the base followed by sandy marls. Then, the “Conglomérat des Coites” show another microconglomerate and pebble sequence followed by another finer unit, the “Silt argileux”. According to Deville et al. (1994), the OMM is constrained locally between the Jura and the Montagne d’Âge frontal thrust (SW continuation of the Salève thrust, see Encl M02), as flexural sequences deposited in front of the pre-existing Montagne d’Âge thrust (formed at the beginning of the Burdigalian transgression). The Gros Foug FT may be considered as a syn-sedimentary structure, developing during the OMM deposition (Deville et al., 1994). The Vuache FZ has clearly also played a role as a barrier between the NE and SW domain during the OMM with the Burdigalian transgression. In this area of the Molasse Basin (Rumilly Basin) the lithological description of the OMM may be simplified with a first sandstone layer overlain by marly sandstones (Figure 2-7; Deville et al., 1994).

The most recent layers of the Cenozoic cover consist of fluvio-glacial deposits from the Quaternary. The two successive glaciations of the Riss and the Würm are associated with two moraine sequences, the basal “Moraine rissienne”, and the youngest “Moraine würmienne”. The fluvio-glacial sandur sediments of the “Alluvion anciens” separate these two layers (Fiore, 2007; Fiore et al., 2011; Lathion & Hauvette, 2020; Vernet & Horn, 1971).

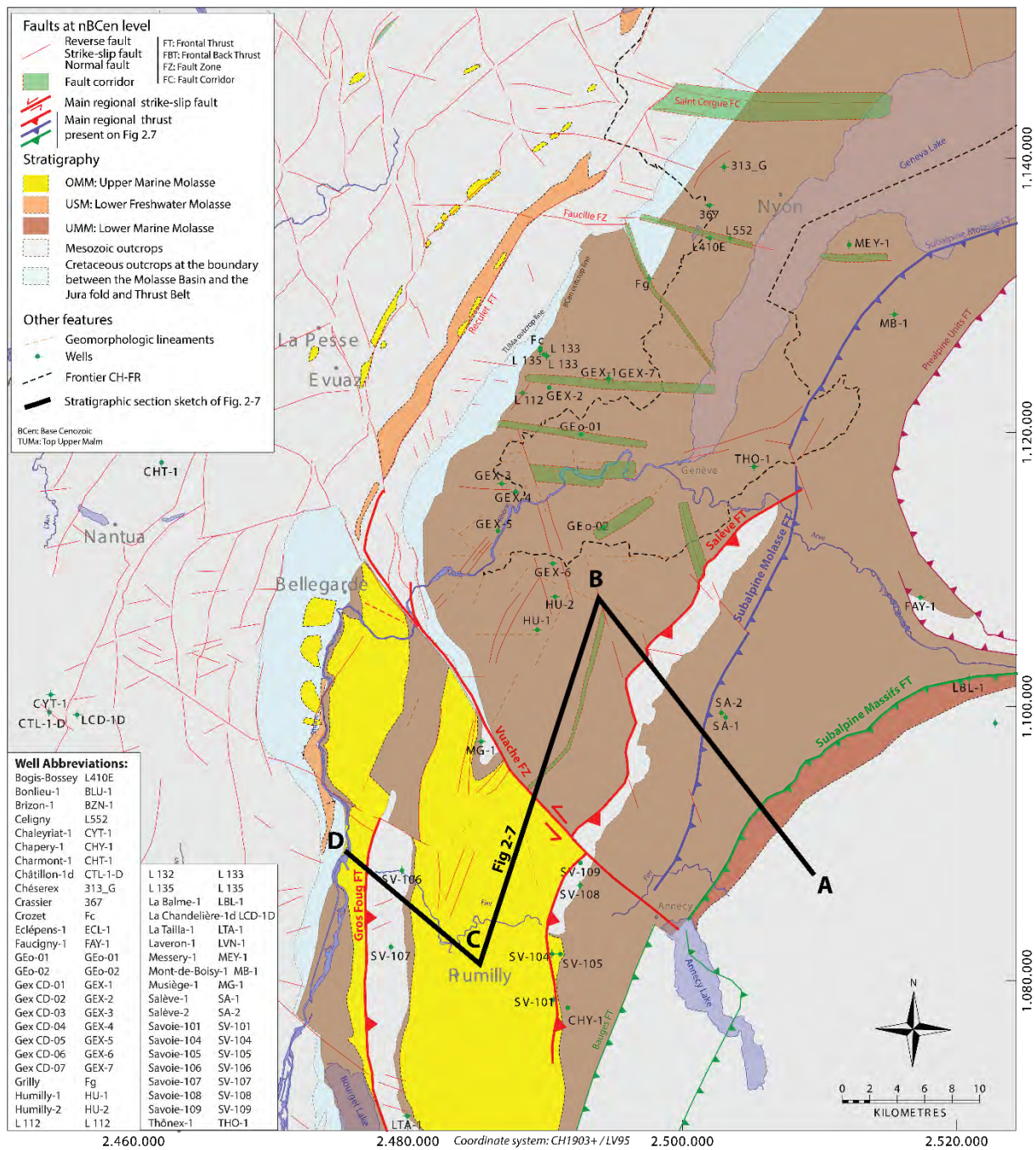


Figure 2-8 : Molasse geological map (without Quaternary deposits) through the Western Molasse Basin. The black line corresponds to the surface trace of the section of Figure 2-7. Note that the Vuache FZ is the northern limit of the presence of the OMM deposits in the western Molasse Basin. However few valley of the Jura host also OMM sediments (Charollais et al., 2006). The UMM is present only in relation to the Subalpine Massif FT. (coordinate system: CH1303+/LV95)

with the deposit of the first USM formation, a ponding of the “Gompholite” unit (Charollais et al., 2007). The latter is distributed across the basin and is considered as strongly diachronous. It was followed by the setting up of a lacustrine environment, with the limestone layers of the “Calcaires d’eau douce inférieurs”. Then, the three next formations of the “Marnes et Grès bariolés”, the “Grès et marnes gris à gypse” and the “Molasse Aquitaniennne” are three marly sandstone layers with the intermediate one formed by an alternance between lacustrine and evaporitic environments (presence of dolomite, gypsum and anhydrite; Rusillon, 2017). Finally, in the studied region, the Molasse unit ends with the Upper Marine Molasse (OMM), characterized by a transgression which started during

2.3 Geodynamics and tectonic evolution

The following chapter summarizes the large-scale geo-history of the area of investigation in relation to the depositional and subsequently tectonic setting of the region (Figure 2-9). Three main tectonic phases marked the geological history of the area; the post-Variscan times and the Permo-Carboniferous continental grabens; the Mesozoic era (Triassic-Jurassic-Cretaceous) with an overall extensional setting and epicontinental depositional environment forming in a rim-basin context with respect to the Alpine Tethys development further to the SE; the Cenozoic era and the Alpine Orogeny that led to the Molasse Basin deposits and the onset and formation of the north Alpine foreland fold-and-thrust belt including the Molasse Basin and the Jura FTB.

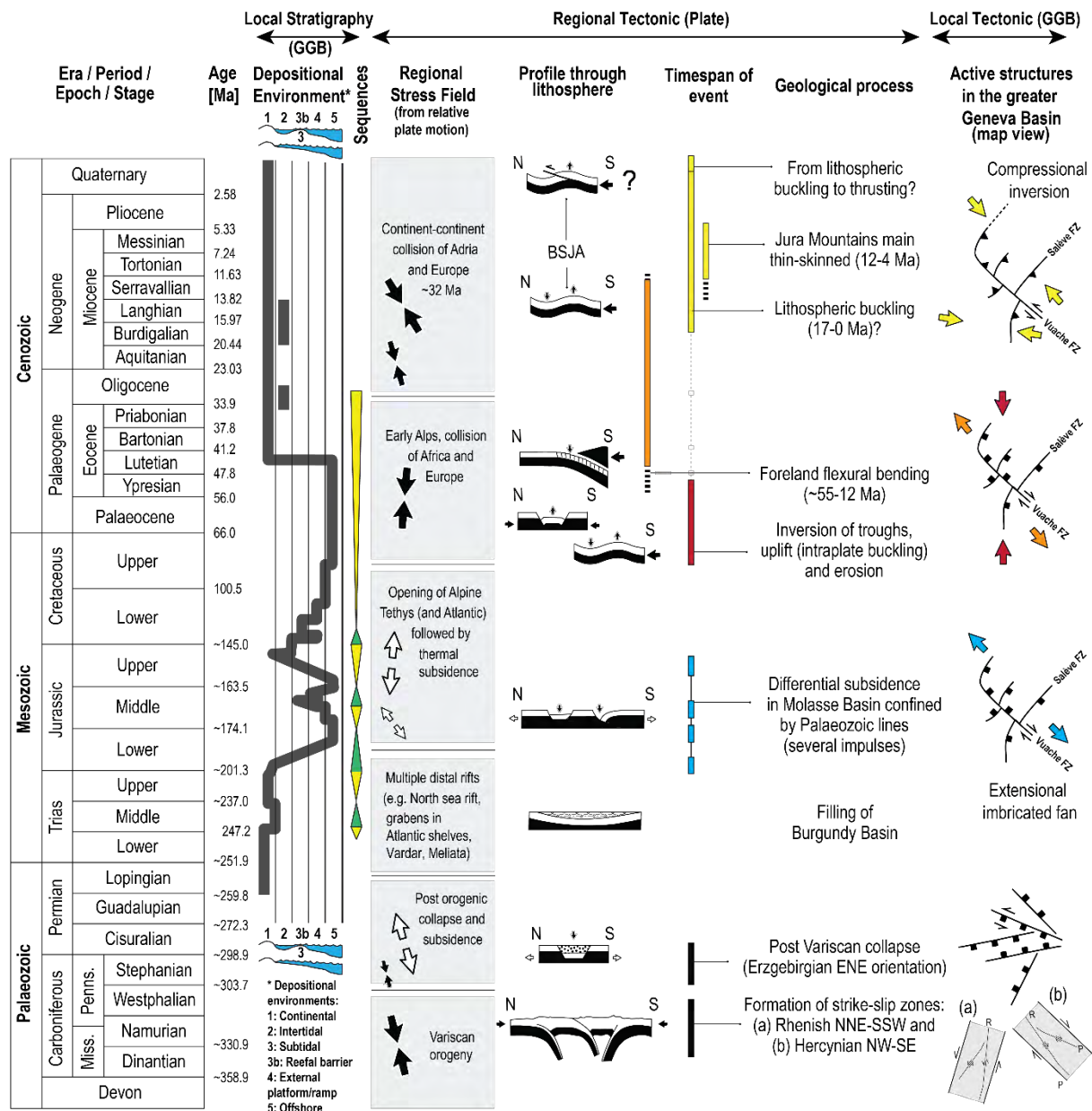


Figure 2-9 : Geodynamic summary of the Greater Geneva Basin, in relation to stratigraphy (left part, of the figure, modified from Brentini (2018) and Rusillon (2017)). The regional context and plate tectonic is shown in the middle of the figure (modified from Schori (2021)) and local tectonic (Greater Geneva Basin (GGB) and the Vuache-Salève FZ explained on following chapters) on the right (arrows represent the tectonic vectors for each main phase).

2.3.1 The Late Paleozoic evolution

The pre-Mesozoic crystalline basement of the WNAF is made of highly deformed metamorphic and plutonic rocks that resulted from the Variscan and prior orogenies. The Variscan orogeny, dated from mid-Devonian to Late Carboniferous times (Stampfli et al., 2001), ended with the complex collision and accretion of the Laurentia and Gondwana continents (Ziegler, 1990), to form the megacontinent Pangea (Stampfli & Borel, 2002). This period is associated with several main fault/shear zone orientations; the sinistral NNE-SSW Rhenish trend, the dextral NW-SE Hercynian, and the NE-SW to ENE-WSW sinistral Erzgebirgian (Schori, 2021).

This compressional phase was followed by an extensional and collapse tectonic period during the Late Carboniferous (Stephanian), and early Permian, which culminated with break-up of Pangea (Schaltegger, 1997). During this period transtensional Permo-Carboniferous troughs, oriented in NE-SW to ENE-WSW (Erzgebirgian) (von Raumer, 1998) were developed. The internal structures of the Permo-Carboniferous infilled grabens are relatively complex (Madritsch et al., 2018), with polyphase transtensional and transpressional tectonics (Diebold et al., 1991), imbricated along the different basement fault orientations. The most detailed example in the WNAF is the Constance-Frick Through in northern Switzerland which developed a E-W striking half graben, with several kilometers of infilled sediments (Naef & Madritsch, 2014). The Permo-Triassic boundary is subsequently characterized by a major erosional unconformity (Signer & Gorin, 1995; Sommaruga, 1999), due to the peneplanation of the entire Late Paleozoic realm, including the Permo-Carboniferous troughs (Bourquin et al., 2011). In the GGB, the orientations of the Permo-Carboniferous troughs are poorly known, but possibly oriented in NE-SW orientation (Signer & Gorin, 1995).

2.3.2 The Mesozoic evolution

Following the post-Variscan extensional phase, and the peneplanation of the area, a transgression phase in the Germanic Basin developed with a relatively low subsidence rate in the WNAF ((Gruber, 2017); Figure 2-11). The shallow Triassic basin that thus developed is also named the Burgundy Trough, whose orientation is linked to inherited early Permian extension (NNE-SSW overall orientation, (Schori, 2021; Ziegler, 1992)). In the Late Triassic, the Germanic Basin, which was previously separated from the Tethys Basin to the South, by the Vindelician land, evolved into an epicontinental evaporitic configuration. The Tethys Basin was still in a marine environment setting, while a restricted environment of the Germanic Basin led to the deposit of a high thickness of evaporites (Ziegler, 1990).

During the Lower Jurassic, a rifting phase occurred in relation with the opening of the Central Atlantic and the Alpine Tethys oceans (Channell & Kozur, 1997; Stampfli et al., 2001). The latter is bordered by the Alemannic land, a topographical high east of the Helvetic and Briançonnais domains, developed in a NE-SW orientation in the SW continuation of the Vindelician land (Lemoine & Trümpy, 1987). Modest normal faulting from Lower to Middle Jurassic developed in the actual location of the WNAF in the far-field of the Alpine Tethys rifting, and differential tectonic subsidence is observed all around the Alemannic land (Figure 2-11). A pervasive thinning and faulting is documented by hydrothermal veins (Allenbach & Wetzels, 2006), or from seismic interpretation (facies and syn-sedimentary thickness variations) according to studies from Burkhard & Sommaruga, (1998) in the Helvetic domain of the Tethys Basin, and from Marchant et al., (2005) for the Rhodanian Basin area. During this rifting period,

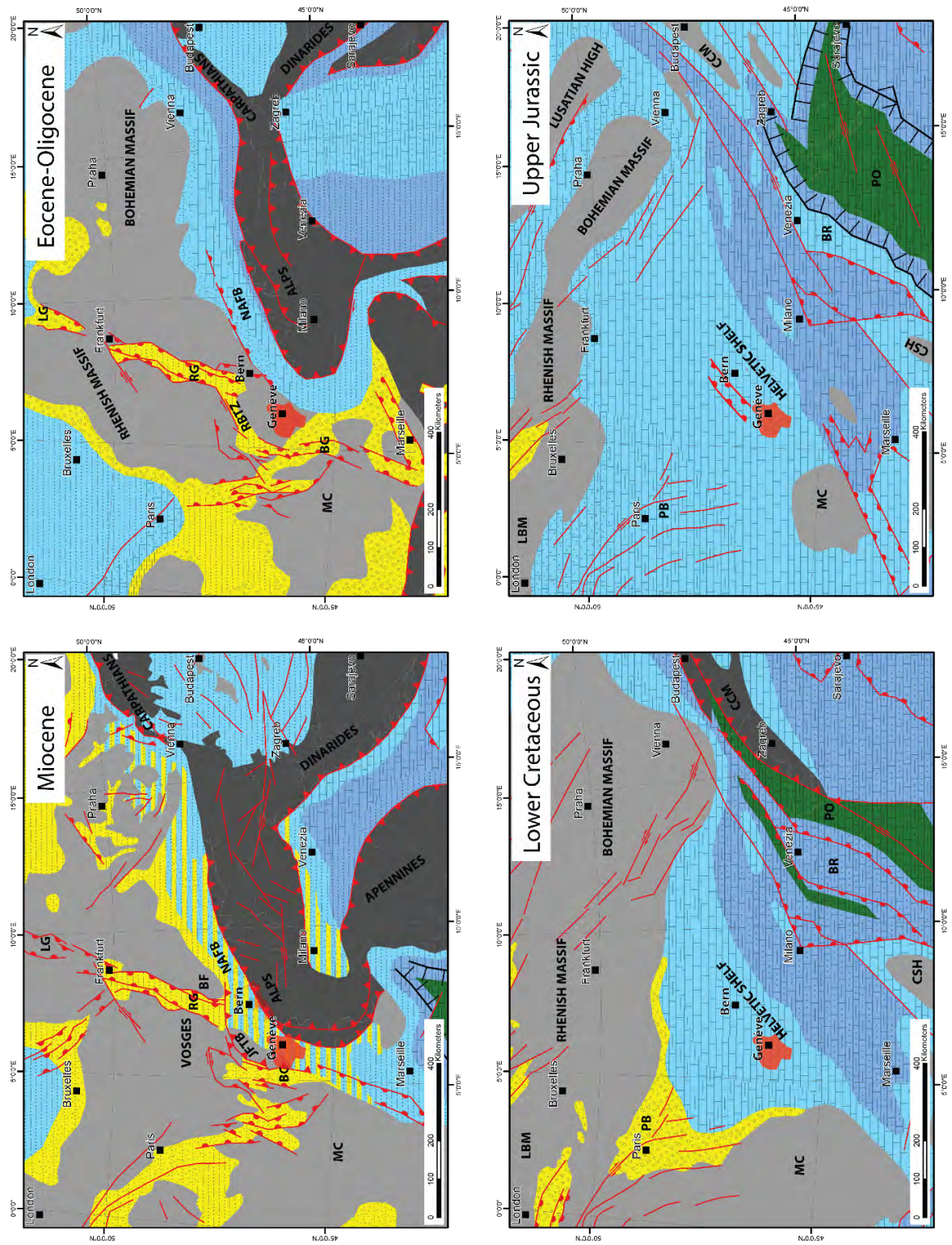


Figure 2-10 : Paleogeographic map of Miocene, Eocene-Oligocene, Lower Cretaceous and Upper Jurassic. This figure is extracted from Gruber (2017), originally redrawn from Ziegler et al., (1998). The study area is located around Geneva.

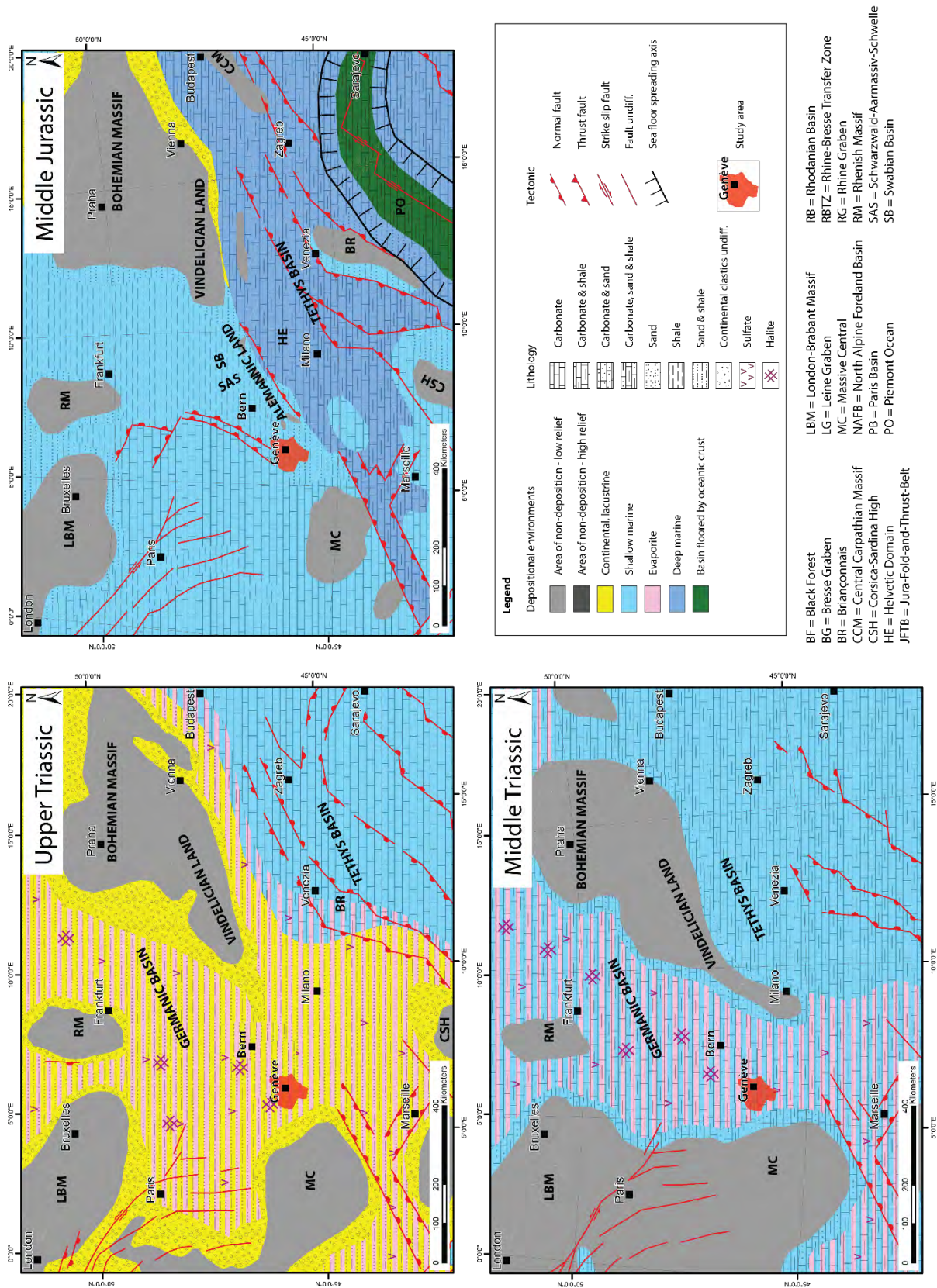


Figure 2-11: Paleogeographic map of Middle Jurassic, Upper Triassic and Middle Triassic. This figure is extracted from Gruber (2017), originally redrawn from Ziegler et al., (1998). The study area is located around the city of Geneva.

certain faults bordering the Permo-Carboniferous troughs are likely reactivated in ENE-WSW (Erzgebirgian) and in NW-SE (Hercynian) and in NNE-SSW striking orientation trends (Ziegler & Dèzes, 2007). This tendency may also continue during the Upper Jurassic period, at least during the Oxfordian (Figure 2-10), as suggested from the interpretation of subsidence curves from Wetzel et al. (2003).

In addition, normal syn-sedimentary faulting rooting in the Triassic evaporites may also occur in the Mesozoic cover only. These may or may not have an indirect link with inherited basement faults (Gruber, 2017; Rusillon, 2017).

2.3.3 The Cenozoic evolution

The extensional tectonics changed into a compressional phase with the first Alpine orogenic event that started during the Upper Cretaceous period. The African and European plates began to collide with a compression oriented N to NNE (Bergerat, 1987), and a subduction of the ocean crust of the Piemont Ocean towards the SE. It progressively closed the Alpine Tethys (Stampfli et al., 1998), and finally, in a continental collision, triggered basement imbrication and uplift of the External Crystalline Massifs (ECM), followed by a partial erosion of the Mesozoic cover (Bourgeois et al., 2007; Debrand-Passard et al., 1984).

First, during the Cretaceous and early Eocene (Figure 2-9, Figure 2-10), the compressional phase of the early Alpine Orogeny was oriented N-S to NNE-SSW. This has led to the inversion of Pre-Mesozoic grabens and therefore the uplift of the related troughs, mostly along the ENE orientation (Erzgebirgian). We can also suppose a reverse faulting of the inherited Variscan strike-slip zones (NNE-SSW or NW-SE). The partial erosion of the Mesozoic cover during this phase is also evidence for intraplate buckling, and long wavelength flexural folding of the lithosphere. The latter flexural large-scale folding of the lithosphere is even extended towards the North of the Paris Basin, as documented by similar increase of subsidence rate observed at that time between the Paris Basin and the Lower Rhône valley (Bourgeois et al., 2007; Dèzes et al., 2004; Schori, 2021).

A second period from the early Eocene until mid-Miocene, concerns the foreland flexural down-bending of the European lithosphere, in relation to its subduction and loading by the orogenic wedge. This tectonic event marks the onset of the foreland basin configuration (from a Flysh-type basin (Homewood & Lateltin, 1988) in Paleocene - early Eocene) with the classical succession of depozones westward of the Alpine front, with foredeep (flexural subsidence), forebulge (flexural uplift), and back-bulge (DeCelles & Giles, 1996). The Alpine foreland basin is supposed to have been initiated around 55Ma, in N-S to NNE-SSW striking orientation passing through northern Corsica, where related Eocene deposits were found (Ford et al., 2006). Then, the foredeep front migrated northward following the Alpine compression, and reached the Helvetic shelf in Late Eocene (Burkhard & Sommaruga, 1998). Finally, at around mid Serravalian (13Ma), the flexural down-bending is supposed to have stopped with the foredeep boundary located along the actual front of the Internal Jura (Pfiffner et al., 2002). Uncertainties remain concerning the dating of these tectonic events, due to a lack of constrain data (sediments lack). The actual foredeep of the northern Alpine foreland is estimated around a 5.5km Cenozoic sediment thickness in front of the Alpine frontal thrust. The flexural mechanism is associated to extensional deformation, with extensional fractures in the forebulge (Bradley & Kidd, 1991), and normal faulting with important offset in the foredeep area (loading vertical compression), likely parallel to the western NAFB in NE-SW striking orientation (Bachmann & Müller, 1992; Nachtmann &

Wagner, 1987)). The latter may either be new crustal features or reactivated inherited faults (DeCelles & Giles, 1996). Considering the Alpine migration of the foredeep, the main extensional phase in the Molasse Basin, is estimated from Late Eocene to Oligocene (Burkhard & Sommaruga, 1998; Ziegler & Dèzes, 2007).

Moreover, during this period, from late Eocene to Oligocene, the European Cenozoic Rift System (ECRIS) was active, leading to the opening of the Upper Rhine Graben (URG) and the Bresse Graben (BG) (see Figure 2-1 for localisation; (Berger et al., 2005)). The latter consists in a reactivation in extension and transtension of Variscan and post-Variscan inherited structures (Dèzes et al., 2004). This event is coeval, during the Oligocene times, with the still ongoing Alpine Orogeny in a general compressional setting. A part of the Cenozoic Molasse sediments were then incorporated into the Alpine wedge, leading to the formation of the Subalpine Molasse thrusting.

The third period concerns the compressional phase that started from the early Miocene and that may still be active. After the Cenozoic rifting phase (ECRIS, late Eocene-Oligocene), from Burdigalian times (17Ma) on, the continent-continent (European-Adriatic) collision induced new long-wavelength elastic lithospheric folds (up to 250 kilometers). This process may explain the 1000m uplift of the lithosphere in the southern part of the URG (Bourgeois et al., 2007; Schori, 2021). Of these lithospheric-scale folds, the closest to our area of investigation is the Burgundy-Swabian Jura Anticline (BSJA). With the constant Alpine compression, this folding is supposed to continue and even to have evolved recently into basement faulting. Indeed, thick-skinned tectonics was interpreted on seismic data (Madritsch et al., 2008; Ustaszewski & Schmid, 2006), and even dated in the northeastern Jura from the Pliocene, using mineral dating by Egli et al., (2017).

The last main tectonic phase, from middle Miocene to beginning of Pliocene, is then overlapping the previous one. Indeed, it is also related to the Alpine compression, but it concerns in this case the formation of the thin-skinned Jura Fold and Thrust Belt. Indeed, during this period, the western NAF was detached from the mechanically more rigid substratum including the basement rocks s.l. and the sandstones of the Lower Triassic along the Middle-Upper Triassic basal décollement level in evaporites (Burkhard & Sommaruga, 1998; Laubscher, 1961). The Molasse Basin was then translated several tens of kilometers (maximum 25-30km) northwestward (Affolter & Gratier, 2004; Schori, 2021), in a thin-skinned tectonic style (“Fernschub” or “distant push” after (Buxtorf, 1916)) that supposedly stopped in the very early Pliocene (around 4Ma (Becker, 2000)). This large-scale decoupling is related to the jump of the Alpine thrust front by some 100km northwestward, in the context of a mechanical wedge. The detachment initiated in Seravallian times, in response (accommodation) to the basement imbrication associated with the exhumation of the External Crystalline Massifs (“Fernschub” hypothesis). This intense deformation phase has triggered all the well-known fold and thrust structures of the JFTB, but it is also recognized in the western NAFB, which evolved into a “wedge-top» configuration. It includes the reactivation of inherited normal or strike-slip faults in the sedimentary cover (Hombert et al., 1999; Radaideh & Mosar, 2021; Schori, 2021). During the transport, it has also created new structures in line with the stress field orientation such as, strike-slips, reverse faults and low-amplitude folding (Ibele, 2011; Sommaruga, 1999). For more details about the deformation style of this period, including evaporites-related structures, please refer to chapter 6.1.

2.3.4 Recent tectonic activity and present-day stress

We have seen in the previous chapter, that thick-skinned tectonic, with reactivation of basement faults is likely happening presently in the Alpine orogen especially on the outer skirt of the orogenic wedge in the Jura FTB. Some seismicity measurements in the western NAF are indeed, located below the detached sedimentary cover in the basement, along the northern and southern edges of the JFTB (Deichmann et al., 2000; Madritsch et al., 2008). In our area, Antunes et al., (2020) has shown recently that the latest earthquakes around Geneva are in pure strike-slip mode, located not far from the Vuache FZ and are possibly rooted in the basement (at around 7 ± 2 km depth below surface).

Much of the seismic activity is however, measured inside the detached Mesozoic-Cenozoic cover, mostly concerning strike-slip systems. For instances, in the Fribourg area with the study from (Vouillamoz et al., 2017), or again in the Vuache FZ (Thouvenot et al., 1998) in relation to the earthquake of Magnitude 5.3 of 1996. Similarly recent studies on seismicity were able to document thrusting events in the detached and deformed sedimentary cover of the Jura along shallow dipping thrusts (Deichmann et al., 2010).

The current tectonic activity supports the idea of an instability of the Alpine orogenic wedge proposed by Mosar (1999) based on wedge modeling. The resulting current overall strike-slip mode (in overall NW-SE S_h max orientation) allows actually to accommodate the compression and rotation of the Alpine foreland (Baize et al., 2011; Gorin et al., 1993; Rabin et al., 2018). Moreover, a possible current combination of thin-skinned and thick-skinned tectonic may be present in the western NAF (Guellec et al., 1990; Mosar, 1999; Philippe et al., 1996; Schori, 2021).

3. DATA INVENTORY – SEISMIC AND WELL DATA

The data inventory of the study area consists of a compilation of geophysical and geological data implemented in GIS softwares (ArcMAP and Petrosys) and in the Kingdom software (IHS). The resulting database represents all the input and knowledge data necessary for the progress of this study. Three main types of data have been collected: seismic data, well data and surface data. See Appendices and Enclosures for complete database details.

Concerning seismic data, except for 2D lines located in the Jura Mountains that were entrusted to the project by the UNIFR, SIG company (based in Geneva) has provided all others 2D lines. Previous seismic interpretation studies carried out on behalf of SIG (Clerc, 2016; Paolacci, 2012) had resulted in a first set of substantial and well organized seismic databases, that were then transferred for the purposes of this study. The latest database (Clerc, 2016) contained complete seismic datasets from Switzerland as well as from France, thanks to a close collaboration between the SIG/UNIGE (Switzerland) and the BRGM (France). As part of the international GEOMOL project led by Swisstopo in Switzerland (Allenbach et al., 2017), this collaboration was made possible. An agreement between UNIFR and the former company Celtique Energie Petroleum Ltd (based in UK) defined the access to the seismic data in the Jura part of our investigation (surveys 80JU-81JU-83JU, see Table 3-1). The north-east part of the Canton of Geneva is adjacent to the Canton of Vaud, whose seismic data are handled by the “Musée Cantonal de Géologie”. SIG via GEOMOL project took care of data sharing between the two Swiss Cantons (surveys 76-VD and 77VD, see Table 3-1). See App_01&02 for complete seismic data tables.

Since 2016, SIG has mandated GGE Company (based in Geneva) for several geophysical and geological studies, including a normalization (Hauvette, 2017) and a valorization through re-processing of the seismic data. In a first step, the normalization consisted mostly 1) in tying seismic 2D lines to a common datum plane (500 or 1125 m a.s.l, see chap 3.2.6), 2) applying a unified nomenclature to all seismic data types (processing versions, see chap 3.2.8) and 3) applying simple amplitude, frequency and dips filtering in order to ease the seismic interpretation (see chap 3.2.8). This step concerned all seismic data in France and in Switzerland. In a second step, the valorization of the seismic data was a more complex process that involved the re-processing of all seismic data located in Switzerland and few seismic lines in France, for those where raw data (acquisition data) were available (see 3.2.7).

Regarding well data, the collaboration between SIG and the BRGM via GEOMOL project has led to an exhaustive database that contains all original well reports and logs (Brentini, 2018; Rusillon, 2017). SIG has also mandated GGE for several studies in the petrophysics domain. The results of these studies (GGE, 2018) were available for this work. See App_03 for complete well data tables.

Surface data used for this study stem from public geological maps, digital elevation maps, and maps published in scientific literature. All data will be displayed in this study according to the more recent Swiss coordinate system CH1903+/LV95.

3.1 Historical context from oil and gas to geothermal exploration data

The interest in oil exploration in Switzerland developed mostly after World War II, along with the increase of consumption (cars and heating) with the aim of reducing the imported amount. It has led to the drilling of 37 deep wells and the acquisition of around one thousand 2D seismic reflections lines (around more than 15000 km total length) during the last century (Sommaruga et al., 2012). Despite interesting oil and gas shows (Molasse in the Geneva area, Eclepens-Yverdon, or Aarau-Oftringen area), no commercially exploitable reservoirs have been revealed (Leu, 2012). It may be explained in a not favorable petroleum system, especially due to a lack of consistent traps, and to relatively low reservoirs quality (porosity and permeability, Gorin (1989), Rusillon (2017)). However, these limitations may also be related to several other factors, including a relatively moderate exploration budget spent by oil and gas companies since the beginning of exploration compared to neighboring countries such as Germany (Frey & Lahusen, 1994). This implies that many seismic sections are outdated in addition to their moderate density. In that sense, several areas in Switzerland may be considered as “under-explored”, with highly scattered or not deep enough wells (potential traps below the Keuper unit). This means that the potential of Switzerland in oil and gas production may still be revised in an optimistic way with a greater financial investment for exploration (more data available).

More recently, along with climate change and ecological issues, new society challenges have raised, including the future exit of nuclear energy production or the expected neutral CO₂ situation. However, the exploration for local fossil fuel could still represent a relatively environmentally friendly solution for a smooth energy transition toward more renewable energies. In that sense, since 2005, two third of the Swiss Molasse Basin and the Jura Mountains are still ruled under eighteen exploration permits managed by seven companies consortium. These different projects are now focused on looking for plays, such as shallow conventional oil and gas in the Mesozoic-Paleozoic section of the Jura Fold belt and in the northern rim of the Molasse Basin (SEAG, PEOS, Celtique Energy (not longer active)), or shallow heavy oil in the Cenozoic unit of the Geneva area (Tethys Oil), or deep conventional and unconventional tight gas plays in the southern part of the Molasse Basin (Petrosvibri, SEAG, GVM). Most of these projects are inactive, waiting maybe for the hypothetical future political discussions around shale gas potential assessment. The latest oil and gas well was drilled in Noville (Noville-1, east of Lake Geneva) in 2011 targeting tight gas in Paleozoic clastic rocks (the results of this drilling will soon become public following the legislation of the Canton de Vaud that authorizes only 10 years of data privacy). This inactivity of the oil and gas exploration is making room for a more promising energy solution: geothermal energy.

Concerning the specific case of the Geneva Basin, neighboring France and Canton of Vaud have also to be considered. Seismic acquisition in the Molasse basin near the GGB started with oil exploration (PREPA, ESSOREP, RAP, BP-France) in France in the 1950's until the 1980's. In the Canton of Vaud, several oil companies (SNPA, BEB SAHL, PREPA, and SHELL) have explored the subsurface during the last decades. Nevertheless, it was already for geothermal exploration that the state of Geneva managed the acquisition of the “GG87” seismic survey in 1987. Thereafter, “les services industriels de Genève” (SIG) took the lead of the subsurface investigation of the Geneva underground for gas and geothermal energy, and started the acquisition of the “90” seismic survey in 1990 (see Table 3-1), followed by the drilling of the first deep exploration well in the Canton Thônex-01, in 1993 (see Table 3-2). Since the 2010's SIG is very proactive in developing the knowledge around the geothermal potential of the GGB. In that sense, forty seismic lines (total length of 358km) were acquired in

collaboration with local contractors Geo2X-Galliego and Geoexperts. During these decades, UNIGE has played a key role in compiling knowledge derived from these seismic lines (e.g. Clerc & Moscariello, 2020; Gorin et al., 1993; Paolacci, 2012; Signer, 1992 and references therein).

3.2 2D Seismic reflection profiles

3.2.1 Principles of seismic reflection (onshore acquisition)

Seismic reflection data are obtained by imaging the subsurface using near vertical artificially generated seismic waves to detect impedance contrasts. In our case of onshore (land) configuration, seismic waves are sent from topographical surface downwards with the help of several kinds of energy sources such as vibrator trucks, dynamites or weigh drops (Figure 3-2). Then, interfaces of sufficient acoustic impedance change in the subsurface allow to reflect the seismic information upward, recorded back to the surface via geophones (detectors). The acoustic impedance represents the opposition that a medium (material, or rock) present to a seismic wave going through it. It is characterized by the velocity of the seismic wave through the medium (rock) multiplied by the density of the medium. In that case, a sharp seismic reflection would be generated for instance from an interface of a clear change of lithology, such as passing from a soft sand to a massive limestone (Figure 3-1).

The first resulting image is usually in the time domain (vertical scale), or two-way-traveltime (TWT) domain that corresponds, to the time that the seismic wave takes to go downwards until the reflection point, then upwards to reach the geophone. It is possible to convert a seismic section from the time domain to the depth domain (from seconds to meters) using a velocity model, see chapter 5.1. The horizontal scale of a seismic image is in meters.

The seismic reflection method provides the highest resolution images of the deep subsurface (several km). As explained by Mooney et al., (2002), there are two reasons for this. The first reason is that this method uses densely recorded data from closely spaced shots (5m-40m in our study, see App_01) and seismic recorders (geophones; 2.5m-30m in our study). The second reason is that the seismic reflection method uses high frequency seismic energy (8–80 Hz for a classic vibrator linear Up-sweep, example of survey “18SIG” relatively similar to the other surveys of this study) which resolves features as thin as 10-15 m at shallow depth (0-500m), and as 20-30m at great depth (500m-3km, SEG Wiki (2018)). The resolution is much higher than refraction imaging, which is more adapted to velocity modeling of shallow targets (0-500m depth, (Frei, 2019)). The seismic reflection image is obtained after a specific data processing that allow displaying acoustic impedance contrast as vertical amplitude trace wiggles (Figure 3-2).

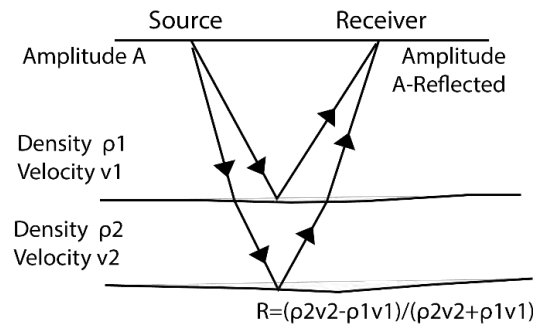


Figure 3-1: Seismic reflection principle: a seismic wave is reflected at a sufficient acoustic impedance contrast (redrawn from Simm & Bacon (2014)).

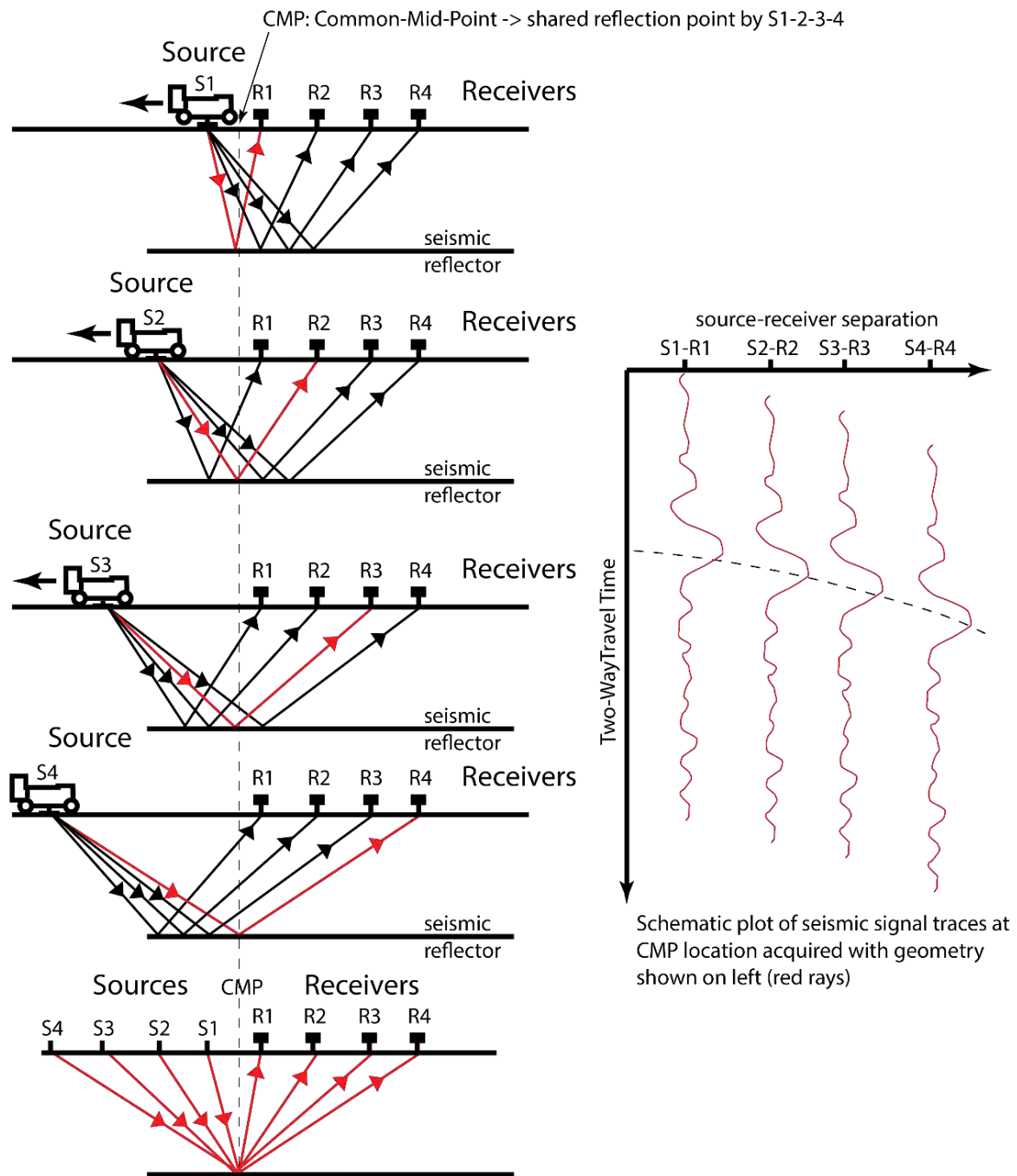


Figure 3-2: Seismic acquisition scheme and resulting amplitude trace wiggles from four folds (redrawn and modified from Simm & Bacon (2014)).

3.2.2 Seismic data resolution and quality types

The type of energy source, and the acquisition scheme/ geometry have a direct control on image resolution, image quality, and depth of penetration (Yordkayhun et al., 2009). Vertical resolution is controlled by the frequency band of the source (Figure 3-3), whereas target depth and acquisition parameters also influence the spatial resolution (Figure 3-1 and Figure 3-4).

Therefore, before a seismic acquisition, choices must be made in terms of:

- Energy power, quantified by the energy density (energy per unit volume) which is proportional to the square of the amplitude within the same medium (Sheriff, 1975; Telford et al., 1990). This means that, the more the energy power is high, the more the amplitude of the reflections will be high.
- Frequency broad bandwidth, characterized by the dominant frequency of the signal. Seismic attenuation, due to absorption increases exponentially with increasing frequency of the seismic signal. This means that, it is possible to obtain a good seismic image at great depth, only if the dominant frequency of the source signal is limited.
- Acquisition scheme, defined by the spacing distance between two sources, and between two receivers. The denser (small spacing distance) it is, the higher the resolution will be at shallow depth (Figure 3-6).

Amplitude depends also on geological factors (subsurface, such as reflector curvature and rugosity (Figure 3-4), but they will not be detailed on this report.

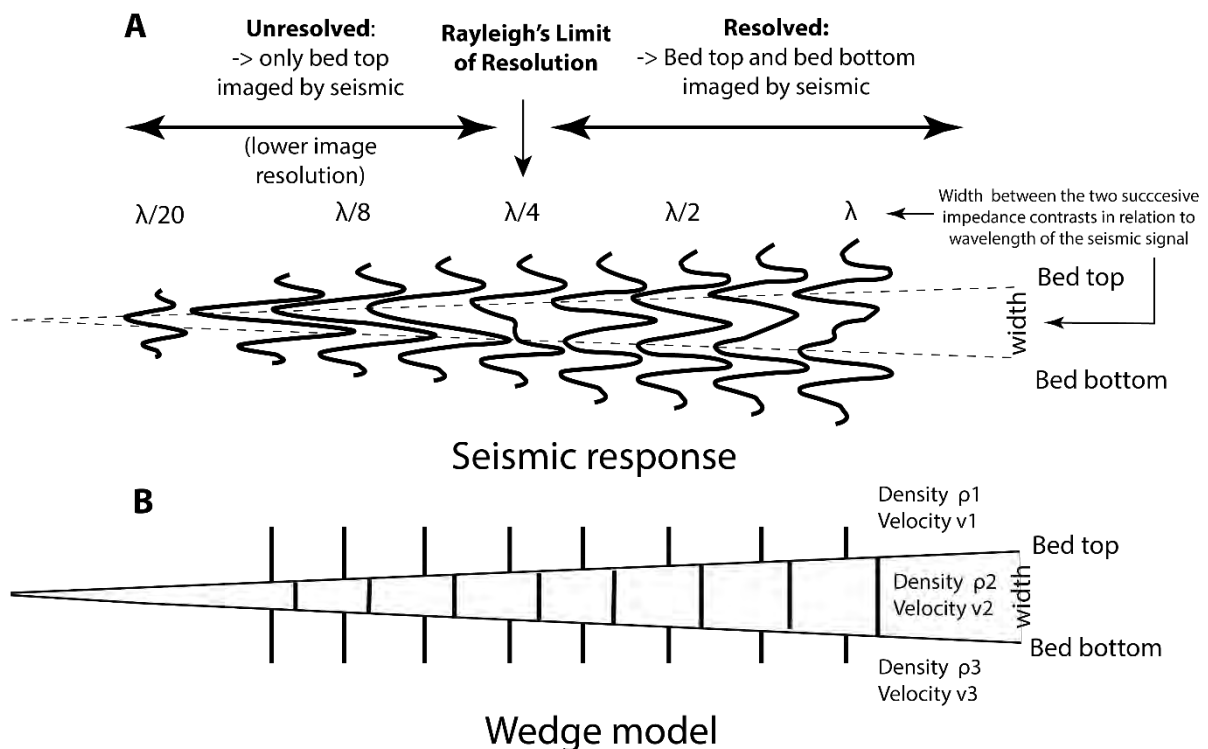
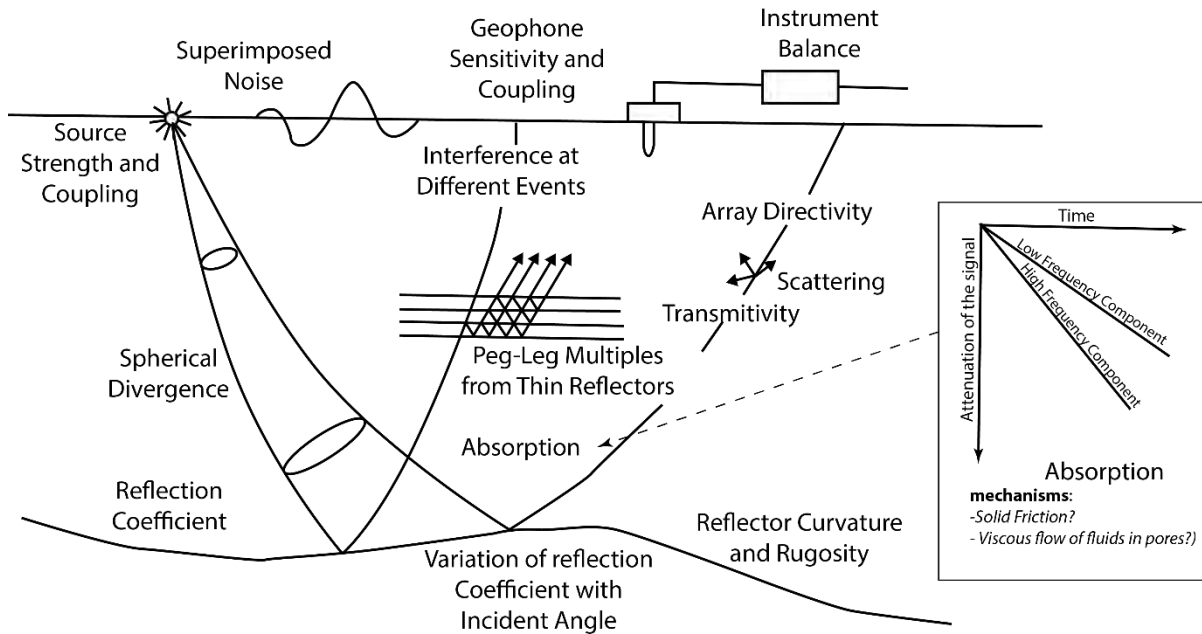


Figure 3-3: The vertical seismic resolution of a seismic reflection image is defined by the Rayleigh's limit that explained that in order to identify two distinct seismic events, they should be separated by the quarter of the wavelength $\lambda/4$ (modified after SEG Wiki (2018)).



Factors which affect amplitude

Figure 3-4 : Signal attenuation is increasing with increasing of the dominant frequency. This figure is modified from Sheriff, (1975).

As a reminder, three main types of energy sources exist for land acquisition; vibrator trucks, dynamite and accelerated weight drops (Figure 3-5 and Figure 3-10). Dynamite (explosives) method has on the one hand, the advantage to be high energy and high bandwidth seismic sources, but on the other hand, it is a financially expensive method with complex permitting operations. These are the main reasons why this method, that was often used before the 1970's, has been progressively replaced by alternatives, such as vibrators or weight drops. The type of seismic source is described for each line of the project in Table 3-1. We can observe on our dataset that dynamite data and vibrator data have quite similar resolutions, even though dynamite data seem to have greater depth penetration (Figure 3-5). As for weight drop data, it allows imaging high resolutions reflections at shallow depth that the two other methods can not produce. These observations are in line with the three main parameters that control the seismic resolution as described above. Weight drop data generates high frequency and relative low energy signals that limits the depth penetration as well as the amplitude value of the signal. Nevertheless, the dense receiver and source spacing gives as a result, high-resolution image at shallow depth. On the opposite, the two other methods described have high resolution and amplitude at great depth, due to high energy and low frequency energy source; but they have limited resolution at shallow depth because of relatively large acquisition bin spacing.

The length of the seismic profiles has a significance in terms of ratio about the number of full fold traces against the cost of the acquisition. As a reminder, a fold (glossary.oilfield.slb.com) is the measure of the redundancy of common midpoint seismic data, equal to the number of offset receivers that record a given data point or in a given bin and are added during stacking to produce a single trace. Typical values of fold for modern seismic data range from 60 to 240 for 2D seismic data, and 10 to 120 for 3D seismic data. The fold of 2D seismic data can be calculated by dividing the number of seismometer groups by twice the number of group intervals between shotpoints.

Indeed, if we consider two seismic lines from the same survey 18SIG_003 and 18CPG_001, the first one having a length twice bigger than the second, as displayed on the Figure 3-7, line 18SIG_003 will have eight times more full fold traces than line 18CPG_001. Even so, these two lines had a very similar cost (only use of several more geophones for the longer line).

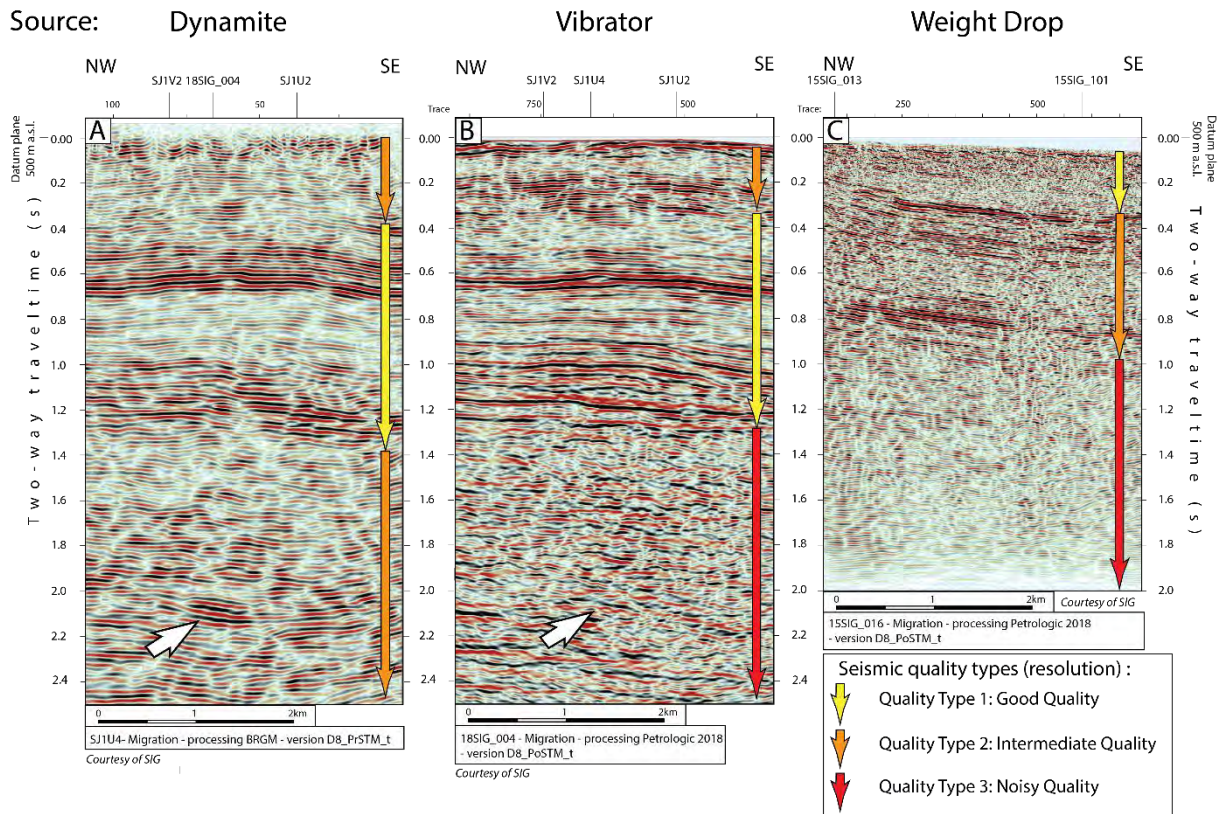


Figure 3-5: Influence of the seismic source type on seismic resolution. Dynamite and Vibrator data have a high resolution (quality type 1) in the TWT interval [0.4-1.2], and limited resolution (quality 2) in the shallow part [0.0-0.4]. Dynamite data is the only of the three methods that highlights seismic reflections (quality 2) in the very deep part [1.4-1.2], whereas Weight drop method is the only method that highlight continuous reflections in the shallow part [0-0.4]. See Figure 3-13 for localisation of the sections. See respectively Encl 76, Encl 22, and Encl 16 for detailed seismic interpretation of lines SJ1U4, 18SIG_004 and 15SIG_016. Seismic quality is here analysed vertically to show the influence of seismic sources on the vertical resolution and wave penetration, whereas Figure 3-8 present the overall seismic quality types (average of the quality types on the whole sections, from shallow to deep parts).

Consequently, acquisition parameters should be adapted to the target depth and resolution. As it is always complicated or even sometimes not possible to have a high resolution at all depth, compromises on the choice of these parameters are usually necessary. As many parameters are involved in the definition of the resolution of a seismic section, it has been decided to use a simple classification of the quality of each seismic data, divided into three groups. The definition of the three quality types (concept following the study of Sommaruga et al. (2012)) is based on visual characteristics of the seismic section, therefore it is a subjective attribution. It allows appreciating the interpretability of a profile, which is the ease to follow a seismic reflection laterally (lateral continuity) during the interpretation process of seismic horizons (Figure 3-8 and Figure 3-9):

- Quality type 1: it corresponds to the best quality type. Such seismic sections, contain an overall good lateral continuity, and therefore a high signal to noise ratio, that enable to pick very easily most of the seismic horizons of the Mesozoic layers. A simple criterion to classify a section in this category is when the autopicking tool can be applied to interpret several seismic horizons.
- Quality type 2: it represents intermediate quality type. The seismic section possesses now seismic noise perturbing the signal, and the automatic picking tool (the Kingdom software) cannot be applied for interpreting seismic horizons. Interpreted horizons segments may be linked manually in order to obtain continuous interpretation through the section. However, all Mesozoic horizons can be interpreted.
- Quality type 3: it concerns very noisy, low resolution seismic lines, that are very difficult to interpret. The continuity of seismic reflections is poor, and only few Mesozoic seismic horizons are able to be interpreted.

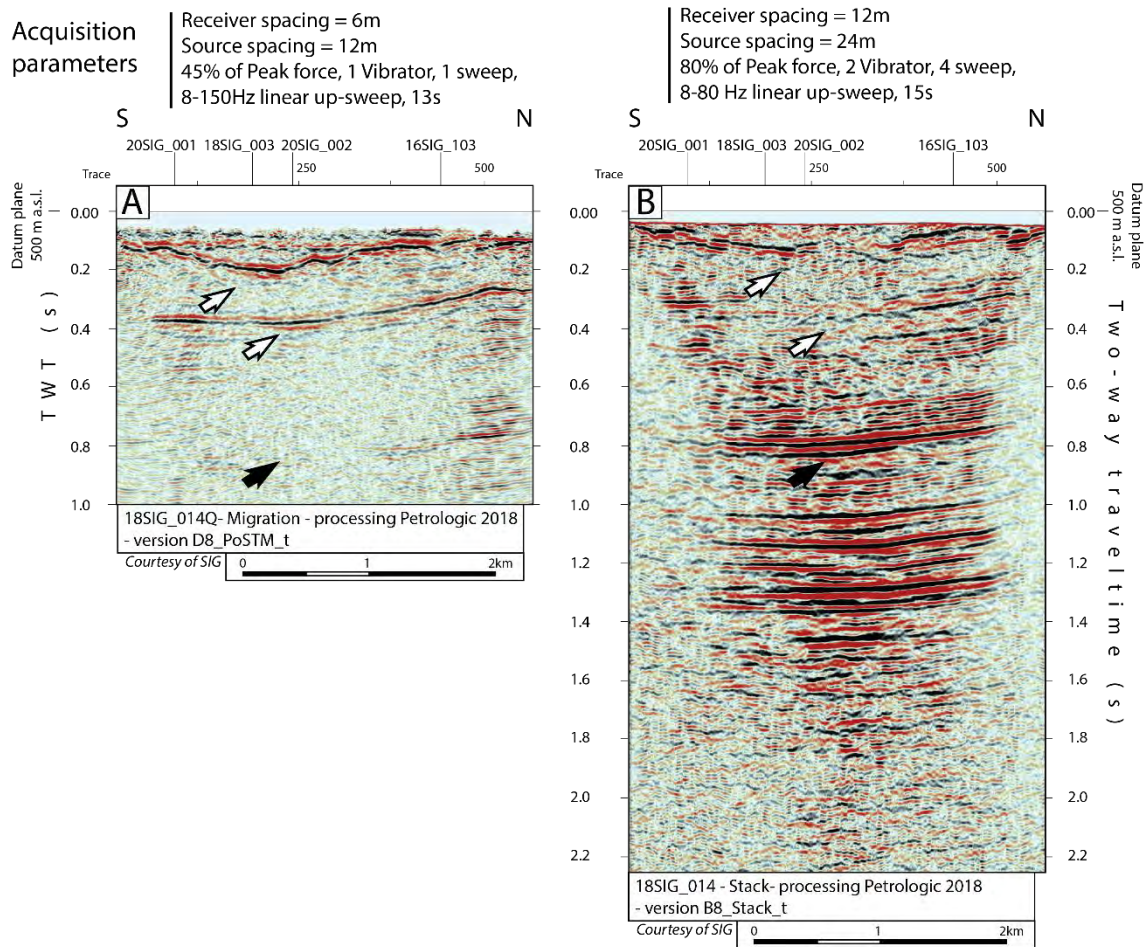


Figure 3-6: Highlight of the influence on seismic resolution and depth penetration of the following parameters; acquisition, bin spacing on the target depth, frequency bandwidth of the signal, and the energy power of the input signal coming for both cases from a the vibrator method. Left image: High frequency and low energy force from the source will increase the amplitude attenuation and depth penetration (black arrow). However, this configuration added to a dense acquisition spacing, allow a high resolution of the shallow part [0-0.4s] (white arrows). Right image: Lower frequency and higher energy force increase the resolution of the image ate greater depth (black arrow), however the larger acquisition bin spacing reduces the resolution at shallower depth [0-0.4s] (white arrows). See Figure 3-13 for localisation of the sections. See Encl 31 for detailed seismic interpretation of line 18SIG_014.

A seismic survey can be defined as a group of seismic profiles that were acquired during the same acquisition campaign using very similar acquisition and processing parameters. Each seismic survey, will then have by definition a specific resolution, following what has been explained in the above paragraphs. The main acquisition and processing parameters are sum up in Table 3-1, and allow to make the link with the actual resolutions of each survey. Here is a description of the column's titles of some of the parameters present in the table:

- Stack data (S, see Table 3-1) corresponds to the first raw result of seismic processing. Migration (M, see Table 3-1) is the main next step tool used in seismic processing to get an accurate picture of underground layers, with a lateral and vertical repositioning of all seismic events at their right locations (see 3.2.7).
- Sample interval in seconds corresponds to the TWT interval in between each amplitude value along seismic trace composing a seismic profile.
- The datum plane defines the elevation in meters corresponding to the vertical origin of the time domain of a seismic section (see chap 3.2.6).

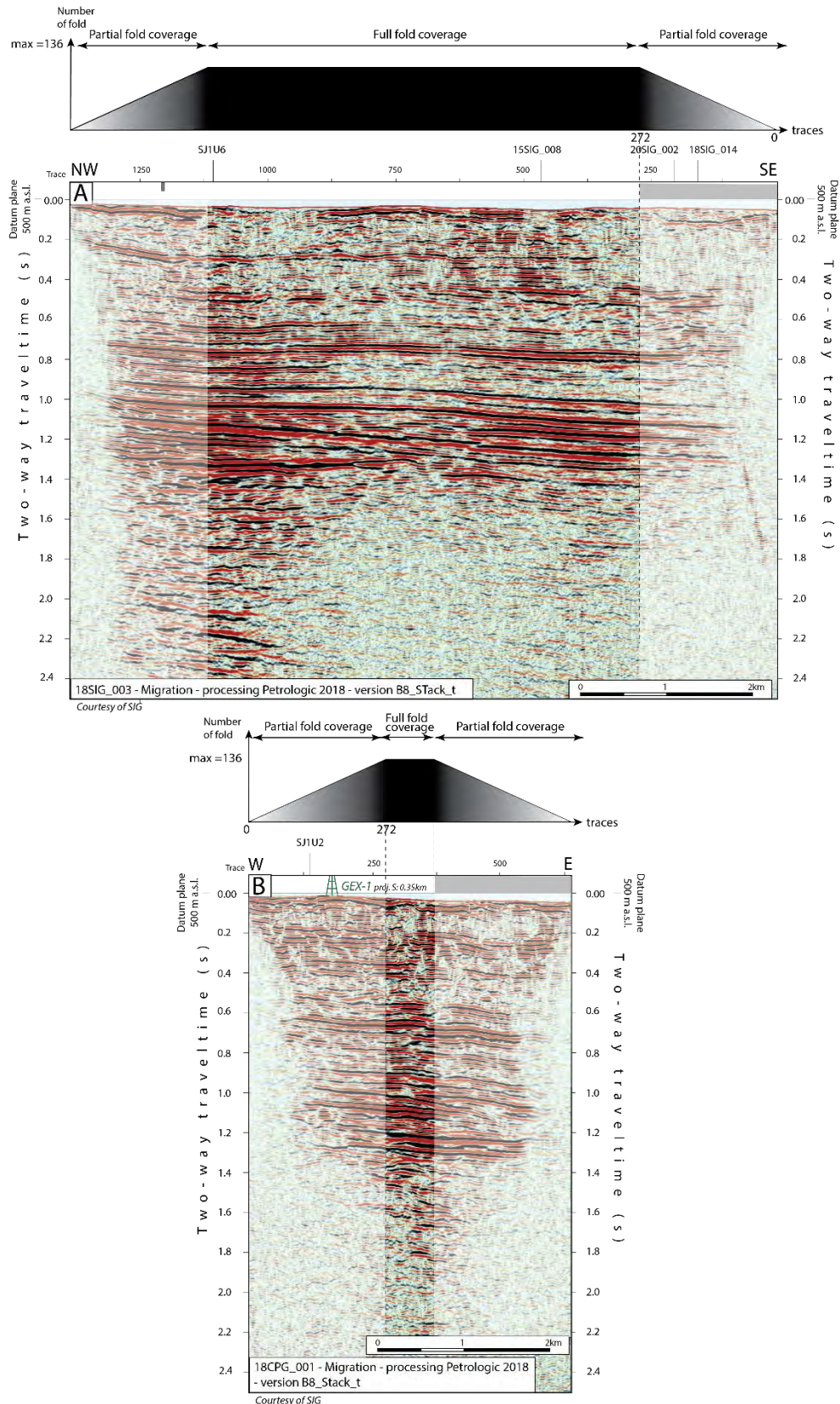


Figure 3-7: Fold coverage of seismic 2D profiles from acquisition in the GGB in 2018. Line 18SIG_003 (A) is approximately twice longer than line 18CPG_001 (B). The acquisition parameters of this survey result in a full fold coverage of 136 traces after the first 272 first traces on each side of the profile. On line 18SIG_003 around 800 traces in the middle part of the profile are full fold traces against only around 100 full fold traces for line 18CPG_001. It shows the advantage of acquiring as long as possible 2D profiles, as for very similar costs seismic line 18SIG_003 is twice longer than line 18CPG_001 and will have around 8 times more full fold traces. See Figure 3-13 for localisation of the sections. See respectively Encl 21 and Encl 33 for detailed seismic interpretation of lines 18SIG_003 and 18CPG_001.

- The replacement velocity is the interval velocity (in m/s, constant value per survey) that is used during seismic processing in between the datum plane and the smoothed topographical surface in the time domain (used during the static correction process).
- Phase shift, in degrees, is the rotation of the phase applied on the whole seismic section. A phase shift of 180 degree corresponds to an inversion of the polarity (sens in which the seismic wiggle is drawn in the seismic profile)
- Energy source is the type of machine used to send seismic signals through the subsurface during seismic acquisition.
- Quality type is a value between 1-3 that describes the resolution of the seismic profile and the interpretability of it. 1 being the best quality type (Figure 3-8).

Seismic line names of one seismic survey begin with the same or similar prefix (survey name) followed by numerical suffix, that differentiates each individual seismic line. For the specific case of 14-15-16-17-18-20SIG survey lines, a specific nomenclature (Hauvette, 2017) has been applied on the numerical suffix. The first digit of the suffix is either 1 for seismic sections acquired with a focus on Quaternary layers (also the case for lines with suffix finishing with the letter Q), or 0 for seismic lines acquired for a subsequent interpretation of the whole Mesozoic layers pile.

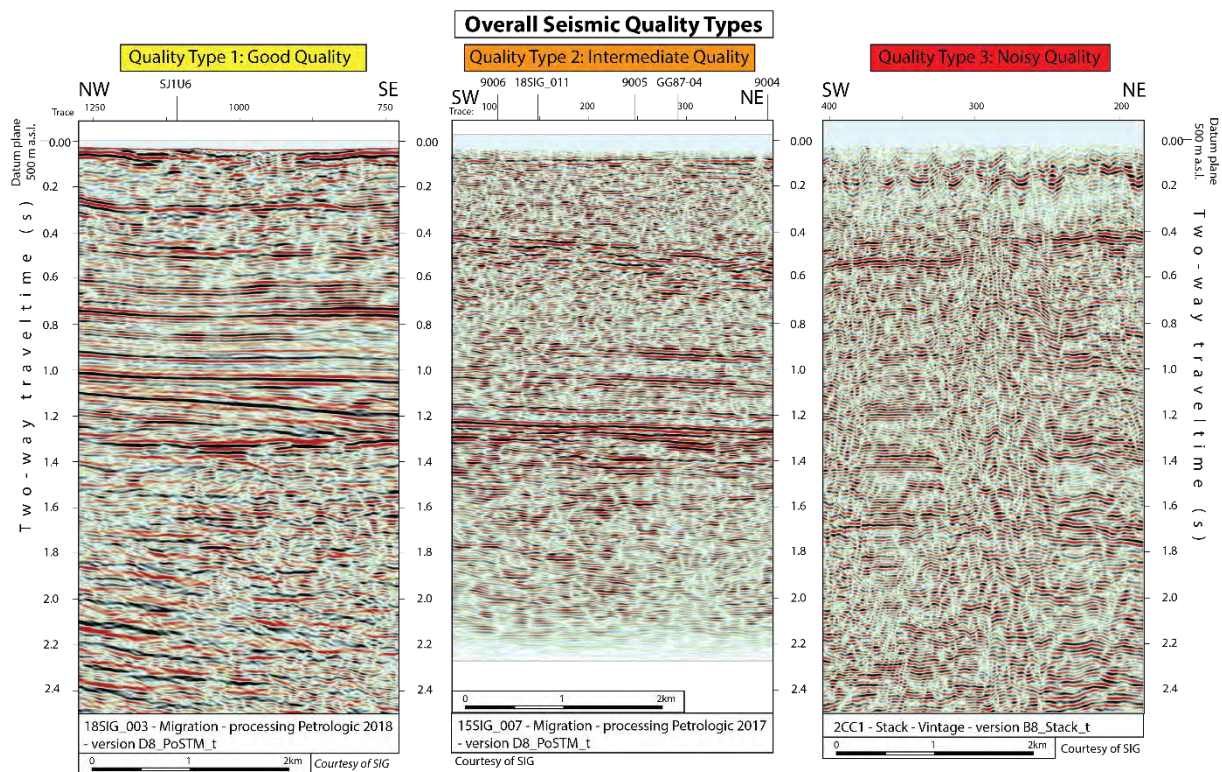


Figure 3-8: Seismic quality classes, 1-2 or 3, respectively on image from left to right. Quality type 1 correspond to seismic images with an overall very good lateral continuity of the reflections in the entire Mesozoic layer. One seismic line can be classified in this quality type 1 if several horizons in the Mesozoic cover can be interpreted using an automatic picking tool (The Kingdom Software). Quality type 2 defines seismic lines that contains a moderate lateral continuity of its seismic reflections. Horizons of the Mesozoic cover may be interpreted in most parts of the seismic line, mostly using a manual picking mode. Quality type 3: seismic lines of this class are very difficult to interpret because of the high noise presence that allow interpreting only partly the horizons. Horizons segments are then sometimes linked together by pure deduction. Note that for the three quality types it does not take into account the resolution of the Cenozoic and Paleozoic layers, as no horizons are picked in these intervals. See Figure 3-13 for localisation of the sections. See respectively Encl 21, Encl 12, and Encl 59 for detailed seismic interpretation of lines 185IG_003, 155IG_007 and 2CC1.

3.2.3 Seismic profiles from Canton Geneva

The seismic acquisition inside the Canton Geneva began several decades after the surrounding areas. This can be explained by the fact that, no oil and gas exploration was run inside this Canton. In 1987, the state of Canton Geneva ordered the acquisition by CGG ("General Geophysical company" based in France, Massy) of seven seismic lines ("GG87" survey, 37km length) in order to find a location for a potential geothermal drillhole. This survey was acquired using vibrators (sources) and processed under a common datum plane of 300m a.s.l and with a replacement velocity of 3000m/s. UNIGE took care of the initial seismic interpretation (Gorin, 1989; Signer & Gorin, 1995). Unfortunately, the original raw

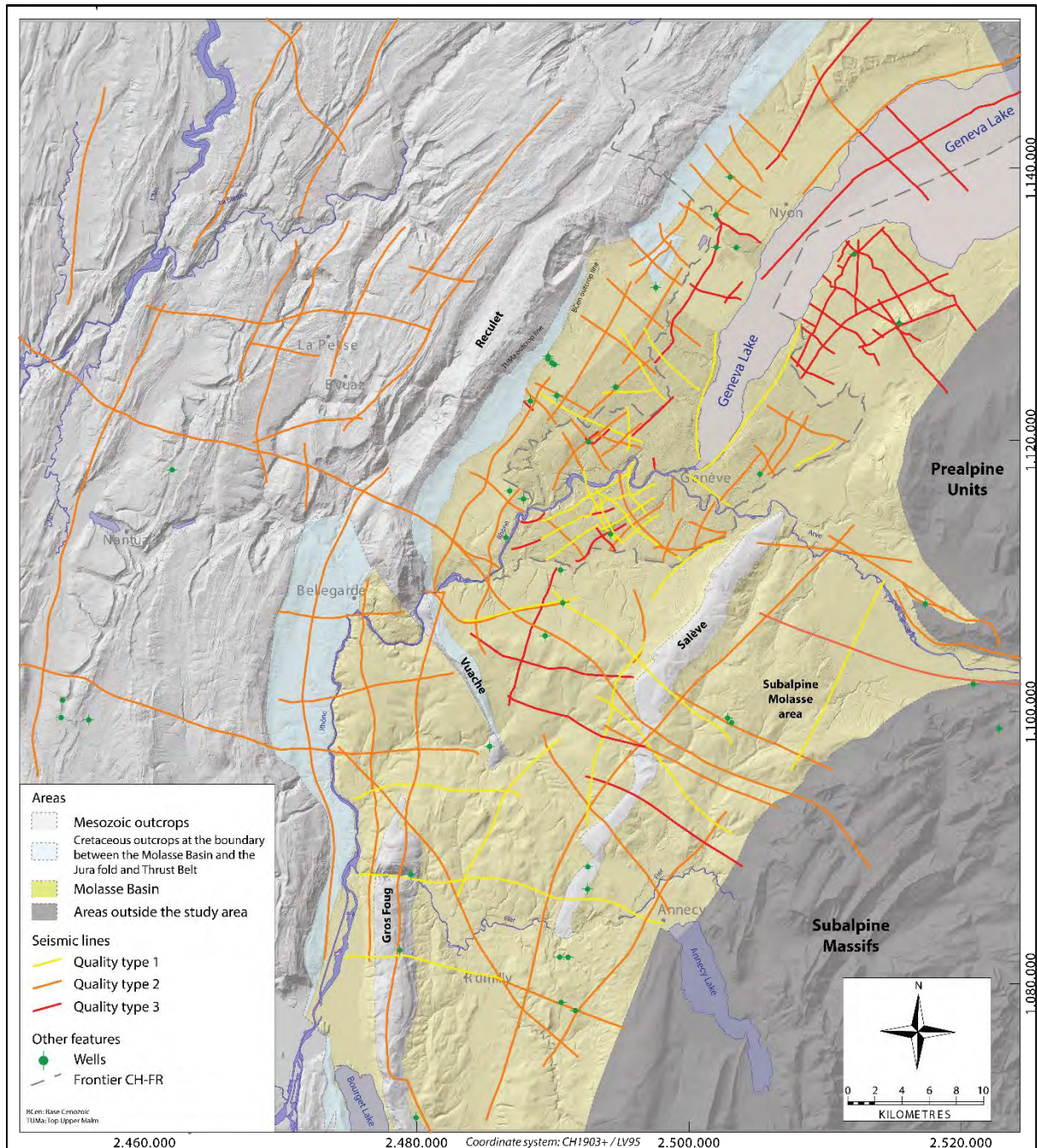


Figure 3-9: Regional map with seismic profiles localisation and division according to their related quality types. Quality type 1: Good quality. Quality type 2: Intermediate quality. Quality type 3: noisy quality. See also Figure 3-8 for examples in section.

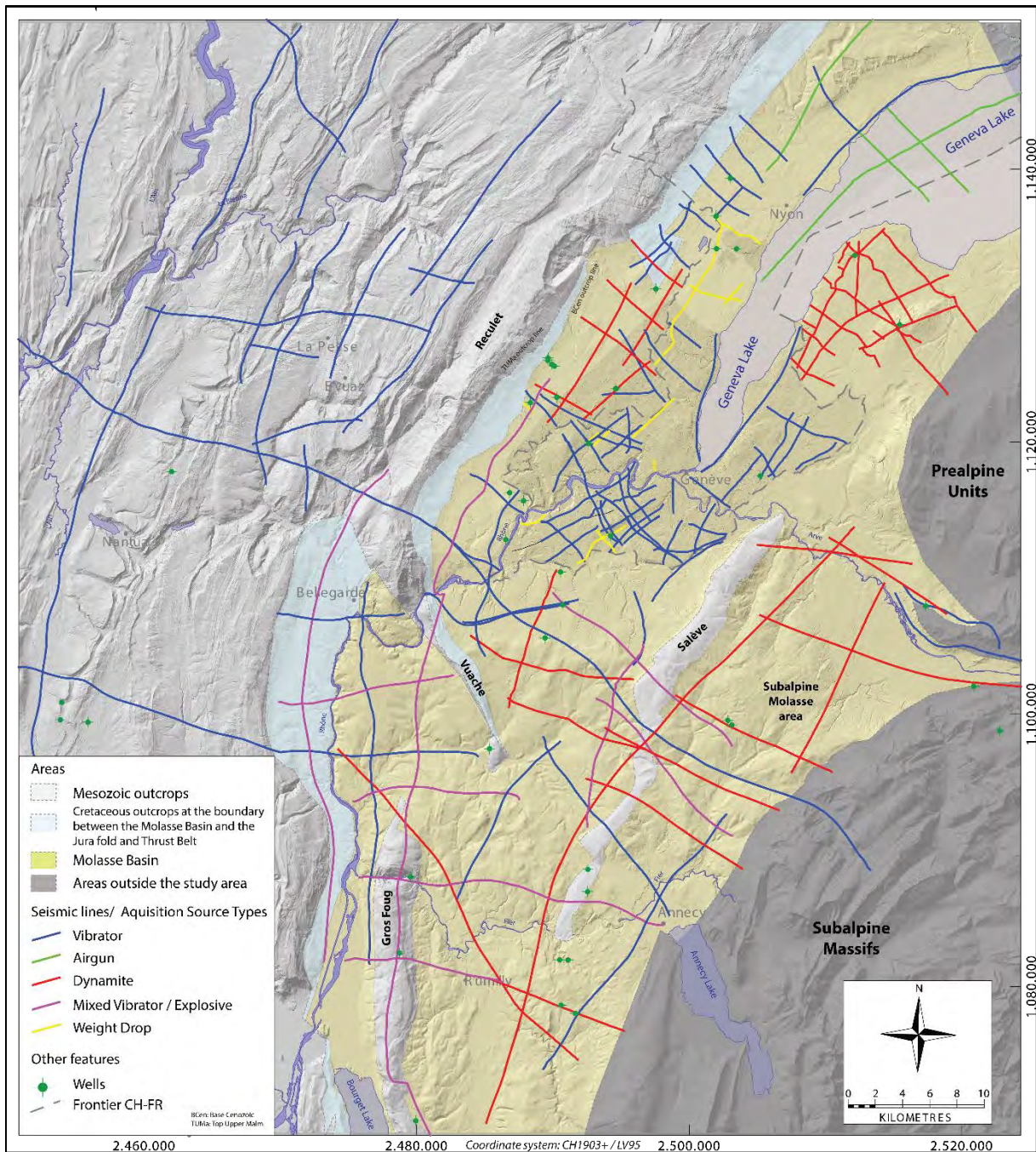


Figure 3-10: Seismic basemap in relation to seismic acquisition energy sources. (coordinate system: CH1303+/LV95). See, Table 3-1 for surveys descriptions and Figure 3-5 for explanations on impacts of seismic source types on seismic image quality.

acquisition data (on tapes) were never found again by SIG or UNIGE during the update of the seismic database. Therefore no reprocessing of the data could be done, but only a digitalization of scans of the paper profiles was achieved. However, these seismic data are of quality type 2 (close to a quality type1).

The second seismic acquisition campaign conducted by Schlumberger (geophysics company, USA), between the villages of Onex and Avully, occurred in 1990, with the same geothermal objective than survey “GG87”, but was led by SIG. The resulting survey “90” (Figure 3-11 and Figure 3-13), which used vibrators as source type, is composed of six seismic 2D lines (38km length), processed originally under common datum plane of 300m a.s.l with a replacement velocity of 2500m/s. This survey was originally

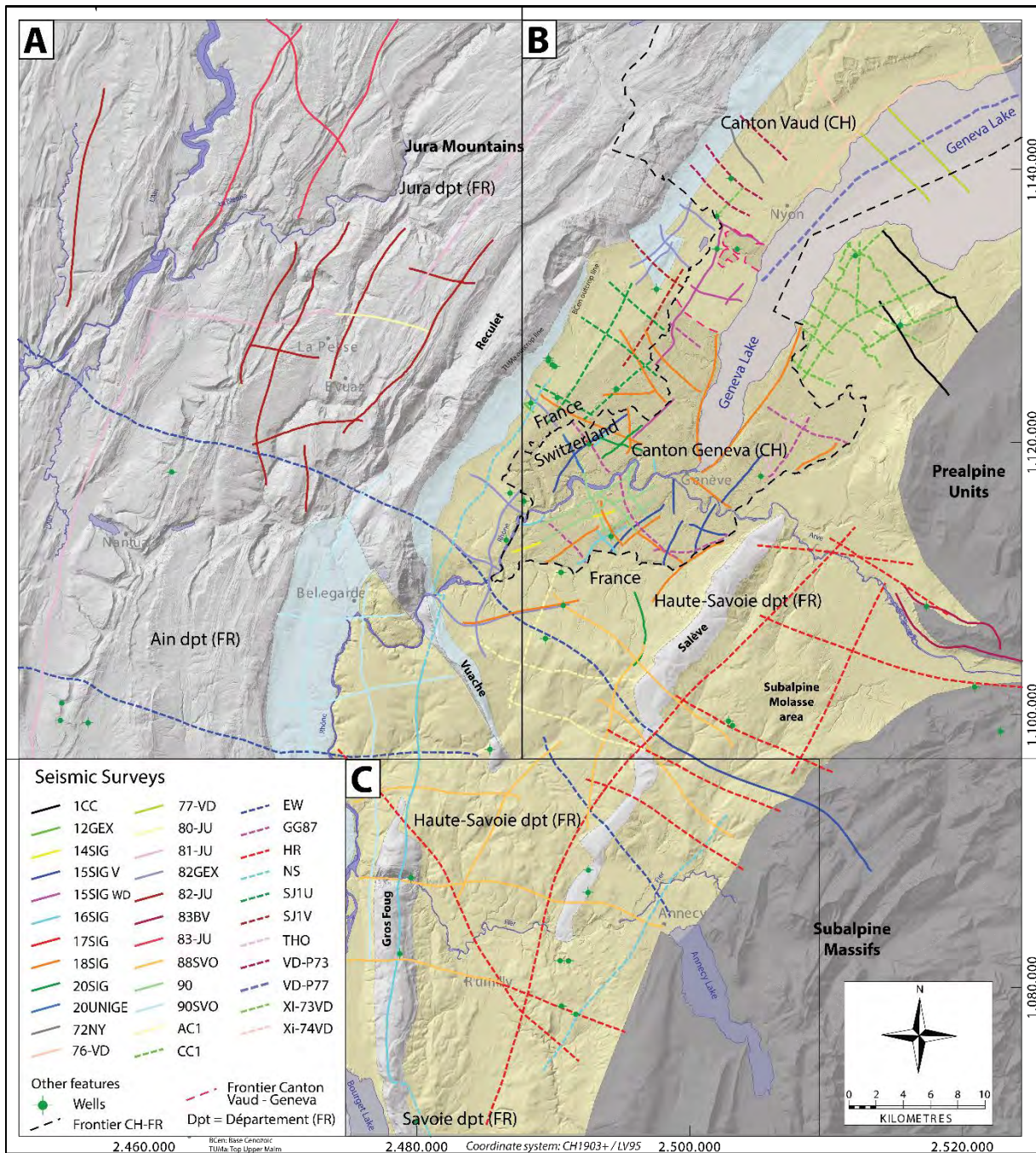


Figure 3-11: Seismic basemap with profiles sorted by survey names.

interpreted by UNIGE (Gorin et al., 1993). The survey belongs to the dataset that was reprocessed in 2017. The "90" survey is set up along the common datum plane 500m a.s.l and replacement velocity 3000m/s defined for this project (except for seismic lines located in the Jura, see chap 3.2.6). Therefore, the original processing parameters of this survey will not be detailed in the rest of the thesis, as it was replaced by a more recent reprocessing from 2017.

The third phase of land seismic acquisition of deep subsurface geothermal exploration, led by SIG, started again with a more sustained rhythm from 2010 to 2020. This impulse in seismic acquisition has been possible thanks to the close collaboration between SIG and the swiss geophysical company Geo2X SA that was in charge of acquiring the following described seismic lines. Two lines from survey "THO" (8km length, quality type 2) were acquired in 2010 with vibrator truck near Thônex-1 well, followed in

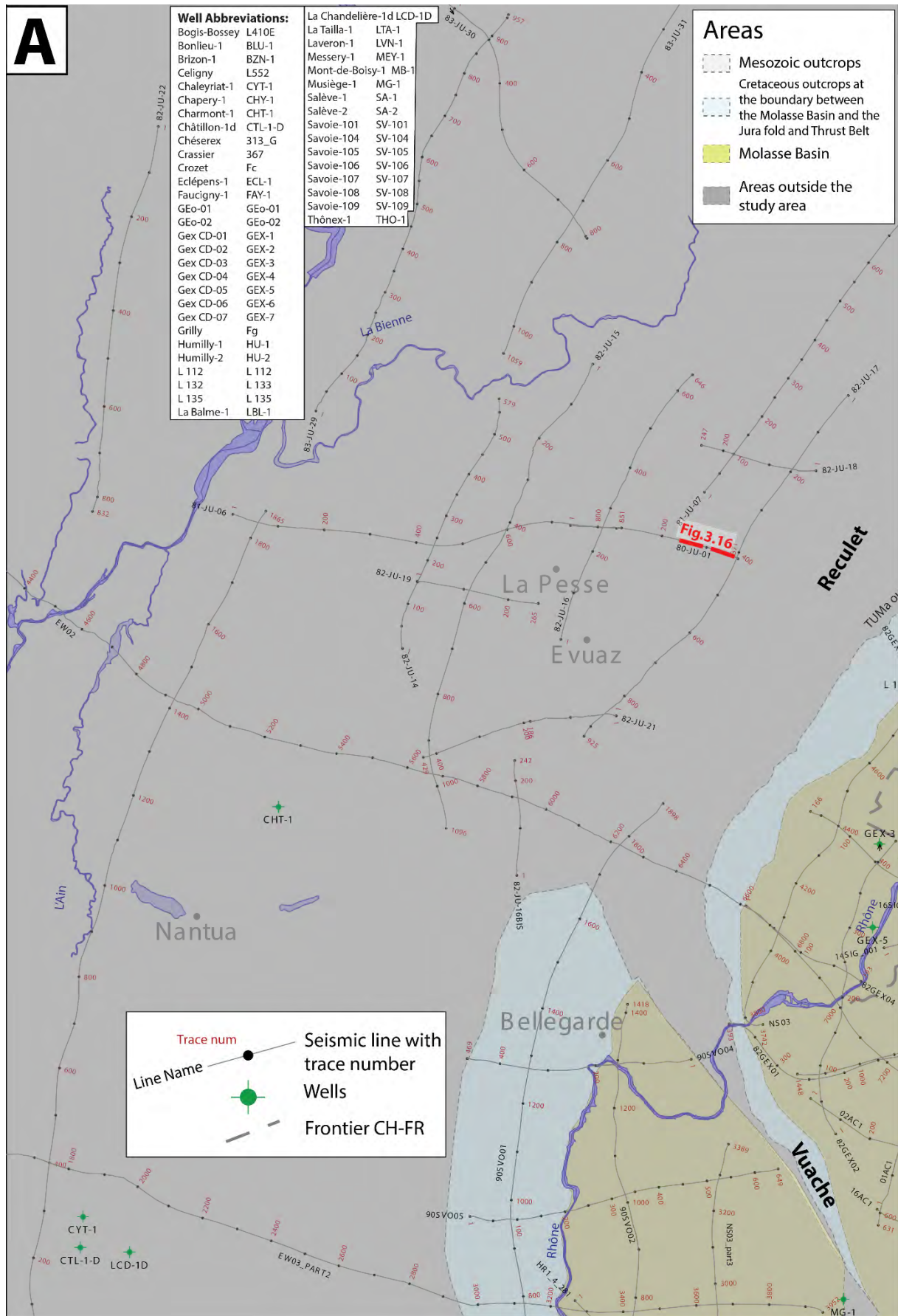


Figure 3-12: Seismic basemap with profiles names and trace numbers. The localisation of figures are highlighted in red.

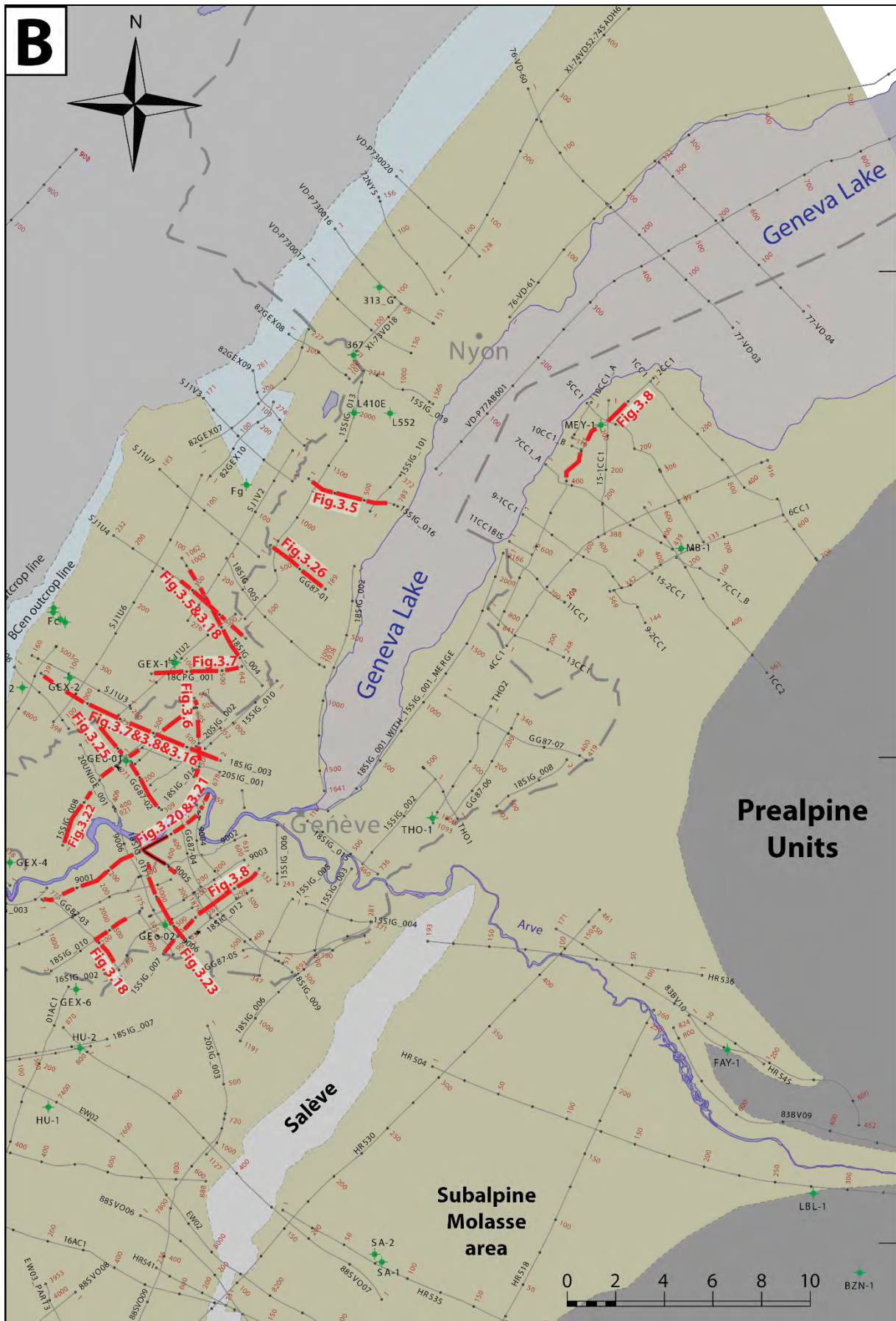


Figure 3-13: Seismic basemap with profiles names and trace numbers. The localisation of figures are highlighted in red. For legend and abbreviation, see Figure 3-12. See the App_01&02 for complete data tables.

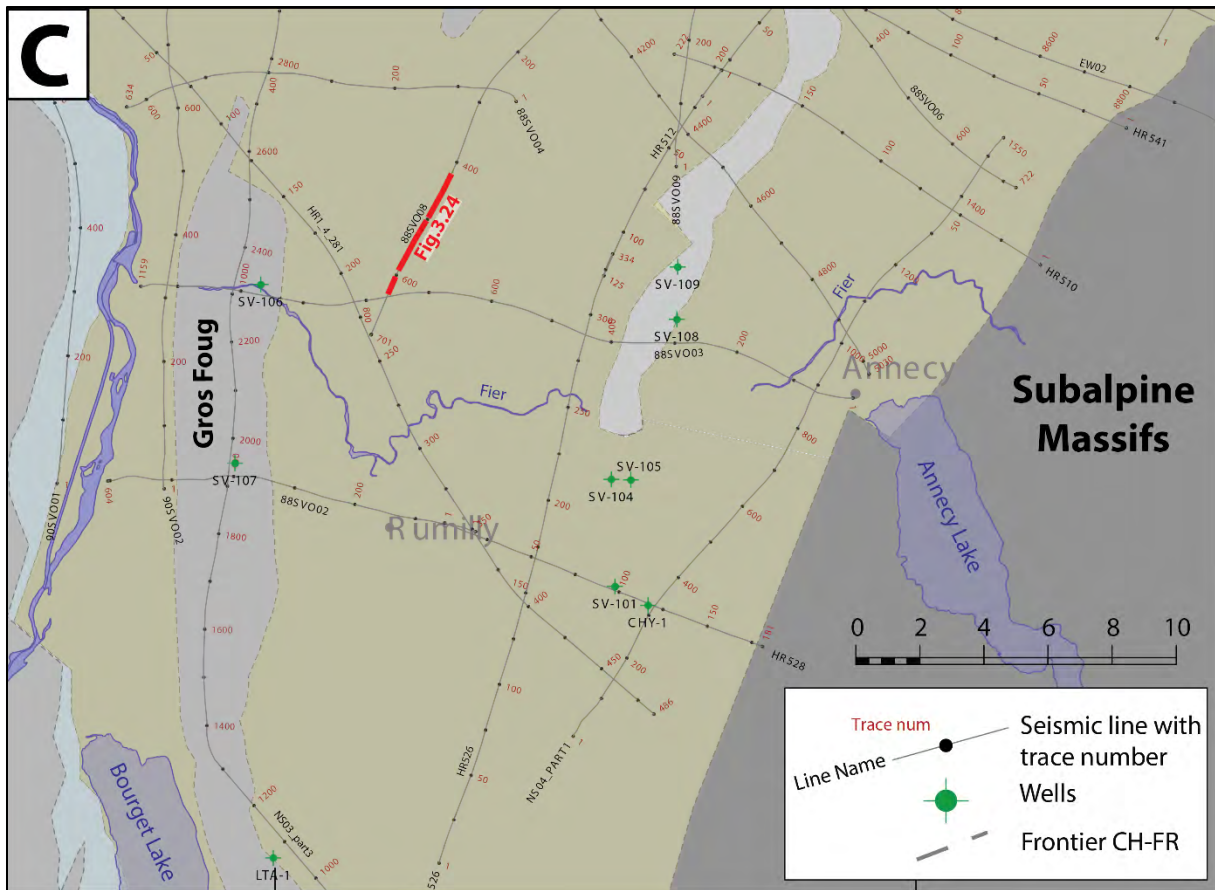


Figure 3-14: Seismic basemap with profiles names and trace numbers. The localisation of figures are highlighted in red. For legend, see Figure 3-12. See the App_01&02 for complete data tables.

2014 by one seismic line in Chancy with a minivibrator, classified in the quality type 3 (Figure 3-11 and Figure 3-13). This line 14SIG_001 mostly aimed at imaging the shallow subsurface (Quaternary layer). In the same perspective, 5 lines in 2015 (25.5km, survey “15SIG WD”) and 6 lines in 2016 (12.5km, survey 16SIG) were computed with the help of weight drops (WD) energy source. These profiles have an interesting resolution for the shallow Cenozoic interval, but are defined by the quality type 3, considering the poor resolution and continuity of the seismic reflectors in the Mesozoic series part. During the same year 2015, an acquisition targeting the deep subsurface with vibrators (V) resulted in 8 seismic lines (30km length, survey “15SIG V”) distributed in the whole Canton Geneva (quality type 2). In 2017, one very short seismic line (0.5km, 17SIG_001) was acquired in the Meyrin area (district around GEO-01 well) with a minivibrator, aimed at calibrating well GEO-01 (2017, see Table 3-2) located in the middle of this small seismic line. It corresponds to a quality type 3, because of the shallow depth penetration, mainly due to the very short geometry of the line. In 2018, a large seismic campaign resulted in 15 seismic lines scattered through the Canton or in France, but very close to the Swiss border. These survey “18SIG” (90km length) has a high resolution (quality type 1) thanks to powerful energy source (20T two vibrator trucks) and adapted acquisition parameters. Indeed, dense source and receiver intervals have resulted in a 6m CMP (Common-Mid-Point, see Figure 3-2) spacing to image the near-surface geology, 0-300 ms. This survey “18SIG” constitutes the main new input data, which enable us to propose a new structural interpretation of the GGB. In 2020, 4 seismic lines (quality type 2) were obtained by vibrator method, 3 lines in the Meyrin area, 20SIG_001, 20SIG_002 and

Acquisition year	Country	Survey	Num. Profiles	Provided by	Data type available Stack (S) / Migration (M)	Line length (km)	Sample Interval (s)	Defined (new) datum plane SRD (m a.s.l.)	Defined (new) replacement velocity VRepl (m/s)	Phase shift (°)	Energy source (see Fig 3-5)	Quality type (1-3) (see Fig 3-8)
2020	CH&FR	20SIG*	3	SIG	S & M	12.8	0.001	500	3000	0	Vibrator	2
2020	CH	20UNIGE*	1	SIG	S & M	3.2	0.001	500	3000	0	Vibrator	2
2018	FR	18SIG*	14	SIG	S & M	89.4	0.002	500	3000	180	Vibrator	1
2017	CH	17SIG*	1	SIG	S & M	0.5	0.002	500	3000	0	Vibrator	3
2016	CH	16SIG*	6	SIG	S & M	12.5	0.002	500	3000	0	Weight Drop	3
2015	CH	15SIG V*	7	SIG	S & M	30.5	0.002	500	3000	0	Vibrator	2
2015	CH	15SIG WD*	5	SIG	S & M	25.5	0.002	500	3000	0	Weight Drop	3
2014	CH	14SIG*	1	SIG	S & M	8.1	0.002	500	3000	0	Vibrator	3
2010	CH	THO*	2	SIG	S & M	8.0	0.002	500	3000	0	Vibrator	2
1990	CH	90*	6	SIG	S & M	37.6	0.002	500	3000	0	Vibrator	1
1990	FR	90SVO	8	SIG (via BRGM)	M	127.3	0.004	500	3000	0	Mixed Vibrator / Explosive	2
1988	FR	88SVO	8	SIG (via BRGM)	M	128.3	0.004	500	3000	0	Mixed Vibrator / Explosive	1
1987	CH	GG87	7	SIG	M	37.1	0.002	500	3000	0	Vibrator	2
1986-88	FR	EW	4	SIG (via BRGM)	M	163.4	0.004	500	3000	0	Vibrator	2
1983	FR	80JU-81JU-83JU	18	UNIFR (via CEP)	S & M	244.6	0.004	1125	4500	0	Vibrator	2
1983	FR	83BV	6	SIG (via BRGM)	M	66.3	0.004	500	3000	0	Vibrator	2
1982-1983	FR	NS	137	SIG (via BRGM)	M	113.5	0.002	500	3000	0	Mixed Vibrator / Explosive	2
1982	FR	82GEX	9	SIG (via BRGM)	M	56.6	0.004	500	3000	0	Vibrator	2
1977	CH	77-VD	2	SIG (via MCG)	S & M	15.8	0.004	500	3000	0	Airgun	3
1977	CH	VD-P77	1	SIG (via ST)	S	25.433	0.004	500	3000	0	Vibrator	3
1976	CH	76-VD	2	SIG (via MCG)	S & M	27.5	0.004	500	3000	0	Vibrator	2
1974	CH	XI-74VD	1	SIG (via ST)	S	29.417	0.004	500	3000	0	Airgun	3
1973	CH	VD-P73	3	SIG (via ST)	S & M	16.059	0.004	500	3000	0	Vibrator	2
1973	CH	XI-73VD	1	SIG (via ST)	S	2.664	0.004	500	3000	0	Vibrator	2
1972	CH	72NY	1	SIG (via ST)	S	4.7	0.002	500	3000	0	Vibrator	2
1970	FR	SJIV-SJ1U	7	SIG (via BRGM)	M	48.4	0.004	500	3000	0	Dynamite	2
1967-1968	FR	HR	14	SIG (via BRGM)	M	506.6	0.002	500	3000	0	Dynamite	2
1957	FR	ICC-CC1-AC1	22	SIG (via BRGM)	S	126.7	0.004	500	3000	0	Dynamite	3

WD=Weight Drop
 V=Vibrator
 Num.=Number of

*reprocessed/processed and adjusted to datum plane 500m a.s.l with replacement velocity 3000m/s during processing.

DEP → Département de l'économie Publique de Genève (Gorin, 1989)
 JVP → Jura Vaudois Pétrole SA (permanently closed)
 ST → Swisstopo
 MCG → Musée Cantonal de Géologie de Lausanne (R. Marchant)
 CEP → Céltique Energie Pétroleum Ltd, London- England (permanently closed)
 BRGM → Actual owner of the data, mostly gathered from oil companies

Table 3-1: Description of acquisition and processing parameters per surveys for this study.

20UNIGE_001 (organized by UNIGE in collaboration with SIG), and one line in France near the city of Beaumont 20SIG_003. This latter is not located in Switzerland, but mentioned in this part as it belongs to the same survey “20SIG”. The contractor company RTS has processed these seismic lines from 2020, whereas the other seismic lines mentioned before have been reprocessed/processed by GGE/Petrologic.

3.2.4 Seismic profiles from France and from Canton Vaud

Seismic lines in France are linked to the oil and gas exploration. The oldest survey of our dataset “1CC-CC1-AC1” dated from 1957, are located mostly in the NE of our area of interest around the well Messery-1 and few lines around Humily-1 well (Table 3-2, Figure 3-11, Figure 3-13 and Figure 3-28). Even so they were acquired using explosives (powerful energy source), they have a very poor resolution (quality type 3). Seismic surveys “SJ1V-SJ1U” acquired in 1970 (7 lines, 48km length) NW of Geneva Canton around well Gex-1 (in the Molasse Basin), have a reasonable resolution (quality type 2). Near the border of the two countries, seismic survey “82GEX” (9 seismic lines, quality type 2) has surely helped placing wells GEX in the early 80’s. Both seismic surveys “HR” and “83BV” cover the Bornes Plateau area between the Salève and the Subalpine Massifs. Survey “HR” acquired in 1967-68 has the highest number of lines of our database (38 lines) for a total length of more than 500 km of seismic data. It has been classified in the quality type 2 because the majority of the profiles have an intermediate resolution; however, some of them have been individually placed in the quality type 3 dataset. In 1988 and 1990 the two seismic surveys respectively “88SVO” and “90SVO” (8 lines each) were computed and placed as a grid scattered in the Rumilly Basin and few near Humilly wells. They have a good resolution (quality type 1-2). As part of academic projects, such as the ECORS (Bois et al., 1986) or ALPS project (Schmid & Kissling, 2000), regional seismic lines were computed by gathering several seismic lines. The resulting “EW” and “NS” surveys have each two very long lines that are divided into several segments. These seismic surveys are of particular interest for the understanding of the regional stratigraphic and structural configuration of the studied areas. In the Geneva Basin, lines EW02 and NS03 are particularly well placed to support the seismic interpretation. Finally, several seismic profiles are located in the Jura part of the study area, forming the surveys “80JU-81JU-83JU”, and allow obtaining significant subsurface information north of the Geneva Basin, which is crucial for proposing a regional structural cross-section. They have a quality type 2, however it has to be noted that these profiles go through significant thrust structures below which the resolution necessarily decrease. Hence, quality type of those lines takes into account the overall resolution of the profiles.

As for the seismic data from the Canton of Vaud, seven surveys (“72NY”, “76-VD”) in our database are dated from the 1970’s, and represent 11 seismic lines for a total length of 150km. Their quality type is between type 2 and 3. Three seismic lines (77-VD-03&04 and VD-P77AB001) have been acquired on the Lake of Geneva (airgun energy source), and are focused on shallow layers (Quaternary lake deposits, quality type 3).

3.2.5 Seismic Profiles Depth Converted (SPDC)

All seismic profiles of the database described in the above paragraphs are processed in the time domain (vertical scale in seconds). A specific workflow has been developed in this study in order to

convert from the time to the depth domain (vertical scale in meters) a selection of seismic profiles among the entire datasets. As the time to depth process is a time-consuming work, it was chosen to apply it only on relevant seismic profiles. For more clarity this selection of seismic lines is named in the study as the Seismic Profiles Depth Converted (SPDC). The choice of the selected seismic lines SPDC was done in collaboration with other members of the tectonic working group of the UNIFR (A. Marro, S. Borderie, A. Sommaruga and J. Mosar), in a way to choose as many as possible seismic lines oriented NW-SE, parallel to the proposed cross sections elaborated by Marro (2021) (see Figure 6-54) and thus parallel to the transport direction in the Alpine foreland. Several seismic lines, oriented NE-SW or E-W were also necessary for the study in order to fully characterize the lithological layer sequence or the tectonic structures, especially in the Internal Jura, in the Salève region, and in the Molasse Basin of our study area in the vicinity of the Jura first chain. The final depth converted seismic lines are intended to constrain:

- The structural interpretation of the Mesozoic cover in the Internal Jura part NW to the Geneva Basin (in collaboration with A. Marro). Here the seismic lines helped identify the geometry of the main thrusts and back-thrusts;
- The depth of the various horizons in the upper most NW part of the Geneva Basin and the depth of the near Base Mesozoic horizon in the Jura part were crucial inputs for the forward modeling process of a NW-SE cross-section performed by A. Marro in the Move software.
- The depth model of the near Base Mesozoic horizon in the whole area (from Subalpine Molasse region to the Jura). It has allowed evaluating the dipping angles of this surface in order to construct new kinematic and balanced cross sections and to investigate the state of stress in the Alpine foreland (in collaboration with S. Borderie).

A total of 44 seismic reflection profiles with a total length of more than 500km, located between the Subalpine Massifs and the Internal Jura have been integrated in the database and depth converted in this study (Figure 3-15). One specific line of the list is a combined seismic lines named EW02_W which is an “arbitrary line” (term used in the Kingdom software), and which means that it is a combination of several parts of various seismic lines. This line is built in great majority with line EW02 (83km out of 89km total length), but slightly deviated in the Salève area, going through very small parts of lines 88SV09, 88SV06, and HR530 (6km long for the three small parts). The composition in traces of this arbitrary line is the following: line EW02 (trace range 1-4284 and 4542-5832), line 88SV09 (trace range 4285-4349), line 88SV06 (trace range 4350-4525), and line HR530 (trace range 4526-4541). This was achieved, in order to avoid artefacts located in this part of seismic line EW02, due to the high lateral velocity contrast created by the Salève structure.

This selection of depth converted profiles (SPDC) can be subdivided into five groups, in relation to their datum plane, their velocity model, and their geographical location (see chapter 5 and Figure 5-3). The group SPDC1 corresponds to the dataset of the Jura Mountains seismic lines with datum 1125 m a.s.l (along with a replacement velocity of 4500m/s). Groups SPDC2 and SPDC3 respectively correspond to the datasets of lines in the Geneva Molasse Basin and in the Subalpine Molasse, both using the datum plane 500 m a.s.l and replacement velocity 3000 m/s. Group SPDC1 and SPDC2 both use only velocity data from well Hu-02 for the subsurface velocity model, whereas the group SPDC3 velocity model is based on velocity information from well FAY-1. SPDC4 and SPDC5 are respectively located in the Rumilly Basin (velocities from well CHY-1) and in the southern part of the Jura of our study area (velocities from LCD-1). The velocity modeling around the depth conversion is detailed in chapter 5.

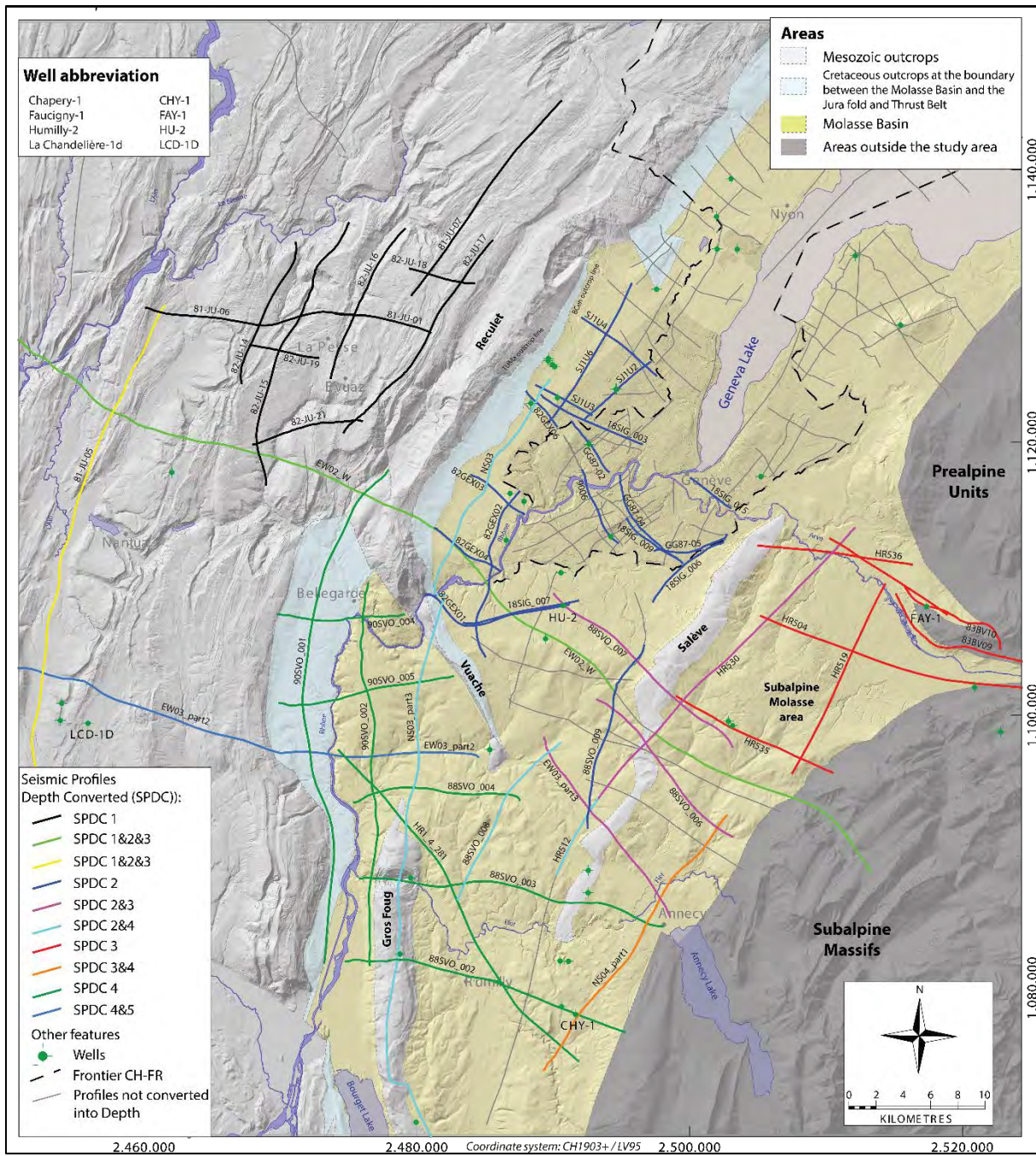


Figure 3-15: Seismic basemap of groups of Seismic Profiles Depth Converted (SPDC) among the entire seismic dataset.

3.2.6 Datum plane and misfit correction

As explained in 3.2.3 and 3.2.4, the seismic dataset consists of several distinct surveys acquired from different periods from the 1950's to nowadays, and processed by different companies. This heterogeneity of seismic surveys in terms of processing and acquisition involves vertical adjustments of each survey in order to consider common datum planes for a correct seismic interpretation. The first step is to consider common datum plane and replacement velocity. In fact, two datum planes were set up; one at 1125 m a.s.l (along with a replacement velocity of $V_{repl}=4500\text{m/s}$) for seismic lines

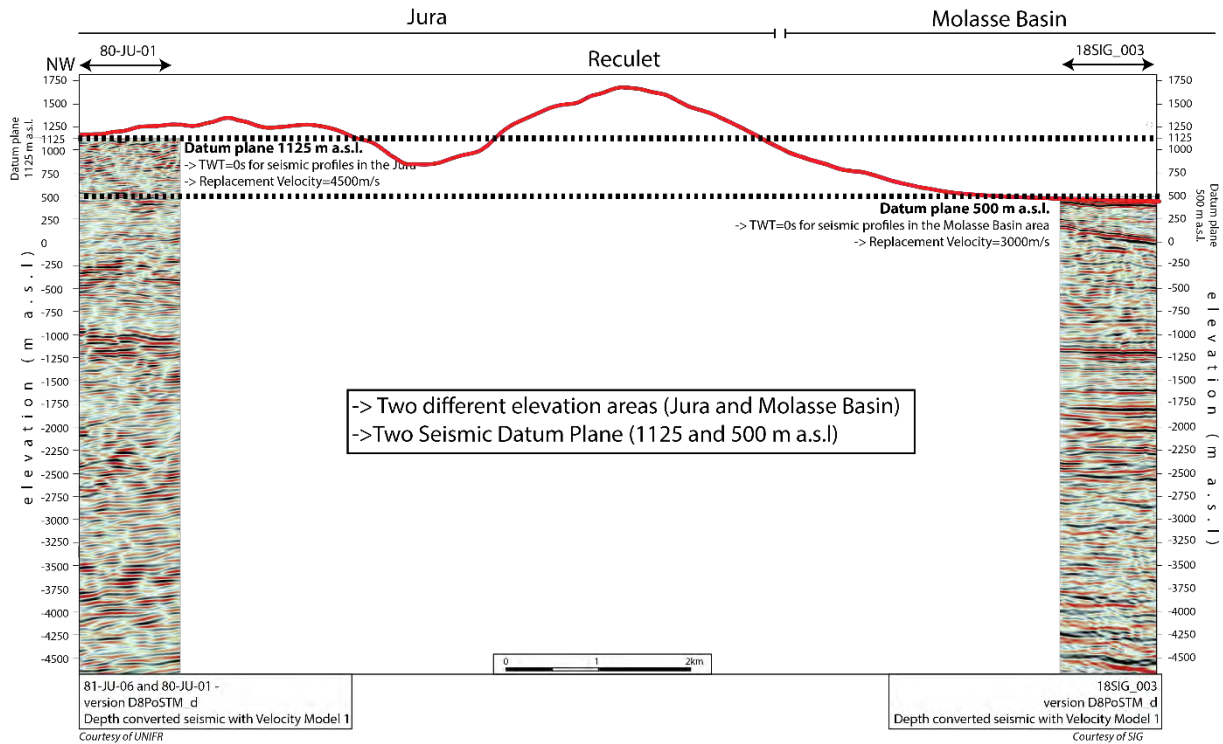


Figure 3-16 : NW-SE cross section going along seismic profile 80-JU-01 (left of the image), and seismic line 18SIG_003 (on the right). We can observe the difference of the topographical elevation between the Jura part (left) with the Geneva Basin (on the right). It explains the difference in the seismic datum planes defined for the project (origin of vertical scale in TWT (s)) from 1125 m.a.s.l in the Jura to 500 m.a.s.l in the Geneva Basin. It allows to have datum planes above the topography and use a replacement velocity in between. See Figure 3-12 and Figure 3-13 for localisation of the sections. See respectively Encl 37 and Encl 21 for detailed seismic interpretation of lines 81-JU-06/80-JU-01 and 18SIG_003.

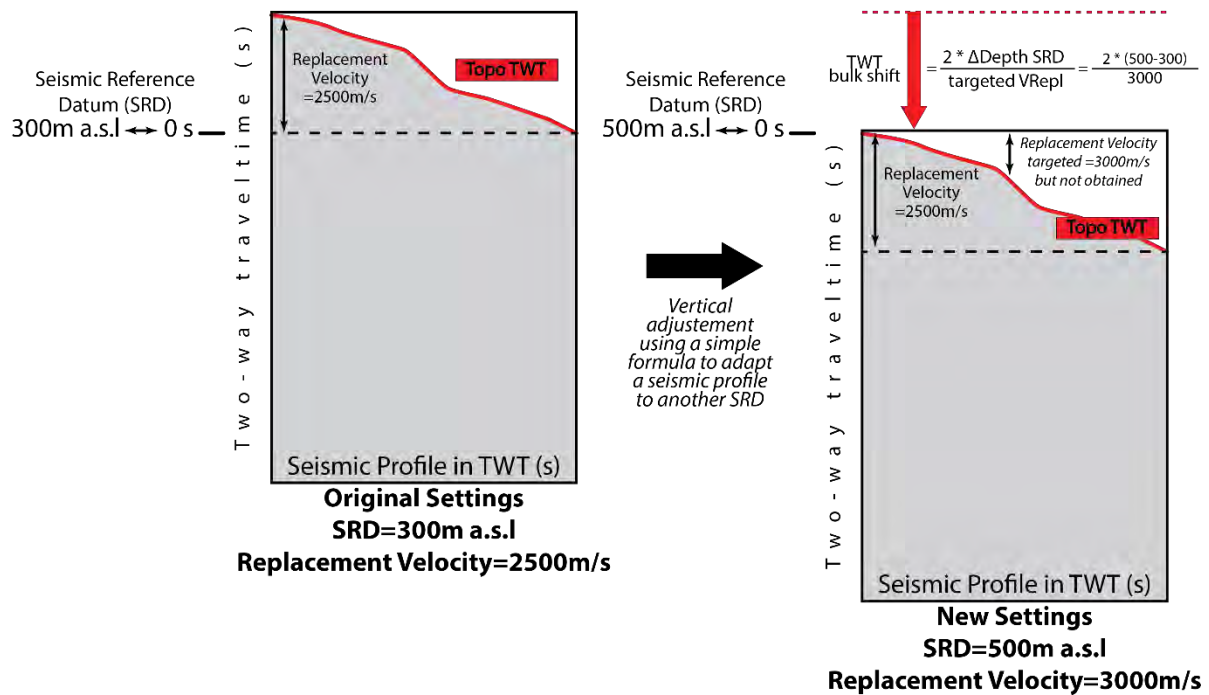


Figure 3-17: Theoretical formula used for a first rough (100ms precision) bulk shift applied on seismic lines that need adjustments; those who have not been processed with the same defined datum plane and replacement velocity than those of this project. This formula does not take into account the replacement velocity of the seismic profile to adjust, hence a manual supplementary bulk shift needs to be applied.

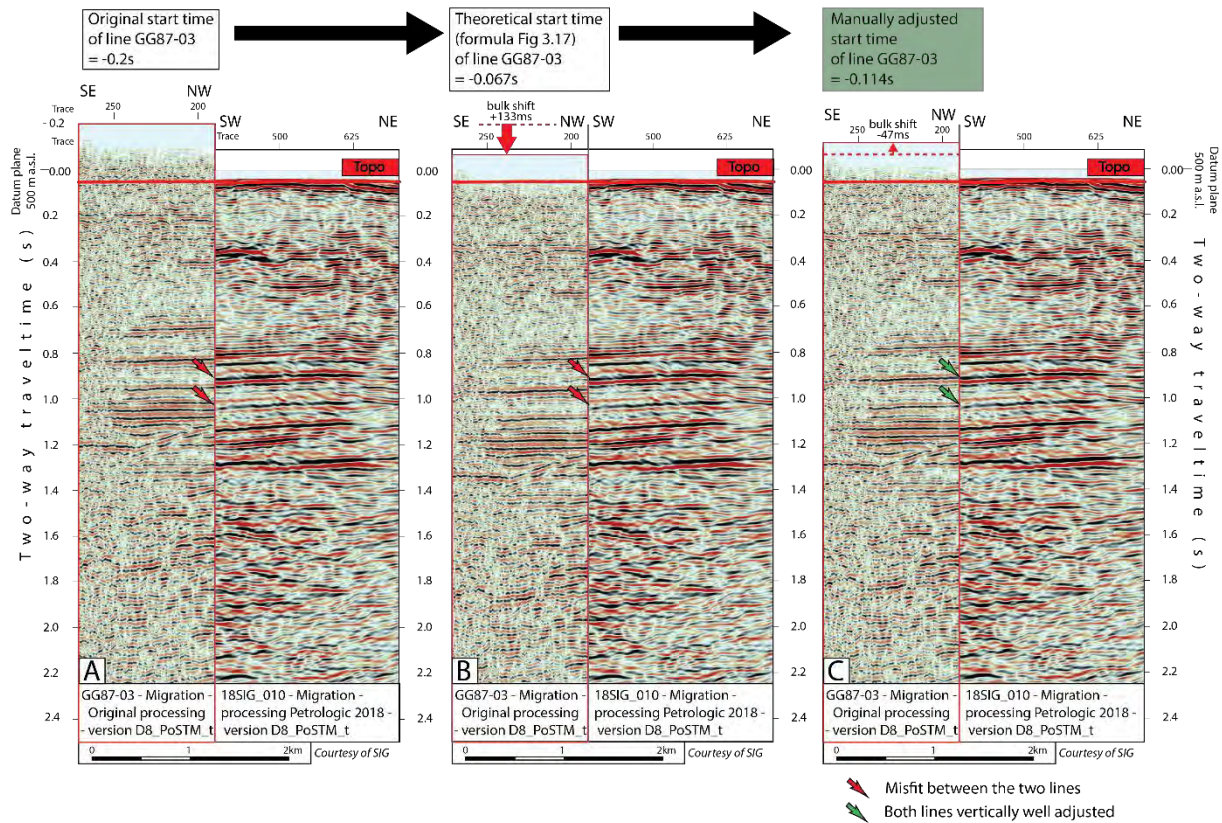


Figure 3-18 : Example of seismic profile GG87-03 (left of each figure), that was processed with the datum plane 300m a.s.l and $V_{repl}=3000\text{m/s}$, and need to be adjusted for the defined datum plane plane 500m a.s.l and $V_{repl}=3000\text{m/s}$. Seismic profile 18SIG_010 (right of each figure) is used as a reference profile for the tie, as it was processed for the defined datum plane and V_{repl} for the project. The first step is to shift the seismic profile using the theoretical calculated value, that bring a first rough value for the tie. The second step corresponds to a manual shifting of the profile GG87-03 based on a visual adjustment to correlate identical seismic reflection together from each profile. See respectively Encl 67 and Encl 28 for detailed seismic interpretation of lines GG87-03 and 18SIG_010.

located in the Jura Mountains, and a second datum at 500m a.s.l (along with a replacement velocity of $V_{repl}=3000\text{m/s}$) for all the rest of the seismic lines (Geneva Basin, the Subalpine Molasse part, Rumilly basin part, see Table 3-1). The replacement velocity is a value of interval velocity used during seismic processing in the layer between the datum plane (origin of the time domain scale of a seismic section) and a near topographical horizon, in order to produce static corrections (vertical shift in seismic to bring a specific point into alignment with some common elevation feature (Marsden, 1993)). The datum plane (also called Seismic Reference Datum: SRD) corresponds to the origin of TWT (TWT=0s) on a seismic section in the time domain. This flat surface (SRD), in the depth domain, is usually placed above the topography in order to ease the processing but also to avoid velocity artefacts in the shallow geology. Considering the average elevation of the topography in the Geneva Basin (400-550 m a.s.l) and in the Jura Mountains (550-1300 m a.s.l) in our study area, it was necessary to use two different datums (Figure 3-16).

In a second step, once the seismic datum planes and replacement velocities are defined for each survey, it is necessary to adjust vertically all seismic lines that were not processed with these two same defined criteria. The best but complex solution to achieve this, would be to change and adapt the whole static corrections (seismic pre-stack processing step), which means correcting vertically and individually each trace of the seismic lines considering the topography/ datum plane/ replacement velocity and weathering shallow layer. Otherwise, the vertical bulk shift method is the easiest and time

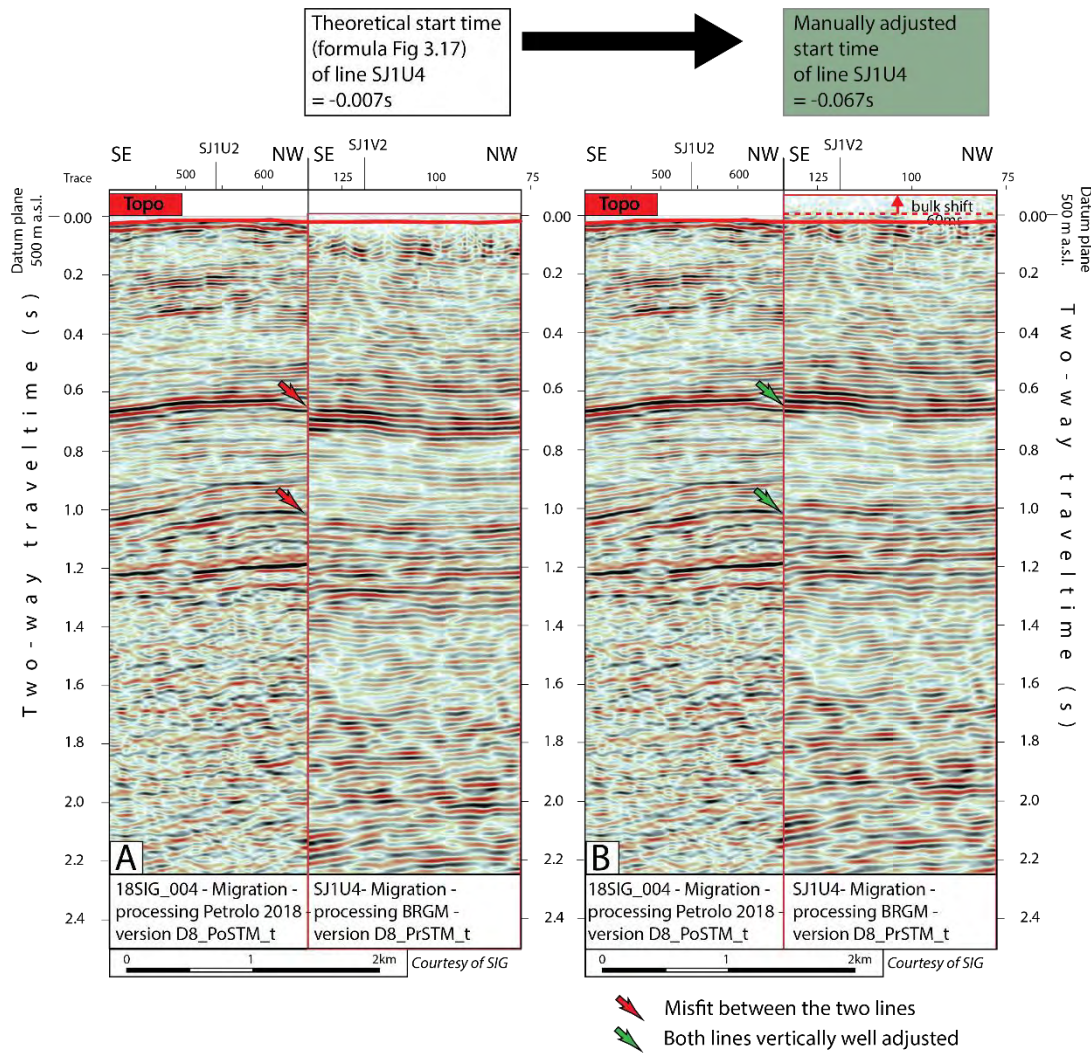


Figure 3-19: Specific case where the theoretical formula for first rough bulk shift can not work; when the datum plane of the seismic line to adjust is the same than the defined datum plane, but with a highly different Vrepl. Here datum plane 500m a.s.l but Vrepl (4000m/s) for SJ1U4 against 3000m/s for the defined Vrepl as 18SIG_004. A manual shift is then necessary. See Figure 3-13 for localisation of the sections. See respectively Encl 22 and Encl 76 for detailed seismic interpretation of lines 18SIG_004 and SJ1U4.

saving post-processing solution for such adjustments, with a precision estimated around 10ms. A first value of bulk shift can be theoretically calculated, using a simple formula that takes into account the defined datum plane (=new SRD) and replacement velocity (Vrepl) with the datum plane that was used during the processing (=old SRD) of the seismic section (Figure 3-17). This formula's main limitation is that it does not consider the replacement velocity of the processed seismic lines, which gives an evaluated 0.1s precision to this first rough theoretical bulk shift method. This lack of precision entails the necessity to apply an extra manual bulk shift based on visual criteria. It consists of taking as references, all seismic lines that were processed along with the defined datum plane and replacement velocity (respectively 500 m a.s.l for and 3000m/s for most of the lines). These reference lines don't need further adjustments as they are already corrected by nature during their seismic processing.

Then, all intersecting seismic lines that need adjustments, are bulk shifted until most of identical seismic reflections on both lines around the intersection are aligned together (Figure 3-18 and Figure 3-19). This process is then achieved iteratively on the next intersecting seismic lines that need an adjustment, following a closed loop if possible.

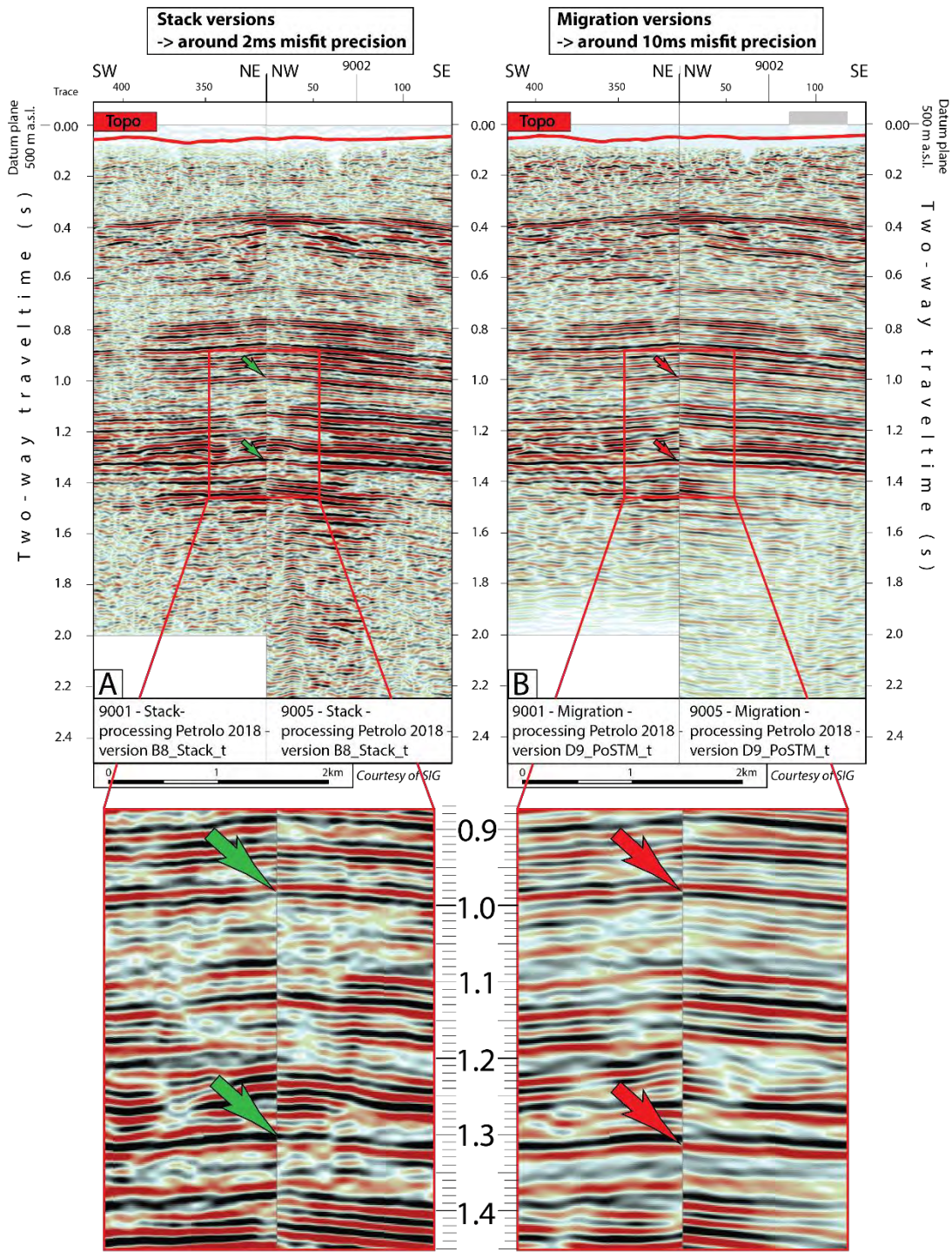


Figure 3-20: Example of remaining misfit between two perpendicular seismic profiles (9001 and 9006), that were both processed under the same defined datum plane (500m a.s.l and replacement velocity 300m/s). We can observe that on the stack version of both lines, seismic reflections are perfectly fitting together on each side of the intersection (A), with a precision less than 2ms. On the migrated version (B), the precision of the match between seismic reflections on both sides of the intersection is increased by 10ms. It comes from the migration tool that moves laterally the image points differently on both lines, and creates this misfit. See Figure 3-13 for localisation of the sections. See respectively Encl 01 and Encl 05 for detailed seismic interpretation of lines 9001 and 9005.

Even after datum planes and misfit corrections applied on all the studied seismic profiles, a remaining misfit can be estimated around 10ms. This misfit seems to be accentuated on migrated versions of seismic lines, compared to stack versions (Figure 3-20). It can be explained by the fact that the migration operator tool is a 2D (XZ) tool that is applied individually on each seismic lines, depending on each velocity model.

3.2.7 Seismic data processing

In 2017, the main assessment made on the seismic database of the GGB of SIG was that each survey were very heterogeneous and not optimized in terms of processing quality, and vertical adjustments. We have seen on the previous part 3.2.6 that even with appropriate datum and misfit corrections, a non negligible uncertainty remains, around 25ms. A common reprocessing applied on all available lines, was the obvious solution to reduce this uncertainty about datum and misfits, but also to homogenize and normalize the seismic images. This would clearly ease the subsequent seismic interpretation, by facilitating the geological correlation of seismic facies or structures from one line to another.

For that, DMT-Petrologic (geophysics/processing company based in Hannover, Germany) with the supervision of GGE (Geophysics-Geology consultancy company based in Geneva) has achieved a reprocessing in 2017 using the same imaging computation sequence for a selection of seismic lines. It concerns all seismic lines inside the Canton of Geneva, except GG87 lines, because no raw seismic tapes could be retrieved (see Table 3-1 for seismic surveys concerned). As a seismic processing always need to be adapted to a targeted depth interval, the Mesozoic unit was chosen as the main focus of this imaging work. However, several seismic profiles, that were acquired with appropriate parameters for shallow imaging (dense source-receivers grid, see 3.2.2) were also reprocessed with a specific focus on the Quaternary and shallow gas in the Molasse interval. Hence, three seismic lines batches were produced with success, notably increasing the resolution for each of the target, in comparison with the original processing (Figure 3-21 and Figure 3-22). Several processing steps have particularly contributed to the improvement of the resolution; - the latest processing algorithm like CRS stacking (Mann et al., 2007) which integrate in the stacking step, neighboring CMP gathers to increase of the reflectivity contrasts ; - shallow layer tomography and statics corrections (Frei, 2019; Marsden, 1993). PostSTM algorithm (post stack migration tool in the time domain) has proved to be the most efficient migration tool, even if PreSTM (pre stack migration tool in the time domain) was also tested, but did not show significant improvements (Cui & Margrave, 2014). The seismic processing is a mathematical task applied on wave physics, which often lack of geological input. That is why this work was done under the supervision of GGE company, so that iterative tests could have been done using geological expertise of GGE, as a complement to the more mathematical part from the processing operator. For concrete examples, advice was given by GGE to DMT-Petrologic to correct velocity anomalies creating wrong geological structures, not in line with the geological settings, or to correct the over-artificial reflector continuity that was hiding geological facies changes or small-scale faults. Concerning another target of imaging, some shallow gas anomalies were also noticed on several seismic profiles (see chapter 4.1.11), matching well hydrocarbon indications. The specific imaging of this is better highlighting the anomalies detected.

Chapter 3

Regarding the data types of the whole database (type of data processing products), stack (named B8_Stack) and/or migration data (named D8_PoSTM or D8_PreSTM) are available (see 3.2.8 for nomenclature), depending on each survey (Table 3-1). In general, migration data is preferred for the interpretation, as it corresponds to the most elaborated data (among other process; removal of diffraction hyperbolas (Figure 3-24) and more correct lateral and vertical placements of the image points). However, when available, stack data were often used in addition to migration data, because it may own sometimes a better geological grain very useful for seismic facies analysis (Figure 3-23).

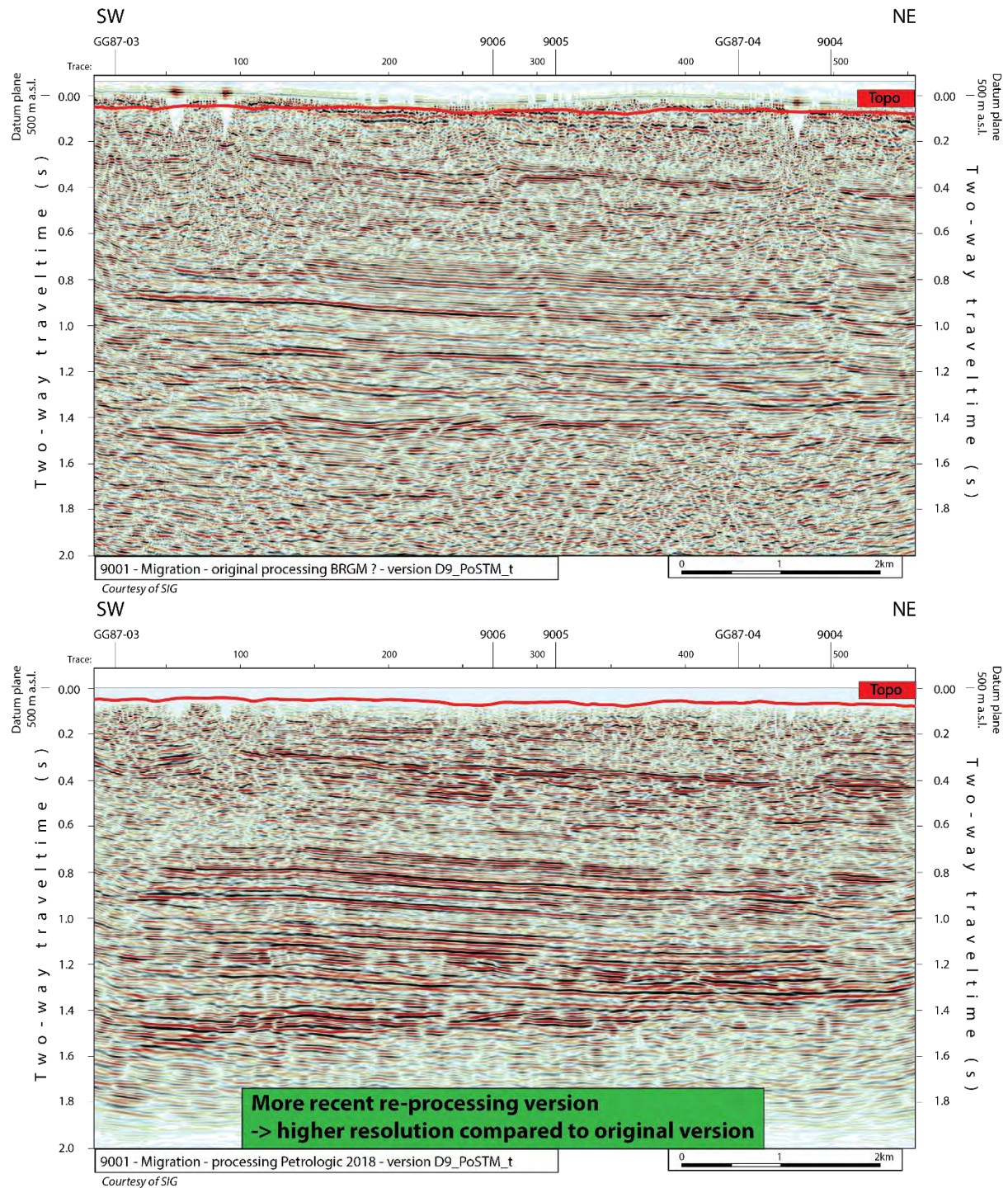


Figure 3-21: Seismic line 9001, before (top) and after (bottom) reprocessing (2018 by Petrologic). On profile 9001, seismic reflections, have an increased vertical resolution, with a better geological grain (facies) of the image. See Figure 3-13 for localisation of the sections. See Encl 01 for detailed seismic interpretation of line 9001.

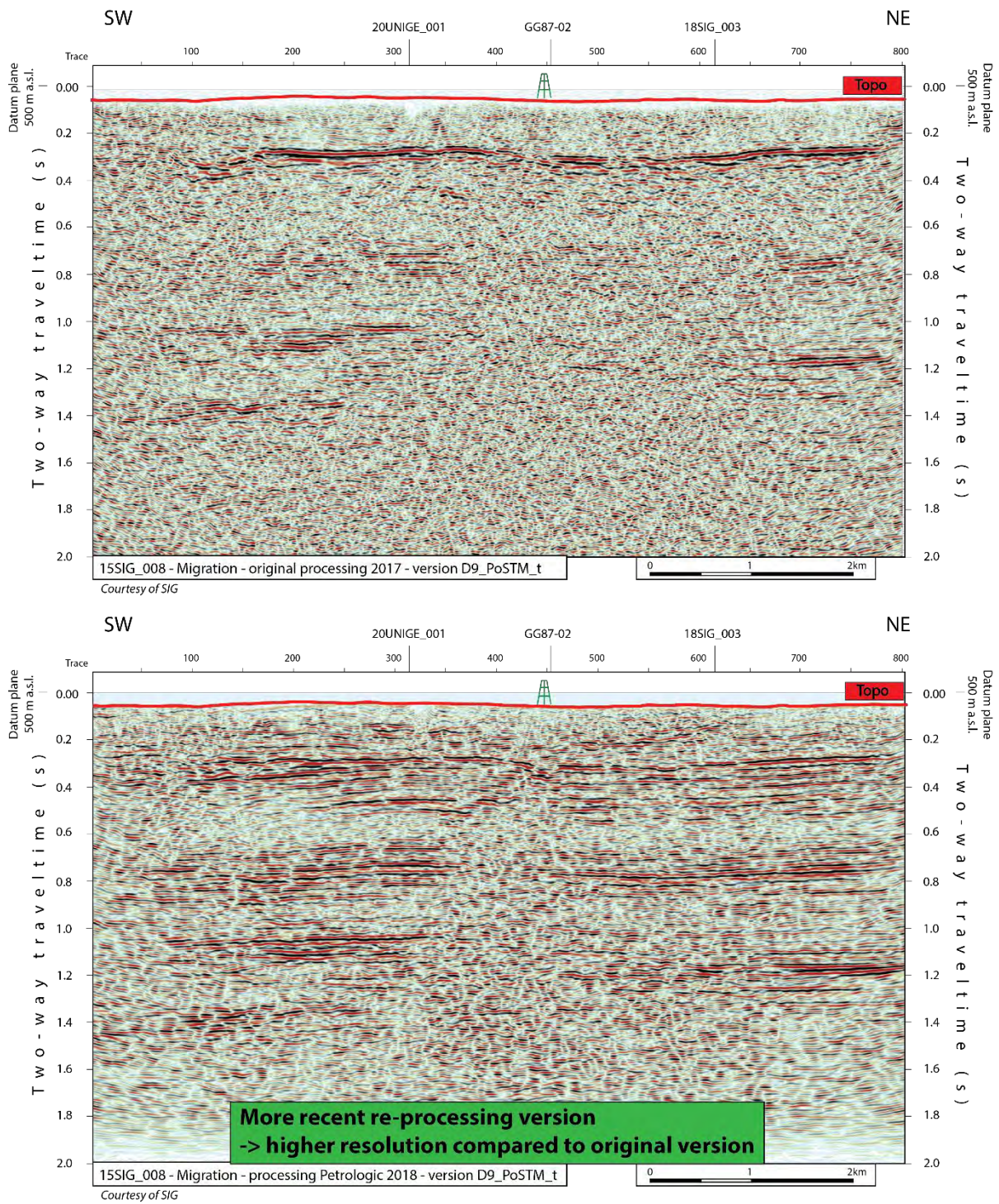


Figure 3-22: Seismic line 15SIG_008, before (top) and after (bottom) reprocessing of 2018 (by Petrologic). On profile 15SIG_008 we can observe that the reprocessing has increased the lateral resolution with a better continuity of seismic reflections. See Figure 3-13 for localisation of the sections. See Encl 13 for detailed seismic interpretation of line 15SIG_008.

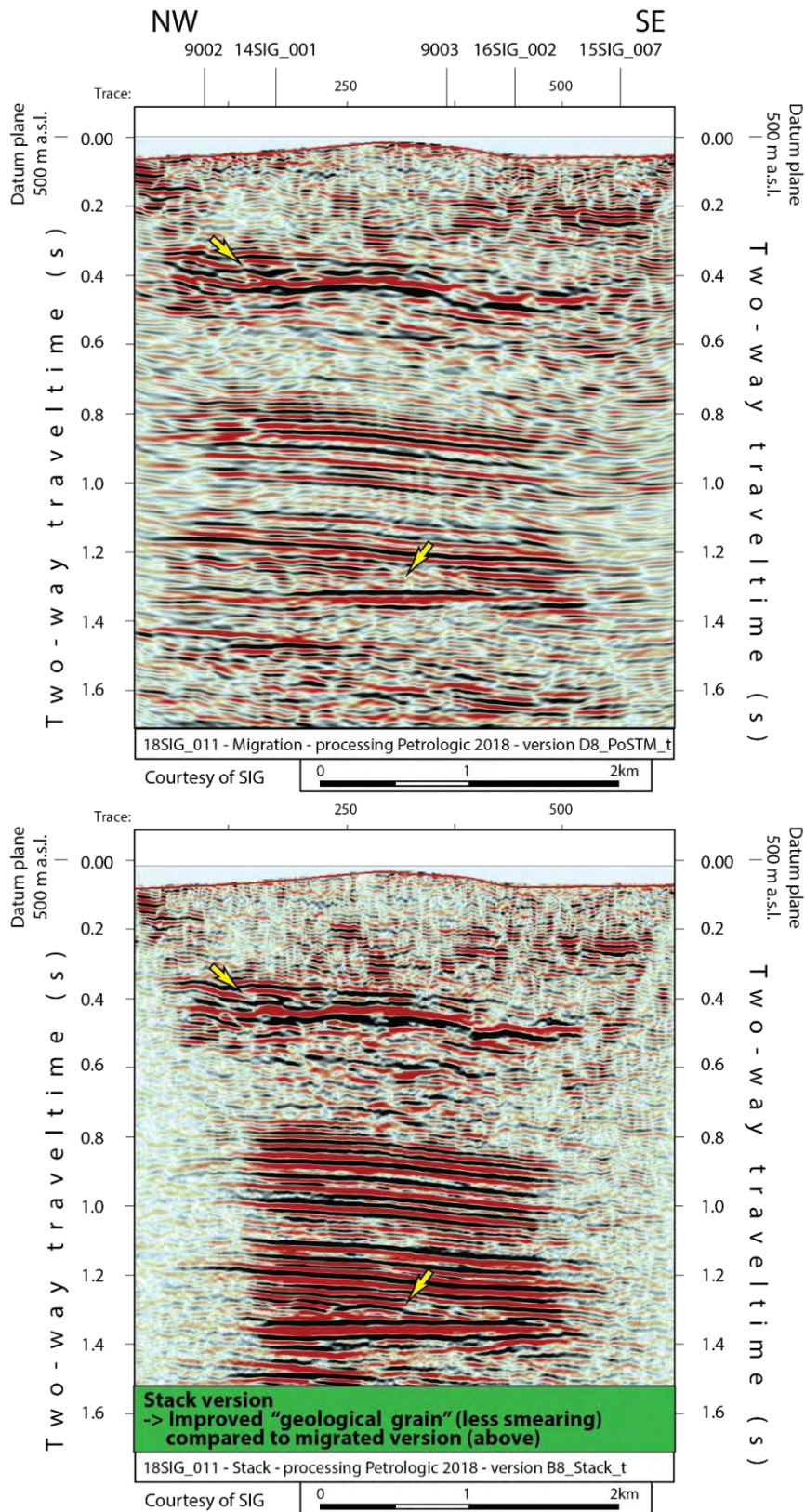


Figure 3-23 : Seismic line 18SIG_010 stack version (B8_stack_t) on bottom and migrated data on top (D8_PoSTM_t). The stack version may have in some part a better geological grain useful for seismic facies interpretation. It can be explained by the fact that migrated algorithm is increasing artificially (and sometimes in excess) the continuity of the reflectors. The yellow arrows are pointing clear clinoform features very sharply imaged on the stack version, in comparison with the migrated data that smooth and increase slightly the continuity of the seismic reflectors. See Figure 3-13 for localisation of the sections. See Encl 29 for detailed seismic interpretation of line 18SIG_011.

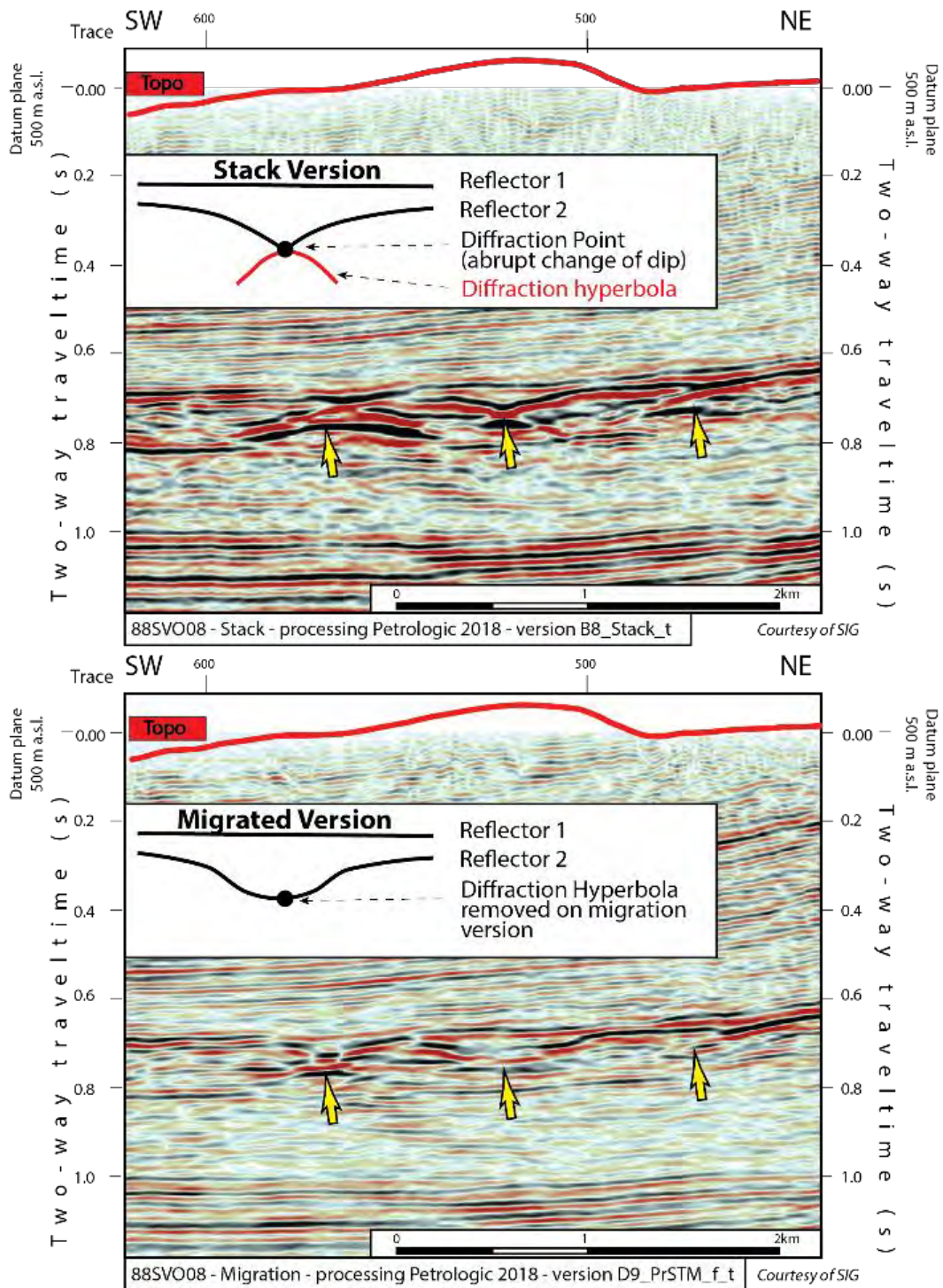


Figure 3-24: Seismic lines 88SV08 stack version (B8_stack_t) on top and migrated data on bottom (D8_PoSTM_t). The stack version contains clearly, on this line, diffraction hyperbolas that are compensated or fully removed on the migration version. Diffraction is created by small scale changes in the seismic reflectivity, such as faults, fractures, channels and rough edges of salt bodies (Bashir et al., 2020). Diffraction hyperbolas on the stack version could lead to a wrong interpretation of the seismic feature. It may appear at first sight on the stack version that shallow thrust are present on the section (yellow arrows / around near Base Cenozoic horizon), but we can see on the migrated version that it looks more like sedimentary infill (Siderolithic channel?, see chapter 4.1.10) on top of an erosional surface. See Figure 3-14 for localisation of the sections. See Encl 52 for detailed seismic interpretation of line 88SV008.

3.2.8 Post-processing filtered seismic data and data nomenclature.

A post processing filter is a fast and efficient way to improve or normalize the image quality of seismic section without going through a long and costly complete new seismic processing.

The frequency range of seismic lines of the database is heterogeneous due to various processing. In order to facilitate the comparison and correlation between seismic lines, it is better to have as many as possible similar frequency ranges for all lines. Hence, we have applied band pass frequency filtering (1-18-60-65Hz) to all available seismic lines that had not been reprocessed (reprocessing of Petrologic in 2018 created also a similar filtered version). This filter consists in removing low frequencies (progressively <18Hz) that may remove otherwise the details of higher frequency ranges. It removes also very high frequencies that correspond usually to ambient noise signal (Figure 3-25).

In the same idea of normalizing as much as possible available seismic data, the AGC tool (Automatic Gain Control) that allow to balance the amplitude along each seismic trace with a time gliding window length of 400ms. In fact, a mean value of amplitude is calculated inside this time window and then a scale factor allows normalizing the amplitude to a constant value, usually equal to 1. This filter yields higher amplitudes in areas of weak amplitude value (usually noisy areas), which improves the quality of the image for an easier interpretation (Figure 3-25)

Another post processing very efficient filter to improve artificially the continuity of the reflections is the dip steered median filter. It was used and applied on all available seismic lines before the reprocessing of numerous seismic sections done in 2017, as explained in part 3.2.7. Technically, it first calculates the dip angle in between identical neighboring seismic reflections throughout the whole seismic section (Figure 3-26). Then it filters all seismic signals that are out of a defined dip angle range (dip angle >70°). It is an edge preserving smoothing filter that enhances laterally continuous events and removes random noise. It is important to keep in mind that these kinds of filtered data may contain artefacts due to the smoothing of the reflections. It is used as a secondary and complementary data type version.

A specific and precise nomenclature has been elaborated in order to characterize all various seismic data processing versions. Here are the major ones:

- B8_Stack_t: Stack version in time domain
- B9_Stack_f_t: Stack version filtered in frequency and AGC in time domain
- B10_Stack_t: Stack version + dip filter in time domain
- B11_Stack_f_t: Stack version filtered in frequency and AGC + dip filter in time domain
- D8_PoSTM_t: Post stack migrated data in time domain
- D9_PoSTM_t: Post stack migrated data + filter in frequency and AGC in time domain
- D8_PrSTM_t: Pre stack migrated data in time domain
- D9_PrSTM_t: Pre stack migrated data + filter in frequency and AGC in time domain
- DB8_d: Stack or migrated data converted into depth domain with velocity model 1 (see chapter 5)

All the mentioned seismic data are loaded and clearly sorted in the Kingdom software interpretation project. A combined use of all different versions and data has been done during the interpretation process.

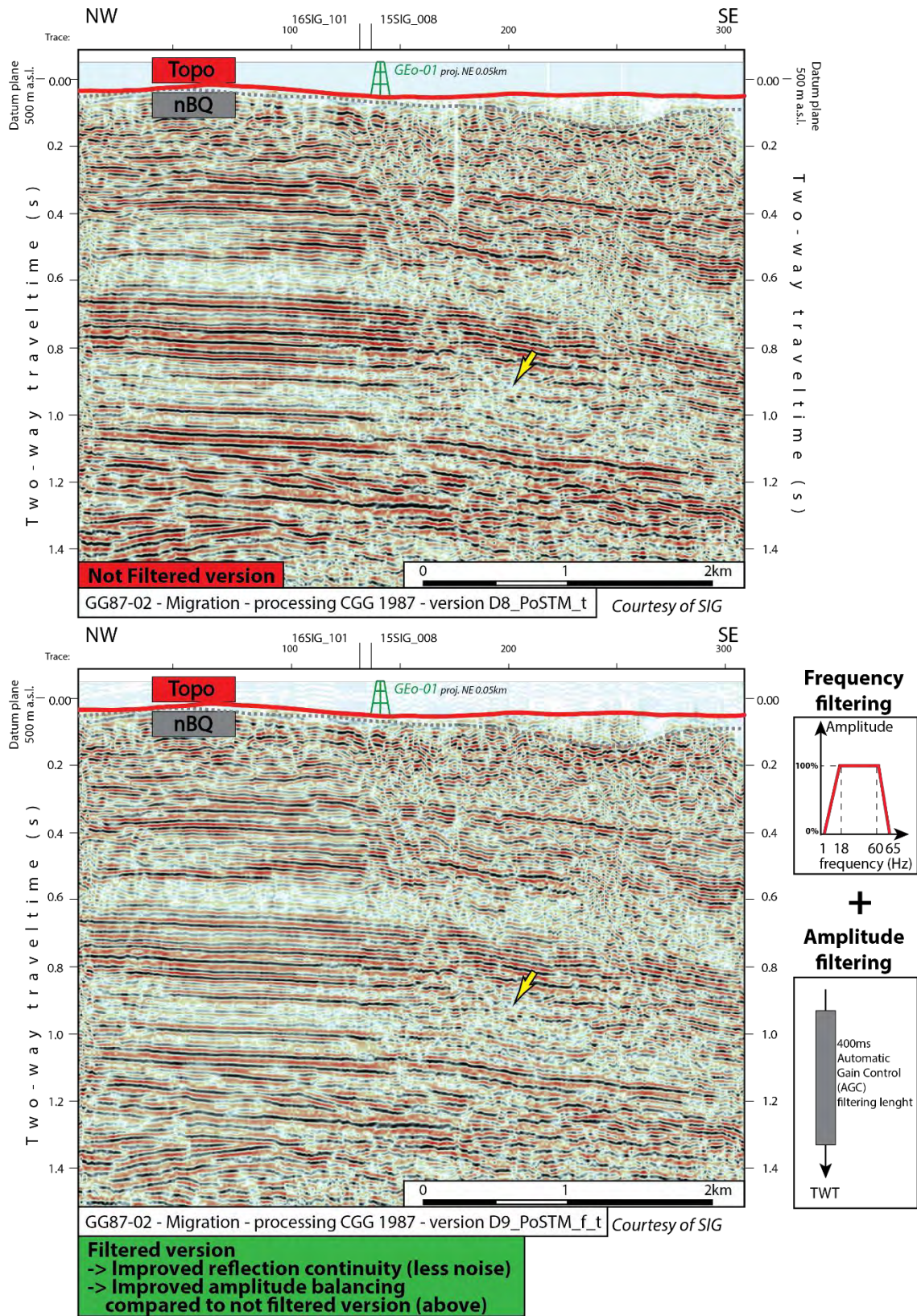


Figure 3-25: Seismic section GG87-02 available processing migrated version D8_PoSTM (top), compared to the same data with an additional frequency and AGC filtering (bottom). We can see on the filtered version that noise is very slightly attenuated (very high frequency range filtered), and that the amplitude is better balanced throughout the whole section. As a consequence in the zone pointed by the yellow arrow, the reflections are slightly clearer. See Figure 3-13 for localisation of the sections. See Encl 66 for detailed seismic interpretation of line GG88-02. nBQ = near Base Quaternary horizon, and Topo = Topographical horizon.

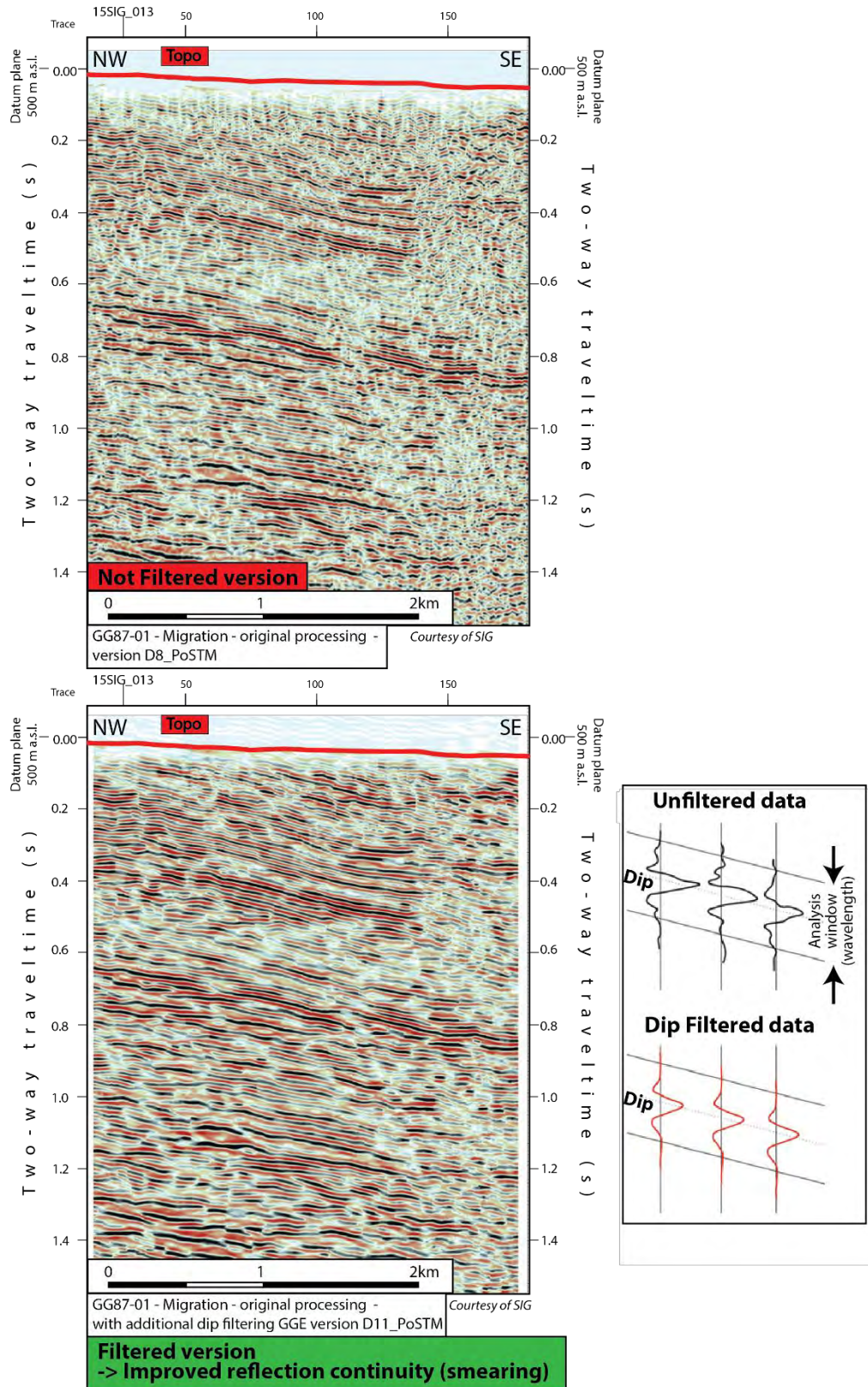


Figure 3-26: Seismic section GG87-01 available processing data (top) compared with the same data with an additional dip steered median filter applied on it (bottom). The filtered data has clearly more continuous reflections, and ambient noise has been very much attenuated. This data is used only as a secondary data, to ease in some specific cases the horizon interpretation. But it is important to keep in mind that this kind of data may bring also artefacts created by these artificial filtering. See Figure 3-13 for localisation of the sections. See Encl 65 for detailed seismic interpretation of line GG87-01.

3.2.9 Incoming 3D seismic (2022)

For several years, SIG has prepared the acquisition of a 3D seismic survey over a major part of the Geneva Canton. When writing the manuscript of this work, this seismic 3D data was not available, as it was acquired from September 2021 until end of 2021, hence it was not intended to be incorporated to this study (DT de Genève & SIG, 2022).

Although the actual density of 2D seismic data is quite high, the uncertainty related to the correlation of fault indications or seismic facies from one line to another remains relatively high. It is mainly due to the singular spatial distribution of 2D seismic lines (not a regular perpendicular grid) and the heterogeneous quality and geometry of the data. A 3D seismic acquisition is the best method for reducing considerably these uncertainties related to spatial geological correlation. In fact, the resolution of seismic sections of a 3D survey (inline or crossline) remains approximatively the same than for 2D seismic section, but it is the quantity of data, which is tremendously higher. It should allow picking up small-scale lateral heterogeneities or discontinuities with a high reliability. For instance, it may help identifying coral reef lateral extensions of the Upper Malm unit, or it should give the exact geometry of all main faults in the Geneva Canton.

Similar to 2D seismic, the 3D acquisition grid scheme needs to be adapted to the depth of the target levels (Figure 3-27, (Ashton et al., 1994; Vermeer, 2003)). As the Mesozoic cover is developed as a monoclinial structure dipping SE under the Geneva basin, a larger acquisition grid of 240mx240m (source-receivers spacing) is considered in the SE part of the survey (deeper target), compared to a 160mx160m bin size in the NW part of the survey (shallower target). Moreover, seismic acquisition inside the city center of Geneva is a great challenge due to the high constraints on roads.

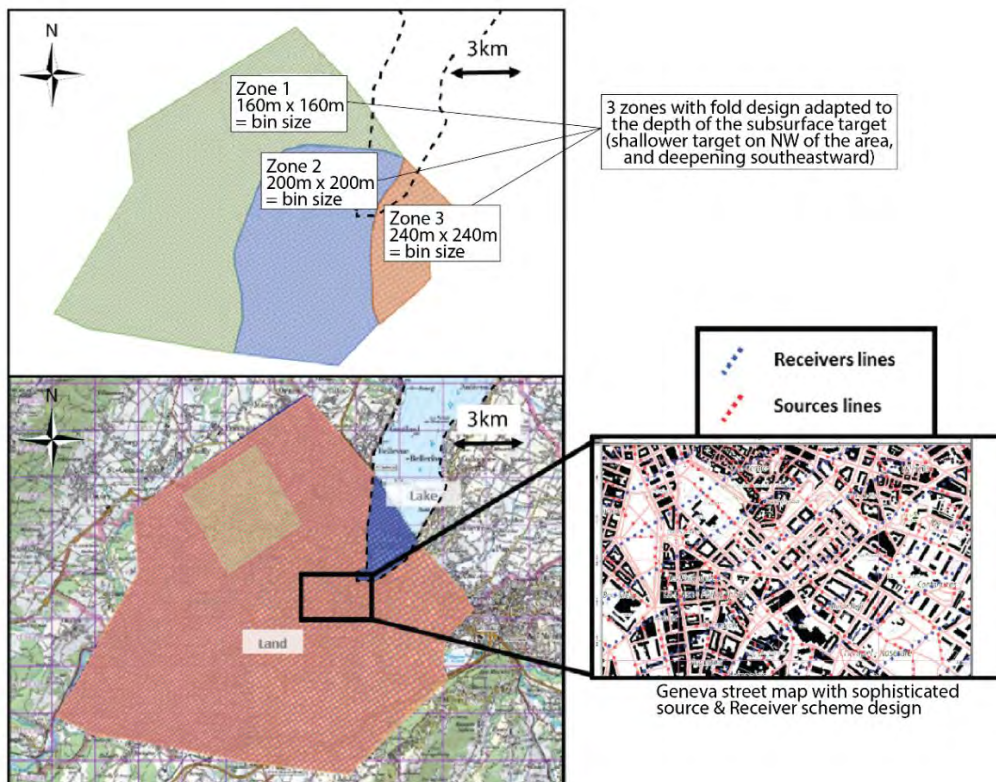


Figure 3-27: On the left part, the proposed 3D seismic survey design (which in the end was chosen slightly differently from the extent of the polygon presented), notional parameters. On the right part the very dense acquisition grid that will tackle all the subsequent surface issues (DT de Genève & SIG, 2022).

3.3 Well data

In Switzerland and in neighboring France, the drilling of deep wells (App_03, Table 3-2 and Figure 3-28) was closely linked to oil and gas exploration (see 3.1). Several companies have followed each other throughout the decades starting from the 1950's, to explore the subsurface of the area of the study. They all placed their wells according to the seismic acquisition and interpretation they had previously completed. For example, Messery-1 and Mont-de-Boisy-1 were drilled northeast of the GGB respectively in 1958 and 1959 in relation with the seismic campaign "1CC-CC1-AC1" acquired in 1957. Similarly, the seven GEX-1->7 wells from 1959 (oil purpose) have followed the seismic acquisition of survey "82GEX" in 1982. As explained in 3.1, the oil and gas exploration concerns only the French area

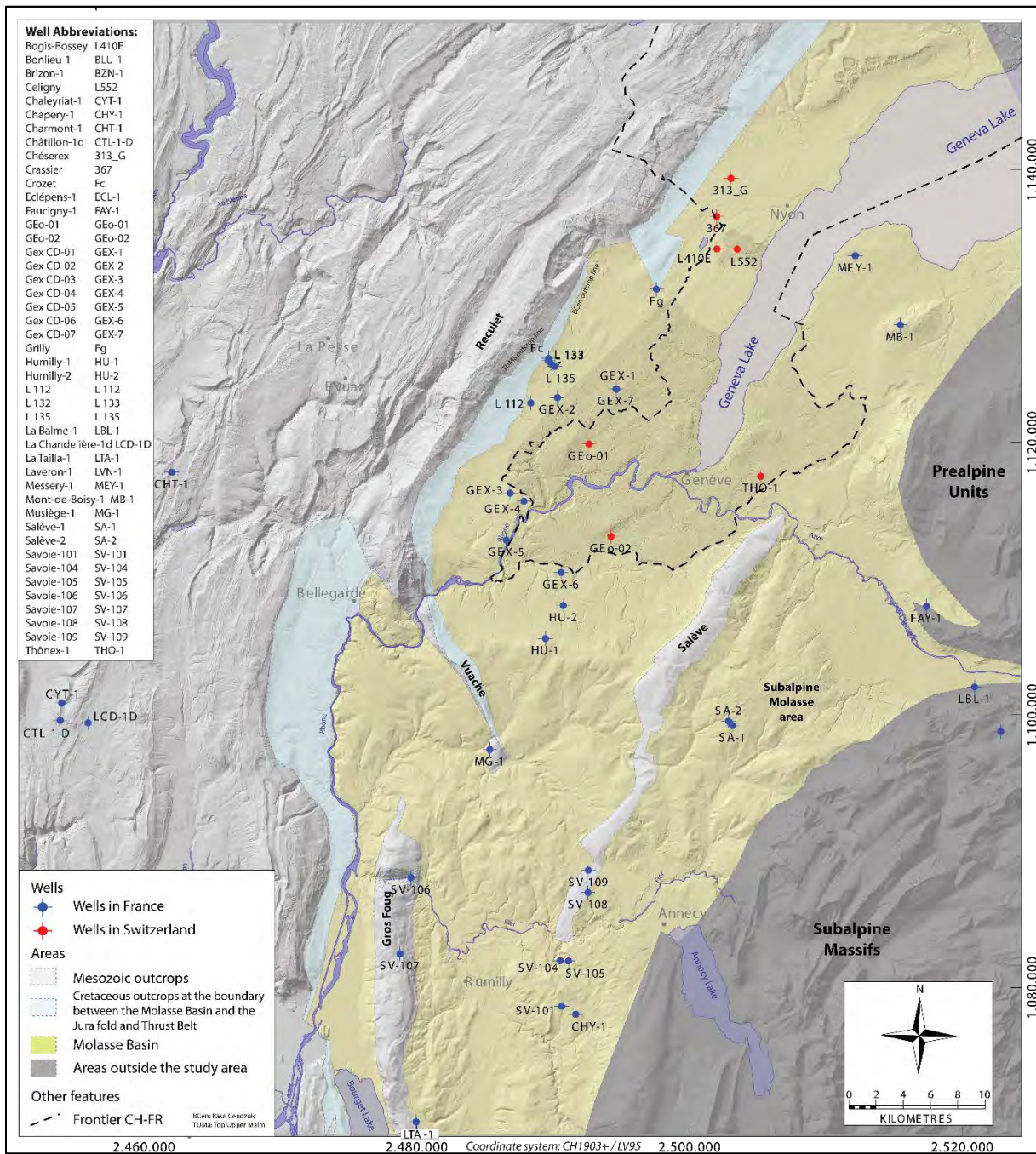


Figure 3-28: Basemap of all deep wells in Switzerland (red points) and in France (blue points).

Well Name	Abr.	Elev Ref (m)	Ref type	Formation at TD	X (CH1903+)	Y (CH1903+)	Total Depth (m)	Spud date	Operator Historical
Bogis-Bossey	L410E	472	GL	Cretaceous	2501999	1134177	180	07.04.2005	Géocadast
Bonlieu-1	BLU-1	809	KB	Paleozoic Meta	2479140	1161130	1862.26	08.05.1982	BP
Brizon-1	BZN-1	1341	KB	Triassic	2522801.54	1098783.81	4416	10.06.1987	Ass oil
Céligny	L552	446.9	GL	Cretaceous - Urgonian	2503477	1134159	126	11.01.2008	GESDEC
Chaleyriat-1	CYT-1	818.4	KB	Permo-Carboniferous	2453950	1100870	1361.9	30.05.1989	ESSOREP
Chapelle-1	CHL-1	764	KB	Cretaceous	2547305	1168359	1530	18.06.1958	SNPA
Chapery-1	CHY-1	616.8	KB	Permo-Carboniferous	2491640.4	1078037.99	4162.3	08.08.1970	ESSOREP
Charmont-1	CHT-1	947.05	GL	Permo-Carboniferous	2462020	1117800	2285.38	01.10.1991	ESSOREP
Châtelblanc-1	CHA-1	1021.6	GL	Permo-Carboniferous	2498120	1170590	2664.3	01.10.1978	Shell
Châtillon-1d	CTL-1-D	911.65	KB	PermoCarboniferous	2453840	1099600	1615.4	09.08.1991	ESSOREP
Chésereux	313_G	520	GL	Cretaceous - Urgonian	2503030	1139345	200	17.07.2012	Geothermal
Crassier	367	471	GL	Cretaceous	2501975	1136560	208	04.01.2013	Geothermal
Crozet	Fc	592	GL	Cretaceous	2489640	1126144	270	05.01.2016	CCPG
Eclépens-1	ECL-1	518.5	KB	Upper Triassic	2533220	1168380	2150	05.09.1981	BEB
Essavilly-101	ESS-101	791.6	GL	Paleozoic Meta	2496130	1182560	2067.4	26.08.1964	SNPA
Essertines-1	EST-1	660.56	GL	Upper Triassic	2539775	1173490	2936.1	01.12.1962	S.A HL
Faucigny-1	FAY-1	766	KB	Permo-Carboniferous	2517360	1107959	4951.3	05.08.1969	ESSOREP
GEO-01	GEO-01	413.84	GL	Malm Sup	2492616.96	1119863.23	744.06	05.10.2017	SIG
GEO-02	GEO-02	410.85	KB	Malm	2494219.19	1113093.85	1455.7	24.10.2019	SIG
GEX_CD-01	GEX-1	471	GL	Cretaceous - Hauterivian	2494640	1123890	290.5	03.01.1983	BP
GEX_CD-02	GEX-2	450	GL	Eocene	2490290	1123270	403.2	22.02.1983	BP
GEX_CD-03	GEX-3	505	GL	Cretaceous	2486830	1116260	293.8	08.02.1982	BP
GEX_CD-04	GEX-4	410	GL	Cretaceous - Urgonian	2487840	1115670	291.7	25.10.1982	BP
GEX_CD-05	GEX-5	365	GL	Eocene	2486550	1112820	560	23.03.1983	BP
GEX_CD-06	GEX-6	452	GL	Cretaceous - Urgonian	2490560	1110450	422	21.05.1983	BP
GEX_CD-07	GEX-7	469.5	GL	Oligocene	2494590	1123900	256	22.06.1983	BP
Grilly	Fg	515	GL	Cretaceous	2497566	1131220	250	29.01.2016	CCPG
Humilly-1	HU-1	643.8	GL	Cretaceous - Hauterivian	2489420	1105600	905	31.01.1958	PREPA
Humilly-2	HU-2	504.12	KB	Permo-Carboniferous	2490720	1108020	3051	01.10.1968	SNPA
L 112	L 112	482	GL	Cretaceous	2488350	1122870	130.5	01.01.1979	CERN
L 132	L 133	570.8	GL	Cretaceous	2489620	1125970	180.5	01.01.1979	CERN
L 135	L 135	527.3	GL	Cretaceous	2489910	1125690	135	01.01.1979	CERN
La Balme-1	LBL-1	451	KB	Malm - Tithonian	2520891.01	1102047.22	1840	17.08.1990	Ass oil
La Chandelière-1d	LCD-1D	839.63	KB	Paleozoic Meta	2455870	1099410	1656.5	03.11.1989	ESSOREP
La Tailla-1	LTA-1	478.9	KB	Paleozoic	2479940.73	1070150.33	3557.2	17.08.1975	ESSOREP
Laveron-1	LVN-1	1079.8	KB	PermoTriassic	2503050	1180240	2485.2	17.09.1959	PREPA
Messery-1	MEY-1	425.3	GL	Cretaceous - Urgonian	2512148	1133678	737.75	05.04.1958	PREPA
Mont-de-Boisy-1	MB-1	678.6	GL	Cretaceous - Urgonian	2515455	1128599	1954.5	26.05.1959	PREPA
Musiège-1	MG-1	465	GL	Dogger	2485340.85	1097461.94	2083	16.02.1962	PREPA
Risoux-1	RX-1	1350	GL	Dogger	2500315	1161048	1958	07.10.1960	PREPA
Romanens-1	ROM-1	947.3	GL	Upper Triassic	2564132.64	1167256.92	4022	19.07.1977	SNPA
Salève-1	SA-1	840	GL	Oligocene - Lower Chattian	2503140	1099220	1175.5	03.05.1959	PREPA
Salève-2	SA-2	813	GL	Cretaceous - Urgonian	2502840	1099540	1985.8	09.11.1959	PREPA
Savigny-1	SAV-1	838	KB	Cretaceous	2546271	1155312	2486	31.05.1960	S.A HL
Savoie-101	SV-101	617.86	KB	Cretaceous - Urgonian	2490605.32	1078627.5	2064	29.11.1951	RAP
Savoie-104	SV-104	505.86	KB	Cretaceous - Hauterivian	2490492.22	1081972.44	1903	03.09.1952	RAP
Savoie-105	SV-105	503.6	KB	Cretaceous - Portlandian	2491102.33	1081952.76	690.7	14.02.1953	RAP
Savoie-106	SV-106	343.7	KB	Keuper	2479550.18	1088056.47	2129.9	11.07.1953	RAP
Savoie-107	SV-107	923	KB	Dogger	2478748.1	1082475.82	2113	12.06.1954	RAP
Savoie-108	SV-108	567.4	GL	Oligocene	2492540	1086970	1260.9	07.05.1956	RAP
Savoie-109	SV-109	513.34	KB	Cretaceous	2492567.25	1088602.75	1203.56	09.09.1959	RAP
Thônex-1	THO-1	428.35	GL	Lower Malm	2505214.81	1117501.95	2690	04.07.1993	OCEAN
Toillon-1	TLN-1	843.79	KB	Lower Keuper	2491640	1173560	1573	01.06.1958	PREPA
Treycovagnes-1	TRE-1	477.9	KB	Permo-Carboniferous	2536135.7	1180273.2	3221.2	22.04.1978	Shell

Table 3-2: Table listing and summary of well information considered in this study. Source: from SIG, GGE database and literature (Gruber, 2017; Schori, 2021). Ref type = elevation reference type (start of depth measurement) between GL= Ground Level, KB = Kelly Bushing (usually few meters above GL), TD = Total Depth. See the App_03 for the excel table and see Figure 3-28 for localization of the wells on map.

and The Canton Vaud. The Canton Geneva has only drilled geothermal wells, such as Thônex-1 in 1993 (based on GG87 survey), or GEO-01&02 in 2017 and 2019. In both oil and gas or geothermal cases, the depth of the drillings are adapted to specific reservoirs targets. Hence the total depths of the wells in the database are quite heterogenous from Cretaceous layer to Paleozoic unit. As our shallowest modeled horizon surface that needs a well tie is near Base Cenozoic, only wells that have reached at least the Cretaceous layer, will be considered (51 wells). Only two wells inside the GGB have reached

the Paleozoic Unit (HU-2 and FAY-1), against ten other wells of the database located outside the GGB have also recorded the whole Mesozoic unit. The spatial distribution of the wells is not homogeneous throughout the area of the study. As reservoirs traps sought consisted mainly in fold anticlines, wells were principally gathered on main tectonic structures of the Molasse Basin (inside our study area). Few wells are in the Jura part of our area of investigation (ex: CHT-1, LCD-1, BLU-1) but also very near to the Prealps (FAY-1) or to the Subalpine massif (La Balme-1 or Brizon-1). These gives crucial constraints points on all edges of our area's polygon.

All basic well information are gathered inside Table 3-2, and are represented on map of Figure 3-28.

The main uses of formerly drilled wells in a seismic interpretation study consists in:

- Tying the interpreted seismic horizon surfaces in depth domain (corresponding to approximations of stratigraphic main boundaries) to their corresponding well formation tops.
- Obtaining time/depth relationships from specific measurements made along boreholes such as checkshots or VSP (vertical seismic profiles). This information is necessary to display well data (in depth domain for the vertical axis, in meters) into seismic section (most of them only in the time domain as vertical axis, in seconds). It also constitutes the major input for time to depth conversion of the seismic interpretation or seismic profiles.
- Analyzing geological information about the stratigraphy or the tectonic settings of the area. This information may be subsequently linked with seismic facies or structural seismic result of interpretation.
- Studying the petrophysical properties and fluid occurrences of reservoirs (if drilled) through well logs or tests, and possibly linking them to seismic specific features or anomalies.

A large part of well data were made available by SIG, after the gathering that was mainly achieved during the GEOMOL project (Robin Allenbach et al., n.d.; Brentini, 2018; Clerc & Moscariello, 2020; Rusillon, 2017). All original useful reports (scanned) were classified by well in the database transferred by SIG. In addition to that, a substantial work was performed by GGE for well petrophysical studies (GGE, 2018), whose results and data were fully available for this study (mainly well log data and result of their interpretation).

3.3.1 Well log data

GGE has compiled, processed, and interpreted most of the petrophysical data of the wells of our database. Hence, all well logs measurements gathered from GGE have been incorporated into the database of the projects and implemented into the Kingdom software Suite from HIS (version 2020).

On the one hand, the seismic profiles have the advantage to be 2D spatial data that allow easily correlating spatially the seismic interpretation results. On the other hand, they are characterized by a relatively low resolution (around 25m vertical resolution at 2000m depth below topography). Moreover, they cannot give any information about petrophysical properties, such as porosity or permeability. On the contrary, drillholes cores have very high resolution (<0.1m) but very limited coverage (cores are often extracted only on few tens of meters). This comparison of resolutions allows introducing the log data that lie just in between seismic data and cuttings or core data in terms of resolution and coverage. We can estimate the coverage of the log data to less than 1 meter, for the

extent of major logs that usually cover the majority of the drilled interval. In the Geneva area, logging acquisitions strongly vary depending on wells and sections. For instance, in GEO-1, the following static conventional logs were recorded (Figure 3-29):

- Caliper Geometric properties of the borehole (diameter, deviation, azimuth)
- Natural radioactivity of the rock (uranium, thorium and potassium content) = Gamma Ray (GR)
- Formation conductivity (RES, induction)
- Spontaneous potential (SP)
- Slowness of acoustic waves in the formation (DTC, part of neutron density separation logs NDS)
- Bulk density (RHOB, part of neutron density separation logs NDS) & photoelectrical factor
- Neutron hydrogen index (NPHI, part of neutron density separation logs NDS)
- Acoustic and optical image logs.
- Photoelectric Factor (PEF and CRIIO)
- Deep and shallow Dual *Laterolog* measurements (RD and RS)

Except from the sonic and density logs, these types of data, are not directly used in this study, however they were all imported into the Kingdom software during the same import process. Therefore, they will not be more detailed. The database is then complete for perhaps further studies.

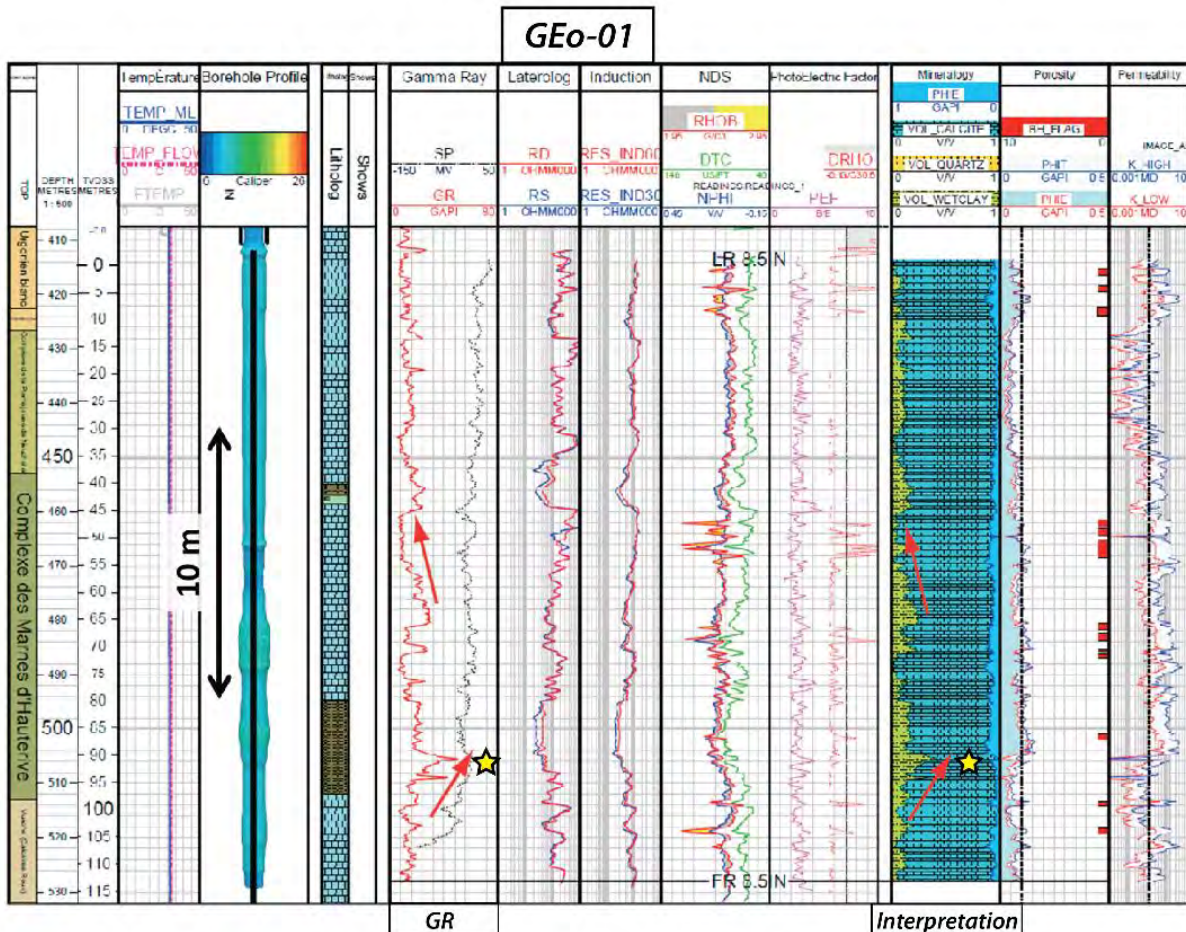


Figure 3-29: Example of well logs display achieved by GGE (Martinuzzi & Sallier, 2018) on a certain interval run in GEO-01 (2018). Yellow stars correspond to increase in gamma ray values (GR), interpreted as increase in clay content (VOL WCTCLAY). Reduction of effective matrix porosity (PHIE) is also interpreted over the same interval. PHI = porosity, K = permeability

GGE has also worked on generating composites logs (calculated, not measured) in order to fill gaps of measurements of log data that can occur in some well sections. They used regional knowledge and geological concepts in order compute them, which gives a complete set of well logs for the majority of

the wells in our database. These complete logs are essential to perform well log correlations through wells in the whole GGB. These are keys for understanding the regional geology, and predict the special changes in rock properties, which cannot be done with seismic data only. The main outcome of this work from GGE that is of our direct interest in this study, is the well formation tops collection for each well that were obtained after high precision well logs correlation (Figure 3-30) (GGE, 2018).

The most important logs for our seismic interpretation study are the sonic (DT in $\mu\text{s}/\text{ft}$) and the density (RHOB in $\text{g}/\text{c}3$) logs. It will be explained in more details in the chapter related to seismic to well tie (see chapter 4.1), but they are essential for synthetic seismogram calculation in relation with calibration of seismic profiles. These data are not always available for all wells.

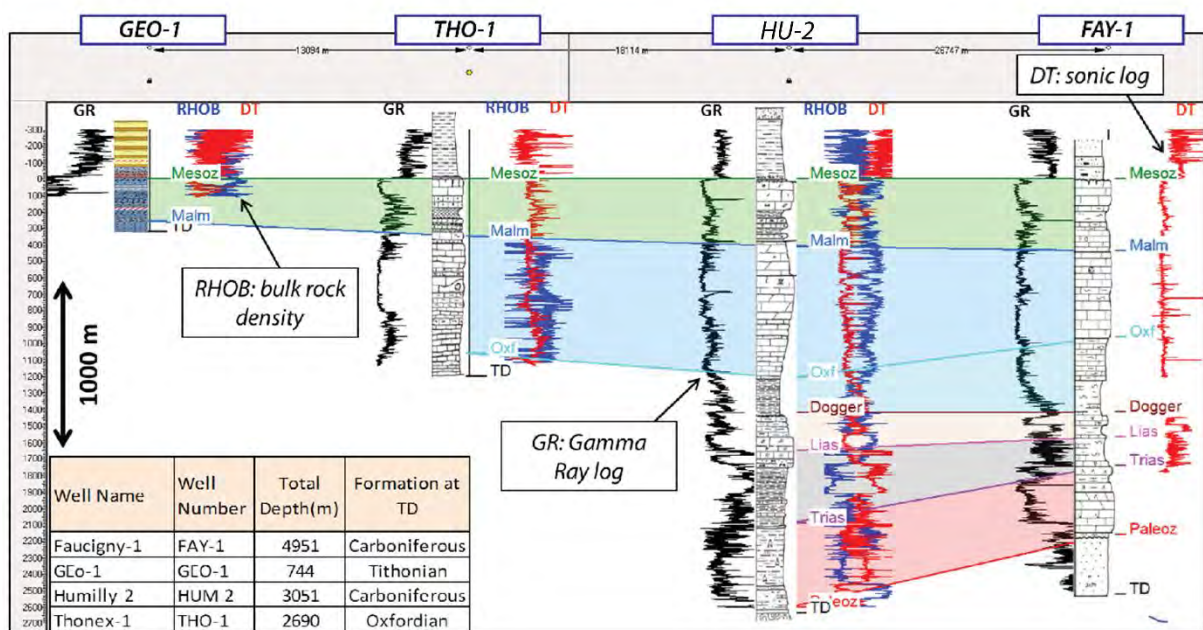


Figure 3-30 : Well log correlation example of the main deep wells around the Geneva area. GGE has generated composite logs for all wells with Mesozoic penetrations to help current and future work. RHOB = bulk rock density, GR = Gamma Ray, DT = sonic log, Oxf = Oxfordian, Mesoz = Mesozoic, Paleoz = Paleozoic.

3.3.2 Image well log data

GGE has also achieved studies related to borehole imagery (BHI) which is a specific log acquisition that gives very high vertical resolution optical and acoustic images of resistivity log (Figure 3-31). It provides detailed structural interpretation and gives key information on nature, orientation and scale of fracture sets and also possible compartments (see example of such interpretation in Lofi et al. (2012) and Wenning et al. (2017)).

As for classic log data description (3.3.1), this petrophysical data are not directly used for our study of seismic interpretation. Nevertheless, the final results of the image log data analysis run by the petrophysical team of GGE, were used and integrated in our structural settings study. Indeed, after an image quality control, GGE can produce a structural interpretation with the following results: a) Beds and regional structure like shale intervals and determine dominant regional dips; b) Faults and unconformities identification (generation of cumulative dip and azimuth vector plots); c) Identify

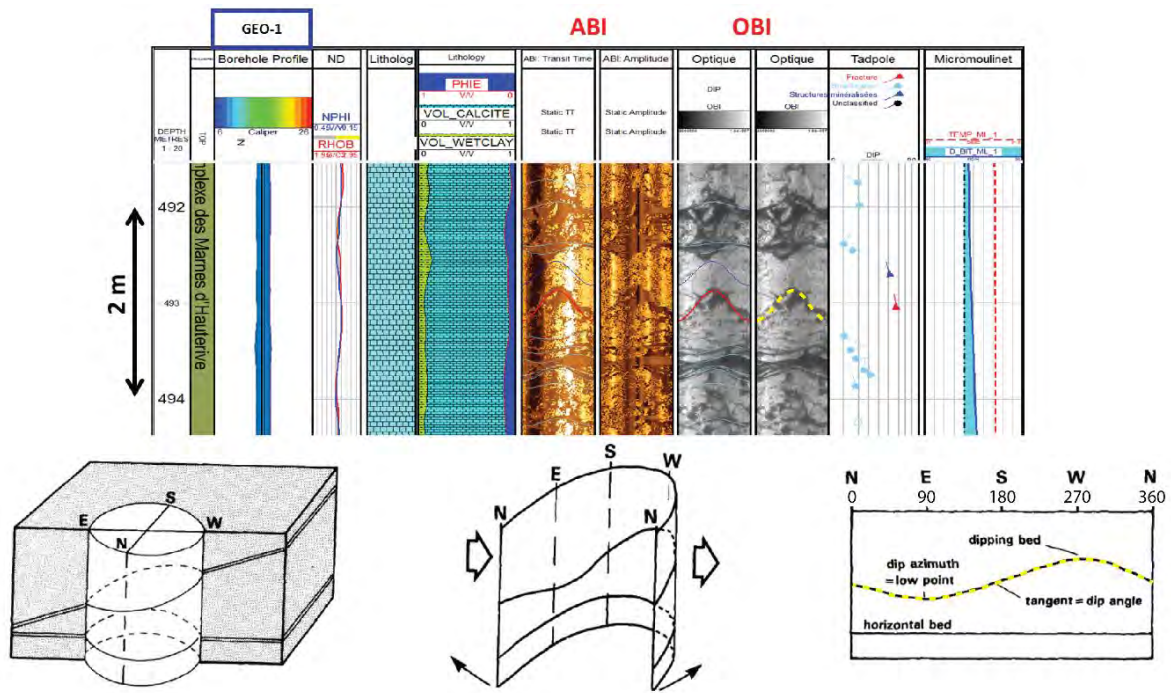


Figure 3-31 : Example of image logs along well GEO-01 well, showing fracture and bedding indications. Display of BHI (BoreHole Image log) are unrolled (360°) and oriented image of the borehole wall. ABI = Acoustic Borehole Image, OBI = Optical Borehole Image.

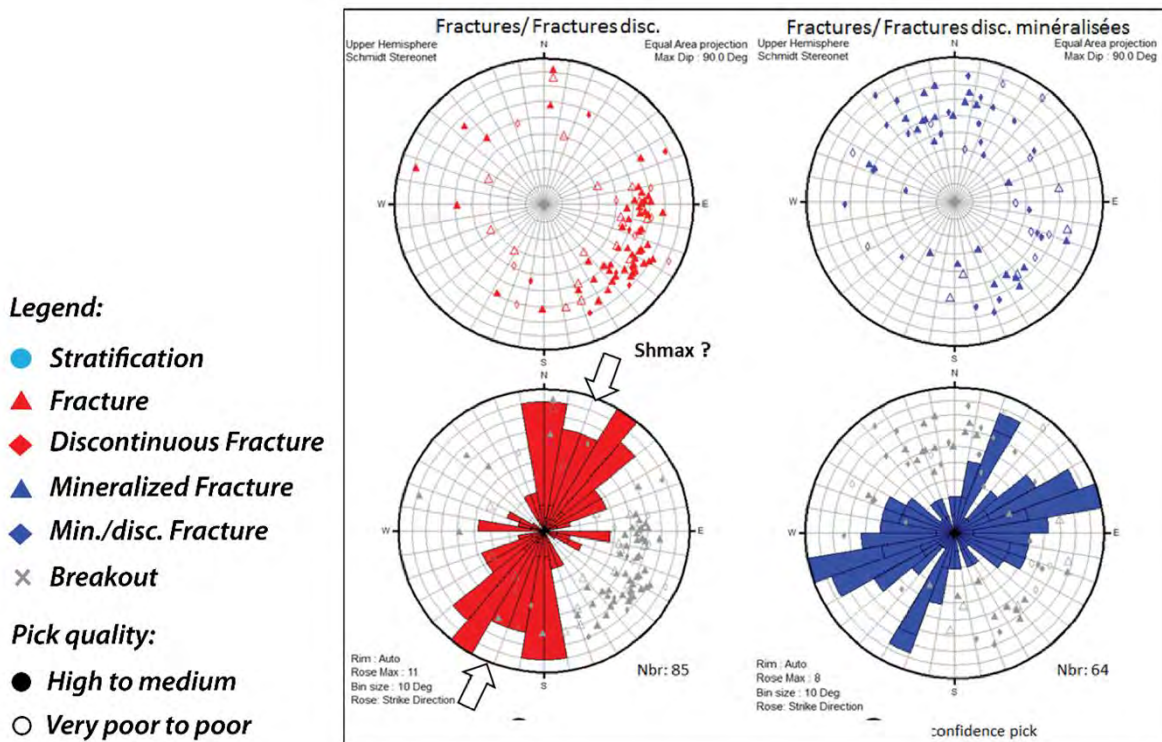


Figure 3-32 : Fractures analysis run along GEO-01 well. Upper hemisphere of a Schmidt stereonet showing the orientations and dips of the fracture planes interpreted in GEO-1. The rose diagrams represent the strike orientation of the fracture planes. The dominant orientation of the fracture plane (strike direction is N-S to NE-SW. Two main orientations of the mineralized fracture planes (strike direction): NE-SW, parallel to the non-mineralized fracture zone, ENE-WSW probably related to a second set of fractures.

fractures and fractures typing (open, closed, healed, etc.). These observations give also consequently the maximum horizontal stress orientation.

The resulting beddings and fractures interpreted with this methodology can then be plotted and classified considering their morphology (continuity, filling, displacement, dissolution, etc.) (Figure 3-32). The orientation and the depth of the visible fractures can be combined with the seismic interpretation to obtain a full integrated study on different scales.

3.4 Surface data

Surface data consists in all the observations or measurements made at the topographical level such as:

- Stratigraphy surface field mapping (map 50k BRGM, or 25k Swiss geocover, (Guillaume et al., 1972; Swisstopo, 2012))
- Structural surface field mapping (dip measures, fault indications, lineaments, geomorphological features, (Charollais et al., 2013; Clerc & Moscariello, 2020; Donzeau et al., 1998; Dupuy, 2006; Mastrangelo et al., 2013; Morend, 2000; Vernet et al., 1974).
- Digital elevation models (DEM) from satellite data (resolution of 5m for the French data (IGN, 2001), and 0.5m for the Swiss data in the Canton of Geneva (DT, 2013; Swisstopo, 2013).

All these data are integrated into the workflow as important additional inputs for the structural investigation and understanding of the GGB (see part 6). The surface data have been collected into the ArcGIS database.

3.4.1 Previous work

Many field measurements and geological observations were conducted in previous years in our area of investigation mainly by the UNIGE or from French geological offices that have led to numerous publications (Favre, 2018). Only few of the latest works of the last decades were fully integrated in our database. Thus, several maps from the literature were georeferenced and saved as Geotiff images in the ArcGIS database originating from articles or reports from (Charollais et al., 2007; Clerc & Moscariello, 2020; Donzeau et al., 1998; Dupuy, 2006; Mastrangelo et al., 2013; Morend, 2000; Vernet et al., 1974).

3.4.2 New surface tectonic map

Our new surface tectonic map (Encl_M02) integrates, in the ArcGIS database, all previously mentioned data adapted or modified for our study:

- Stratigraphical mapping layer including an update and harmonization of the stratigraphical data coming from heterogeneous inputs (French maps from 74, 73, 01 departments, Swiss maps from canton of Geneva and Vaud. The harmonization is based on (Brentini, 2018; Rusillon, 2017). The stratigraphical spatial distribution of the Molasse sediments under the Quaternary deposits is proposed in this study, based on (Charollais et al., 2006, 2007) and our own interpolation of Molasse information from outcrops and well data.

- Structural layers, such as dips data from several sources (no measurements have been collected in the field for this study), fault/lineaments indications made by digitalizing lineaments observed on the DEM or in the literature. The Jura part NW of the Geneva Basin structural information comes also from collaborations at the UNIFR with colleagues of the tectonic groups that were also involved in the study of this part of the Jura Mountains (Marro, 2021; Schori, 2021).
- The dips of the bedding were interpolated in this study throughout our area and saved as shapefiles. This work has allowed to draw our proposed fold axis of the Molasse unit, linked also sometimes with Mesozoic bedding information.

4. SEISMIC INTERPRETATION: METHODOLOGY

The seismic interpretation was performed on computer station from the UNIFR using the Kingdom software from IHS Markit, with the license package Geophysics-Geology (Advanced). A project was created in version 2020 of the software (named "01_Kingdom_Geneva_LH_PhD_Final.tks") and set up with the Swiss coordinate system CH1903+/LV95. All seismic and well data were imported into the dedicated project as SEGY format, and well data as ascii or las format. Georeferenced maps (from ArcMap or Petrosys softwares) have also been integrated into the Kingdom project as Geotiff files.

A conventional methodology was carried out for seismic interpretation (Figure 4-1). After the calibration of seismic profiles using well data, seismic horizons are associated to specific seismic reflections. Then they can be interpreted (picked) in relation with fault sticks along each seismic line. This interpretation will follow stratigraphic and structural defined concepts. As already mentioned in part 3.2.5, a disadvantage of 2D seismic profiles concerns misfits in between intersecting 2D sections. The residual misfits entail necessarily horizon misties that can be corrected by a post-interpretation method. Each step owns a certain range of uncertainty related to the vertical scale (TWT(s) or depth(m)), that can be estimated in order to evaluate an overall uncertainty of the seismic interpretation process.

4.1 Calibration of seismic profiles

4.1.1 Seismic to well tie

The seismic to well tie aims at associating a specific seismic reflection to an approximation of a stratigraphic boundary. As a reminder, a seismic reflection corresponds to a contrast of acoustic impedance (velocity-density factor, see chapter 3.2.1), and is characterized by an amplitude value, a frequency and a phase along a seismic trace wiggle (Figure 4-2).

Few definitions for clarification of the terminology used about seismic image in this work (<https://glossary.oilfield.slb.com>):

A trace is the seismic data recorded for one channel. A trace is a recording of the subsurface response to seismic energy passing from the source, through subsurface layers, and back to the receiver.

A wiggle trace is a common seismic display that shows trace amplitude versus time as an oscillating line about a null point.

Amplitude (A) is the difference between the maximum displacement of a wave and the point of no displacement, or the null point. The common symbol for amplitude is a .

Acoustic impedance (AI) is the product of density and seismic velocity, which varies among different rock layers, commonly symbolized by Z . The difference in acoustic impedance between rock layers affects the reflection coefficient.

A sonic log is a display of traveltime of acoustic waves versus depth in a well, or acoustic logs display velocity (usually in $\mu\text{s}/\text{ft}$ or in m/s).

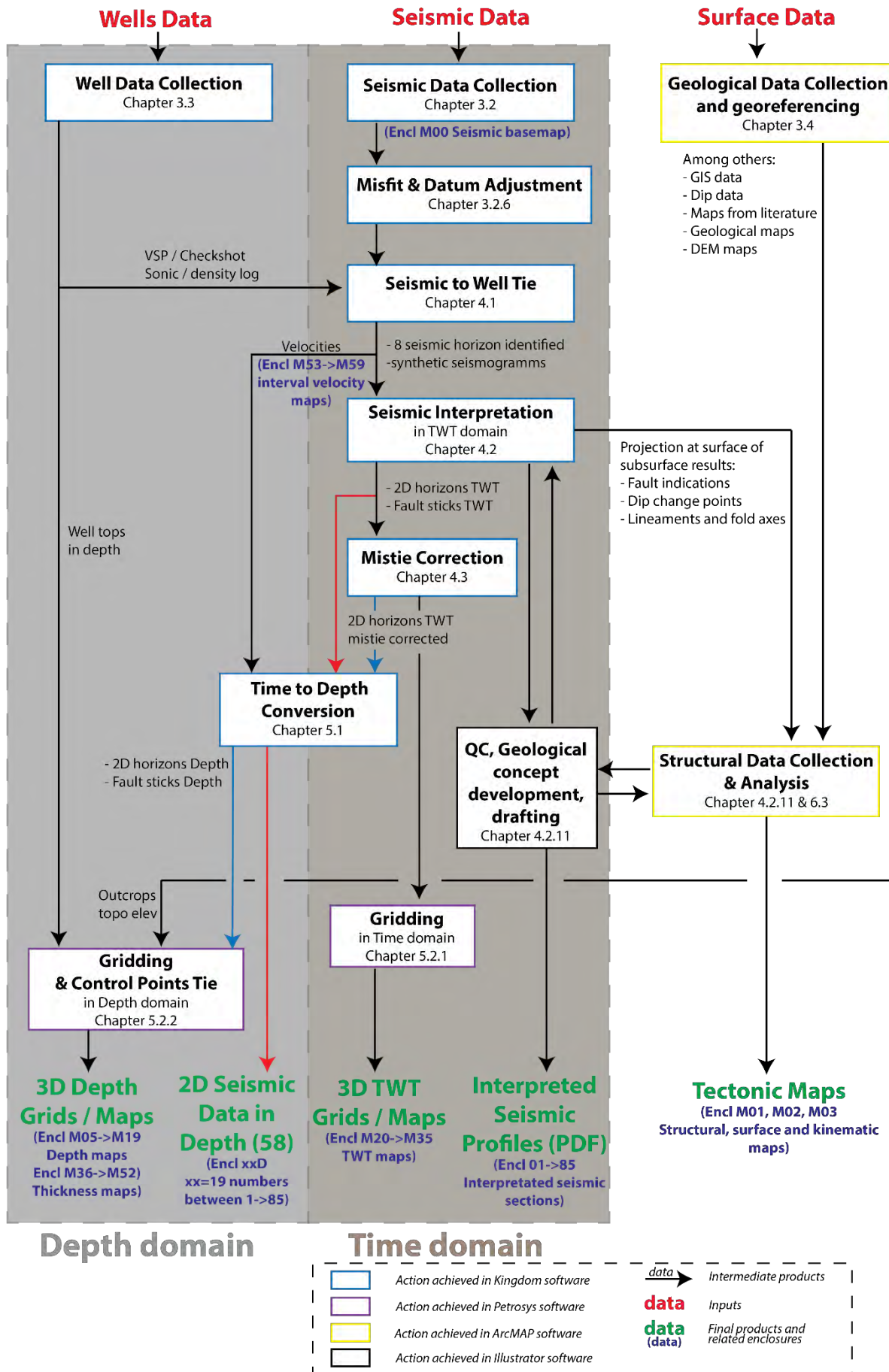
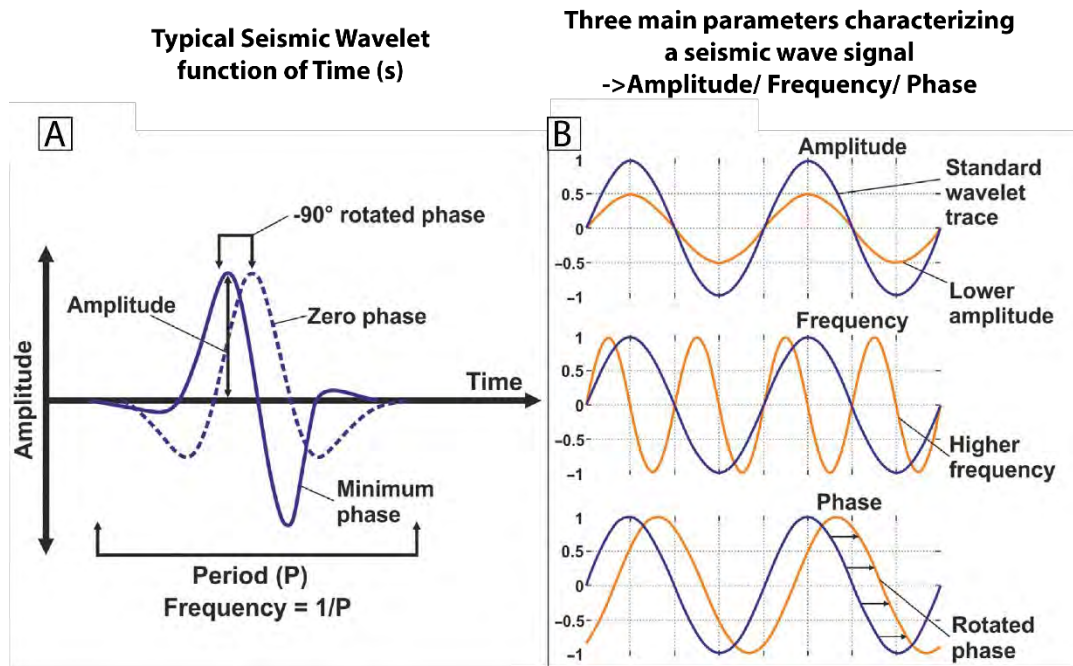


Figure 4-1 : Flow chart of each methodological steps followed in this study.



For one Acoustic impedance (AI) contrast, several way to represent it with a seismic signal

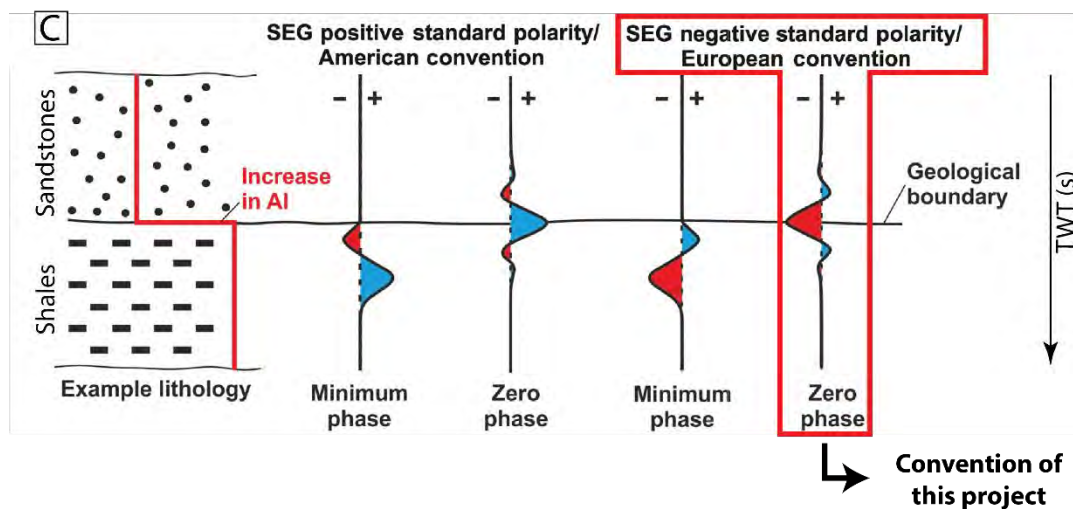


Figure 4-2 : A and B: a seismic wave signal is characterized by a amplitude value, a frequency (inverse of period) and a phase. C: a polarity convention is needed for associating an acoustic impedance contrast with a related seismic signal. In our case, the European convention (SEG negative standard polarity) zero phase has been defined for the polarity of seismic profiles (modified after Cox et al., (2020)).

An amplitude **peak or trough** correspond respectively to a positive and a negative maximum of amplitude. A **zero+ and zero-** are both associated to zero crossing amplitude (value of 0 amplitude) respectively from a peak to a trough and from a trough to a peak.

The polarity conventions clarify the association between a seismic reflection and an acoustic impedance contrast, in relation to the amplitude (sign) and the phase of the signal. Indeed, the polarity of the raw seismic data may vary according to acquisition parameters (types of source/recorder), and processing procedures. However, before acquisition a procedure of testing geophone could help understand the polarity response. Moreover, during seismic processing, the polarity of the data can be guessed by looking at the polarity of first breaks of the direct downgoing P wave near zero offset

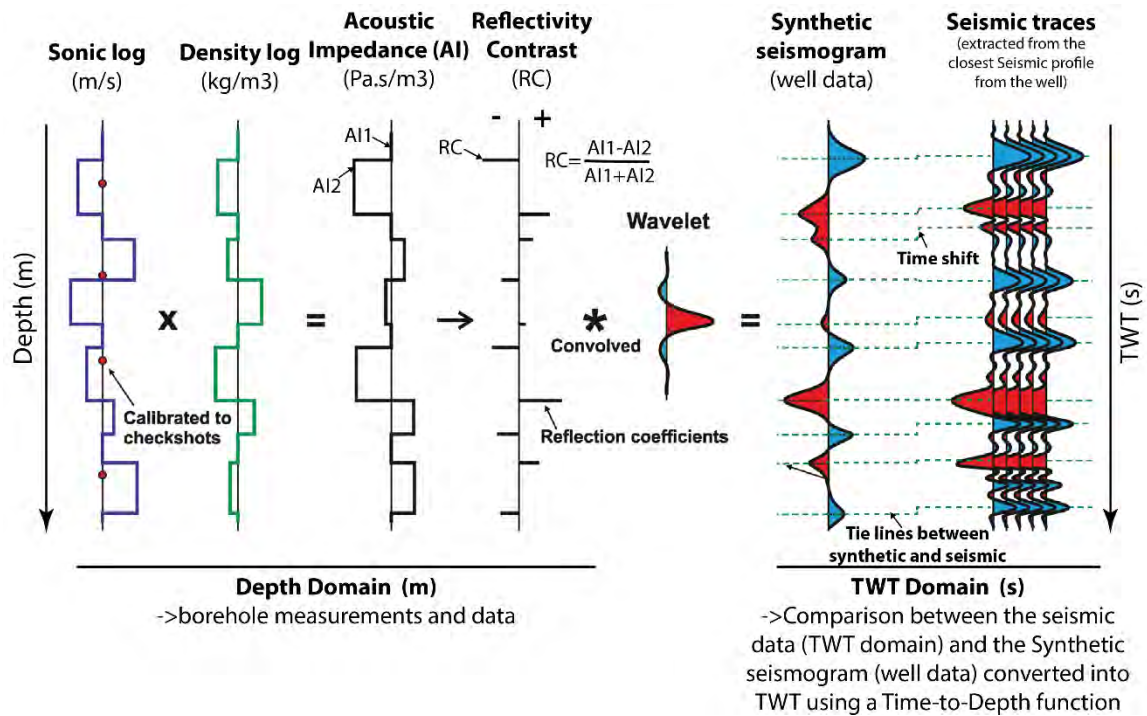


Figure 4-3 : Seismic to well tie workflow scheme. The acoustic impedance curve is the product of sonic and density logs. A reflectivity series is obtained by a simple derivation of the acoustic impedance curve, and when convolved with a defined seismic wavelet, it is possible to obtain a synthetic seismogram (trace) from well log data. This synthetic trace is then compared with a seismic trace extracted from the closest seismic profile to the well. Note that the reflection coefficient (RC) is calculated at each acoustic impedance (AI) contrast with the simple formula displayed in the middle of the figure (modified after Cox et al., (2020)).

on common-receiver gathers (Brown et al., 2000). This verification remains uncertain, since it is applied on land data, and noisy responses may often interfere with the first break signal. On the contrary marine acquisition data gives usually very clear polarity results from first break picking due to the very sharp reflection between seawater and first sediments. In our case (land), the reprocessing of a major part of the seismic profiles located inside the Canton Geneva in 2017 has led to the conclusion that all these reprocessed lines follow the European polarity convention (written in the headers of the seismic profiles). This means that an increase of acoustic impedance downward corresponds to a negative amplitude (red reflection with our seismic colorbar, see Figure 4-2 and Figure 4-3). After this reprocessing from 2017, the rest of the dataset (not reprocessed data) was at that time compared with the reprocessed seismic lines that had a defined polarity. By following loops of comparison from one line to another intersecting 2D profiles, it has been observed and concluded that the rest of the seismic data will be treated in relation to the European polarity convention. Only few seismic lines had to be phase rotated (by 180°, applied by myself in the Kingdom software) to be in line with the polarity of the other profiles (see Table 3-1). Seismic data acquired in 2018 by SIG (survey 18SIG) have been processed in the SEG standard polarity (inverse of European polarity). In order to remain consistent in terms of polarity of the whole dataset, the seismic survey 18SIG profiles have been phase rotated by 180° to match the define polarity.

The seismic processing allows to give a first estimate of the polarity of the seismic profiles, that will be confirmed or not during the seismic to well tie. This latest process consists of comparing a synthetic seismogram generated from digital logs acquired along the borehole, with an actual seismic trace from the closest seismic profile to the well (Figure 4-3 and Figure 4-5). Seismic data are usually first

Area	Well Name	Abr.	Density Log (even not complete)	Sonic log	Checkshots/ VSP	Nearest seismic line	Synthetic seismogram	Seismic to Well Tie feasibility
Jura	Chaleyriat-1	CYT-1	Yes	Yes	No	EW03_part2	OK	NO
	Châtillon-1d	CTL-1-D	Yes	Yes	No	EW03_part2	OK	NO
	Charmont-1	CHT-1	Yes	Yes	No	EW02	Ok	NO
	La Chandelière-1d**	LCD-1D	Yes	Yes	Yes	EW03_part2	OK	YES
RUM	Chapery-1**	CHY-1	Yes	Yes	No	HR528 & NS04_part1	OK	YES
SAM	Faucigny-1**	FAY-1	No	Yes	Yes	83BV10	OK	YES
GVA Basin	GEo-01	GEo-01	Yes	Yes	No	GG88-02 & 15SIG_008	OK	YES
	GEo-02	GEo-02	Yes	Yes	Yes	9006 & 18SIG_011	OK	YES
	Humilly-2**	HU-2	Yes	Yes	Yes	885VO07 & 18SIG_007 & 82 GEX01	OK	YES
	Thônex-1	THO-1	Yes	Yes	Yes	TH02	OK	YES

RUM: Rumilly Basin

SAM: SubAlpine Molasse area

See Figure 4-7

* either too far from the nearest line, or pertubated by faults or seismic resolution of nearest seismic line not sufficient.

** wells used for deep calibration

Table 4-1 : Listing of wells that have been well tied according to the availability of sonic, density logs and checkshots/VSP data. Green boxes show wells with data, whereas orange boxes wells without data.

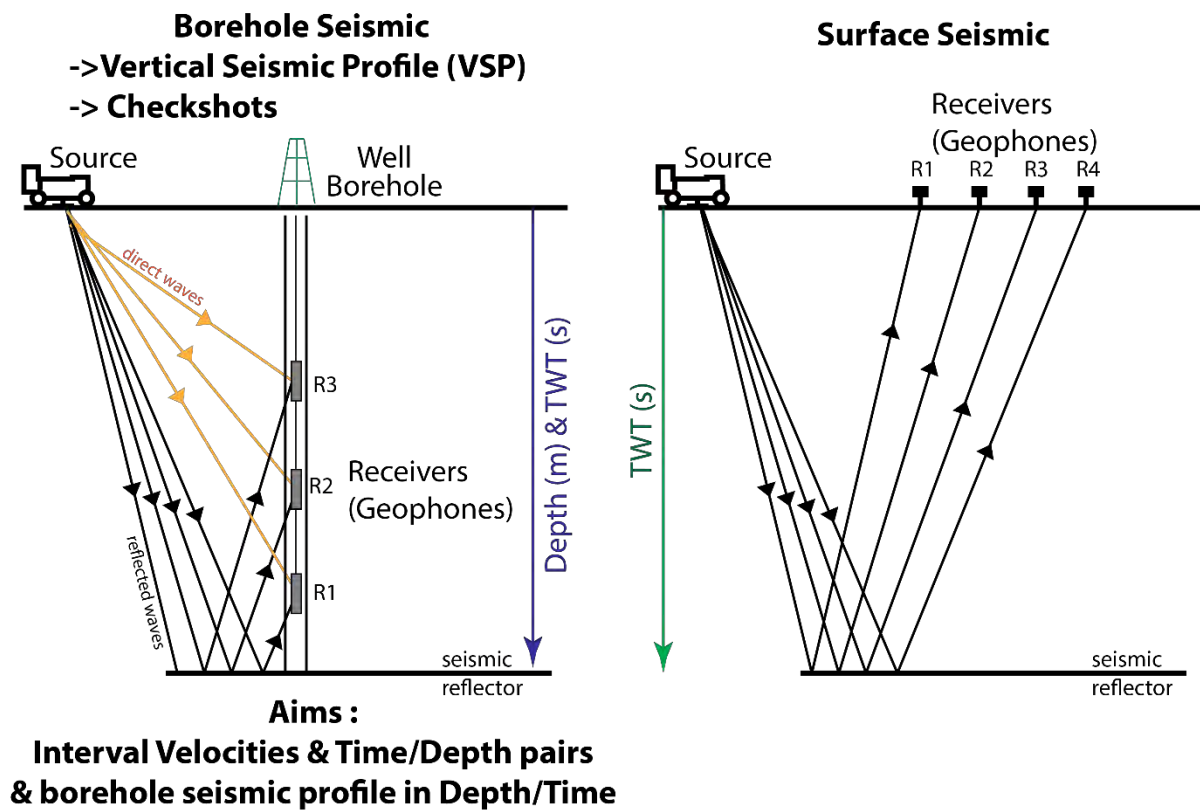


Figure 4-4 : VSP and Checkshots are methods of borehole seismic imaging (left) where geophones are recording along the borehole the seismic signal, which is the opposite of surface seismic that acquire data from topographical surface (right). Figure inspired from Mokhtari & Pourhossein (2003).

processed in the time domain (vertical scale in two-way travel time, TWT (s)); whereas well data are all recorded in the depth domain (meters). A time to depth relationship is hence needed for comparing the well data (synthetic seismogram in depth domain) with the seismic data (nearest seismic trace from the well in time domain). The comparison is often carried out in the time domain. As the seismic profiles are already adjusted vertically, it is the seismic seismogram trace in time domain that will be shifted, stretched and squeezed relatively to the seismic trace (Cox et al., 2020). This corresponds in fact to a modification of the time to depth relationship. The tie between the two will be obtained when most of major seismic reflections are aligned together and resulting in the highest correlation coefficient as possible (Figure 4-3 and Figure 4-5).

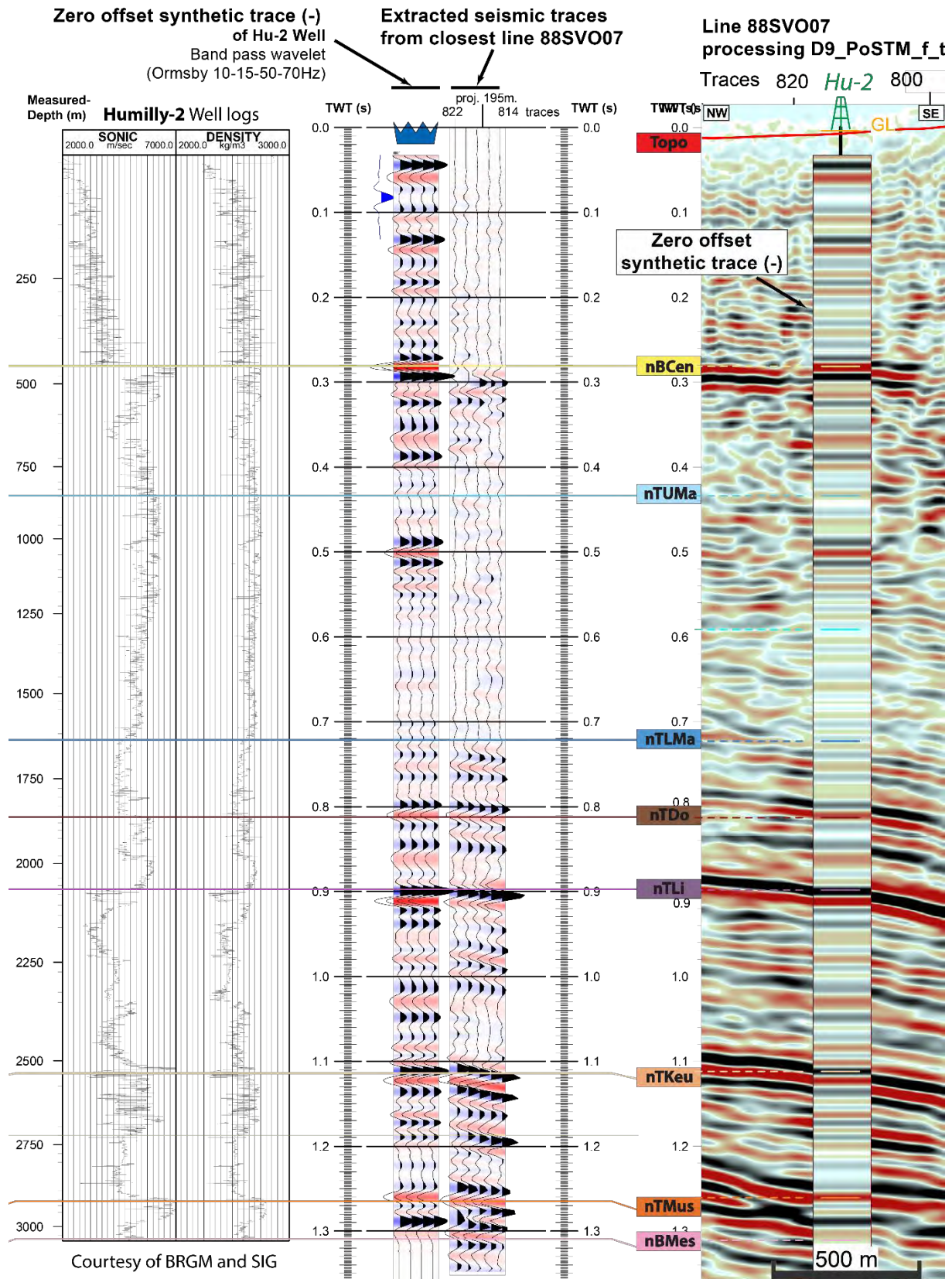


Figure 4-5 : Example of seismic to well tie results of well Humilly-2, achieved with comparison with the closest seismic line from the well, 88SVO07. The software is automatically calculating a positive and a negative convolution synthetic seismograms. In order to follow our defined European polarity convention (SEG negative), the negative convolved synthetic trace is compared to the seismic trace from line 88SVO07. Synthetic seismogram can also be displayed in the Kingdom software as raster log (right image), which means that it will have the same appearance as the seismic profile. See Encl 38&85 for detailed seismic interpretation of line 88SVO07. See Figure 4-7 for location of well and seismic line.

Calculation of a synthetic seismogram from well log data, requires at least a sonic log to begin the process. As it is a velocity information, a simple mathematical integration of it gives a first time/depth relationship. Then, if a density log is available (if not, a constant value is taken, such as 2500 kg/m³ which is a generic value), it is multiplied with the sonic log to produce an acoustic impedance log in the depth domain, which allows producing a reflectivity log. This latter highlights each acoustic impedance contrast, and when it is convolved with a seismic wavelet (approximation of the same seismic source signal than the one used during acquisition of the seismic profile), it gives as a result a synthetic seismogram. The wavelet may be adapted in shape and frequency content (proposed in the Kingdom software) along with frequency filters applied on the synthetic seismogram, to obtain comparable characteristics (frequency, amplitude and phase) between the two traces to be compared. In order to check again the polarity of the seismic profile, two synthetic seismograms with opposite polarity (seg positive and negative) are computed. They are both compared with the actual seismic trace, and the one that gives the highest correlation coefficient is kept and hence inform about the actual seismic polarity (see Figure 4-5, for HU-2 well, the very high visual correlation between the two shows clearly a negative resulting polarity).

A synthetic trace will be calculated only along the sonic log intervals, that is why the digital well logs should cover as much as possible depth intervals to allow a reliable seismic to well tie. It should at least reach the first main seismic horizon to adjust, for instance in our study area only wells that have a sonic log that goes beyond near Base Cenozoic will be considered (Table 4-1).

The use of sonic log is not the only way to run a seismic to well tie. Other geophysical measurements, such as checkshots or Vertical Seismic Profiles (VSP) are perfectly adapted to such tasks. Both methods consist in seismic acquisition, but unlike surface seismic acquisition, they use geophones along the boreholes instead of at the surface (Figure 4-4). The VSP method has greatly evolved during the last decades to produce nowadays high-resolution seismic images along the borehole in time and depth domain (calibrated with synthetic seismogram). This technique brings a substantial additional constrain to the calibration of the subsurface model. However, during most of well drillings of our project, the VSP technology was not yet available. Checkshots were at that time acquired, that follow approximately the same principle of acquisition along the borehole than VSP but gives as a result only interval velocity information along with a deducted time-depth relationship (Table 4-1). Unlike VSP method, which is achieved along with a precise calibration between the VSP, the synthetics seismogram and the closest seismic image, the checkshot method is obviously less accurate. Checkshots usually has the main role of easing the seismic to well tie by bringing a first estimate of the time to depth law.

In our study, we have considered 16 wells that have reached at least Base Cenozoic series and have sufficient data to carry out the time-depth adjustment of the seismic horizon (Table 5-3). For deep seismic horizons, each of the main four areas (Jura, Rumilly Basin, Subalpine Molasse area and Geneva Basin) contain at least one well with the total depth below Base Mesozoic and that allow an accurate a seismic to well tie (Table 4-1 and Figure 5-3):

The Geneva Basin has the well Humilly-2 that gives a precise tie of the complete Mesozoic cover as well as a confirmation of the seismic polarity statement previously mentioned (Figure 4-5). The comparison between reprocessed (from 2018) seismic line 88SV07 that crosses the well with the generated synthetic seismogram lets us conclude that the European polarity will be the only polarity

convention used in this study, as the negative synthetic seismogram gave a higher correlation coefficient than the positive one. In the Geneva Basin, all other wells give only tie information until at best Top Lower Malm series, but they are all consistent with the results of the calibration of well Humilly-2. Uncertainties related to these adjustments will be described in more details in 4.4.

In the Subalpine Molasse part, well Faucigny-1 is the reference well of the area that has also reached the Paleozoic units, and contains relevant geological information. This well highlights the fact that the thickness and velocities of the Mesozoic sub-units in this region are quite different from Humilly-2 well. A seismic to well correlation was possible with seismic line HR545 and 83BV10 and is nearly as accurate as in Humilly-2 (App_04_to_07 and Encl_47).

In the Rumilly Basin it is well Chapery-1 drilled until Paleozoic unit that let the possibility to adjust the geology of the area, which is relatively different from the Geneva Basin and Subalpine Molasse areas in terms of thickness of the Mesozoic sub-units. Well La Tailla-1 has reached Base Mesozoic but it does not own a continuous record of the whole Mesozoic cover, as it is crossed by several faults.

Several deep wells have been drilled in the Jura Mountains area, but only well La Chandelière-1d is not faulted and allows calibrating the full continuous Mesozoic rock column in this area. However, all wells of this part of the study process high quality sonic logs for accurate synthetic seismogram processing. Well Charmont-1 could not be adjusted in relation to its nearest seismic line EW02, which has a too poor resolution in this area for a proper calibration. Nevertheless, the synthetic seismogram of this well was projected into farer seismic profiles that are in a similar geological and tectonic context such as line 81-JU-06.

4.1.2 Seismic horizon definition

A seismic horizon is picked along a specific seismic reflection, which corresponds to a significant change of acoustic impedance (AI, dependent of petrophysical properties of the rocks). It is usually not

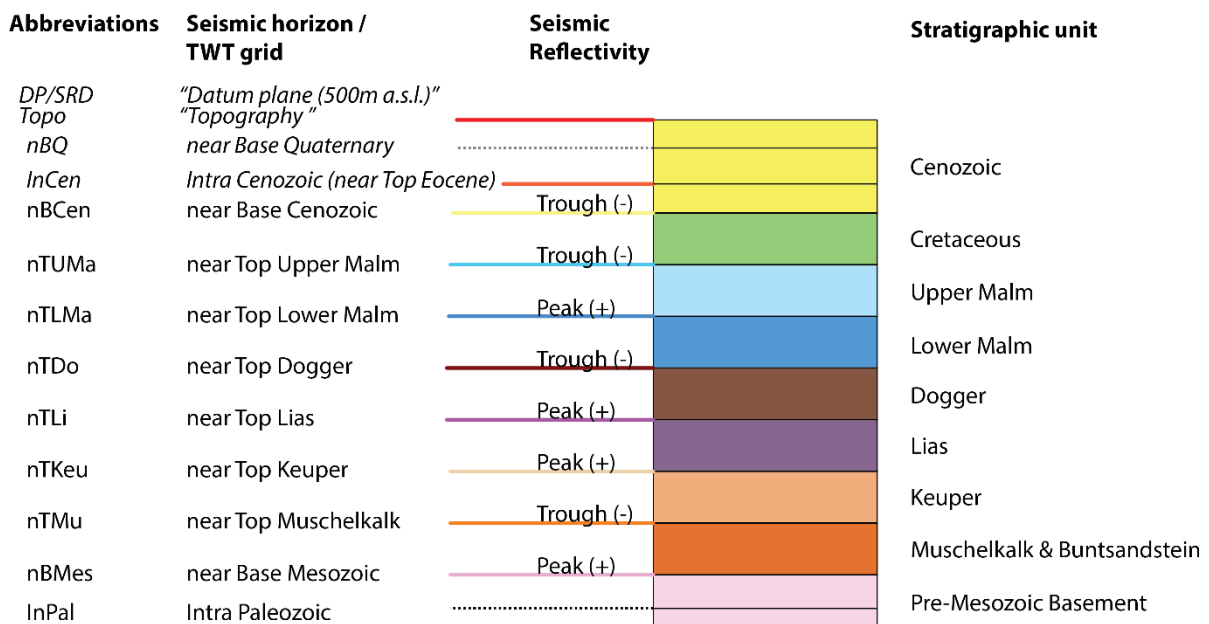


Figure 4-6 : Seismic horizon correspondence with seismic reflectivity and stratigraphic units.

complicated to link a seismic reflection to a well-known stratigraphical boundary (or the nearest approximation of it), on the condition that it corresponds to a sufficient lithological (therefore petrophysical) contrast. The stronger this petrophysical contrast, the easier will be the interpretation. Indeed, it is always easier to follow a very strong amplitude reflection than the opposite. The lateral continuity of this contrast is also crucial in helping the interpretation process. For instance, an erosive surface may be more difficult to pick than a regular “layer cake” stratigraphical surface because the characteristic of the seismic reflection will constantly evolve laterally in relation to the modification of the acoustic impedance contrast.

Eight major stratigraphical boundaries (Figure 4-6) have been targeted for dividing the interpretation of the Mesozoic cover (same boundaries selected than in Gruber (2017) and Sommaruga et al., (2012)). These geological limits correspond in fact to the main changes of depositional ages, and most of them are fortunately marked by significant lithological contrast. The interpretation of these geological boundaries is associated to seismic horizons (and therefore to seismic reflections). The uncertainty around the calibration between the two requires to add the prefix “near” before the naming of each of these eight seismic horizons.

Three other seismic horizons, visible along seismic sections, are treated differently. Firstly, the topographical line displayed on seismic profiles is not a seismic interpreted horizon. It comes simply from the topographical grid (3D surface) converted from depth to time using the replacement velocities. Then, the “near Base Quaternary” horizon may be displayed on several seismic profiles but in fact it is the intersection of the profiles with the grid (3D surface) of this boundary created during a project run by GESDEC in collaboration with GGE in 2020 (Lathion & Hauvette, 2020). This horizon has not been interpreted during this work and is simply displayed (converted into TWT with $V_{int}=3000\text{m/s}$), mainly in order to quality check the possible artefacts that Quaternary channels may produce on the seismic image below. Indeed, this layer of low velocity may create push down effects (due to high lateral velocity variations) or signal absorption that decreases the resolution of deeper reflections (Sheriff, 1975). Finally, prominent Intra Paleozoic reflections have been highlighted, but no continuous and systematic interpretation has been achieved on our seismic dataset.

The seismic to well tie procedure explained in 4.1.1 gives as a result for each well the link between each seismic horizon and a corresponding seismic reflection. The characteristics of the seismic reflections (peak (+), trough (-) , zero+ or zero-) associated with the eight main seismic horizons are summarized in Figure 4-6.

It is important to keep in mind that these characteristics, taken from the seismic to well tie procedure, may vary from one well to another. Indeed, lateral changes of the lithological contrast of each boundary may occur. Seismic to well tie is a local calibration, whereas lithologic/sedimentologic properties necessarily evolve laterally at regional scale. A second reason of the differences in the reflection events of one seismic horizon on several wells comes from the uncertainty related to the seismic to well tie procedure. This uncertainty is dependent on several factors, but the major ones may be the resolution and quality of the well log data and the petrophysical interpretation produced as a result. If the stratigraphical boundary is not placed at the right depth, consistently between all wells based on the accurate identification of the same petrophysical signature event, the seismic horizon will then be placed inevitably along different seismic events depending on wells. In our case, we have a regional petrophysical study that has been carried out by GGE on behalf of SIG (GGE, 2018), and that

should have interpreted consistently the major stratigraphical boundaries along a majority of the wells of our database. However, several well log data have vertical intervals of data gaps and sometimes through one or more main stratigraphic boundaries. That is why some of the seismic horizons are not defined in terms of reflectivity for some wells. For all these geological (lateral variation of the seismic facies) and technical (uncertainties) reasons, we have observed that certain seismic horizons have different seismic reflectivity characteristics depending on wells. For consistency and simplicity of the seismic interpretation, a convention of picking is established and precises one unique reflectivity event for each of the eight seismic horizons for all areas.

4.2 Interpretation of seismic profiles

The seismic interpretation of a profile consists in picking three kinds of features. First, seismic horizon picking allow the vertical subdivision of the sedimentary cover. Then, seismic facies analysis may suggest lateral stratigraphic distribution within each subunit. Finally, the fault segment picking reflects the structural configuration of the interpreted profile.

The next part 4.1.3 describes the methodology of the first two aspects of seismic horizons and facies interpretations. A seismic stratigraphic catalogue will then be presented to summarize the related seismic interpretation. In the part 4.1.13, it will be the structural interpretation methodology that will be similarly explained.

4.1.3 Stratigraphic interpretation: methodology

Once the nearest seismic line from one well is tied, the interpretation of seismic horizons can be easily propagated from one line to another. In order to interpret the eight main seismic horizons through all the seismic dataset, the methodology entails starting from the main deep wells of each areas (4.1.1 and) and then propagate the interpretation following loop (Figure 4-7), once the following conditions are maintained:

- there is a lateral continuity between seismic lines (intersecting each other)
- there is a sufficient resolution and continuity of the seismic reflections in between profiles.

Otherwise, if these conditions are not observed, the method of correlation polygon may be used along with the regional geological knowledge of the area. It consists in extracting a rectangle portion of one calibrated seismic profile (with its interpreted seismic horizons) and overlay it on top of another profile that needs a calibration (Figure 4-8). It is essential to extract a vertical column as long as possible in order to be able to compare as many as possible seismic reflections together. Hence, in order to use properly this method, we may set the condition of extracting a stratigraphically continuous column containing at least three of the main seismic horizons and be able to calibrate them. The calibration is finished once enough identical seismic reflections are laterally aligning between the correlation polygon and the seismic profile to calibrate. It can also be particularly useful on a single profile in case of major fault perturbing the whole Mesozoic unit, seismic horizons can then be propagating from one side to another of the fault, using this method.

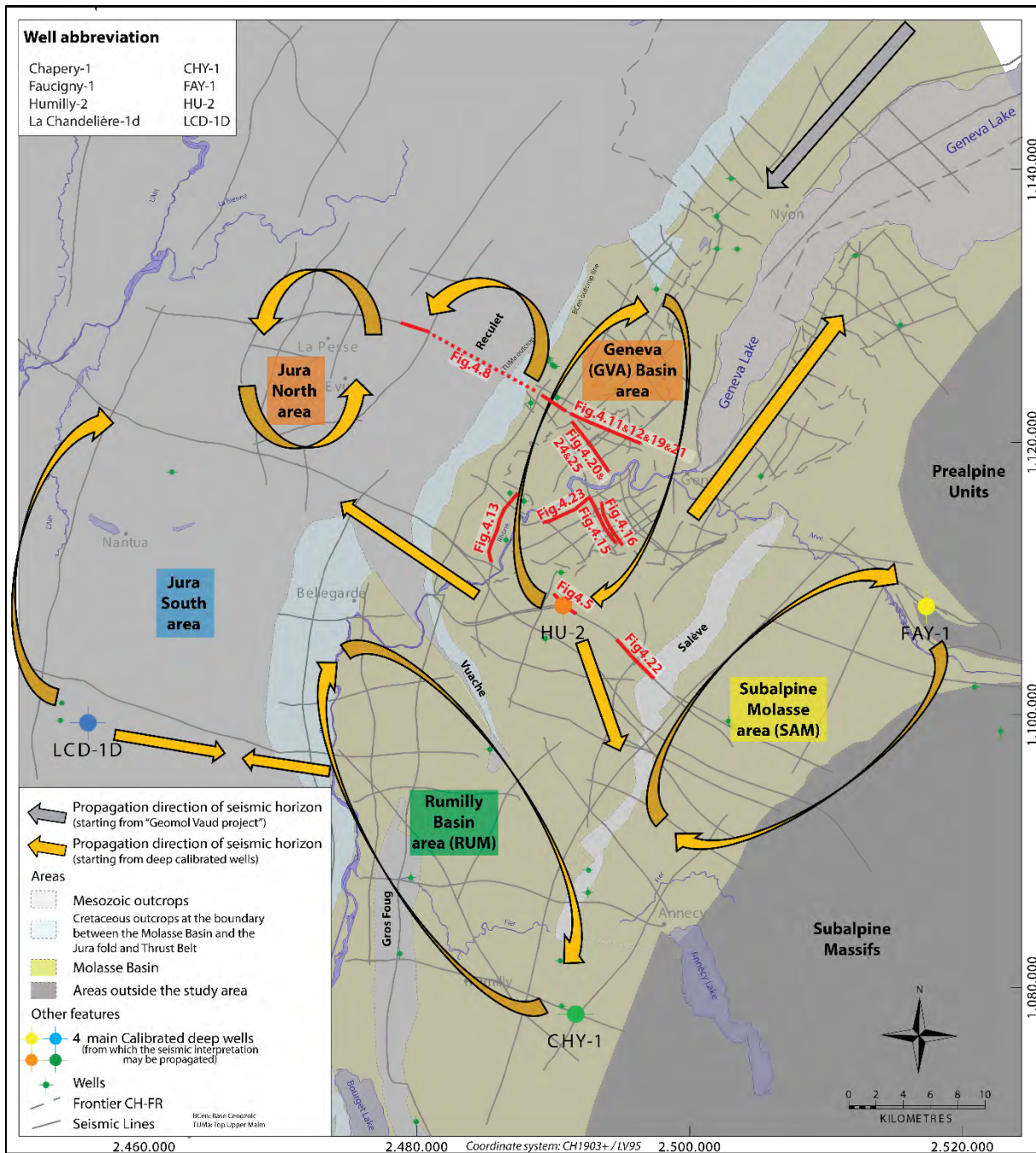


Figure 4-7 : Map with schematic loops of the propagation of seismic horizon picking starting from deep wells and expanded through all the seismic dataset. Note that location of seismic profiles from figures of this chapter is indicated on this map (red lines).

The resolution of seismic profiles plays an important role in the interpretation process. The methodology of seismic horizon picking depends on the classification of the quality of the section defined in part 3.2.2. Indeed, along seismic profiles of best quality type 1, the autotracker (automatic) picking tool (Kingdom software) was often used. It consists in defining a vertical TWT guide window in which the picking will be propagated automatically along a defined seismic event. This data driven interpretation allows to have an accurate interpretation that follows exactly the amplitude oscillation of the seismic reflection. However, it is important to qualitatively check this automatic interpretation, and adapt manually the picking if necessary. These manual corrections may be needed for instance on locally noisy areas or on the edges of the profiles where the resolution necessarily decreases due to

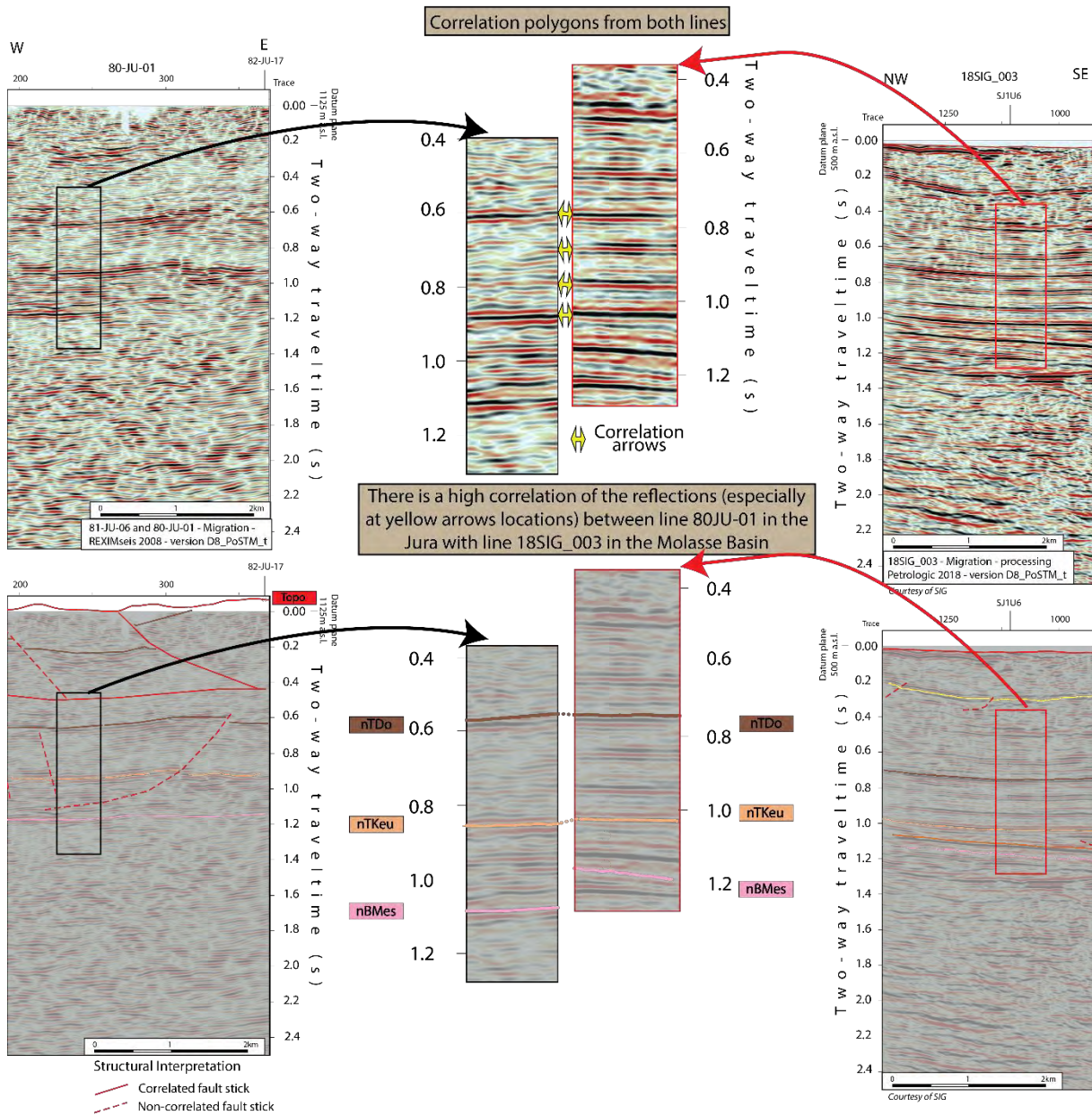


Figure 4-8 : The interpretation of seismic horizons can be propagated from a calibrated seismic profile (on the right, line 18SIG_003), into a not calibrated seismic profile (on the left, 80-JU-01) using the method of polygon correlation that consist in extracting a portion of one profile (with its interpretation of the horizons) and overlay it on top of the other profile. It is particularly useful in the case of isolated seismic profiles, not intersecting another profile. See respectively Encl 37 and Encl 21 for detailed seismic interpretation of lines 81-JU-06/80-JU-01 and 18SIG_003. See Figure 4-7 for location of seismic lines. This figure is modified from L. Hauvette et al. (2021).

less fold coverage and/or migration artefacts. For seismic profiles of quality type 2, the autopicking is used approximatively in half of the sections against half of manual picking. Concerning seismic profiles of quality type 3, the manual picking is fully required.

In some cases, it may help the interpretation of seismic horizons along one seismic profile to consider jointly the different versions of processing seismic data. The characteristics of the seismic reflections might vary slightly between two data types. For instance, artefacts from migration of data such as migration smileys may mislead the interpretation or conversely diffraction hyperbolas may affect wrongly the judgment of the interpreter (see chapter 3.2.7 and Figure 3-24).

It is noted that the range of two-way-time (TWT) of the seismic horizons to interpret has an influence also on the interpretation. The very shallow interval (<0.2s) is usually poorly imaged due to a lack of fold coverage (Figure 3-6), therefore the uncertainty linked with the interpretation is very much higher. It is the case for near Base Cenozoic layers in the Molasse Basin in the vicinity of the major thrusts (Jura first high chain or near the Salève Mountains), or also the case of other Mesozoic series seismic horizons close to the topographical surface in the Jura part.

In the Paleozoic part of the sections, no continuous horizons have been picked as there is not a continuous stratigraphic regional boundary to interpret. Grabens developed in the crystalline basement are filled with clastic deposits from Paleozoic times. These sediments may be interpreted as locally oblique, semi-continuous high amplitude reflections (Gruber, 2017). A correlation of these reflections is very difficult to achieve, hence they are only drawn individually and referred as “Intra Paleozoic” (InPal) reflections.

When the interpretation of seismic horizons becomes difficult to run due to weaker resolution (quality types 2 or 3) or because of the reflection events (contrast of acoustic impedance) that simply have a less pronounced amplitude appearance, the use of the seismic facies for each unit may be of great support. A seismic facies is a group of seismic reflections with specific reflection signatures related to the continuity and geometry of the reflections and their frequency, phase, amplitude, and polarity content (Roksandic, 1978). Analyzing seismic facies can then help understand the stratigraphic deposition of an entire sub-unit in comparison to units above and below, and hence support the interpretation of its boundaries (seismic horizons). For instance if it is accepted that a unit is composed of cross bedding dips and is deposited and overlapped by subparallel layering deposits, its top and base seismic horizons (angular unconformity) will then be easily deduced from the obvious contrast of seismic facies between these units (Figure 4-9).

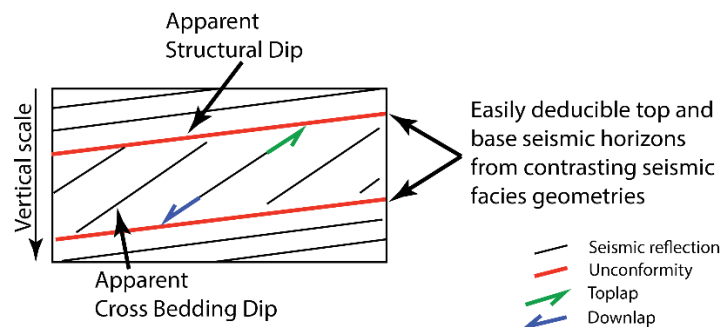


Figure 4-9 : Schematic principle of seismic facies helping for seismic horizon interpretation.

In addition to helping the seismic horizon picking, the facies analysis has many other interesting purposes aimed at predicting lithology, fluid content, petrophysical properties (porosity...), type of stratification or identifying specific geological bodies (Roksandic, 1978). In our case, it will improve the overall geological knowledge of the Mesozoic deposits, in relation to the structural history of the area. One particular useful application of this analysis is the identification of reefal seismic reflection patterns within the Upper Malm unit (Hauvette, 2020), which is a very interesting potential geothermal target in the Geneva Basin (identified highly porous reservoir (Brentini, 2018; Rusillon, 2017)). Another major focus of this seismic facies study is the mapping of the highly variability of thickness of the Triassic unit, and especially the identification of the pure salt bodies that are key for understanding a majority of the main folded and faulted structures within the Molasse Basin. A third facies has been

raising many geological questions for decades in the Geneva Basin; it is the Eocene deposits of the Siderolithic that may correspond to continental fluvial deposits lying on top of the erosive surface (nBCen) of the Cretaceous unit (Conrad & Ducloz, 1977). During the recent drilling of the Geo-02 well (Chablais & Savoy, 2021), an unexpected thickness of 140m of Eocene deposits was observed instead of the max 40m of generally accepted thickness in the Geneva Basin (Brentini, 2018; Rusillon, 2017). Seismic facies analysis may then give the beginning of an answer. A classification of the seismic facies per sub-units will be described in detail in the next parts from 4.1.4 to 4.1.12.

A seismic facies may be described with several criteria related to various characteristics of the seismic image. This study will only take into account visual-based seismic information. Indeed, 2D seismic profile does not allow following modern workflow that classify seismic facies automatically using algorithms such as clustering or machine learning. Our qualitative criteria used for seismic facies identification are the following:

- Amplitude: *high, moderate or low* amplitude value of seismic reflections relatively to the amplitude range value of the analysed seismic profile (Figure 4-2).
- Frequency: *high, moderate or low* frequency content of a seismic reflection. In a practical manner, it corresponds to the TWT(s) “thickness” (vertical extent) of the seismic reflection, and therefore may provide information for instance about bed thickness (Figure 4-2).
- Continuity: *continuous, semi continuous, discontinuous, chaotic*. The continuity criteria may relate to the depositional or structural settings of the seismic facies. However, it may also be linked to the resolution of the image (Figure 3-8).
- Internal geometry: *Sigmoid, oblique, shingled, subparallel, parallel-even, divergent, mounded, deformed, chaotic, reflection free and Hummocky* (Figure 4-10). These various types inform about the depositional processes.
- Termination patterns: *onlaps, toplaps, downlap, and erosional* (Figure 4-10). This also gives information about the geological and kinematic relationship with neighbouring seismic facies units.

As explained in chapter 3.2, the seismic dataset of this study is heterogeneous; since each seismic survey has been acquired and processed differently. Therefore, the resolution and the seismic reflectivity content is inevitably varying from one survey to another. This concerns all the criteria defining a seismic facies, as discussed in the above paragraph. The quality type of the seismic profiles is obviously the major criteria to estimate the capacity of a seismic image to highlight a seismic facies. In that sense, only the best quality profiles of type 1 and 2 were selected to run such tasks (Figure 3-9). Noisy seismic parts of sections are avoided during the seismic facies analysis, or always taken into account in the uncertainty evaluation. It is noted that this kind of analysis is usually carried out on 3D seismic surveys, that have most of the time a higher resolution than 2D seismic, and because seismic facies may easily be mapped or laterally correlated. Therefore, in our case this analysis applied on 2D seismic sections does not intend to bring clear answers about the lateral seismic facies development or about the exact geometries of their associated depositional environments. Rather, it was possible to propose a seismic facies catalog for the entire sedimentary cover that present the basic concepts and first applications around this kind of study.

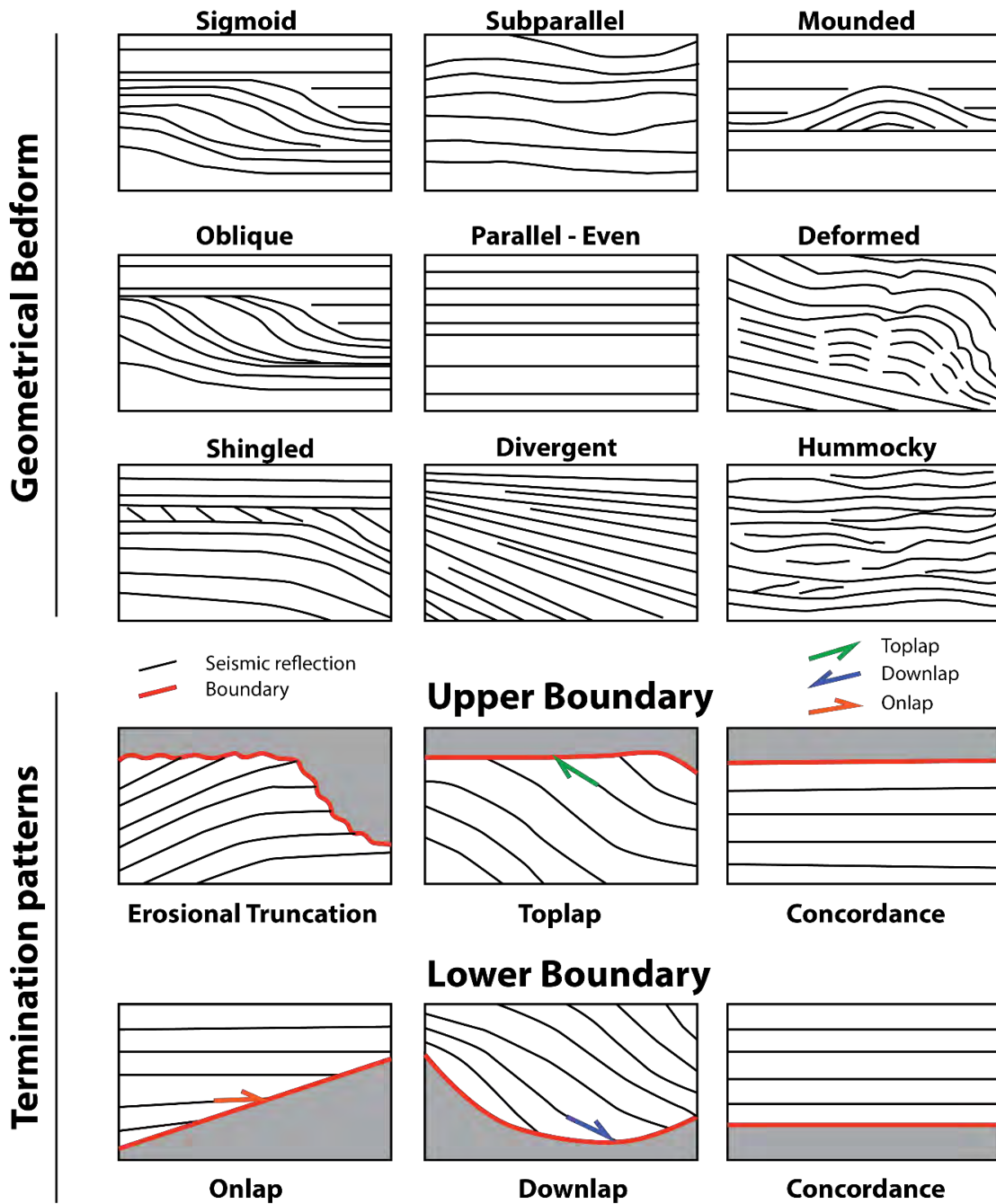


Figure 4-10 : Types of geometrical bedform (top, modified from Ramsayer (1979)) and termination patterns (bottom, modified from (Chopra & Marfurt, 2005 and Vail, 1987) for seismic facies analysis.

Seismic attributes are particularly suitable for supporting the seismic facies analysis. The Kingdom software proposes a set of seismic attribute (IHS Markit, 2017) very easily calculated from a seismic section (instantaneously). A seismic attribute is a quantitative measure of a seismic characteristic of interest (Chopra & Marfurt, 2005). It is a quantity extracted or derived from seismic data that may enhance information in order to highlight specific geological features. For our study, only three types of seismic attributes were used (Figure 4-12), especially for characterizing carbonate platform seismic facies of the Upper Malm unit (Hauvette, 2020):

Pseudo relief seismic attribute is derived from the amplitude seismic by applying RMS calculation in addition to Hilbert transform (Chopra & Marfurt, 2008). It brings a sort of relief to high amplitude

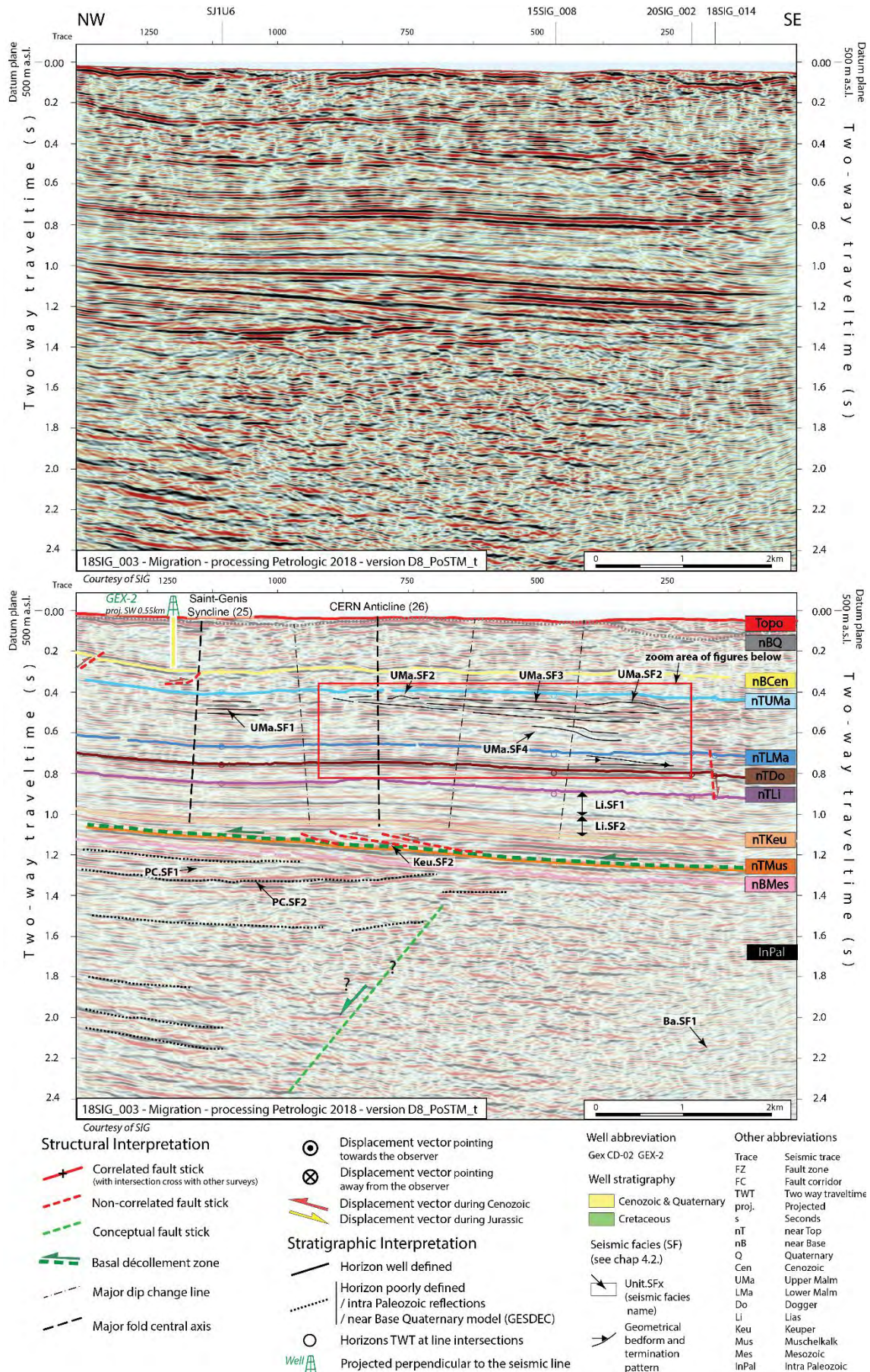


Figure 4-11 : Seismic profile 18SIG_003 uninterpreted (top) and interpreted (bottom) along with seismic facies analysis. See Encl 21 for detailed seismic interpretation of line 18SIG_003. See Figure 4-7 for location of seismic line.

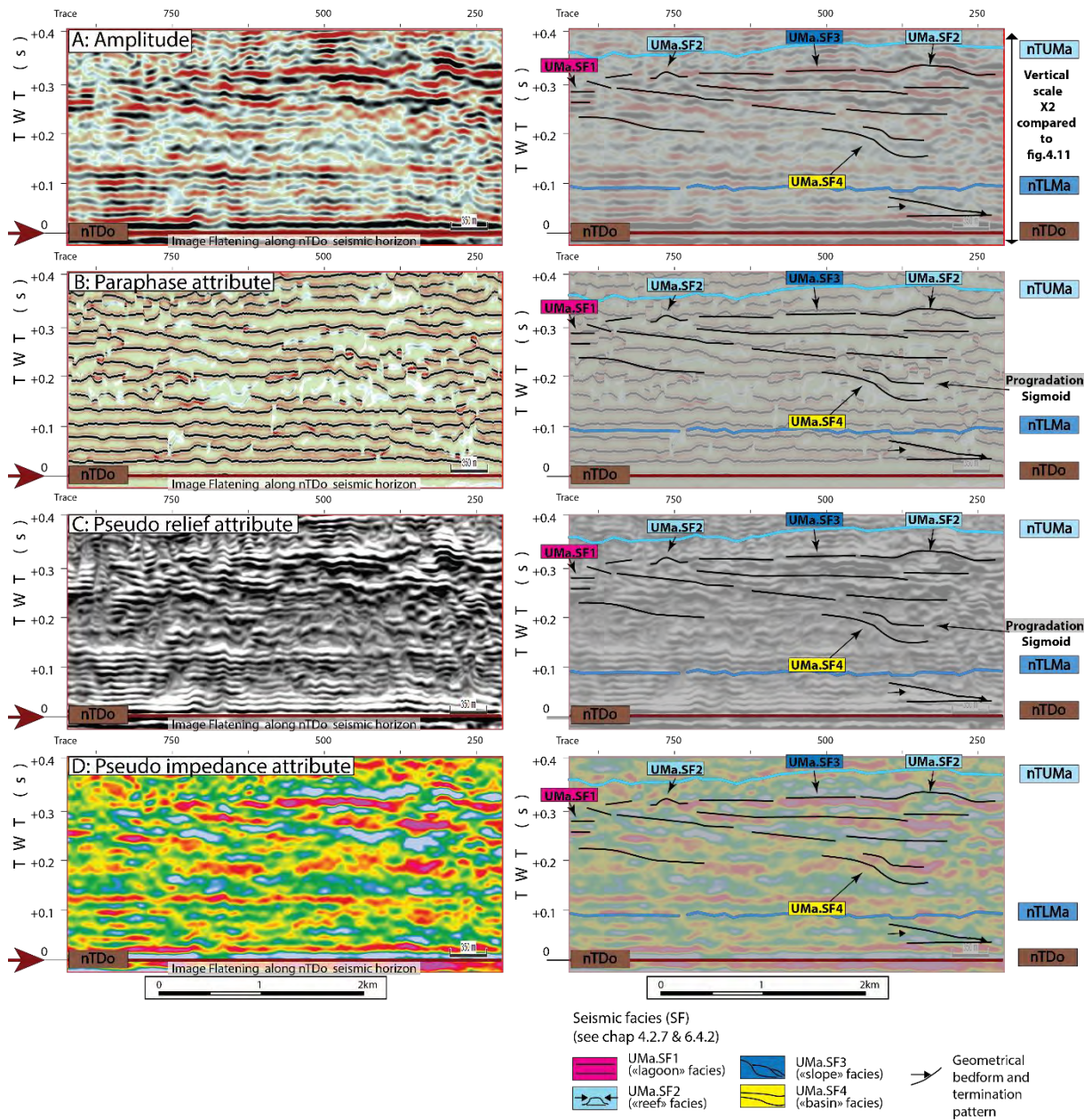


Figure 4-12 : Example of seismic attributes that help for the seismic facies analysis. The four left images are different versions of attributes displays without any interpretation of profile 18SIG_003 (see polygon extraction on Figure 4-11). A: amplitude, B: Paraphase attribute, C: Pseudo relief attribute, D: Running sum or pseudo-impedance attribute. The four right images are the same data as left but with the seismic facies interpretation on top of them. Geometries of seismic facies are highlighted with black lines. Arrows are indicating terminations, and a tentative interpretation of the depositional environments has been proposed. This will be detailed in more details in the next parts. Note that the figures are flattened along nTDo seismic horizon to analysis the seismic facies nearly parallel to the stratification of the Malm. See Encl 21 for detailed seismic interpretation of line 18SIG_003. See Figure 4-7 for location of seismic line.

contrast reflections and may emphasize geological features such as faults, channels and bright spots (Figure 4-12).

Paraphase seismic attribute shows the instantaneous phase and removes the reflective background component in between change of phase. It appears to be a very useful attribute for interpreting the geometry and the termination of a seismic facies (Medina et al., 2018) (Figure 4-12).

Running Sum or pseudo-impedance attribute (Subrahmanyam & Rao, 2008) provides an approximation to acoustic impedance. The algorithm applies a simple formula on the amplitude that approximates an

integration of the trace with a half-sample time shift. On the contrary to full seismic inversion, there is a lack of the of the low frequency trend. However, it may give an idea about the impedance (velocity*density) trends, which is very interesting for a seismic facies analysis (acoustic impedance inform about the lithologies) (Figure 4-12).

The tool of *flattening* was often used as well. It consists in taking a seismic horizon as a temporary new flat datum. This tool gives the possibility to observe or interpret a seismic profile parallel to a seismic horizon; therefore, it removes any structural trend. This is particularly adapted for stratigraphical interpretation (Figure 4-12).

In the following parts from 4.1.4 to 4.1.12 each Mesozoic sub-unit is described in detail in terms of seismic facies according to the criteria defined above. This catalogue is a descriptive overview of the seismic characteristics of each stratigraphical unit. It can be seen as a tool for the next seismic interpretation studies. The discussion and conclusion that come out of these descriptions are presented in chapters 6 and 7. The naming of the seismic facies is composed of the abbreviation of the stratigraphic unit (refer to the stratigraphic column on Figure 2-3) followed by a numbering of seismic facies (SF).

4.1.4 Paleozoic interval

The domains of the Paleozoic units that can be interpreted on the seismic profiles are comprised between the near Base Mesozoic horizon down to the end of the profiles. Considering the depth penetration of seismic data, approximately 7,5km of thickness of the Paleozoic units can be imaged in the best case. Indeed, on seismic profile HR530 (Encl_70), which is a good representation of the deepest seismic reflection imaging, we can see that in a range of approximately 3s TWT below near Base Mesozoic it is still possible to indentify seismic reflections. Taking into account the average velocity of 5000m/s for this interval (Gruber, 2012; Sommaruga et al., 2012), this 3s TWT range corresponds to a 7,5km depth range. This Pre-Mesozoic interval may be divided into two subunits, the crystalline basement and the Permo-Carboniferous through deposits. The latter is composed of deltaic siliciclastic deposits infilling half-grabens (or grabens) developed in the basement (Rusillon, 2017; Signer & Gorin, 1995). This continental deposit contains in some parts organic matter rich layers which create high amplitude reflections corresponding to seismic facies PC.SF2 (Table 4-2). The rest of the deposits is represented by seismic facies PC.SF1 with low amplitude and marked by erosional truncation along near Base Mesozoic (nBMes) and by onlaps and dowlaps along the faulted top basement. The crystalline basement is represented by chaotic low reflectivity seismic facies Ba.SF1 (Figure 4-11).

The **near Base Mesozoic (nBMes)** horizon in the Geneva Basin can be identified fairly easily as a peak with relatively high amplitude and low frequency, as it is an erosional surface (toplaps below and concordance on top). Indeed, the transition between the sandstone dominated facies of Permo-Carboniferous age with the Triassic evaporites may produce a high acoustic impedance contrast. It is not clear if the Triassic Buntsandstein siliciclastic unit that has a regular thickness in the GGB around 15m (Rusillon, 2017), which is below the seismic resolution, may be present just below the near Base Mesozoic seismic horizon.

Seismic facies	Reflection characteristics	Lithological Interpretation	Sedimentological Interpretation
	<p>PC.SF1:</p> <ul style="list-style-type: none"> - Amplitude: Low - Frequency: Intermediate to low - Continuity: Semi-continuous to discontinuous - Geometry: Subparallel to Hummocky - Termination: <ul style="list-style-type: none"> ->Near Top: Erosional truncation ->Near Base: Downlaps/onlaps to concordance 	Sandstones to argillaceous sediments	Continental deposits Deltaic
	<p>PC.SF2:</p> <ul style="list-style-type: none"> - Amplitude: High - Frequency: Intermediate to low - Continuity: Semi-continuous - Geometry: Oblique - Termination: <ul style="list-style-type: none"> ->Near Top: Toplaps to erosional truncation ->Near Base: Downlaps/onlaps to concordance 	Coal-bearing sandstones to argillaceous sediments	Continental deposits Deltaic
	<p>Ba.SF1:</p> <ul style="list-style-type: none"> - Amplitude: Low - Frequency: High - Continuity: Discontinuous - Geometry: Chaotic 	Crystalline basement	Rifting

Table 4-2 : Seismic facies description of the Pre-Mesozoic unit. Sedimentological interpretation is based on Brentini (2018) and Rusillon (2017). See respectively Encl 70 and Encl 19 for detailed seismic interpretation of lines HR530 and 18SIG_001.

A more complex facies distribution of the Permo-Carboniferous deposits had been proposed by Naef & Madritsch (2014) and Nagra (2014) among others, with three types of infill (upper, middle and lower Sub-units) in northern Switzerland. Since in our area, the two main wells Humilly-2 and Faucigny-1 (Figure 4-7) have barely penetrated the Permo-Carboniferous unit, it was not possible to calibrate such complex Paleozoic facies distributions. It would have been too much subjective to attempt such interpretation of this unit. In addition, the seismic resolution of our dataset does not allow to interpret with enough certainty the top of the basement or even continuous layering of the clastic deposit on top, therefore only Intra-Paleozoic (InPal) segments of reflections have been picked. This makes it possible to obtain a general insight into the location of the main half grabens or grabens structures, when observing interpreted seismic sections of this study.

4.1.5 Triassic interval

The **near Top Muschelkalk (nTMu)** seismic horizon is placed in between the evaporites (gypsum and halite) of the Upper Triassic Unit (Keuper) and the dolomites of the Middle Triassic Unit (Lettenkohle). It is represented by a trough based on Humilly-2 seismic to well tie. The thickness of the Middle Triassic unit is relatively constant over our area (around 135m (Brentini, 2018; Rusillon, 2017), even so it is supposed to increase northeastward (Figure 2-5), according to the thickness maps from (Sommaruga et al., 2017). Therefore, the Muschelkalk seismic interval appears as a regular doublet of low frequency and high amplitude reflections (Mu.SF1, Table 4-3). This strong Muschelkalk internal impedance contrast may be produced by contact between the Muschelkalk anhydrite layers overlain by the

Seismic facies	Reflection characteristics	Lithological Interpretation	Sedimentological Interpretation
	<p>Mu.SF1:</p> <ul style="list-style-type: none"> - Amplitude: High - Frequency: Low - Continuity: Continuous to semi-continuous - Geometry: Parallel - Termination: <ul style="list-style-type: none"> ->Near Top: Concordance ->Near Base: Concordance 	Dolomite and anhydrites (evaporites) dominated unit	Supratidal/ intertidal deposit

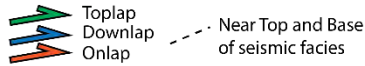


Table 4-3 : Seismic facies description of the Muschelkalk unit. Sedimentological interpretation is based on Brentini (2018) and Rusillon (2017). See Encl 20 for detailed seismic interpretation of line 18SIG_002.

Seismic facies	Reflection characteristics	Lithological Interpretation	Sedimentological Interpretation
	<p>Keu.SF1:</p> <ul style="list-style-type: none"> - Amplitude: High - Frequency: Moderate to low - Continuity: Continuous - Geometry: Parallel - Termination: <ul style="list-style-type: none"> ->Near Top: Concordance ->Near Base: Concordance to onlaps 	Dolomite and anhydrites (evaporites) dominated unit	Supratidal/continental deposit
	<p>Keu.SF2:</p> <ul style="list-style-type: none"> - Amplitude: High - Frequency: Moderate to low - Continuity: Semi-continuous - Geometry: Deformed, duplexes - Termination: <ul style="list-style-type: none"> ->Near Top: Concordance / faulted (thrusts) ->Near Base: Concordance 	Dolomite and anhydrites (evaporites) dominated unit	Supratidal/continental deposit
	<p>Keu.SF3:</p> <ul style="list-style-type: none"> - Amplitude: Low - Frequency: Low - Continuity: Discontinuous - Geometry: Mounded, deformed - Termination: <ul style="list-style-type: none"> ->Near Top: Concordance to toplaps ->Near Base: Concordance to onlaps 	Halite dominated unit	Carbonate platform deposit

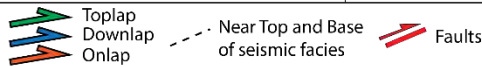


Table 4-4 : Seismic facies classification of the Keuper unit. Sedimentological interpretation is based on Brentini (2018) and Rusillon (2017). See respectively Encl 21, Encl 38&85, and Encl 20 for detailed seismic interpretation of lines 18SIG_003, 88SVO07 and 18SIG_002.

dolomites of the Lettenkohle (see stratigraphic column on Figure 2-3). This unit is in concordance with top and base seismic horizons.

The **near Top Keuper (nTKeu)** marks the transition from the evaporite alternations (dolomites, anhydrites and shales) to the siliciclastic Rhaetien layers (sandstone and clay unit) (Clerc, 2016; Gorin et al., 1993; Paolacci, 2012). The contrast corresponds to a very strong peak clearly visible on most lines and seismic to well ties. In terms of seismic facies, the gypsum and halite deposits may be detected by pillow mound-like shapes with internal “transparent” texture (Keu.SF3, Table 4-4), when it may have been subject to halokinetic movements or lateral migrations in relation to deformation. Otherwise, if it was deposited in a conformable layering, overlain by the anhydrite-dolomite

alternations it would be associated to seismic facies Keu.SF1 (Table 4-4). The main décollement level is placed at the bottom of the Keuper unit, as a consequence a major part of compressive structures (thrusts) have termination just on top of near Top Muschelkalk horizon. Several intra-Triassic thrusts (not developed above near Top Keuper) forming duplexes in some cases are interpreted in our area, as proposed Sommaruga et al., (2012). The resulting “deformed” seismic facies around these structures is represented by Keu.SF2 (Table 4-4). The thickness of the overall Triassic unit is increasing northward (Schori, 2021), in the Jura direction, corresponding to the most deformed areas (duplications of Triassic layers, see Figure 6-7).

4.1.6 Liassic interval

The **near Top Lias (nTLi)** corresponds to a high amplitude peak from our seismic horizon convention (Figure 4-2 and Figure 4-6), which depicts the boundary between the Toarcien shaly interval and the limestone layering of the Aalenien-Bajocien (Dogger) series. The Lias beds interval may be vertically divided into two parts roughly equal in thickness. The lower part is a limestone dominated unit embodied by seismic facies Li.SF2 (Table 4-5) showing usually either two or four high amplitude reflections, depending on the frequency content of the seismic profile. The upper part is a shale dominated layer with alternations of limestones deposits. The related seismic facies is often displayed as a succession of seismic reflections moderate in frequency and amplitude (Li.SF1, Table 4-5). The overall Lias Unit is highly varying in thickness throughout the area of study. These variations seem to be linked in some cases to the main NW-SE and E-W strike-slip faults (syn-sedimentary faulting) or to major normal faulting oriented NE-SW (observed in the Humilly area, see chapter 6.4.1). Several seismic profiles seem to confirm the trend given by the Humilly-2 well and the correlation with the Haute-Chaine (Brentini, 2018; Rusillon, 2017), which suggests that thickness variations of the Lias Unit are mostly coming from the lower limestone dominated unit (Figure 4-13).

Seismic facies	Reflection characteristics	Lithological Interpretation	Sedimentological Interpretation
	<p>Li.SF1:</p> <ul style="list-style-type: none"> - Amplitude: High to moderate - Frequency: Moderate - Continuity: Semi-continuous to continuous - Geometry: Parallel to subparallel - Termination: <ul style="list-style-type: none"> ->Near Top: Concordance to few toplaps ->Near Base: Concordance to few onlaps 	Shale dominated unit	Marine deep offshore
	<p>Li.SF2:</p> <ul style="list-style-type: none"> - Amplitude: High to moderate - Frequency: Low - Continuity: Continuous to semi-continuous - Geometry: Parallel to subparallel - Termination: <ul style="list-style-type: none"> ->Near Top: Concordance to toplaps ->Near Base: Concordance to downlaps 	Limestone dominated unit	Carbonate platform deposit

Table 4-5 : Seismic facies description of the Lias unit. Sedimentological interpretation is based on Brentini (2018) and Rusillon (2017). See Encl 38 & 85 for detailed seismic interpretation of line 88SVO07.

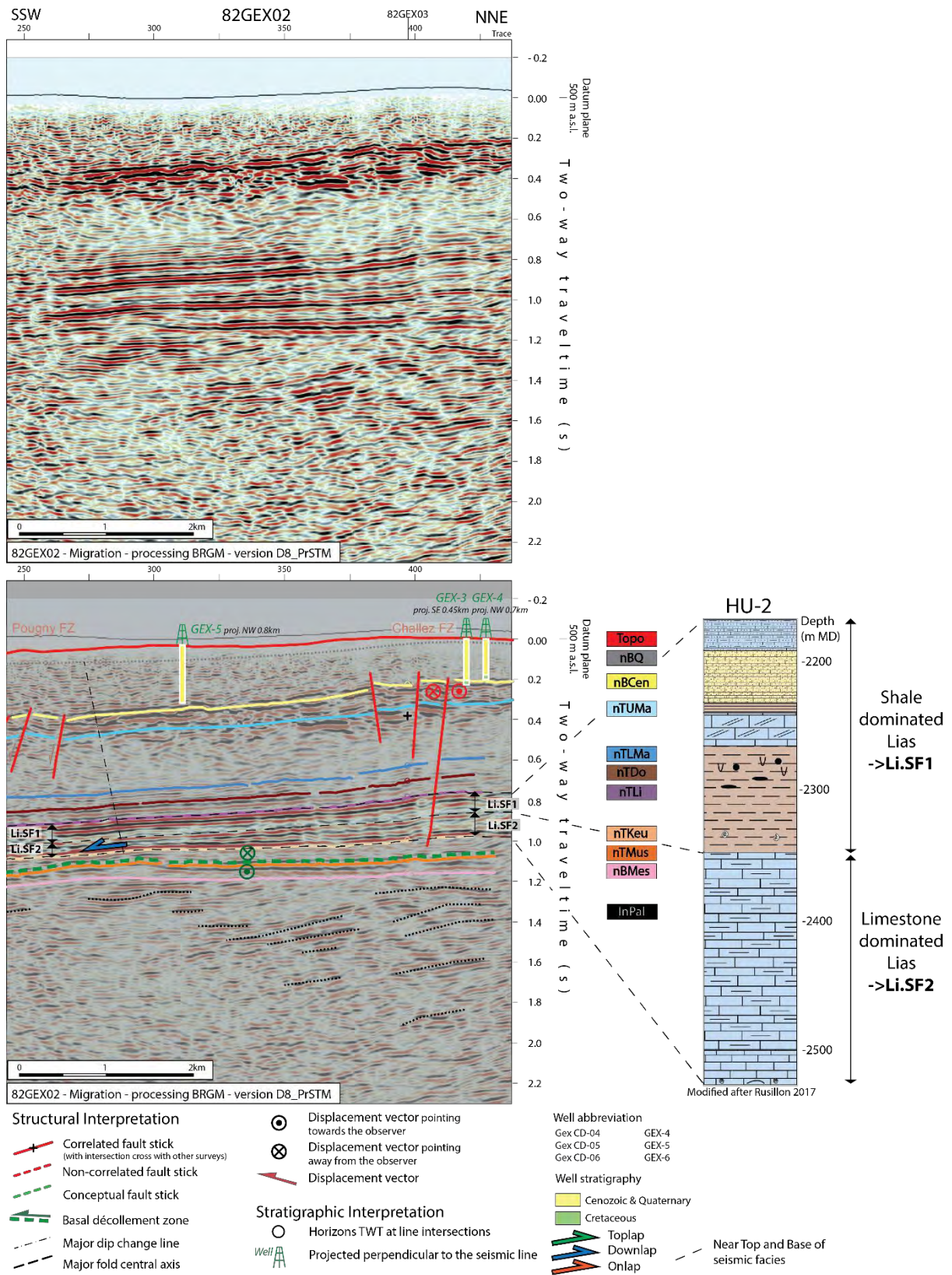


Figure 4-13 : Division of the Lias unit into two seismic facies that one may correspond to a more shaly interval (upper part) and the other one to a limestone dominated part (lower part). This latter seems to be the most varying in thickness of the two, in relation to main strike slips faults systems (Clerc & Moscariello, 2020; Rusillon, 2017). See Encl 39 for detailed seismic interpretation of line 82GEX02. See Figure 4-7 for location of seismic line.

4.1.7 Dogger interval

The **near Top Dogger (nTDo)** is represented as a trough seismic reflection according to Humilly-2 seismic to well tie (Figure 4-5) and is pointing to a contrast between the Oxfordian marls and the overlying bioclastic limestones of the Callovian. The Dogger interval is a highly limestone dominated unit with several marly alternations that yield a moderate amplitude and frequency, parallel seismic facies (Do.SF1, Table 4-6). The reflections are mainly onlapping the near Top Lias horizon along NE-SW lineaments in relation to the orientation of the sedimentary basin. However, major faults may also play a role in the thickness changes of the unit (Rusillon, 2017; Signer & Gorin, 1995).

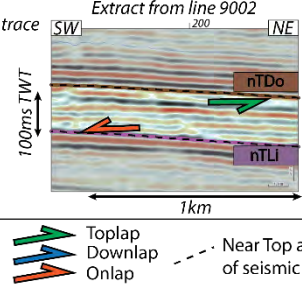
Seismic facies	Reflection characteristics	Lithological Interpretation	Sedimentological Interpretation
	Do.SF1: - Amplitude: Moderate - Frequency: Moderate to low - Continuity: Continuous - Geometry: Parallel to Sigmoid - Termination: ->Near Top: Concordance to toplap ->Near Base: Concordance to onlaps	Carbonate dominated unit with mud intercalation	External platform/ramp / marine deep offshore

Table 4-6 : Seismic facies description of the Dogger unit. Sedimentological interpretation is based on Brentini (2018) and Rusillon (2017). See Encl 02 for detailed seismic interpretation of line 9002.

4.1.8 Lower Malm interval

The **near Top Lower Malm (nTLMa)** was attributed to the transition between the Oxfordian marls (“Couches d’Effingen-Geissberg”) and the overlying massive limestones of the Upper Malm Unit. The marly facies of the Lower Malm Unit are visible on the seismic profiles as a thin continuous layering of seismic reflections (high frequency, high to moderate amplitude, LMa.SF1, see Table 4-7). The near Top Lower Malm Unit may be confused in some areas with relatively similar seismic facies of the overlying “Calcaires lités”. Few downlaps have been witnessed of the thin bedding of this layer in relation to its base seismic horizon (near Top Dogger).

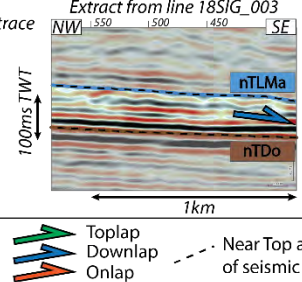
Seismic facies	Reflection characteristics	Lithological Interpretation	Sedimentological Interpretation
	LMa.SF1: - Amplitude: High to moderate - Frequency: High - Continuity: Continuous to semi-continuous - Geometry: Paralell to slightly sigmoid - Termination: ->Near Top: Concordance ->Near Base: Concordance to few downlaps	Alternations marls/ limestones	Marine deep offshore

Table 4-7 : Seismic facies description of the Lower Malm unit. Sedimentological interpretation is based on Brentini (2018) and Rusillon (2017). See Encl 21 for detailed seismic interpretation of line 18SIG_003. See Table 4-11 for stratigraphic details.

4.1.9 Upper Malm interval

The **near Top Upper Malm (nTUMa)** is certainly the most difficult seismic horizon to interpret, as it separates similar lithological layers of the Tithonian limestones and dolomites and the Berriasian limestones. However, the overall seismic facies contrast between Cretaceous deposits with Upper Malm deposits still gives an approximate positioning of this interface. Indeed, some parts of the “*complexe récifal*” may have a relatively lower amplitude of seismic reflections than the Cretaceous unit that has more consistently higher amplitude (Table 4-8 and Table 4-9).

We can divide vertically and laterally the Upper Malm Unit by several types of seismic facies. First the seismic facies UMa.SF4 (Table 4-8) has a “transparent” texture (low amplitude and frequency), and is located approximately from the “*Calcaire lités*” (that may look like LMa.SF1 as explained in 4.1.8) until the base of the “*Complexe récifal*” (see stratigraphic column on Figure 2-3). This texture may be explained by the massive nature of the limestones that define this part. The overlying layers are represented by three seismic facies that may vary laterally across this layer, in relation to their depositional environment along the carbonate platform (Figure 4-14). The polarity of the sedimentary basin remains NW-SE respectively for the proximal and distal parts. As this unit is marked by a major marine regression with a progradation of the sequences towards SE, we may expect seismic facies with

Seismic facies	Reflection characteristics	Lithological Interpretation	Sedimentological Interpretation
	<p>UMa.SF1: </p> <ul style="list-style-type: none"> - Amplitude: High - Frequency: Moderate - Continuity: Continuous - Geometry: Parallel to subparallel - Termination: <ul style="list-style-type: none"> ->Near Top: Concordance ->Near Base: Concordance 	Dolomite dominated unit	Lagoon Inner platform
	<p>UMa.SF2: </p> <ul style="list-style-type: none"> - Amplitude: Low to moderate - Frequency: Low - Continuity: Discontinuous to semi-continuous - Geometry: Mounded - Termination: <ul style="list-style-type: none"> ->Near Top: Concordance to toplap ->Near Base: Downlap 	Bioconstructed Limestone unit	Reef
	<p>UMa.SF3: </p> <ul style="list-style-type: none"> - Amplitude: High to moderate - Frequency: High to moderate - Continuity: Continuous to semi-continuous - Geometry: Sigmoid / clinofolds - Termination: <ul style="list-style-type: none"> ->Near Top: Toplap ->Near Base: Downlap 	Limestone dominated unit	Slope of carbonate platform
	<p>UMa.SF4: </p> <ul style="list-style-type: none"> - Amplitude: Moderate to low - Frequency: Moderate to low - Continuity: Semi-continuous - Geometry: Subparallel to sigmoid - Termination: <ul style="list-style-type: none"> ->Near Top: Concordance ->Near Base: Concordance 	Limestone dominated unit	Carbonate platform deposit

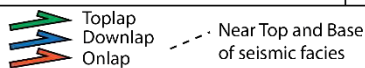


Table 4-8 : Seismic facies classification of the Upper Malm unit. Sedimentological interpretation is based on Brentini (2018) and Rusillon (2017). See Encl 21 for detailed seismic interpretation of line 18SIG_003. See Table 4-11 for stratigraphic details.

clinoform geometries dipping in this direction. The seismic facies classification of this unit is rather more conceptual than a proven and accurate demonstration. Indeed, only few wells give complete information about this layer (Thônex-1 and Humilly-2) and allow calibration of the seismic facies. Even for these two latter cited wells, the calibration of the seismic facies is difficult to achieve. An attempt of seismic facies interpretation was nevertheless realized, very much inspired by the detailed work of Paumard et al., (2017), which gives very meaningful examples of reefal depositional environment interpretation. Even so, our seismic facies related to the “Complexe récifal” is not accurately interpreted, it may foster thoughts for facilitating the future interpretation that will be done on the incoming 3D volume. In that sense, UMa.SF1 (Table 4-8) is characterized by high amplitude continuous and parallel seismic facies and may represent dolomitic lithologies corresponding to lagoon (inner platform) deposits (Figure 4-14). Seismic facies UMa.SF2 (Table 4-8) with a mound shape geometry and destructured internal seismic reflections may depict a reef platform margin or patch reef. As for depositional slope environment of carbonate platforms, we may define it seismically with seismic facies UMa.SF3 (Table 4-8). It is described as continuous to semi-continuous relatively high in amplitude and frequency with sigmoidal clinoforms for its geometry. As it has been detailed and proposed, in Meyer (2000); OCEN (1994); Rusillon (2017), we give in Figure 4-14 the approximative association of depositional environments related to carbonate platform with the stratigraphical formations present in the GGB. It is noted that patch reefs developed preferentially on inherited structural highs (Rusillon, 2017), therefore faults may give indications about the location of these sedimentary features (see chapter 6.4.2).

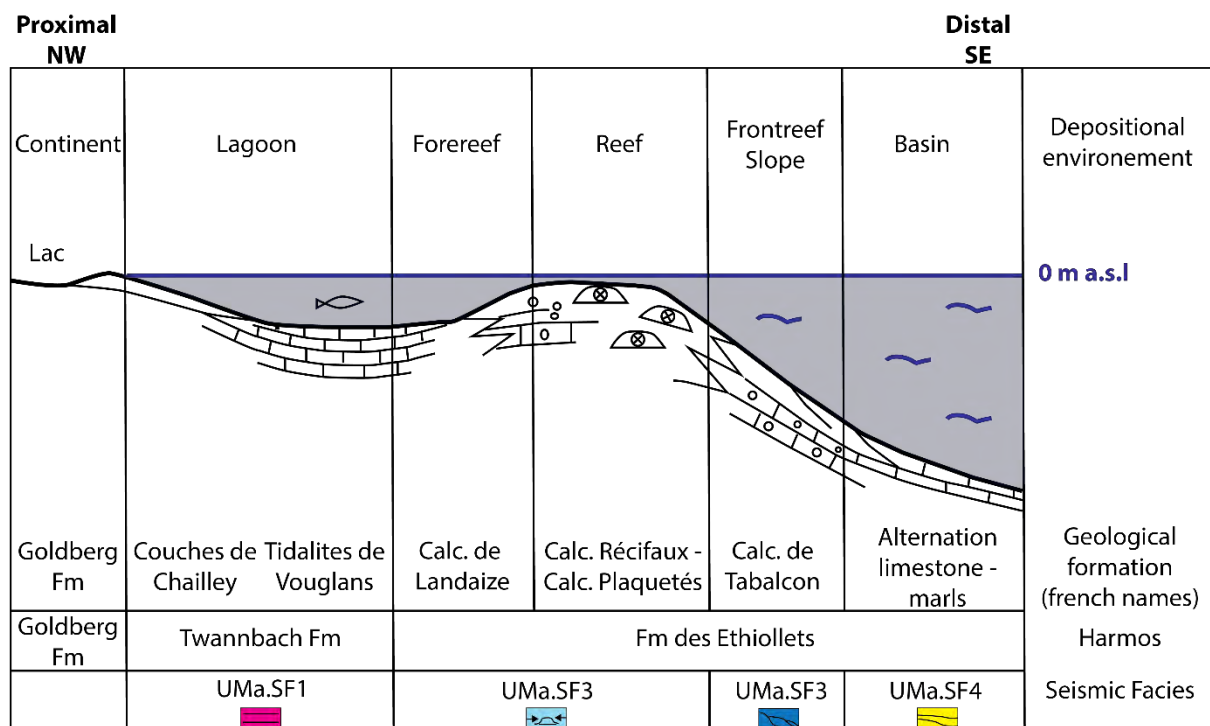


Figure 4-14 : Scheme of the depositional environments associated to the formations of the “complexe récifal” of the Kimmeridgian unit in the Fm des Ethiollets (HARMOS), inspired from the detailed work of Paumard, 2018 that gives clear seismic facies classification for each part of a reefal carbonate platform. See Figure 2-3 and Table 4-11 for complete stratigraphy.

4.1.10 Cretaceous and Eocene interval

The **near Base Cenozoic (nBCen)** seismic horizon corresponds to the transition between the siliciclastics from the Cenozoic unit and the massive limestones of the Cretaceous unit (Table 4-9). It is a complex boundary, as it is the result of the significant erosion of the Mesozoic cover in addition to the complicated Cenozoic deposits on top of it. First, it means that this horizon is marked by a non regular geometry (truncation) usually of the Urgonian Unit. However, it may be expected that the erosion has reached underlying formations (GEO-02 well has encountered directly the “Grand Essert” Formation while reaching the Cretaceous unit). Secondly, the Cenozoic deposits in contact with the Cretaceous unit may be variable, as it may be either (1) sandstones of the Siderolithic or (2) poudingue of the Gompholite unit or (3) the “Calcaires d’eau douce inférieurs” unit or (4) directly the “Marnes et grès bariolés”. Therefore, the impedance contrast of the Cretaceous-Tertiary unconformity may be highly heterogeneous, depending on the different possibilities of lithological contacts. In all cases, the corresponding seismic reflection should theoretically be a trough (cf seismic to well tie of Humilly-2 on Figure 4-5 and seismic polarity convention on Figure 4-2) as all Cenozoic deposits should have a smaller acoustic impedance value than the massive limestones of the Urgonian Unit (even for underlying formations in case of more important erosion of the Cretaceous unit). The strength of the amplitude and the frequency content of the near Base Cenozoic (nBCen) seismic horizon may nevertheless be variable. The surprising results of recent drilling of GEO-02 well (Chablais & Savoy, 2021) have allowed adding another interpretation related to this seismic horizon (Figure 4-15 and Figure 4-16). Indeed, as previously mentioned in this paragraph, the well has not reached the Urgonian limestones at this boundary but directly penetrated the underlying “Grand Essert” formation. If we consider the mean thicknesses of the Cretaceous formations over the Geneva Basin (Table 4-11), we can estimate the gap of the Cretaceous unit missing to around 147m of thickness. The drilling has witnessed a surprising 140m thickness of sandstones of the Siderolithic unit instead of the Cretaceous limestones, whereas these Eocene deposits were estimated before the drilling to a maximum of 40m thickness in the area. Therefore, a deep infill of possibly 140m thickness of Siderolithic in a topographic depression is very likely. The depression may have a tectonic and/or erosional origin, and the Siderolithic sandstones could be fluvial deposits (Figure 4-16), as suggested by Conrad & Ducloz, (1977) and Weidmann (1984). It also cannot be excluded that it consists in an accumulation of wind dune deposits (Chablais & Savoy, 2021). Such deposits were often supposed to be present, mostly in karsts or along fault planes (Serneels, 1993). These two cases are also possibilities that could replace the others hypothesis, but it has been decided to give a higher probability to the idea of a strong erosional event at nBCen horizon level creating large (several km) and deep (possibly 140m depth) depressions infilled by fluvial Siderolithic deposits (Figure 4-16). Indeed, the seismic to well tie of GEO-02 well using a VSP corridor stack (powerful calibration tool), suggests now a deeper seismic reflection of nBCen seismic horizon than it was proposed before the drilling (Figure 4-15). This seismic reflection is no longer the first high amplitude reflection underlying the low amplitude discontinuous seismic facies of the Molasse sediments (Cen.SF1, see 4.1.11), but would correspond to the very high amplitude and low frequency trough from one to three reflection loops below. This new definition of nBCen seismic horizon seems more coherent with the erosional truncation geometry that characterizes it, which is particularly well represented on seismic profile 18SIG_011 (Figure 4-15 and Figure 4-16). The interval including one to three seismic reflection loops above it would correspond to the Eocene deposits (Eoc.SF1, see Table 4-10). The new main interpretation about nBCen seismic horizon mentioned above is then supported by the seismic to well tie of GEO-02,

Seismic facies	Reflection characteristics	Lithological Interpretation	Sedimentological Interpretation
<p>Extract from line 15SIG_008</p> <p>trace</p> <p>100ms TWT</p> <p>0.5km</p> <p>nBCen</p> <p>nTUMa</p>	<p>Cre.SF1:</p> <ul style="list-style-type: none"> - Amplitude: High to moderate - Frequency: Low to moderate - Continuity: Continuous to semi-continuous - Geometry: Parallel - Termination: <ul style="list-style-type: none"> ->Near Top: Concordance to erosional truncation ->Near Base: Concordance 	Limestone dominated unit	Subtidal to external carbonate platforme/ rampe
<p>Extract from line 9001</p> <p>trace</p> <p>100ms TWT</p> <p>0.5km</p> <p>InCen</p> <p>nBCen</p> <p>nTUMa</p>	<p>Cre.SF2:</p> <ul style="list-style-type: none"> - Amplitude: Moderate - Frequency: Low to moderate - Continuity: Semi-continuous to discontinuous - Geometry: Deformed - Termination: <ul style="list-style-type: none"> ->Near Top: Concordance to erosional truncation ->Near Base: Concordance 	Limestone dominated unit	Subtidal to external carbonate platforme/ rampe

Table 4-9 : Seismic facies description of the Cretaceous unit. Sedimentological interpretation is based on Brentini (2018) and Rusillon (2017). See respectively Encl 13 and Encl 01 for detailed seismic interpretation of lines 15SIG_008 and 9001. See Table 4-11 for stratigraphic details.

Seismic facies	Reflection characteristics	Lithological Interpretation	Sedimentological Interpretation
<p>Extract from line 18SIG_011</p> <p>trace</p> <p>100ms TWT</p> <p>0.5km</p> <p>InCen</p> <p>nBCen</p> <p>nTUMa</p>	<p>Eoc.SF1:</p> <ul style="list-style-type: none"> - Amplitude: High to moderate - Frequency: High to moderate - Continuity: Continuous to semi-continuous - Geometry: Oblique to Hummocky to subparallel - Termination: <ul style="list-style-type: none"> ->Near Top: Concordance to toplap ->Near Base: Downlap/Onlap 	Sandstone unit	Fluviatile?

Table 4-10 : Seismic facies description of the Siderolithic (Eocene) formation. Sedimentological interpretation is based on Brentini (2018) and Rusillon (2017). See Encl 29 for detailed seismic interpretation of line 18SIG_011.

but also, by the erosional geometry of the newly defined seismic reflection and finally by the characteristics of the seismic facies attributed to the Eocene fluviatile deposits. This seismic facies Eoc.SF1 consists in relatively high amplitude and high frequency seismic reflections with hummocky to subparallel geometries, which are typical seismic characteristic of fluviatile deposits (Gong et al., 2013; Morend, 2000). Seismic profile 18SIG_011 is showing a nice representation of this seismic facies geometry, with possible seismic features corresponding to laterally stacked channels (Figure 4-16).

These new information increases nevertheless the uncertainty related to nBCen seismic horizon, by at least the maximum thickness in between the new nBCen seismic horizon and the approximation of the supposed top horizon of the Eocene deposits. When they are continuous enough, the seismic reflection at the top of seismic facies Eoc.SF1 (Table 4-10) was picked and named as “Intra Cenozoic” horizon, or InCen. As we have only few information about the relationship between the erosion of Cretaceous interval and the Siderolithic deposits, it is still possible that this horizon InCen could corresponds to nBCen seismic horizon, and that the presence of Siderolithic deposits in Geo-02 is explained by either an infill of a Karst feature or a fault plane. The most probable scenario remains the case of a stratiform deposition of the Siderolithic on top of highly eroded Cretaceous unit (Figure 4-16).

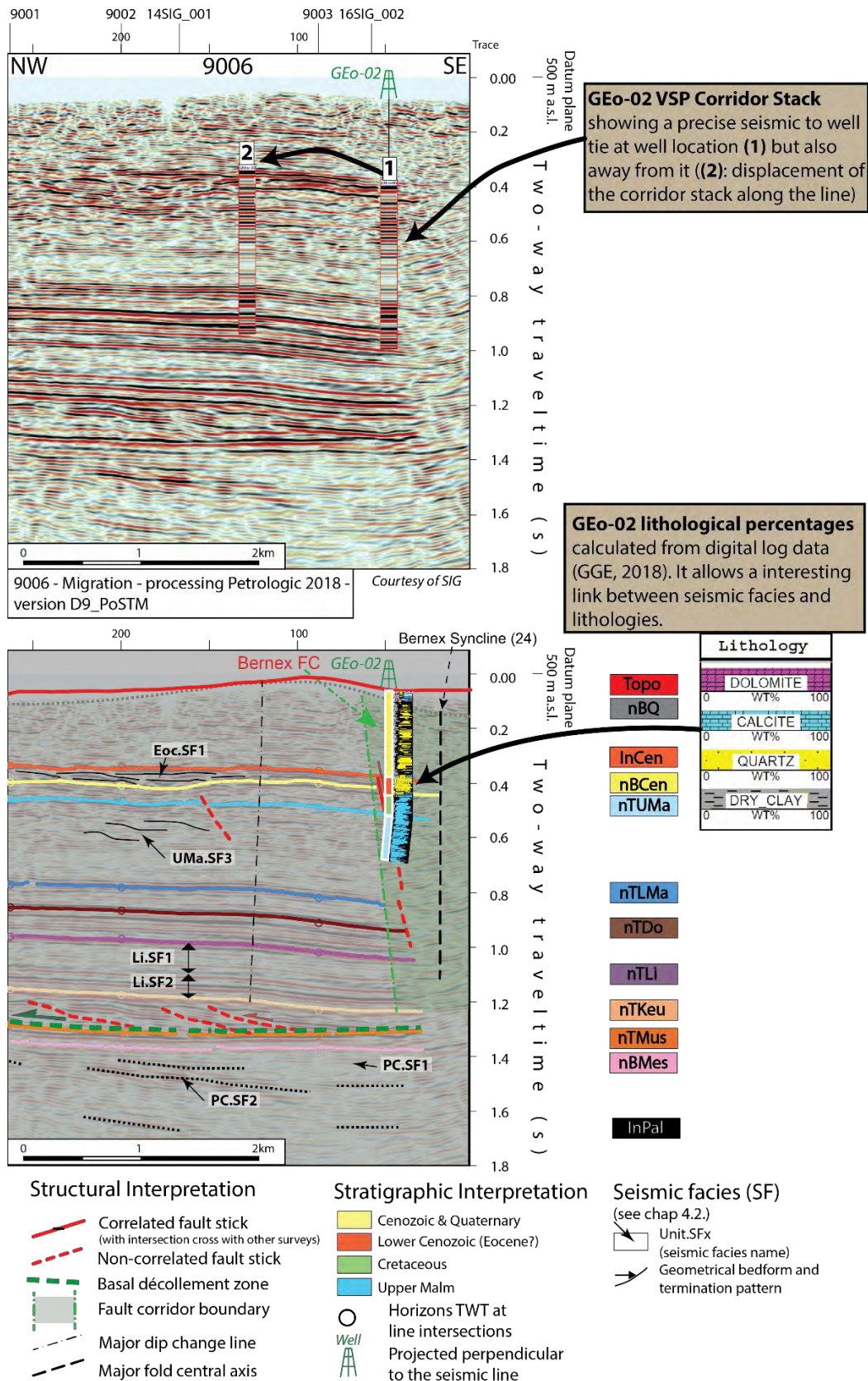


Figure 4-15 : Seismic (line 9006) to well tie of well GGeo-02 with the use of a corridor stack (top section) that support the hypothesis of a major unconformity along nBCen seismic horizon with large (km) and deep infill of sandstones of the Siderolithic deposits (possibly 140m thickness, bottom section). Hence, seismic facies Eoc.SF1 is proposed for characterizing this possible fluvialite deposits. With this new information about the possibly thick Eocene layer, the uncertainty around nBCen has increased and correspond now to the difference of depth between the two possibilities around nBCen. See Encl 06 for detailed seismic interpretation of line 9006. See Figure 4-7 for location of seismic line.

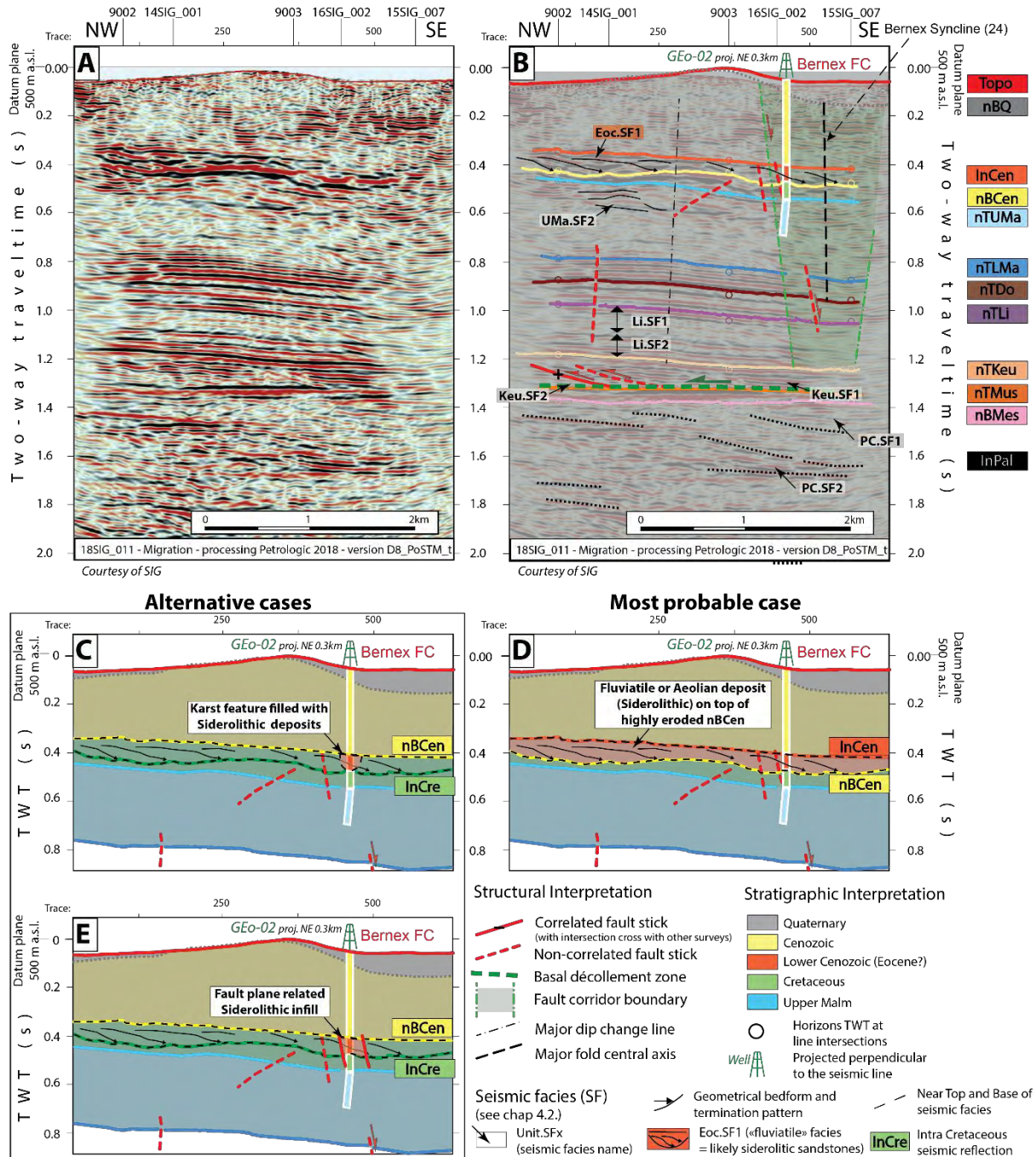


Figure 4-16 : Seismic profiles 18SIG_011 uninterpreted (A: top left) and interpreted (B: top right). The new information (Geo-02) about the Siderolithic formation allow reconsidering the positioning of near Base Cenozoic seismic horizon. The corresponding seismic horizon initially interpreted before the drilling was picked along the first high amplitude seismic reflection below the low amplitude and discontinuous seismic facies of the Molasse unit. However, according to seismic to well tie of GGeo-02 that made use of a VSP corridor stack (Figure 4-15) for accurate results, we can consider nBCen seismic horizon three loops of seismic reflections below the previous interpretation. Moreover, on both profiles 18SIG_011 and 9006 (Figure 4-15) the newly interpreted nBCen seismic horizon has clearly a geometry of erosional truncation. Both sections may contain geometries of laterally stacked channels inside seismic facies Eoc.SF1. Below the seismic section are conceptual geological models of the Siderolithic deposition (C, D and E), based on seismic interpretation of seismic profiles 18SIG_011 and 9006 jointly with geological and geophysical results of drilling GGeo-02. A: The most probable case (D) assumes an important erosion of nBCen horizon (possibly up to 140m thickness of erosion, as observed in GGeo-02 well) with an infill of approximately the same thickness of Siderolithic deposits. This could be the case at least in the area around GGeo-02 well. C: Another possibility could be that the Siderolithic unit observed in the GGeo-02 well corresponds to an infill of a karstic feature such as a doline. E: Another considered scenario would be that GGeo-02 well was drilled inside a fault plane (target of the drilling) with an infill of Siderolithic deposits. See Encl 29 for detailed seismic interpretation of line 18SIG_011. See Figure 4-7 for location of seismic line.

Chapter 4

Stratigraphical Units	True Thickness LEP wells (m)			Known Thickness GVA Basin (m)			Geo-01	Thônex-1	Humilly-2	Geo-02
	min	max	mean	min	max	mean				
M&G bariolés	8.7	86.9	47.8	250	955	602.5	308	954.6	363	571
Calcaires inférieurs	8.7	38.6	23.65	0	30	15	68	?	?	21
Gompholite	1.40	42.1	21.75	0	50	25	3.5	-	-	-
Sidérolithique	0	0	0	0	40	20	0	12.1	7.5	139.9
Aptien à orbitoline	8.3	8.7	8.5	0	10	5	-	-	-	-
Urgonien B+J	85	130	107.5	80	132	106	19	94	124.5	-
Grand Essert	21.3	91	56.15	90	100	95	87	121.8	105	54
Calc-AR			0.8	0	12	6	n.d.	n.d.	n.d.	n.d.
Calc-Roux	5.3	39.3	22.3	10	40	25	18.5	21.2	25	37
MArz-Guiers	1.30	11.30	6.3	15.00	27.00	21	23	14.60	23.00	22.00
Chambotte	3.20	20.70	11.95					16.50		
Vions	31.9	52.4	42.15	20	30	25	45	16.4	37	24
Pierre Châtel	24.1	30.1	27.1	30	45	37.5	14	39.2	60	41
Goldberg	13.6	17.5	15.55	30	38	34	33.5	23.8	34	30
TOTAL Thick. Cretaceous	194	401	298.3	275	434	354.5	240	347.5	408.5	208
Tidalites	-	-	-	80	120	100	96.56	143.4	163	122
Landaize	-	-	-	20	150	85	-	43.6	141	27
Calcaires récifaux	-	-	-	20	30	25	-	93	149	62
Tabalcon	-	-	-	20	30	25	-	80	121	62
Ccéphalo/Cmicr. beiges (Couvaloup)	-	-	-	50	100	75	-	97.4	252	76
Alt. Calc.&marnes/Calc. Pseudolitho	-	-	-	80	120	100	-	235.6	85	23.7

Thickness in italic : biased by erosion, faults, uncomplete drilled units (TD), or being described only in one well

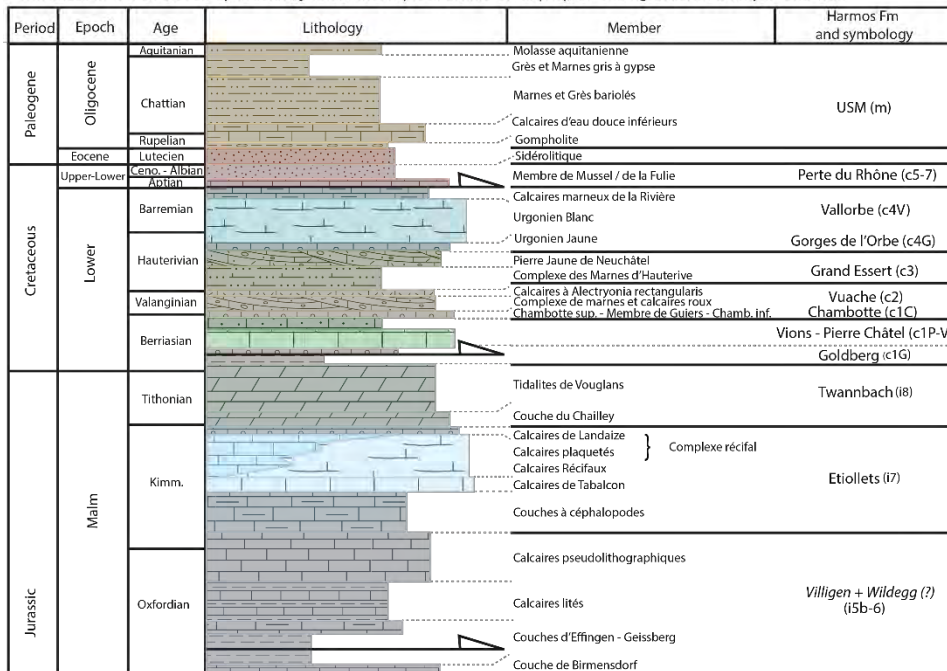


Table 4-11 (above) and associated stratigraphic column (below): This table taken from Chablais & Savoy (2021) compiles the thickness values of each formation that have been reached by well Géo-02, in comparison to surrounding wells in the GGB. We can see the thickness gap of the Urgonian formation in addition to a part of the Grand Essert formation. This gap corresponds exactly to the thickness of the overlying sandstones of the Siderolithic. An erosion of such thickness of the Cretaceous unit may be supposed with an infill on top of it of the same thickness of Eocene fluvial deposits. The presence of a karst doline or a fault plane infill may also be possibilities (Figure 4-16). On bottom of the image is the lithological column of the Upper Malm, Cretaceous and Lower Cenozoic units (black horizontal arrows represent likely décollement zones). LEP wells are a serie of wells drilled in the west of the GVA Basin, among with L112, L132 and L135 wells (see Table 3-2 and Figure 3-28 for localization and details about these wells).

Away from Géo-02 well, the nBCen horizon may also be overlain by the lowest part of the Molasse formation, which may vary throughout the Geneva Basin from the “Gompholite”, to the “Calcaires d’eau douce inférieurs” or directly the “Marnes et Grès bariolés” (see Figure 2-7 for stratigraphy of Cenozoic unit). The two first candidates for the formation in contact with nBCen seismic horizon owns a maximum potential thickness of 30m for the “Calcaires d’eau douce inférieurs” and 50m for the

“Gompholite” formation (Table 4-11 from Chablais & Savoy (2021)). This implies that a thin layer of approximately 30ms in the time domain may be present and contrasting with the Cretaceous unit below and with the “Marnes et Grès bariolés” above. We estimate that is not possible to distinguish these layers with the potential Eocene deposits, as they are too thin and should have the same pinch out geometry (thinning with onlap terminations) on top of nBCen seismic horizon. In consequence, the previously mentioned Intra Molasse reflection (InMol) can be drawn on the interpreted seismic profile and could also correspond to a near seismic horizon of the top of these two other formations.

4.1.11 Cenozoic and post- Eocene intervals

The Cenozoic interval is overlain by Quaternary deposits in major part from the Geneva Basin, except for few Molasse outcroppings in some topographically elevated areas. Where Quaternary layers are present, the **near Base Quaternary (nBQua)** marks the erosional truncation of the Molasse sediments during the glacial ages. This surface has not been the subject of this study, therefore it has not been interpreted. However, it was interesting to know the approximate location of thick glacial valleys to evaluate possible imaging artefact present on the underlying layers (velocity push down effect, see Figure 3-6). Therefore, we have used a grid of nBQua (Figure 4-18) produced by Lathion & Hauvette (2020), and converted into the time domain with constant velocity of 3000m/s (=Vrepl). On our seismic dataset, which was not processed adequately for focusing the Quaternary layer (see Figure 3-6), the nBCen seismic horizon corresponds roughly to a high amplitude peak and low frequency seismic reflection. The Molasse seismic reflections, when they are visible, are toplaping logically nBQua horizon.

The rest of the overlying Molasse sediments is represented by seismic facies Cen.SF1 (Table 4-12) that is composed of moderate to low amplitude semi-continuous to discontinuous seismic reflections. The Molasse part was not the subject of this study, moreover the resolution of the seismic dataset does not allow a proper interpretation of this layer, hence a simple seismic facies classification of this unit has been proposed. For a more detailed classification, we can suggest the reading of the thesis of Morend (2000) who analyzed this unit in the western Swiss Molasse Basin.

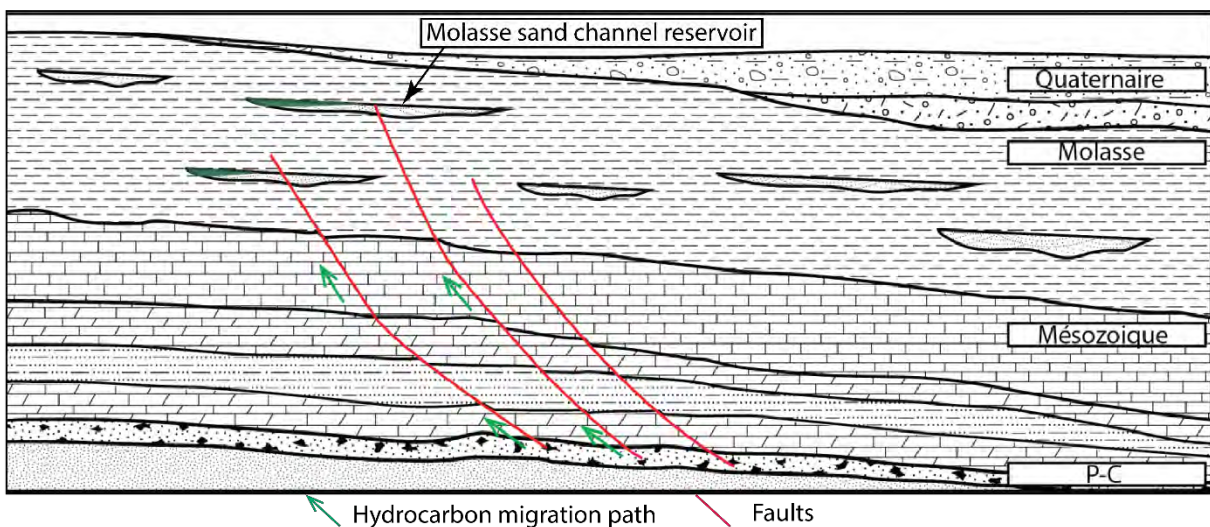


Figure 4-17 : Conceptual scheme explaining the principle of hydrocarbon migration from Carboniferous coal bearing layers to fluvial sandstones reservoir in the Molasse interval. Figure modified from Hauvette et al. (2018).

Seismic facies	Reflection characteristics	Lithological Interpretation	Sedimentological Interpretation
	<p>Cen.SF1:</p> <ul style="list-style-type: none"> - Amplitude: Moderate to low - Frequency: High to moderate - Continuity: Semi-continuous to discontinuous - Geometry: Hummocky - Termination: <ul style="list-style-type: none"> ->Near Top: Erosional truncation ->Near Base: Onlap to concordance 	Sandstone-shale dominated unit	Continental marine-fluviatile deposits
	<p>Cen.SF2:</p> <ul style="list-style-type: none"> - Amplitude: High - Frequency: Moderate - Continuity: Semi-continuous to discontinuous - Geometry: Bright spots - Termination: <ul style="list-style-type: none"> ->Near Top: Concordance to toplap 	Sandstones reservoir (filled with Gas)	Continental channels

Table 4-12 : Seismic facies description of the Molasse formations. See respectively Encl 29 and Encl 14 for detailed seismic interpretation of lines 18SIG_011 and 15SIG_010.

An additional distinction has been made about the seismic facies of the Molasse unit concerning bright spots that are amplitude anomalies (very high) and may be associated with gas pocket infill inside sandstone channels of the Molasse unit (Hauvette et al., 2018; Gorin et al., 1995; Morend, 2000). The migration of the hydrocarbon originates from the Carboniferous coal bearing layers to the fluvialite reservoir of the Molasse, possibly through faults or fractures corridors (Figure 4-17, Table 4-12).

4.1.12 Quaternary interval

Quaternary infill of glacial erosional valleys may be visible on certain seismic profiles, even though the seismic processing of our seismic dataset was not achieved with a specific focusing on this (see Figure 3-6). Indeed, it would be required for detailed interpretation of internal seismic facies of this layer. However, we can attribute seismic facies Qua.SF1 (Table 4-13) to the overall infill of the Quaternary channels, which appears usually as a low amplitude and low frequency seismic facies (“transparent” texture).

Seismic facies	Reflection characteristics	Lithological Interpretation	Sedimentological Interpretation
	<p>Qua.SF1:</p> <ul style="list-style-type: none"> - Amplitude: Low - Frequency: High to low - Continuity: Discontinuous - Geometry: Hummocky - Termination: <ul style="list-style-type: none"> ->Near Top: erosional truncation ->Near Base: downlaps/onlaps 	Moraine and fluvialite deposits unit	Continental glacial deposits

Table 4-13 : Seismic facies description of the Quaternary unit. See Encl 31 for detailed seismic interpretation of line 18SIG_014.

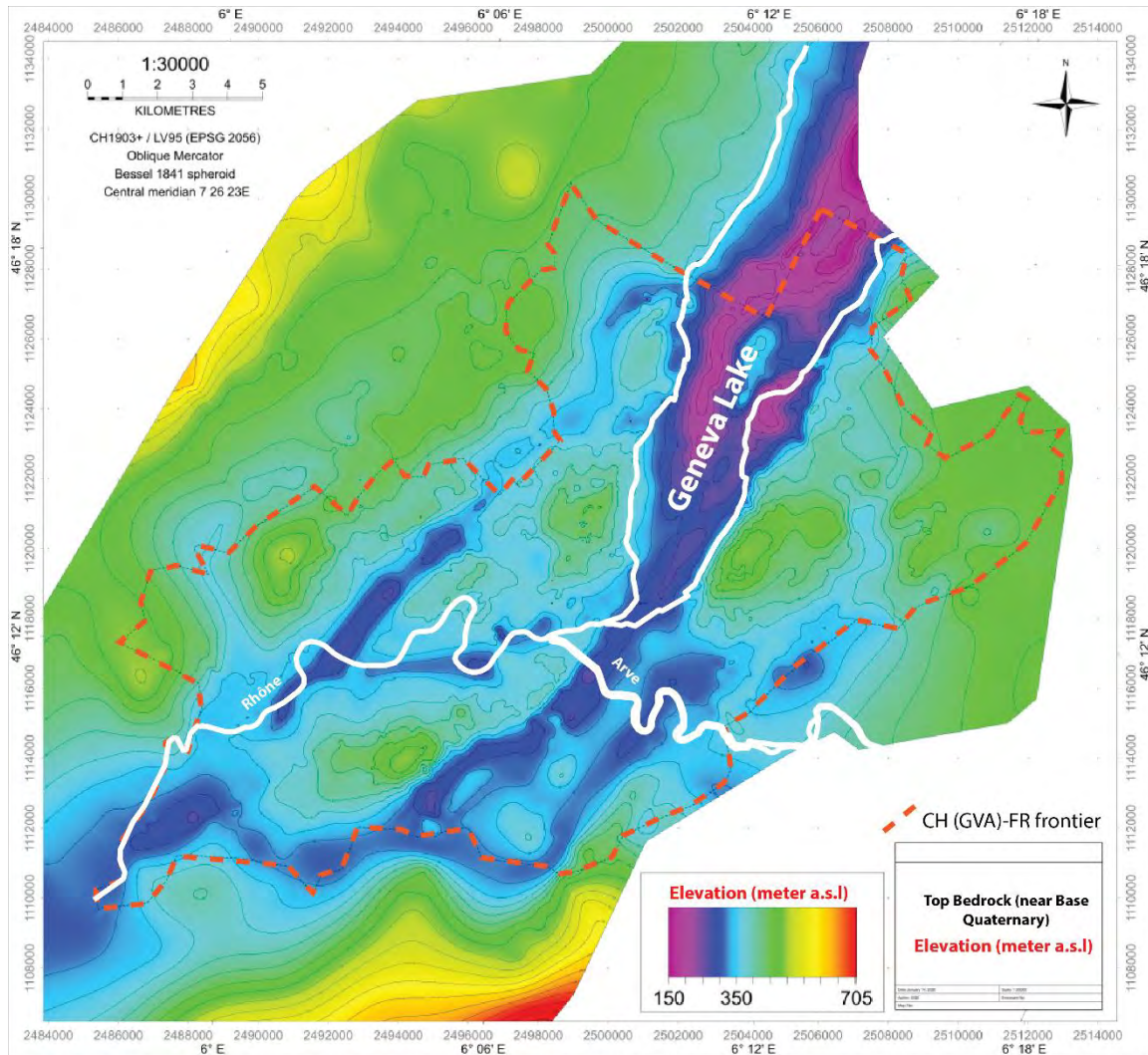


Figure 4-18 : near Base Quaternary elevation grid (Lathion & Hauvette, 2020).

4.1.13 Structural interpretation

Given the differences in seismic line quality, spatial resolution (density of lines), processing issues and a complex structural context, it was necessary to define a systematic way for the interpretation of these lines to obtain a structural concept that is homogeneous throughout the area of investigation, with the same level of detail (“precision”) and relevance. The interpretation of the seismic lines in terms of structural features is thus guided by the following main concepts (Figure 4-19, Figure 4-20):

- **Décollement zone:** the Mesozoic cover series are detached from the undeformed underlying basement s.l.. The décollement horizon is defined as a surface located near the bottom of a broader zone of deformation (décollement “zone”) associated with the Triassic evaporites of the Keuper Group for this area (Affolter & Gratier, 2004; Guellec et al., 1990; Philippe, 1995; Sommaruga et al., 2017). Thus, implicitly, the Muschelkalk Group and Buntsandstein Series are not detached and can be considered as part of the mechanical basement or basement s.l.. Numerous smaller reverse/thrust faults (or duplexes) were interpreted in the Triassic evaporite zone to account for thickness changes and the changes in dip of the seismic horizons.

- **Main folds** affecting Mesozoic and Cenozoic layers are defined by changing dip domains, where bedding has a different inclination. The dip domains are separated by major dip change lines. These surfaces, represent axial surfaces, and can be recognized and shown on seismic lines, and partially also on existing surface maps where enough dip data of the Mesozoic series, and the Cenozoic Molasse layers are recorded.
- **Steep to subvertical faults** s.l. are ubiquitous features and can be observed on seismic lines. They are considered discrete discontinuities when an obvious offset of layers (continuous reflections on seismic lines) can be recognized. Faults are, however, difficult to correlate, both in one seismic line (top to bottom) and across several lines. Reflections which are not continuous show in many cases small offsets, due either to the seismic line quality or to the nature of the faulting process. Thus, in clay-rich layers such as the Lias and Dogger units, faults may not be expressed on the seismic lines unlike in more competent interlayered limestone series. It may therefore be difficult to assess the presence of a fault. We observe and define only relevant faults of modest extent and define fault sets, often conjugated. In addition, faults are frequently arranged in broader zones. Therefore, rather than drawing single large faults we decided to define fault corridors (the width of which may range from decameters to several hundred of meters (up to 500m) where we observed a higher density (more than 3 faults on average) of faults and which can be correlated across seismic lines. We prefer the term fault corridor to fault zone which refers to a narrow zone with an individual fault or fault set. Fault corridors may host brittle and/or plastic-cataclastic deformation processes depending on the rheology of the layers affected. Fault corridors have been systematically represented on seismic profiles by two external boundaries that stop vertically downward near nTKeu seismic horizon. Indeed, these faults appear not to cut the basal décollement and root in the ductile Triassic evaporite rich layers. A rough estimate of the length of the fault corridors interpreted can be given by the two occurrences in the Meyrin area (see chapter 6.3.1), which have an approximate lateral extent of 13-15km long. Faults inside the fault corridors have an apparent 60-70° dip on the interpreted 2D seismic lines. The real dips must, therefore, be higher by probably 10-20°, depending on the angle between seismic lines and the azimuth of the fault corridors. Fault corridors appears often on strike seismic sections as a chaotic seismic facies with an overall “transparent” appearance (relatively low amplitude zone). Further descriptions about interpreted fault corridors in this study are given on chap 6.
- Concerning the **vertical offsets** of the faults observed, it is possible to estimate it around 20ms, as an average between the numerous faults interpreted.
- **Reverse faults** were difficult to demonstrate and arise from an interpretation of the bedding dips, hence the inclination changes of continuous seismic reflections and the kinematic understanding of the structures interpreted. Reverse faults are thus associated with large-scale folds (fault-bend folds and fault-propagation folds), imbrication and duplication of layers (seismic horizons). Major thrust faults with larger offset are observed in the Jura area and, in the Salève mountain area and in the Gros Foug area.
- **Inherited normal faults** (listric). Listric synsedimentary normal faults can be identified by a combination of an offset of seismic reflections and a change of thickness of lithostratigraphic units along and across the fault. Offsets of reflections along the fault may show both normal and reverse movement. This is diagnostic of inversion along an inherited normal fault (Figure 4-20). An additional criterion is the progressive curving and flattening of these faults in the

vicinity of the detachment level which is pointing to a listric normal fault geometry typical of extensional synsedimentary settings.

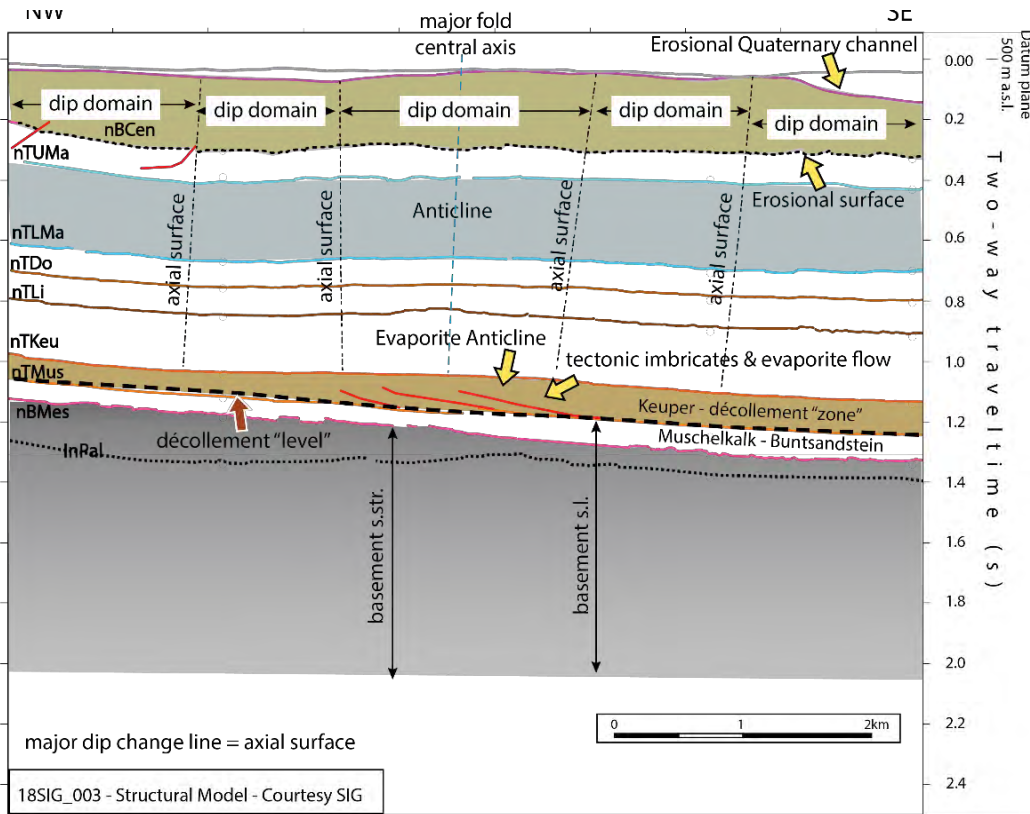


Figure 4-19 : Sketch of major structural concepts used in structural interpretation of the seismic lines, based on 18SIG_003.

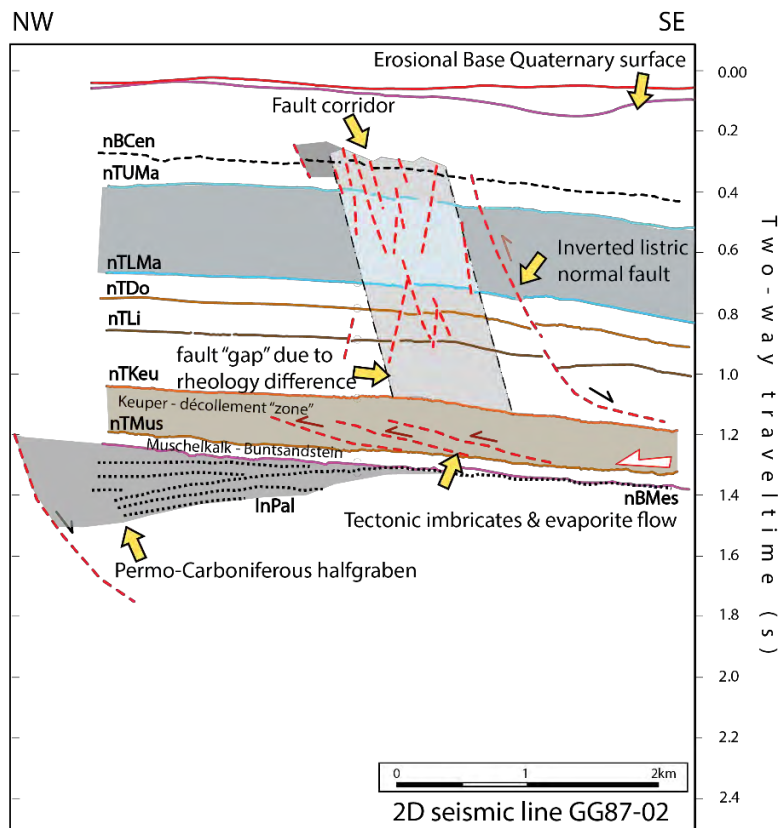


Figure 4-20 : Simplified sketch of structural features interpreted on seismic lines in the study area, based on section GG88-2.

4.3 Horizon mistie correction

As already mentioned in part 3.2.6, a disadvantage of 2D seismic profiles concerns misfits in between intersecting 2D sections. These misfits have been corrected as much as possible during the preparation of the data, using the simple methodology of vertically bulk shifting each seismic profile when necessary. This was achieved in order to have a maximum of identical seismic reflections aligned together at the intersection of profiles. However residual misfits always remain, hence the usefulness of the mistie correction. The intersections of seismic lines and respective “corrections” for associated measures are an integral part of geophysical measures. To assess the offsets of interpretation across a seismic line grid, misties (offsets values) can be calculated and subsequently corrected. The procedure to minimize errors has been accomplished in two steps as follows (Figure 4-21):

- A first a constant shift applied on each interpreted horizon that minimizes the mistie between the lines.

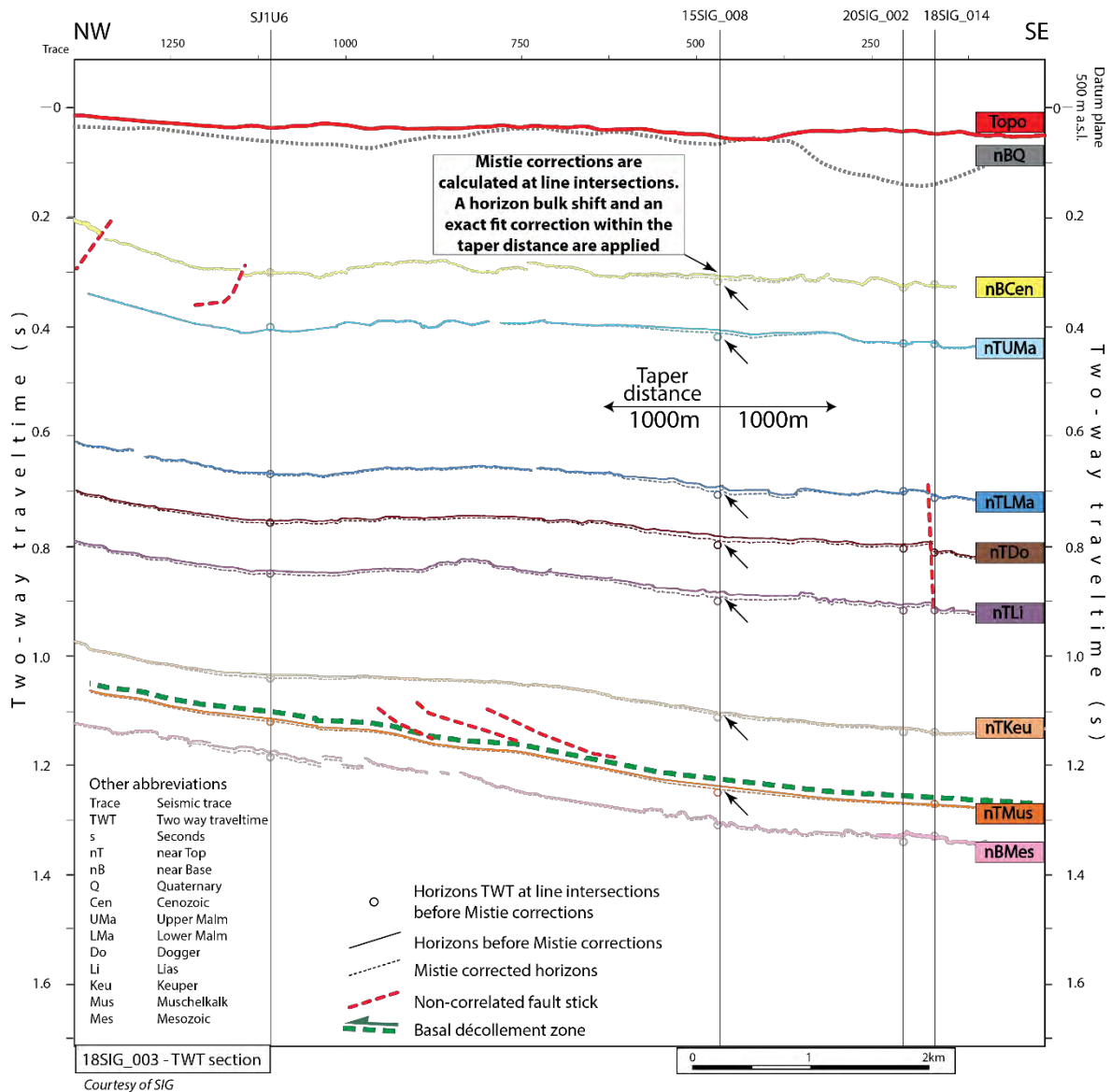


Figure 4-21 : Mistie corrections example on seismic line 18SIG_003, intersecting line SJ1U6 along the black dashed line on the left, and line 15SIG_008 along the black dashed line on the right. The mistie correction represent only few milliseconds, usually 2-8ms corrections (black arrows).

- Then local corrections are made on seismic horizons around still existing mistie points (1000m taper distance) created by small local distortions.

Seismic profile misfits and misties of seismic horizons at intersecting sections are mainly caused by the limitation of seismic processing velocity modeling in the time domain. Indeed, processing velocity analysis may influence the dipping angle of the reflections, or artefacts such as pull up or push down effects. Therefore, we can suppose that, when horizon mistie corrections are needed between two intersecting lines, it may improve in fact the reality of the interpreted geological structures along sections. Indeed, it compensates the lack of precision of the processing velocity modeling of one profile compared to the other one.

This process of horizon mistie correction has allowed decreasing all misties values greater than 0.02s before the correction to residual mistie values less than 0.02s. A great majority of the residual mistie values are even less than 0.01s. These remaining misties can be discarded, as they are less than the resolution of the seismic lines.

4.4 Uncertainty of the seismic interpretation in the Geneva Basin

The accuracy of the interpretation process depends on several factors. First, each data used during the seismic interpretation (wells, seismic, GIS) owns inherent uncertainties, due to their quality varying laterally and vertically. The density of the data (spatial distribution) has also a significant role to play in the uncertainty evaluation. Then, each step achieved by the interpreter will also include possible errors (seismic to well tie, horizon picking), that are very complex to quantify with precision. Indeed, by definition an interpretation may be biased by the subjectivity of the operator/interpreter. Therefore, it is very difficult to quantify and assign a unique and global uncertainty value to the final results. It could be possible to assess such a summary value locally in the frame of a preparation of a well drilling, but it is not feasible for a regional evaluation. The lateral and vertical variability of uncertainty is too large for such task.

However, we propose to attribute a rough uncertainty range to each possible source of error involved in the interpretation process. It can give some keys to estimate the total uncertainty. The order of magnitude given in the following paragraphs and in Table 4-14 and Table 4-15 may be applied thereafter locally for future well planning in the area. We give examples of uncertainties measured along certain profiles (the most representative profiles are named on Table 4-14).

The uncertainty related to seismic data is described in part 3.2. By definition of the seismic reflection data, the vertical resolution is given partly by the Rayleigh's limit (see part 3.3.2 and Figure 3-3) and it can be rounded to the TWT range of 5-8ms (10-15m) for the first 0-500m below topography and of 8-12ms (20-30m) for deeper seismic reflections. Any seismic interpretation can thus not produce results with an evaluated uncertainty below this range. The following uncertainties may then be added to this range value. It corresponds to an average range value but in fact, the acquisition parameters may increase this range, mainly depending on the strength and the frequency content of the energy source used.

Seismic processing entails several uncertainties:

- A geometry of the line along the topography is calculated in the first steps of the processing. It consists in placing regularly along a relatively smoothed line at surface the traces that will

constitute the seismic profile. The smoothing of the line is a simplification made in order to attenuate crooked geometries that come from a complex acquisition scheme. This causes lateral uncertainties that can be measured along particularly affected profiles. It is the case for instance of seismic line 18SIG_001 on which we observe traces located 250m away from source or receiver points. Hence, a large average lateral uncertainty range of 20m-300m.

- Static corrections intend to adjust all traces vertically to the main datum plane. This includes velocity modeling of the shallow interval. Seismic lines 18SIG_014 and 18SIG_014Q are two independently acquired profiles along a common outline (Figure 3-6). Two completely different static solutions were used for these two sections, one to highlight the Mesozoic units and the other one for the Quaternary interval. It is a good extreme example, to allow evaluating the static uncertainty with the average value measured along this profile of 45ms. It corresponds to the TWT difference at near Base Cenozoic level of the same seismic reflection visible on both profiles.
- During seismic processing, a velocity modeling is achieved and applied during stacking and migration processes. The calculation of these velocity models is driven by manual picking of the operator that may create vertical shifts of the seismic image points. Seismic profile 88SVO07 has two very different versions of processing (GGE-Petrologic 2017) that were produced as part of an iterative process to improve the imaging. The main difference between these two versions concerns the velocity model applied during the time processing. Near the Salève Thrust the velocity may be difficult to assess accurately. We can measure along this line the TWT difference generated between the two versions around 25ms (Figure 4-22). As it is an extreme case it gives a realistic uncertainty value to this processing step.
- The migration process allows improving the lateral and vertical positioning of the image points of a seismic profile. In the same way, and again along seismic line 88SVO07 (extreme case in front of the Salève mountain) the uncertainty related to the migration versus stack versions can be estimated by measuring the lateral and vertical TWT difference between the two. This gives an uncertainty of 15ms vertically in time domain and 100m laterally. This uncertainty may be particularly important in laterally highly variable velocity areas (fault area, salt pillow, etc.).
- As explained in 4.1, it is complicated to know the exact polarity of seismic data. Therefore, the related uncertainty corresponds to the time difference between a peak and the following trough reflection. Considering the lower frequency of the interpreted seismic horizons (near Top Muschelkalk horizon), the time difference does not exceed 15ms.

In part 3.2.6, we have seen the issue linked to datum plane and misfit correction that affect seismic profiles that have not been processed under the same combination of datum plane and replacement velocities defined for this present study (see Figure 3-18). A theoretical vertical adjustment was applied on the profiles that needed a correction, followed by an additional manual bulk shifting to optimize the adjustment. This technique has proven to be relatively efficient in terms of misfit corrections, as the resulting remaining misfits at profile intersections range between 0.01s to 0.06s (range of horizon mistie values before correction). After the horizon mistie correction the residual horizon mistie values are less than 0.02s (uncertainty related to mistie correction). However, this needs to be distinguished from the adjustments of profiles in relation with the defined datum plane of this study. We have decided to assess the corresponding uncertainty of the latter, by considering an average value

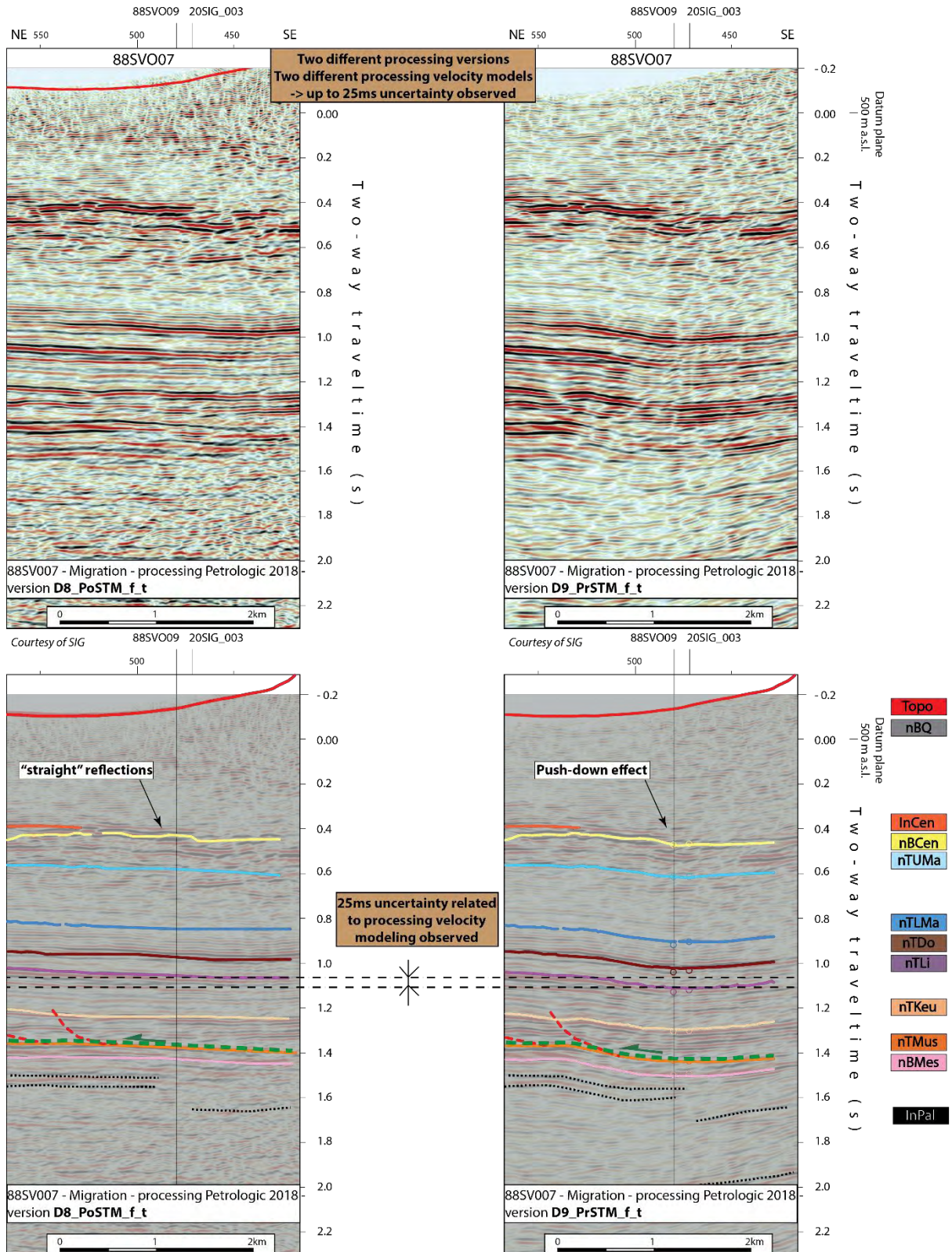


Figure 4-22 : Seismic profile 88SV007 (traces range 375-525) with two versions of time migrated data produced using two different processing velocity modeling (by the processing center Petrologic in 2018). In this area in front of the Salève Mountain it may be difficult to assess accurate velocities. This extreme case highlights well the uncertainty related to seismic processing. The yellow and red arrows are pointing at the same image point but with different vertical positioning. See Encl 38&85 for detailed seismic interpretation of line 88SV007. See Figure 4-7 for location of seismic line.

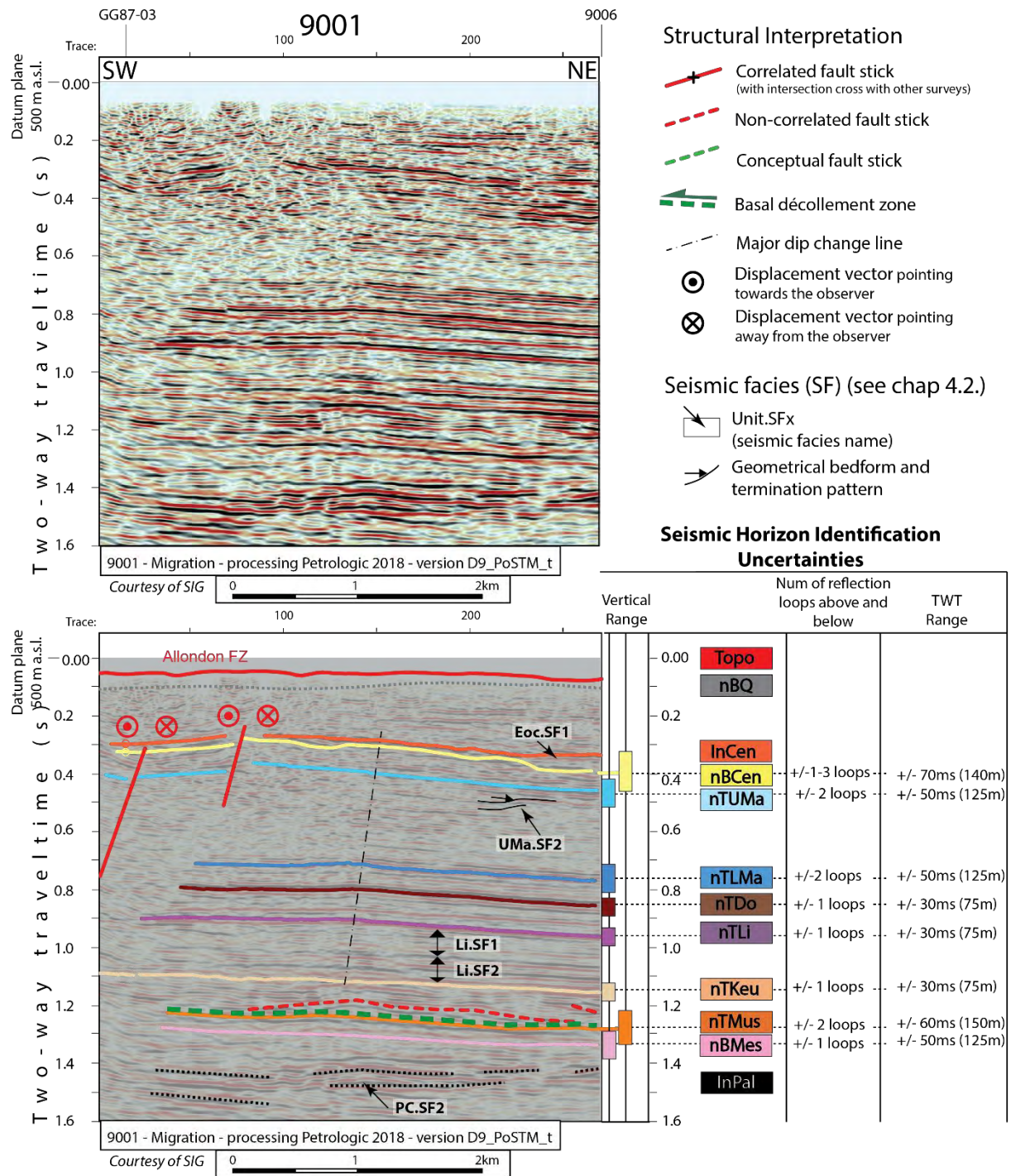


Figure 4-23 : Uncertainties related to the seismic horizon identification according to the strength of their signal signature. The uncertainties is estimated based on the number of reflections loops of possible error above and below each seismic horizon. See Encl 01 for detailed seismic interpretation of line 9001. See Figure 4-7 for location of seismic line.

of the difference between the theoretical approximated first adjustments with the final adjustment (with the manual bulk shifts). This gives a value of 100ms, which is dedicated to seismic lines away from well tied profiles and from sections calibrated during processing to the defined datum plane of this study.

The uncertainty concerning the horizon picking can be divided into three parts. First, when interpreting a seismic horizon, one need to identify the right reflection. Away from control points (wells or outcrops), the calibration of profiles may include errors when propagating the interpretation from line

Source of uncertainty	Details	Measured or estimated uncertainties are in grey boxes and calculated equivalence (in TWT or in depth domain) are in white boxes		Average Lateral uncertainties (m)
		Equivalence TWT (ms)	Equivalence depth (m)	
		Average Vertical uncertainties TWT (ms), depth (m)		
Seismic data	Geometry lateral positioning			20m-300m
	Resolution of seismic data (0-500m TVD)	5-8 ms	10-15m	
	Resolution of seismic data (500m-3km TVD)	8-12ms	20-30m	approx 25m
	Static corrections	5-45ms (1)	12-112m	
	Processing velocity modeling	5-25ms (2)	12-60m	
	Migration vs non migrated data	+/-15ms	+/-37m	10-100m(2)
	Polarity	5-15ms	12-37m	
Misfit and datum plane	Limit of vertical adjustments to datum plane	100 ms (6)	250m	
Mistie correction	Limit of vertical adjustments in between seismic lines	60ms (7)	150m	
Horizon Picking	Seismic reflection identification on each profile (cf table)	30-70ms	75-175m	
	On seismic profile Quality 1 (following of reflections)	10ms	24m	
	On seismic profile Quality 2 (following of reflections)	30ms	75m	
	On seismic profile Quality 3 (following of reflections)	100ms (3)	250m	
	Around fault structures (fault throw understanding)	20ms-200ms (4)	50-500m	100m
Well data	Stratigraphical well top identification (Petrophysics)	0.4-2ms	1-5m	
	Seismic to well tie	0-150ms (5)	0-300	

- (1) maximum measured line on 18SIG_014
- (2) maximum measured on line 88SVO07
- (3) example given with 02AC1 or 2CC1 profile (see Fig 3.8)
- (4) maximum case measured on line 18SIG_001
- (5) according to Sommaruga et al.2012 (analogous study), which is confirmed by our study.
- (6) this concerns only profiles not originally processed under the defined datum plane/ repl vel of the present study (approx 146/191 lines) the theoretical formula and the manual bulk shift contain limits (see Fig.3.16)
- (7) based on residual horizon mistie corrections that still remains after ajustement (see Fig.4.21)

Table 4-14 : Evaluation of uncertainties related to each possible source of errors involved in the interpretation process.

Seismic horizon	Seismic horizon (abbrev)	Strength of the associated seismic reflection (+, ++, +++)	Number of well calibration points in the Geneva Basin	Average uncertainty TWT(ms)	Uncertainty Equivalence in Depth(m)	Equivalence in number of reflection loops above and below	Details
near Base Cenozoic	nBCen	+++	7	+70ms/-30ms	+/-140m	1-3 loops	Uncertainty given by the thickness of Eocene in Geo-02
near Top Upper Malm	nTUMa	+	4	+/-50ms	+/-125m	2 loops	Very weak seismic reflection signature
near Top Lower Malm	nTLMa	+	3	+/-50ms	+/-125m	2 loops	Weak seismic reflection signature (help using seismic facies)
near Top Dogger	nTDg	++	2	+/-30ms	+/-75m	1 loop	Strong seismic reflection signature
near Top Lias	nTLi	++	2	+/-30ms	+/-75m	1 loop	Strong seismic reflection signature
near Top Keuper	nTKeu	+++	2	+/-30ms	+/-75m	1 loop	Very strong seismic reflection signature
near Top Muschelkalk	nTMu	+	2	+/-60ms	+/-150m	2 loop	Poor knowledge on underlying unit Mu in the Geneva Basin
near Base Mesozoic	nBMes	+++	2	+/-50ms	+/-125m	1 low freq loop	Erosional truncation well visible

Table 4-15 : Estimation of the uncertainties related to the interpretation of each seismic horizon away from seismically calibrated wells. This type of uncertainty is increasing with the distance to control points (calibrated wells, outcrops), but depends also with the vertical identification of the correct seismic reflections that should corresponds to each of these boundaries. Taking into account the strength of each seismic reflection observed at seismic to well tie locations (strength of the amplitude value), and the number of calibrated points in the Geneva Basin (wells), it allows evaluating uncertainty values.

to (intersecting) line. A quality check is done during the interpretation considering the signal signature of each seismic boundary. Unfortunately, some seismic horizons have weaker reflection characteristics such as the near Upper Malm Unit that is hardly distinguishable on many profiles (see part 4.2). It means that the identification of the adequate seismic reflection depends on the properties of each seismic horizon. In that sense, an uncertainty value is given to each boundary in relation with the strength of its associated seismic reflection in combined with the number of control well points (Figure 4-23 and Table 4-15). The defined criterion of calculation is the following:

- nBCen uncertainty corresponds to the Eocene thickness observed at GEO-02 (140m), as discussed in 4.2.1.7.
- a weak reflection signature may introduce a possible error of 2 reflection loops above and below the interpreted seismic horizons (nTUMa and nTLMa nTMu)

- A strong reflection signal may introduce a possible error of 1 reflection loop above and below the interpreted seismic horizon (nTDo, nTLi, and nBMes).

Once a seismic reflection is selected to pick a seismic horizon, one needs to be able to follow accurately the seismic reflection. This will depend directly on the quality type of the interpreted seismic profile. A visual analysis on each type of data has led to the estimation of an additional uncertainty of 10ms, 30ms and 100ms for respectively quality types 1, 2 and 3.

Around major fault structures in the Geneva Basin, such as the Coligny Fault zone, a lateral positioning error may be present. Therefore, the seismic horizon picking may be placed in this “corridor” zone on the wrong side of the fault. In this case, the related vertical uncertainty is equal to the fault throw of the fault. The Coligny fault zone having one of the major fault throws visible on seismic profile 18SIG_001 in the Geneva Basin, we can use it to define the upper value of the average uncertainty range of 200ms for horizon picking in highly deformed area.

As mentioned in part 4.1.2, the uncertainty proper to stratigraphic identification of well tops (petrophysics), is estimated between 1-5m (same estimation than Sommaruga et al., (2012)). Following the same source, the seismic to well tie uncertainty may reach 150ms for wells of limited quality data.

Last but not least, an uncertainty particularly interesting for this study concerns the subjectivity of structural interpretation (Bond et al., 2007). Each seismic interpreter may produce results biased by his knowledge and the geological concepts that he may be inclined to apply and possibly by a forcing during the interpretation. In our case, the two major opposed structural concepts of thin-skinned and thick-skinned tectonics have been applied by several interpreters at different times on the same data (Figure 4-24). For instance of seismic profile GG87-02, a major near vertical fault was interpreted (G. E. Gorin et al., 1982) crossing the whole Mesozoic cover and reaching the Paleozoic unit (thick-skinned tectonic). The authors had also interpreted several flower structures. These two types of structures are also interpreted on all the other profiles of the Geneva Basin by Gorin (1989); Gorin et al. (1993); and Signer & Gorin (1995).

In a different interpretation and with a different structural style, Sommaruga et al., (2012) interpreted the same central vertical fault on the same seismic section GG87-02, to stop in the Muschelkalk Unit. No offset of nBMes is drawn, hence the thin-skinned tectonic concept is respected. Another specific characteristic to the interpretation of Sommaruga et al., (2012) is the interpretation of intra-Triassic duplexes occurring along the main décollement level (above nTMu horizon). This example of variability of interpretation of seismic section GG87-02 highlights very well the human biased seismic interpretation. The present study has the advantage that several seismic interpretations have been proposed in the past. Therefore, it was possible to learn from these different structural solutions and keep the best of each model, in consideration also of all the additional knowledge from more recent studies and from the literature brought since these interpretations. In that sense, based on the available seismic lines and surface map data, it was locally possible to propose alternative scenarios for a structural model. We therefore made a selection of the most suitable models based on a serie of external criteria (Figure 4-25):

- Consistency with the regional kinematic and tectonic model;
- Apply the principle of parsimony and opt for the “simplest” solution;
- Interpret fault zones (fault corridors) rather than large single faults;
- Use thickness changes of interpreted layers to define structures.

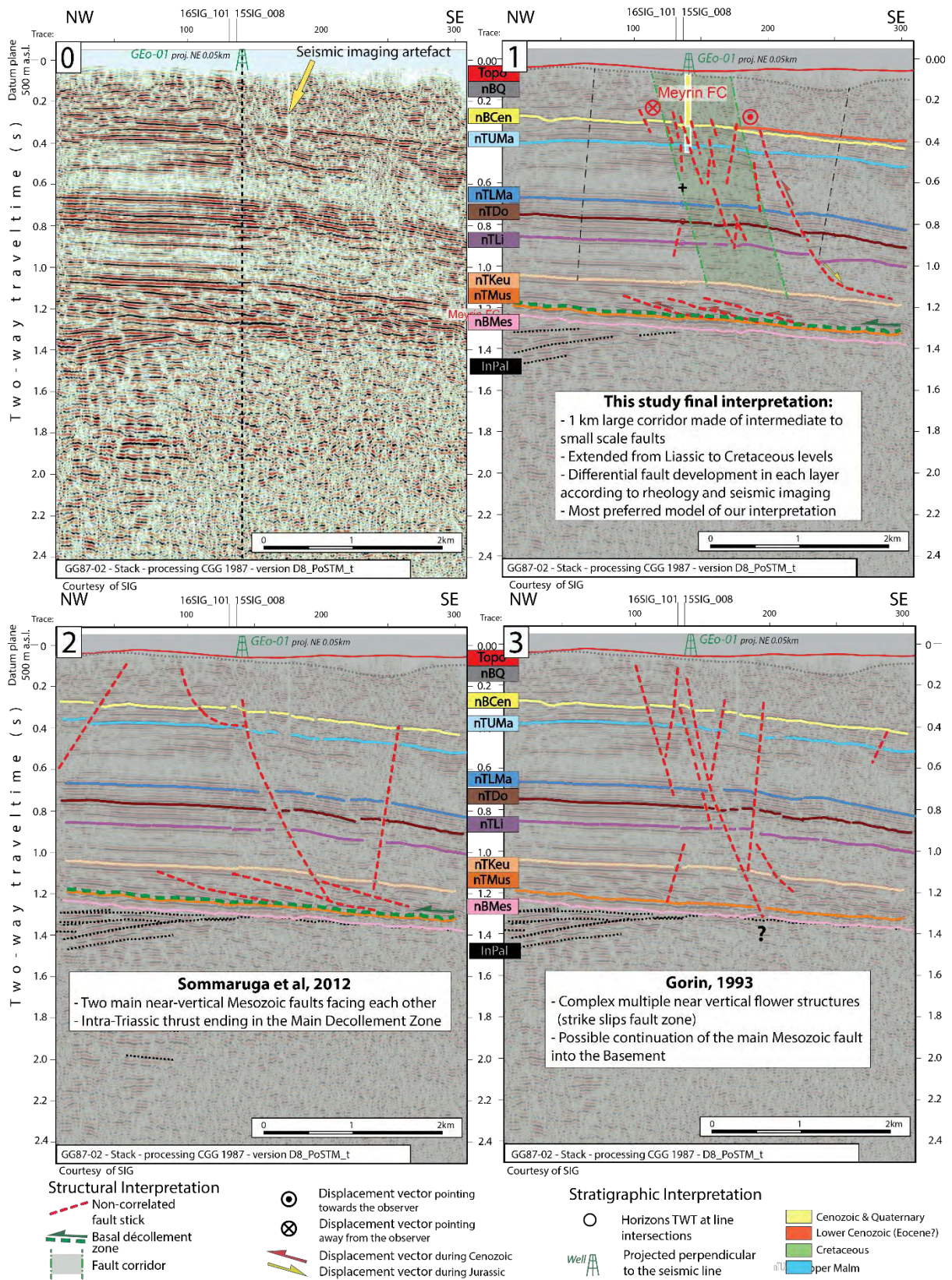


Figure 4-24 : Example of variability of seismic interpretation of seismic profile GG87-02, that may be biased by the conditioning of the interpretation knowledge and geological concepts that each interpreter may be tempted to apply, sometimes by forcing interpretation. See Encl 66 for detailed seismic interpretation of line GG87-02. See Figure 4-7 for location of seismic line.

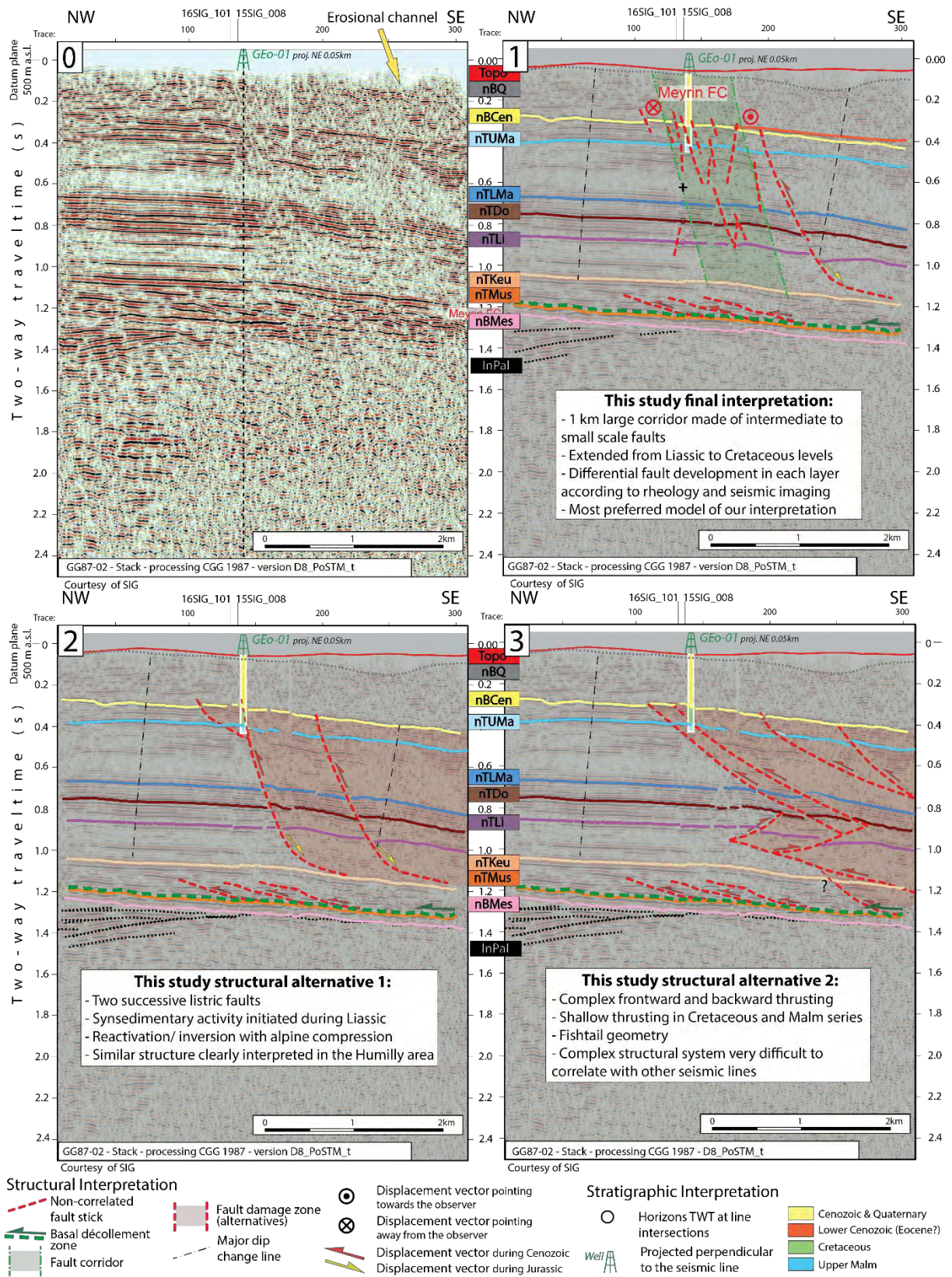


Figure 4-25 : Structural concepts in seismic interpretation: alternative solution are evaluated against different criteria. See Encl 66 for detailed seismic interpretation of line GG87-02. See Figure 4-7 for location of seismic line.

5. MODELLING AND 3D GEOLOGICAL MODEL

The resulting seismic horizons interpreted in the “time” (more precisely in TWT) domain are converted into the depth domain using specific time/depth relationships extracted from well data. During the process of time/depth conversion a selection of seismic profiles are also converted into the depth domain. Final maps correspond to the spatial interpolation of the horizons in the time and in the depth domain (gridding), in relation to main interpreted faults. These different processes of time/depth conversion, gridding and mapping are necessarily associated with artefacts and uncertainties that will be discussed in the parts 5.1.5 and 5.2.4.

5.1 Time to depth conversion

5.1.1 Methodology

The seismic interpretation is achieved in our case along seismic profiles processed in the time domain (chap 4, and see flowchart of Figure 4-1). It results in 2D seismic horizons and fault sticks in twt, whereas the main objectives of the study are to obtain:

- 3D depth grids (maps) at different stratigraphical levels (8 boundaries: nBCen, nTUMa, nTLMa, nTDo, nTLi, nTKeu, nTMu and nBMes).
These grids or maps, computed in relation to faults will represent the main tool for the geothermal exploration. Indeed, the main criteria for placing a geothermal well are the presence of faults (high permeability), and the depth of the different stratigraphical boundaries.
- 2D Seismic Profiles Depth Converted (SPDC).
This allows to quality check the time to depth conversion process, and to better understand the possible artefact that it can produce. This may also highlight limitation of seismic section in the time domain, but the main utility is to be able to have depth visualization of seismic data into a 3D depth model project in software such as Move, Petrel or OpenDTECT.

The elaboration of the targeted products justify the necessity to convert from the time domain into the depth domain the results and seismic profiles obtained from the interpretation. For this task, velocity models are needed, as they represent the only link between the two types of vertical scales (from TWT to depth, Figure 5-1). We have used three different velocity models to reach our goals (Figure 5-2). Each of them has a specified resolution that depends on the area it was applied to, and on the types and resolution of the targeted products. Indeed, the first regional velocity model 1 has an intermediate complexity and resolution that suits the objectives of obtaining large scale structural and stratigraphical trends. The velocity model 2 is centered around the Geneva Basin, where a highest resolution is needed for the geothermal exploration in this area. A third very simple model 3 was also used, only for quality checking and comparison purposes. This latter has not produced any final results for this study, only intermediate products.

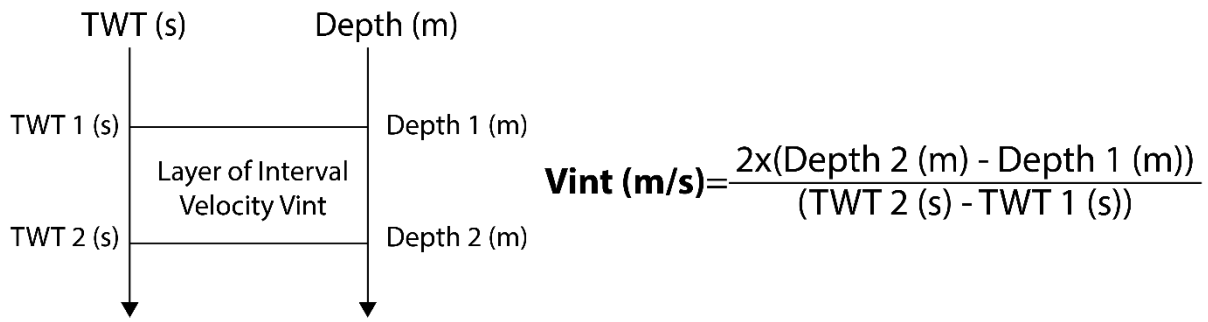


Figure 5-1 : Scheme of the relationship between time and depth domain given by the definition of interval velocity. Vint = interval velocity, TWT = Two Way Time.

An important remark is that the time depth conversion process was applied on 2D interpreted seismic horizons, and not on 3D grids (surface). The resulting 2D depth horizons are gridded in a second step (5.2.2). This procedure is supposed to be more efficient than converting directly 3D TWT grid into depth (detailed in 5.2.2).

The velocity modeling and depth conversion were performed on « the dynamic depth conversion and map update » module of Kingdom 2020 software. This tool uses constant interval velocities in between interpreted horizons, to build the velocity model that will be used as input for the time to depth conversion. This allows creating multi-layer velocity models for each of the seismic lines. It has been achieved for the so-called regional model 1, with one different velocity function per group of seismic lines. The module of Kingdom software also proposes to use velocity grid as conversion tool. This give the opportunity to create more complex and precise velocity model, which was the case of the model 2 centered around the Geneva Basin. In order to have a comparable basis for evaluating the benefit of this model 1 and 2, a very much simpler model 3 (only one interval velocity below topography) was generated and only applied on certain profiles. This comparison also allows evaluating the uncertainties related to this time to depth conversion method.

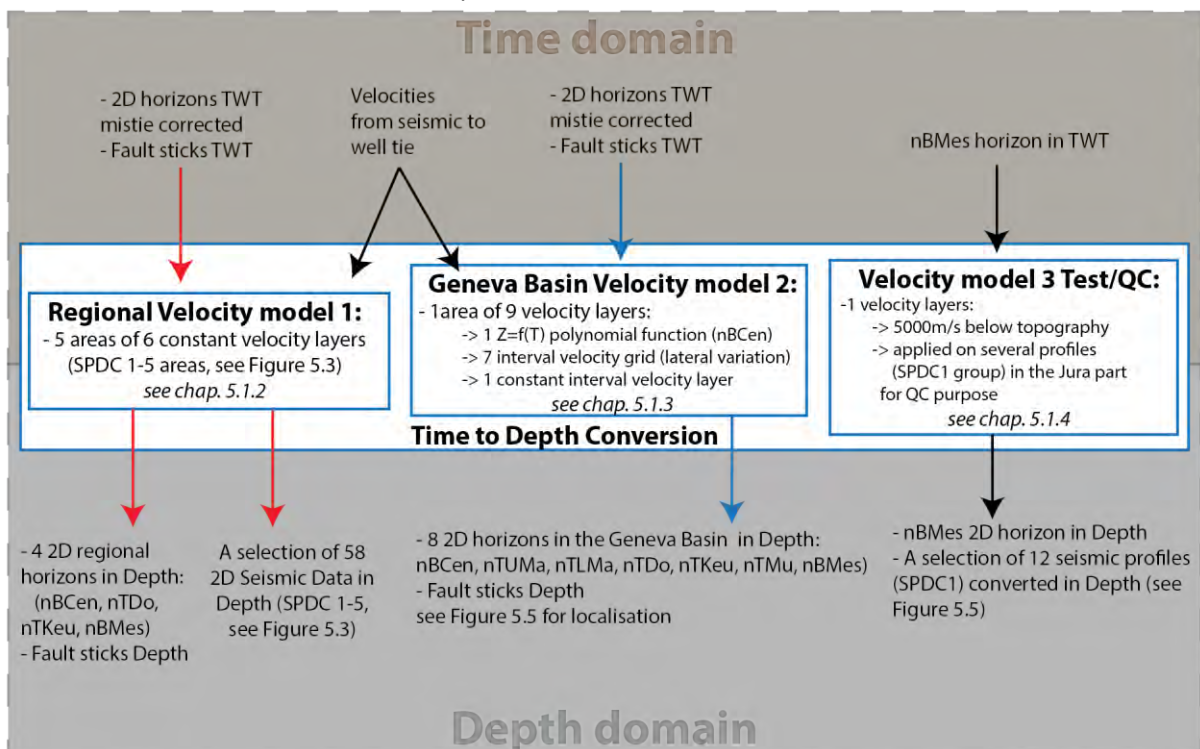


Figure 5-2 : Time to depth conversion flowchart. See Figure 5-3 and Figure 5-5 for localization of the three velocity models.

5.1.2 Regional velocity model 1

The main goal of this regional velocity model is to obtain an overview of the structural and stratigraphic setting of the Geneva Basin and its surrounding areas. This was achieved as part of a team project within the tectonic group of the UNIFR. Indeed, a selection of seismic profiles (SPDC 1, 2 and 3, see Figure 5-3 for location) to convert into depth was prepared to support the structural investigation of the Jura part in the master thesis of Adeline Marro (Marro, 2021), and to support the study of Sandra Borderie concerning the stress configuration of the whole area. For these purposes, it was necessary to consider seismic profiles in the Jura part NW of the Geneva Basin (SPDC1), in the Geneva Basin or the “plateau molassique” (SPDC2), as well as profiles southeast of the Salève in the Subalpine Molasse

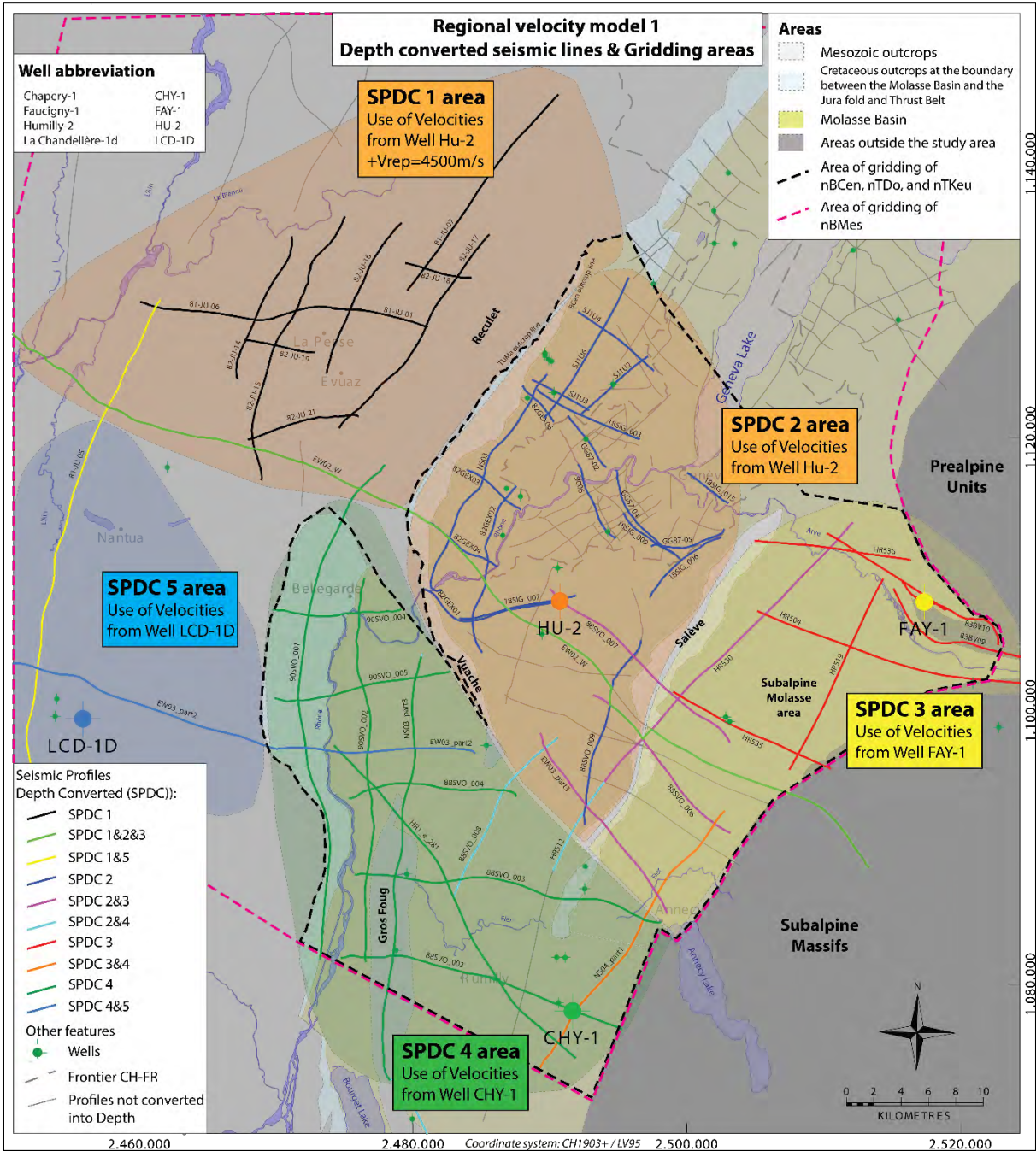


Figure 5-3 : Map of the lateral distribution of regional velocity (model 1) throughout the regional area in relation to the main deep wells from which the velocity models are extracted. SPDC means Seismic Profiles Depth Converted. For well and velocity information see Table 4-1 and Table 5-1. SPDC 1/ 2 areas are both colored orange, as they share the same well velocity data.

		Velocity model	Model 3 test	Model 1 Regional					
		Seismic reference datum	SRD 1125 m.a.s.l	SRD 1125 m.a.s.l	SRD 500 m.a.s.l	SRD 500 m.a.s.l	SRD 500 m.a.s.l	SRD 1125 m.a.s.l	
		Reference well for velocity modeling	Theoretical	HU-2	HU-2	FAY-1	CHY-1	LCD-1d	
		Group for velocity modeling	SPDC1	SPDC1	SPDC2	SPDC3	SPDC4	SPDC5	
Group of stratigraphic intervals used for the velocity modeling	Stratigraphic intervals	Abbreviation of interval top horizons on seismic profiles	Jura part North part	Jura part North part	Plateau Molassique	Subalpine Molasse part	Rumilly Basin	Jura Mountains South part	
From SRD to Topography	From SRD to Topography	SRD	4500	4500	3000	3000	3000	4500	
Cenozoic	Cenozoic	Topo	5000	No Cenozoic	3300	3918*	3660	No Cenozoic	
		Topo+0.3s			4000		4482		
		Topo+0.7s							
Cretaceous+ Malm	Cretaceous	near Bcen Trough (-)			5340	5340	5617	5721	4109
	Upper Malm	near TDo Trough (-)			4520	4520	5132	4851	4429
	Lower Malm								
Dogger+ Lias	Dogger	near Tkeu Peak (+)			5101	5101	6302	5172	4470
	Lias								
Triassic	Keuper Muschelkalk	near Bmes (Peak +)			5000	5000	5000	5000	5000
Paleozoic / Precambrian	Paleozoic /Precambrian	near Bmes (Peak +)							
-> 6 Velocity layers		-> 4 seismic horizons							

*3300 m/s velocity was used to model shallow parts at the back of the Salève FT

Table 5-1 : Table summarizing the vertical distribution of the regional velocity model 1 divided per areas and groups of profiles (SPDC 1-5) that are depth converted using these models.

part (SPDC3). These three areas cover a NW-SE trending region passing through the Geneva Basin and encompassing the main structural domains of the study area. Two other areas have been added to the study to extend the analysis west of the Vuache fault. Therefore, seismic profiles were selected in the Rumilly Basin (SPDC 4), but also in the meridional Jura part (SPDC 5).

Each of the five groups of selected Seismic Profiles Depth Converted (SPDC) are located in distinct structural and stratigraphic setting. Indeed, they are all separated by major fault systems that often mark the position of major changes in the stratigraphy linked to changes in the depositional environment. For instance, across the Vuache fault important thickness variations on several Mesozoic or Cenozoic layers can be observed. The Salève Mountain separates the Geneva Basin to the Subalpine Molasse part, which are two areas of distinct stratigraphy. This inherent segmentation of our study area into five areas requires necessarily adapted velocity modeling for each part (Figure 5-3). Four deep wells that have reached the Paleozoic units and are tied to seismic give velocity information for each of the areas. However, in the area of the Jura FTB just NW of the Geneva Basin (SPDC1) the velocity data were obtained from the well Humilly-2 located in the Geneva Basin. It was done this way, because these two areas are adjacent, and Humilly-2 well was the closest drilling tied to seismic and having accurate velocity information. The well Charmont-1 located in the mentioned area was not adjusted to its closest seismic profile (too low resolution of closest line EW02), hence it could not provide enough confidence in its velocity curve. Moreover, this well is crossed by a major backthrust in the Jura FTB, and it is usually preferable to derive the velocity modeling from an undisturbed Mesozoic column (not the case of well CHT-1).

For this regional velocity model 1, velocity information will not be interpolated laterally into interval velocity grids, but the interval velocity values of each of the four wells will be propagated as constant values along seismic profiles inside each of the delimited areas (Figure 5-3). It is the most logical way to spread laterally the well velocity data in our case. Major faults are segmenting these five stratigraphically different regions and only one well is present per area (except for SPDC1). For the case of seismic lines crossing two areas, the profiles have both SPDC naming. Then the velocity model

of both areas will be respectively attributed on the section on both sides of the faults dividing the two areas.

The velocity modeling of the different areas is based on four wells that penetrated the whole Mesozoic cover without any major stratigraphic duplication due to major deformation. Only the Triassic unit shows internal structures triggering tectonic thickening, but these do not affect the velocity of the unit. In terms of velocity modeling, the distribution is the following (Figure 5-3 and Table 5-1):

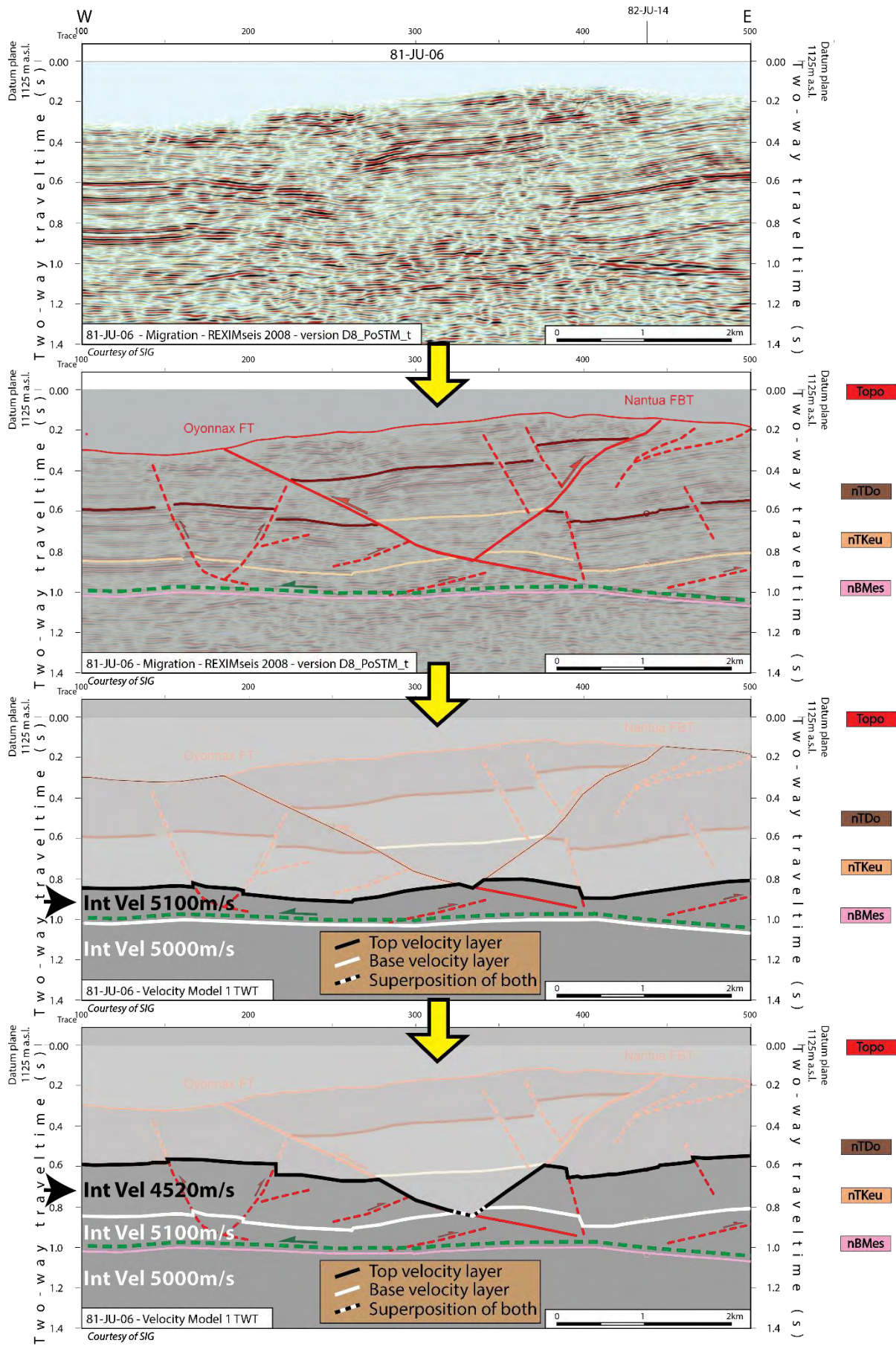
- The Geneva Basin (SPDC 2) and the Jura part (SPDC1) are represented by the well Humilly-2 (HU-2),
- The Subalpine Molasse part (SPDC3) is represented by the well Faucigny-1 (FAY-1),
- The Rumilly Basin (SPDC4) is represented by the well Chapery-1 (CHY-1),
- The Jura Meridional (SPDC5) is represented by the well La Chandelière-1d (LCD-1d).

Eight Mesozoic horizons are interpreted along seismic reflection lines in the Molasse Basin (see part 4.1.2). However only four horizons were integrated into the workflow of regional velocity model 1 and time to depth conversion: near Base Cenozoic, near Top Dogger, near Top Keuper and near Base Mesozoic. This involves five layers of constant interval velocity that are integrated into the model 1: Replacement velocity layer/ Cenozoic and layer/ Cretaceous+Malm/ Dogger+Lias/ Triassic/ Paleozoic. This multi-layer velocity model 1 was applied to each of the seismic datasets (Table 5-1), but the values of velocities in the model differs from each of the five groups of datasets SPDC (Figure 5-3). For group SPDC 1 and part of SPDC 5, the SRD 1125 m a.s.l and the replacement velocity of 4500 m/s were set up, whereas group SPDC 2, SPDC 3, SPDC 4 and part of SPDC5 datasets have been adjusted to SRD 500 m a.s.l along with a replacement velocity of 3000m/s (Figure 5-3).

The Mesozoic layers have quite limited thickness variations compared to the Cenozoic unit layer; hence, they may be easily associated with constant interval velocity unlike the Cenozoic layer that has a non-negligible gradient of velocity. These assumptions about velocities are confirmed by well data (Table 5-3 and Figure 5-7). In order to take into account the important thickness change in the Cenozoic series (Sommaruga et al., 2012), the velocity of the Cenozoic layer has been adjusted manually by adding a second intra Cenozoic layer in order to match as much as possible this velocity gradient (Table 5-1 and Figure 5-12). Quaternary sediments are included in the Cenozoic layer during seismic processing (static corrections) in terms of velocity association (that is why it this layer is not represented in Table 5-1). This was especially relevant in the Molasse Basin with the seismic lines of groups SPDC 2, SPDC 3 and SPDC 4. Pre-Mesozoic constant velocity of 5000m/s was chosen in accordance with the methodology of Sommaruga et al. (2012).

The main advantage and innovation of the method developed in this time to depth conversion workflow, is that the duplications of layers are taken into account in the modeling process. This has required to adapt the workflow in the Kingdom software. The conventional way of using this depth conversion tool, proposes only to configure "layer cake" velocity models, which means that each horizon can have only one depth or TWT vertical positioning value at each lateral location point. Our adapted method consists of creating a submodel for each of the duplicated thrust structures (Figure 5-4). This technique allows obtaining more realistic depth converted sections, by avoiding fault shadow artefacts (Figure 5-4 and Figure 5-11). The outputs of the regional velocity model 1:

- 4 seismic horizons converted into depth (near Base Cenozoic, near Top Dogger, near Top Keuper and near Base Mesozoic) along numerous seismic profiles in the 5 areas,
- A selection of seismic profiles converted into depth (SPDC 1-2-3-4-5, see Figure 5-3).



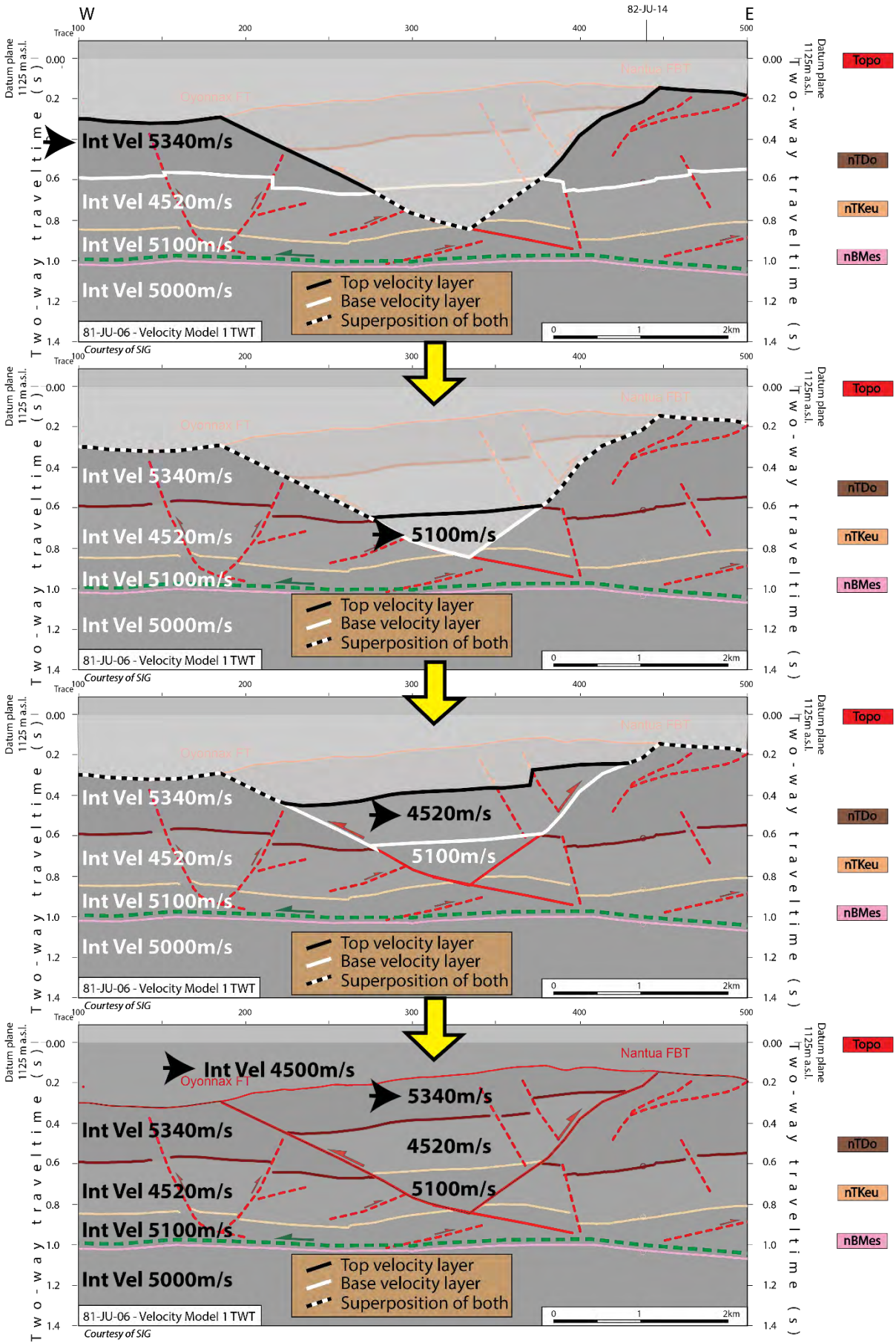


Figure 5-4 : Velocity model building of seismic section 81-JU-06 (trace range 100-500 see Figure 5-5 for localisation of the part of the line). This line belongs to SPDC1 (located in the Jura part, see Figure 5-3). The four seismic horizons are picked, near Base Cenozoic, near Top Dogger, near Top Keuper, and near Base Mesozoic. Several structural duplications are present, and handled in the velocity modeling 1, but not in the conventional modeling of velocities in the Kingdom software. Each section of this figure is highlighting the picking of each velocity boundary from the deeper layers (top left figure) to the shallower units (bottom right), using the faults sticks and the topography, in order to allow the modelling of the duplication (see location of the section in Figure 5-5). See Encl 37 for detailed seismic interpretation of line 81-JU-06.

5.1.3 Geneva Basin velocity model 2

This second velocity model is intended for converting into depth the eight main seismic horizons in the Geneva Basin with the highest precision as possible (Figure 5-6). For that, all wells available inside the area that own velocity information were gathered into the velocity model 2. However, the velocity modeling was achieved differently for nBCen horizon than for the seven following Mesozoic horizons. Indeed, for nBCen seismic horizon, a polynomial law ($Z=f(TWT)$) was calculated from velocity information (apparent velocity) extracted for 16 wells located inside the area and that reached at least nBCen level (Table 5-3, Figure 5-5 and Figure 5-7). The extracted apparent velocity information corresponds to actual depth of the formation top (nBCen) from the wellbore divided by the TWT value extracted from the final TWT grid at the intersection with the well. Note that the formation top depth is actually related to the SRD as reference level for calculation, in order to be in line with the twt values also calculated from this datum. This fact would give very similar results than if the calculation were made from the ground level, since the thickness between the topographical surface and the SRD is relatively constant and thin (both surfaces are approximatively around +500m m a.s.l). This kind of velocity allows considering all 16 wells of the area containing at least a nBCen formation top depth value. Indeed, if we would use only wells that have been tied to seismic, the number of velocity information would be much less (5 wells only), and therefore the accuracy of velocity modeling would decrease. After having collected the 16 (TWT; depth(Z)) pairs data, a tendency curve was produced to fit as best as possible the raw data (Figure 5-7). The best result was obtained using a 6th degree polynomial function that gives a correlation coefficient R^2 of 0.9989, which proves the accuracy of the modeled curve. The resulting velocity curve begins around 2500m/s near the topographical surface and velocity increases relatively linearly until reaching an approximate asymptote of 4000m/s from around 1000m depth below SRD. The velocity function is modeling very coherent values, considering the modeled Cenozoic layer which is mainly constituted of marly sandstones (Morend, 2000; Signer & Gorin, 1995) from the Molasse USM formation. The linearly increasing first part of the curve represents the progressive compaction of the layer with depth. The second part, with a more constant value, corresponds either to the maximum compacted marly sandstones part of the Molasse, or to the higher velocity layer such as the limestones of the "Calcaires d'eau douce inférieurs" or the Siderolithic deposits (velocity around 4000m/s attested by GCo-02 VSP data). The polynomial velocity curve was then directly used to convert the TWT grid into a depth grid. In this process, each TWT grid point value will be associated to a unique resulting velocity value. The higher the TWT value is, the higher will be the resulting velocity value. It means that the velocity grid, is dependent on the structural configuration of the interpreted TWT grid. This approach is very realistic in terms of velocity modeling, in comparison to other technique such as the classical interpolation/extrapolation of interval velocity from well data. Indeed, for the latter, outside the area near the input well data, velocity is independent of local structures (highs or lows) in relation to the surface to convert into depth (Figure 5-8). The technique of velocity modeling (polynomial function) was only applied to convert into depth the nBCen

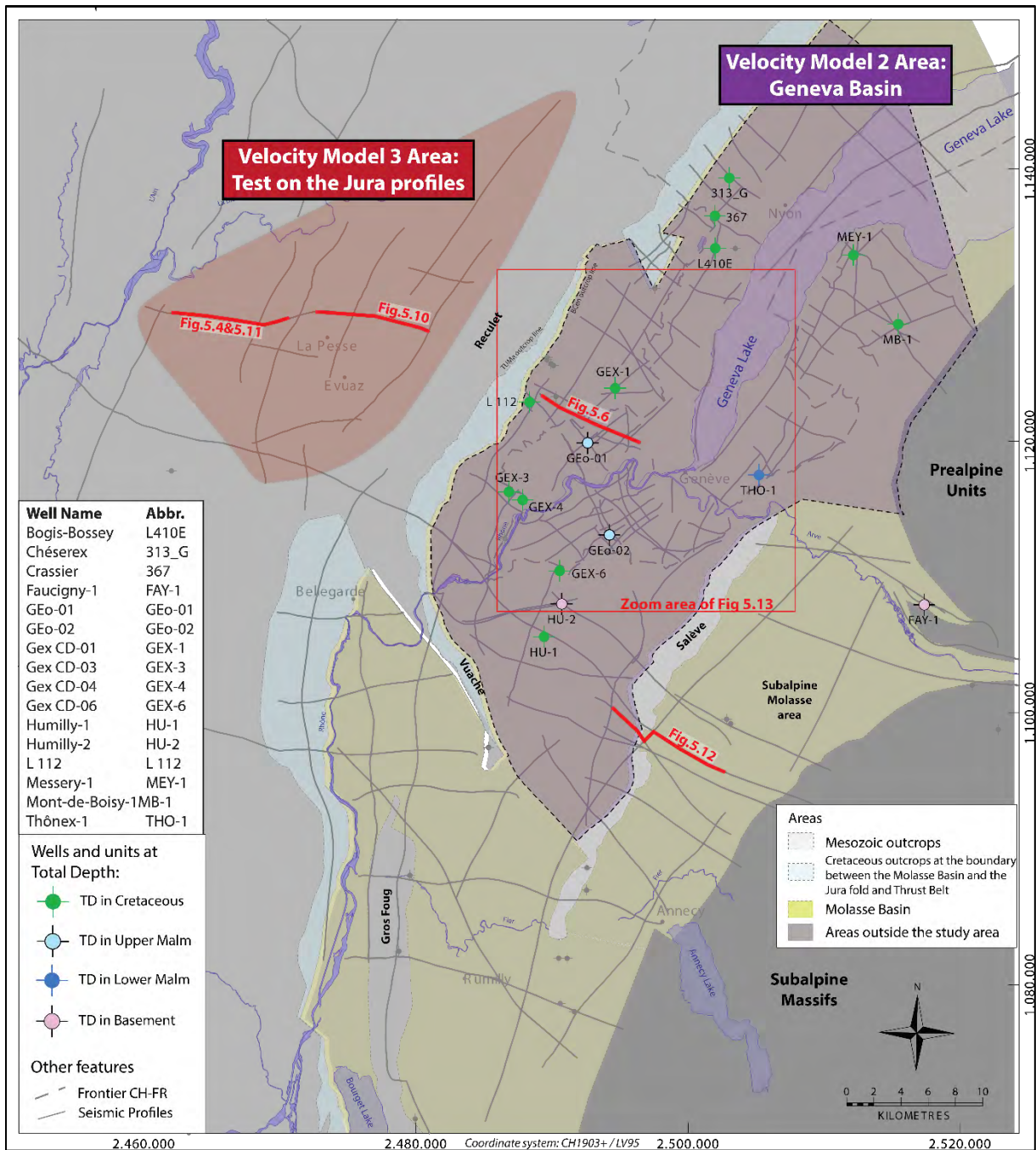


Figure 5-5 : Map showing the polygon in which grids are computed after depth conversion of seismic horizons using velocity model 2 inside the Geneva Basin. The main wells ,from which the velocity model 2 is extracted, are represented on this map in relation to their deepest seismic horizon reached by the drillings. Location of sections of several figures of this chapter are represented along red lines.

seismic horizon, because a sufficient number of wells reaching this horizon was available (16 wells). However, for the following deeper horizons, the number of available well data was not enough to accurately model a velocity tendency curve. Moreover, the Cenozoic layer is known to have a relatively important velocity gradient (2500-4000m/s velocity range) in addition to a highly variable thickness through the basin (0-2500m thickness range). The method used for this horizon was then specifically adapted, whereas the seven following Mesozoic intervals are varying more gently in thicknesses and are thus less affected by compaction than the Cenozoic layer. In that sense, a classical interpolation/extrapolation of interval velocity for the seven Mesozoic units was judged to be the most

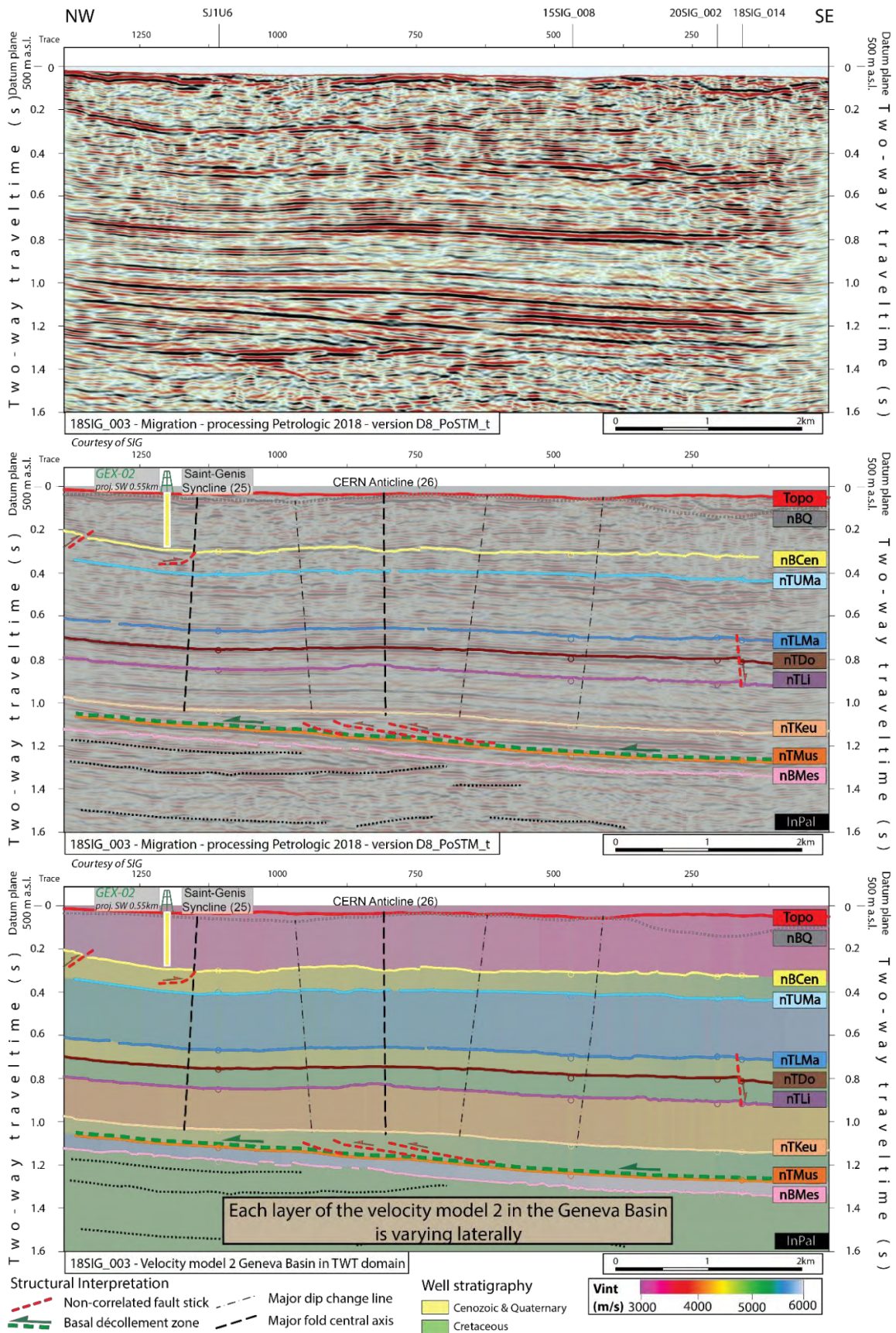


Figure 5-6 : Velocity model 2 applied on seismic profile 18SIG_003, in which 9 interval velocity layers are set up. Each layer is modeled with laterally varying velocities according to available well data and interval velocities from Vaud Canton (Marchant, 2016). We can observe well that velocity is increasing in SE direction, which is consistent with the structural and stratigraphical regional trend (see location of the section in Figure 5-5). See Encl 21 for detailed seismic interpretation of line 18SIG_003.

Interval	Abbreviation of interval top horizons on seismic profiles	Polarity of the seismic reflection	Velocity Model 2 Geneva Basin					Number of input velocities for velocity modeling of each layer	Type of velocity modeling
			Wells with interval velocities (m/s)						
			GEO-01	GEO-02	Hu-2	FAY-1	THO-1		
Cen int	SRD	Nothing	T=f(Z)	T=f(Z)	T=f(Z)	T=f(Z)	T=f(Z)	16	T=f(Z) function*
Cret int	near BCen	Trough (-)	4833	5974	5345	5733	5676	5 + Vaud**	Interval velocity Grid
Uma int	near TUMa	Trough (-)			5532	5750	5831	3 + Vaud**	Interval velocity Grid
LMa int	near TLMa	Peak (+)			4718	5370		2 + Vaud**	Interval velocity Grid
Do int	near TDo	Trough (-)			5400	5135		2 + Vaud**	Interval velocity Grid
Li int	near TLi	Peak (+)			4165	5130		2 + Vaud**	Interval velocity Grid
Keu int	near TKeu	Peak (+)			5101	6302		2 + Vaud**	Interval velocity Grid
Mu int	near TMu	Trough (-)			5101	4355		2 + Vaud**	Interval velocity Grid
Pal int	near BMEs	Peak (+)			5000	5000		1	Constant interval velocity
-> 9 Velocity layers	-> 8 seismic horizons							** Interval Velocity gridding was controled from NE by results from GEOMOL Vaud (Marchant, 2016)	

Table 5-2 : Table summarizing the vertical distribution of the velocity model 2 in the Geneva Basin in relation to the main inputs.

appropriate tool for velocity modeling (Table 5-2 and Figure 5-5). To increase the number of input data for the interval velocity gridding, control points from outside the GVA area (but in the vicinity) were used and integrated into the process. Indeed, the well Fauigny-1 that contains a complete Mesozoic column and related interval velocities was considered, as well as the interval velocity information from the GEOMOL project of the Canton de Vaud (Marchant, 2016). For the latter values, the velocity grids of the neighboring canton project were cut in the northern part of our area and directly incorporated in the gridding process in combination with the other well data. This allowed to better constrain the regional trends.

The interval velocities used are the result of the seismic to well tie procedure of the various wells (see 4.1). The classical algorithm of minimum curvature was used for gridding the interval velocities values of the different wells. The geometry of the resulting grid was adapted to the density of data with a relatively large bin size of 200mx200m. The final velocity grids are shown in Encl_M53 to Encl_M59.

We can observe on the interval velocity grids that the regional structural and stratigraphical trend is respected. The Mesozoic cover is dipping regionally towards SE direction, and compaction is increasing in the same direction, and therefore also the velocity trends. These velocity tendencies may also be related to the overall sedimentary basin orientation of each unit (see paleogeographical maps (Figure 2-11). Indeed, it usually influences the thickness trends and even the lithological trends (for diachronous deposits for instance), and therefore this can be highlighted by the interval velocity lateral variations.

For the Pre-Mesozoic interval, no direct velocity information are given by wells in the region of the study. We considered a constant velocity of 5000 m/s for this part, as proposed by Sommaruga et al. (2012) and confirmed by measurements made by Hefny et al. (2020) based on Humilly-2 data. All Pre-Mesozoic lineaments interpreted are depth converted using this velocity.

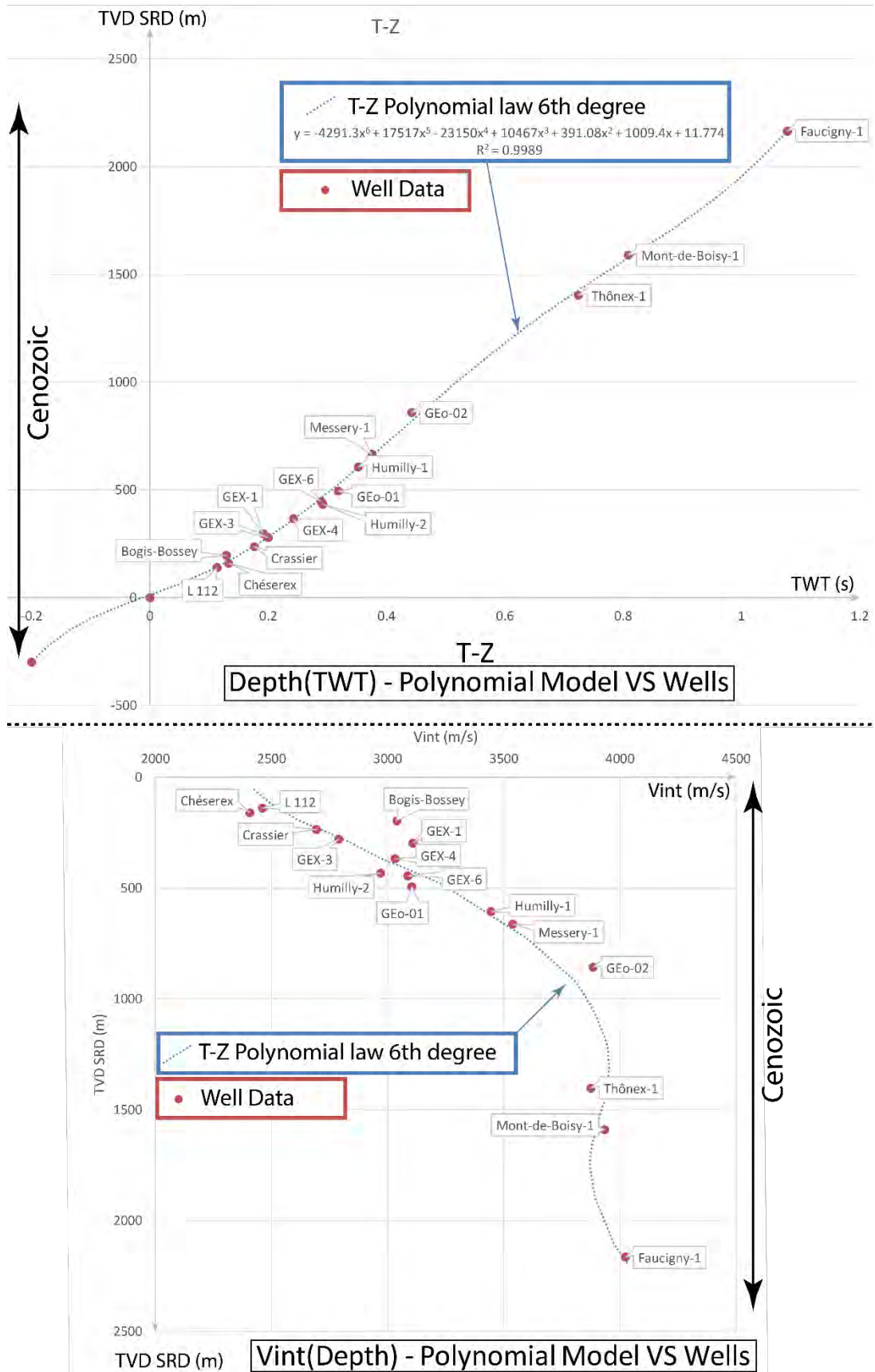


Figure 5-7 : Velocity modeling of the Cenozoic unit (from SRD). The 6th degree polynomial function (dashed blue line) is chosen as the tendency curve modeling the 16 Well data (T,Z) pairs (top image) that reached nBCen horizon. This function is then used for converting the nBCen seismic horizon from Time to depth domains. On bottom image is the resulting velocity curve in blue overlying the well velocity data.

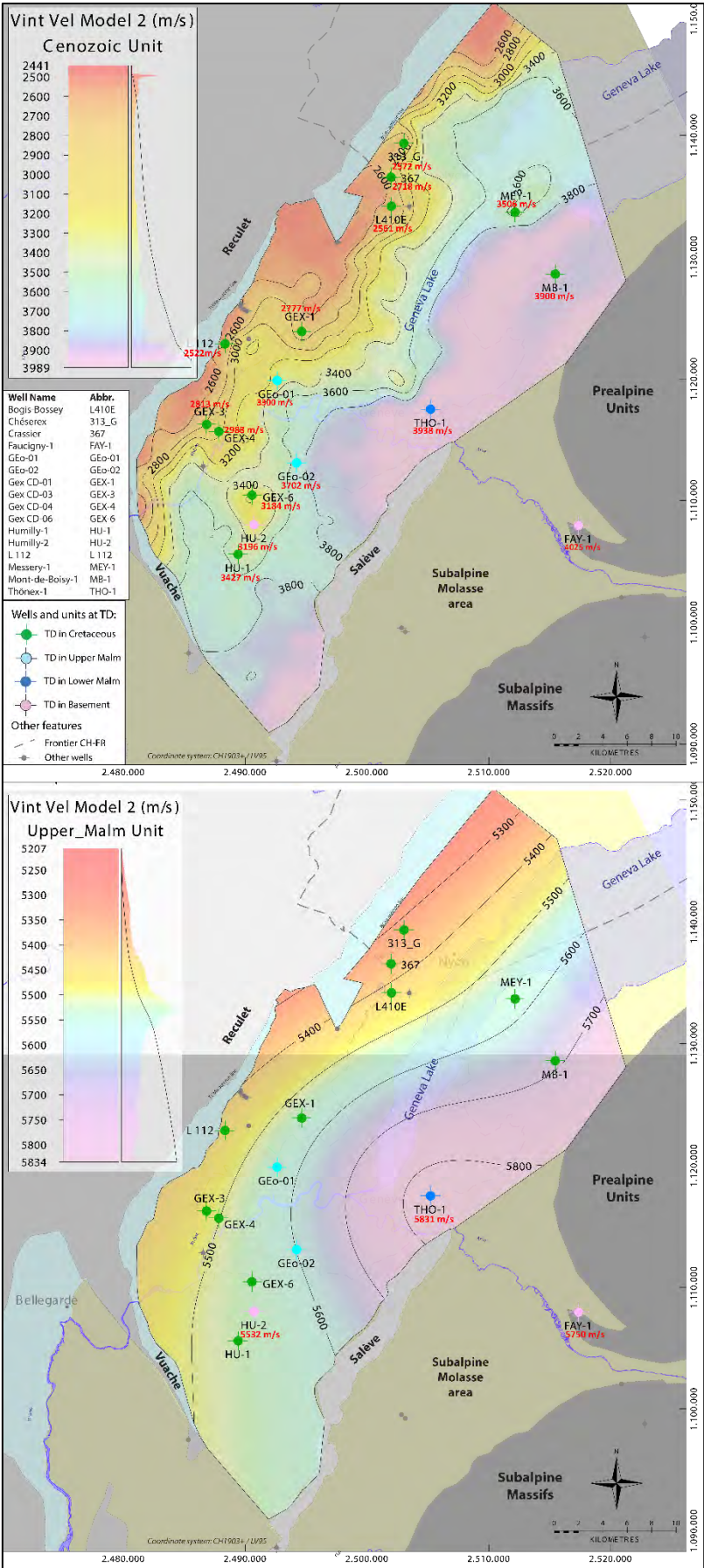


Figure 5-8 : Example of velocity grid of the polynomial law for nBCen (top image), and interval velocity grid for nUMa (bottom). See enclosures from Encl M53 to Encl M59 for all velocity maps used for Geneva velocity model 2.

Data of nBCen or Cen interval	Well Data			Polynomial Model 6th degree		Absolute Difference between Well Data and Polynomial Model	
	TWT (s)	TVD SRD (m)	Int Vel (m/s)	TVD SRD (m)	Int Vel (m/s)	TVD SRD (m)	Int Vel (m/s)
Bogis-Bossey	0.129	196	3039	165	2561	31	478
Chésereux	0.133	160	2406	171	2572	11	166
Crassier	0.176	237	2693	239	2718	2	25
Faucigny-1	1.077	2166	4022	2167	4025	1	2
GEo-01	0.318	494	3105	525	3300	31	195
GEo-02	0.442	858	3884	818	3702	40	183
GEX-1	0.191	297	3110	265	2777	32	333
GEX-3	0.2	279	2790	281	2813	2	23
GEX-4	0.242	367	3033	362	2988	5	45
GEX-6	0.289	446	3087	460	3184	14	98
Humilly-1	0.352	606	3444	603	3427	3	17
Humilly-2	0.292	434	2970	467	3196	33	226
L 112	0.113	139	2460	142	2522	3	61
Messery-1	0.375	664	3540	657	3506	6	33
Mont-de-Boisy-1	0.808	1589	3934	1576	3900	14	34
Thônex-1	0.724	1402	3874	1426	3938	23	64
						16	124
							Mean diff

Table 5-3 : Table of velocity information of well data in the Geneva Basin related to nBCen horizon and calculated for Velocity Model 2. These data are compared to the velocity information given by the polynomial function 6th degree (Figure 5-7) used for modeling at best as possible the well data.

5.1.4 Velocity model 3 test

The velocity model 3 test is applied only within the dataset group SPDC1 (Figure 5-3 and Figure 5-5), and consists in building the first replacement velocity layer with 4500 m/s along with the datum of 1125 m a.s.l, in exactly the same way as for model 1 for this layer (Figure 5-4). In the seismic section, below the topography, a constant interval velocity of 5000 m/s is attributed, which represents a quite realistic compromise for modeling any Mesozoic layers in the Molasse Basin or in the Jura FTB (Sommaruga, 1999; Sommaruga et al., 2012). This model is named “test” because it was only a model used in order to produce intermediate products. The resulting depth-converted section

		Velocity model	Model 3 test
		Seismic reference datum	SRD 1125 m a.s.l
		Reference well for velocity modeling	Theoretical
		Group for velocity modeling	SPDC1
Stratigraphic intervals	Modeled intervals	Polarity of the seismic reflection	Jura North part
From SRD to Topography	SRD		4500
Cenozoic	Topo		5000
Cretaceous			
Upper Malm			
Lower Malm			
Dogger			
Lias			
Keuper			
Muschelkalk			
Paleozoic /Precambrian	near BMes	Trough (-)	
	-> 1 seismic horizon		-> 2 Velocity layers

Table 5-4 : Table summarizing the vertical distribution of the velocity model 3 in the Jura part (SPDC1, see Figure 5-3 for localization). One constant velocity of 5000m/s is used below topography. See Figure 5-5 for localization.

using this very simple model, gives an interesting comparative basis for evaluating the uncertainties related to other velocity models such as velocity model 1 (Figure 5-10).

5.1.5 Discussion about the velocity models and uncertainties

An interesting comparison point between the regional model 1 and model test 3 results consists in analyzing the resulting elevation of near Base Mesozoic horizon in depth of the two models. It has been observed that a maximum of 200 meters (approximation) may be present between the two types of results (Figure 5-10) in the Jura FTB part at around 3000 meters below topography. This value gives then an idea for quantifying the uncertainty about this time depth conversion method, or more precisely about the possible increase of precision of the resulting depth horizons from our model 1.

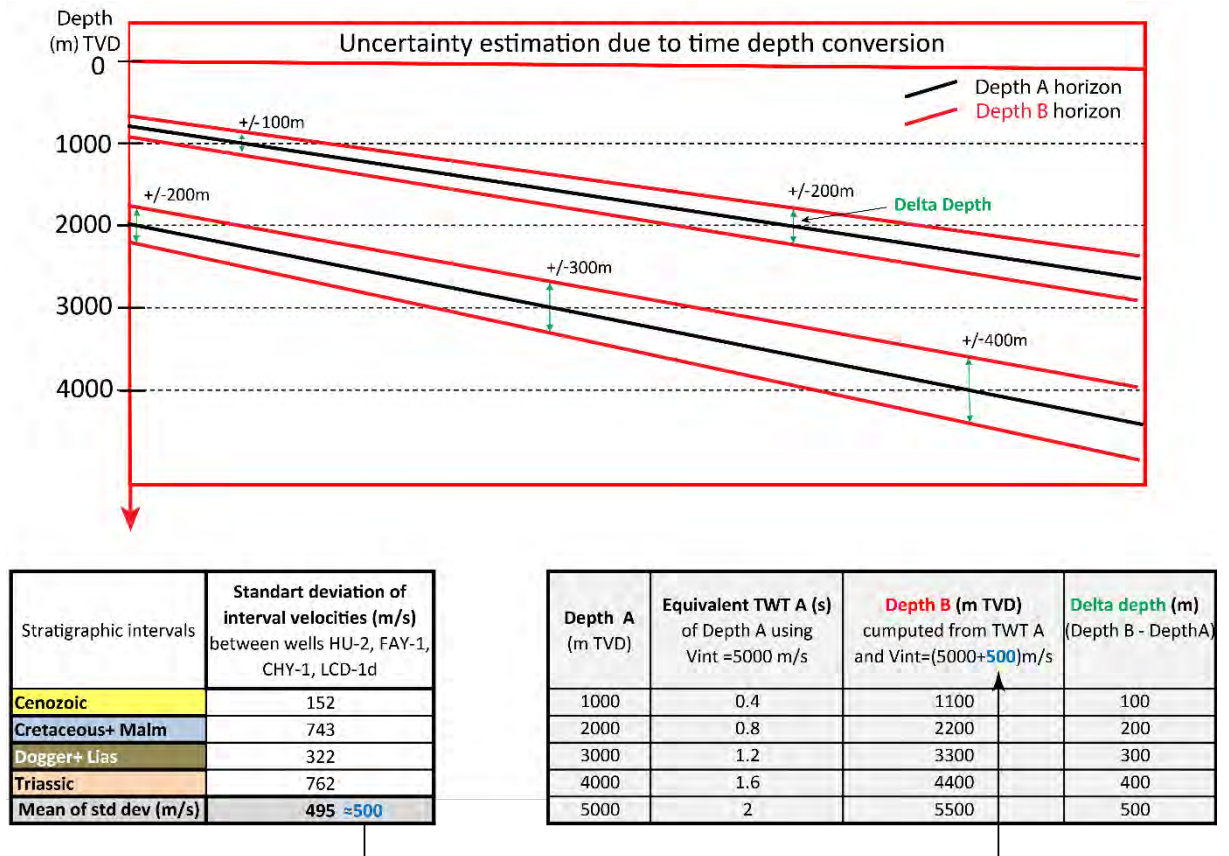


Figure 5-9 : Uncertainty estimation linked to the velocity modeling and to the time to depth conversion process.

We can verify this uncertainty value by a calculation. In Figure 5-9, we have computed the standard deviation of interval velocity between the different areas for each sub layer of regional velocity model 1. This gives a mean of standard deviation of interval velocity (in between all sub layers and sub regions of regional velocity 1) of 500 m/s. The four wells are separated by a distance of more than. This means that away from wells (for instance in between wells at 12,5km distance from one well), the velocity of each modeled layer could be potentially overestimated or underestimated by 500 m/s. If we consider depth values as multiple of 1000m/s (depth A in table of Figure 5-9), we can calculate the equivalent TWT values of these depths with the simple formula of the velocity (Figure 5-1), taking into account the mean velocity of 5000 m/s below topography. Then we can calculate back the equivalent depth with the same velocity (5000 m/s) added up with the standard deviation velocity mean value of 500

m/s. The difference between the two depth types (depth A and depth B) gives the uncertainty value of time to depth conversion using our velocity modelling method. This uncertainty increases with depth, which is logically inherent from the velocity formula (Figure 5-1). Away from wells and at the depths of 1000m and 4000 m below surface the time to depth conversion may contain vertical errors of respectively 100m and 400m (Figure 5-9).

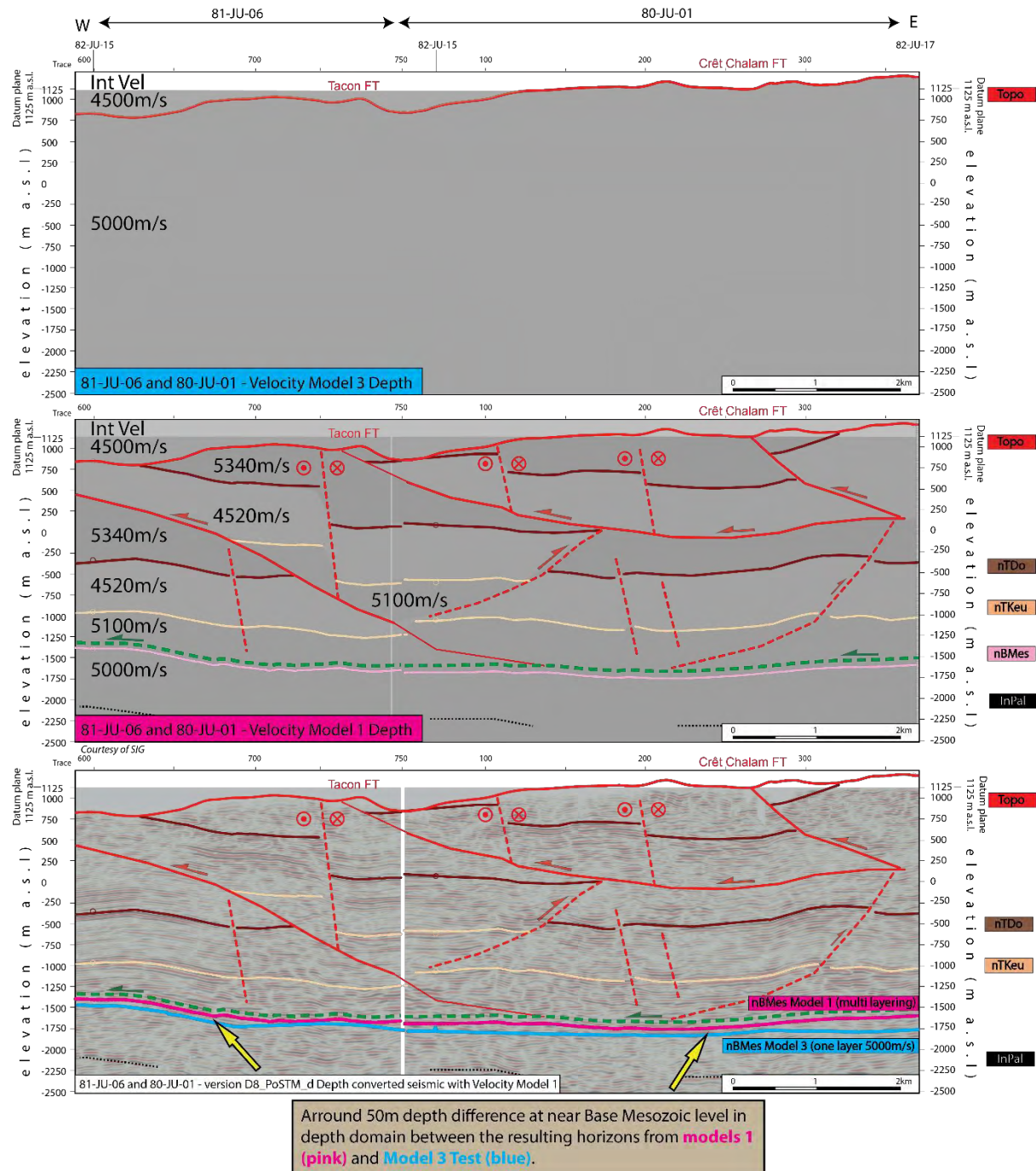


Figure 5-10 : Comparison between velocity model 1 et 3 and their resulting depth conversion. At near Base Mesozoic level, a maximum of 200 meters depth difference can be measured between two models (50m average difference) (see location of the section in Figure 5-5). See Encl 37 for detailed seismic interpretation of lines 81-JU-06&80JU-01.

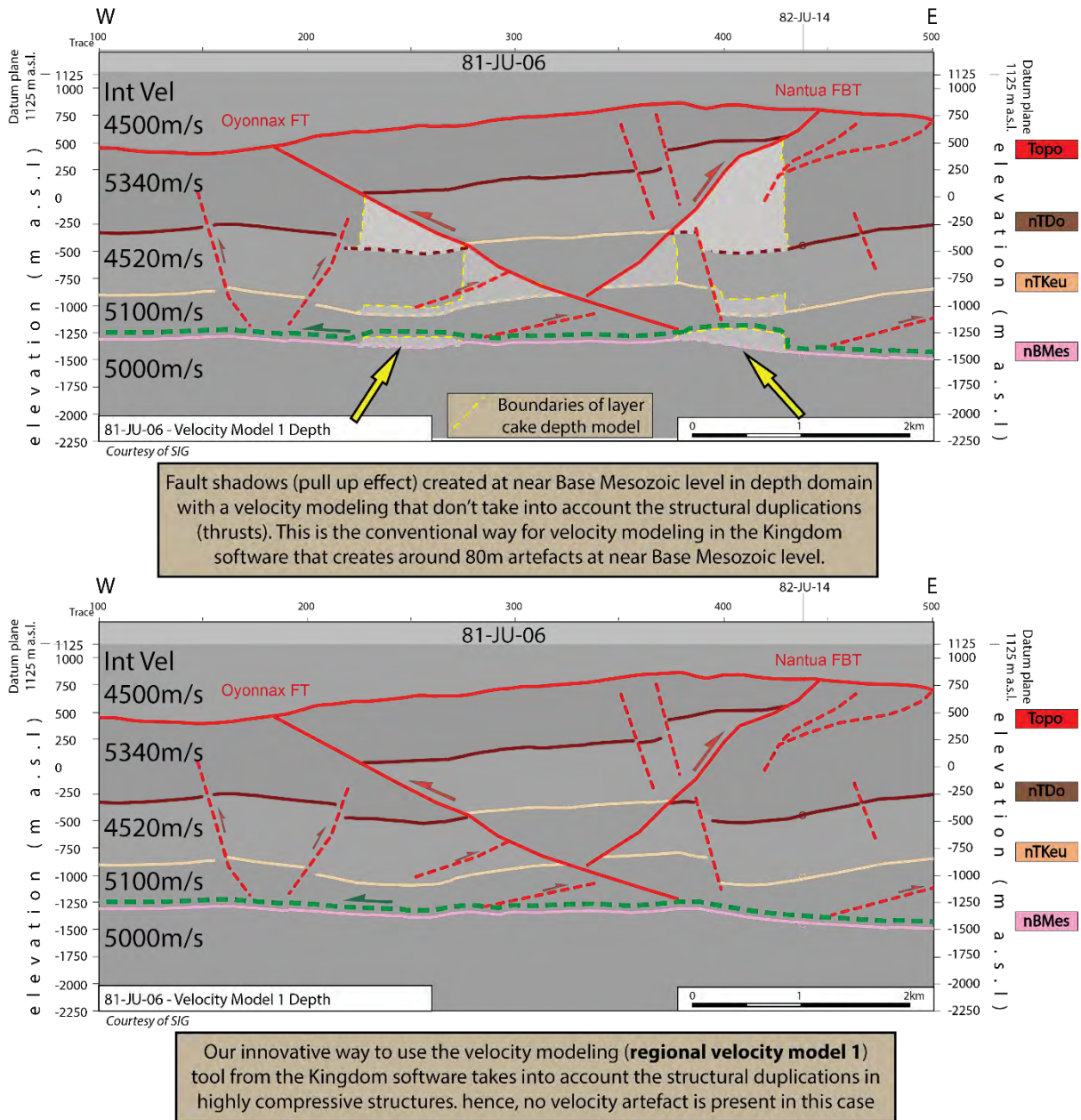


Figure 5-11 : Comparison between our modeling technique (down) that takes into account geological duplications into the modeling workflow with the conventional “layer cake” technique (above). The latter generates fault shadows artefact into nBMes seismic horizon (see location of the section in Figure 5-5). See Encl 37 for detailed seismic interpretation of line 81-JU-06.

The use of four seismic horizons to build the velocity model 1, compared with the use of eight seismic horizons (velocity model 2) will generate very similar results, due to the fact that the overall interval velocity of the Mesozoic layers will be nearly the same in both cases (depending only on slight lateral thickness variations of each layer). The maximum depth difference uncertainty between the two time to depth methods (Model 1 and Model 2) can be estimated around 5-10m.

In general, sections in depth domain avoid artefacts, such as “pull up” or “push down” effects. These artefacts in time domain are due to major lateral velocity heterogeneities and to structures, which generate a bending upward or downward of all seismic reflections below these major heterogeneities (Li & Mitra, 2020). Major thrusts, such as the Salève Mountain, create exactly this kind of velocity

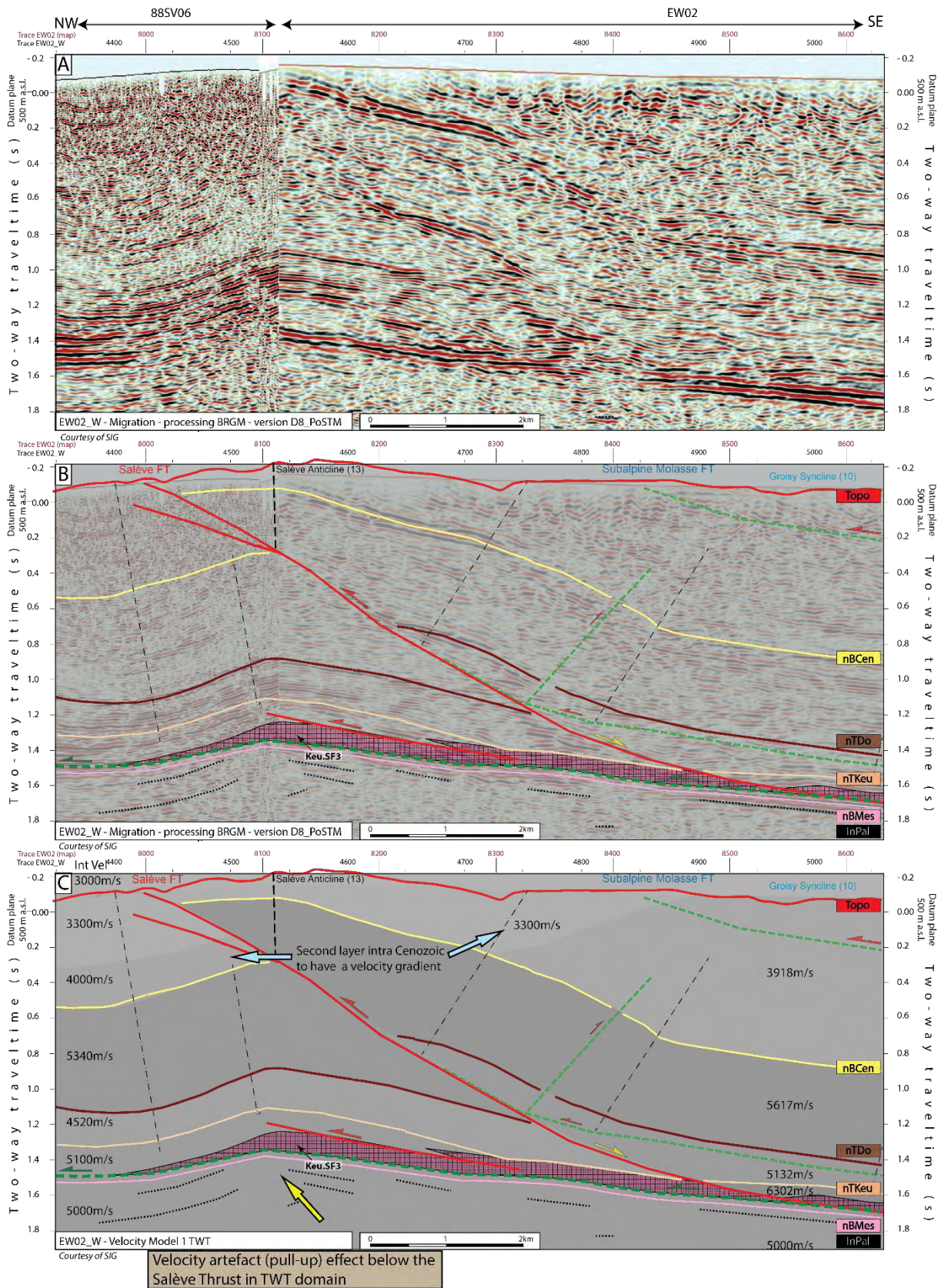


Figure 5-12a : Our modeling technique and resulting time to depth conversion allows removing pull-up effect below high lateral velocity variations. Here is the example of the Salève area with seismic section EW02_W (see location of the section in Figure 5-5). A: twt uninterpreted section, B: twt interpreted section, C: twt velocity modelling section (regional velocity model 1, see 5.1.2). See Encl 61 for detailed seismic interpretation of line EW02_W_SAM.

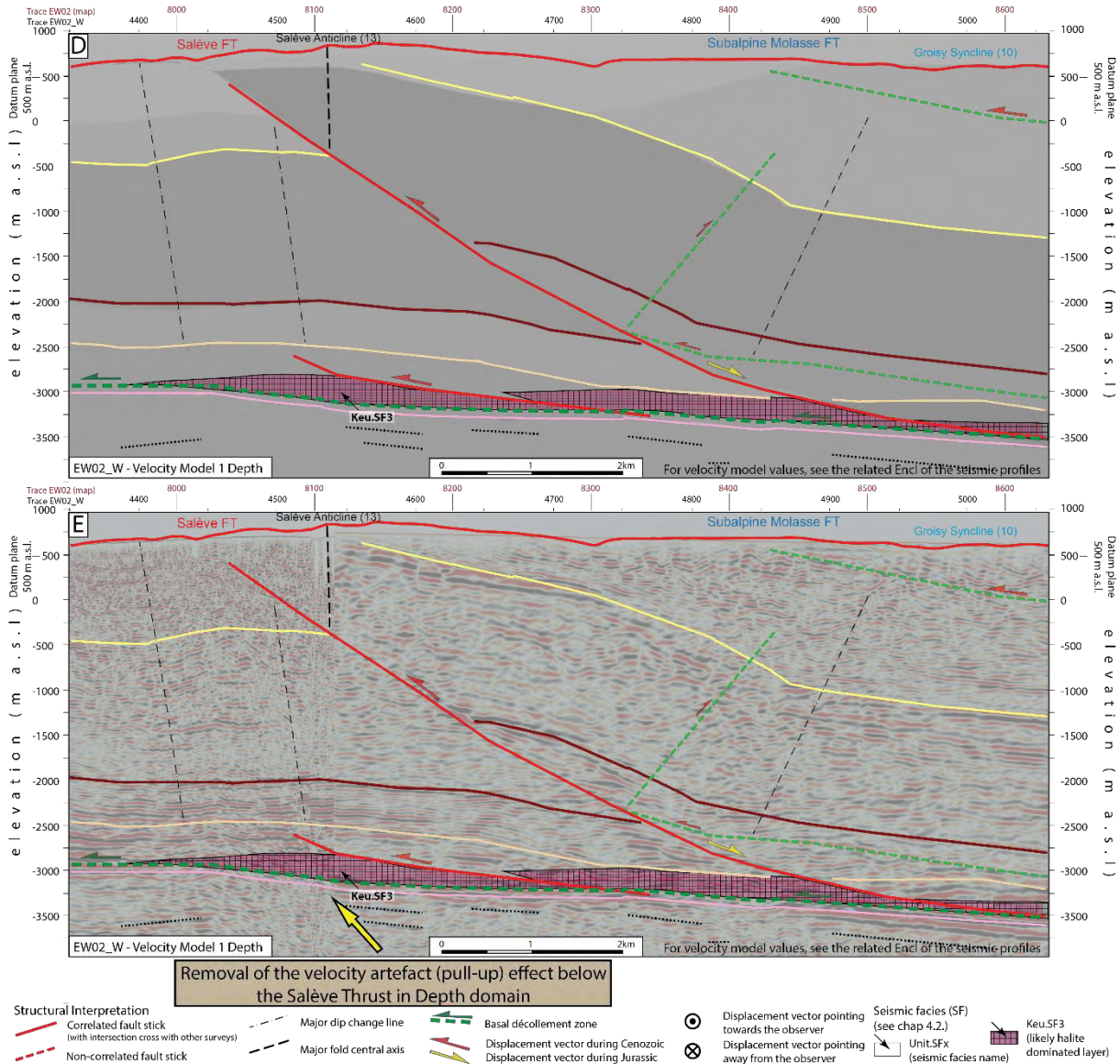


Figure 5-12b: Our modeling technique and resulting time to depth conversion allows removing pull-up effect below high lateral velocity variations. Here is the example of the Salève area with seismic section EW02_W (see location of the section in Figure 5-5). D: depth velocity modeling section (regional velocity model 1, see 5.1.2), E: depth converted seismic section with above velocity model (regional velocity model 1, see 5.1.2). See Encl 61 for detailed seismic interpretation of line EW02_W_SAM.

heterogeneity, hence a resulting pull up effect. Our methodology for time depth conversion gives results that seem to compensate very well this artefact (Figure 5-12). Another advantage of our workflow of model 1, is that the duplications of layers are integrated into the modeling. This allows to convert into depth compressional tectonic structures with accuracy by removing fault shadow artefacts (Figure 5-11). The explanations given in this chapter is mentioning mainly the time to depth conversion of seismic horizons. However, fault sticks were also converted into depth following the same methodology, also in the “dynamic depth conversion and map update” tool of the Kingdom software.

Some suggestions for improvements of our methodology may be proposed this way:

- Additional layering of the velocity model may be computed (especially for model 1),

- The relevance of the constant velocity modeling of each layer may be revised (especially for model 1). If needed, interval velocity maps varying laterally may be used. Seismic processing velocities may also be incorporated into the modelling. The velocities derived from the coming 3D seismic processing in the Geneva Basin may be of a particular interest (for model 1 or 2),
- Concerning the particular case of the Cenozoic layer, the next well drilling reaching near Base Cenozoic in the Geneva Basin may bring crucial velocity information that could help improving the velocity law of the Cenozoic layer,
- More well velocity information may be incorporated into model 1 (such as Charmont-1 for model 1) even if they have duplications (not continuous Mesozoic column), and even if their seismic to well tie is not optimum.

These actions would have the effect of decreasing the dispersion related to the velocity modeling, hence reducing the related uncertainty.

5.2 Gridding methods

Gridding consists in interpolating together the 2D seismic horizon values (TWT in seconds or depth in meters) along seismic profiles in order to create 3D surfaces. These surfaces are called grids because the interpolation is achieved along a regular cellular (square) grid, in which one value (depth (m) or TWT (s)) is attributed to each cell. The bin size of the computed grids reflects the resolution of the resulting model and should be adapted to the input data resolution. Considering the scattering of the interpreted seismic profiles, we have chosen a bin size of 50m for all computed grids. This calculation of the grids was done in Petrosys software which is a software fully dedicated to gridding and mapping. We have used the classical algorithm of minimum curvature for gridding which is known for optimizing the interpolation (Figure 5-13). An intermediate smoothing of the grids was also added for a better visualization. Faults can be integrated into the gridding using “faults polygons” (considered as barriers) which correspond to fault traces at the intersection between faults surfaces and the grids. The width of these fault polygons represents either the lateral offset of the seismic horizon induced by a normal faulting, or the lateral positioning uncertainty of the fault trace for any fault. No gridding is computed inside fault polygons. By default, the fault polygons were drawn with a width of around 50 meters. In some areas fault corridors have been identified and include numerous small-scale faults that could not be correlated in between seismic profiles (see 4.1.13). These fault corridors may have length of more than 10km and width of 500m. As they don't correspond to sharp structural boundaries compared with fault polygons, fault corridors (also polygons) are taken into account in the gridding process (contours stop at their edges), but the inside of the corridors is gridded (Figure 5-13). After the gridding process, contours can be added, and consists in isovalue lines (elevation) that allow characterizing the structural configuration of the 3D seismic horizons grid.

5.2.1 TWT grids

The input data for TWT gridding are the seismic horizons in TWT domain after mistie correction (see part 4.3). They are produced in relation to fault polygons and fault corridors (Figure 5-13). Manual corrections were locally applied on the computed grids, by smoothing certain contours in Petrosys

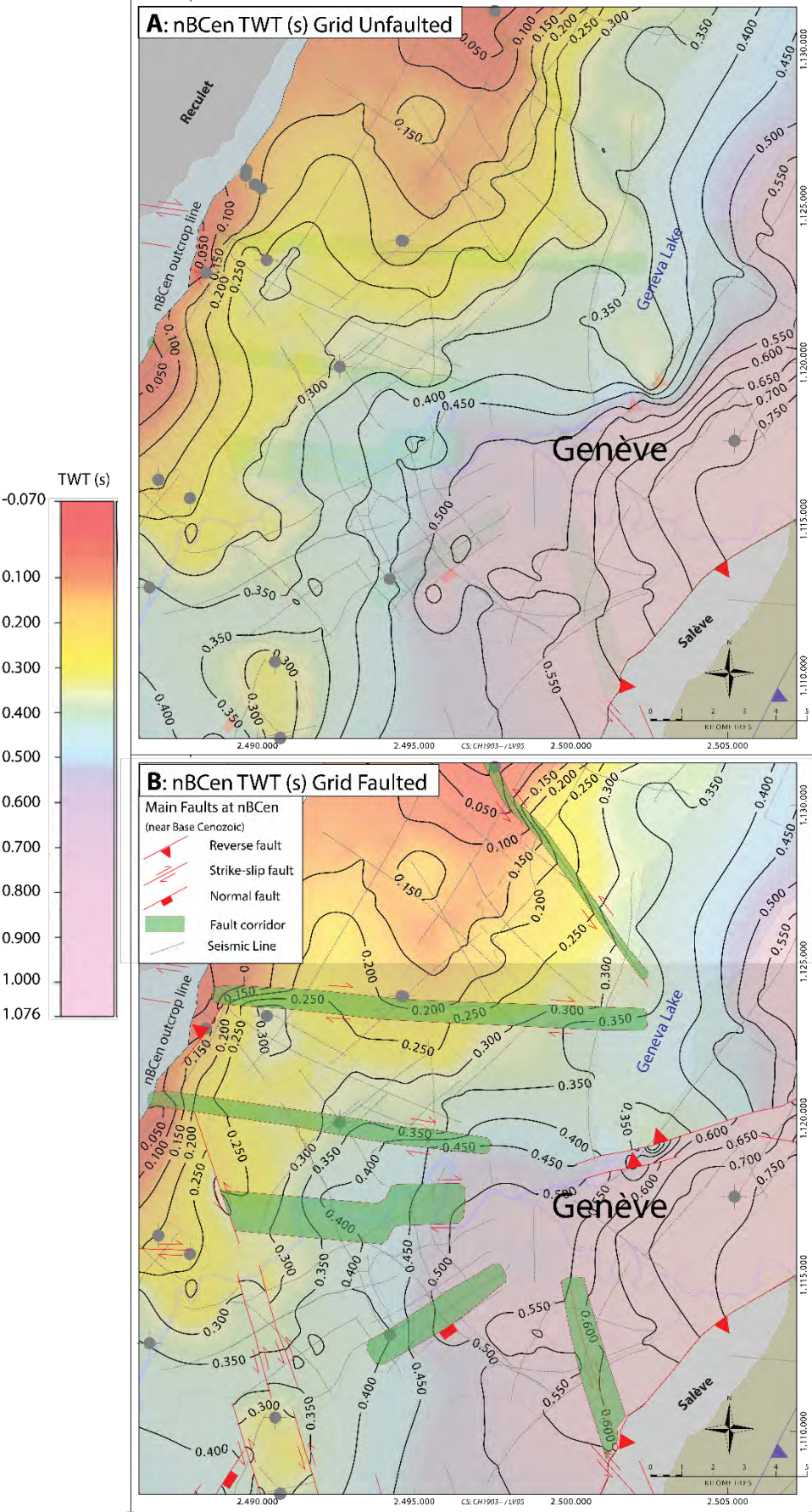


Figure 5-13 : Mapping example of twt gridding (nBCen) with (bottom) and without (top) fault polygons and fault corridors. See Encl from Encl M20 to Encl M35 for complete TWT grid results.

software followed by a second gridding with the manually adjusted contours as input data. The resulting grids don't go through any further adjustments according to well data or outcrops line, as these corrections make sense only in the depth domain (see Figure 4-1 for localization of the TWT grids in the project flowchart and see from Encl M20 to Encl M35 for final TWT grid results).

These results may be interesting for the structural analysis as they represent the raw interpretation data (only few adjustments) in comparison to the depth grids. For this task, it may be interesting to analyze the major change of directions of the contours that characterizes actually the major dip change, and possibly major tectonic directions. In the methodological workflow (see flowchart of Figure 4-1) the gridding in TWT domain has no further steps, the TWT grids will then not be used as input for further calculation such as the depth gridding.

Time (TWT) "thickness" grids ("isochrone") may be produced between two grids, by subtracting the deepest grid from the one above. It gives the possibility to observe vertical variations in time between two seismic horizons on the resulting isochrone map.

5.2.2 Depth grids

Depth grid results are compiled in enclosures from Encl M04 to Encl M19. See Figure 4-1 and Figure 5-2 for position of depth grids in the flow chart of the project.

In several parts such as in the Jura, Vuache, or Salève areas, the Mesozoic cover is partly outcropping. It has been possible to extract in ArcMAP from the topographical surface (SRTM), elevation values along the outcropping lines of the corresponding seismic horizons. This concerns the seismic horizons nBCen, nTUMa and nTDo, for which the depth modeling will need to take into account these outcropping elevation values.

To obtain depth grids, two main approaches are possible. The first method (approach A in Figure 5-14) consists in first computing TWT grids that are then converted into depth grids using a time to depth algorithm, such as the technique of interval velocity grid. The resulting 3D depth grid needs usually adjustments to control points such as well tops and/ or outcrops line elevations. The second approach (method B in Figure 5-14) consists in implementing the gridding step in a different order in relation to the time to depth process. First, the 2D seismic horizons (interpretation along seismic profiles in TWT) are converted into depth using a velocity modeling along each seismic sections (see part 5.1). The resulting 2D depth horizons are then gridded simultaneously with the control points (well tops depth and outcrops line elevations). The main difference between the two methods is that in the method B, the seismic horizons are taken as hard data, in a way that the final 3D grid will match closely the 2D seismic horizons in depth domain along the 2D depth converted seismic profiles. Only the smoothing of the gridding and the secondary well adjustments could generate small differences (few milliseconds) between the two. By contrast, the final depth grids resulting from approach A, could possibly be different than the depth converted data before adjustment to control points (outcrops line for instance) along 2D seismic profiles (Figure 5-14). Therefore, it has been decided to follow the approach B, so that the final depth grids would fit better the depth converted seismic profiles. Moreover, we think also that this approach produces more realistic results as it is less artificially modified by the gridding adjustments to control points.

After this process, a final supplementary well-tie is achieved. It involves slightly modifying the 3D grid (minimum curvature algorithm) within a distance of 2km around wells, so that it reduces at best the vertical discrepancies between well tops and the corresponding near seismic horizon (<5m residual discrepancies).

The regional velocity model 1 resulted in four 3D seismic horizons grids (nBCen, nTDo, nTKeu, nBMes), whereas the velocity model 2 located in the Geneva Basin has allowed producing eight 3D seismic horizon grids (nBCen, nTUMa, nTLa, nTDo, nTLi, nTKeu, nTMu, and nBMes).

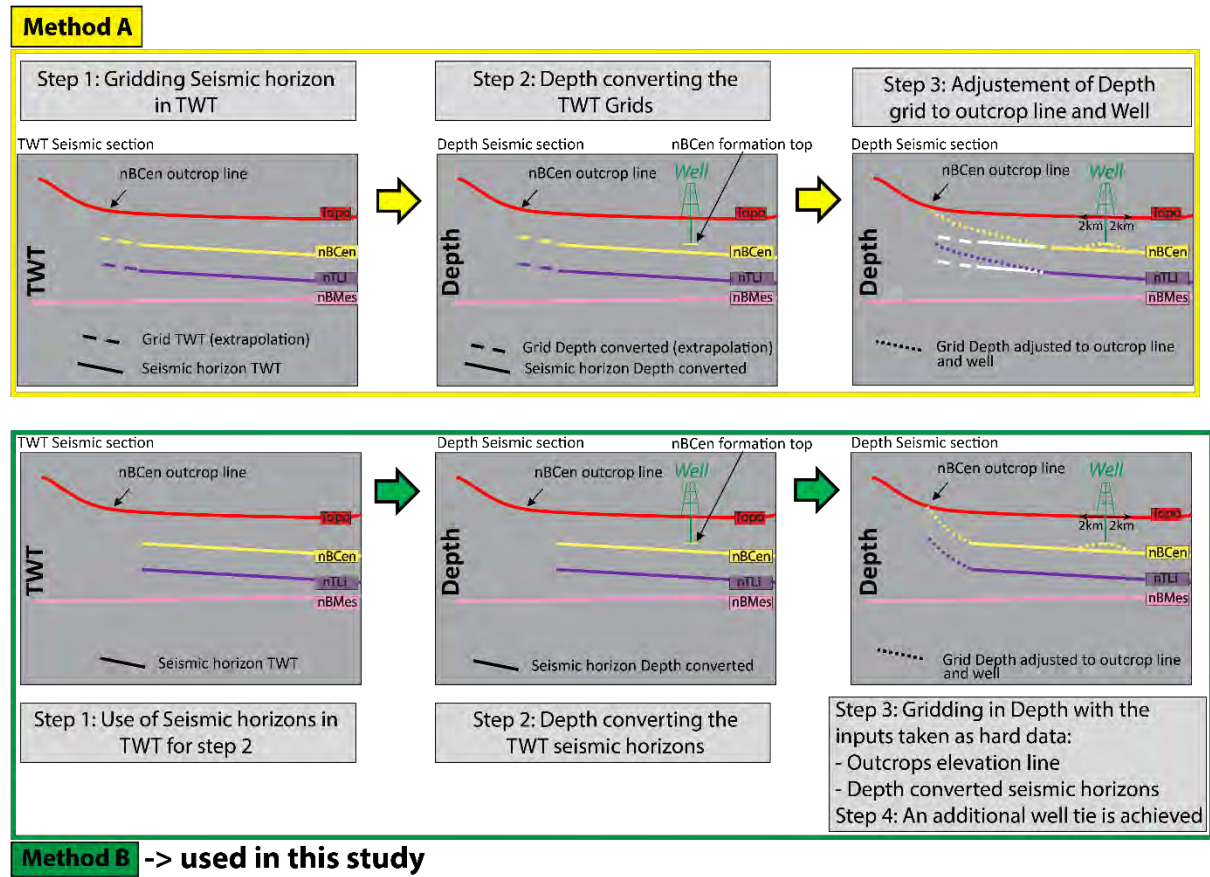


Figure 5-14 : Two possible approaches to transform 2D seismic horizon in TWT into 3D depth grids. We have used approach B for more realistic results that respect better the seismic interpretation picking geometries. Indeed, on approach A the final 3D grids could be modified on during the final adjustment to topographical lines and then mismatch the depth converted seismic profiles. See Figure 5-13 for grid display, which corresponds to interpolation of seismic horizon (ribbon data along interpreted seismic lines) in lateral direction resulting in 3D surface.

5.2.3 Interval thickness grids

Interval thickness grids are compiled in enclosures from Encl M36 to Encl M52.

The eight 3D seismic horizons grids produced in the Geneva Basin offer the possibility to compute vertical thickness grids (isochore). They represent “vertical” thickness (Figure 5-15) since they are computed from the subtraction of two seismic horizon grids. This differs from the “stratigraphic” thickness (isopach thickness) in areas of dipping bedding (Figure 5-15). Therefore, the isochore thickness maps may show decrease of values along the crest of folds (anticlines or synclines) compared

to the flanks. Nevertheless, it is possible to observe the major regional thickness changes of stratigraphic intervals that are higher than the “artificial” vertical thickness variations due to folding.

The thickness grids were still calculated in Petrosys software with the same parameters than the TWT or depth gridding.

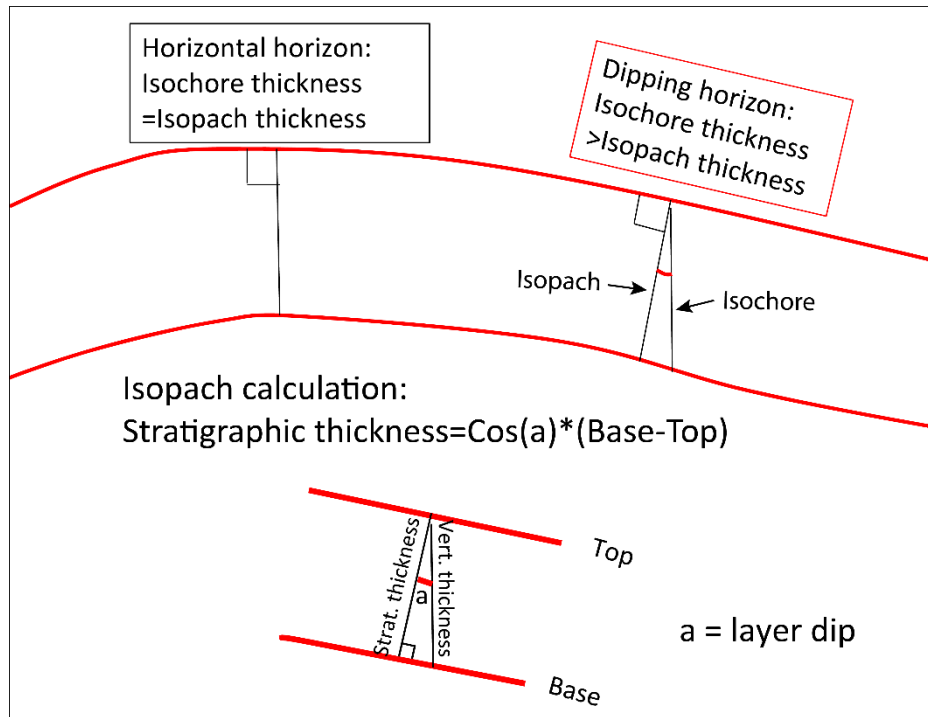


Figure 5-15 : Sketch defining the notion of isochore and isopach thickness. In our study, only isochore thickness maps are obtained after the seismic interpretation which differs from isopach thickness which represents the stratigraphic thickness (perpendicular to the bedding).

5.2.4 Uncertainty of gridding

The uncertainty of final depth grids owns the cumulative uncertainties of all previous steps that have already been addressed in previous paragraphs. We can particularly mention again the following uncertainties related to (see part 4.4):

- Seismic data and its misfits and datum plane adjustments,
- Seismic interpretation,
- Well data,
- Time to depth conversion.

Concerning the uncertainty of the final step of the gridding process, this corresponds in fact to the resolution of the grids, or to its bin size. Therefore, the gridding process is introducing a 50m lateral uncertainty, and for the vertical uncertainty we may consider that it is included into the uncertainty of the time to depth conversion that has been detailed in 5.1.5. Indeed, this previously mentioned uncertainty takes into account the notion of an increase of it away from wells.

6. SEISMIC INTERPRETATION RESULTS

This chapter summarizes the seismic interpretation results of this study. Firstly, the structural configuration of the investigated area, divided into five structural domains, is discussed. Each domain is characterized by one major specific structural feature that differentiates it from neighboring domains. These differences mostly concern the tectonic setting of the detached Mesozoic cover and that has deformed independently from the mechanically more rigid underlying mechanical basement s.l. The essential role of the evaporite-rich Triassic layers will be introduced as a preamble. The results will be addressed along with tectonic maps and cross sections. Secondly, selected, relevant stratigraphic observations will be discussed, e.g. main thickness variations and relevant seismic facies. This chapter will present a selection of local maps and seismic sections, but the complete set of results are available in Enclosures.

For each structural area, fault zones and main folds will be described in detail in the following. Fault zones and corridors are characterized by their name, location, type, geometry (lateral and vertical length, orientation), vertical and horizontal displacement, indication of syn-sedimentary activity. Age constraints will be discussed whenever possible. Folds will be described and the kinematic link to faulting and thrusting assessed. In order to guarantee a proper reading of the following parts, the main definitions and nomenclatures related to fault and fold characteristics are briefly discussed in part 6.1.

6.1 Structural styles

Hereafter a selection of the most common structural features, relevant for our work, is briefly introduced.

Nomenclature linked to folds and folding (Figure 6-1): A *fold* is a curved or bent planar structure of bedding plane, foliation, or cleavage, formed due to deformation (Saklani, 2008). An *Anticline* is a fold with older rocks in its core, and a *syncline* is a fold with younger rocks in its core (Fleuty, 1964).

Fold axis is defined as the nearest approximation to the line which, moved parallel to itself in space, generates the form of the fold (Donath & Parker, 1964). *Axial surface* (or axial surface plane, if it is planar) is the virtual surface, which passes through the hinge lines of the successive folded surfaces composing a fold. Implicitly the axial surface separates zones with different bedding inclination, called dip domains. Fold axis may plunge and form periclinal lateral closure associated with the fold termination. Folds may further be characterized by their asymmetry in limb length and inclination. Thus, the vergence (McClay, 1987) indicates the direction of movement that occurred during deformation. The concept of vergence of movement may be applied to asymmetric folds. Fold also may be open and broad to tight and isoclinal.

Frequently folds are associated with faulting and thrusting such as in fault-bend folds or fault-propagation folds (Mosar & Suppe, 1992). Folds may also be associated with salt flowage and/or result from duplexing in underlying horizons such as the Triassic evaporite series. Thus, the following main types of folds can be recognized (Figure 6-4):

- Monoclines: regularly dipping bedding panels.

- Fault-bend folds (FBF) (A in Figure 6-4): the classic fault-fold system where a fold develops over a tectonic ramp at the transition between two flats (upper and lower flats). Several fault-bend folds may develop in a multiple ramp-flat system. Fault-bend folds have to terminate towards the surface either by breaking through to the surface and being exposed to erosion, or by transforming displacement into a fold such as in fault-propagation folds.
- Fault-propagation folds (FPF) (B in Figure 6-4): in this model an anticline and syncline develop simultaneously over the propagating thrust ramp. The propagating ramp terminates at the lower tip of the syncline. A fault-propagation fold may evolve with the ramp breaking through, either the anticlinal or synclinal limb. The fold geometry is constrained by the ramp angle, which typically is around 30° but may be shallower or steeper. Fault-propagation folds show a strong asymmetry in their overall built, with a backlimb often parallel to the ramp and a steep forelimb indicative of the transport direction. A typical example of such a structure is the Salève thrust and fold in our study area. A special type of thrust and fold propagation are tri-shear folds. The tri-shear concept is similar to the fault propagation fold in that a syncline and anticline develop at the tip of a propagating ramp and over the ramp, respectively. However, in the tri-shear model the fold geometry is not constrained by the ramp and ramp angle, which allows for more complex geometries.
- Folds with direct contact to the décollement horizon and without connection to thrusts ramping upward through the sedimentary pile:
 - Folds with evaporite pillows filling (F in Figure 6-4): such folds are linked to the development of evaporite pillows (gentle antiforms) and may be due to evaporite flowage and/or development of tectonic duplexes (Sommaruga, 1997, 1999). The geometry of the fold developing over this type of structure is not directly linked to the décollement geometry but rather to the pillow geometry.
 - Detachment folds (C in Figure 6-4): detachment folds are located within an incompetent or at the boundary with a competent unit. The fold forms in the competent layers and can be understood as due to lateral compression and vertical fold development. Detachment folds are not directly related to any specific faults/thrust geometry. (see also Mitra (2003)). Lift-off faults and Box folds are similar to detachment folds, of which they may be considered as a special case. Lift-off and box folds are rather symmetric. Box folds are special cases of lift-off folds and exhibit a typical box-shaped geometry of limbs and flat top. Box folds typically are known from the eastern Jura FTB.

Main fracture/fault types observed in our area of investigation include:

Normal faults (Figure 6-3): normal faults may have different origins. They may be due e.g. to a syn-sedimentary extensional setting as in our study area and may be planar or listric shaped. Similarly, *reverse faults* may come as steeply dipping faults and/or more shallow dipping faults. *Thrust faults* are among the dominating tectonic features in our area of investigation. They include the main décollement level as well as thrusts related to the fold development. Steeper *ramps* develop in the mechanically stronger levels and may connect thrust flats. Frontal ramps are defined to be perpendicular to the transport direction (often derived from the trend of the fold axis); whereas lateral or oblique ramps are at a different angle to the transport direction. Lateral ramps (oblique ramps sensu stricto) occur on numerous thrust and reverse fault terminations or at the transition from strike-slip faults to thrust zones, or along inclined strike-slip faults. They have gently to steep inclinations. This type of oblique convergence leads to the formation of transpressional zones, often with

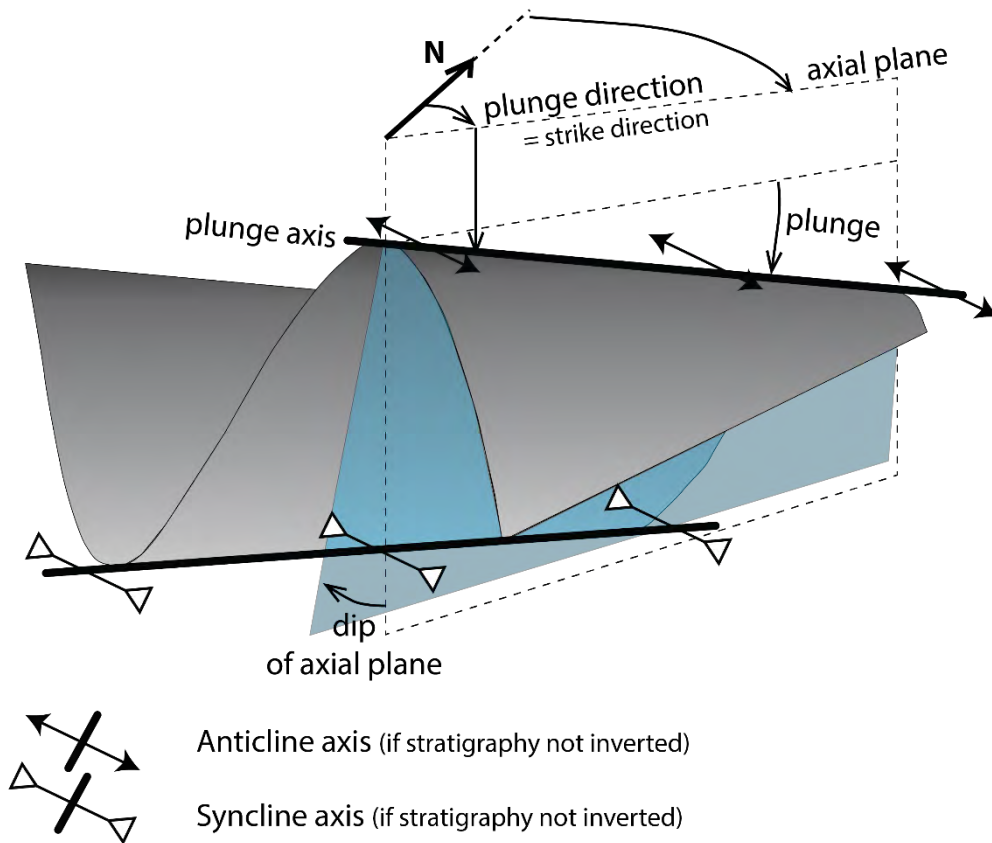


Figure 6-1 : Fold definitions of axial plane, plunge direction and angle, and fold dip angle. Here is an example of a syncline followed by an anticline.

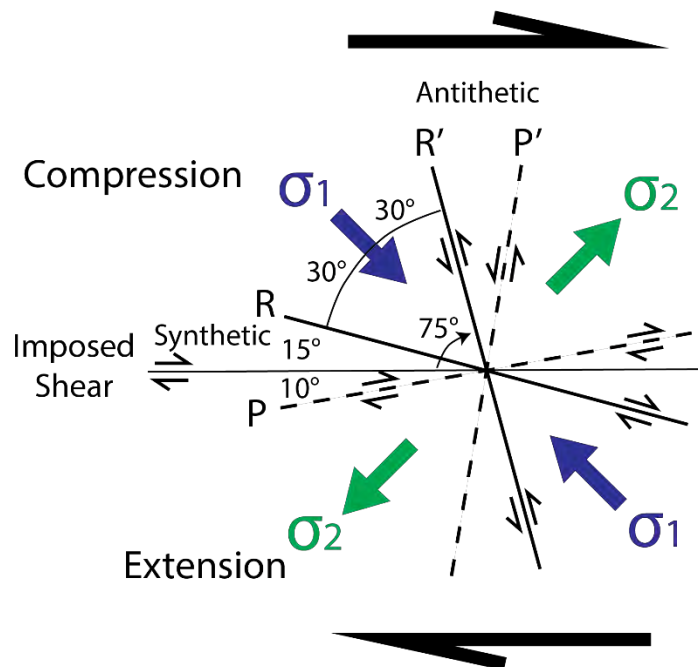


Figure 6-2 : Riedle faults system along a larger dextral strike fault zone (principal displacement zone). Riedle -shears (R) are necessarily present in this system, and often conjugated with P-shear (synthetic). The antithetic system R' and P' are conjugated shears symmetrical to R and P with respect to the main compression direction (blue arrows).

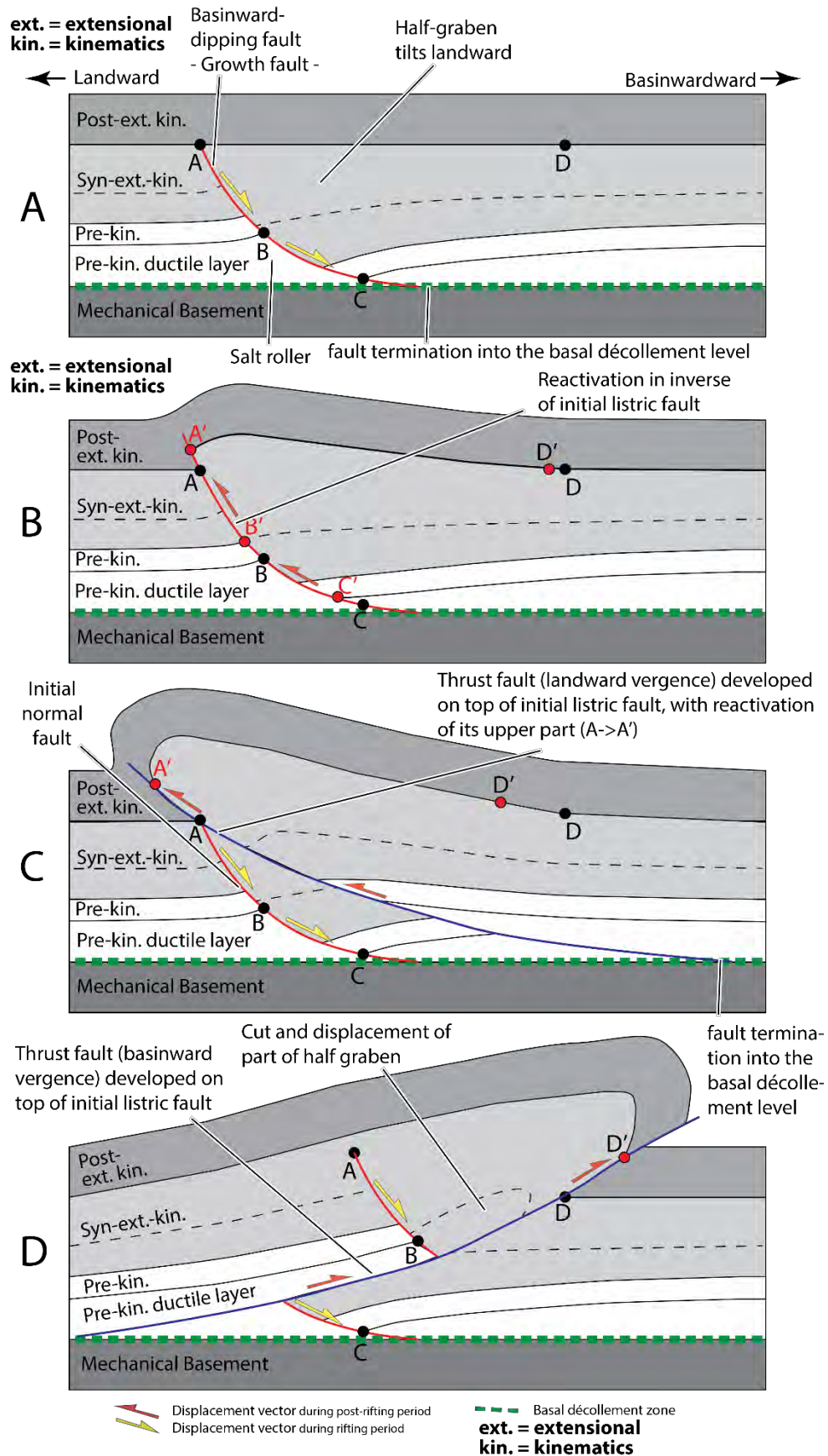


Figure 6-3 : Growth fault and reactivation: A: formation of the syn-sedimentary listric normal fault system. B: reactivation in inverse of the same listric fault. C: Thrust fault development on top of the listric fault system of A (same vergence). D: Thrust development on top of the listric fault (from image A) but with opposite vergence. Figure modified from Jackson & Hudec (2017b) and Pace et al. (2014).

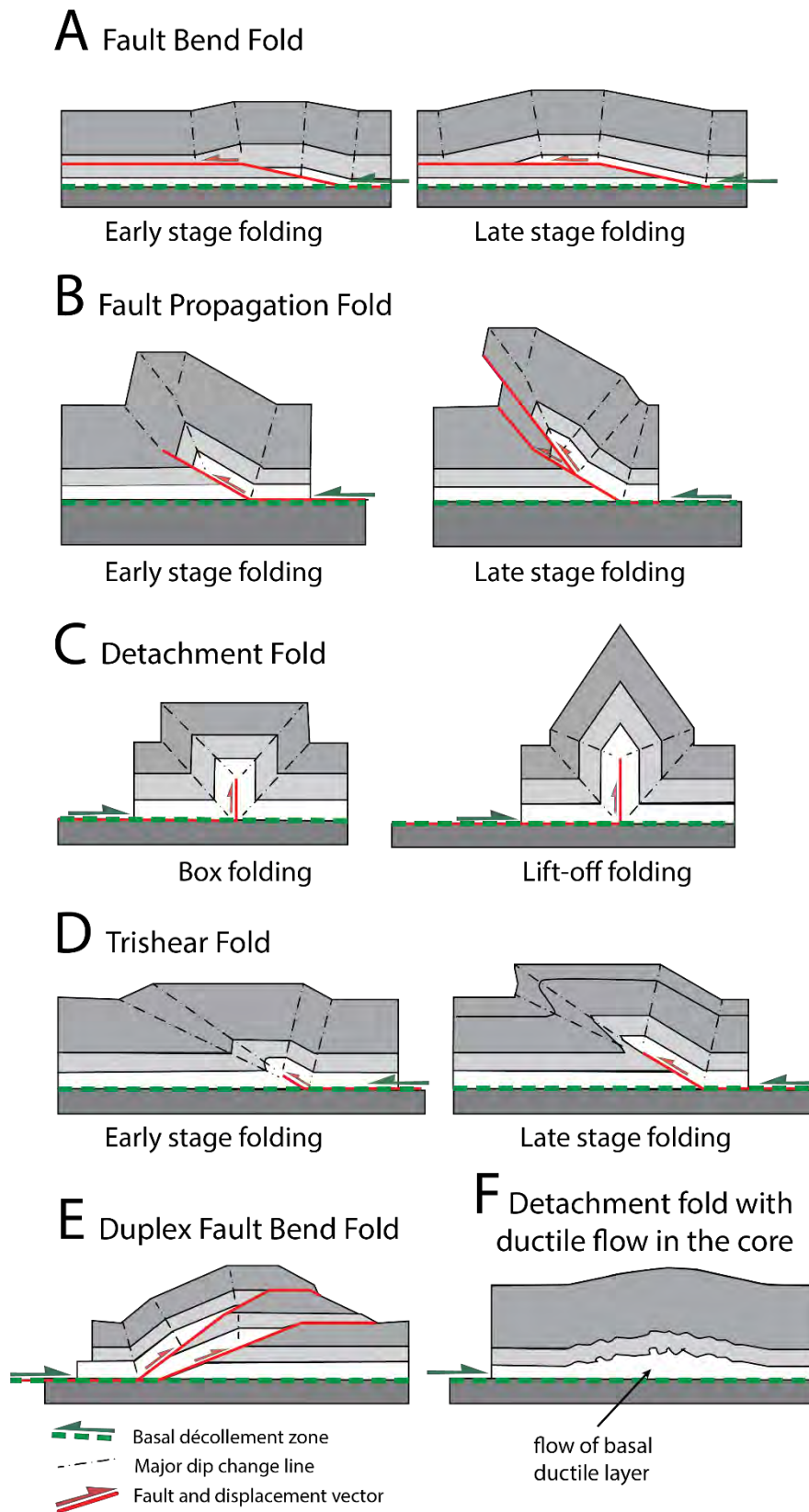


Figure 6-4 : Fault related folds types and associated fold geometries. Note that these cases may be compared to the geology of our study area with the following association of layers (from bottom to top): dark grey = mechanical basement, white = Keuper more ductile layer with major décollement layer at its base, middle/light greys above sedimentary cover. Figure modified from Medwedeff (1992) and Mitra (1986).

obliquely oriented folds and thrusts of smaller order. Lateral ramps are also frequently found in lateral transfer zones and associated with tear/transfer faults (lateral (vertical) ramps *sensu stricto*).

Strike-slip fault (Figure 6-2): subvertical to vertical fault in which the displacement is in the horizontal plane, parallel to the strike of the fault (Peacock et al., 2016). Strike-slip faults are widespread in compression tectonics of brittle solid rocks. They are ideally formed at an angle of around 30° (with small material-specific variations) to the main stress direction. In an Andersonian state of stress, as given in the rather shallow Alpine detached foreland fold-and-thrust belt, the main stress direction is approximately horizontal and the intermediate stress orientation, given by the lithostatic overburden only, is vertical. Strike-slip faults and tear faults, though two distinct terms will be used in the following as synonyms. Strike-slip systems may be formed by several major faults strings defining a broad zone of deformation. This type of broad zone is defined in this work as fault corridor. It hosts a family of faults which represent the brittle behaviour inside the fault. The fault corridor may develop as a Riedel shear system (Davis et al., 2000).

Growth fault (listric fault, Figure 6-3) according to Brun & Mauduit (2008) : Type of normal fault with an upward concave movement surface that transforms steeply plunging displacements at the surface to nearly horizontal ones at depth. Growth fault/rollover systems are extremely common structures of thin-skinned extensional systems resulting from gravity gliding above salt. A growth fault has a limited lifetime during which it controls the deposition of new layers and their downward displacement and rotation in a synsedimentary extensional setting.

Reactivation (Figure 6-3): renewed displacement on a fault that has undergone a prolonged period of inactivity. The different displacement events may or may not be of the same sense (Peacock et al., 2016). We define *Inversion* as a reactivation of a fault in opposite direction of fault throw. Thus, locally steep (around 60° dip) listric shaped reverse faults can be documented (seismic lines). Which can be interpreted to be inverted, inherited synsedimentary normal faults. Alternatively, the steep faults may result from a younger deformation process of Eocene to Oligocene age (rifting, foreland flexuring), that have subsequently been inverted or that have preserved on original offset along a fault that is steeply inclined.

6.2 The Triassic, basal décollement zone and mechanical basement

This chapter addresses the basal décollement zone in Triassic evaporite-rich units and its structural development in connection with the configuration of the mechanical basement. The Mesozoic-Cenozoic series are detached above the main décollement horizon and deformed and transported in a mechanical tapered wedge (Sommaruga et al., 2017). The displacement is explained by the “Fernschub” hypothesis initially proposed by Buxtorf (1916), which introduces the notion of “distant push” of the Alpes. This distant push originates in the antiformal stacking of the External Crystalline Massifs that subsequently led to the displacement of the foreland sedimentary cover on top of the mechanical basement and the formation of the Alpine detached foreland including the Jura Fold and Thrust Belt (Burkhard & Sommaruga, 1997)(Figure 6-5). The amplitude of the structures in the foreland basin part is lower than in the JFTB due to the larger load of the Tertiary sediments inhibiting the deformation of the cover (Sommaruga et al., 2017; Sommaruga et al., 2012). This tectonic phase also

includes the transition from a flexural foreland basin to a “wedge top” configuration. The large-scale decoupling and implicit thin-skinned deformation of the Jura FTB has been supported by numerous studies, based on outcrop and subsurface investigations (e.g. Laubscher, 1961), but also using balanced cross-sections (Burkhard, 1990; Burkhard & Sommaruga, 1998; Rime et al., 2019; Schori, 2021; Marro et al., 2023), as well as retro deformation analysis (Affolter & Gratier, 2004). All these studies underscore the documented existence of a décollement horizon, and the necessity of a shortening and a displacement in a detached cover. The geometry of near top basement, the position of the main décollement and the link between the Triassic evaporite thickness, and the deformation was supported by seismic interpretation and borehole data in Sommaruga (1997) and Sommaruga et al., (2017).

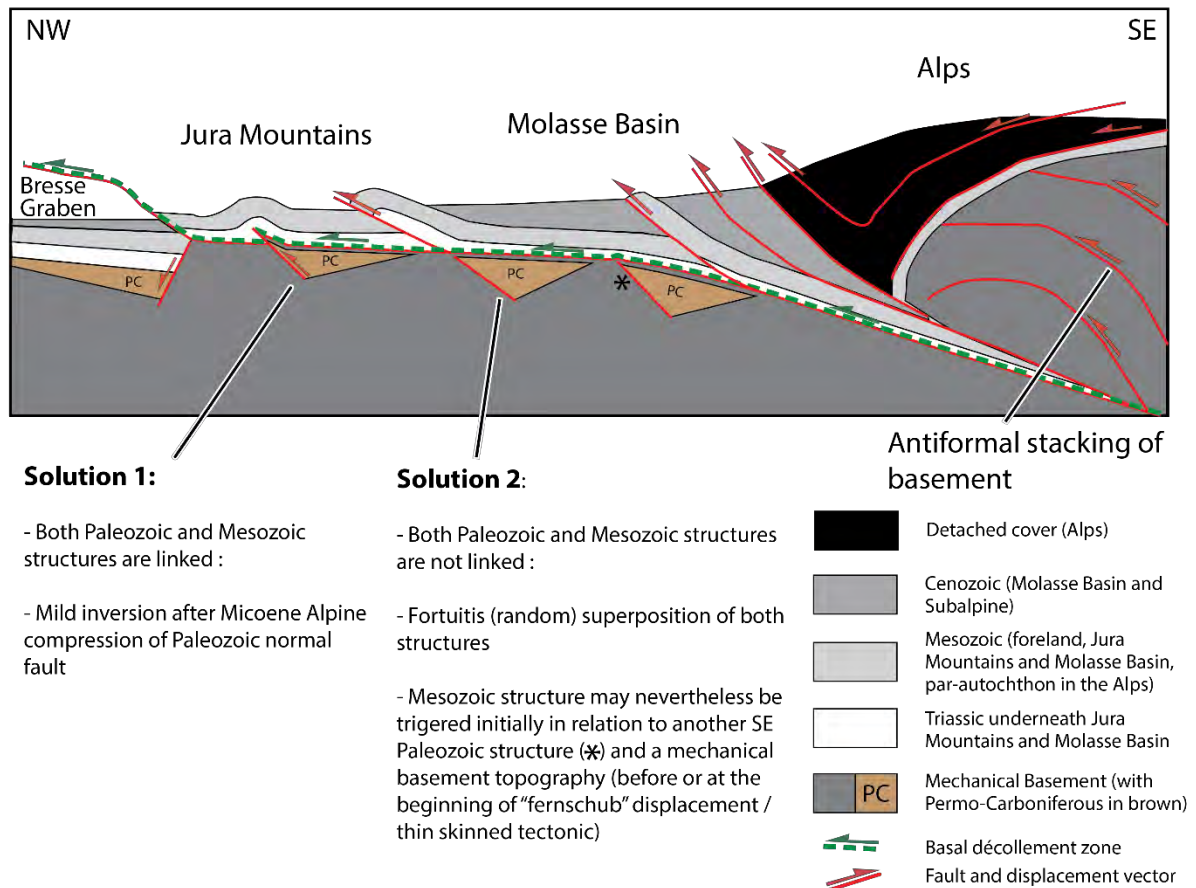


Figure 6-5 : Fersschub or distant push concept from the external Crystalline Massifs in the SE and detachment of the foreland basin and the Jura Mountains in the NW (modified after (Ibele, 2011)). This shows the two main hypotheses regarding the possible link between faults in the mechanical basement and in the sedimentary cover.

Minor involvement of the basement s.l. in a late stage of the orogenic evolution has been discussed in , Madritsch et al. (2009), Malzer et al. (1983), Mosar (1999), and Schori (2021), but are not relevant for the bulk of displacement and deformation in the thrust belt development. However, inherited basement topography is an important feature that can be linked to the initiation and formation of thrusts in the detached cover (e.g. thrust mills of H. P. Laubscher, 1986; Schori, 2021). In that sense, if a structure in the sedimentary cover is located on top of a pre-Mesozoic fault seen on seismic data, two scenarios are then considered:

- o *Both structures in the Pre-Mesozoic and in the Mesozoic-Cenozoic layers are linked:* In such a case, where the deformation is in situ, the implication is that its development post-dates the emplacement of the foreland FTB. It means that it would have occurred after the Miocene Alpine

compression and the major displacement of the detached sedimentary cover that led to the formation of the Jura FTB (after Serravallian (Mock & Herwegh, 2017)). This may thus involve an active structures in the basement and the cover; which can be attributed to mild inversion (Mosar, 1999; Naef & Madritsch, 2014).

- *Both structures in the Pre-Mesozoic and in the Mesozoic-Cenozoic layers are not linked.* The superposition of the two independent structures may be considered fortuitous and due to the relatively regular lateral distribution of the supposed/expected basement faults (roughly around 5-10 km spacing between faults (Schori, 2021)) and the displacement/spacing on major structures in the detached cover series, with a magnitude of around 10km northwestward in the center of the Jura Mountains and around 25-30km in the Molasse Basin). This coincidence does not mean that this structure in the cover cannot be related with different basement structures. It is possible, and even likely, that structures in the detached cover have been initially triggered in relation to a basement faulting before or during the Miocene compression (Laubscher, 1965; Laubscher, 1986; Schori, 2021). Indeed, top basement is an irregular surface with possible offsets along graben bounding faults of inherited Permo-Carboniferous grabens that may lead to stepping down or up the basal décollement, and therefore initiate tectonic structures during the distant-push (Sommaruga et al., 2017, Laubscher 1986: thrust mills). In that case, applying retro-deformation of the Miocene displacement would be needed to locate the initial possible triggering Pre-Mesozoic fault location. Schori (2021) has demonstrated in analogue laboratory modeling that basement faults with greater vertical offset than 400m, are initiating oblique ramps and associated fold, the specific geometry of which can, subsequently, be clearly identified in the Jura FTB. Alternatively, such basement steps may also trigger recent to present deformation, in a way post-dating the main tectonic events of the Jura FTB (e.g. in the Rhenisch Jura). This cannot be excluded, and reflects on the sequence of deformation in the foreland, and has been discussed and suggested in recent works (see Rabin, 2016; Radaideh & Mosar, 2021).

Also, the detailed inspection and interpretation of our seismic database does not show any major throughgoing structures from cover to basement across the main décollement horizon. Therefore, we favor scenarios of the second type, where the Jura FTP and the whole Alpine foreland is detached along a major décollement level in Triassic evaporites and propagates to the foreland over inherited basement topography.

The main structural concept being stated, we will discuss in the following its application in our investigation area. A key issue with the detachment and wedge concept is the presence of a laterally continuous and highly viscous layer (or alternatively very low friction and/or high fluid pressure), separating the two decoupled layers; the basal décollement horizon. In the Alpine foreland this décollement level has been demonstrated to be a highly viscous salt-rich evaporite layer in the Triassic series (Sommaruga et al., 2017 and ref. therein). This horizon can be identified in well cores, on outcrops or even on seismic data as a highly deformed layered zone (Jordan, 1992; Sommaruga, 1999). The vertical position within the Triassic units may vary laterally across the Alpine foreland. Sommaruga et al., (2017) and Gruber (2017) have mapped, at the scale of the Alpine foreland, the different sub-units of the Triassic layer and have concluded that the main deformation zone is located in the Muschelkalk Group in the E-NE part of the alpine foreland, whereas it is located in the Keuper Group in the W-SW Part (the approximate N-S transition line going through Vevey-Moudon-Estavayer-le-Lac in Switzerland, see maps on page 99 of Gruber (2017) for localization).

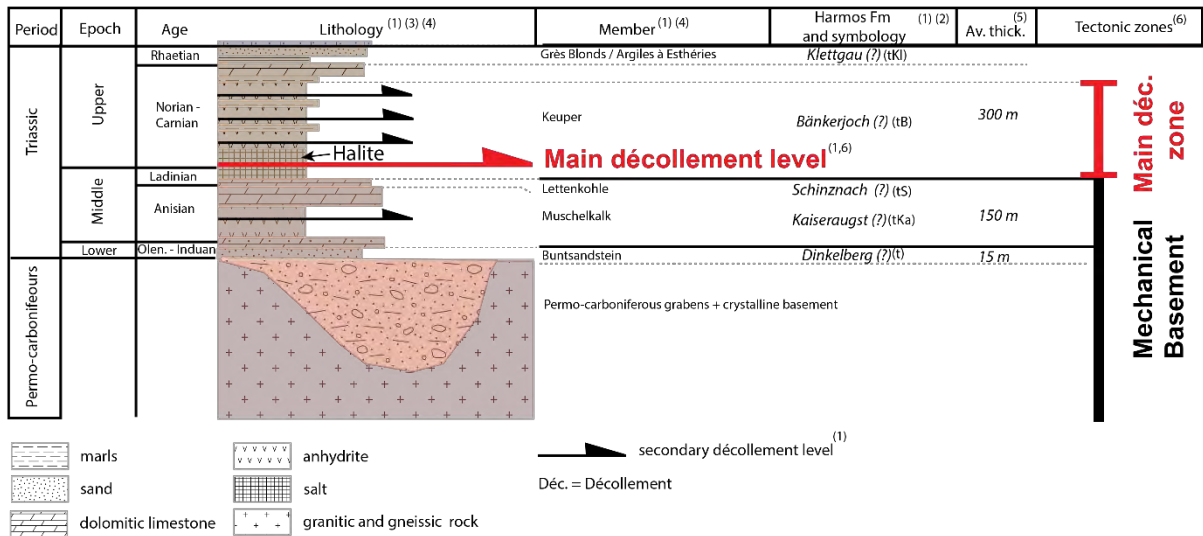


Figure 6-6 : Lithological log of the Triassic unit in our study area, and supposed identification of the basal décollement zone at the base of the halite layer just above near Top Muschelkalk horizon. Figure modified from Marro, 2021.

The well data, such as Humilly-2, in our study area confirm the presence of a thick evaporite-rich layer in the Keuper Group (100-400m), compared to a lower thickness of the Muschelkalk Group (less than 120m (Rusillon, 2017), see Figure 6-6). The lower Triassic consists of the modest Buntsandstein unit (around 15m). Our seismic interpretation, and the resulting mapping of the different seismic horizons, shows the detailed lateral thickness distribution of the entire Triassic Unit (Figure 6-7) and its sub-units in our area. We observe that the Muschelkalk Group can be interpreted with a relatively constant thickness through the GVA Basin, whereas the Keuper Group and thus the entire Triassic Unit is thinning southwestward. This assessment considers that the thickness of the Triassic layers above the basal décollement zone are higher in the more deformed areas, due to duplications of layers (thrusting) or halokinetic movements caused by the faulting. Indeed, the original depositional thickness of the Triassic layer is in fact relatively homogeneous laterally, around 200m for the Keuper and Muschelkalk Groups each (Sommaruga et al., 2017). In that sense, if we remove the local increases of thickness below structures such as the Vuache FZ or the Gros Foug FZ, the overall Triassic unit is indeed thinning southwestward. The thicker Triassic layers are located in the NE part of the investigation area in the Canton Vaud, which is coherent with results from Gruber (2017), Schori, (2021) and Sommaruga et al., (2017) who place the center of the deformation and therefore the greatest Middle and Upper Triassic unit thicknesses in the center of the arc-shaped Jura FTB (just north of the city of Nyon in between St-Cergue FZ and Pontarlier FZ).

In terms of lithology, the Lower to Middle Triassic units (composing the approximated near Muschelkalk seismic unit), are mainly made of dolomite and anhydrite (evaporite, see Figure 6-6). Two parts are recognized in the Keuper Group; the lower one with massive halite and gypsum/anhydrite layers is overlain by a sub-unit formed of alternating dolomite, anhydrite and argillaceous layers similar to the Muschelkalk Group (Brentini, 2018; Rusillon, 2017). Ductile salt layers of the lower part of the Keuper Group are here a perfect candidate to act as the basal décollement zone. The well Humilly-2 is showing a thickness of massive halite of around 150m, despite the fact that regionally this salt content is decreasing southwestwards (see cross sections of Figure 2-4, Figure 2-5 and Figure 2-6). In addition, in well Humilly-2, deformation has been described in several tectonised levels inside the Keuper Group

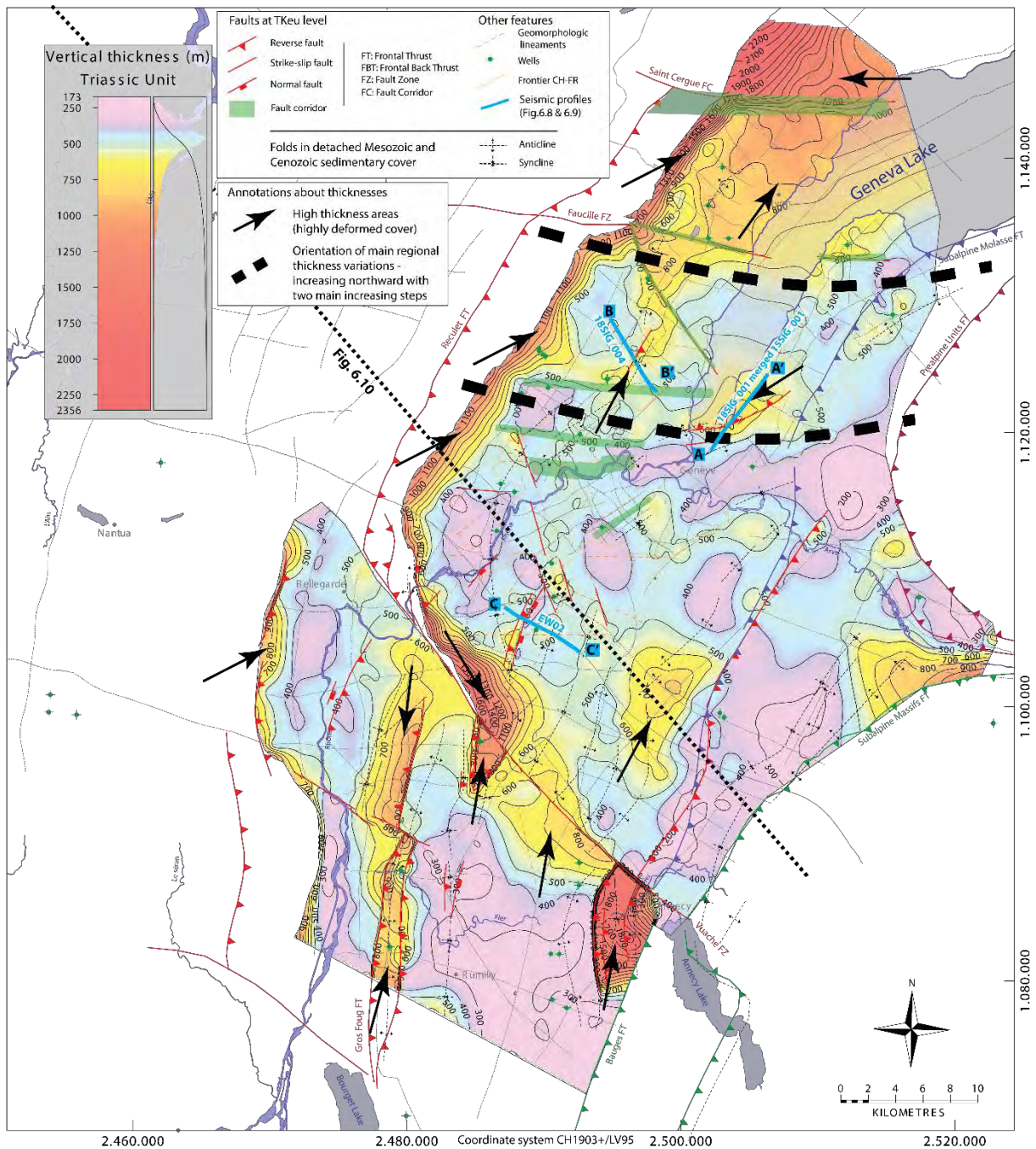


Figure 6-7 : Regional thickness map of the entire Triassic unit. High thickness areas are pointed out by black arrows, which correspond in most cases to structural thickening (highly deformed sedimentary cover). There is an overall increase of the entire Triassic unit northeastward. Note that localization of sections of Figure 6-8 and Figure 6-9 are represented as blue lines.

(S.N.P.A, 1969), suggesting that the deformation is partitioned along secondary décollement levels within the lower part of the Keuper Group (Figure 6-6).

Similar observations also apply to the Jura part of our study with a relatively high thickness of the Keuper Group noticed in the Bonlieu-1 well (378m) or Tolon-1 well (more than 465m), while it is clearly decreasing southwestwards with only 122m measured in La-Chandelière-1d. The location of the basal décollement level in the Jura FTB part is also positioned near the base of the Keuper Group, just below the salt layers.

In order to better assess the subsurface structures, seismic interpretation remains an important tool, in particular to determine the position of the basal décollement zone. Massive halite can be recognized

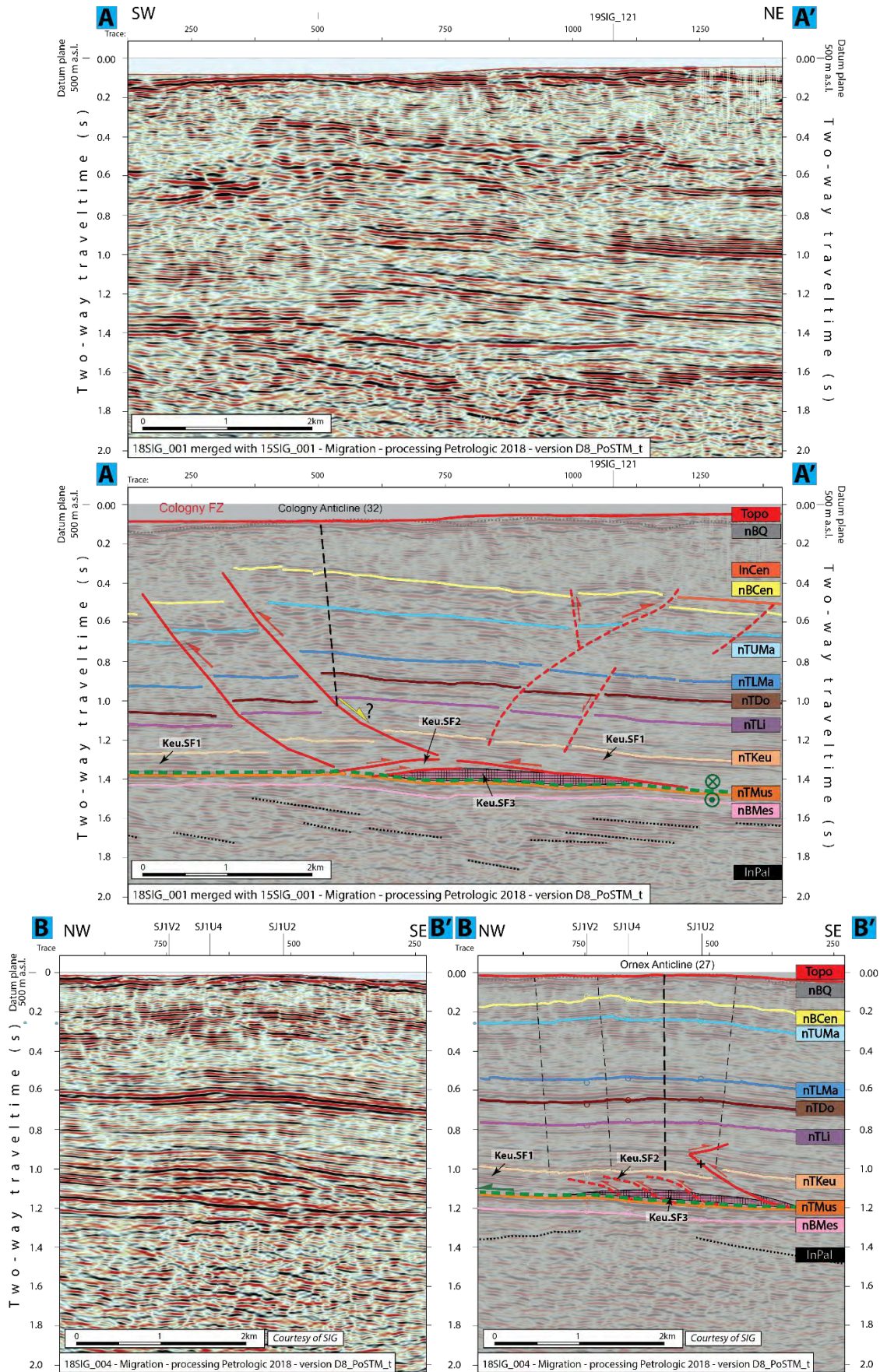
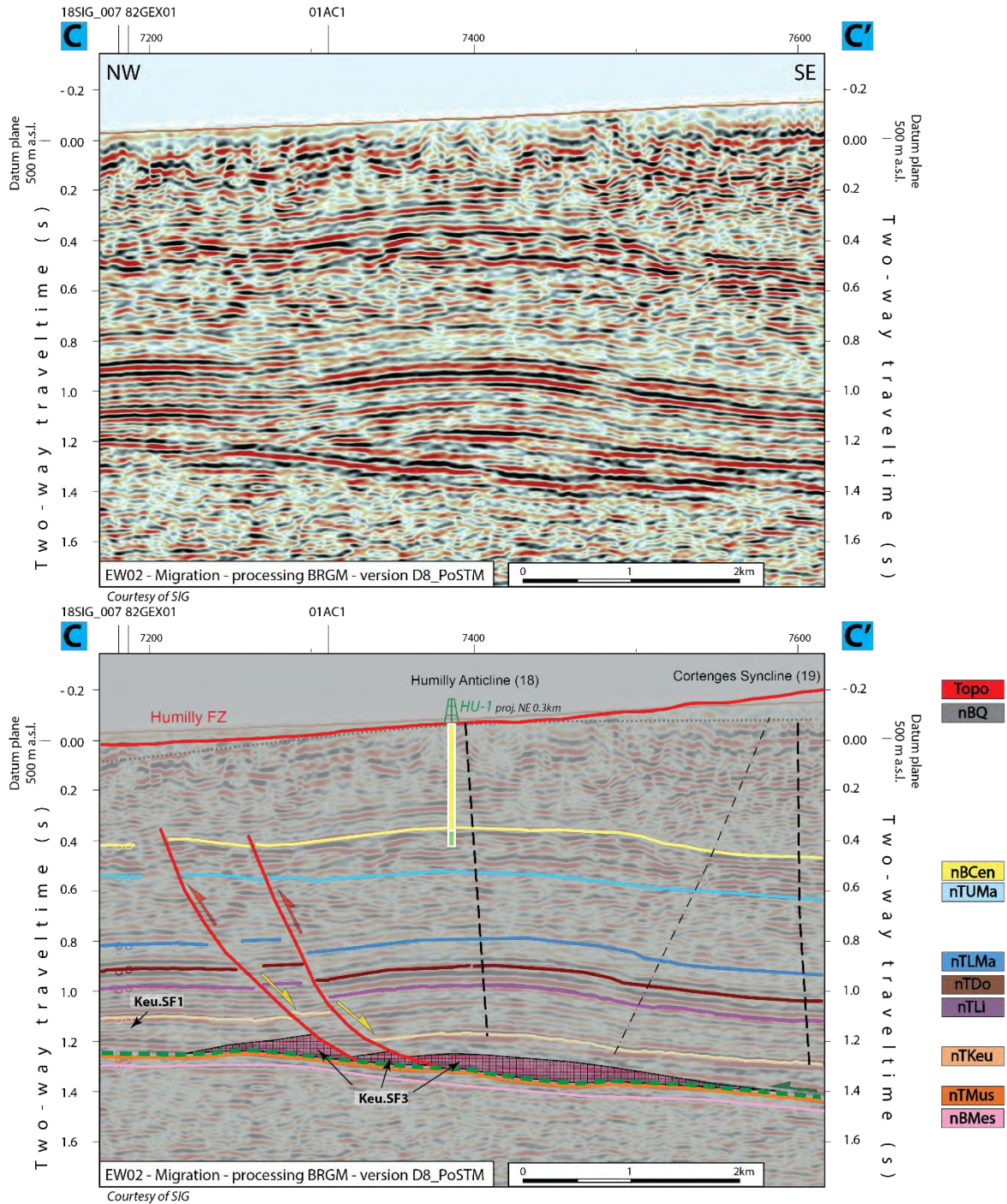


Figure 6-8 : The two top images represents the pop-up Cologny FZ on line 18SIG_001 (AA'), and bottom images shows the intra Triassic duplexes formed at the base of the Ornex Anticline on line 18SIG_004 (BB'). Localization on Figure 6-7. See respectively Encl 19 and Encl 22 for detailed seismic interpretation of lines 18SIG_001 and 18SIG_004. Legend on Figure 6-9.



Structural Interpretation

- Correlated fault stick (with intersection cross with other surveys)
- Non-correlated fault stick
- Basal décollement zone
- Major dip change line
- Major fold central axis
- Displacement vector pointing towards the observer
- Displacement vector pointing away from the observer
- Displacement vector during Cenozoic time
- Displacement vector during Jurassic time

Stratigraphy

- Well
- Cenozoic & Quaternary
- Cretaceous
- Keu.SF1 (undeformed evaporites dominated layer)
- Keu.SF2 (likely thrustured evaporites dominated layer)
- Keu.SF3 (likely haalite dominated layer)

Abbreviations

- | | | | |
|-------|---------------------|-----------|-----------------|
| Trace | Seismic trace | Keu | Keuper |
| FZ | Fault zone | Mus | Muschelkalk |
| FC | Fault corridor | Mes | Mesozoic |
| TWT | Two way travelttime | InPal | Intra Paleozoic |
| proj. | Projected | Humilly-1 | HU-1 |
| s | Seconds | | |
| nT | near Top | | |
| nB | near Base | | |
| Q | Quaternary | | |
| Cen | Cenozoic | | |
| UMa | Upper Malm | | |
| LMa | Lower Malm | | |
| Do | Dogger | | |
| Li | Lias | | |

Figure 6-9 : Seismic interpretation of the Humilly FZ (growth fault) on line EW02 (CC'). Localization on Figure 6-7. See Encl 60 for detailed seismic interpretation of line EW02.

by a typical “transparent seismic facies” (see chapter 4.1.5, and section A in Figure 6-8), that may form salt pillow shapes, often present locally near fault zones, and which may amplify the fault-related folding. The convex salt pillows are usually correlated with an increase of Triassic thickness which is often creating gentle anticlines in the Mesozoic cover (evaporite related pillow/anticline or detachment fold). We may suppose halokinetic processes (salt flow) in relation to the development of thrusts, duplexes, fishtails structures, or listric normal faults. The presence of onlaps on top of the structure allows an understanding of the kinematics and timing of the salt flow (Figure 6-9).

Several deformation styles with an involvement of Triassic evaporite-rich series are thus identified in our study area, such as thrusting or listric extension/inverted faults (Figure 6-9). Thrusts rooting in the basal décollement zone are observed on seismic sections; oblique reflectors fading and bending horizontally close to the suspected basal décollement zone near Top Muschelkalk Group seismic horizon are diagnostic of such zones. Vertically stacked reflectors within the Triassic Unit are interpreted to be imbricates separated by thrusts, forming intra-Triassic duplexes (section B in Figure 6-8). They consist of a system of ramp-related anticlines, with linked floor and roof thrusts (Shankar Mitra, 1986). We have also interpreted fishtail structures (B in Figure 6-8), which are thrusting faults with a lower part rooted along one décollement level and an upper part (linked to the lower part) composed of a thrust with opposite vergence (in comparison to the lower part) and detached along another shallower décollement level.

Locally, the intra-Triassic unit duplexes and thrusts may be linked to larger thrusts/reverse faults that affect the whole detached Mesozoic-Cenozoic cover to form large-scale structures (section A in Figure 6-8). Thus, it was possible to identify and interpret inherited, original listric, normal faults, with a gently rollover geometry associated with thickness changes in the underlying evaporite horizons. Thickness changes were linked to salt flow associated with the original extensional setting ((Jackson & Hudec, 2017c), see Figure 6-9). In Humilly FZ, this kind of structure has been clearly identified on several seismic sections, and salt flow is thought to have occurred within the Triassic layer likely, on both sides of the listric fault. This process has increased the concave-up fault-bend-folding and the amplitude of the rollover anticline in the hangingwall part of the fault. These faults have then, subsequently suffered inversion during the alpine deformation and detachment of the cover series.

The mechanical basement, over which the Mesozoic-Cenozoic cover is detached (Figure 6-6), transported and deformed is considered to be *insitu*. It is composed of two parts (see Figure 2-9 geodynamic explanations):

- the pre-Mesozoic units associated with the crystalline basement. This basement is composed of pre-variscan deformed and metamorphosed rocks, igneous series of late variscan age and older and faulted (grabens or half-grabens) and filled with Permo-Carboniferous sediments (trough infill), and
- the Mesozoic series below the basal décollement zone, which correspond to the units below the near Top Muschelkalk seismic horizon and thus include the Buntsandstein-Muschelkalk-Lettenkohle layers.

We thus define the mechanical basement or basement *s.l.* as all the units beneath the décollement level (Figure 6-6). Based on seismic interpretation, we can assume that the top of the mechanical basement surface can be approximatively correlated with the position of nBMes seismic horizon, and which, in this work, has been interpreted on a regional scale (unlike nTMu horizon which was

interpreted only in the GVA Basin area)(see also Marro et al., 2023). It was thus possible to propose a new refined grid of the nBMes seismic horizon. This surface shows a measured dip angle around 3.25° towards the South-East below the Western Molasse Basin, and some 1.7° below the neighboring Internal Jura (Figure 6-10).

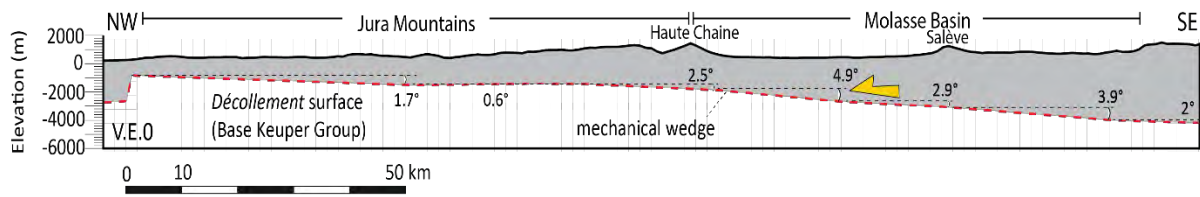


Figure 6-10 Simplified wedge geometry of the western Alpine foreland in the Geneva region. Shown are the newly defined detachment horizon (derived from the near to basement seismic line interpretation and new depth conversions of this project). Topography is an average swath profile (10 km wide) from the Jura Mountains across the Geneva area, the Salève and into the subalpine chains. Topography and décollement dips are in $^\circ$ angle. Figure from Borderie et al. (2022), as part of common team project of tectonic group at the UNIFR. Localization of the section on Figure 6-7.

Thus, the first high chain of the Jura FTB reflects a major change of dip of the mechanical basement. Even if this surface is considered as an overall “smoothed” horizon that allows the decoupling with the cover, several slight irregularities in its top basement topography are thought to be present. Indeed, the existence of Permo-Carboniferous troughs has been proven and testified by several deep wells in the entire Alpine foreland, such as Treycovagnes-1 (475m thickness of PC sediments), or in our studied area in Charmont-1 (498m of PC thickness), or Faucigny-1 (363m of PC thickness) (see also Schori (2021) for detailed discussion, and Figure 2.4 for localization of the wells). These remarkable geological structures have also been investigated on seismic data (Heuberger et al., 2016; Naef & Madritsch, 2014), and their NE-SW dominant orientations have been identified (at least in the NE part of the Swiss Molasse Basin) by many studies using a combination of different sources such as gravimetry, well data, seismic data (Altwegg, 2015; Meier, 2010). In our investigation area, Signer & Gorin, (1995) had proposed the existence of NE-SW oriented Permo-Carboniferous half-grabens; below the High Chain of the Jura FTB and below the Salève Chain. More recently, Schori (2021) proposed, in addition to the above mentioned orientation, the existence of NW-SE oriented basement normal fault (below the Vuache Fault zone and below the GVA Basin), based on results from analogue modelling and lineament restoration using retro-deformation in relation to the formation of ramps (oblique) in the JFTB. Our seismic interpretation provides indications of seismic facies corresponding to Permo-Carboniferous sediments, as well as, possible location of basement faults. Although these results of seismic interpretation of the mechanical basement remain highly uncertain (due mainly to the resolution of seismic data), it is supporting the interpretation and statement concerning the basement fault mapped out by Schori (2021), whose final map is used in our study (see chapter 7). We have used the irregularities of the top mechanical basement to deduce the location of the basement faults (up to 400m fault throw). These faults are likely inherited from the Variscan orogeny and post-Variscan extensional setting, with the following orientations, NW-SE, NNE-SSW, ENE-WNW (Schori, 2021). The ramp triggering effect of this top basement offsets is thus very likely in this study.

6.3 Tectonic interpretation

The zone of investigation has been divided into five structural areas illustrating each a newly observed or confirmed tectonic concept. Each of these five tectonic styles/features are explained according to

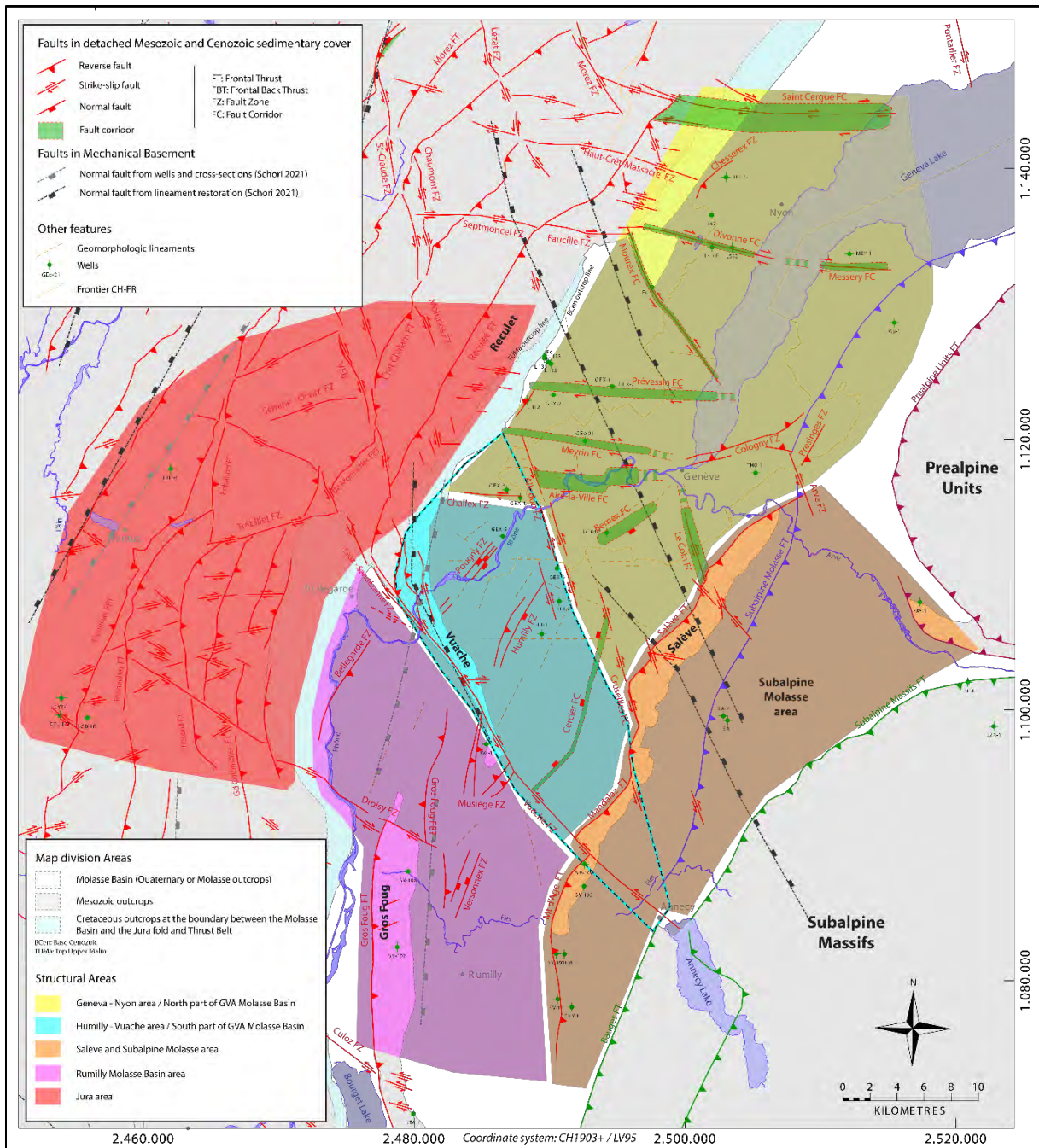


Figure 6-11 : Simplified tectonic map showing the main analyzed structural domains, described in detail in the text. See Encl M01 for detailed structural map.

their geometry and kinematical evolution. The transition between the different areas may not be clear cut and structural specificities of one area may overlap slightly with adjacent areas. It is to be noted that certain areas may show common structural features with other areas, and that the division presented hereafter of five polygons was proposed in order to facilitate the summarizing of the structural setting of the whole area. The more regional tectonic setting and kinematic development of the region will be discussed in a subsequent chapter 7.

The identified structural domains are separated by some of the major, overarching structural features in our region of investigation; e.g. the Jura FTB, the Vuache fault and the Salève mountain (see Figure 6-11, Encl M01 and Encl M02):

- The Geneva-Nyon area or the northern part of the Geneva Molasse Basin (chapter 6.3.1) is dominated by ESE-WNW and NNW-SSE conjugated strike-slip fault zones. This fault system is similar to the one observed in the Jura FTB.
- The Humilly-Vuache area or the southern part of the Geneva Molasse Basin (chapter 6.3.2) is mainly composed of a former Jurassic extensional fault systems, with NE-SW oriented normal faults terminating against the NW-SE Vuache fault; which also exhibits syn-sedimentary tectonics. This fault system has been reactivated during the alpine deformation, and is slightly affected by the same strike-slip system than observed in the northern part of the Geneva Molasse Basin described above.
- The Salève and Subalpine Molasse (SAM) area (chapter 6.3.3) includes the whole Salève ramp related fold (Mt Salève - Mt Mandallaz and Mt d'Âge), which has also been associated with a synsedimentary growth fault initiated during the Jurassic period and subsequently inverted. It comprises also the Molasse Basin part between this major structure and the Alpine Nappes, and is characterized by the Subalpine Molasse thrusts.
- The Rumilly Molasse Basin (RUM) area (chapter 6.3.4) located to the west of the Vuache fault, is marked by compressive structures such as thrusts and back thrusts with a N-S orientation, as well as conjugated strike-slip faults, mainly with a NW-SE direction.
- The Jura area (chapter 6.3.5) forms a fold and thrust belt, to the north of the Geneva and Rumilly Basins, and is also affected by conjugated strike-slip systems similar to those mentioned before in the other areas (Figure 6-11). The main specificity of this area is the formation of large fault related folds, yielding a distinct topography, the Jura Mountains (see also Marro, 2021)

6.3.1 Geneva – Nyon area / North part of GVA Molasse Basin

The Geneva – Nyon area / North part of GVA Molasse Basin is a structural area mainly dominated by conjugated strike-slip faults more or less with a ESE-WNW / SSE-NNW striking direction, that are interpreted to be initiated by the Miocene NW-SE compression leading to the foreland detachment. Since this work focuses on the seismically interpreted structures inside the Molasse Basin, the Jura faults will be mentioned but will not be fully described if they were not interpreted on seismic sections. A more detailed interpretation can be found in Marro (2021) and Marro et al. (2023). Several wells were drilled in the Nyon area, such as Messery-1, or Grilly wells, that only reached nBCen horizon, provide crucial tying points for the mapping of this horizon. For convenience of display and description, they will be presented (maps and sections) in a north/south order (Figure 6-12).

Nyon area

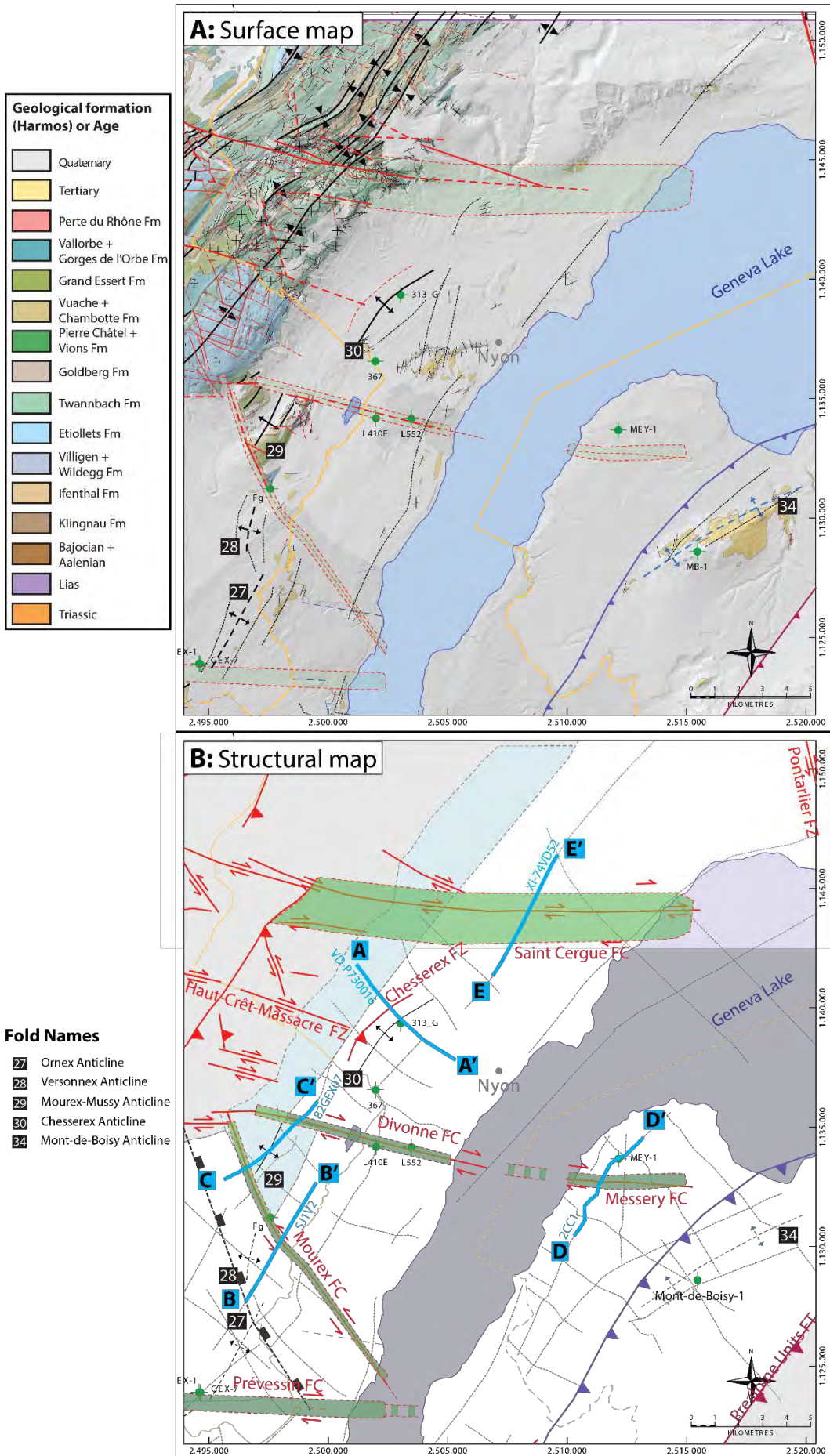
The Nyon area is composed of three strike-slip fault corridors (FC), which extend into clearly outcropping strike-slip zones in the Haute Chaîne of the Jura FTB to the NW (Figure 6-12). One can discriminate the E-W oriented Saint Cergue FC, the WNW-ESE oriented Divonne FC with its likely eastern prolongation into the more E-W oriented Messery FC, and the NW-SE oriented Mourex FC. An additional NE-SW striking thrust fault (Chesserex FZ) is completing the structural setting in between Saint Cergue FC and Divonne FC. The E-W oriented Prévessin FC to the S, will be described in the following with the Geneva area. All the major fault corridors, as well as the thrust faults are interpreted hereafter to root in the basal décollement zone.

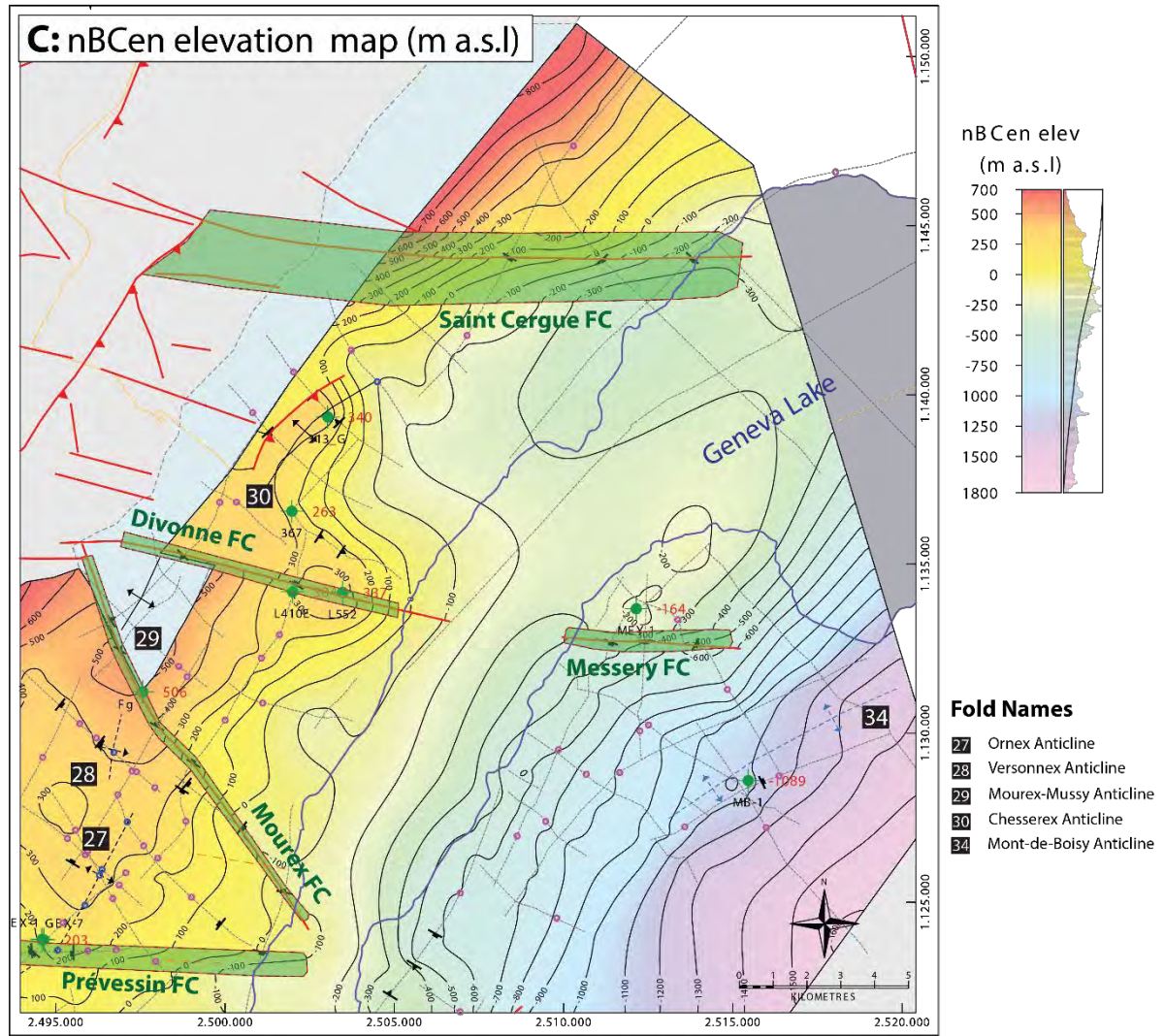
The **Saint Cergue FC** is a dextral strike slip-fault that has been observed in outcrops in the Jura FTB, and has a measured horizontal offset of around 1km, decreasing eastwards (Arn et al., 2005). This fault corridor has also been interpreted (or at least represented) by several authors on seismic data and often named in their studies as the St. Cergue-Luins strike-slip fault zone (Arn & Conrad, 2005; Dupuy, 2006; Marchant, 2016; Paolacci, 2012). This fault zone can be interpreted on seismic sections (see section E on Figure 6-14 and localization on Figure 6-12) as a large 2km wide strike-slip fault corridor, with a near vertical central fault (interpretation similar to the one from the GEOMOL project of the Vaud Canton from Marchant (2016)) surrounded by irregularly spaced smaller scale faults and/or a network of fractures (not represented at the scale of a seismic section). This fault corridor appears on strike seismic sections as a chaotic seismic facies with an overall “transparent” appearance (2km large), but with smaller scale offsets of seismic reflections suggesting the existence of smaller scale faults. Although the resolution of the seismic data in this area is of intermediate quality, the large fault corridor appearance is depicting the actual deformation style described above. The fault corridor itself is interpreted here to root in the basal décollement zone. This structurally remarkable feature is showing a moderate vertical offset with the NE side rising up compared to the SW compartment. The eastern extent of the fault corridor has been stopped near border of Geneva Lake, since no seismic line inside the lake was able to confirm the continuation eastward of the fault (seismic lines acquired on the lake usually show a poor deep resolution).

The **Divonne FC** is a dextral WNW-ESE striking, steeply SSW dipping strike-slip fault corridor, with a width up to 500m width, and up to 10km length. Across Lake Geneva in France, another strike-slip fault corridor, the **Messery FC** has been identified in the exact continuation southeastwards of Divonne FC (see map of Figure 6-12 and section D in Figure 6-14). The two fault corridors strings appear to have an opposite vertical (modest) offset, which may be related to gentle plunges (up or down by 1-5°) of the transport direction. The lack of deep seismic data in Lake Geneva does not allow confirming the continuous link between the two fault systems. A more complex picture with multiple smaller blocks, separated by vertical faults has been proposed by Vernet et al., (1974), based on seismic interpretation (shallow seismic data), beneath Lake Geneva. Globally they corroborate our interpretation but are not integrated into this work because of very different nature of the seismic interpretation.

The **Mourex FC** has a similar geometry as the Divonne FC, but a more NNW-SSE orientation and a sinistral strike-slip component. The Mourex and Divonne FC form a conjugated fault system, leading to the development of the pop-up like Mourex-Mussy Anticline in the (NW oriented) compressional corner, located SE of their intersection just at the boundary between the Jura Haute Chaîne and the Molasse Basin (see map of Figure 6-12 and section C in Figure 6-13). The consequent thickening of the Triassic layer beneath this pop-up structure implies the presence of highly ductile evaporite layers, such as salt pillows. The Mourex-Mussy anticline is oriented NE-SW with a NW vergence. Thus the Mourex FC shows a modest reverse component in its NW segment whereas further to the SE this component appears to be slightly normal (see map of Figure 6-12 and section B of Figure 6-13).

The three major FC described here are important regional structures, as they represent perfect examples of the continuation of clearly visible conjugated strike-slip systems in the Jura FTB (outcrops) into the Molasse Basin part. The extension of these faults in the Molasse Basin has already been suggested by several authors (Clerc & Moscariello, 2020; Marchant, 2016; Rigassi, 1957; Signer & Gorin, 1995), although the faults are not exactly traced the same way as proposed in this work. In the Jura FTB part, near the Nyon area, it is possible to interpret numerous smaller-scale conjugate fault





Legend Surface Map (A)

Faults in detached Mesozoic and Cenozoic sedimentary cover

- Jura - Salève - Cd Foug - Mt Vuache
 - Visible main Thrust
 - Suspected main Thrust
 - Primary visible Strike-slip fault
 - Primary suspected Strike-slip fault
 - Secondary visible Strike-slip fault
 - Secondary suspected Strike-slip fault
- Molasse Basin
 - Fault at nBCen level interpreted on seismic data
 - Fault corridor nBCen level interpreted on seismic fault

Other features

- Geomorphologic lineaments
- Interpolated trace of bedding strike
- Bedding dip (source from respectively FR 50k geol map (black), CH25k geol map (purple), literature (blue))

Coordinate system: CH1903+ / LV95

Legend Structural Map (B)

Folds in detached Mesozoic and Cenozoic sedimentary cover

- Anticline visible on surface and on seismic data (blue -> only in Cenozoic cover)
- Syncline visible on surface and on seismic data (blue -> only in Cenozoic cover)
- Anticline visible only on seismic data (blue -> only in Cenozoic cover)
- Syncline visible only seismic data (blue -> only in Cenozoic cover)

Main Faults at nBCen (near Base Cenozoic)

- Reverse fault
 - Strike-slip fault
 - Normal fault
 - Fault corridor
- FT: Frontal Thrust
 FBT: Frontal Back Thrust
 FZ: Fault Zone
 FC: Fault Corridor

Areas (maps (B) and (C))

- Molasse Basin (Quaternary or Molasse outcrops)
- Mesozoic outcrops
- Cretaceous outcrops at the boundary between the Molasse Basin and the Jura fold and Thrust Belt

Faults in Mechanical Basement

- Normal fault from wells and cross-sections (Schori 2021)
- Normal fault from lineament restoration (Schori 2021)

Legend nBCen elev Map(C)

- Intersection of major dip change line with the map
- Intersection of major fold central axis with the map
- Intersection of reverse fault with the map
- Intersection of normal fault with the map
- Value of Well formation top elevation (GEO-01)

Common features to three maps

- Seismic lines
- Wells (GEO-01)
- Frontier CH-FR
- Bauges and Subalpines Massifs Front Thrust
- Prealpine Units Front Thrust
- Subalpine Molasse Front Thrust

Other features

- Geomorphologic lineaments
- Seismic profiles (Fig.6.13 & 6.14)

Figure 6-12 : Maps of structural interpretation results of the Nyon area. It includes the Saint Cergues FC, the Chesserex FZ, the Divonne FC, the Mourex-FC and the Messery FC. These structures are described in detail in the text of part 6.3.1. See Table 3-2 for well abbreviations. Sections of Figure 6-13 and Figure 6-14 are represented on structural map B as blue lines. Coordinate system : CH1903+ / LV95. Geological map A is based on Marro (2021).

systems, but only the higher resolution of a 3D seismic survey could allow to consider interpreting this kind of faulting/fracturing inside the Molasse Basin.

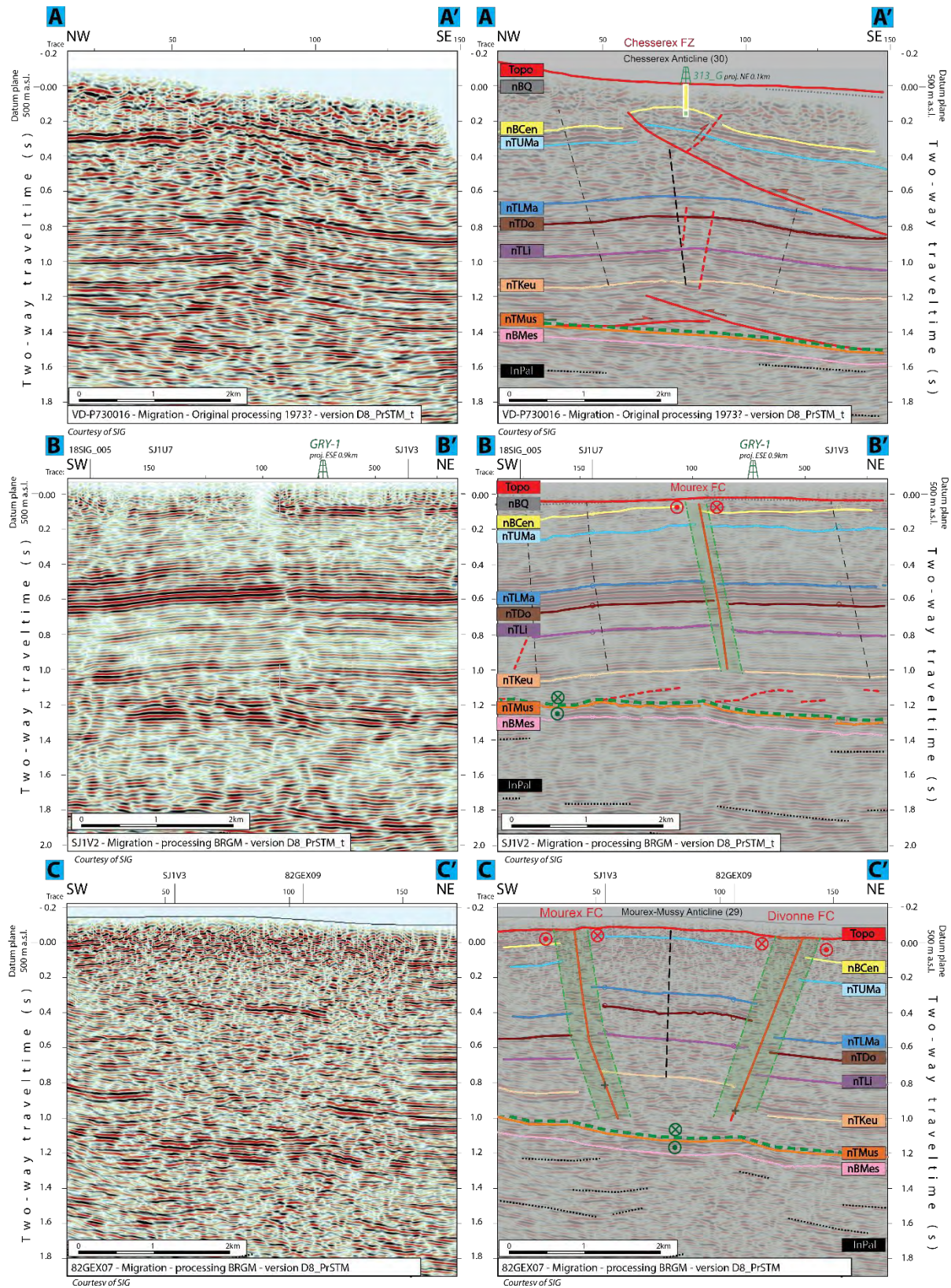


Figure 6-13 : Seismic interpretation (twt) of the Chesserex FZ on seismic line VD-P730016 (top image and section AA'), the Mourex FC on seismic line SJ1V2 (middle image and section BB'), the Divonne FC (and again the Mourex FC on seismic line 82GEX07 (bottom image and section CC'). See Figure 6-12 for localization of the sections. See respectively Encl 83, Encl 79, and Encl 42 for detailed seismic interpretation of lines VD-P730016, SJ1V2 and 82GEX07.

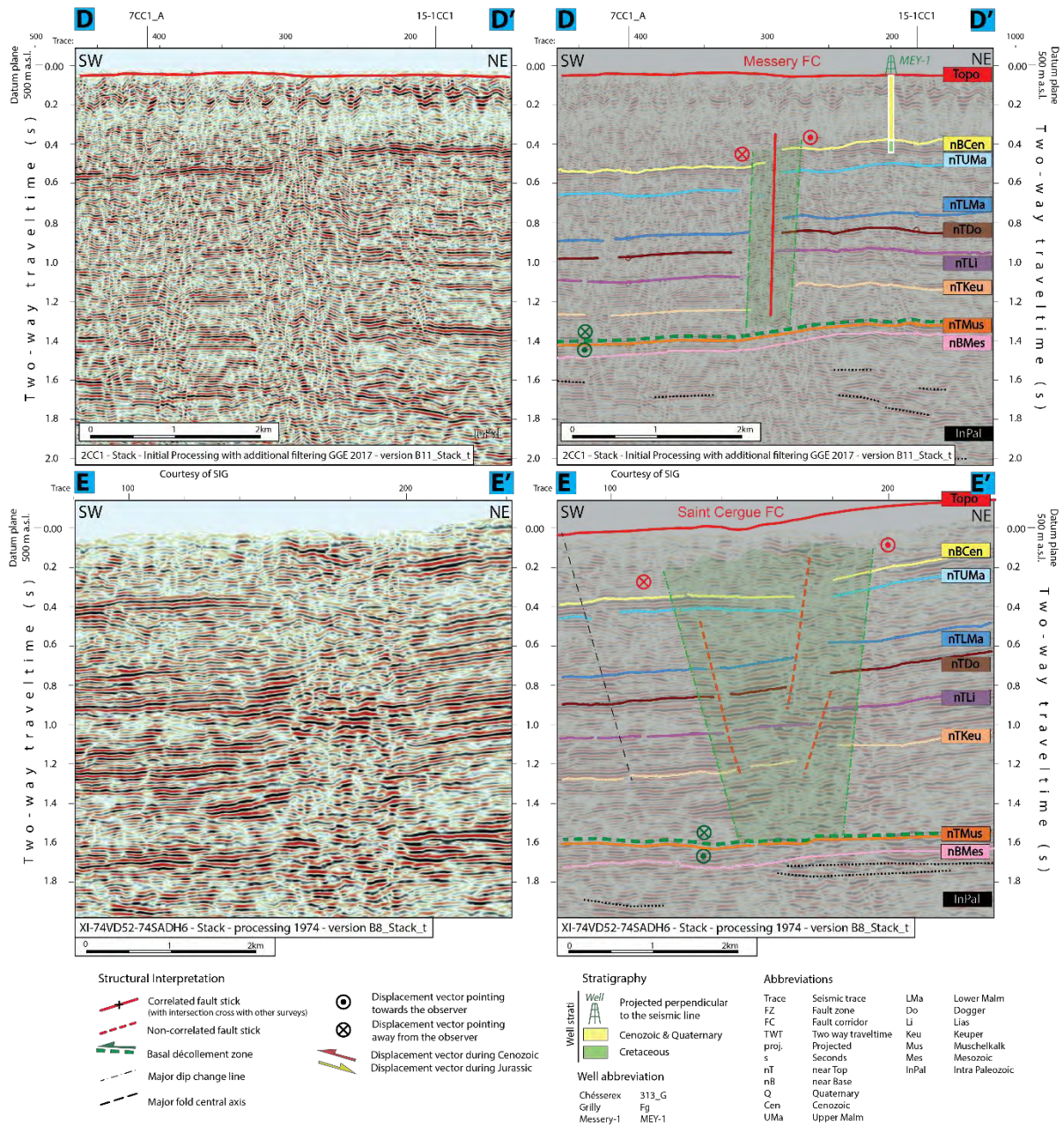


Figure 6-14 : Seismic interpretation (tw-t) of the Messery FC on seismic line 2CC1 (top image and section DD’), the Saint Cergue FC on seismic line Xi-74VD52-74SADH6 (bottom image and section EE’). See Figure 6-12 for localization of the sections. See respectively Encl 59 and Encl 84 for detailed seismic interpretation of lines 2CC1 and line Xi-74VD52-74SADH6.

The **Chesserex Fault Zone** is located between the Saint Cergue FC and the Divonne FC, NW of well 313_G, and is a NE-SW striking thrust fault, with a top-to-the-NW thrust direction (see map of Figure 6-12 and section A in Figure 6-13). Clear oblique strong amplitude seismic reflections can be identified and associated with the fault plane that has been rooted in a shallower décollement level than the basal décollement level, in fact in the Effingen marls of the Lower Malm unit. The Chesserex FZ is a blind thrust forming a fault-propagation fold associated to the Chesserex Anticline, that was drilled by well 313_G, which confirms the shallow presence of nBCen horizon. In addition to the shallow thrust splay, the deeper part of this structures is related with imbricates formed in the Triassic series and leading to a local tectonic thickening. The recent study from Marchant (2016), in the frame of the GEOMOL project (applied for the Vaud Canton and swisstopo), is drawing another ESE-WNW strike-slip fault similar to the Saint Cergue FC and the Divonne FC, just between the two latter, and called the

Bonmont-Yvoire fault. However, we were not able to recognize this in our seismic interpretation study; instead, we identified the Chesserex Fault Zone.

In the area around Mont de Boisy, SE of Lake Geneva, the outcropping Molasse series, in combination with seismic interpretation, are providing information to confirm the presence of the **Mont-de-Boisy Anticline** with a NE-SW striking orientation. This anticline is located just SE of the Subalpine Molasse frontal thrust. This latter thrust surface is visible on seismic profiles as a clear, oblique and bent, strong seismic reflection that appear to be rooted in a near base Cenozoic décollement level. The thrust Molasse pinches out underneath the Alpine nappes, and thrusting could involve both USM and UMM deposits (Gorin et al., 1993). In addition, other thrusts carrying the UMM at the front of the Subalpine Massifs have been clearly interpreted based on outcrops (Charollais, 1986)(see tectonic map on Encl_M01).

Geneva area

The southern part of the Geneva-Nyon area is formed by the Geneva area sensu stricto (Figure 6-15). It is a complex structural area characterized by several E-W oriented strike-slip fault corridors (Prévessin FC, Meyrin FC, Aire-la-Ville FC), several NW-SE oriented strike-slip fault corridors (le Coin FC) and more discrete fault zones (Arve FZ, Cruseilles FZ, Allondon FZ), a ENE-WSW backthrusting Cologny FZ, a shallow NE-SW oriented thrust fault in the Presinge FZ, and a NE-SW graben fault corridor, the Bernex FC. In following we will discuss these different structures and possible kinematic links.

In the northern part of the Geneva area, the E-W striking **Prévessin fault corridor** is a right lateral strike-slip fault zone with a width of more than 750m and a length of more than 12km (Figure 6-15 and section A and B in Figure 6-17). Its northern part is characterized by shallower Mesozoic units due to a thickened Triassic unit. This creates an apparent normal component across the steeply south dipping fault corridor. This fault system shows several main fault segments (2-3 main fault sticks of around 0.2 second apparent vertical extent interpreted on each seismic section crossing the corridor) accommodating the deformation in addition to smaller scale faults/fractures. The faults represent the brittle expression that is probably associated to a more plastic/brittle behaviour in the evaporite-rich layers of the Triassic. In addition, the differences in lithostratigraphic rheology favor/inhibit the development of clear discrete brittle faults. Thus, for instance the very massive limestones of the Upper Malm unit behaved very differently to the deformation (brittle behavior) than the very marly layers of the Lower Malm (Effingen unit) or of the Dogger or Lias units (more diffuse and ductile behavior) where a clearcut fault is more unlikely to develop. The various fault segments cannot be correlated between each seismic line intersecting the tectonic structure, and the high complexity of this system cannot be fully captured by few interpreted fault correlations. Therefore, it is important to consider the overall fault corridor geometry (correlated between sections) more than smaller-scale individual structures (not correlated). Concerning the lateral extent of this fault system, faults and structural lineaments with the same orientation have been observed in the continuation of the corridor westward in the Jura Haute Chaîne (Marro, 2021). Also, this FC may be seen as conjugated with the Mourex FC at its eastern termination. This latter fact could create a triangular shaped uplifted structural area west of the intersection of the two fault corridors, following a similar configuration than the Mourex-Mussy anticline area (Figure 6-20).

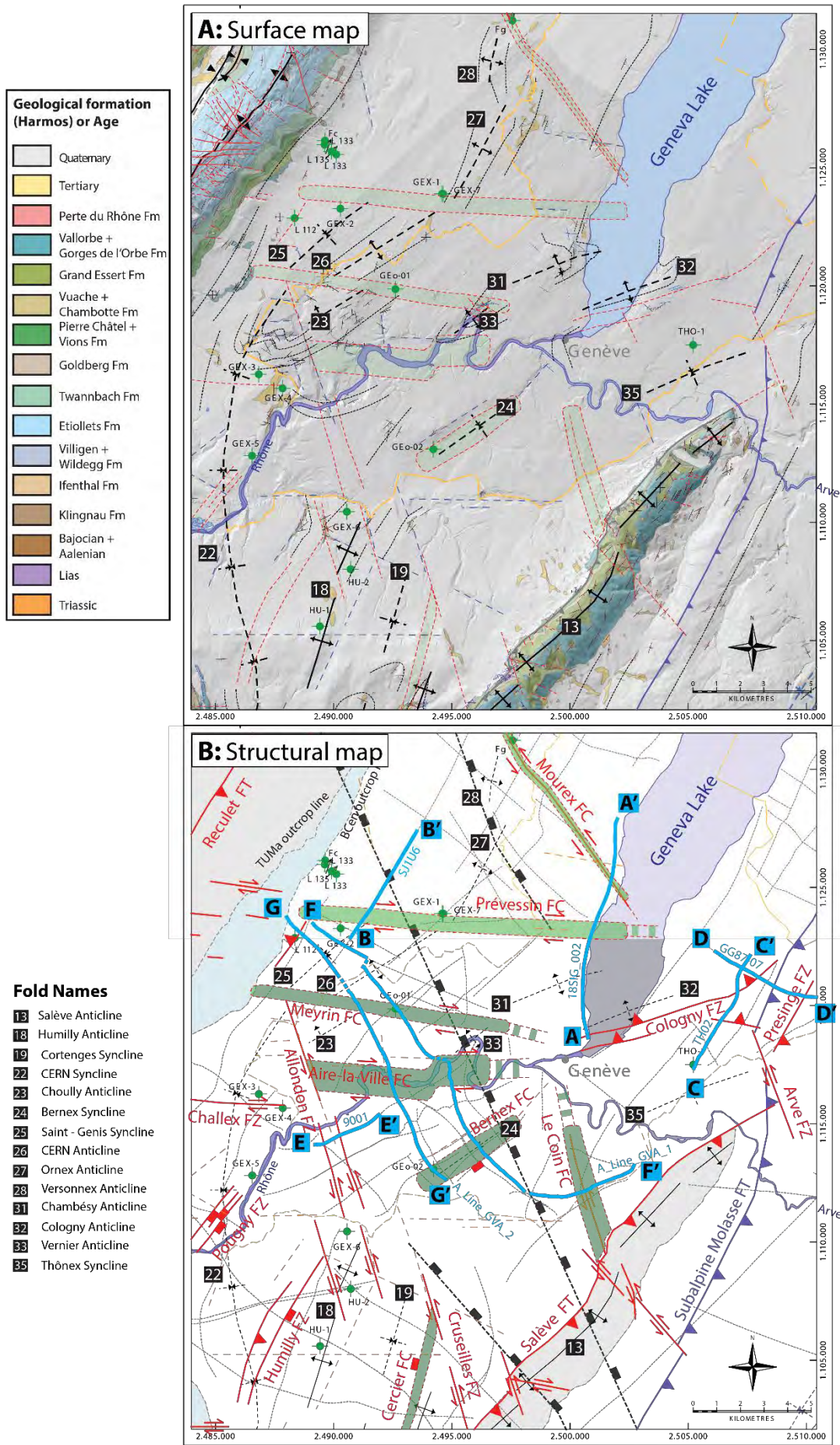
It is important to note that all mentioned fault corridor boundaries are represented on seismic profiles by two external boundaries that stop vertically downward near nTKeu seismic horizon. Although the

Keuper Unit should play a role in the structural setting of the strike-slip fault corridors, the ductile behavior of this layer and the associated thrusting structures cannot be incorporated in these boundaries. Indeed, the intra-Triassic thrust faults are too different to the steep strike-slip fault segments interpreted on the overlying Mesozoic layers.

In the overall triangle area (on map view) located in between Mourex FC, Prévessin FC and the Jura Haute Chaîne, we have interpreted two NE-SW gentle folds; the **Ornex and Versonnex Anticlines**, which are typical evaporite related structures with intra-Triassic duplexes and possible salt pillow/anticline increasing Triassic thickness in the NE-SW direction and correlated with a Mesozoic-Cenozoic anticlines on top of them (Figure 6-7 and section B in Figure 6-8). The same concept is applied on major dip change axis displayed on seismic profiles. The **Meyrin fault corridor** has a very similar structural configuration to the Prévessin FC (Figure 6-15). It is also a wide (500m width) and long (around 10km long) ESE-WNW strike-slip fault corridor and is located just 5km to the south of the Prévessin FC (Figure 6-15) to which it is parallel. This structure is following the same structural principles of a fault corridor (diffuse deformation) described on the above paragraph (or see chap 4.1.13). For reminder, they have been defined to avoid tracing excessively long single faults that cannot be confirmed and correlated laterally. Fault corridors have been identified and correlated across several seismic lines. The section F (Figure 6-18, see location on Figure 6-15) and section G (Figure 6-19, see location on Figure 6-15) are intersecting the Meyrin fault corridor just around GGeo-01 well location that was drilled in 2018 (Chablais & Savoy, 2019). The fractures/faults analysis of this well (Koumrouyan, 2019; Martinuzzi & Sallier, 2018), based on petrophysical logging measurements, is highlighting N-S to NNE-SSW fracturation (Figure 6-21). Strike-slip fault corridors are thus complex fault systems associated with many kinds of subsidiary structures in the damage zone around the main strike slip faults (Jackson & Hudec, 2017d; Massironi & Kim, 2015). The slip is mostly horizontal, but it may also be oblique leading to segmented straight or gently curved faults. The strain may vary along the length with alternating transpression or transtension configuration, leading to switches of the uplifted side of the fault along it, due to gentle changes in dip of the transport direction. We consider that the seismic interpretation is indicating the orientation and the geometry of the overall fault corridors, although the internal structural configuration cannot be directly deduced. The image log information of GGeo-01 suggests the following interpretation (1D analysis at well location, Figure 6-21):

- The N-S to NNE-SSW striking discontinuous open fractures could be related to antithetic Riedel shears.
- The fold axis is oriented along NE-SW, confirmed by the seismic interpretation in this area.

It is all the more difficult to understand the secondary faulting and fracturing of the Meyrin FC since the analysis of the contouring of the gridding and mapping of the Mesozoic seismic horizons is indicating that GGeo-01 well is placed in a transition area in relation to the uplifted parts of the faults. Indeed, eastward of GGeo-01 well, the northern block of the fault appears uplifted in comparison to the southern block, whereas westward of GGeo-01 well the trend is switched with the southern block uplifted in relation to the northern block. Several seismic profiles located on both sides of GGeo-1, are confirming this configuration. Seismic line 20UNIGE_001 (West of GGeo-01, see section on Figure 6-19 and map on Figure 6-15) is showing a north-vergent reverse fault, while 20SIG_002 (East of GGeo-01) display the Meyrin FC as an overall apparent normal fault system dipping South. Along GGeo-01 well, the fault corridor appears on seismic profiles GG87-02 NW-SE oriented) with an overall transtensive system, whereas on seismic line 15SIG_008 (NE-SW oriented) it has an apparent overall transpressive configuration. This confirms the ambivalent structural location of GGeo-01 well along the Meyrin FC.



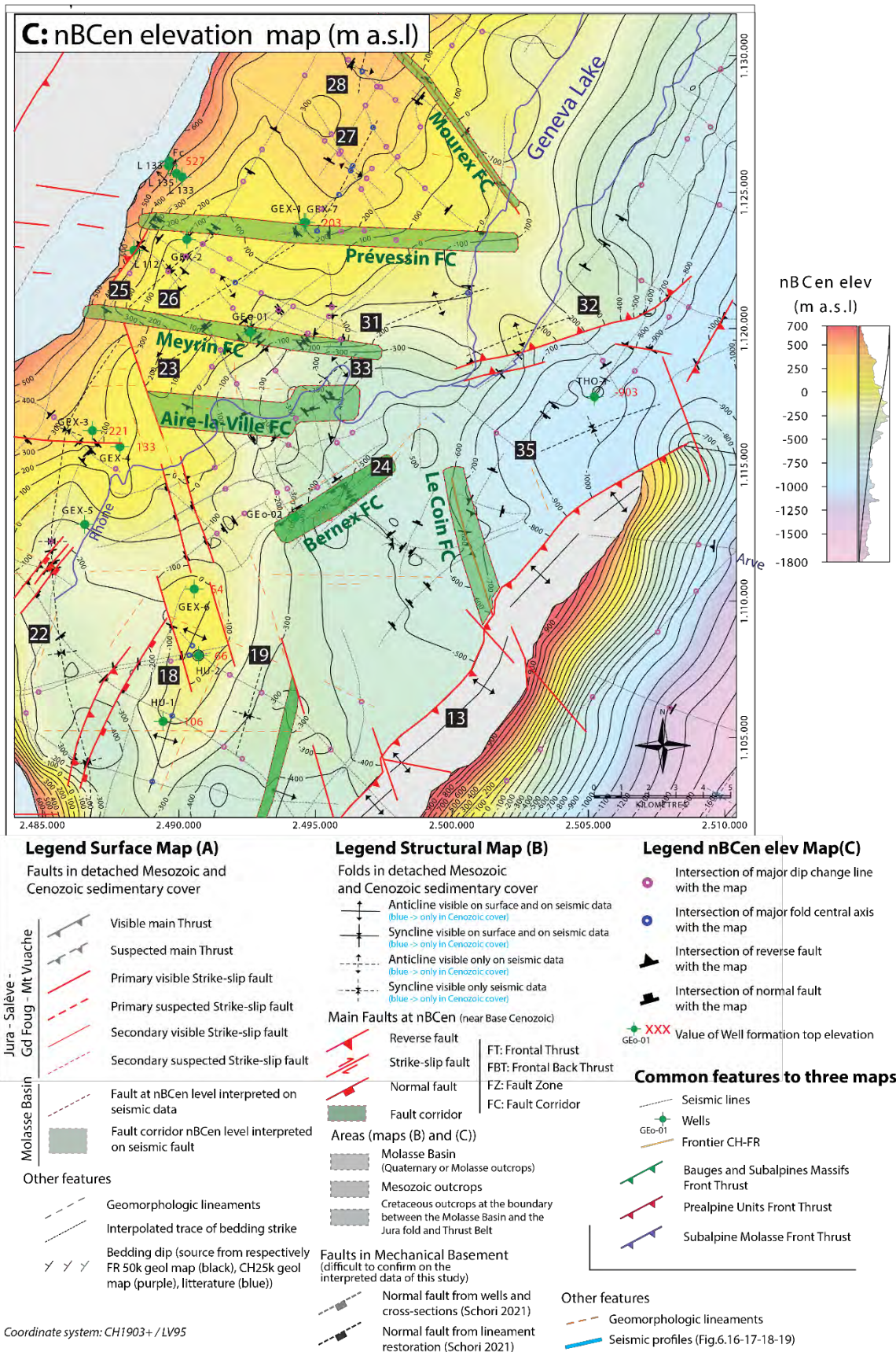


Figure 6-15 : Maps of structural interpretation results of the GVA Molasse Basin area. It includes the Mourex FC, the Prévessin FC, the Meyrin FC, the Aire-la-Ville FC, the Bernex FC, the Allondon FZ, the Le Coin FC, the Cologny FZ, and the Présinge FZ. These structures are described in details in the text of part 6.3.1. See Table 3-2 for well abbreviations. Sections of Figure 6-16, Figure 6-17, Figure 6-18, and Figure 6-19 are represented on structural map B as blue lines. CS: CH1903+/LV95. Geological map A is based on Marro (2021).

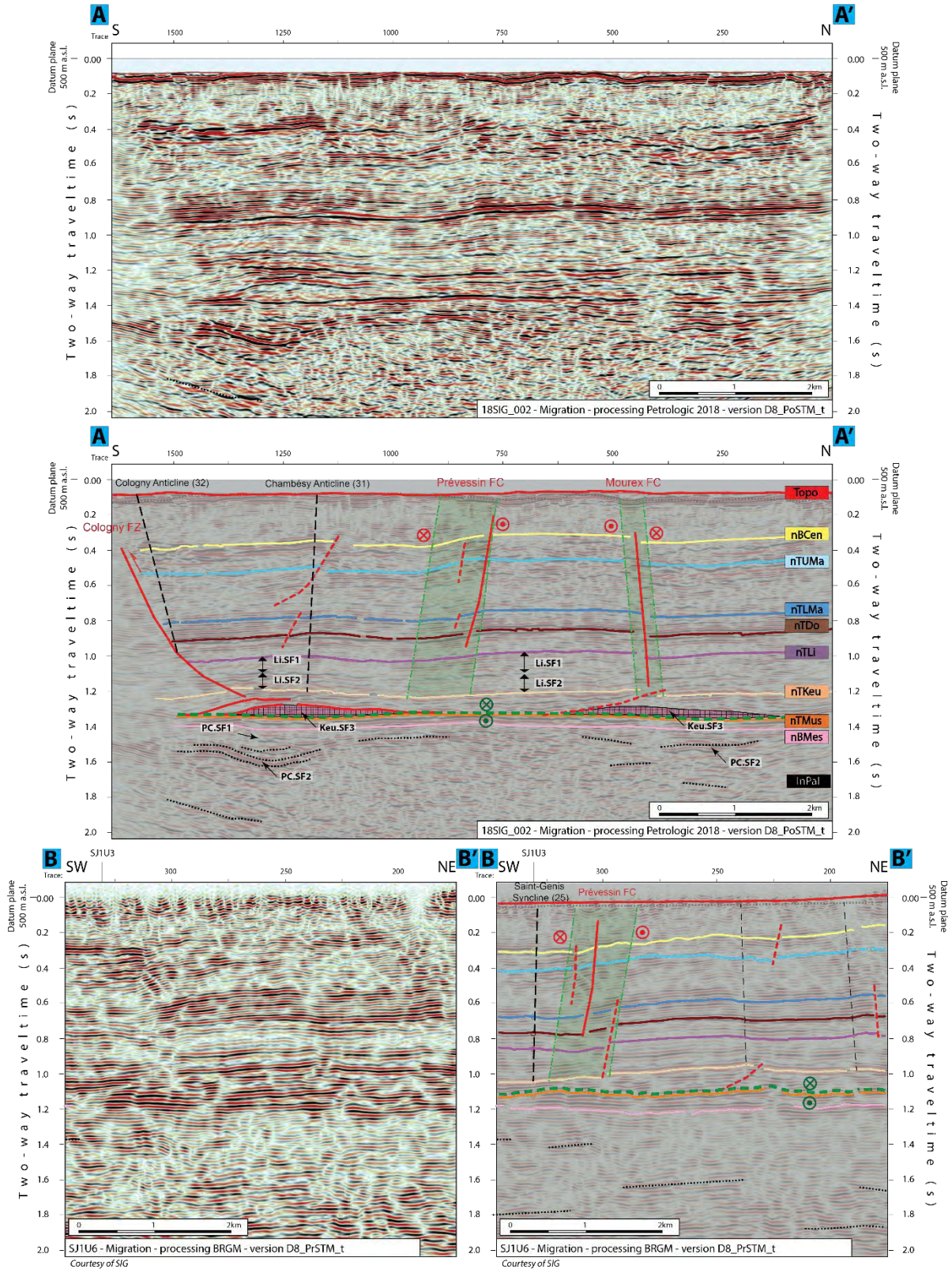


Figure 6-16 : Seismic interpretation (twf) of the Prévessin FC and the Mourex FC on seismic line 18SIG_002 (top image and section AA'), the Prévessin FC on seismic line SJ1U6 (bottom image and section BB'). See Figure 6-15 for localization of the sections. See respectively Encl 20 and Encl 77 for detailed seismic interpretation of lines 18SIG_02 and SJ1U6.

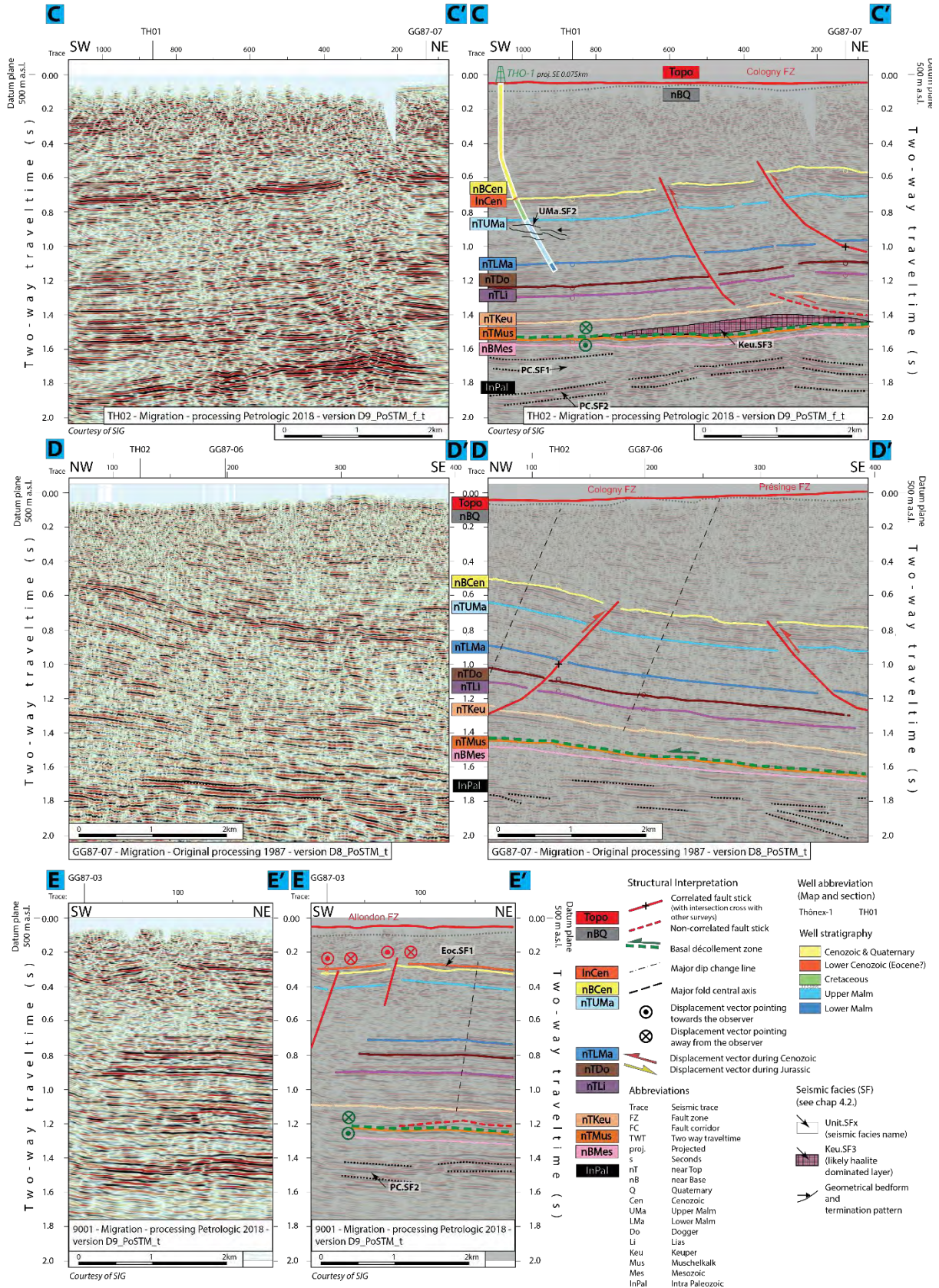


Figure 6-17 : Seismic interpretation (tw) of the Coligny FZ on seismic line TH02 (top image and section CC'), the Présinge FZ and Coligny FZ on seismic line GG87-07 (middle image and section DD''), and the Allondon FZ on seismic line 9001 (bottom image and section EE'). See Figure 6-15 for localization of the sections. See respectively Encl 82, Encl 69, and Encl 01 for detailed seismic interpretation of lines TH02, GG87-07 and 9001.

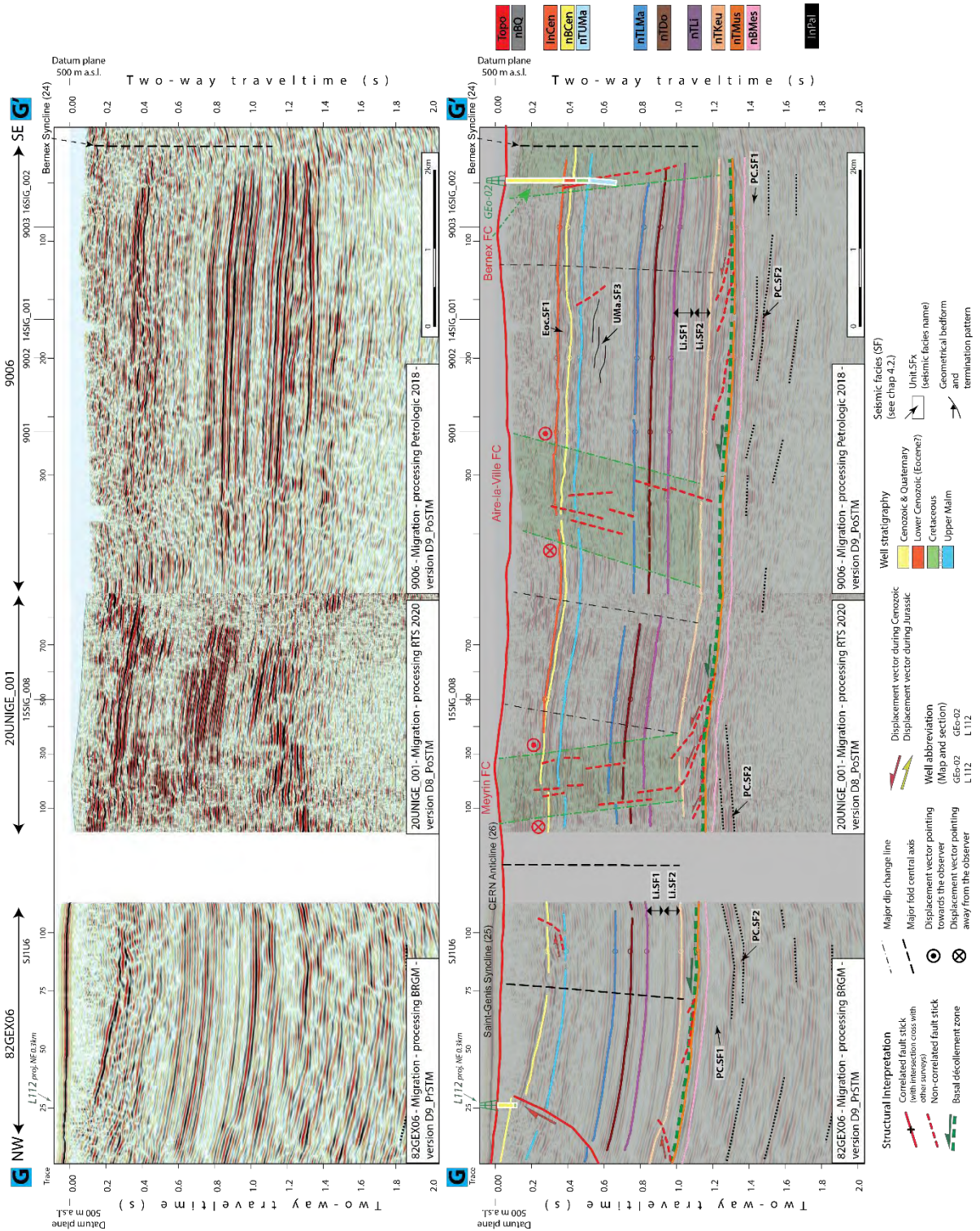


Figure 6-19 : Seismic interpretation (tw) of the Meyrin FC, the Aire-la-Ville FC, and the Bernex FC on seismic lines (from NW to SE) 82GEX06, 20UNIGE_001 and 9006 (section GG'). See Figure 6-15 for localization of the sections. See Encl 06 for detailed seismic interpretation of the lines of this figure.

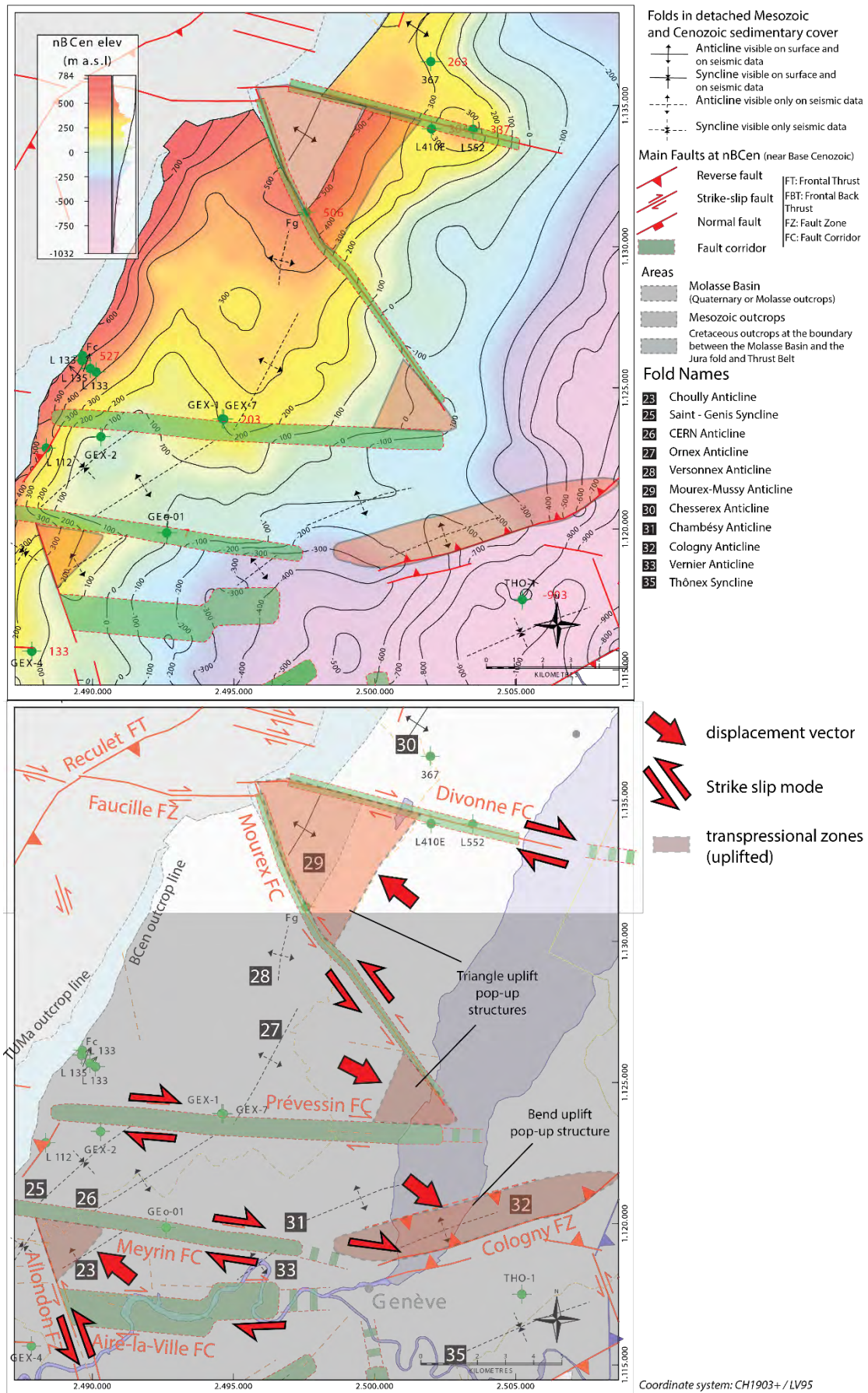


Figure 6-20 : kinematic scheme of uplifted triangles (or bend zone) structural areas (red areas) in relation to conjugate strike-slip fault systems.

In the westward continuation of the Meyrin FC, fault or structural lineaments in the Jura High Chain are present in the same orientation than the fault corridor that provide additional confidence to the interpreted tectonic structure. Towards the eastern part of Meyrin FC, no seismic data is available until 2D seismic profile 18SIG_002 bordering the SW part of Lake of Geneva. This lack of data does not allow linking the fault with the Cologny FZ, although this correlation is likely present according to the mapping of Mesozoic seismic horizons (vertical offset visible on the contouring along this likely fault continuation).

The **Aire-la-Ville FC** is another replica of the E-W striking fault corridors described above (Meyrin FC, Prévessin FC, Divonne FC and Saint-Cergue FC). It is located just 4km south of the Meyrin FC, and has the particularity of being interpreted with a larger width (more than 1km) than the two other northern fault corridors (section F on Figure 6-18 and section G on Figure 6-19, see location on Figure 6-15). It is following the Rhône River along a length of around 7km and is likely to stop laterally against the Allondon FZ (NW-SE strike-slip fault system, described below) in its western part and could not be continued towards its eastern part due to an insufficient number of seismic profiles in the area inside the city of Geneva. The “Z” shape (on map view) of the corridor with a northward shift of the eastern part of the structure may be due to a NW-SE sinistral strike-slip fault, not identified on the current interpretation. A link with Le Coin FC or Cologny FZ is not excluded but is elusive. The geometry and even the presence of this fault corridor remains quite speculative, as only one seismic profile is continuously crossing it (the Rhône River being a logical obstacle to seismic acquisition). Moreover, in this context, the other segments of seismic images displaying the supposed fault corridor consist of extremities of seismic profiles that usually are of limited resolution in comparison to centers of the profiles (see part 3.2.2). However, the seismic representations of this area are characterized by the same seismic facies typical of fault corridors, with “transparent” texture, discontinuous oblique reflectors, and vertical offset of seismic horizons or main dip changes along the lateral boundaries of the corridors. The strike-slip fault system appears with an overall very steep dipping-north normal faulting configuration, with several small-scale fault segments (0.1-0.3 second of apparent vertical extent) in the most competent layers such as the massive limestones of the Upper Jurassic unit.

The **Cologny Fault Zone (FZ)** is a structural variation of the E-W (approximated orientation) strike-slip faults presented in the above paragraphs. It appears as an ENE-SSW striking SE-vergent reverse fault bending toward a striking NE-SW trend in its upper most northern part. However, its orientation and the possible continuation westward into the Meyrin FC, are strong kinematic arguments in favor of incorporating this fault zone into an overall E-W strike-slip regime. In that sense, it would consist of a restraining bend uplift or to a pop-up structure (see maps on Figure 6-20 and Figure 6-15, and section A of Figure 6-8, section A of Figure 6-16, and sections C and D on Figure 6-17). It is considered as a fault zone (FZ) and not as a fault corridor, because it has been interpreted as two en-echelon oblique reverse faults with clear, sharp and high fault throw (around 0.2 seconds) on the intersected seismic profiles. There is a north-vergent reverse fault facing and associated to the Cologny Fault zone, but it was not possible to map the trace of this complementary fault zone that gives a pop-up style along seismic profile 18SIG_001 (see A of Figure 6-8). Additional seismic data in the lake of Geneva and in the Cologny area would be necessary in order to identify the exact geometry of the entire Cologny structure (north and south-vergent faults). The main Cologny south vergent reversed fault is clearly rooted along the basal décollement zone passing on top of what looks like an evaporite-rich (probably salted) pillow. This suggests a lateral migration of the ductile Triassic layers towards the center of the Cologny anticline (evaporite-related fold).

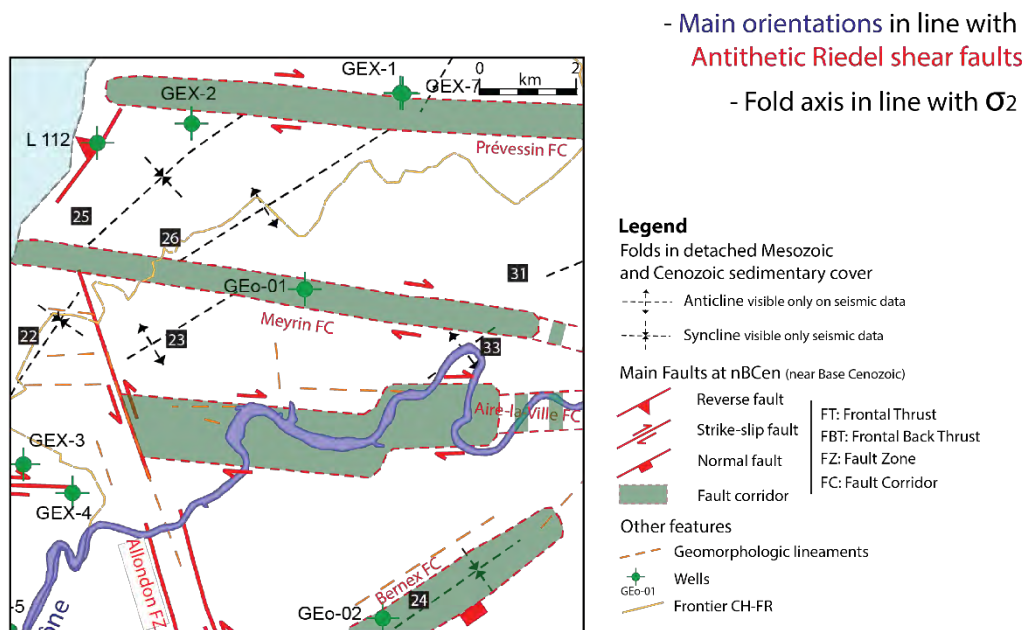
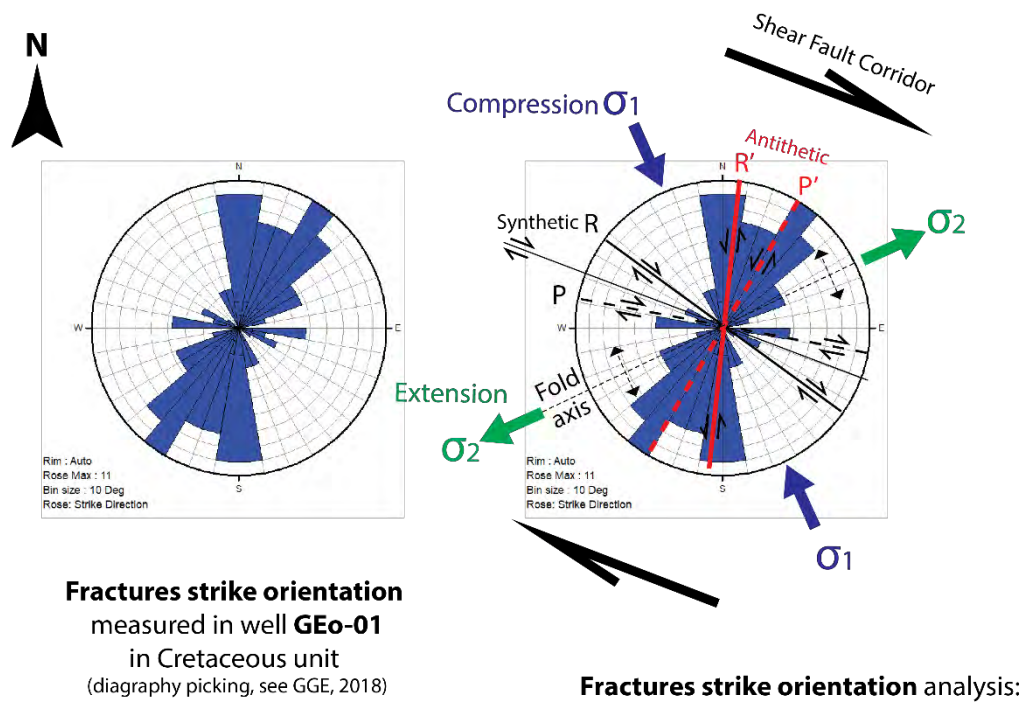


Figure 6-21 : GEO-01 fracture identification on petrophysical logging measurements (top images). GEO-01 is located in the center of the Meyrin Fault Corridor (map on bottom part), and shows antithetic Riedel fractures in N-S to NNE-SSW orientation. It confirms the fold orientation in NE-SW orientation.

This interpretation of the Coligny FZ is a new structural approach in this area, proposing this orientation and fault presence. Previous authors had noticed and mapped a NE-SW Coligny anticline parallel to the Lake Geneva (“Coligny-Vandoeuvres-Choullex” hill for Signer & Gorin (1995), or just “Coligny” Anticline for Rigassi (1957), and in addition to that Morend (2000) had mapped the USM distribution with new dip data of the outcropping Molasse in the Coligny area in line with our interpretation of this Mesozoic-Cenozoic structure (ENE-WSW strike). More recently Clerc & Moscardiello, (2020) have supposed an E-W structural “convergence zone” (of around 5 km wide and 30km long) going from the Jura High Chain toward the area near the northern outcropping extremity of the Salève FT. This structural strip passing just south over the Meyrin FZ and the Coligny FZ, is

dividing (according to Clerc & Moscariello (2020)) the structural setting into two parts, with to the north of this strip, a dominant overall E-W right lateral strike-slip trend, and to the south of the strip, a dominant left lateral NW-SE strike-slip trend. The interesting point of this latter citation is that our entire structural framework proposed and described above in our study (north to this “convergence zone” of Clerc & Moscariello (2020)) is in agreement with the interpretation of this author. Indeed, the overall E-W structural orientation is dominating this area in our study (with several fault corridors drawn), even if the exact fault scheme and the number of interpreted faults are different in Clerc & Moscariello (2020).

If we consider the area in between the four parallel E-W Prévessin, Meyrin, Aire-la-Ville FC and the Cologny FZ, as deformed zones in between large-scale strike-slip fault corridors, we can kinematically and mechanically assume the presence of large-scale passive *en échelon* folds in the Mesozoic-Cenozoic cover with a trend around 45° to the shear direction. Indeed, simple shear and buckling during compression deforms the layered overburden above evaporite-rich (and salt-rich) Triassic unit, to form kind of en-echelon wrench folds that can be later stretched and rotated by continued shear to orientations of 20 to 30 degrees to the shear direction (Jackson & Hudec, 2017d). In that sense, NE-SW striking gentle to open folds are developed in between the E-W strike slip fault corridors, such as the Chouilly Anticline, Saint-Genis Syncline, CERN Anticline, Ornex Anticline, Chambésy Anticline, Cologny Anticline, Vernier Anticline and Thônex Syncline (see map of Figure 6-15). These folds are mainly the result from a combination of deformation by flowage and tectonic imbrication (duplexes) within the Triassic Unit (above the basal décollement level) as explained several paragraphs above concerning both Versonnex and Ornex anticlines (see also link between folds and Triassic thickness on Figure 6-7). In general, and as a reminder, folds axis have been drawn on the final tectonic map by combining the results of seismic interpretation using the main dip change axis (presented along each seismic profiles concerned), with the surface data analysis using principally the dip data (outcrops of the Molasse formation) and DEM lineaments.

The **Le Coin FC** is a NNW-SSE oriented strike-slip fault laterally offsetting the Salève FZ with a left lateral displacement (map of Figure 6-15, and section F in Figure 6-18). The outcrops of this fault in the Mont Salève are detailed by Joukowsky & Favre (1913). It has been described structurally by Signer & Gorin (1995), as a wrench fault zone continuing towards NW into the Geneva area up to the Jura FTB, as a flower structure, and aligned along a supposed basement fault. Our seismic interpretation, confirms its continuation northwestward from its outcrop in the Salève FT. However, we rather considered it as a fault corridor following the same principles as the other fault corridors interpreted, such as a wide (up to 500m) strike slip zone with a complex internal, smaller-scale fault distribution. Evidence on seismic profiles of this corridor are clear, with a notable dip change of the layered Mesozoic-Cenozoic cover from one side to another of the corridor, as well as the discontinuous and strong amplitude reflections inside it, that underline the complex internal faulting. The central main internal fault has been correlated and its trace represented on the tectonic map. Moreover, the continuation of this fault in the Geneva area has been revised in relation to the available data that delimit it until the Arve River. A possible link of this fault with one of the northern E-W fault corridors (Cologny FZ or Meyrin or Aire-la-Ville FC) is likely. The kinematics of this fault system remains uncertain, but it appears to initiate as a lateral ramp near the Salève Thrust and then continues as a tear fault into the Geneva Basin. One crucial observation about this fault corridor is that the Lias unit is showing a slight thinning in the NE part of the fault in comparison to the SW part (around 20ms of twt vertical apparent variation, see section F in Figure 6-18). Two hypotheses can be proposed about this thickness variation. Firstly, a stratigraphic thinning during deposition according to the fact that the thinning is relatively gradual and following a suspected thinning trend of this layer (transition from platform to basinal settings southeastward (Signer & Gorin, 1995; Ziegler, 1990)). A second hypothesis would be that it is related to a tectonic syn-sedimentary activity meaning that this fault is a re-activated inherited fault dated

from at least the Lower Jurassic period. The second hypothesis is less probable mainly because the fault does not seem to extend vertically along the entire Lias unit and from the fact that it does not have the similar shape as the other Liassic extensional faults observed in our studied area (see the Humilly area, in chap 6.3.2). If the second hypothesis was proven to be verified in future studies, it should be analyzed in relation to the Salève middle to Lower Jurassic structural inheritance that will be discussed in following parts (see 6.3.3 and chapter 7). As for the Triassic unit, an internal structure has been interpreted near Le Coin FC justifying a local thickening. Signer & Gorin, (1995) have interpreted in their study, a NW-SE basement faulting and a Permo-Carboniferous graben infill just below Le Coin fault. Our interpretation suggests also the presence of Permo-Carboniferous seismic facies in this area, that would likely correspond to the NNW-SSE normal basement fault proposed by Schori (2021) based on lineament restoration and located just 2km west of Le Coin FC (see Encl_M01 structural map). However, no direct connection between basement structures and cover structures can be interpreted.

In the area around Le Coin FC, we can furthermore observe that the Mesozoic horizons are dipping northeastward (with a NNW-SSE strike, parallel to Le Coin FC and Allondon and Cruseilles FZ, see map of Figure 6-15), with the same plunging orientation as the Salève ridge. Since the sedimentary cover is dipping southeastward in the majority of the Swiss Molasse Basin, this observation could be an argument in favor of the structural analysis of Clerc & Moscariello (2020) who see in the southern part of the so-called E-W "Convergence Zone" (extending from the Jura High Chain to the Salève ridge, passing south of the axis Meyrin-Cologny), a dominant trend of NW-SE strike-slip faulting.

In addition to the Le Coin FC, the Salève ridge is crossed by several other NNW-SSE strike-slip fault system (see map of Figure 6-15), including the suspected **Arve FZ** (Clerc & Moscariello, 2020; Signer & Gorin, 1995). This fault could not be interpreted clearly along seismic profiles, due to a lack of subsurface data in this area, in that sense it is rather a conceptual fault than an observed one. Its presence is supposed and mainly deduced from the regularity of the lateral distribution of NW-SE strike-slip fault along the Salève ridge (approximately every 10km). Its structural role is also justifying its presence. Indeed, this fault is marking the northeastward termination (lateral ramp?) of the Salève ridge but is also laterally offsetting (sinistral movement), by approximately 2km, the Subalpine Molasse Front Thrust.

The **Cruseilles FZ** is similar in its configuration to Le Coin FC and Arve FZ (NNW-SSE striking), but is clearly shifting in a sinistral strike-slip movement the Salève ridge with a higher offset than the two others faults. The outcropping fault is showing up to 4 km lateral offset from the Mandalaz FT to the Salève FT (see Figure 6-23). The continuation of this fault northwestward is also more conceptual than proven by seismic interpretation. Indeed, only modest fault throw is visible on seismic profiles crossing the fault segments just above the Salève Front Thrust, but being a strike-slip fault, it should not necessarily show vertical apparent fault throw. Geomorphological lineaments observed on the DEM images helped tracing this segmented strike-slip fault. Near Humilly-2 well, seismic interpretation is however indicating in a clearer way a vertical offset with an uplifted eastern part of the fault segments. This structural setting of the Cruseilles FZ is accommodating the deformation by several 3-5km fault segments organized in lateral relay setting. North of well Gex-6, the fault system is continuing and relayed by the Allondon FZ (see section E in Figure 6-17). The resolution/quality of the interpreted seismic images intersecting the Allondon FZ is poor (quality type 2 in lateral extremities of 2D lines), but they are nevertheless representing these faults with relatively shallow vertical extent (down to Lower Malm), with still an uplifted eastern part of the faults. The northern segment of the Allondon FZ is not proven by seismic interpretation, but the very strong geomorphological incision of the Allondon in this specific NNW-SSE direction might be an interesting argument to support this hypothesis. The mapping of seismic horizons allows confirming the kinematically logical uplifted triangle zone in the southeastern part of the intersection between the Allondon FZ and the Meyrin FC (Figure 6-20).

The above description discusses the several conjugate strike-slip fault systems (NNW-SSE and ESE-WNW striking), which are developed in the same way in the entire area Geneva area (eastward from Cruseilles-Allondon axis) as in the Canton Vaud area. They were very likely generated in the same structural setting and strain field. However, the intensity of the deformation seems to increase northward with higher uplifts (vertical fault throw component of the strike slips fault corridors), and higher Triassic thicknesses observed in the Nyon area than in the Geneva area.

Two structures developed in the Geneva area differ from the strike-slip systems described above. The **Présinge FZ** which is located east of the Cologny FZ (see map of Figure 6-15) is a hypothetical NE-SW striking reverse fault (thrust) possibly rooted in the Lower Malm Unit (Effingen marls). Its interpretation remains relatively uncertain, taking into account the minor fault throw observed (around 30ms), and the limited number and lengths of seismic lines used to identify it (see section D of Figure 6-17). This fault is oriented and placed in the continuation of the Salève FT with a slight NW lateral shift, and can be seen as the termination to the NE of the Salève FT, shifted laterally by the Arve FZ. The well Thônex-1 was drilled in 1993 (Jenny et al., 1995; OCEN, 1994) less than 5km south-west of the Présinge FZ and appears to be located in a structurally calm area (in the Thônex Syncline area) with no fault on its path observed on seismic profiles.

The second non-strike-slip FZ in the Geneva area is the **Bernex FC** (see section F of Figure 6-1818 and section of Figure 6-19), which has a NE-SW structural graben appearance in the Mesozoic part on several seismic lines. The seismic expression of the hangingwall is a chaotic and “transparent” facies with an apparent vertical offset of approximately 20-30ms along nBCen horizon. A great uncertainty remains around the presence of this fault, since a thick Quaternary channel (more than 100m thickness) is overlying just along the interpreted structure (Lathion & Hauvette, 2020). The above Quaternary valley is attenuating the seismic signal during acquisition and therefore may decrease the resolution of the underlying seismic reflections (see part 3.2.2). Nevertheless, we favor the idea of a fault system. The surface geomorphology may be described by the two NE-SW axis known as “Bernex-Configny hill” and “Sillon du Petit Lac” (Signer & Gorin, 1995). In the context of the program GEothermie 2020, the well GGeo-02 was drilled in 2020 (Chablais & Savoy, 2021), and was targeting the NW part of this supposed graben, that may have been reached near nBCen seismic horizon (uncertain structural interpretation based on logging). The faulting and fracturing distribution inside this fault corridor remains unclear and very difficult to interpret on seismic data (chaotic seismic facies). This explains the attribution of the fault type “fault corridor” to this zone. Nevertheless, the main outputs of the fracture analysis along this well is a set of fractures in the Upper Mesozoic unit striking NNE-SSW dipping WNW and an ovalisation (see definition in Beghoul (2004)) in N-S to NNE-SSW directions which indicate an approximation of the maximal horizontal shear direction in WNW-ESE (Chablais & Savoy, 2021). These results are not bringing any strong arguments for confirming any exact fault geometries. Concerning the kinematics, the characteristics of this fault with its particular orientation and mechanism suggest that it is not a strike-slip fault and that it has a different origin and dating. Several facts can be discussed; the apparent normal component of this fault corridor, the orientation (NE-SW) and the fact that no Mesozoic syn-sedimentary activity seem to have occurred, but rather an Eocene syn-sedimentary activity is probable (high infill of Siderolithic deposits (140m) over the hangingwall of this fault). These arguments seem to coincide with the flexural period of the Alpine foreland Basin, due to a bending of the European lithosphere in the subduction process during the Eocene/Oligocene times. This kind of fault system has been observed NE of Lake of Geneva by Gruber (2017). Another lead has also been investigated, and concerns the fact that this fault corridor is located

in the NE continuation of the Humilly FZ, and geomorphological lineaments may suggest a possible link between both fault systems. This second assumption is ruled out as there is not enough evidences to prove it. The high thickness of Siderolithic deposits (140m) mentioned above and observed in this well will be recalled in part 6.4.3.

Outside the latter described fault zones or corridors, several individual fault indications have been interpreted along the numerous seismic profiles available in the Canton Geneva. Unfortunately, no correlation of these fault sticks could be achieved. These indications are still marked on seismic horizons maps (see Encl_M05 to Encl_M35).

6.3.2 Humilly – Vuache area / Southern part of the Geneva Molasse Basin

This structural area is comprised between the Allondon-Cruseilles FZ axis to the east and the Vuache FZ axis to the west (Figure 6-23). In the northern part, the **Challex FZ** striking in a E-W direction is a strike-slip fault that is part of the dominant conjugate strike-slip system dissecting the whole Geneva-Vaud area and discussed in detail in the above part. The Challex FZ has been interpreted as a very steep fault with a slight uplift of the northern part. Two other shallower (Cretaceous-Malm reflector extent) fault sticks have been also been interpreted on seismic sections just south of the main Challex fault zone, but could not be correlated. Another structural alternative was appraised and would imply replacing the strike-slip fault interpretation by a normal fault zone dipping SE and following the orientation and the axial trace of the CERN syncline. Only new additional seismic data can help resolve this uncertainty. The second option could be included in the dominant NE-SW normal faulting interpretation of the Humilly-Vuache area, described in the next paragraph.

The **Pougny FZ** is bordering the Rhône River in a NE-SW orientation. It is composed of two main normal faults dipping SE with up to 50ms fault throw applies on all Mesozoic layers above the basal décollement level (see map of Figure 6-23 and sections A of Figure 6-24). No syn-sedimentary activity has been detected in this fault zone, unlike the Humilly FZ described in the next paragraph. In the westward continuation of this fault zone are very similar indications of faulting near the Mount Vuache, along seismic profile 82GEX_01 (see western border of section B in Figure 6-25). A link between these two traces is very likely and would form a structural branch of the large-scale normal Vuache-Humilly fault system. The density of the seismic lines in our database is not sufficient to ascertain an extension eastward of this fault zone, but if we take into account the important fault throws of these faults, a fault scaling fault length vs. offset would surely support an extension towards the Allondon FZ.

In the center we find one of the most remarkable structures in the Greater Geneva Basin, **the Humilly FZ**. The geometry, type, and history of this fault register information on its geological evolution that are not common in the region. It can be demonstrated, based on the seismic interpretation that this NE-SW striking listric normal fault can be linked to synsedimentary activity during the Lower Jurassic periods (growth fault) (see map of Figure 6-23 and sections A and B in respectively Figure 6-24 and Figure 6-25). Indeed, bedding shows a rollover geometry (smooth decreasing of the dip of the fault downwards) and the fault has a listric geometry rooting in the basal décollement level. In addition, thickening of the Liassic unit is visible along the hangingwall of the fault. There is a major dip change axis facing the fault southeastward, and both (the fault and the major dip change axis) delimit the rollover anticline (Humilly Anticline). Offsets along the fault are taken as indicator for an inversion in

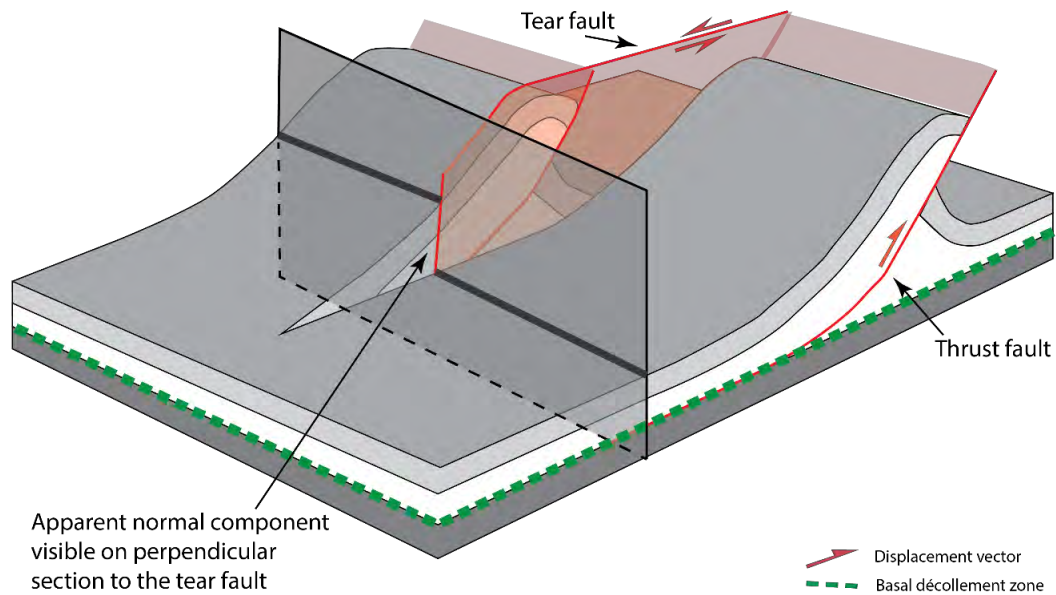
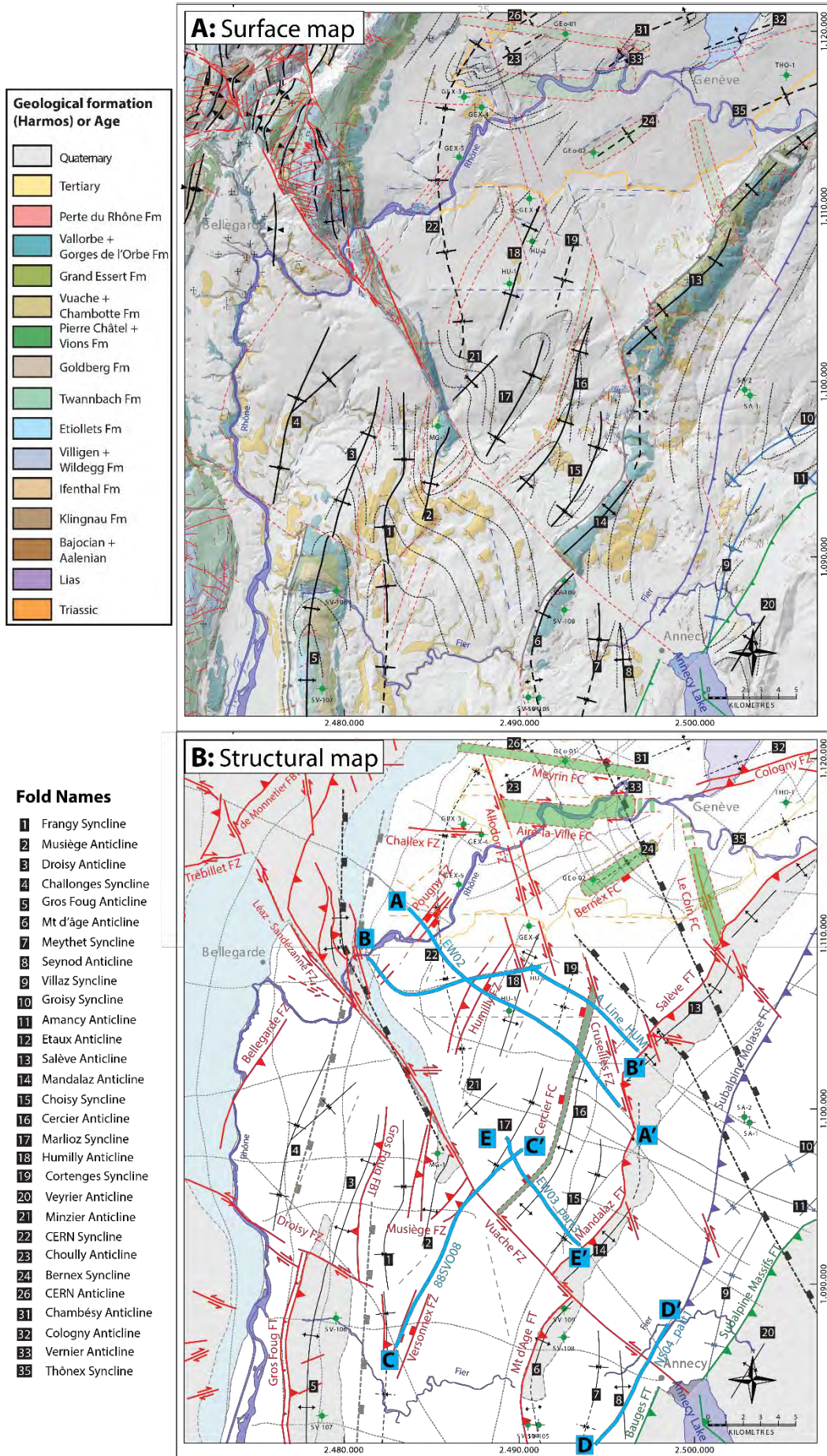


Figure 6-22 : Scheme for geometrical understanding of the backlimb of ramps laterally shifted by a tear fault (see Vuache FZ – Mt d'Âge FT – Mandallaz FT on map Figure 6-23 and section D of Figure 6-27 & Figure 6-28).

compression of the originally extensional growth fault. The well Humilly-2 and Humilly-1 were drilled during the 1950ties for oil exploration, and were targeting possible structural oil traps along this Humilly Anticline. Humilly-1 has reached only the nBCen horizon, but Humilly-2 penetrated Permo-Carboniferous sediments beneath the basal décollement zone and is an invaluable source of geological information. This well also represents the reference data for all petrophysical and geophysical studies since decades in this area. In our case, it allows tying all Mesozoic seismic horizons in the hangingwall of this fault, and it particularly indicates the presence of a thick salt layer (around 120m thickness) in the evaporite layers of the Keuper Group. This information helped to understand the location of the basal décollement layer, but also corroborates the possibility of salt flow mechanisms in the extensional rollover evolution. Indeed, the Humilly Anticline has now a compressional shape, but it was initiated during the extensional phase (Jurassic). It possibly happened in relation with salt flow and a migration towards both sides of the fault, specifically towards the center of this anticline (Humilly) forming a salt pillow/anticline (Jackson & Hudec, 2017c). On section B of Figure 6-25, we can notice the NW continuation of a branch of the Cruseilles FZ crossing in segments the Humilly FZ (see also Figure 6-23). Geomorphological lineaments oriented parallel to the Humilly FZ/Anticline, in addition to the surface (and subsurface) dip data support the idea that the entire Humilly structure likely continues southwest by joining the Vuache FZ and the Minzier Anticline. This fault zone is interpreted to be actually part (as a lateral branch) of the large-scale Vuache-Humilly extensional fault system (active in Jurassic times and inverted later during Alpine compression, see Figure 6-30).

The Humilly FZ was interpreted in a similar way by Gorin et al. (1993), with an extensional mechanism and a thickening of the Lias unit, but with the main difference is that these authors root the fault into the mechanical basement. However, as mentioned prior, no evidence of such a throughgoing fault can be observed on seismic lines; in addition, the regional thin-skinned tectonic (Miocene) concept and balanced cross sections show the inconsistency of such a model. In more recent studies (Clerc & Moscariello, 2020; Paolacci, 2012), this remarkable structure was not fully explored/considered (or in a very different interpretation style).



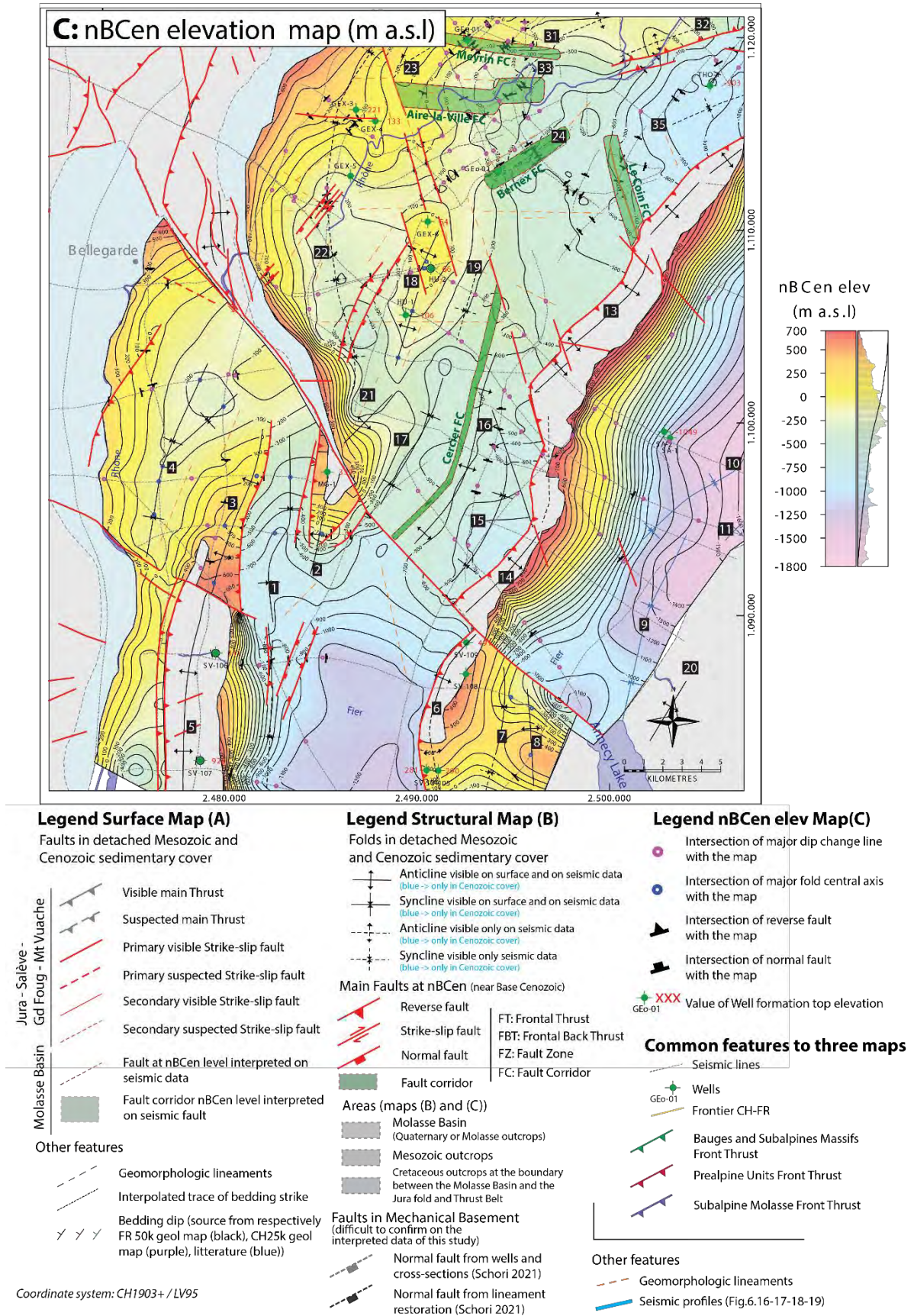


Figure 6-23 : Maps of structural interpretation results of the Humilly - Vuache area. It includes the Pougny FZ, the Humilly FZ, the Cercier FC, the Cruseilles FZ, and the Vuache FZ. These structures are described in details in the text of part 6.3.2. See Table 3-2 for well abbreviations. Sections of Figure 6-24, Figure 6-25, Figure 6-26, Figure 6-27, Figure 6-28 and Figure 6-29 are represented on structural map B as blue lines. CS: CH1903+/LV95. Geological map A is based on Marro (2021).

The **Cercier FZ** consists of a narrow normal fault corridor developed south-east of the Humilly FZ and with a parallel strike orientation in NE-SW in its southern part and bending to reach a more NNE-SSW orientation in its northern part. The horizontal trace is in fact following the same curvature (parallel) than the Mandalaz FT, further to the S (see Figure 6-23). We can observe a Triassic evaporite anticline made of intra-Triassic NW-vergent duplexes (or successive thrusts), forming a Mesozoic-Cenozoic anticline on top of it: the Cercier Anticline (see section E of Figure 6-29). Thus, this structure has a compressive Miocene component. In addition, and by similarity with the Humilly FZ, the Cercier FC may also have an extensional inheritance, although clear syn-sedimentary-activity cannot be resolved on the seismic lines. On a regional scale, we suggest that this fault corridor may have been triggered simultaneous to the Humilly FZ during the Lower Jurassic times, and has been reactivated and slightly reshaped in compression during the Alpine distant-push (Figure 6-30).

The **Vuache FZ** forms the western boundary of the Geneva Basin, and with its 11km length striking NW-SE from Annecy (France) to the Lons-Le-Saunier area (external Jura FTB) allows linking the Subalpine Massifs and the thrusts and folds of Jura FTB (Chauve et al., 1980). This remarkable tear fault system has played a major role in the structural evolution of the region. It has a clear geomorphological signature, with a first meridional NW-SE segment extending from the Lake of Annecy to the Rocher de Léaz. The fault thus cuts the Salève ridge with a left lateral offset; lateral shift of the northern Mandalaz FT with respect to the more southerly located Mt d'Âge FT, and forms the northern termination of Musiège Anticline (Figure 6-23). The second, northern segment of the Vuache fault system (north of the Rocher de Léaz) is divided into two branches: the NW-SE Léaz-Sandezanne FZ in the continuation of the southern segment, and the NNW-SSE Vuache-Forens-Les Bouchons FZ (VFB) in the northern part. A structural triangle zone stands out from the zone, in between the two latter branches and is bordered in the north by the Monnetier backthrust. This triangular zone, called the relais de faille de Léaz-Champfromier, is a shear transfer zone with transpressional structures (Donzeau et al., 1998). The eastern branch of this zone is considered to be a lateral ramp merging northward with the Crêt Chalam Thrust and the Reculet Thrust. Meyer (2000) analyzed the structural configuration of this transpressional zone, and proposed a development in two phases of successive opposite-vergence thrusting, hiding a common thrust volume. This may explain the local uplift of the area. The Jura part of this fault is examined in more details by Marro (2021) and Marro et al. (2023), whereas in our study, we focused more on the part of the Vuache FZ located towards the Molasse Basin. North of the Musiège FZ (in the Rumilly Basin), the Vuache FZ appears as SW-vergent reverse (thrusting) strike-slip fault system. This outcropping (Mesozoic) part is geologically described in detail by Charollais et al. (2013), but also from a structural and kinematic point of view by Blondel (1988). The latter proposed a deformation in four stages, with a start of the deformation during the Eocene (N-S compression phase) and re-activations during the Oligocene (E-W extension), Miocene inf (NE-SW shortening), Miocene sup (shortening NW-SE). This proposed kinematic evolution will be fully revised in our study, by proposing among other, an older tectonic inheritance from the Lower Jurassic. Indeed, based on our seismic interpretation of the blind part of the fault (fault not outcropping, recovered by Quaternary sediments), south of the Musiège FZ, we can observe that the Vuache FZ is composed of one main NW-SE fault surface dipping NE with a vertical extent across the Mesozoic-Cenozoic layers above the basal décollement zone (see map of Figure 6-23 and sections C and D of respectively Figure 6-26 and Figure 6-27&Figure 6-28). In the area in between the Mont Musiège and the Mt d'Âge – Mandalaz FT, the Vuache FZ has an apparent overall reversed offset. On the other hand, we clearly can identify a syn-sedimentary activity of the fault during the Liassic period, with a higher thickness of the Dogger-Liassic

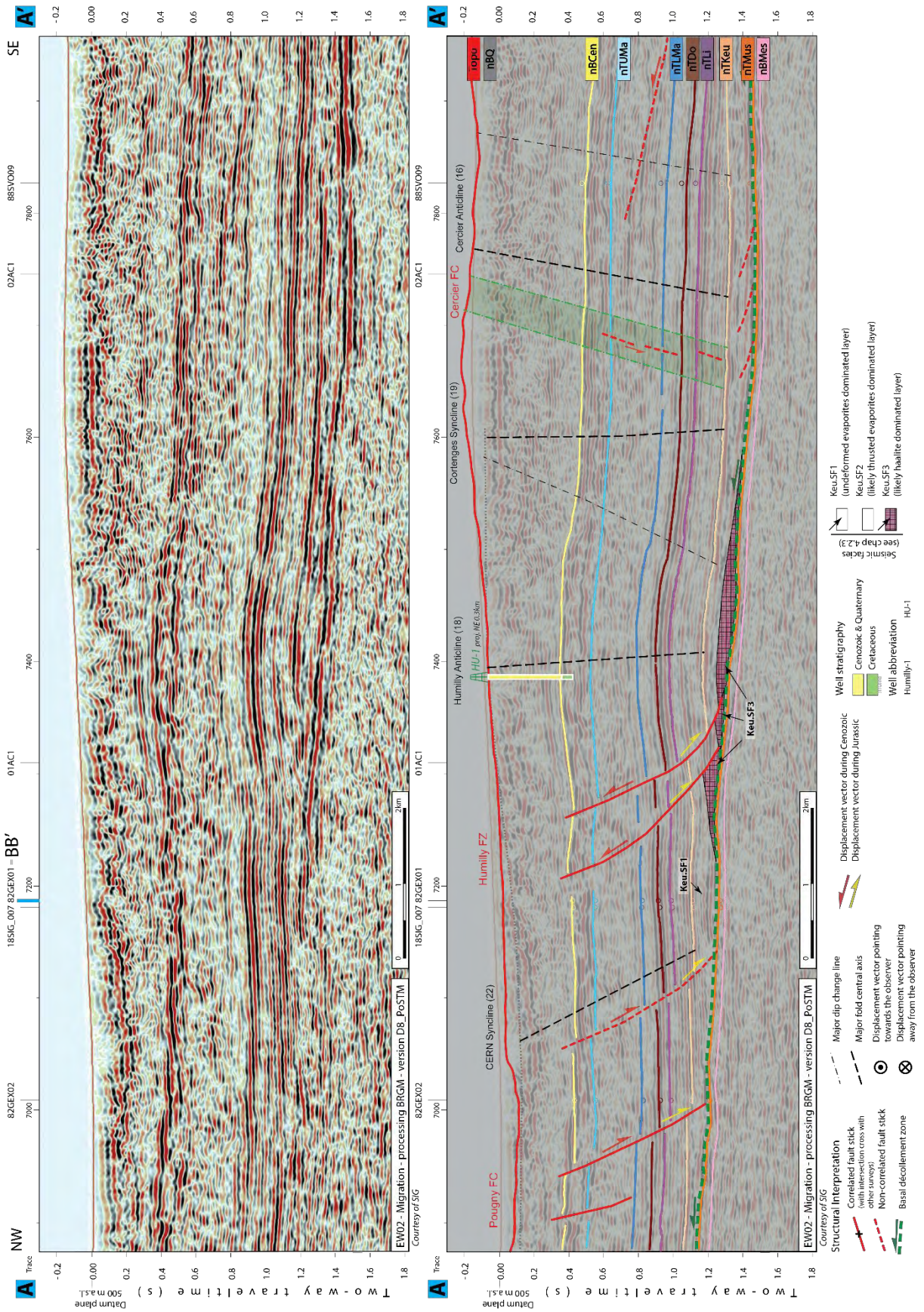


Figure 6-24 : Seismic interpretation (tw) of the Pougny FC, the Humilly FZ, and the Cercier FC on seismic line EW02 (section AA'). See Figure 6-23 for localization of the sections. See Encl 60 for detailed seismic interpretation of line EW02.

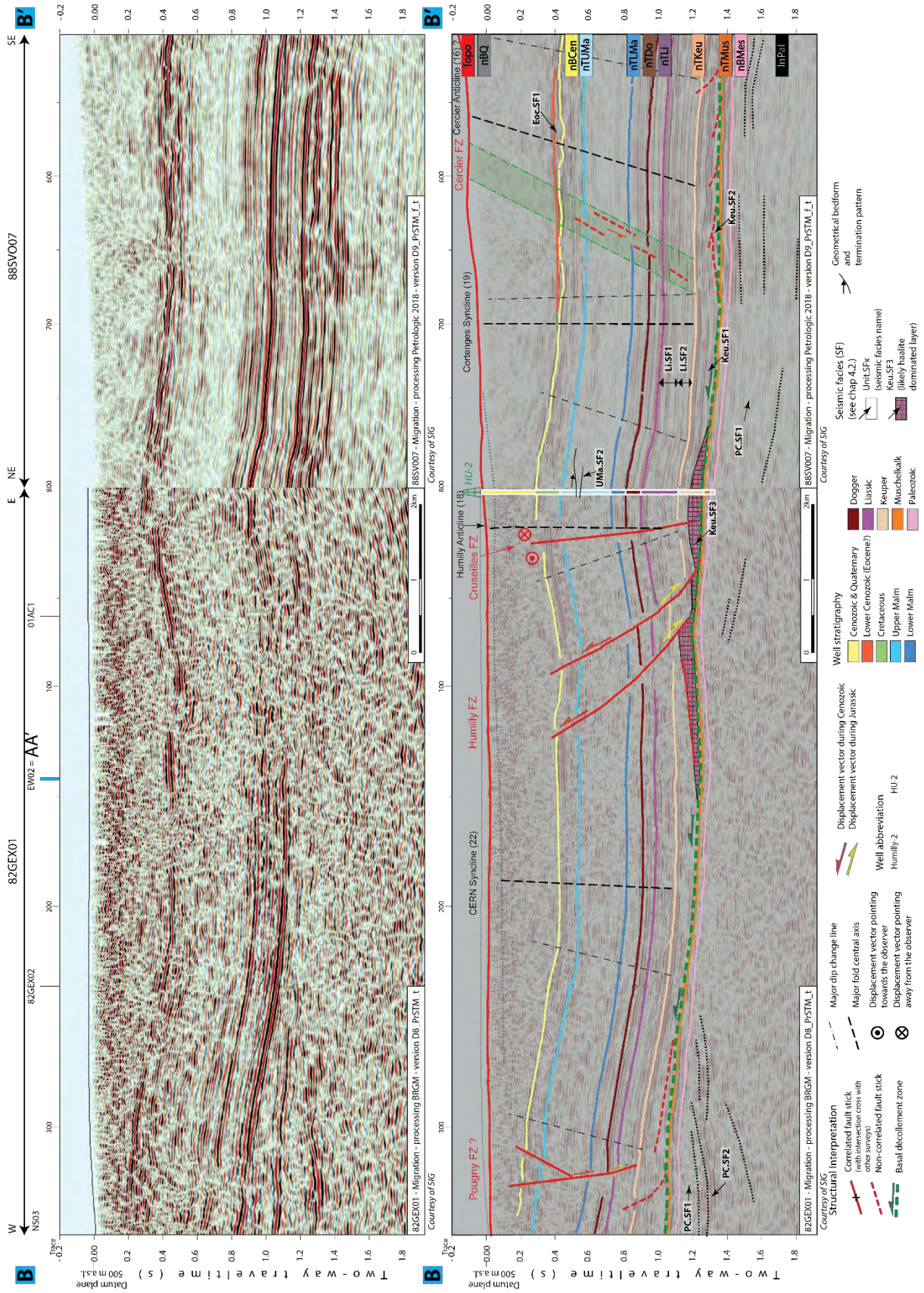


Figure 6-25 : Seismic interpretation (twT) of the Pougny FC, the Humilly FZ, the Cruseilles FZ, and the Cercier FC on seismic line (from NW to SE) 82GEX01 and 88SV007 (section BB'). See Figure 6-23 for localization of the sections. See Encl 38 for detailed seismic interpretation of the lines of this figure.

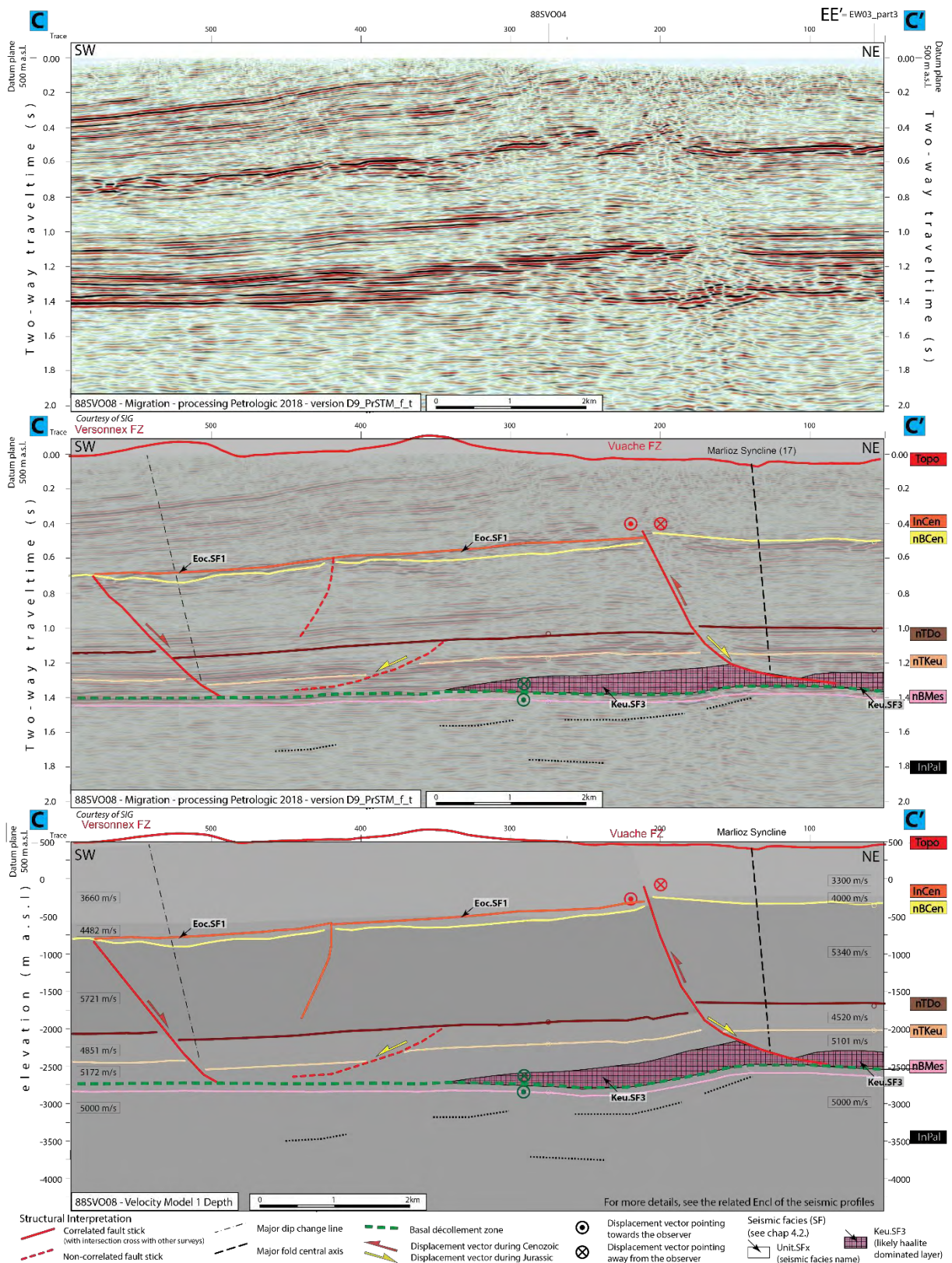


Figure 6-26 : Seismic interpretation (in twt on top two images and the depth velocity model 1 on bottom image) of the Vuache FZ and the Versonnex FZ on seismic line 88SVO08 (section CC'). See Figure 6-23 for localization of the sections. See Encl 52 for detailed seismic interpretation of line 88SVO08. In the Paleozoic part below the Vuache FFZ, the resolution of the seismic data does not allow locating with enough certainty a basement fault (as calculated by Schori (2021)). Note also that a velocity modeling and time-to-depth conversion issue and therefore a misleading geometry of the nBMes seismic horizon in the depth domain may not be excluded.

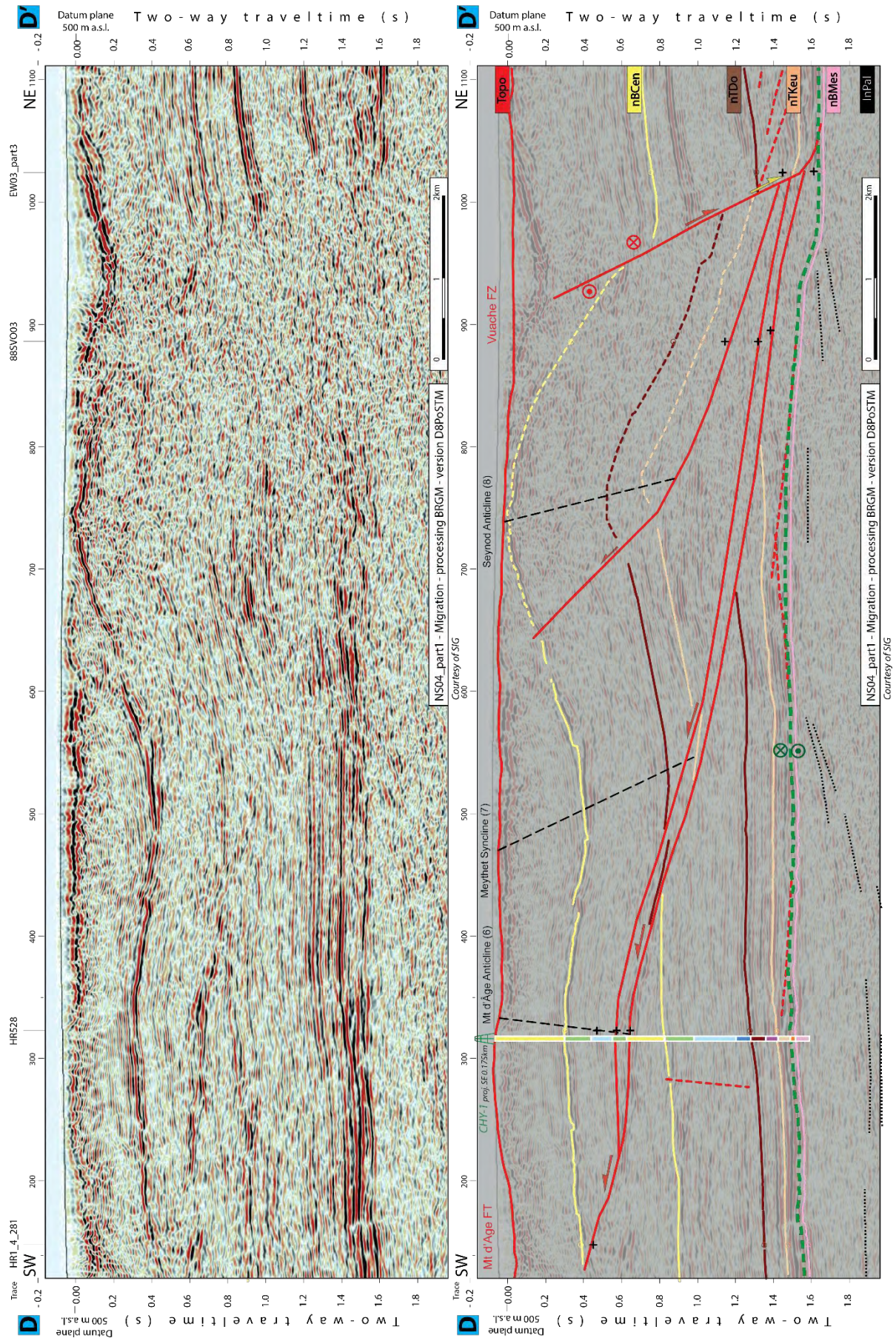


Figure 6-27 : Seismic interpretation (in twt) of the Vuache FZ on seismic line NS04_part1 (section DD'). See Figure 6-23 for localization of the sections. See Encl 73 for detailed seismic interpretation of line NS04_part1.

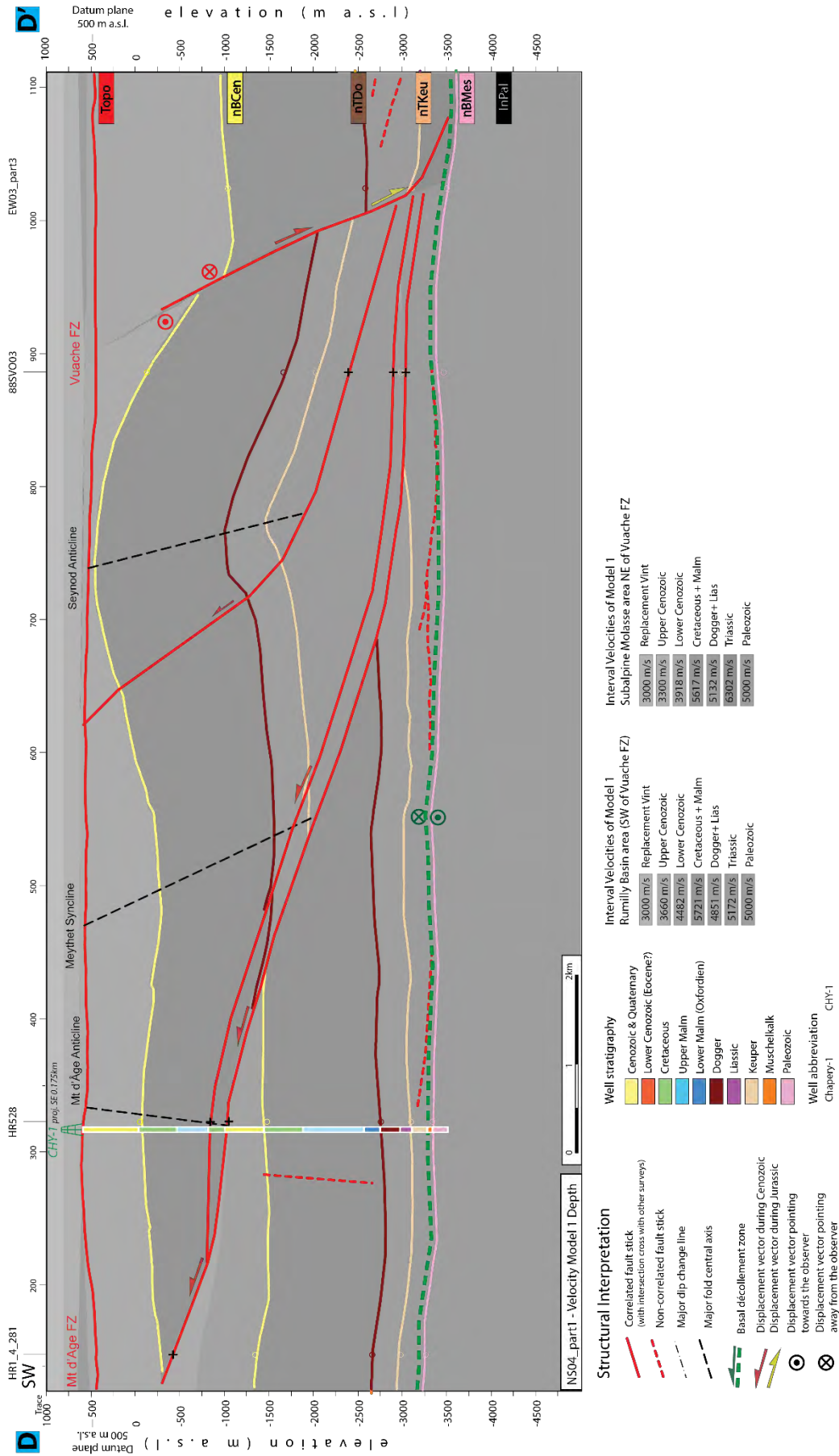


Figure 6-28 : Seismic interpretation (depth velocity model 1) of the Vuache FZ on seismic line NS04_part1 (section DD'). See Figure 6-23 for localization of the sections. See Encl 73 for detailed seismic interpretation of line NS04_part1.

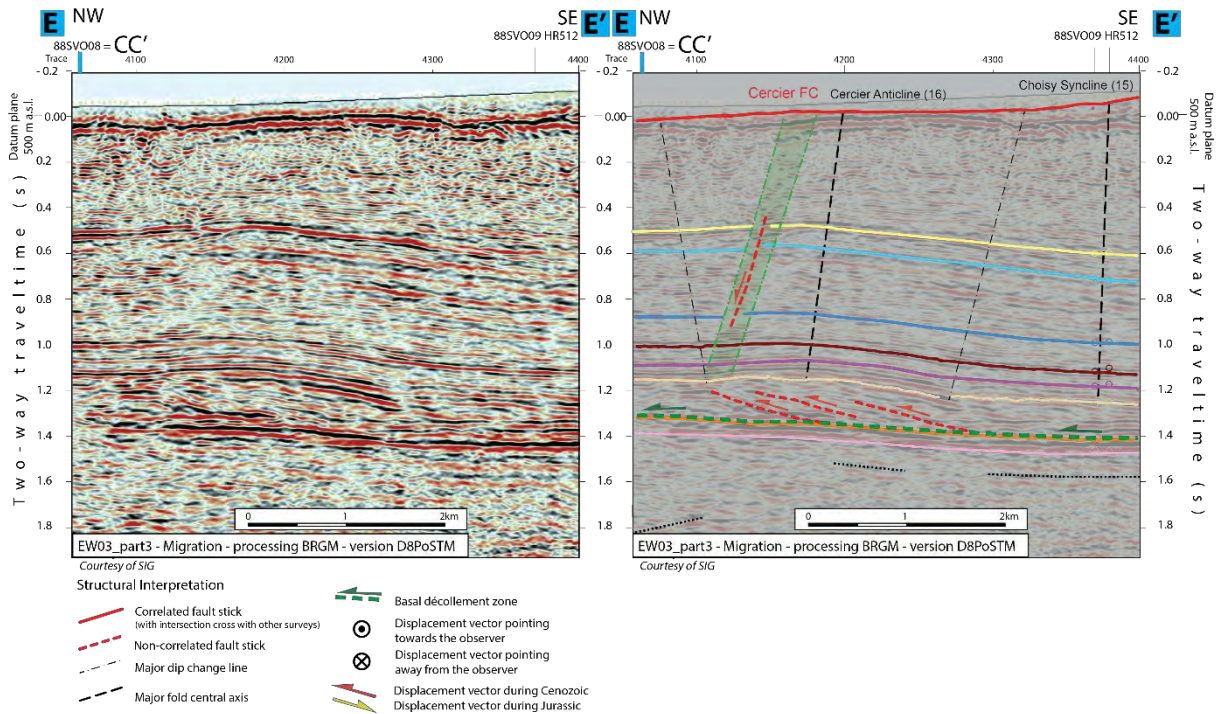


Figure 6-29 : Seismic interpretation (in twt) of the Cercier FC on seismic line EW03_part3 (section EE'). See Figure 6-23 for localization of the sections. See Encl 64 for detailed seismic interpretation of line EW03_part3.

intervals (regional model including both) on the northern part of the fault (hangingwall). We can also observe that the Triassic evaporite unit has a variable thickness across the fault, meaning that it has influenced and co-evolved with fault kinematics, probably by salt flow or evaporite imbrications. The Vuache FZ has actually a similar configuration as the Humilly FZ. Both are extensional faults from the Jurassic period and affect the entire vertical extent of Mesozoic reflectors, and were re-activated, and inverted later on during Alpine compression. Moreover, they have intra-Triassic structures in relation to the development of the major overlying fault system. Finally, their perpendicular orientations and their likely merging supports the idea of a large-scale common extensional en-echelon fault system, with lateral NE-SW lateral branches (Pougnny FZ - Humilly FZ – Cercier FC) merging into the main fault, the Vuache FZ. We can also notice a normal component of the Vuache FZ south of Mandallaz FT (section D of Figure 6-27 and Figure 6-28). This structural difference in comparison to the area north of the Mandallaz FT (reversed fault), comes from the fact that the left-lateral movement of this tear fault implies that on a perpendicular section, the backlimb of the Mt-d'Âge in the Southwestern part of the Vuache FZ appears uplifted in comparison to the northeastern part (Figure 6-22).

Thus, we interpret the Vuache FZ together with the Pougnny, Humilly, Cercier FZ and probably the Mandalaz Thrust as an inherited mixed strike-slip-inverted normal fault system. This fault system originated a transtensional synsedimentary strike-slip system with minor halfgraben development (Figure 6-30). The Vuache FZ thus originated as the main lateral boundary with a normal and strike-slip displacement. The other faults originated as steep normal faults laterally branching into the bounding Vuache Fault Zone. The system originated in Liassic times and roots in the Triassic evaporite décollement. The whole system was, subsequently inverted during the Alpine compression (Figure 6-30).

In the Pre-Mesozoic units, a vertical offset of some 300-400m can be interpreted below the Vuache FZ (see Figure 6-26). According to Schori (2021), the corresponding NW-SE basement fault present below

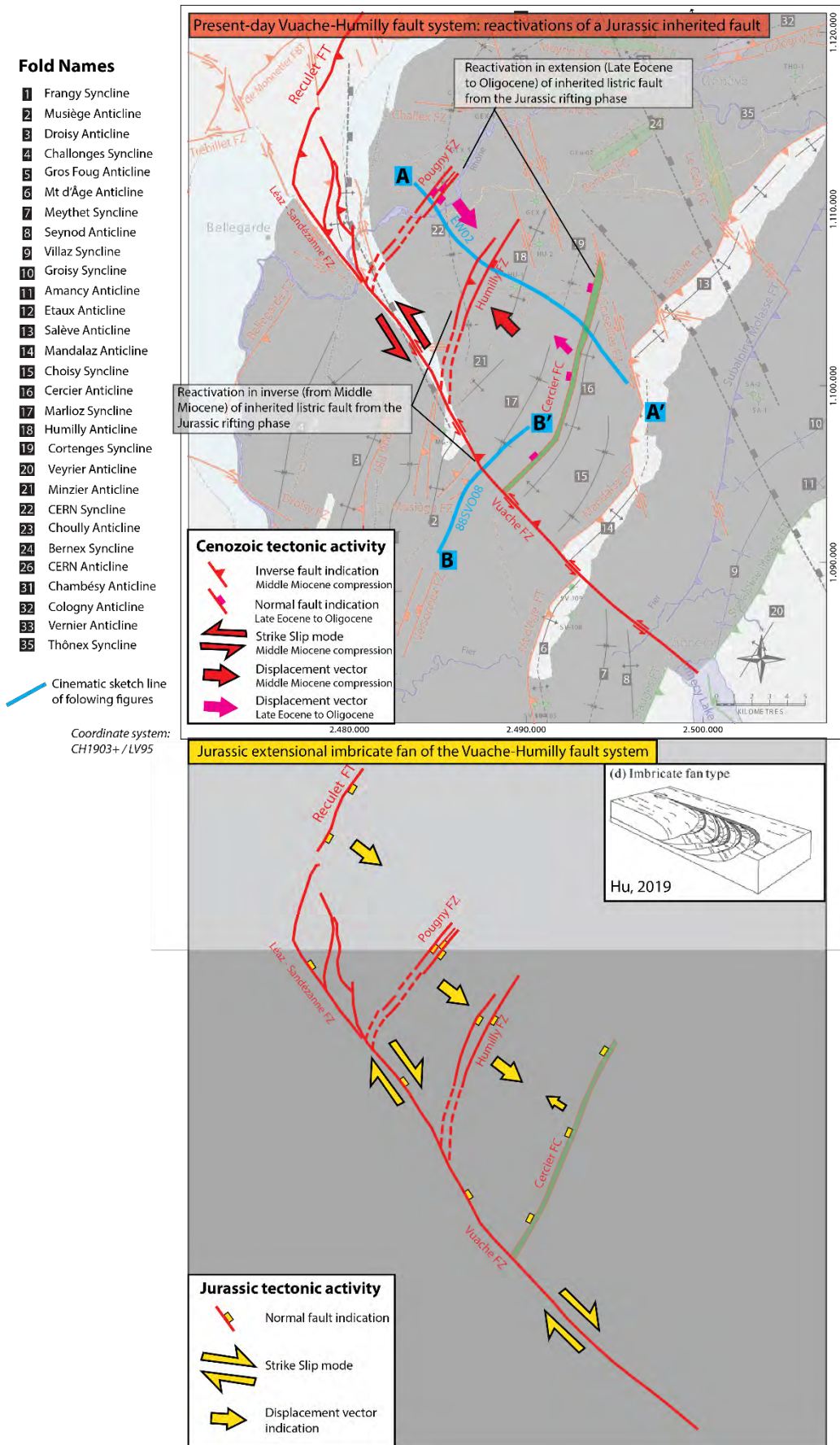


Figure 6-30a: Structural mapping scheme of the Humilly-Vuache fault system, as an extensional imbricated fan during Lower Jurassic period (bottom image) and as an inverted system during later compression (top image). Next sections as blue lines.

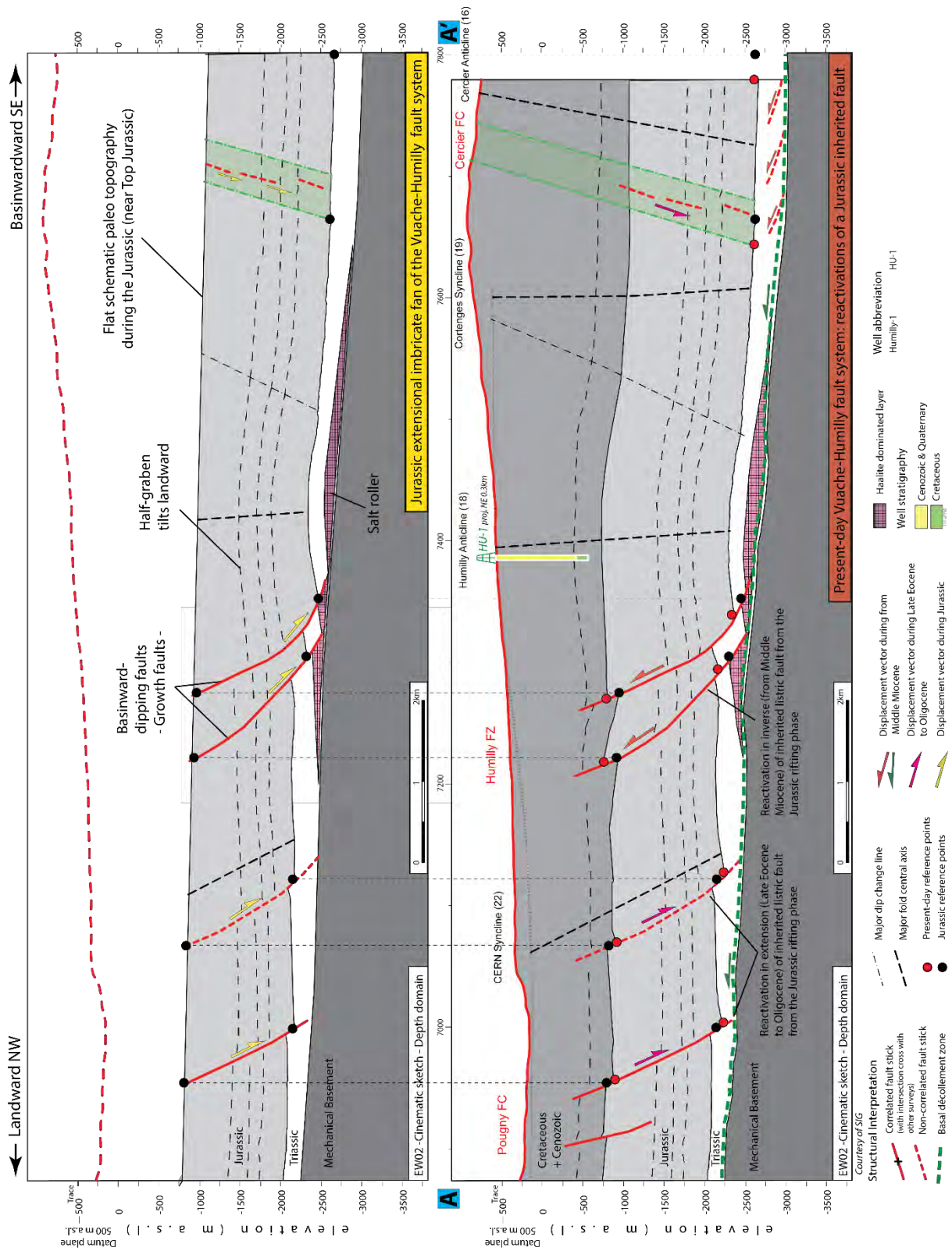


Figure 6-30b: Structural scheme section (NW-SE) of the Humilly-Vuache fault system, as an extensional imbricated fan during Lower Jurassic period (left image) and as an inverted system during later compression (right image). See localization of section AA' on Figure 6-30a.

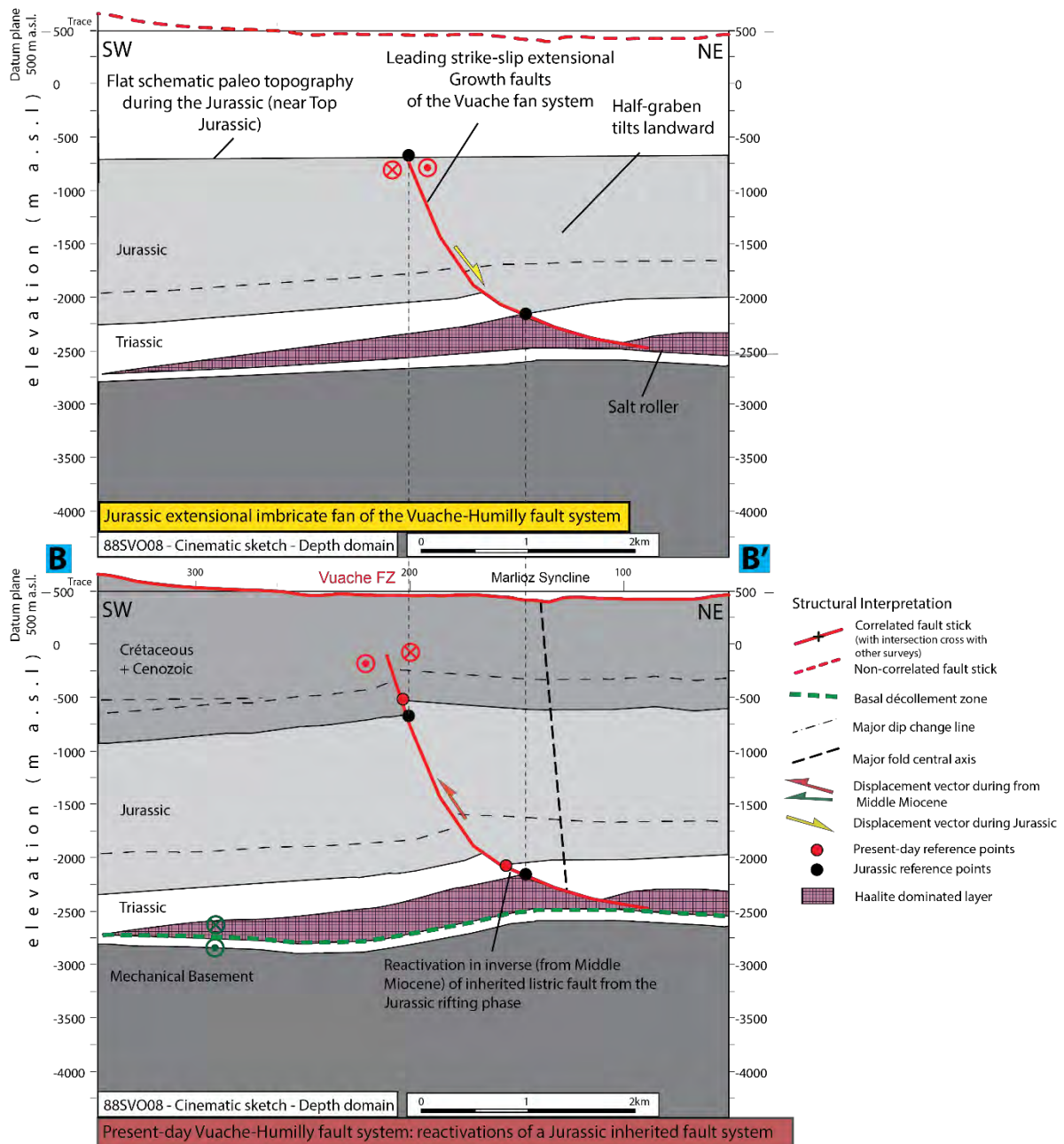


Figure 6-30c : Structural scheme section (SW-NE) of the Humilly-Vuache fault system, as an extensional imbricated fan during Lower Jurassic period (top image) and as an inverted system during later compression (bottom image). See localization of section BB' on Figure 6-30a.

the Vuache has induced the presence of another lateral ramp thrust and fold structure (not included in our study – Schori et al., 2021) now located several kilometers northwestward of the present-day location of the Vuache Fault due to the general transport of the Jura FTB. Indeed, during the thin-skinned tectonic and the formation of the JFTB, irregularities in the basement may initiate lateral ramps in the Mesozoic-Cenozoic cover that are subsequently displaced (km away from basement fault) during the tectonic process.

Along the same line, the present day basement fault below the Vuache FZ cannot be related to the overlying Vuache structure in the cover as noticed by De la Taille (2018) who moreover concluded of a lateral offset of 1,5km southwestward between the Vuache FZ in the cover and the non-related near basement fault. The latter is moreover nowadays visible with a downward step southwestward. Even

if a velocity artefact might be present (push-down effect leading to this apparent downward step), it is more likely that this vertical offset of Base Mesozoic corresponds to a possible reversed re-activation of this latter fault happened after or in a late phase of the formation of the Jura. Schori (2021) and Schori et al. (2021) restored the possible triggering basement fault (offsetting vertically the mechanical basement up to 400m) that is supposed to have allowed the onset of the lateral ramping of the Vuache FZ, and located it few kilometers west of the Le Coin FZ in NNW-SSE striking orientation (see chapter 7 and Figure 7-1). Slight indications on seismic profiles in this area may support this idea. Nevertheless, since we propose in our study another origin of the Vuache FZ, with a Lower Jurassic initiation, this restored basement lineament becomes unnecessary (see also discussion in Chapter 7).

6.3.3 Salève and Subalpine Molasse area

The Salève Mountain forms a prominent topographic ridge separating the Geneva and Rumilly Basins northwestward, with the Subalpine Molasse area in south (area in front of the Subalpine Massifs and Bauges FT). It consists of an imposing ridge culminating at 1379m a.s.l., stretching in a NE-SW direction for more than 40km long, between the Montagne d'Âge in the SW and Arve River valley in the NE (Figure 6-31). This major topographical structure of the Western Swiss Molasse Basin is the result of a remarkable NW-vergent ramp and fault propagation fold, that brings Cretaceous/Upper Malm layers to the surface. The entire ridge is segmented into three main parts by NNW-SSE and NW-SE strike-slip faults. From South to North, it is composed of the Mt d'Âge FT (and Anticline), the Mandalaz FT (and Anticline), and the Salève FT (and Anticline) separated respectively by the NW-SE Vuache FZ, the NNW-SSE Cruseilles FZ, and the Le Coin FZ. The extreme northern part of the structure is thought to terminate against the NNW-SSE Arve FZ. A possible continuation into the Presinge thrust cannot be excluded (described in 6.3.1, Figure 6-15). For simplicity, in the following paragraphs, the term "Salève" is used to refer to the entire structure (the three parts of Mt d'Âge - Mandalaz - Salève FT and anticlines).

On top of the Mesozoic cover, Siderolithic deposits are often observed within or on top of karstified and fractured Cretaceous series. In the region north of Le Coin FZ, an angular discordance (around 20°) between the stratified Siderolithic deposits and the Cretaceous layers is observed and measured (Mastrangelo et al., 2013). This possibly indicates an existing structuration (uplift) of the Salève (prior to the Eocene deposits), as proposed by Blondel et al. (1988) in the Vuache FZ. However, Mastrangelo et al. (2013) propose to explain this foredeep unconformity by a flow of the Siderolithic deposits into the Cretaceous karstic features, after their initial deposit (or during the erosional karst formation). This argument means that the uplift of the Salève Mountain may in fact have occurred after the Eocene, likely during the Alpine compression (Miocene). This idea is more in line with our tectonic concepts applied on this area.

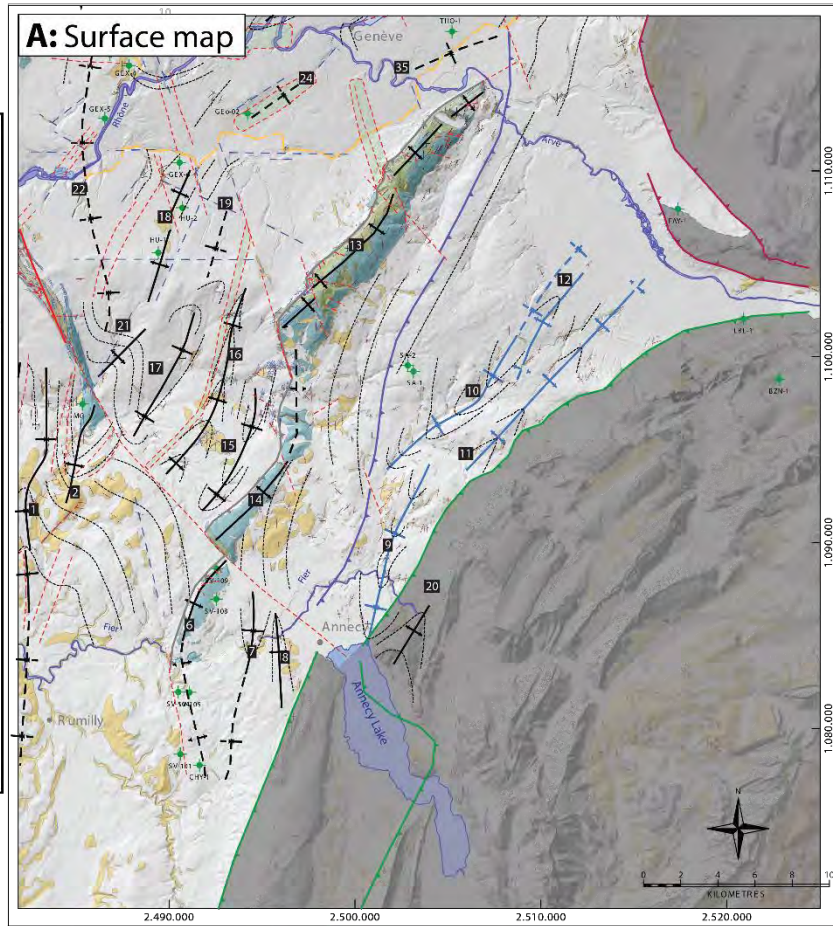
Our seismic interpretation confirms that the frontal ramp of the the whole Salève structure roots in the basal décollement. Oblique reflectors ending downward on top of the Muschelkalk unit are clearly visible. A debate remains to know if the Salève structure belongs to the Subalpine Massifs (Beck et al., 1998) or the JFTB (Philippe, 1995). We consider that the thin-skinned tectonic principles applied on this structure to be the same as for the JFTB.

The density of our seismic database allows obtaining a full geometry of the fault plane (Mt d'Âge-Mandalaz-Salève FT) along sections perpendicular to the frontal thrusts (see map of Figure 6-31 and

sections AA' of Figure 6-32, BB' of Figure 6-33 and Figure 6-34 and DD' of Figure 6-36), but also with oblique seismic lines such as seismic line HR530 running almost parallel to the anticlinal structure. The main new observation about this structure concerns the Lower and Middle Jurassic layers (both layers grouped in the regional model) thickening on the hangingwall of the thrust, consistently interpreted on several seismic profiles. We suggest that the main thickening occurred during the Liassic period, in a similar manner as was demonstrated for the Humilly-Vuache FZ (GVA model giving more vertical details). The Triassic layer is also varying in thickness from one side to the other of the fault. On the footwall part, we have a significant Triassic structure with a pillow geometry that could be the result of either halokinetic flowage or tectonic imbrications within the Triassic. This highlights in fact two stratigraphical possibilities concerning the setting of the the Jurassic (Lower and Middle) layer thickening and its structural relationship to the later thrusting (Figure 6-37). First, like in Humilly FZ, an extensional growth fault installed during Lower Jurassic involving a salt flow process, with a movement away from the fault plane on both sides. This could imply an uplift of the footwall part and an accentuation of the hangingwall rollover anticline. Subsequently, the same fault plane is inverted to form the frontal thrust, well visible on the surface. Alternatively, a salt pillow in the Keuper Group may have been set up and welded prior to deposition of the Jurassic layers in the current position of the footwall of the fault. This would subsequently have influenced the thickness of the Liassic and/or Dogger units with an increase of thickness as the sequestered salt pillow is thinning progressively. Later on, the thrusting may onset on the extremity of the welded salt pillow (or anticline) that will continue to be evacuated towards its center (Jackson & Hudec, 2017a). We consider this second possibility as less probable and retain the option including the development of a Jurassic extensional fault, which better explains the significantly higher thickness of Jurassic (Lower and Middle) in the hangingwall of the fault.

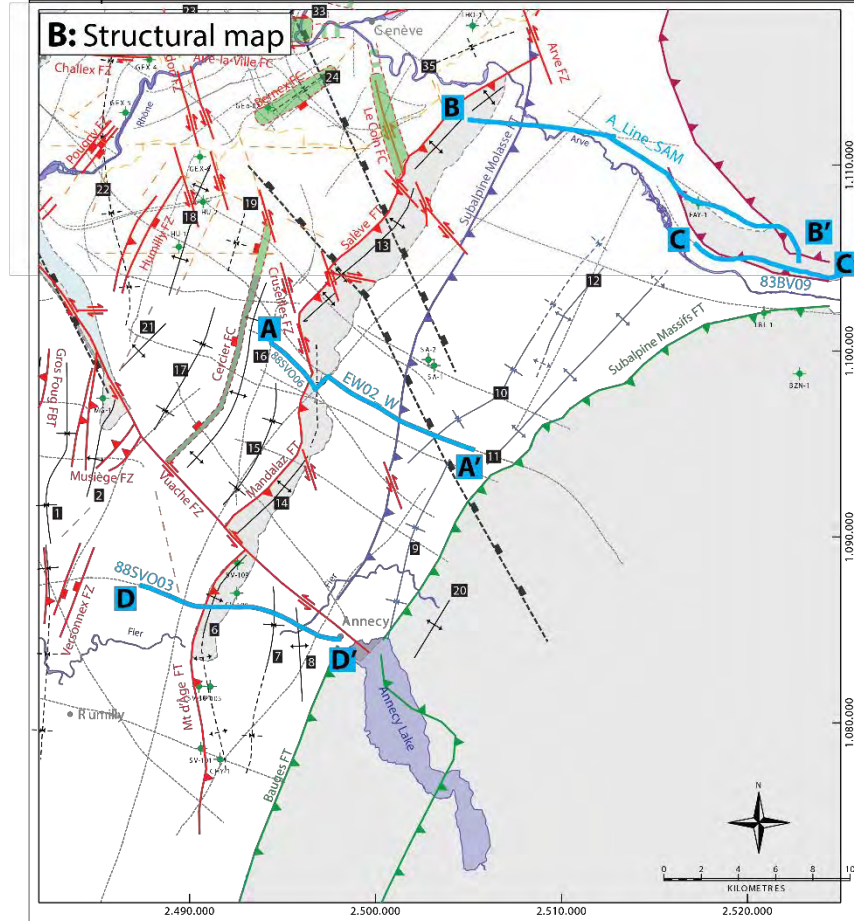
Seismic interpretation also reveals the possible presence of a secondary décollement level rooted in the shally Liassic layer, allowing an imbrication (second ramp thrust) forming locally a duplex-like structure. This imbricate can be recognized well on near strike-line (HR530, Encl.70) and on sections perpendicular to the Salève structure (Figure 6-32, Figure 6-33 and Figure 6-34). The imbricate terminates in the SW near the Cruseilles FZ and extends all the way to the NE up to the Arve Valley. The related fault plane is attached in its upper part top the main Salève thrust. This interpretation is considered as uncertain and therefore annotated as conceptual tectonic on all seismic sections.

The time-depth conversion process of the seismic sections and the resulting depth visualization, gave the possibility to compensate the limitations of the time imaging that may be biased by velocity artefacts. Indeed, a very high velocity gradient is present just northwestward of the frontal thrust, between the low velocity of the Cenozoic sediments in the Molasse Basin (3000-4000 m/s) and the higher velocity of the outcropping Mesozoic unit (5000-6000 m/s). This creates a significant pull-up effect of all thrust layers below the Salève belt in the time domain (0,1-0,2s). In the depth domain, our resulting images show a relatively smoothed nBMes seismic horizon and accentuate a pillow-shaped anticline of the Triassic layers, increasing in thickness in the footwall part of the fault. The seismic resolution is relatively poor in the Pre-Mesozoic part, and it is then very difficult to interpret Permo-Carboniferous seismic reflections (InPal), below the Salève. No apparent vertical offset of nBMes seismic horizon is visible, and it thus remains difficult to confirm or infirm the presence of a Permo-Carboniferous graben located just front of the ridge, as was suggested in the past by Signer & Gorin (1995). However, we notice slight topographical variations of nBMes in the opposite orientation, west of Le Coin FC (see HR530 seismic interpretation). This would be approximatively in line with the



Fold Names

- 1 Frangy Syncline
- 2 Musiège Anticline
- 6 Mt d'Âge Anticline
- 7 Meythet Syncline
- 8 Seynod Anticline
- 9 Villaz Syncline
- 10 Groisy Syncline
- 11 Amancy Anticline
- 12 Etaux Anticline
- 13 Salève Anticline
- 14 Mandalaz Anticline
- 15 Choisy Syncline
- 16 Cercier Anticline
- 17 Marlioz Syncline
- 18 Humilly Anticline
- 19 Cortenges Syncline
- 20 Veyrier Anticline
- 21 Minzier Anticline
- 22 CERN Syncline
- 24 Bernex Syncline
- 35 Thônex Syncline



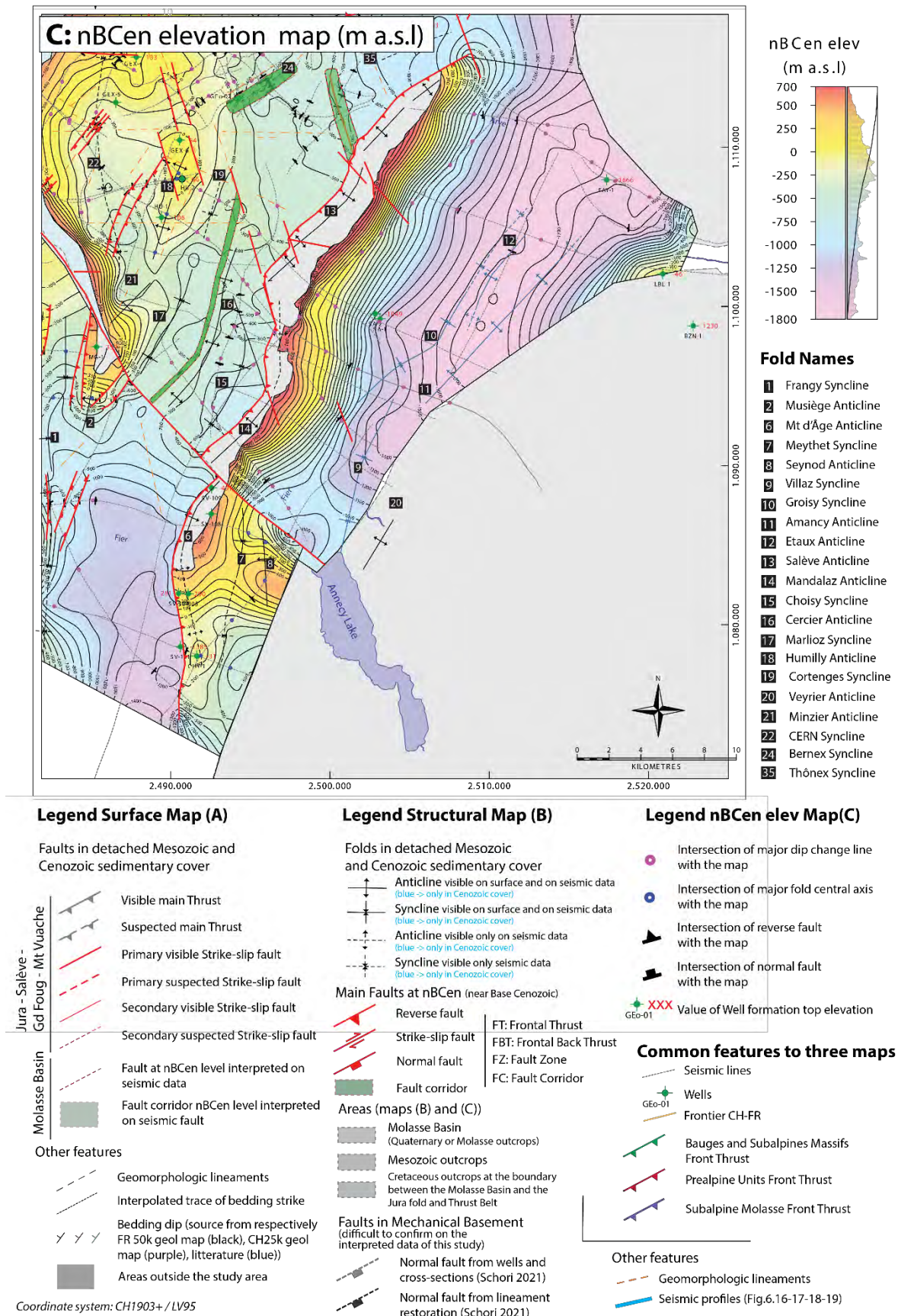


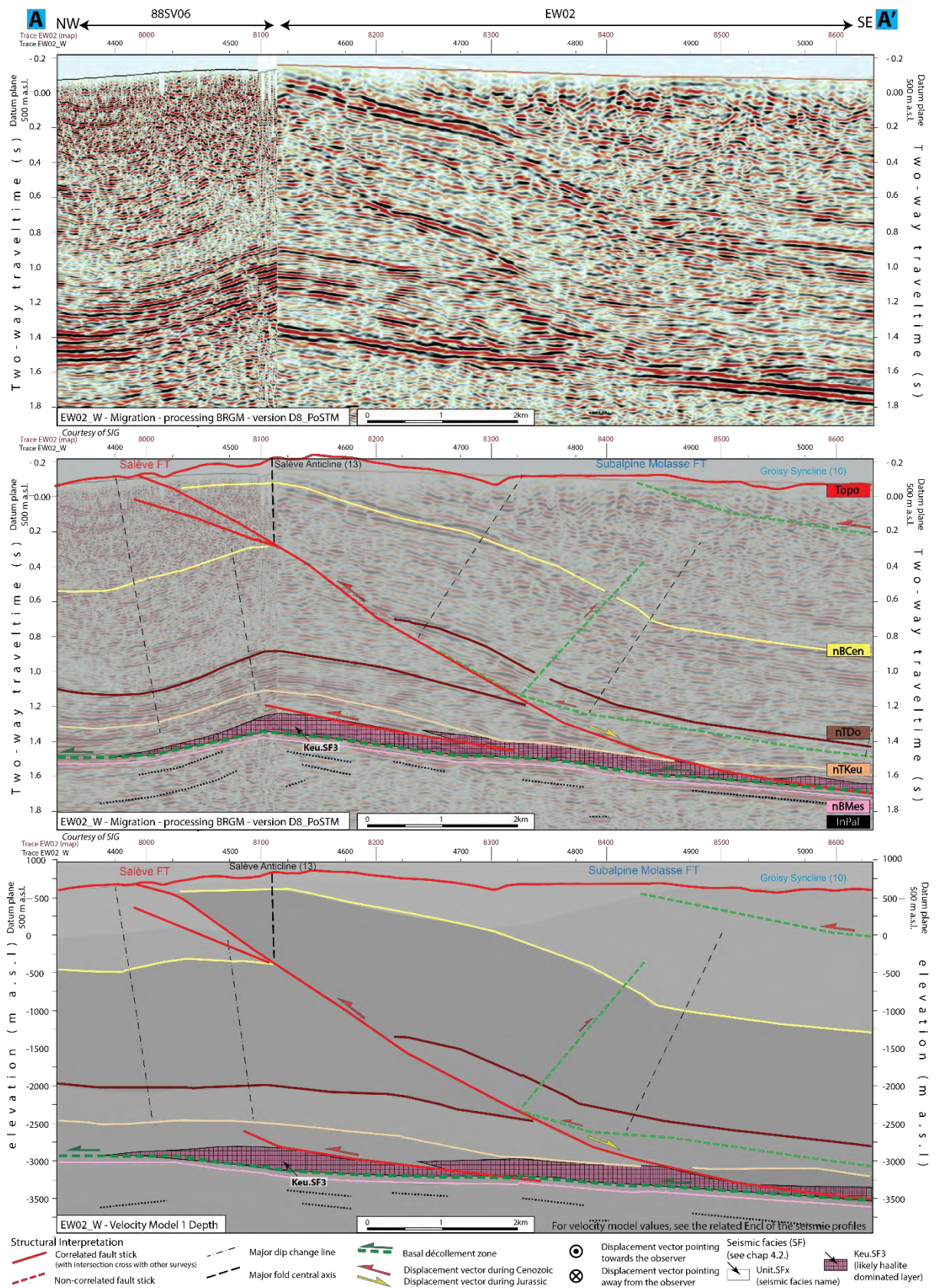
Figure 6-31 : Maps of structural interpretation results of the Salève and Subalpine Molasse area. It includes the Salève FT, the Mandalaz FT and the Mt d'Âge FT. These structures are described in details in the text of part 6.3.3. See Table 3-2 for well abbreviations. Sections of Figure 6-32, Figure 6-33, Figure 6-34, Figure 6-35, Figure 6-36 are represented on structural map B as blue lines. Coordinate system: CH1903+/LV95. Geological map A is based on Marro (2021).

basement structures suspected by Schori (2021) (lineament restoration), consisting in NNW-SSE downward step linked to a fault dipping ENE located west of Le Coin FC (see Encl_M01 structural map).

An important tying point for the seismic interpretation and mapping in the southeastern termination of the backlimb of the Salève structure are the two wells Salève-1 and Salève-2 (common surface location), with the latter reaching nBCen horizon. These wells are, incidentally, located just in between the two suspected basement faults from Schori (2021). The well information also show that the Molasse deposits of the UMM (Lower Marine Molasse unit) are resting against the nBCen horizon (Deville et al., 1994). By comparison with regional wells, especially those located inside the GVA Basin, we can then confirm the approximate correlation between the termination northwestward of this lower Molasse unit UMM from Rupelian (older than USM from Chattian-Aquitainian) against the backlimb of the Salève structure (near the surface trace of the Subalpine Molasse Front Thrust, (Gorin et al., 1993)). The Subalpine Molasse FT is interpreted using seismic indicators (oblique seismic reflections along the fault trace) visible on several cross sections. This frontal thrust of Subalpine Molasse in the Cenozoic series is laterally segmented and shifted by the major sinistral NNW-SSE strike-slip system of the Arve FZ, Le Coin FC, and Cruseilles FZ. To the SW, the Subalpine Molasse stops near or against the Vuache FZ. The upper most part of the Cenozoic layer is considered to be decoupled from underlying Mesozoic layers (by the Subalpine Molasse trusting). In that sense, the folds interpreted with surface dip data concern Cenozoic series only (Charollais, 1986). They are interpreted as part of the Subalpine Molasse FT. These structures cannot be extended confidently northeastward into the Arve valley because of the significant footprint of the Arve glacier that took this path during the Quaternary (Charollais et al., 1998). The presence of the UMM Molasse against the meridional limb of the Salève ridge and its absence in the GVA Basin, supports the proposition of a pre-existing basin boundary (Salève fault system). Indeed, such a normal fault (Salève Jurassic fault system) may have been re-activated during the Oligocene flexure of the Basin.

In the vicinity of the Prealpine Units, the well Faucigny-1 was drilled in 1969 reaching Permo-Carboniferous sediments. The well is an important velocity guidance for the local area. Thus, we can notice a thinner Keuper unit in comparison to the Muschelkalk unit, when getting closer to the Prealpine Units. The well is surrounded and even crossed in its upper most part by frontal thrusts coming from the neighboring allochthonous massifs (see map of Figure 6-31 and section C of Figure 6-35).

To the west of the Vuache FZ, the Mt d'Âge FT shows a significant displacement of the sedimentary cover, and a noticeable uplift of the Mesozoic-Cenozoic units above a thick Triassic unit (map of Figure 6-31 and section D of Figure 6-36). Indeed, we have interpreted more than 1500m of Triassic series thickness due to multiple thrusting of complex imbrications. The prominent anticline in th Mt d'Âge continues with a N-S orientation to the south in parallel to the Mt d'Âge FT. In absence of conclusive evidence, we have stopped this thrust in the Molasse Basin. Other authors such as Deville et al., (1994) extend the thrust to the south up to the Subalpine Chains, where it is cut obliquely by the Bauges FT (Semnoz). As pointed out by Deville et al. (1994), the area in between the Mt d'Âge FT, the Vuache FZ and the Bauges FT is overlain by Molasse sediments from the Chattian-Aquitainian (USM), unlike in the Rumilly Molasse Basin area where younger Marine Molasse sediments of the OMM (Burdigalian) are deposited. This triangle area represents thus a distinct paleogeography with the beginning of the Burdigalian transgression (or late Oligocene-early Miocene (Beck et al., 1998)).



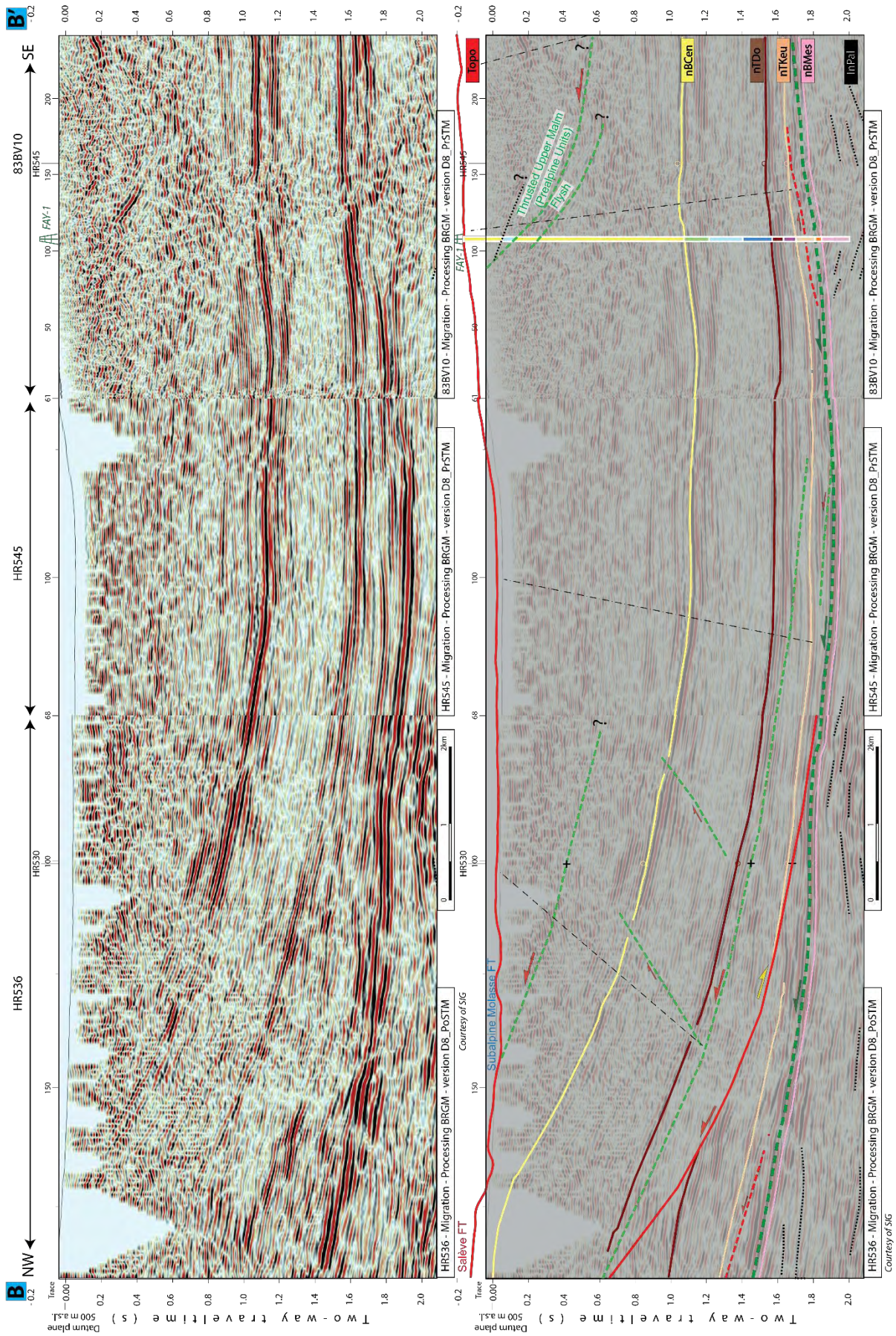


Figure 6-33 : Seismic interpretation (in twt) of the Salève FT on seismic line HR536 (section BB'). See Figure 6-31 for localization of the section. See Encl 47 for detailed seismic interpretation of the lines of this figure.

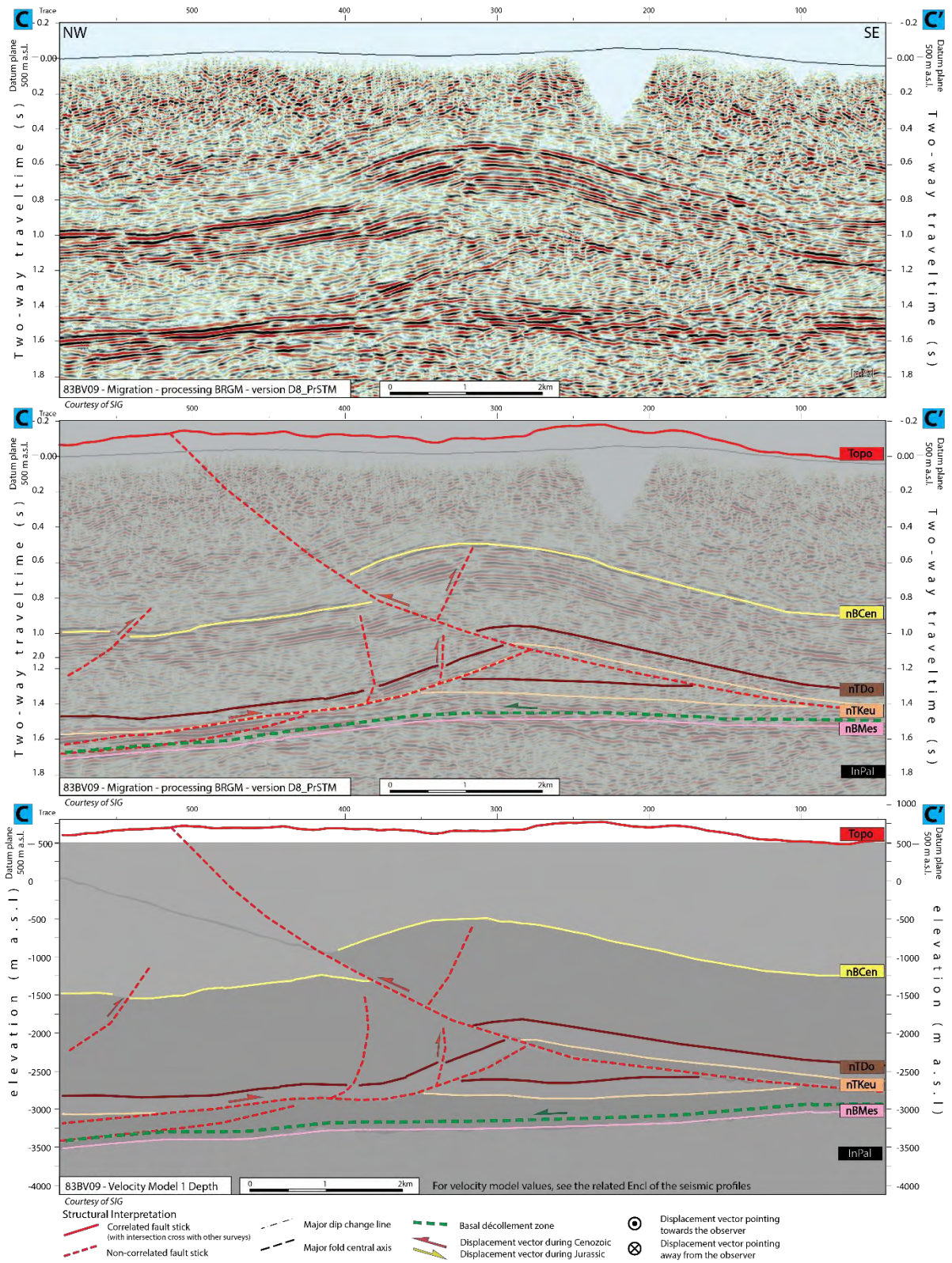


Figure 6-35 : Seismic interpretation (in twt for the two upper images and depth velocity model 1 in bottom image) of the Prealpine units FT on seismic line 83BV09 (section CC'). See Figure 6-31 for localization of the section. See Encl 46 for detailed seismic interpretation of line 83BV09.

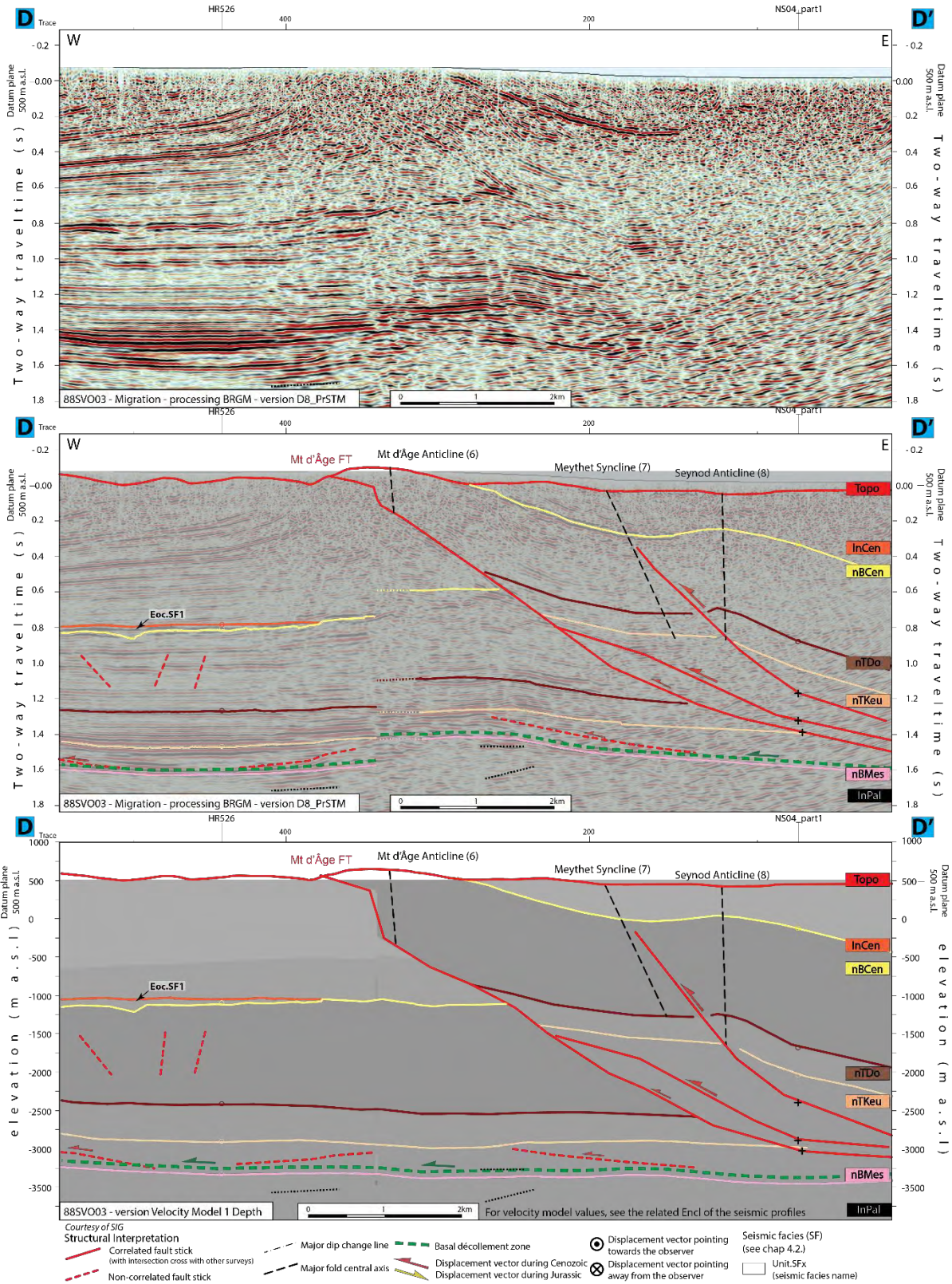


Figure 6-36 : Seismic interpretation (in twt for the two upper images and depth velocity model 1 in bottom image) of the Mt d'Âge FT on seismic line 88SVO03 (section DD'). See Figure 6-31 for localization of the section. See Encl 49 for detailed seismic interpretation of line 88SVO03.

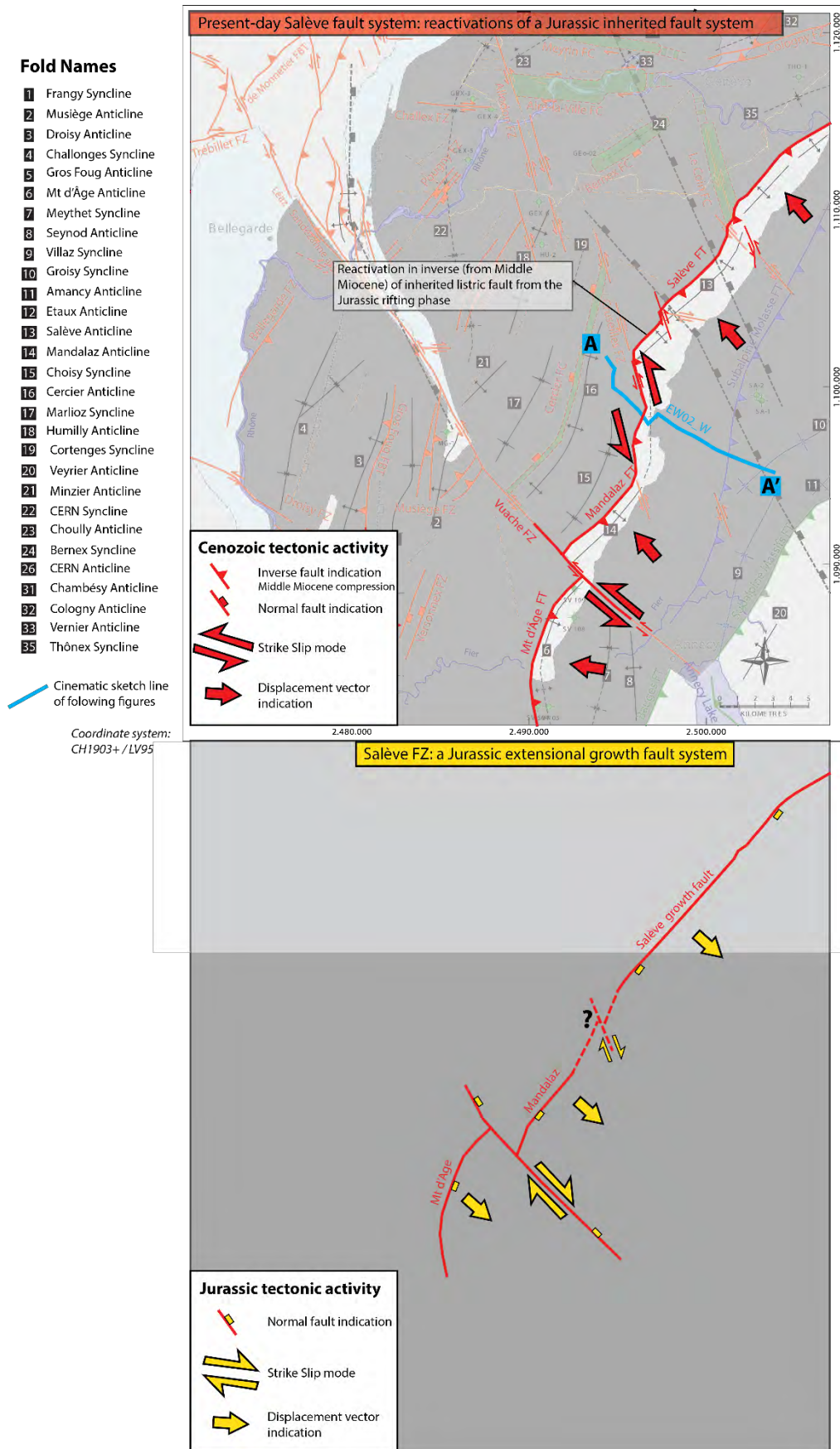


Figure 6-37-a : Structural mapping scheme of the Salève fault system (extended SE with Mt d'Âge and Mandalaz structures), as an extensional growth fault during Lower Jurassic period (bottom image) and as an inverted system during later compression (top image). Next section as blue lines. Note that the "?" on bottom image show a conceptual fault location.

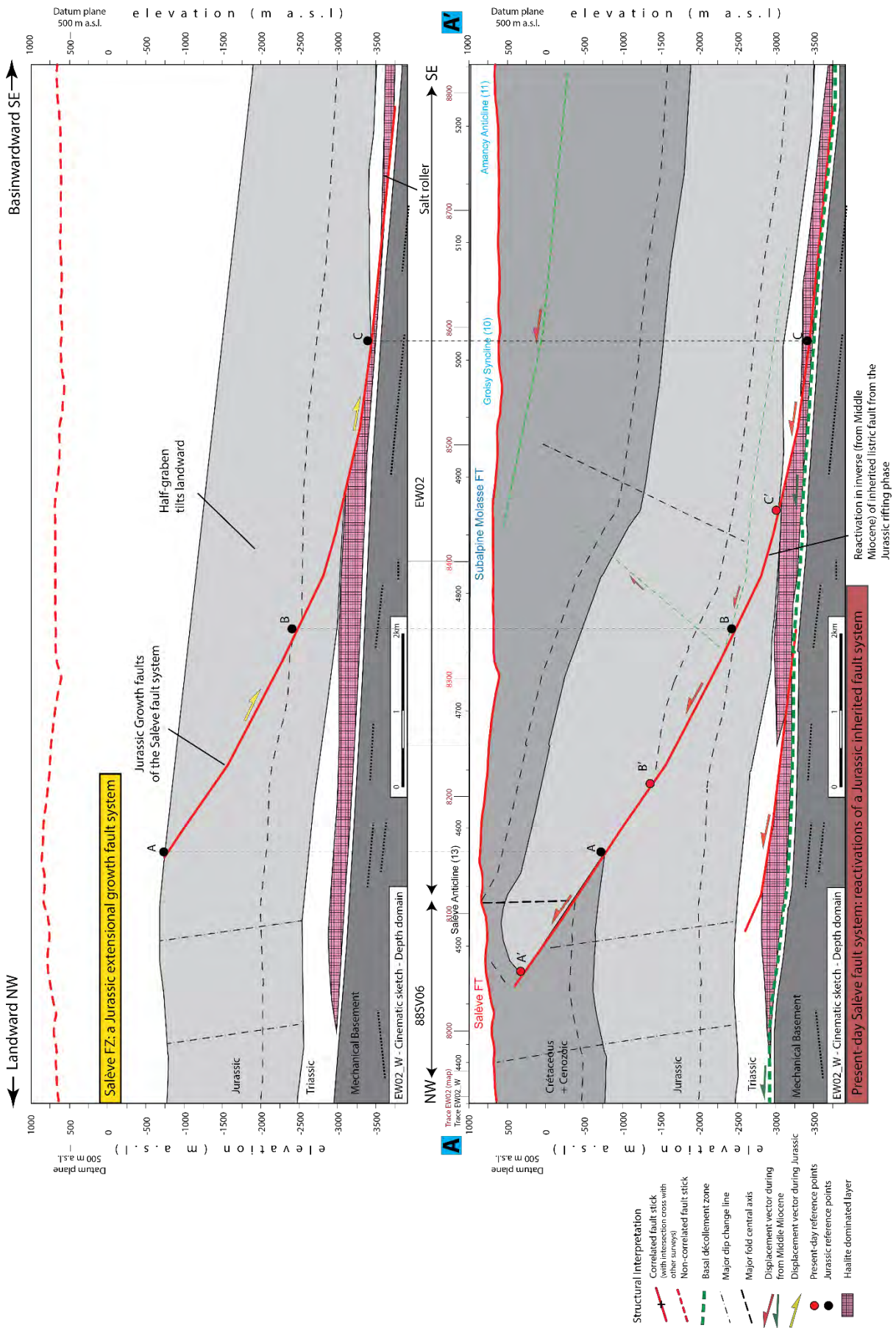


Figure 6-37b : Structural scheme section AA' (NW-SE) of the Salève fault system, as an extensional growth fault during Lower Jurassic period (left image) and as an inverted system during later compression (right). See localization on Figure 6-37a.

6.3.4 Rumilly Molasse Basin area

The Rumilly Molasse Basin area is part of the Savoy Tertiary Molasse Basin as described by (Deville, 2021; Deville et al., 1994), and extends from the Geneva area to the Chambéry area between the Bauges FT at the edge of the Chaines Subalpines and the Jura Mountains FTB. We will focus on the northern part, the Rumilly Molasse Basin, between the Vuache FZ in the north to the Culoz FZ in the south. The area between the Mt d'Âge and the Bauges FT (see previous discussion) can be distinguished from the western part of the Rumilly Molasse Basin by the presence of different age Molasse deposits. Thus, the OMM (Upper Marine Molasse) is found only in the Rumilly Molasse Basin westward of the Mt d'Âge FT, whereas USM (Lower Freshwater Molasse) is deposited eastwards only (see part 2.3.3, Figure 2-7).

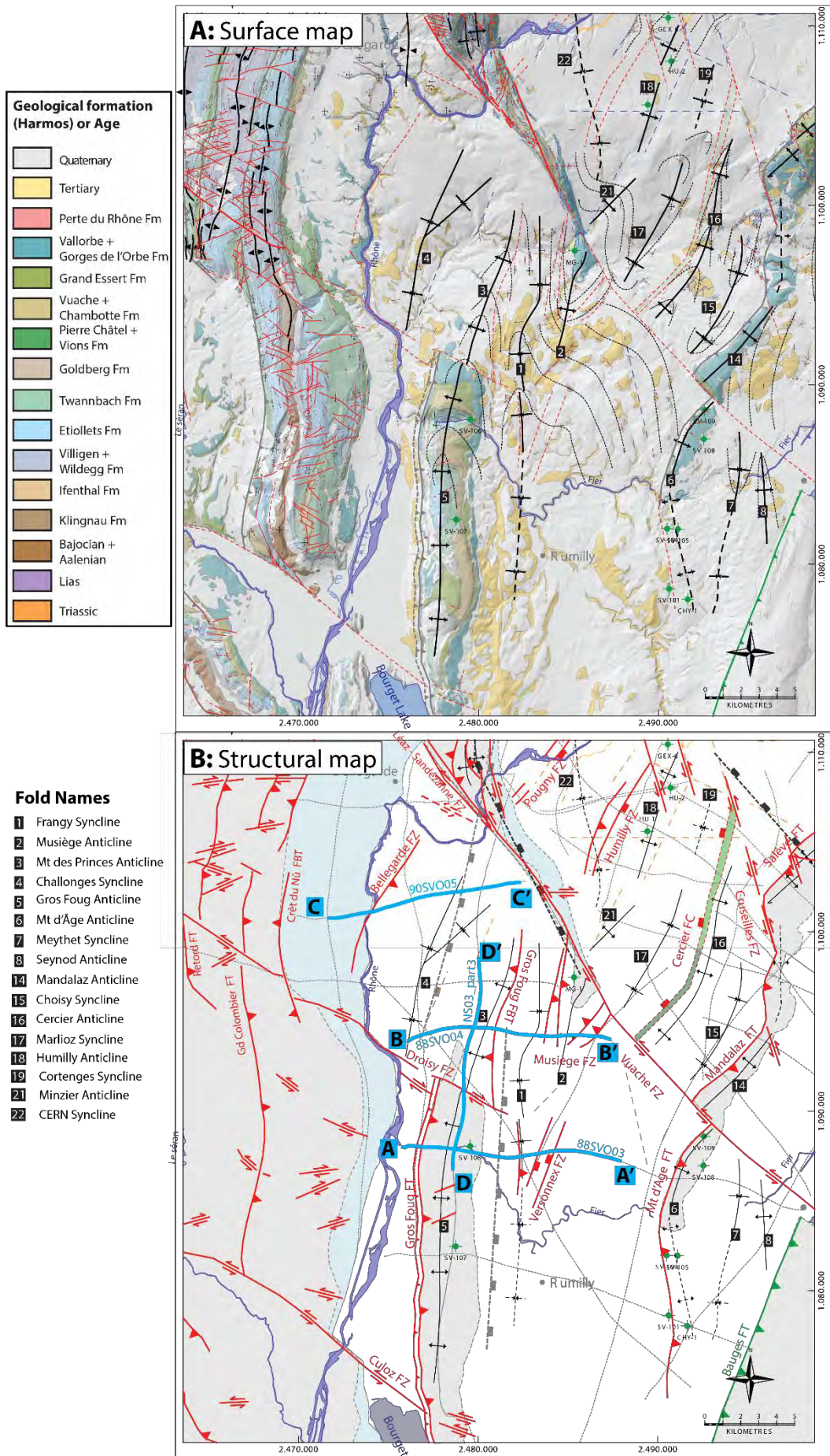
Aside from the Mt d'Âge, the most prominent structure of the area are the **Gros Foug FT** and the associated fault-propagation style anticline forming an important N-S oriented topographic ridge. The structure is formed by a N-S striking, west-vergent frontal ramp. In its central segment between the Culoz FZ to the Droisy FZ (18km length), Cretaceous and Malm units are outcropping on a wide band (3km) that allows obtaining the exact geometry of the main anticline and give access to lineaments and fracturation information on outcrops. In addition, several seismic profiles are crossing the fault zone in perpendicular and longitudinal directions (see map of Figure 6-38 and sections A and D of respectively Figure 6-39 and Figure 6-42&Figure 6-43). The Droisy FZ in its northern part acts as a tear fault north of which the main thrust and anticline change their kinematic (Figure 6-38). We have interpreted a W-vergent duplex thrust system rooted along the basal décollement zone. These faults in the Mesozoic series are facing an intra-Triassic series E-vergent thrust or imbrications, justifying the high Triassic series thickness. A slight back thrusting may be present along the backlimb of the uppermost main ramp. Two wells, SV-106 and SV-107 (respectively Keuper and Dogger formations at TD) drilled along the crest of the anticline give control points to support this interpretation. The advanced time-depth conversion of the seismic profiles further contributes to the geometrical consistency of the interpreted structure. Prior studies have proposed alternative interpretation considering the Gros Foug fault as one simple ramp rooting in the Triassic décollement level (Beck et al., 1998; Deville et al., 1994; Kalifi et al., 2021; Philippe, 1995). In our study, we refined the interpretation of the high Triassic thickness below the main structure and observed that it does not involve significant vertical offset of the basement. This follows a similar structural interpretation proposed by Clerc & Moscariello, (2020); Meyer, (2000); Paolacci, (2012). Our depth model nevertheless highlights a change of dipping of nBMes reflectors along the Gros Foug ridge, along with a relatively flat topography westward of the Gros Foug and east-dipping by approximately 6°. We can wonder if a N-S basement fault step dipping eastward, located at this change of angle could be present, thus marking the transition from the Plateau Molasse to the Internal Jura FTB. Such a fault is proposed in the basement modeling of Schori (2021). Concerning the age of formation of the anticline, Deville et al., (1994) have estimated the onset of the décollement during the Burdigalian to Langhian, taking into account thrust Tertiary deposits in the footwall.

The **Droisy FZ** is a WNW-ESE strike-slip fault bordering the Gros Foug structure, as a tear fault to the north. Affolter & Gratier, (2004) have considered this fault zone as a major regional strike-slip fault. It can be subdivided, into several segments, with the main part continuing westward into the Jura Mountains, crossing and offsetting several regional thrusts, such as the Gd. Colombier FT. It has an apparent sinistral movement along the majority of the fault zone, except in the part bordering the Gros

Foug FT. Indeed, in this area, the northern part of the Droisy FZ is composed of a block verging southeastward (backward), which leads to an inversion of the Droisy FZ kinematics into a dextral configuration. The strike-slip fault roots into the basal décollement zone in a complex interaction with an east-vergent imbricate system in the lower Mesozoic units (Triassic and Lower-Middle Jurassic units) in this area (see map of Figure 6-38 and section D of Figure 6-42&Figure 6-43). The fault system is however developed with a near vertical configuration further northwestward. The southeastward termination of the fault is difficult to assess but it is likely disappearing shortly eastward of the intersection with the Gros Foug FBT.

As already alluded, N of the Droisy FZ the Gros Foug structure is expressed mainly by an eastward vergence in connection with a back-thrust oriented NNE-SSW and located in the exact continuation northeastward of the Gros Foug. Its most uplifted part (of the Mt des Princes Anticline) is clearly situated against the Droisy FZ, and could not be prolonged further northward due to a lack of evidence (not enough seismic profiles), but there is a possible link with the Léaz-Sandezanne fault (Deville et al., 1994). Surface lineaments in the back limb of the structure confirm the logical NNE-SSW orientation of the structure that may be connected to the Vuache FZ. Seismic profiles in this area that are of high resolution, show clear indications for an Intra-Triassic series west-vergent thrusting facing the main Mesozoic series east-vergent Gros Foug FBT (see section B of Figure 6-40). The Frangy Syncline is slightly crooked by the influence of the Musiège FZ. It is to be noted that the Gros Foug FT and FBT are not necessarily part of a common large-scale faulting mechanism. It is true that they have approximately common axial traces, but the orientation is not exactly the same (N-S and NNE-SSW) and they have opposite vergence and thus different kinematics.

The **Musiège FZ** is a NNE-SSW pop-up structure developed along a main NE-SW SE-vergent reversed fault. The structure is attached to the Vuache FZ where the outcropping Cretaceous layers were mapped in detail by Charollais et al. (2013). This outcropping area was drilled by well Musièges-1 that reached the Dogger unit, but was unusable for seismic to well tie, not being located along any seismic profile. The Musiège Anticline appears as very similar system as the Gros Foug FBT (similar geometry, and fault angles, see section B of Figure 6-40). The difference lies in the serie of back reversed faulting of the Musiège FZ, which testify of a higher compressional rate (coming surely from the connection with the Vuache FZ). We have not noticed any indications of syn-sedimentary activity along these two fault zones. However, it could have been different if more data in this area was available, including well calibrations. Our methodology of seismic interpretation may have biased the results. Indeed, when we interpret such a fault zone without well calibration on both sides of the fault, we logically tend to correlate similar thicknesses in the hangingwall and in the footwall (conservative approach). It means that we cannot exclude a synsedimentary activity of certain faults. In this case, the two faults of the Gros Foug FBT and the Musiège FZ seem to be both attached to the Vuache FZ and are dipping westward. These various arguments lead us to imagine a structural possibility that would include them into the large-scale Vuache-Humilly-Salève extensional system. There is no proof of syn-sedimentary activity of these faults during the Liassic period (like in the Vuache-Humilly-Salève FZ), but if it happens to be the case, they would belong to a laterally hidden strike-slip as described theoretically by Hu et al., (2019) (see Figure 6-44). The time-depth conversion process of the last two structures yielded very interesting results. Seismic profiles of this zone have a high resolution, especially for the nBMes seismic horizon level. The very strong push down effect along the Frangy Syncline was completely attenuated highlighting a more realistic topography of the nBMes seismic horizon. It resulted in a near straight seismic horizon in depth domain, removing any possibility of basement step in this sector (see section



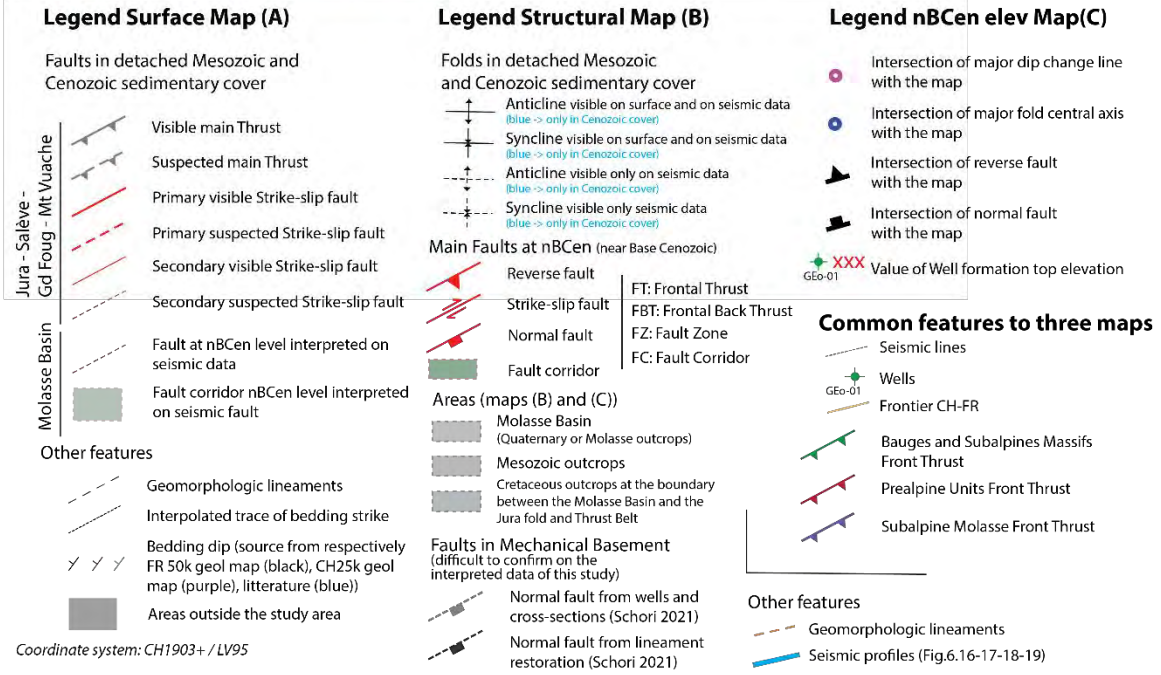
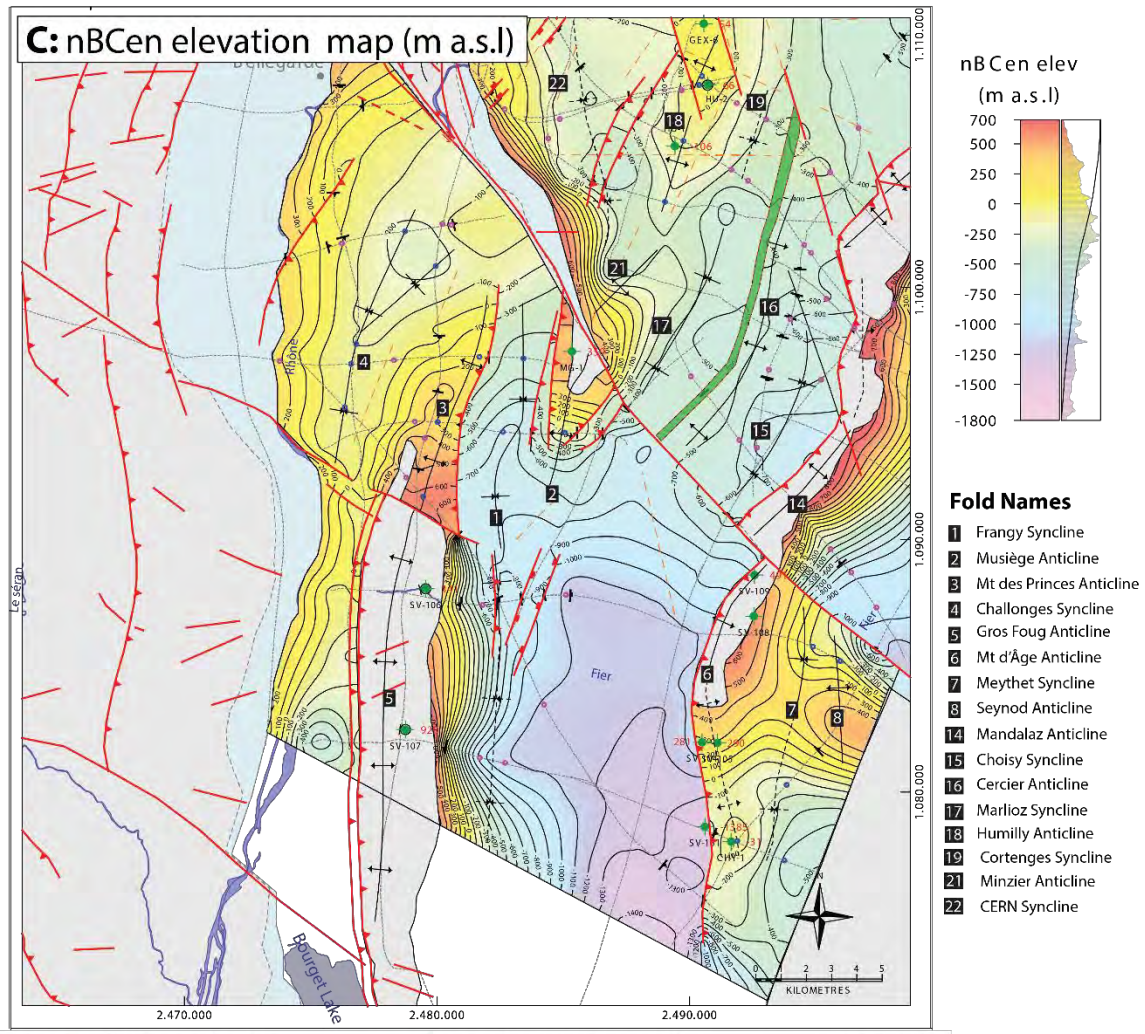


Figure 6-38 : Maps of structural interpretation results of the Rumilly Molasse Basin area. It includes the Bellegarde FZ, the Gros Foug FT and FBT, the Droisy FZ the Veronnex FZ and the Musiège FZ. These structures are described in detail in the text of part 6.3.4. See Table 3-2 for well abbreviations. Sections of Figure 6-39, Figure 6-40, Figure 6-41, Figure 6-42, and Figure 6-43 are represented on structural map B as blue lines. Coordinate system : CH1903+/LV95. Geological map A si based on Marro (2021).

B of Figure 6-40). Northwestward of the Gros foug FBT, the Challonges syncline is located at the termination of the backlimb of the Mt des Princes Anticline. We can notice the presence of a suspected NNE-SSW normal basement fault (from Schori (2021)) superimposed on the Challonges syncline (see map B on Figure 6-38).

The **Bellegarde FZ** is a NNE-SSW oriented, compressive structure characterized by very modest vertical offset. It is marking the transition of the Molasse Basin with the Internal Jura part, northwest of the Challonges Syncline (see section C of Figure 6-41). The compressive part of this fault zone is overlying a normal faulting in the Jurassic layers. We can note also a slight change of dip of nBMes seismic horizon below the fault zone.

The **Versonnex FZ** is composed of two normal fault segments, and one compressive fault. The fault system is rooted along the basal décollement zone. The kinematics of the fault show an original normal component (likely in Jurassic) that it was reactivated in reverse mode during the Alpine compression. It is located in the continuation southwestward of the Musièges FZ, suggesting a possible link between the two fault zones.

Upper Cretaceous sediments are outcropping in the area of study only in the Valserine-Bellegarde area (see part 2.2.2). Moreover, Donzeau et al. (1997) also observed reworked Upper Cretaceous sediments in early Cenozoic deposits on the oriental side of the Vuache Mountain. From these observations, the heterogenous erosion of this layer, support the idea that an early structuration and uplift of the foreland Basin was more pronounced in the GVA Basin (Est of the Vuache Mountain) (that led to a bigger erosion bulge) than in the Bellegarde-Rumilly Basin where it has been more preserved (Scolari, 1956; Charollais et al., 2013).

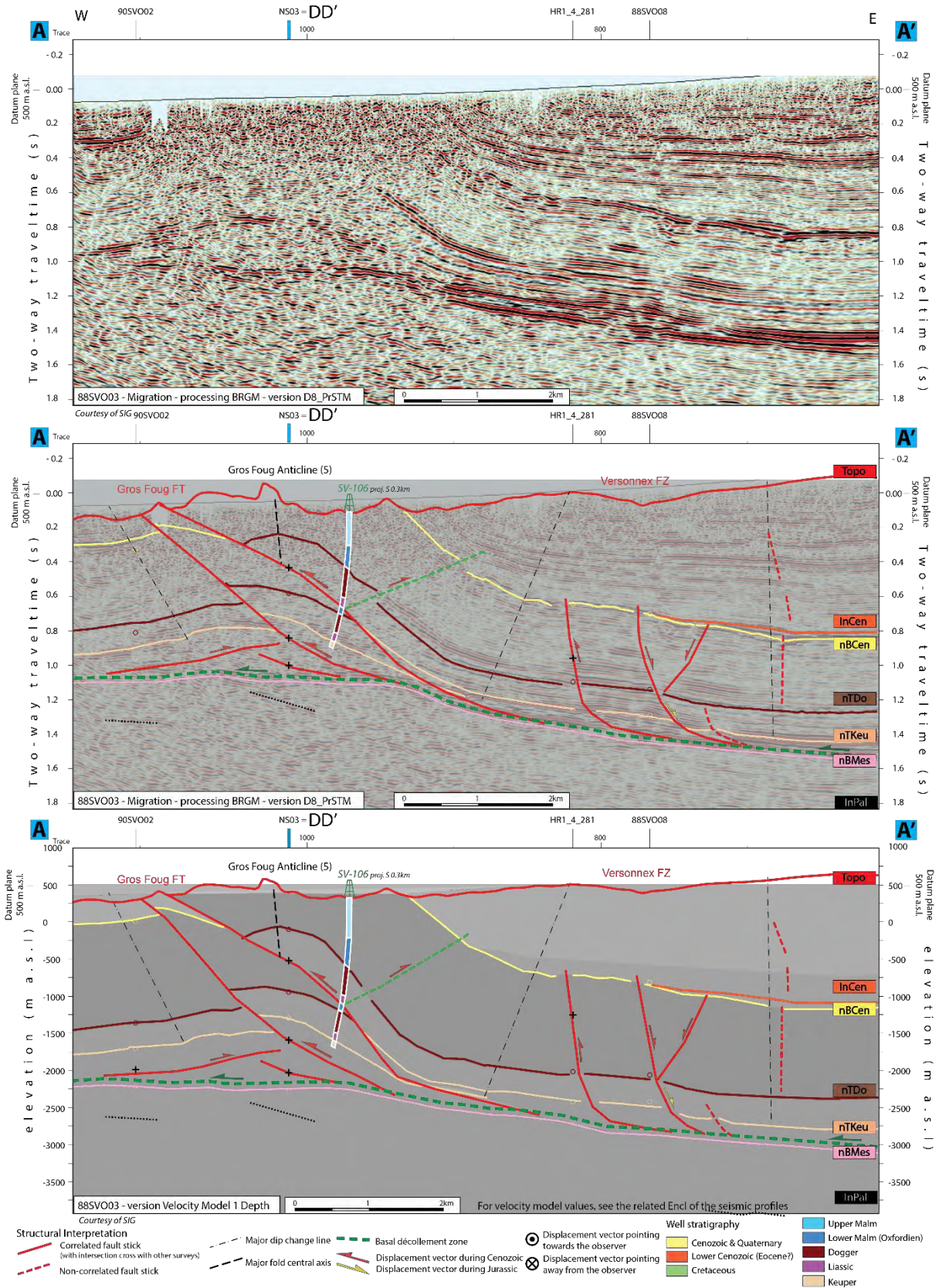


Figure 6-39 : Seismic interpretation (in twt for the two upper images and depth velocity model 1 in bottom image) of the Gros Foug FT and the Vernonnex FZ on seismic line 88SVO03 (section AA'). See Figure 6-38 for localization of the section. See Encl 49 for detailed seismic interpretation of line 88SVO03.

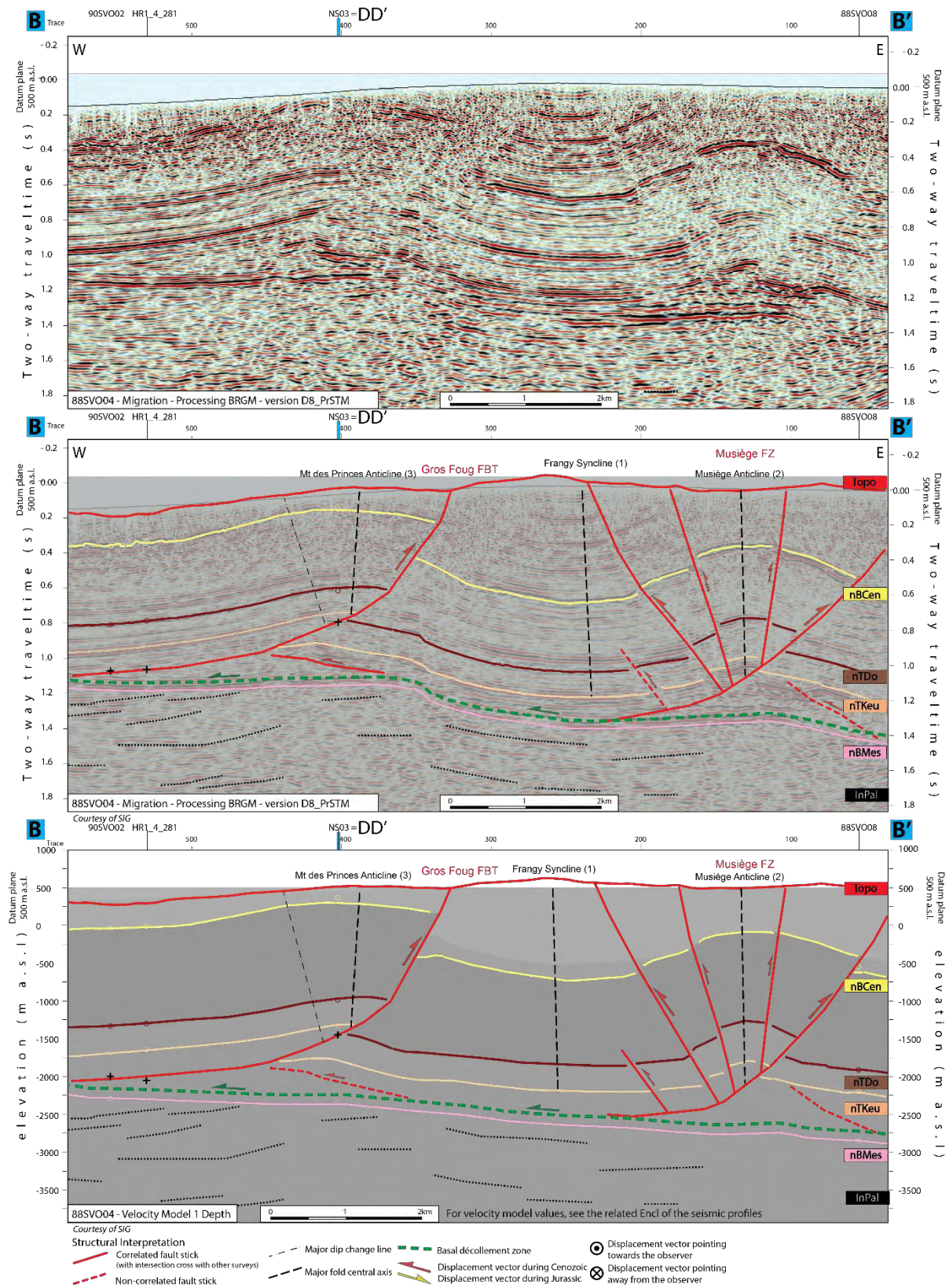


Figure 6-40 : Seismic interpretation (in twt for the two upper images and depth velocity model 1 in bottom image) of the Gros Foug FBT and the Musiège FZ on seismic line 88SV004 (section BB'). See Figure 6-38 for localization of the section. See Encl 50 for detailed seismic interpretation of line 88SV004.

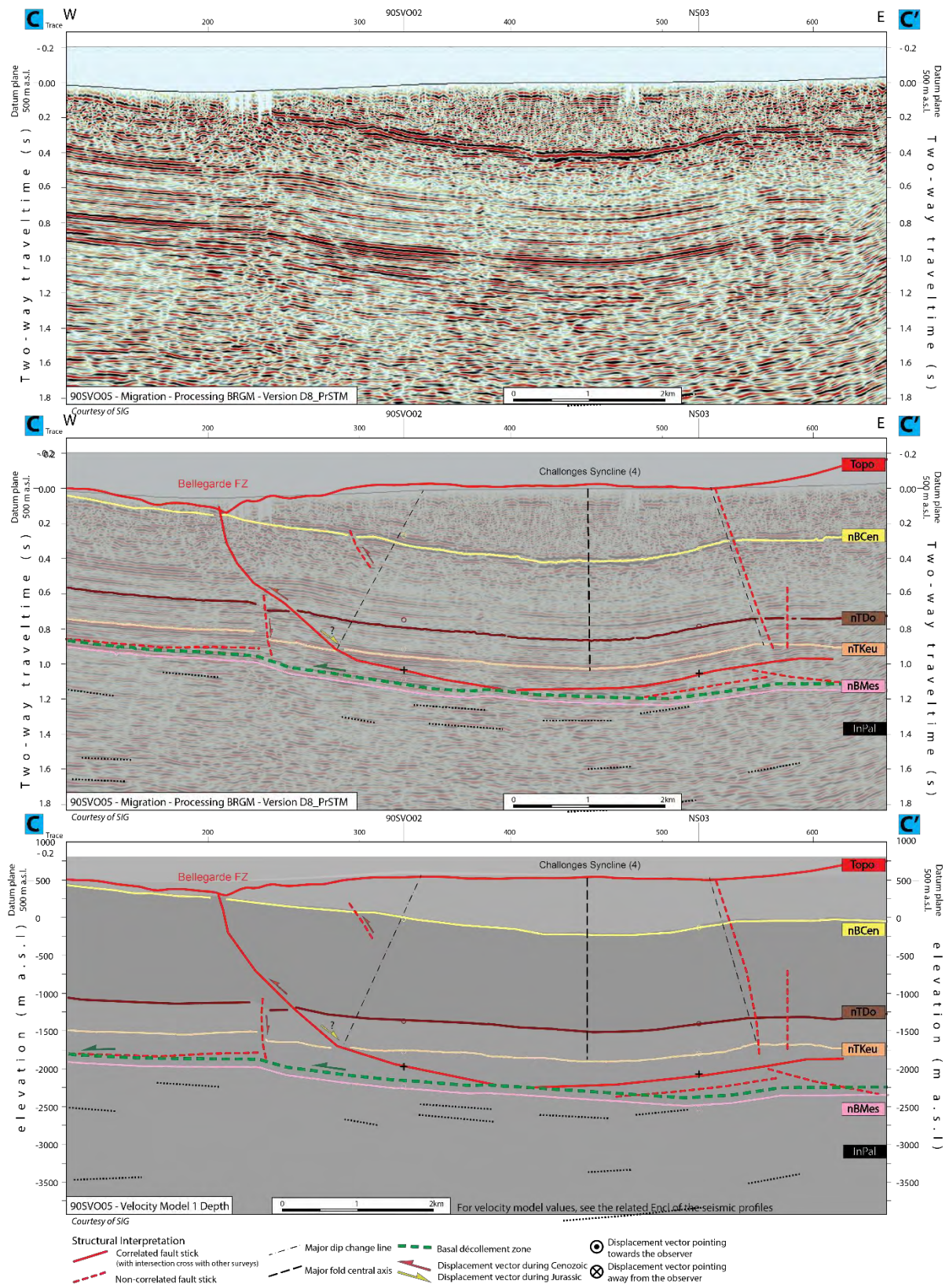


Figure 6-41 : Seismic interpretation (in twt for the two upper images and depth velocity model 1 in bottom image) of the Bellegarde FZ on seismic line 90SVO05 (section CC'). See Figure 6-38 for localization of the section. See Encl 55 for detailed seismic interpretation of line 90SVO05.

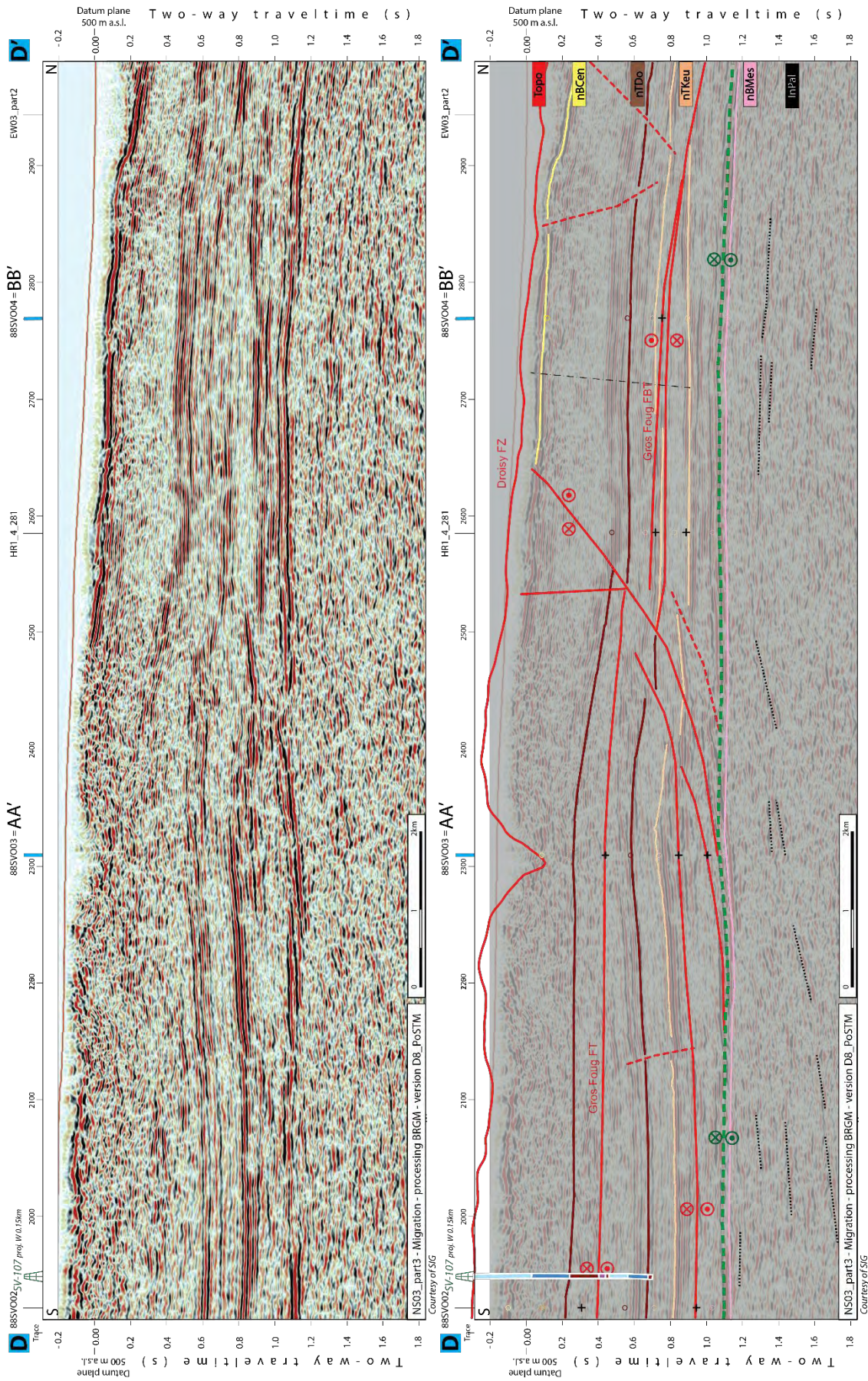


Figure 6-42 : Seismic interpretation (in twt) of the Gros Foug FT/ FBT and the Droisy FZ on seismic line NS03_part 3 (section DD'). See Figure 6-38 for localization of the section. See Encl 71 for detailed seismic interpretation of line NS03_part3.

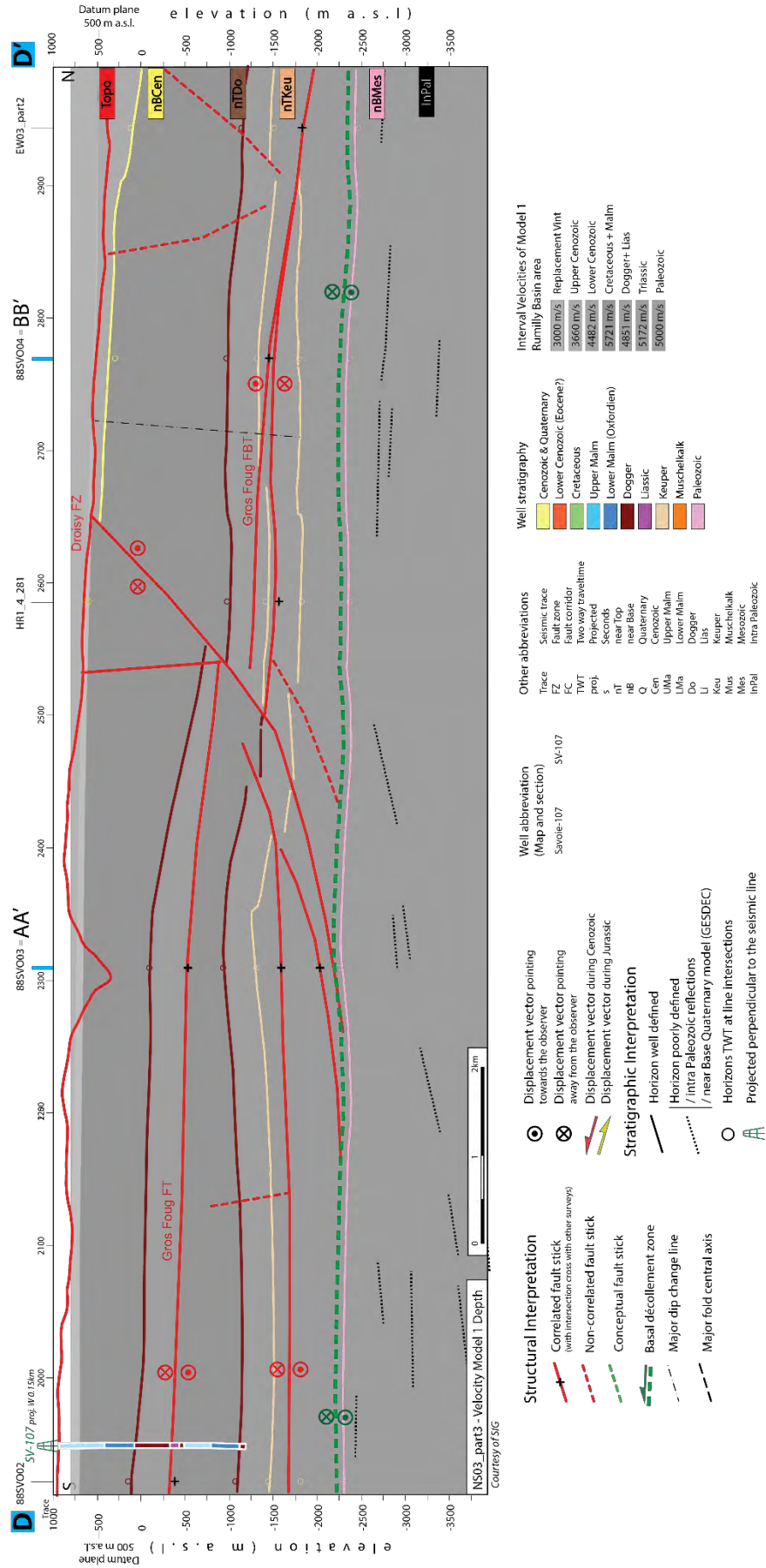


Figure 6-43 : Seismic interpretation (depth velocity model 1) of the Gros Foug FT/ FBT and the Droisy FZ on seismic line NS03_part 3 (section DD'). See Figure 6-38 for localization of the section. See Encl 71 for detailed seismic interpretation.

Fold Names

- 1 Frangy Syncline
- 2 Musiège Anticline
- 3 Droisy Anticline
- 4 Challonges Syncline
- 5 Gros Foug Anticline
- 6 Mt d'Âge Anticline
- 7 Meythet Anticline
- 8 Seynod Anticline
- 9 Villaz Syncline
- 10 Groisy Syncline
- 11 Amancy Anticline
- 12 Etaux Anticline
- 13 Salève Anticline
- 14 Mandalaz Anticline
- 15 Choisy Syncline
- 16 Cercier Anticline
- 17 Marlioz Syncline
- 18 Humilly Anticline
- 19 Cortenges Syncline
- 20 Veyrier Anticline
- 21 Minzier Anticline
- 22 CERN Syncline
- 23 Chouilly Anticline
- 24 Bernex Syncline
- 26 CERN Anticline
- 31 Chambésy Anticline
- 32 Cologny Anticline
- 33 Vernier Anticline
- 35 Thônex Syncline

Coordinate system:
CH1903+ / LV95

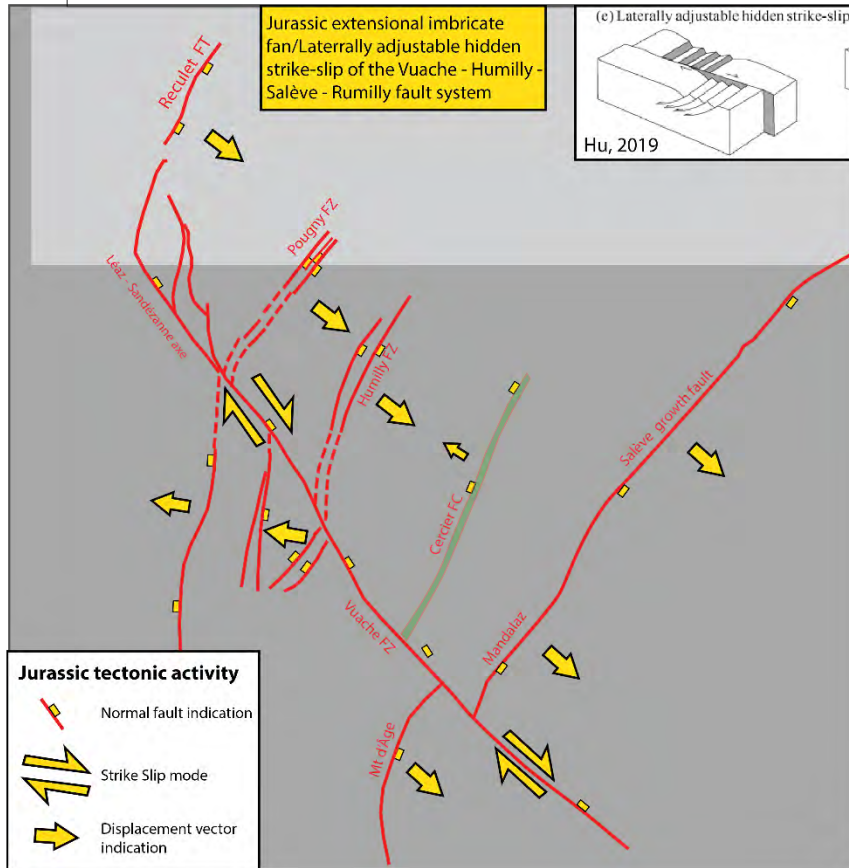
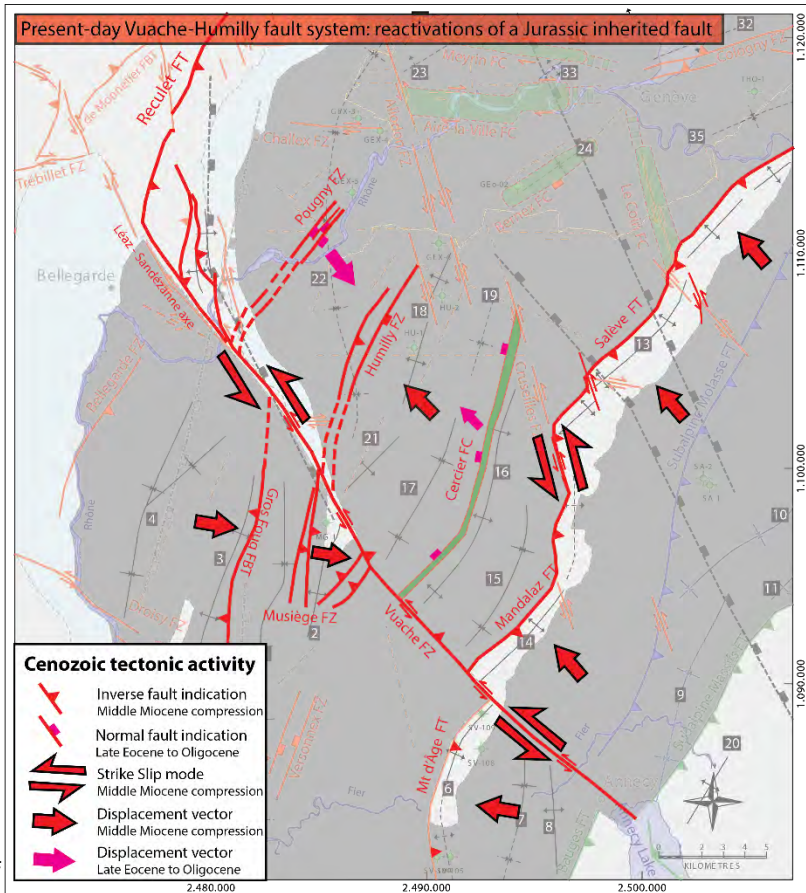


Figure 6-44 : Structural mapping scheme of the Humilly-Vuache-Salève fault system, as a laterally adjustable hidden strike-slip during Lower Jurassic period (bottom image) and as an inverted system during later compression (top image). Next sections as blue lines. Note that this structure is a combination of structures seen on Figure 6-37 and Figure 6-30.

6.3.5 The Jura area

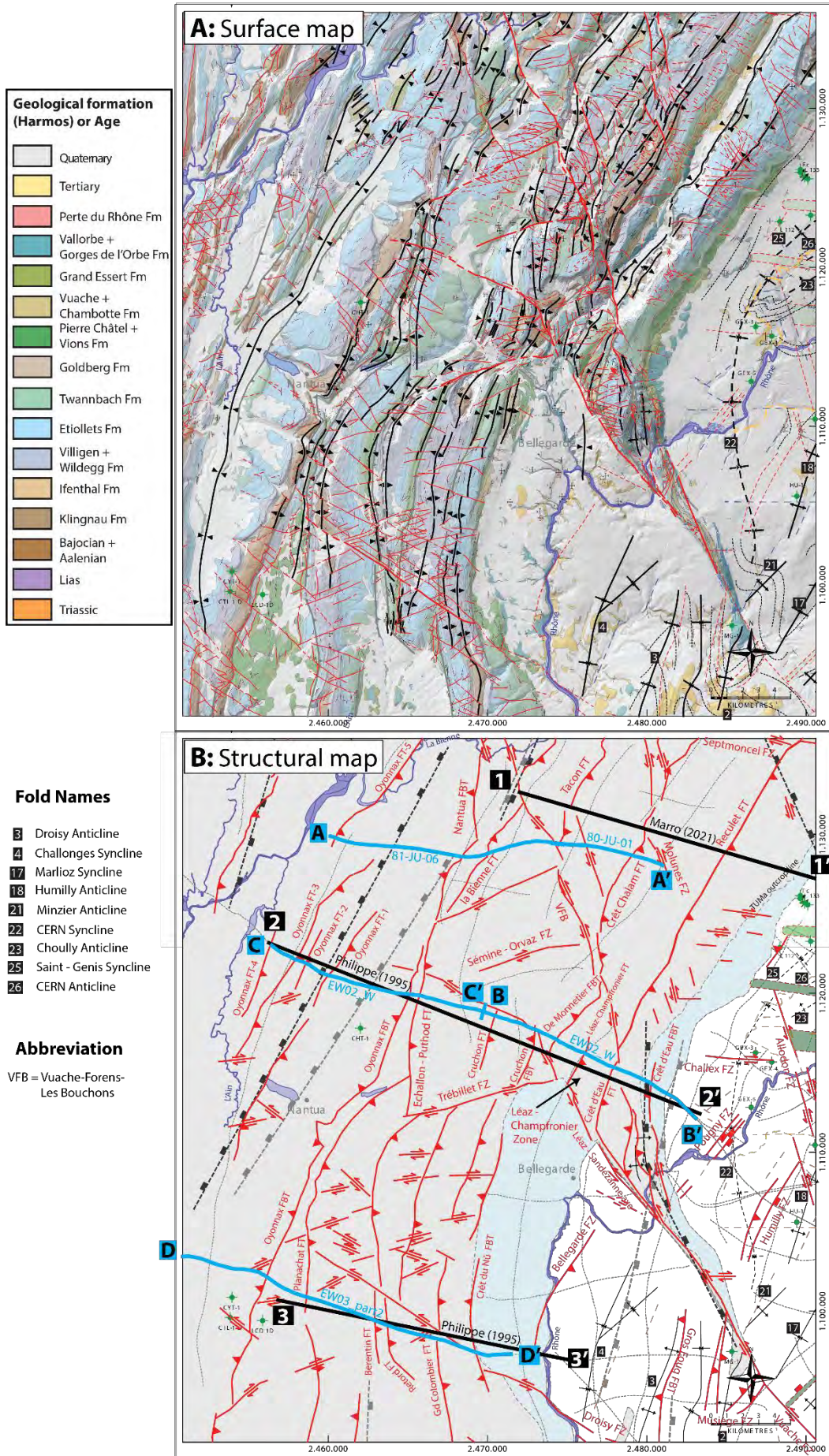
The seismic and structural interpretation of the Jura area may be summarized with three main regional NW-SE sections: the northern section A of Figure 6-46 and Figure 6-47, the intermediate combined sections B and C of respectively Figure 6-48 and Figure 6-49 and Figure 6-50 and Figure 6-51 and the southern section D of Figure 6-52 and Figure 6-53 (see localization map of Figure 6-45). The sections presented in this chapter are based exclusively on seismic and well data, in line with information from the literature and in agreement with geological surface data (maps). The interpretations are inspired and controlled by the near cross sections from Affolter & Gratier (2004); Guellec et al. (1990); Philippe (1995) (section 22', see Figure 6-45); Schori (2021); Wildi & Huggenberger (1993). The section A was interpreted in collaboration with A. Marro (2021) and Marro et al. (2023) whose work provides a more detailed structural analysis of this area.

This chapter gives an insight of the internal part of the Jura FTB, delimited westward by the Oyonnax structures FT/FBT and eastward by the Reculet and Crêt de la Neige FT along the Geneva Basin, and by the Grand Colombier and Crêt du Nû FT along the Rumilly Molasse Basin (see Figure 6-45). The internal Jura or Haute Chaîne is, in our region, the eastern or innermost part of the arc-shaped Jura FTB, and is therefore composed of a succession of ramp-flat thrusts and associated imbricates and folds, forming a series of anticlines and synclines parallel of the thrust faults (thrust-related folds), and formed of outcropping Cretaceous to Jurassic rocks. These structures are developed with an overall N-S orientation south of the Léaz-Sandezanne FZ (see Figure 6-45), and with a more NNE-SSW (to NE-SW) east of the northern continuation of the Vuache FZ. Our study confirms that all major thrusts root in the basal décollement zone (Triassic evaporites).

The seismic interpretation could not resolve the structural detail of local, secondary folding, and focusses on the large-scale structural configuration. Although, Molasse type sediments are found in some valleys (approximately 300m thickness in La Pesse, (Charollais et al., 2006)), usually along synclines in front of main thrusts faults (helping constrain the onset of the tectonic events), these thin, near surface layers cannot be imaged and characterized on seismic lines. We only consider seismic horizons of Mesozoic series in the interpretation of the profiles.

The two orientations of the thrusts and folds cited above indicate the two main shortening (compressional) orientations; E-W orientation for the area South of Léaz-Sandezanne FZ and NNW-SSE (to NW-SE) for the part east of the Vuache FZ. The transition between these two zones occurs across the transpressional triangle zone of Léaz-Champfronier already described along with the Vuache FZ analysis (6.3.2).

Associated with the thrusts are two main conjugate strike-slip systems, with N of the Vuache FZ axis, numerous sinistral NNW-SSE oriented strike-slips conjugated with dextral ESE-WNW strike-slips. South of the Léaz-Sandezanne FZ, we observe a counter-clockwise rotated system with sinistral NW-SE oriented strike-slip conjugated with NE-SW oriented dextral strike-slips (see Figure 6-45). Certain faults have more vertical offsets than others, and may appear in some cases as oblique ramps (Schori, 2021). We can notice that these strike-slip fault systems are nearly identical of the neighbouring systems interpreted on the Molasse Basin part. It confirms the idea that the Internal Jura area has a structural continuity with the Molasse Basin.



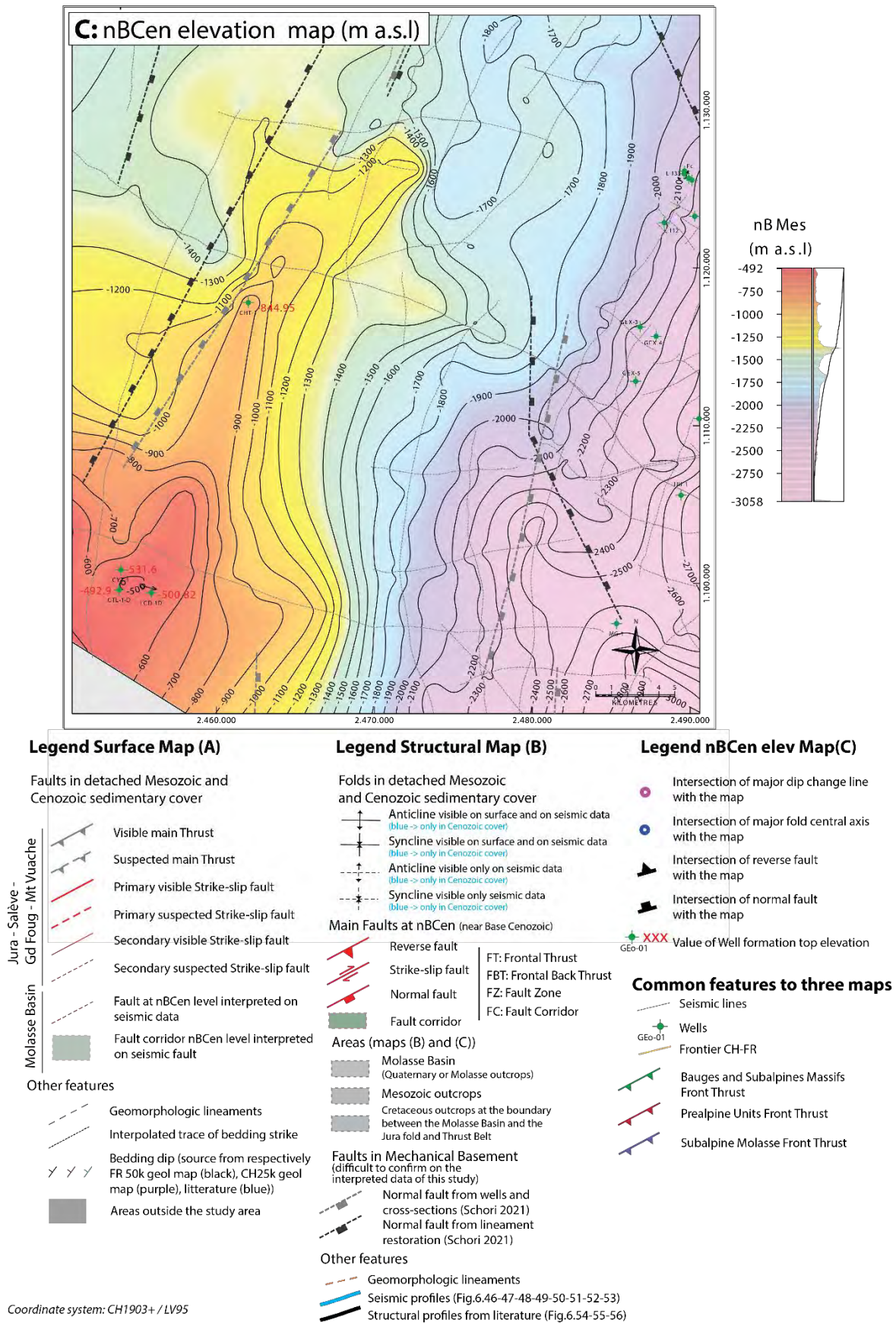


Figure 6-45 : Maps of structural interpretation results of the Jura area. It includes a succession of thrusts and backthrust from the Haute-Chaine area in the SE to the Oyonnax FT in the NW. These structures are described in details in the text of part 6.3.5. See Table 3-2 for well abbreviations. Sections of Figure 6-52, are represented on structural map B as blue lines. Coordinate system : CH1903+/LV95. Geological map A si based on Marro (2021).

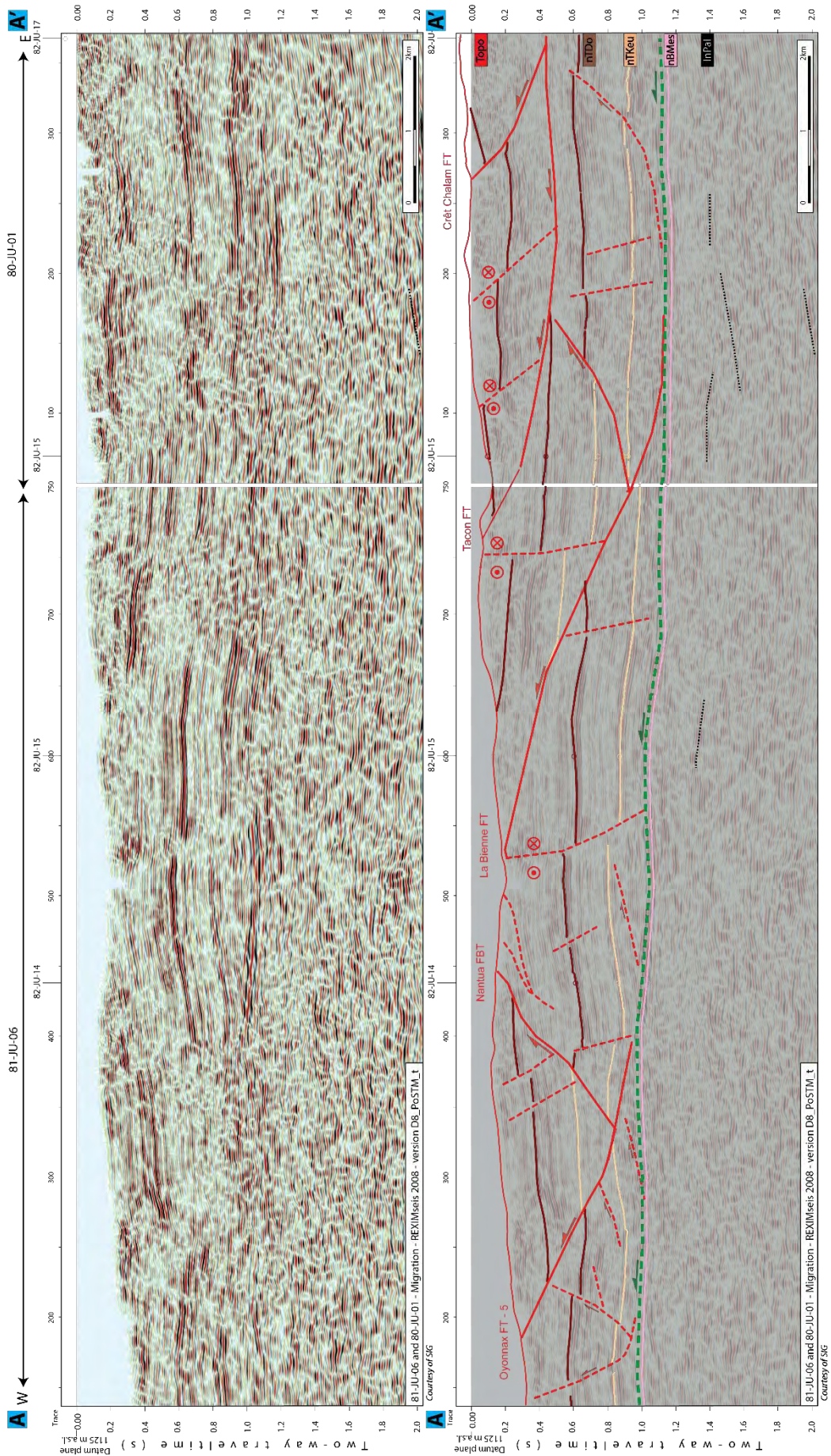


Figure 6-46: Seismic interpretation (twt) of the Northern Jura on lines 81-JU-06&01 (section AA', see Figure 6-45 and Encl 37).

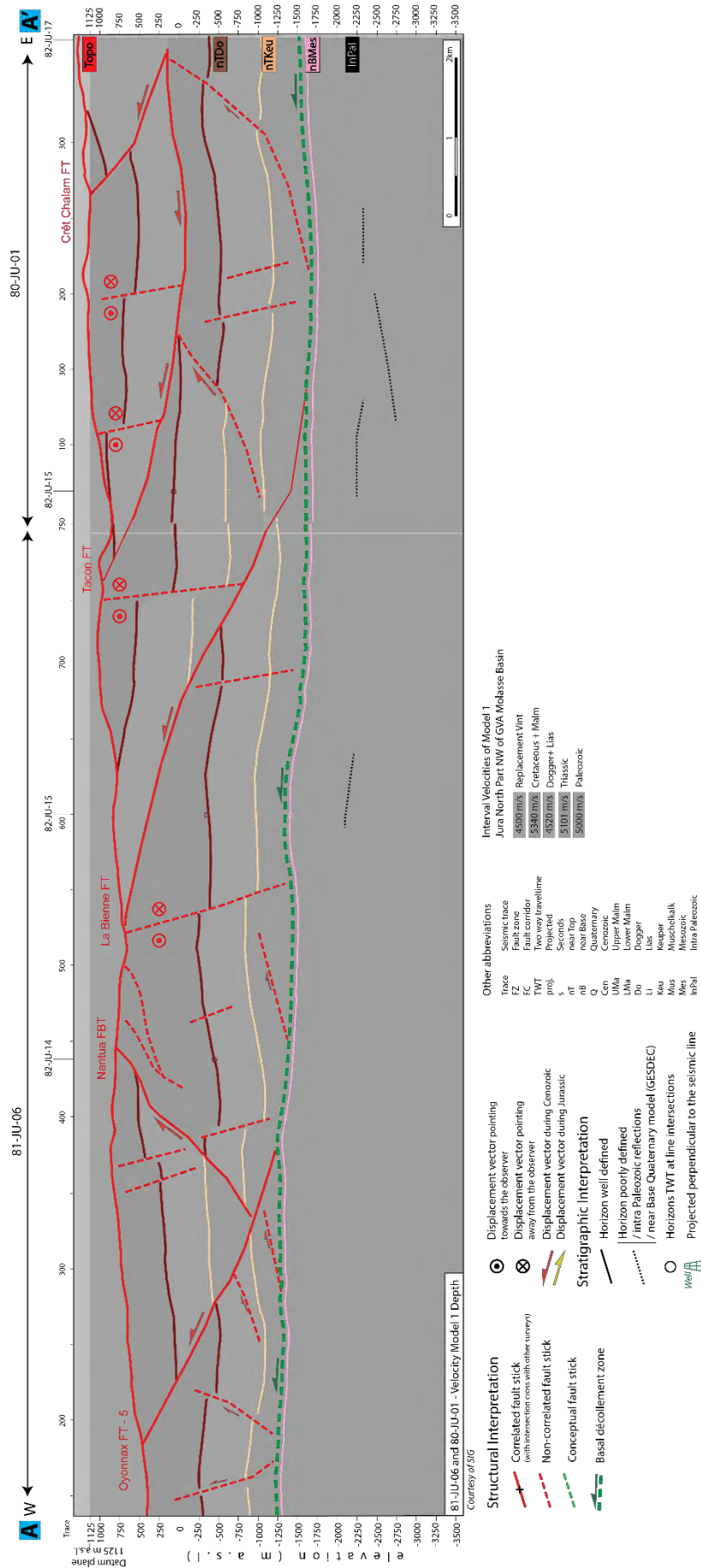


Figure 6-47 : Seismic interpretation (depth) of the Northern Jura area on lines 81-JU-06, 80-JU-01 (section AA', Figure 6-45).

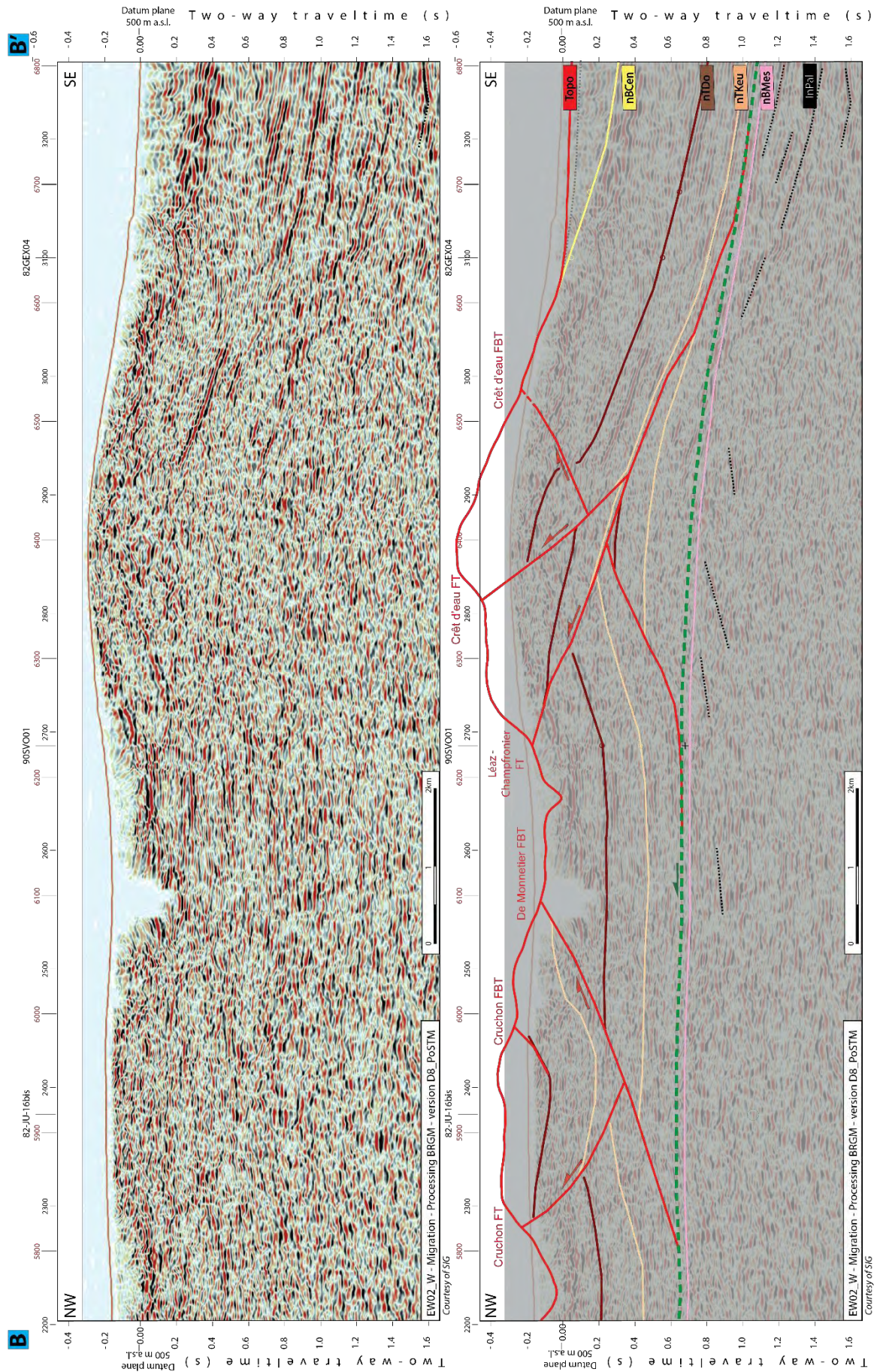


Figure 6-48: Seismic interpretation (twT) of the Central Jura area on lines EW02_W (section BB', see Figure 6-45 and Encl 62).

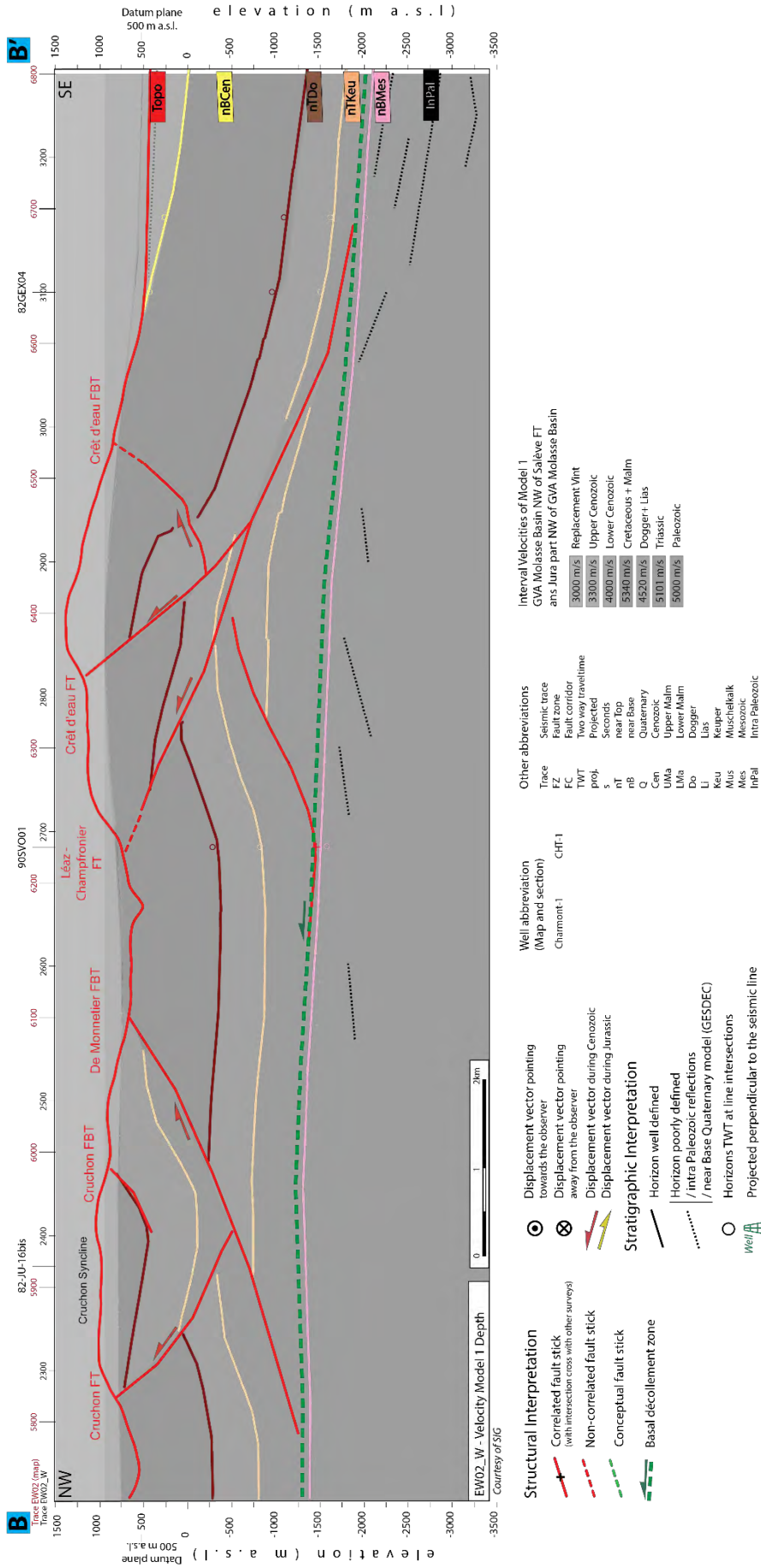


Figure 6-49: Seismic interpretation (depth) of the Central Jura area (South) on lines EW02_W (section BB', see Figure 6-45).

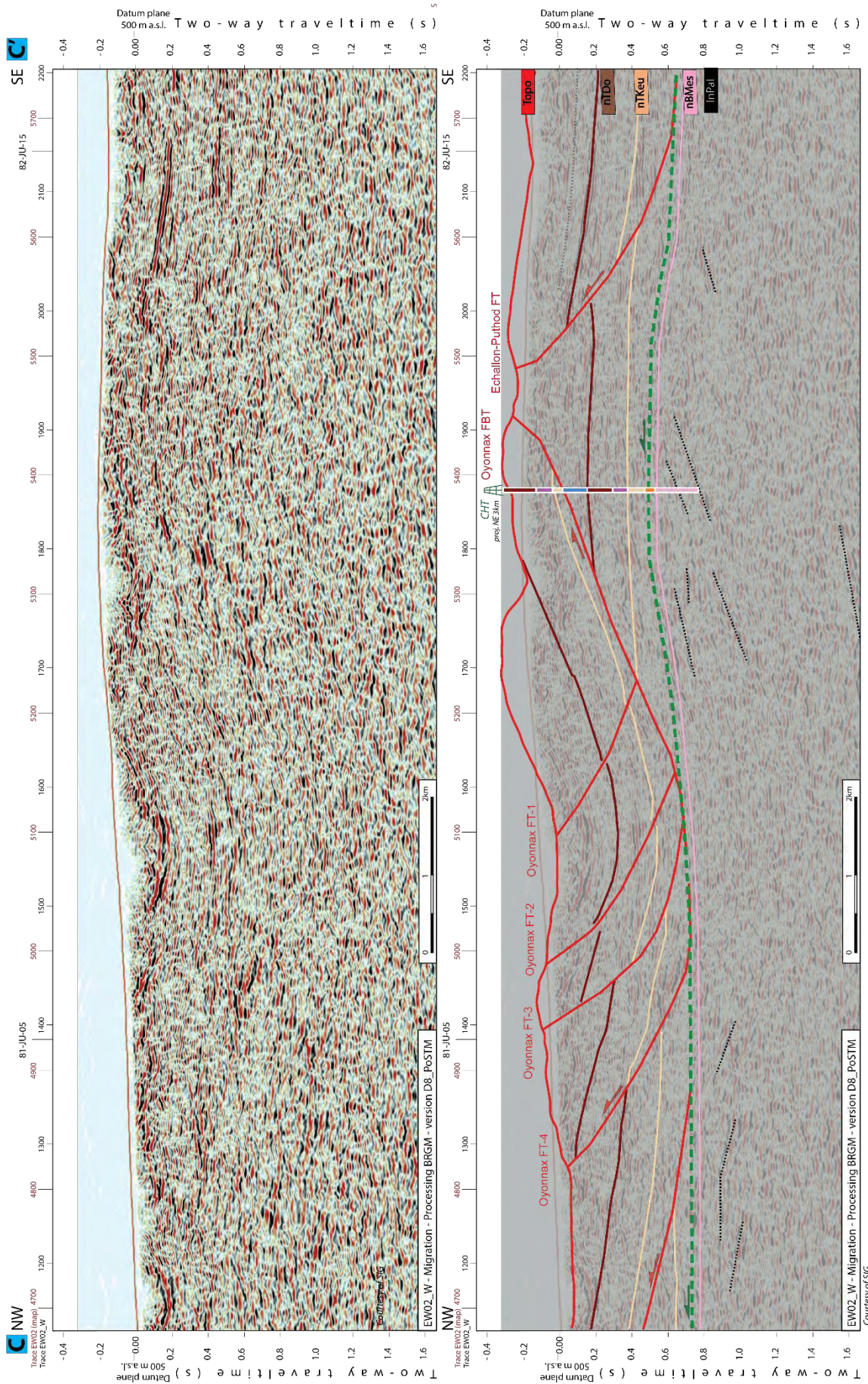


Figure 6-50: Seismic interpretation (tw) of the Central Jura area on lines EW02_W (section CC', see Figure 6-45 and Encl 62).

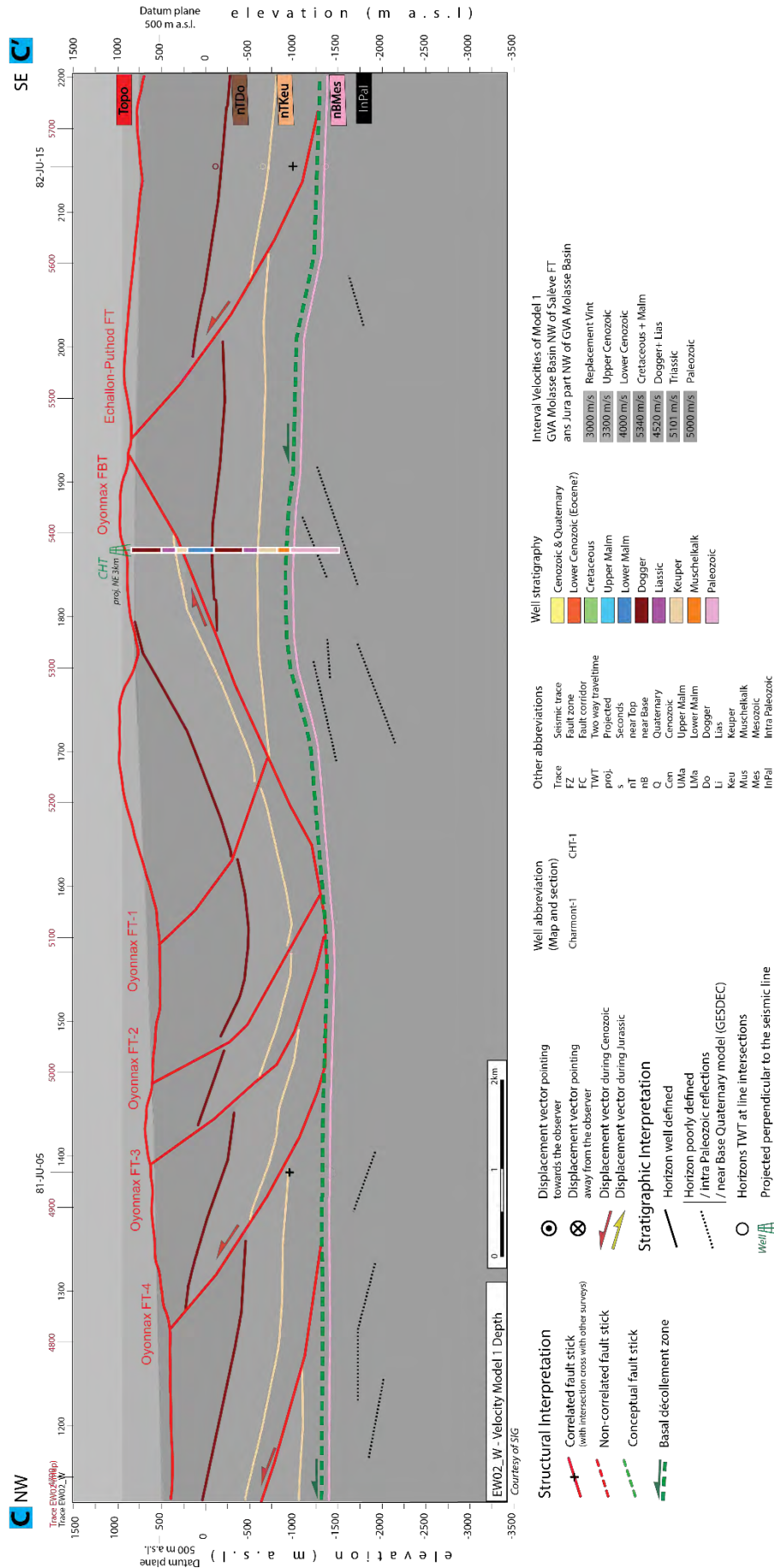


Figure 6-51: Seismic interpretation (depth) of the Central Jura area (North) on lines EW02_W (section CC', see Figure 6-45).

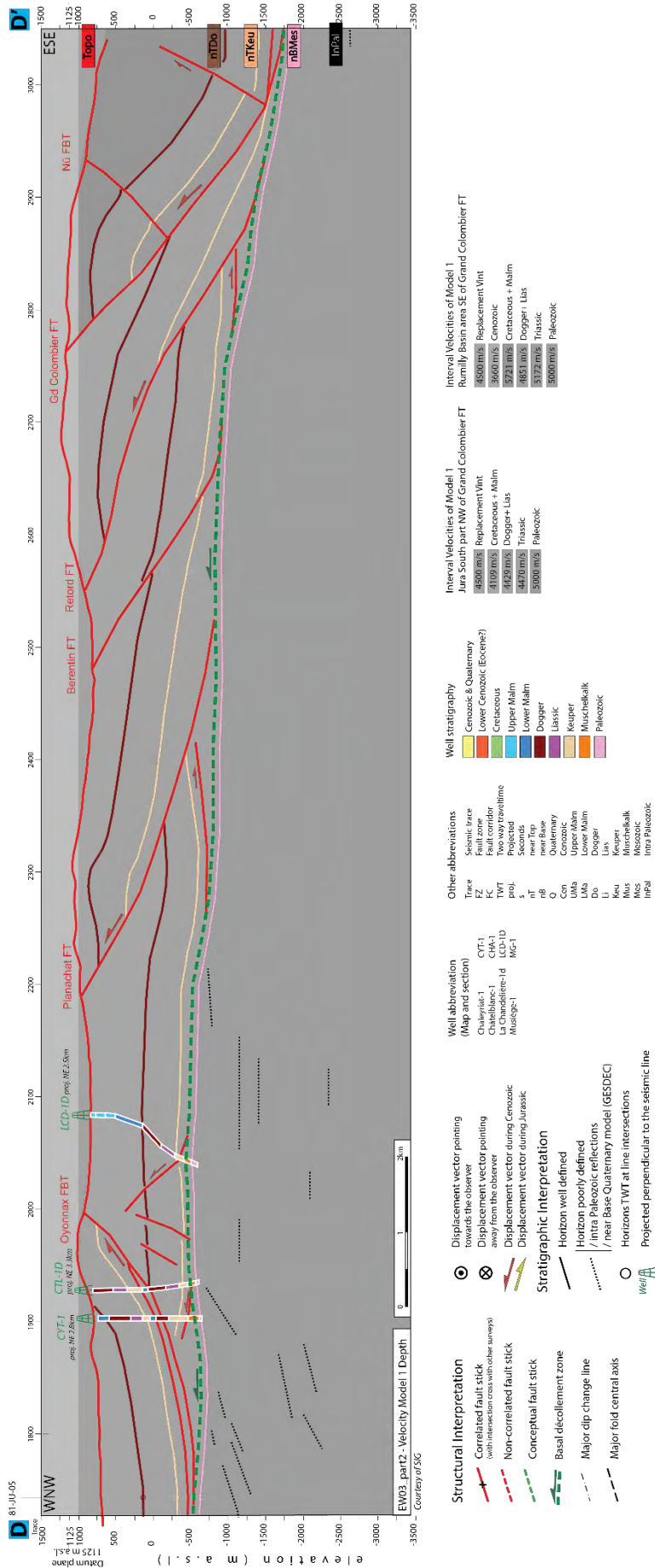


Figure 6-53: Seismic interpretation (depth) of the Southern Jura on seismic line EW03_part2 (section DD', see Figure 6-45).

Another main objective of the expansion of the seismic interpretation into the Jura, was to obtain a new and coherent regional map of the nBMes seismic horizon (Figure 6-45). The velocity modeling and time-to-depth conversion methodology of our study provides the opportunity to increase the resolution of such a map, in comparison to previous studies. Indeed, it allows getting rid of velocity artefacts (pull-up and push-down effects), and it models the velocities of the layers in a more realistic manner than a “layer-cake” model (see part 5.1.5). These technical improvements are relevant when assessing the structural configuration of the basement. It provides at least the main basement highs and lows and the related dipping angles of the top of the mechanical basement.

The Sections A of Figure 6-46 and Figure 6-47 are presenting the Internal Jura part bordering the Geneva Basin. There is a data gap between seismic data inside the Geneva Basin and inside the Internal Jura (Figure 4-8). Therefore, it was not possible to directly correlate the results of interpretation of both parts. However, the correlation polygon method was used to link the two areas (see part 4.2.1). Moreover, the seismic interpretation of this section A was used as input for the elaboration of the balanced cross-section of Marro (2021) and Marro et al. (2023)(Figure 6-54), in order to achieve a continuous structural model from the Basin to the Jura. According to this work, the high topographic position of the Crêt de la Neige and Crêt au Merle anticlines is explained by a possible imbrication of a ramp flat geometry involving a secondary décollement level at the Dogger-Lias boundary (“facies de transition”). The fault-bend folding principles of Suppe (1983) were used to explain the angle of the Reculet thrust in relation to the angle of the underlying hidden ramp of the Crêt de Chalam Thrust. The geometry of the Reculet thrust obtained with this method, is then in line with the interpreted back thrusting (or top to the south movement) on the back-limb of this major thrust towards the Geneva Basin (on seismic profiles, (Paolacci, 2012; Signer & Gorin, 1995)). It is to be noted, that Intra-Paleozoic seismic reflections associated to Permo-Carboniferous units can be interpreted on seismic profiles at the NW extremity of the Geneva Basin and the presence of a Permo-Carboniferous half graben, developed along a NE-SW oriented, and SE dipping normal basement fault (uncertain) can be proposed. The Crêt Chalam frontal thrust is preceding an imbrication of numerous secondary thrusts, linked to the disharmonic folds in the Dogger units along the Crêt Chalam anticline. The high dip angles of the bedding measured in the backlimb of the Crêt du Merle anticline is justified on the model of Marro, (2021) by an underlying imbrication (following principles of Suppe, (1983)). This part corresponds to the start of our seismic interpreted section A of Figure 6-46 & Figure 6-47. It was possible to locate the ending of the Crêt Chalam Thrust on the southeastern part of the seismic profile. Then we can see with higher certainty, the detachment of the underlying thrust above the Dogger Unit, proposed to be inside the Effingen-Geissberg marls. This underlying flat ramp belongs in fact to the Tacon frontal thrust rooted along the basal décollement zone (Marro, 2021; Marro et al., 2023). The detachment of the Tacon flat ramp may be linked with a secondary underlying backthrust, located below the Crêt au Merle and that is relatively obvious on the seismic image. The flat Tacon Thrust was also clear to interpret on seismic; the thrust is supposed to be positioned above the marly Goldberg formation at Cretaceous-Jurassic boundary (Marro, 2021). The following structure northwestward, is the Bienne FT overlapping a complete Mesozoic series, that was tied (correlation polygon method) with a projection of Charmont-1 well. A NW-SE strike-slip fault is interpreted just below the surface signature of the Bienne Thrust. It is dipping NE, crossing the entire Mesozoic cover and showing thickening of the Triassic series likely due to Intra-Keuper Group imbrications in its vicinity. The domain west of this fault appears uplifted due to the lateral sinistral movement shifting the related folding. This strike-slip fault belongs to the large Vuache-Léaz-Sandezanne transpressional system (see

map of Figure 6-45). The next structure to the NW is the Nantua-Oyonnax structure also shown in the cross-section of Marro (2021) and Marro et al. (2023) (Figure 6-54). This major NNE-SSW oriented structure contributes to an important topographic uplift (500-1000m vertical offset) and is composed of the frontal thrust of Oyonnax and the regionally important backthrust of Nantua. Several secondary faults (compressional and strike-slip) are surrounding this remarkable fault system. This development and geometry of this structure is in agreement with analogue modeling results of Schori (2021), which highlight very similar pop-up thrusting structures in wedge-propagation systems. Indeed, the northwestward tilting of the uplifted triangle block is typical of such structural settings. In addition, this classical pop-up configuration does not require any basement step to be triggered (Schori, 2021, Schori et al., 2021).

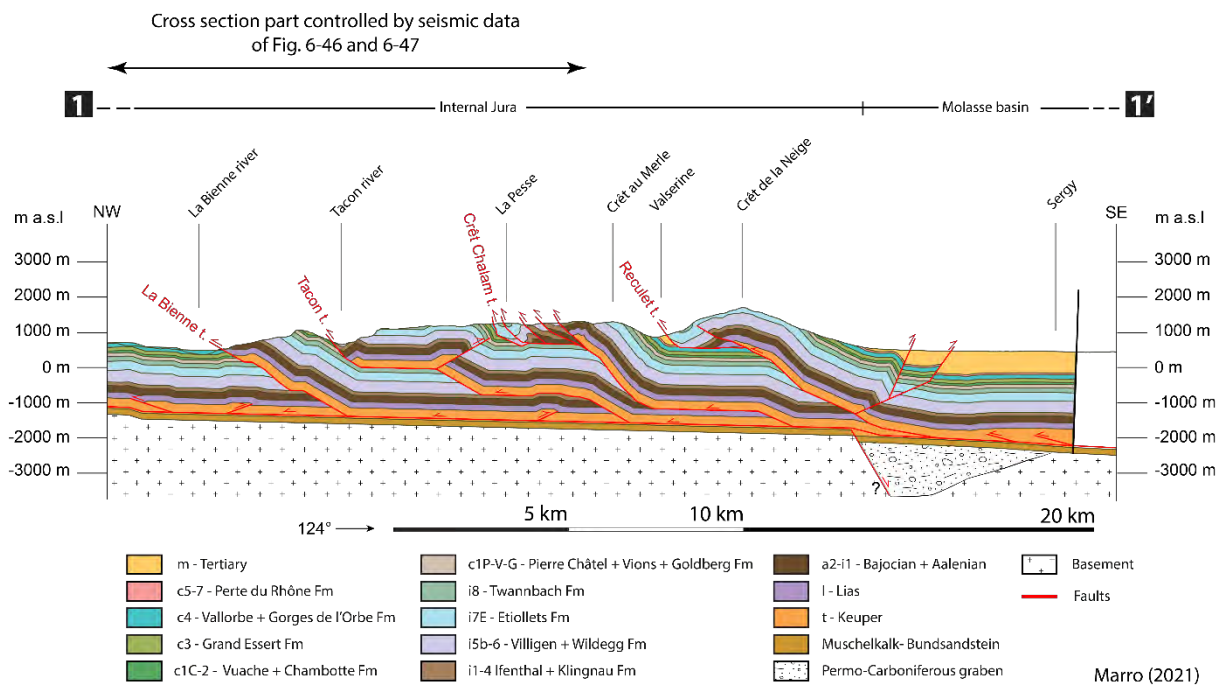


Figure 6-54 : Final Cross-section of Marro (2021) and Marro et al. (2023), with the western part (west of the Crêt Chalam FT) constrained by the seismic interpretation of this study (section A of Figure 6-46 & Figure 6-47). See localization of this section 1'1' on Figure 6-45.

USM and OMM deposits are outcropping in the two main valleys of the Valserine and La Pesse synclines in the Haute Chaîne Jura (Charollais et al., 2006; Wildi et al., 1991), although it is not relevant for seismic interpretation, it suggests that the Crêt Chalam Thrust must have developed after the OMM (Upper Marine Molasse) age (Langhian, 16-14Ma (Charollais et al., 2006)). In addition, the altitude of these valleys, which is higher than the Molasse deposits in the Geneva Molasse Basin, can be explained by thrust imbrications (Marro, 2021; Marro et al., 2023; Schori, 2021), or alternatively linked to uplift of the basement. Philippe (1995), thus suggested the presence of an inverted half-graben developed along normal basement fault dipping SE, below the Crêt Chalam structure. It is not excluded that the Permo-Carboniferous seismic facies observed at the NW extremity of the Geneva Molasse Basin could be associated with such a graben structure. Therefore, we suppose a normal basement fault dipping with the classical angle of 60° southward below the backlimb of the Reculet Thrust, with an estimated 180m vertical offset of the mechanical basement. We can also notice a change of dipping angle of nBMes seismic horizons along the basement fault. It is dipping SE with an average angle of 2.7 degrees in basin part of the section and decreasing to 1.3 degrees below the Internal Jura.

The Sections B/C of respectively Figure 6-48 and Figure 6-49, and Figure 6-50 and Figure 6-51 (see map of Figure 6-45), is an excerpt from the NW-SE oriented ECORS profile (Guellec et al., 1990), intended to image the deep structures from the Western Alps to the Bresse Graben, crossing the Vuache FZ in the Geneva Basin. The section links the deep wells Hu-02 in the Geneva Basin with Charmont-1 well in the internal Jura area. The seismic interpretation of the Mesozoic layers is based on the work from Philippe (1995)(Figure 6-55). The seismic resolution is relatively poor (mountainous environment for acquisition), however, the image allows identifying the geometry and curvature of the seismic reflections of the main Mesozoic series. The first structure SE of section B is the SW continuation of the Reculet FT inside the transpressional Vuache FZ. The Crêt d'Eau FZ corresponds to a subdivision of the main Reculet Thrust into two ramps with a pop-up structure developed on the southeastern flank of the crest. In the footwall of the fault, the NW dipping Mesozoic layers are indicating the presence of back-thrust, probably internal of the Triassic unit. Philippe (1995) proposed a continuation upward thus forming a fish tail structure (Figure 6-55) which is an elegant and probable solution considering the several secondary detachment levels of the Mesozoic cover. This entire structure better fits the complex structural configuration of the transpressional triangle zone (Léaz-Champfronier), than the simpler fault-bend fold interpretation of Guellec et al. (1990). Indeed, the doubly verging structure, with a frontward and backward thrust conceals a triangular volume as proposed in the interpretation of the Vuache FZ by Meyer (2000). The next structure to the NW is a large-scale pop-up thrust structure (10km width), in between the de Monnetier FBT and the Echallon-Puthod FT. The entire uplifted block is tilted NW, with a secondary pop-up ramp (Cruchon FZ) along the upward extremity of the De Monnetier FBT. The latter is justifying the high elevation of the Cruchon Syncline (see Figure 6-55). The main evaporites-rich Triassic décollement zone is used for detachment of these faults. The sections B/C is crossing the continuation southwestward of Nantua-Oyonnax structure described on section A. However, the vertical amplitude, offsets, and NW tilting of the pop-up ramp are amplified in this area. Moreover, it is preceding another serie of two other frontal ramps that can be interpreted as a large-scale imbricated pop-up system. Geometrical similarities with modeled compressional systems from Schori (2021), suggest that this type of structures resulting from a detachment initiating over an upward step in the basement. The mechanical basement was relatively difficult to identify along this seismic profile and its interpretation and the identification of related faults and Permo-Carboniferous infill remain highly speculative. We can, nevertheless, observe a change of dip of this surface between the Molasse Basin and the Internal Jura parts, as well as a basement high SE of the Oyonnax FBT (Figure 6-45). The large-scale analysis of this profile B/C, is highlighting a topographic and structural uplift of the mechanical basement in between the Reculet FT and the Oyonnax FBT. Philippe (1995) explained this topographical anomaly by inversion of a Permo-Carboniferous graben with the bordering basement fault below the Reculet FT and the Oyonnax structure Figure 6-55. Guellec et al. (1990) proposes two hypothesis either with a recent thick-skinned thrusting of the basement, or a horst that may be as is insitu or could be also reactivated along its normal faults. Schori (2021) supports the idea of a horst configuration with the southeastern flank that may have triggered an oblique ramp structure subsequently transported during deformation and presently observed further NW of the Reculet-Vuache area. Based on modelling from Marro (2021) and Marro et al. (2023) along section A, we know that a basement step, linked with a normal fault offset towards the SE between the internal Jura FTB and the Molasse Basin is a viable kinematic solution to explain the anomalous uplift of the internal Jura area. Moreover, our time-depth conversions, especially of near top basement surface (Figure 6-45) corroborate the presence of the basement uplift, and a horst configuration seems the most

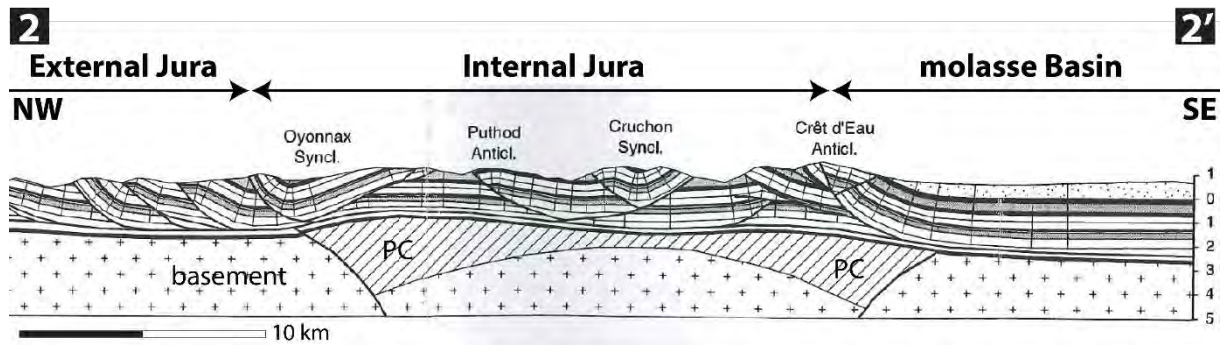


Figure 6-55 : Cross-section from Philippe (1995), passing along sections B/C of this study, see Figure 6-45 for localization. Note the structural solution proposed in the basement with two reactivated basement faults bordering half grabens. In our study, we are more in favor of the structural solution of Schori (2021) that supposes a horst structure. See localization of this section 22' on Figure 6-45.

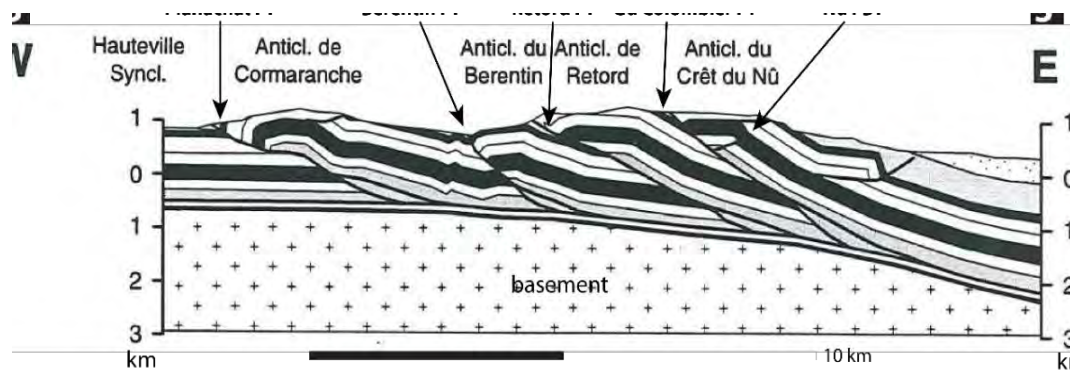


Figure 6-56 : Cross-section from Philippe (1995), passing along section D of this study, see Figure 6-45 for localization. The Berentin FT was not identified on our seismic data (EW03_part2, Figure 6-52 and Figure 6-53). See localization of this section 33' on Figure 6-45.

reasonable. As pointed out by Schori (2021), and already alluded to prior, the basement steps do not imply, nor need a recent reactivation, but may be developed before the Jura FTB formation.

The Section D of Figure 6-52 & Figure 6-53 starts from the Rumilly Molasse Basin and crosses the internal Jura FTB parallel to the two other sections in NW-SE orientation. In the SE part of section D, the internal Jura FTB is made of a series of stacked ramps and associated folds. The first one is the Grand Colombier FT, which may have a small-scale pop-up with a back-thrust near the crest, but which could not be resolved on the seismic line, and therefore we here “only” show a classical fault-bend fold shape. We have noticed larger back-thrusting along the SE termination of the backlimb of this Grand Colombier FT, where the seismic image begins to be fuzzy. The next major structure to the NW is the Retord FT also detached along the basal décollement zone. The seismic response along the fault plane is relatively clear. As for the the Berentin FT (related to Berentin anticline), even if it was not so obvious as for the other main thrusts, it has been identified the same way as Affolter & Gratier (2004) and Philippe (1995) have drawn it on their cross-section (Figure 6-56). The Planachat FT is the southwestern continuation of the Echallon FT and of the La Bienne FT, and has a configuration of a fault-bend fault. In the area between this westward propagating thrust and the Oyonnax backthrust, Cretaceous rocks are outcropping on top of an undeformed horizontal, complete Mesozoic series. The well La Chandelière-1D, drilled in this zone, is a crucial tying point, which provides a tie in time and in the depth domain of the seismic horizons, as well as velocity information for the velocity model building. In addition, in this zone the near Base of the Mesozoic horizon is showing the same positive

topographical anomaly than observed along strike in the other section. The basement high area between the Oyonnax FBT and the Grand Colombier FT may be explained by a regional horst, with vertical offsets forming inherited basement steps.

6.4 Main Stratigraphical observations

During the seismic interpretation, we were also able to re-assess the stratigraphy of different layers, based on horizon interpretation, seismic facies analysis and by creation of thickness and depth maps.

It has to be remembered, that a high thickness area may be related to either an increase of the depositional rate during the period of the analyzed interval and hence a thicker sediment package or to a later tectonic activity that led to duplication of the layer or flowage if evaporite (salt)-rich layers are involved. Also in areas of dipping layers, where the vertical thickness measured after seismic interpretation may differ from the stratigraphic thickness, which is measured perpendicular to the strata dip (usually lower, see part 5.2.3).

6.4.1 *The Liassic and Dogger intervals*

Note that the Triassic stratigraphical observations are presented in previous chapter 6.2.

In the regional analysis (velocity model 1, see 5.1.2), we have merged the near Liassic and the Dogger seismic intervals for practical reasons (for further description of seismic horizons and facies of nTDo and nTLi, see 4.1.6 and 4.1.7). These two units can be considered to pertain to the same paleotectonic and basin evolution event associated with the period of rifting initiation and rifting during the opening of the Alpine Tethys. Both the regional results (velocity model 1, see 5.1.2) and the more detailed, local analysis (Geneva Basin velocity model 2, see 5.1.3) suggest an increased activity (syn-sedimentary paleotectonic structures) particularly during the Liassic period in our area of study.

In the Greater GVA basin, the Liassic unit corresponds to marly carbonates and shales, whereas the Dogger unit is showing alternating bioclastic carbonates and muddier facies (Rusillon, 2017). This highlights the depositional trend, with a Liassic deepening eastward of the NE-SW striking basin in our area of study, followed by a shallower environment along the carbonate platform during the Dogger. The main depocenter zone of the Liassic unit of the western Molasse Basin lies in between Pontarlier-Oyonnax-Geneva-Fribourg (Figure 6-57, (Schori, 2021)). On the other hand, the Dogger unit has its highest thicknesses around Nyon or Pontarlier. In that sense, the higher thickness heterogeneity of our grouped Liassic-Dogger interval in our area of study are actually more influenced by the Liassic layer than by the Dogger layer. Schori (2021) noticed substantial tectonic thickening along major strike-slip faults such as the Pontarlier FZ, La Lance FZ (Vaud), but also along the Vuache FZ. As he assumes a Mio-Pliocene origin of these faults, he then supposes that the high thickness values of the Liassic Unit are linked to tectonic duplications rather than sedimentary processes. However, our seismic interpretation is showing a Liassic-Dogger syn-sedimentary tectonic activity east of the Vuache FZ and in the Salève area (growth faults, see 6.3.2 and 6.3.3). This goes along with Rusillon (2017) who pointed out the likely sedimentary trend influenced by syn-tectonic activity during the Liassic-Dogger times along the NW-SE trending fault lineaments in the Greater GVA Basin. Our Liassic-Dogger regional thickness map is highlighting this activity (Figure 6-58) with higher thicknesses of the Lias-Dogger units in the

hangingwall of the interpreted large-scale extensional faults from Liassic-Dogger (Vuache-Humilly-Salève FZ, see 6.3.2 and 6.3.3). These fault zones are prone to later reactivation, and may have an impact on diachronous depositional trends, such as for the Upper Malm reefal complexe (see 6.4.2).

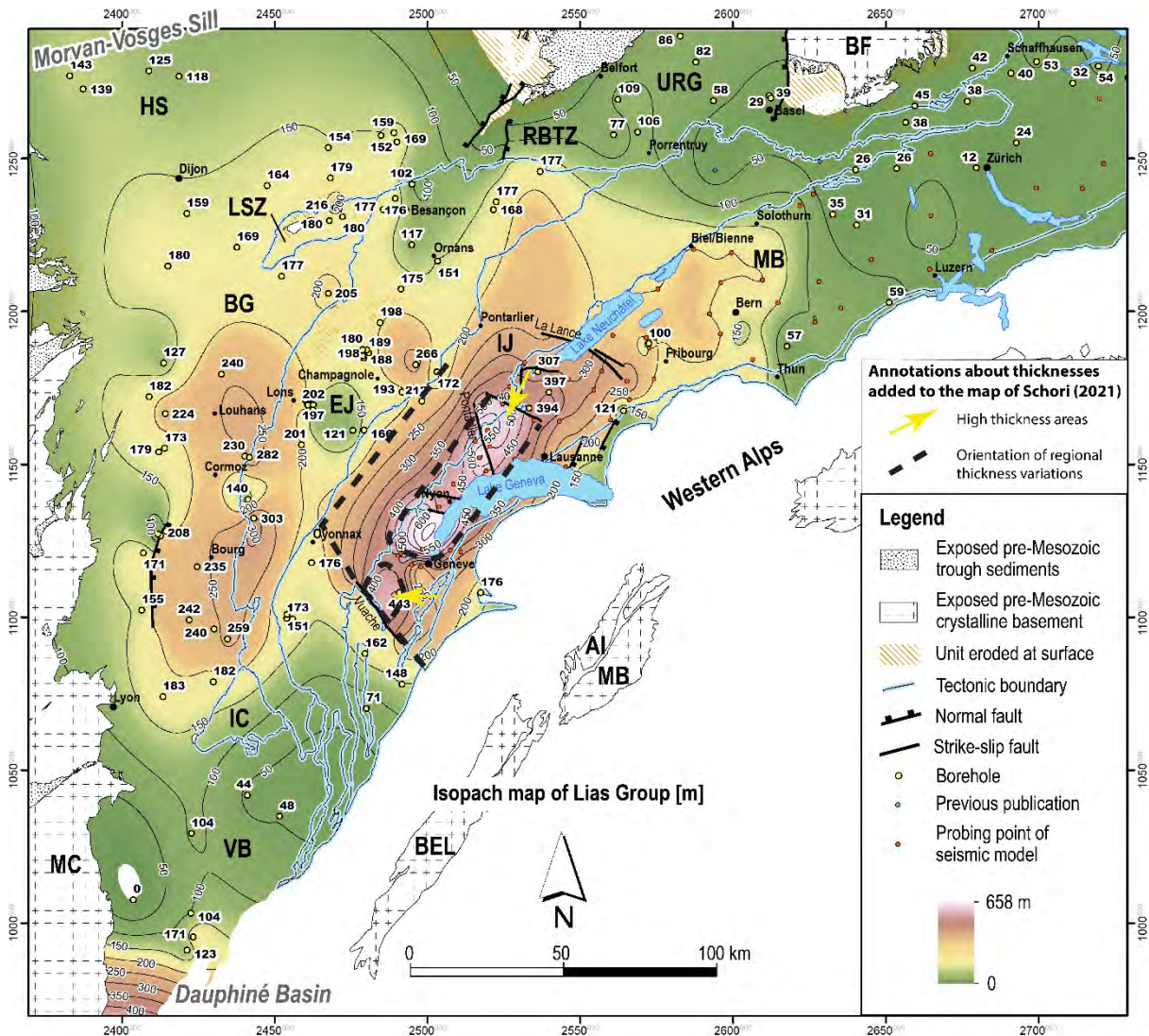


Figure 6-57 : Regional Isopach (from well data) of the Lias unit from Schori (2021). High thicknesses are located in between Pontarlier-Oyonnax-Genève-Fribourg. The Vuache FZ is clearly playing an important role in the deposition of this unit (higher thicknesses on the NE part of the fault). These observations are in line with our seismic interpretation results that suppose an extensional origin (Lias-Dogger) of the Vuache FZ with syndepositional activity during that period (growth fault).

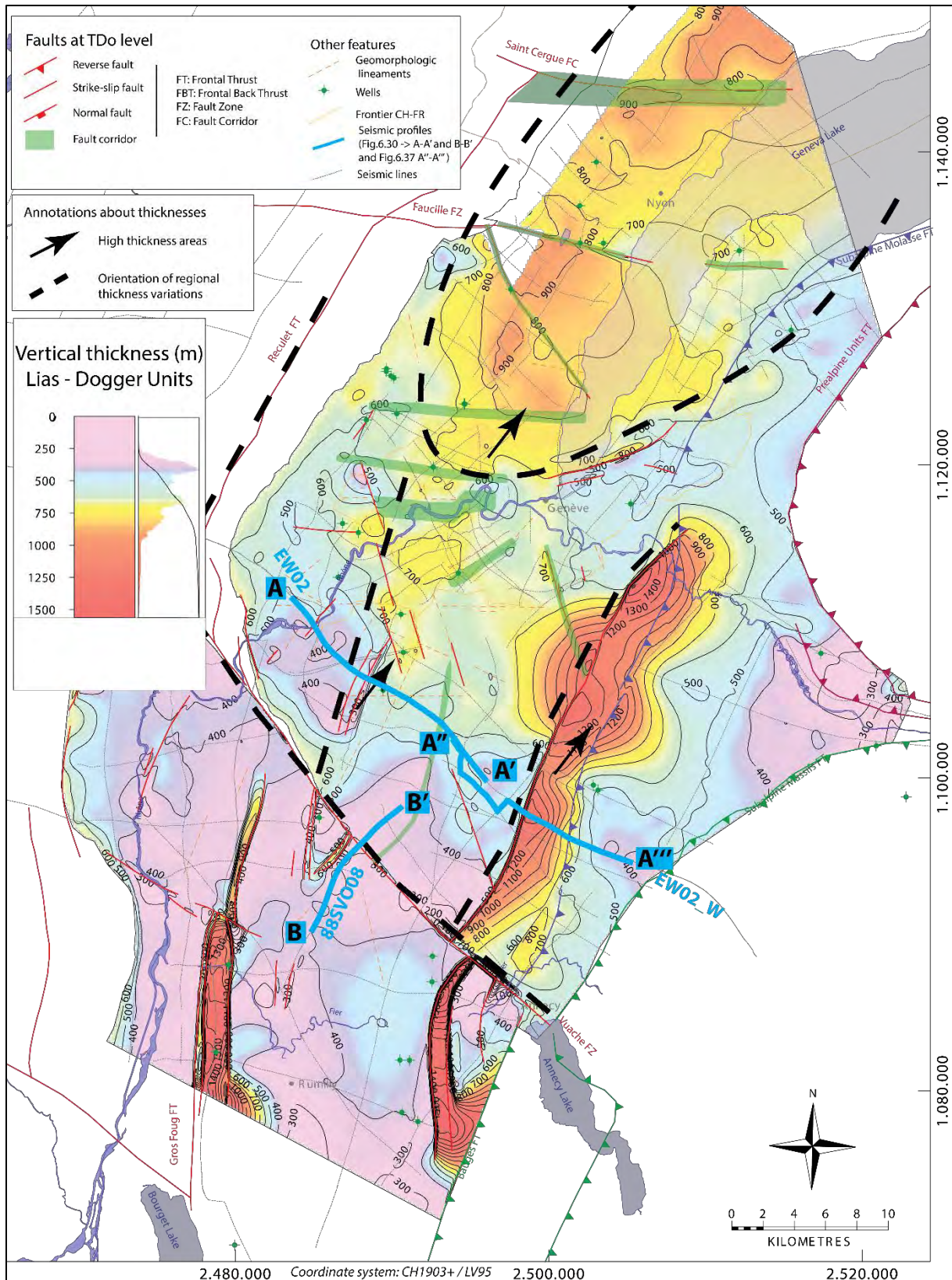


Figure 6-58 : Regional thickness map of the Lias-Dogger units resulting from our seismic interpretation work. Higher thicknesses are visible along the Vuache-Humilly-Salève structure, linked to syn-sedimentary extensional activity during the Liassic-Dogger interval (see 6.3.2 and 6.3.3). The high thicknesses observed along the Gros Foug and Montagne d'Âge are linked to tectonic duplications. For further description of seismic horizons of nTDo and nTLi and seismic facies of Dogger and Lias intervals, see 4.1.6 and 4.1.7. See Figure 6-30 for localisation of sections AA' and BB', and Figure 6-37 for localisation of sections A''A''' (called AA' on Figure 6-37).

6.4.2 The Malm reef complex

The results of our investigation on the Malm reef complex is specifically detailed in this part, because it represents a promising geothermal reservoir (high porosity-permeability properties, (Meyer, 2000; Moscariello et al., 2020; Rusillon, 2017)).

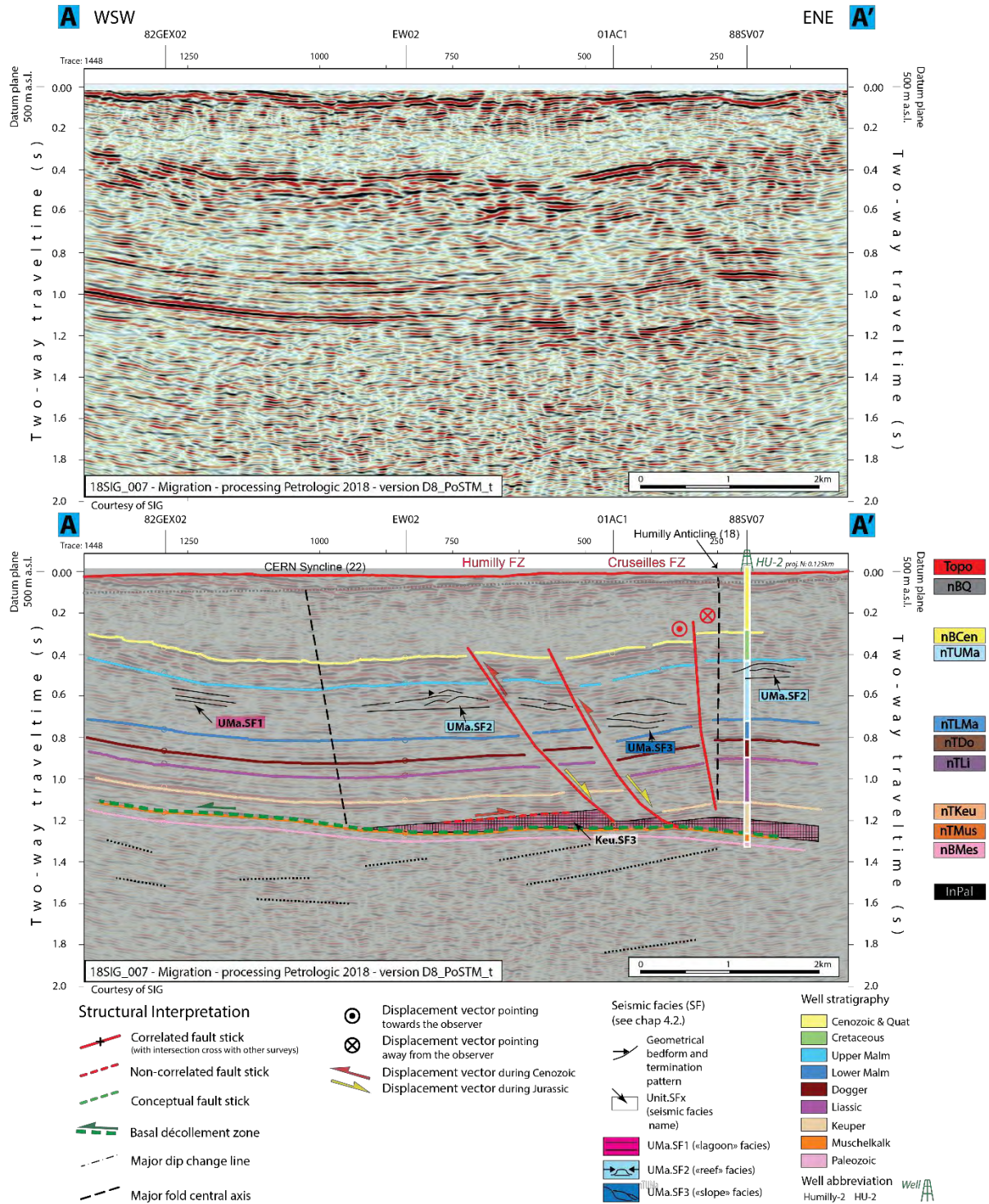


Figure 6-59 : Seismic interpretation of line 18SIG_007 located in the Humilly area (see structural results on part 6.3.2 and localization on Figure 6-62). Seismic facies of the Upper Malm unit are drawn on this section, and highlighting the favorable development of reefal complex (UMa.SF2) along paleo-topographical highs (here on the footwall of the Jurassic extensional Humilly FZ, or on the associated rollover Humilly anticline). See Encl 25 for detailed seismic interpretation of line 18SIG_007. For further description of seismic horizons of nTLMa and nTMa and seismic facies of Malm interval, see 4.1.8 and 4.1.9.

Reef complexes are part of the Upper Malm Unit, more specifically from the Kimmeridgian/Tithonian age. They are part of an overall regressive trend of the Upper Jurassic that starts with the deep marine environment of the Oxfordian and ends with continental deposits at the beginning of the Cretaceous. The main reef complexes belong to the “Ethiolet Formation” according to the recent HARMOS classification (Brentini, 2018; Rusillon, 2017)). This Formation consists of diachronous deposits developed on a large, shallow carbonate platform (coral-microbial patch reef system, Rusillon (2017)). We attempted to associate a seismic facies to this type of complex, (UMa.SF2, see 4.1.9) with a mound-shape geometry and low amplitude/frequency texture (Paumard et al., 2017). This approximation consists of linking geophysical data (seismic facies) with a lithological interpretation (bioconstructed limestone), and a sedimentological interpretation (reefal depositional environment). As very few wells control this interpretation, there is therefore a very high uncertainty attached to this interpretation. In order to help the identification of reefal seismic facies, we use the surrounding seismic facies that the sedimentology proposes. In that sense, we tried to interpret UMa.SF1 (see 4.1.9) seismic facies that corresponds theoretically to a lagoon environment, and UMa.SF3 matching a slope of carbonate platform environment. The succession of these three seismic facies allows characterizing the entire sedimentological context.

The Carbonate platform is supposed to be oriented along an axis striking NE-SW with a deepening of the basin southeastward. The Jura Haute Chaîne appears as a sedimentary boundary dividing a more proximal environment in the NW to a more distal position in the Greater Geneva Basin (GGB). The isopach map of the Upper Malm of Schori (2021) is clearly supporting this trend, with the highest thicknesses of the unit inside the GGB following the Haute-Chaîne of the Jura (Figure 6-61). Meyer (2000) and Rusillon (2017) agree on the fact that the patch reefs developed initially on inherited structural highs, such as footwall of normal faulting (Figure 6-59). Therefore, the understanding of the structural configuration at the time of the deposition may help identify favorable patch reef growth areas. Conversely, the identification of patch reefs and the trends of deposition may provide information about the topography and structural highs during the Upper Malm units, and therefore could bring details about possible tectonic inheritance. We have interpreted most of the seismic lines of the GVA basin, regarding the seismic facies of the Upper Malm (Hauvette, 2020). To do so, we have used seismic attributes (pseudo-relief, paraphase, and running sum, see 4.2.1 for details) for additional support of the interpretation. Indeed, it may help to characterize the geometry and the texture of the seismic facies. Two concepts are confirmed by our interpretation. First, it has been observed that the basin is oriented NE-SW, with a deepening of the system southeastward. Indeed, our final thickness map of the Upper Malm (Figure 6-62) is following this trend, with a large band of higher thickness located in the middle of the basin in the same orientation. This band may correspond to the highest depocenter axis of the carbonate platform. The polarity is in line with the theory, with the classical succession of seismic facies UMa.SF1 (lagoon), UMa.SF2 (reef), UMa.SF3 (slope of carbonate platform), developed mainly from NW to SE (Figure 6-60). This orientation of the basin is also confirmed by the clear presence of progradation sigmoids dipping southeastward (Figure 6-60). The second main result concerns the structural inheritance of the sedimentary trend of the growth of the patch reefs. We have observed in several locations, that reef indications may be developed preferentially in relation to the footwall of the normal faults present at the time of the deposition. Indeed, the region was in an extensional rifting phase during the entire Jurassic period. We have seen in previous parts, the identification of a large-scale extensional system initiated during the Liassic period; the Humilly-Vuache-Salève FZ. We have particularly analyzed the Humilly structure. The Humilly rollover anticline

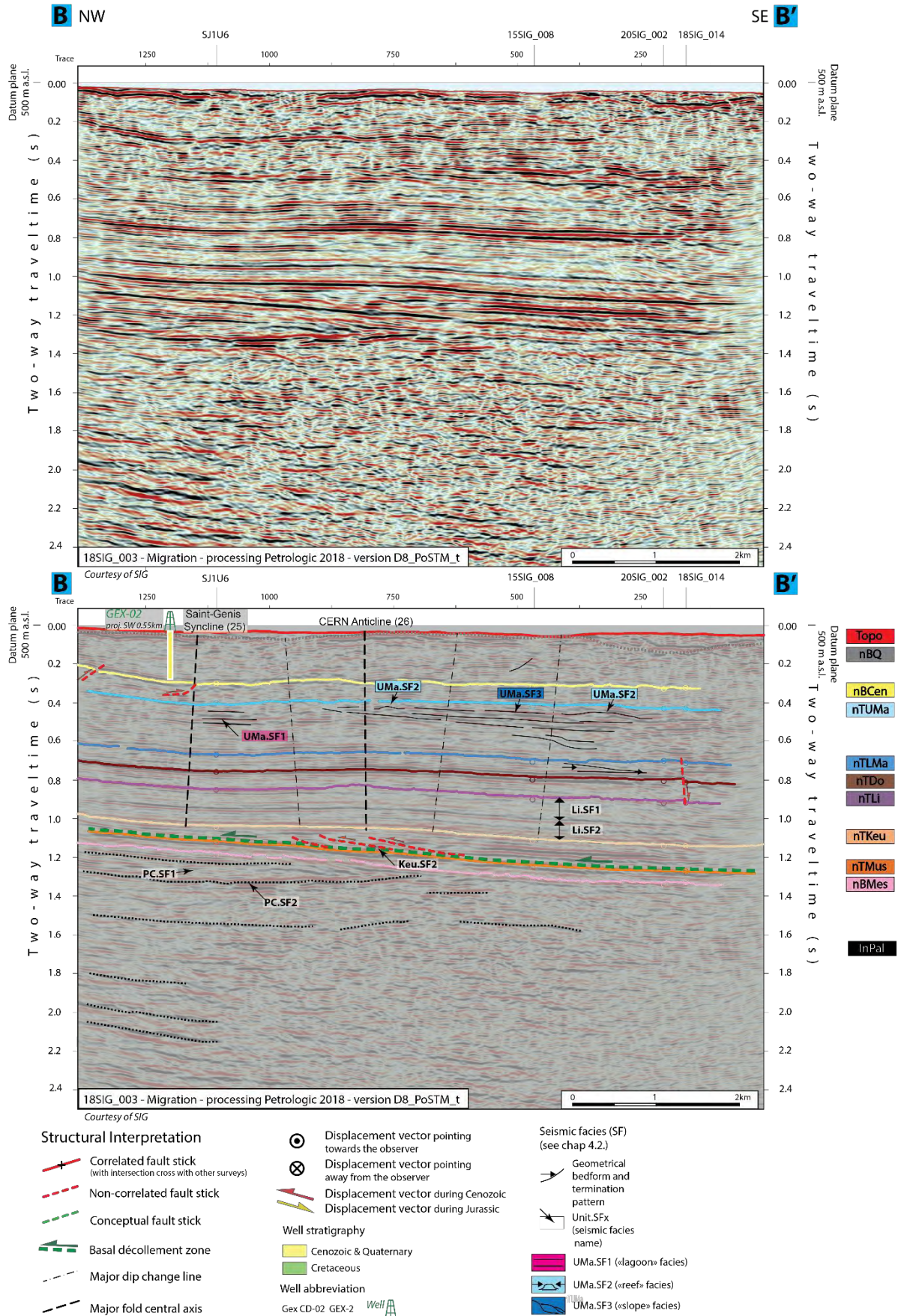


Figure 6-60 : Seismic interpretation of line 18SIG_003 (localization on Figure 6-62). Seismic facies of the Upper Malm unit are drawn on this section, and highlighting a classical succession of "lagoon-reef-slope" related seismic facies from NW to SE. See Encl 21 for detailed seismic interpretation of line 18SIG_003.

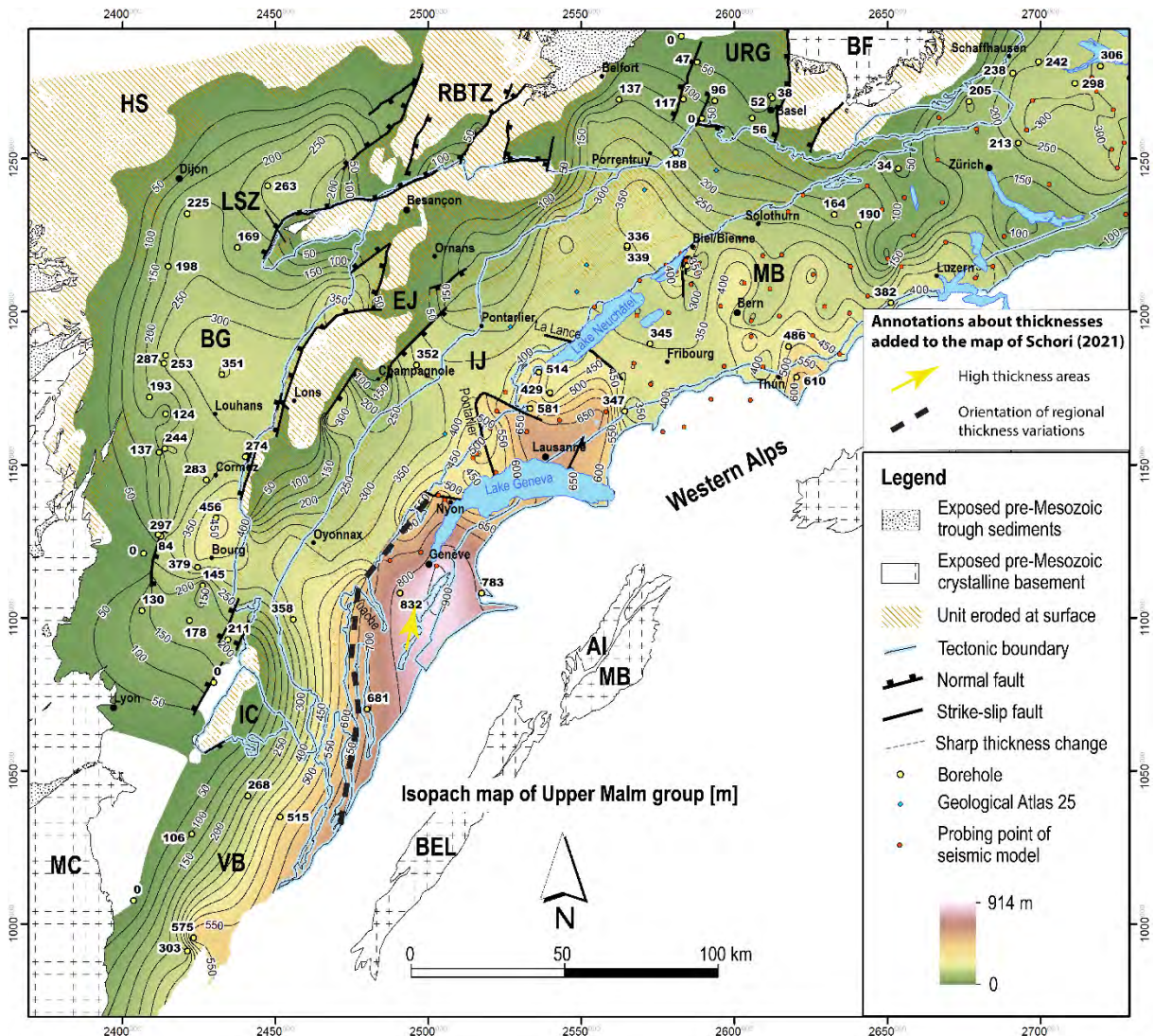


Figure 6-61 : Regional Isopach of the Upper Malm Unit from Schori (2021), based on well data. It confirms the position of the depositional basin during the Upper Malm period with deeper depositional rate in the Greater Geneva Basin with an overall NE-SW striking orientation (polarity with proximal NW pole and distal SE pole).

is drilled by Humilly-2 (Hu-2) well in which reef structures have been interpreted in the Kimmeridgian series (Rusillon, 2017) (see Figure 6-59). Alongside this observation, the seismic facies corresponding to a reef (UMa.SF2) is interpreted around the Hu-2 reefal indices, but also along the footwall of the normal growth fault (Figure 6-59). Moreover, the regional paleogeographical mapping from Meyer (2000) proposed a bending of the basin along the Vuache FZ, attributing therefore to this fault zone a structural inheritance in relation to the development of the carbonate platform. In that sense we can conclude that reefal barriers or patch reefs may developed preferentially along the strike orientations of the interpreted extensional large-scale system of the Vuache-Humilly-Salève FZ. The footwall part of these normal faults and the faulted rollover anticlines represents favorable inherited highs for the growth of reefal structures.

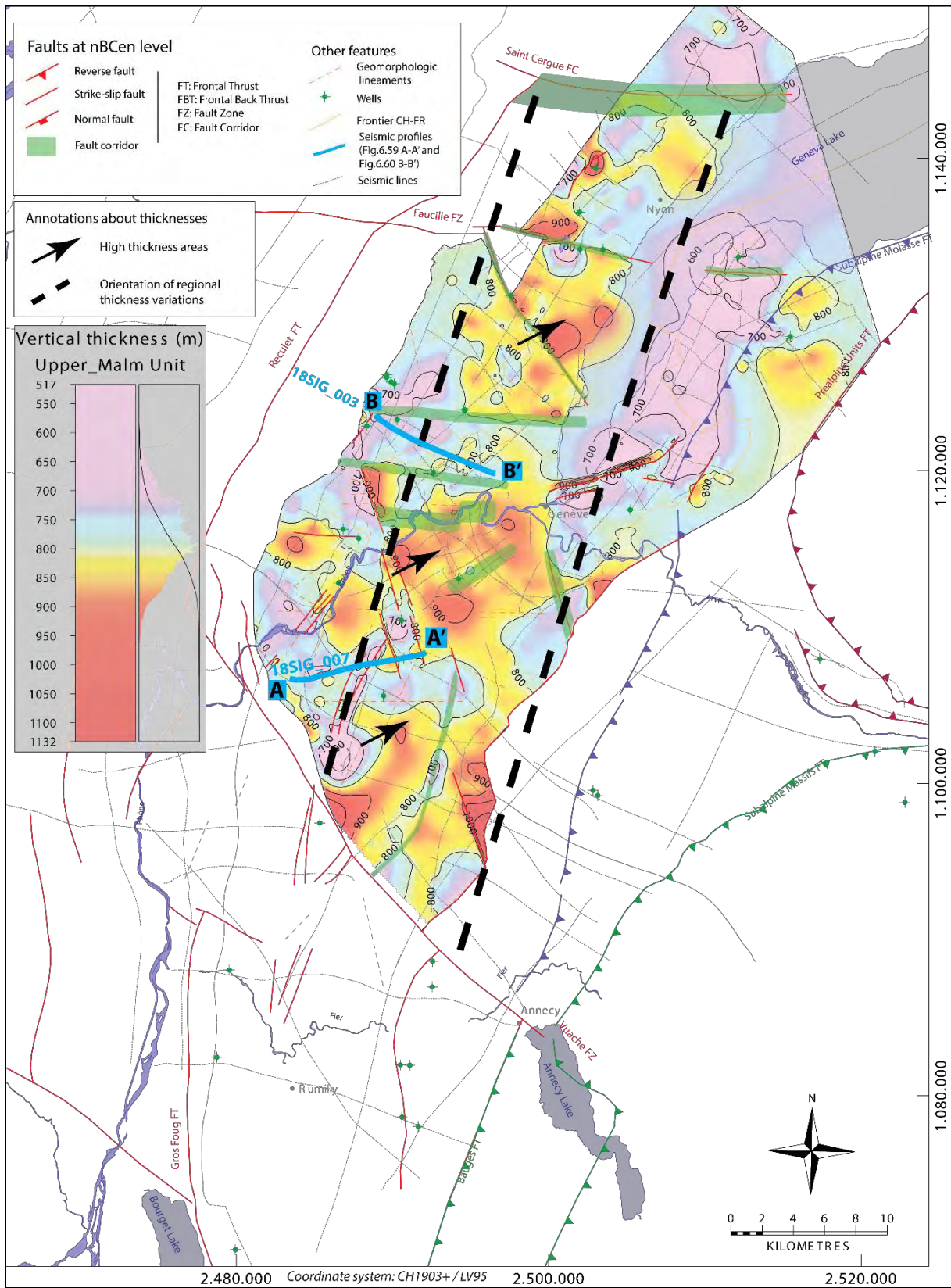


Figure 6-62 : Malm thickness map resulting from the seismic interpretation inside the Geneva Molasse Basin (Geneva Molasse Basin Velocity Model 2). It confirms the overall NNE-SSW striking orientation of the sedimentary Upper Malm basin (polarity with proximal NW pole and distal SE pole). Localization of Figure 6-59 and Figure 6-60 are represented as blue lines.

6.4.3 The Mesozoic-Cenozoic boundary and the Siderolithic deposits

A major geodynamic change occurs at the transition Cretaceous-Tertiary. Indeed the European platform, including the broader Jura realm is witnessing the arrival of the orogenic wedge and is progressively subjected to flexural bending of the lithosphere under the influence of the orogenic load. The sedimentary and erosional changes of this transition are recorded in the “Siderolithic series” dated from the Eocene period. The deposits are unevenly spread, and very varying in thickness. They often lie on the erosional surface on top of the Cretaceous series, inside karst systems, along fault planes or in topographical depressions (Serneels, 1993). However, a stratiform deposition has also been observed, and therefore a fluvial origin is suggested by several authors (Conrad & Ducloz, 1977; Weidmann, 1984). Wind dune deposition is also a possible hypothesis (Chablais & Savoy, 2021; Conrad & Ducloz, 1977). The discovery of the unexpected high thickness of 140m of these sediments in the recent well G_{Eo}-02 in 2017 (Chablais & Savoy, 2021), in the center of the GVA basin, has relaunched an interest in the geological understanding of this layer.

As discussed, paleotopography may be strongly linked to inherited structures such as faults, possibly inverted or/and newly formed. Thus, during the late Eocene, the Siderolithic erosional “event” can be assessed in the frame of extensional faulting due to flexural bending of the Alpine foreland (Gruber, 2017; Schori, 2021), which may create, locally, important surface variations and offsets. Moreover, the flexural bending of the lithosphere may reactivate inherited extensional structures (Jurassic). The faults may be subject to intense karst dissolution processes during this period and therefore form privileged depositional traps for Siderolithic sediments.

Thanks to the surprising occurrence of the Siderolithic in well G_{Eo}-02 (140m thickness), we were able to identify on neighboring profiles a potential seismic facies (Eoc.SF1, see 4.1.10) corresponding to these Eocene deposits. It consists of oblique to hummocky geometries of seismic reflections with high to moderate amplitude and frequency appearance. This seismic facies is typical of fluvial deposits (Ge et al., 2018; Moscardelli et al., 2012), and represents stacked channels on top of eroded valleys. We have used this signature to interpret several seismic profiles in three areas, where potentially a certain thickness of Siderolithic (up to around 150m thickness) is expected (see map of Figure 6-63 and seismic interpretation on Figure 6-64 and Figure 6-65). The first area is comprised in between the “Allondon FZ - Cruseilles FZ” axis, the “Meyrin FC - Cologny FZ” axis and the Salève FT. The interpretation of seismic facies Eoc.SF1 was propagated from well G_{Eo}-02 Siderolithic indices and stopped against the three main structural axes mentioned above. This delimitation remains relatively arbitrary, as there is not enough systematic drilling occurrences to constrain more accurately this boundary. Indeed, several wells (GEX CD-2-3-4-5-6, Hu-02, Th-01) outside our central seismic facies area, have encountered Siderolithic sandstones at the Cretaceous-Cenozoic boundary, but very often with thicknesses below the seismic resolution (less than 25m). We have mapped areas of the presence of substantial thicknesses of seismic facies Eoc.SF1 (up to 150m). Inside this central zone, it seems that a series of fluvial channels are developed in the NE-SW direction as section A of Figure 6-64 is highlighting. These sedimentary features are parallel to the Bernex FC that probably influenced the paleotopography and therefore the transport of the sandstones. The second area is located north of Mourex FC (see section C of Figure 6-64), where a very strong truncation of Cretaceous layers is interpreted. A logical depression then appears above the truncation that stops southwestward against the Mourex FC. There is no drilling to confirm this interpretation, which is therefore very speculative.

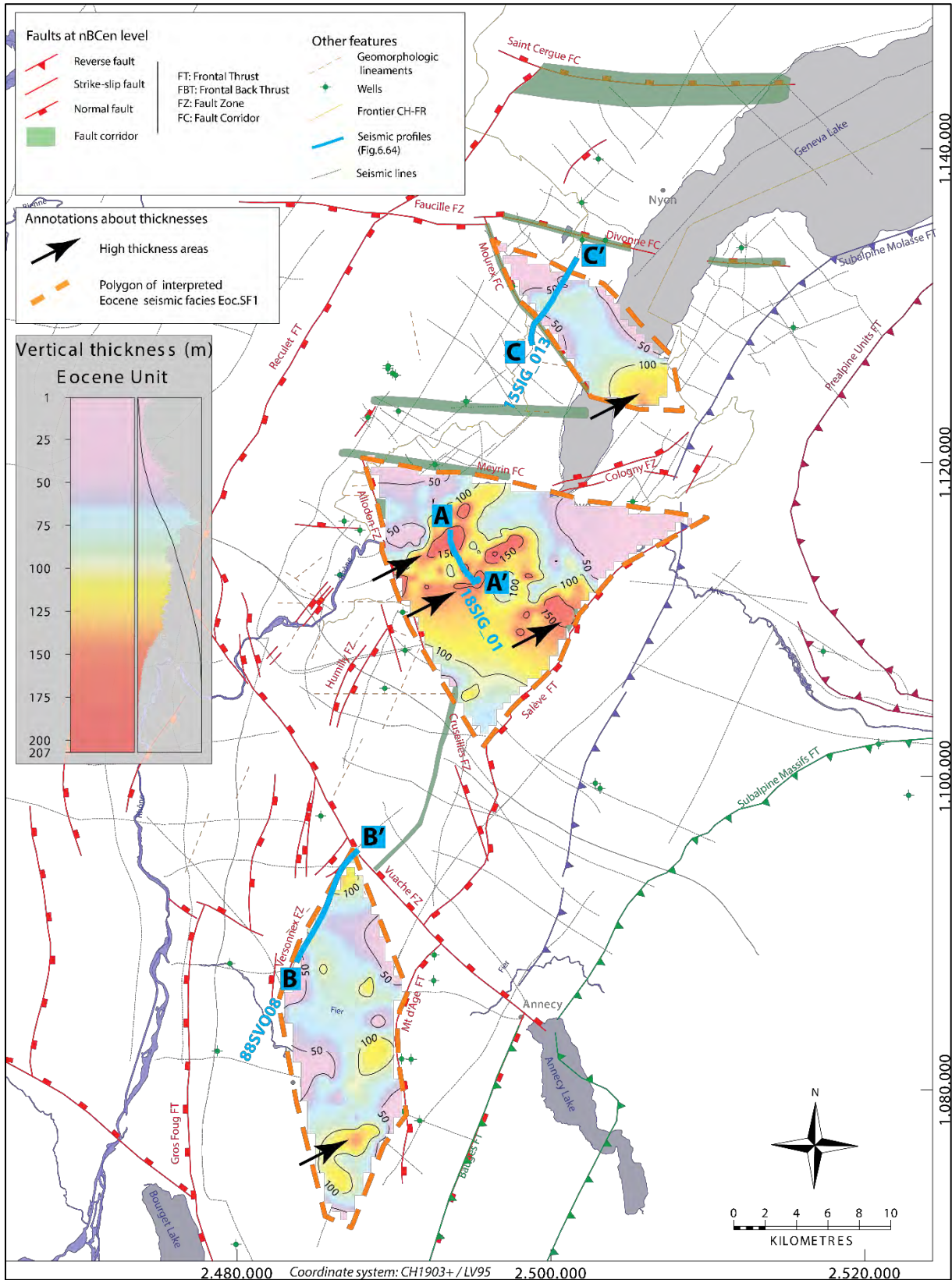


Figure 6-63 : Orange dashed lines: Areas of interpreted seismic facies related potentially to the Siderolithic deposits. The thickness in meters of this interpreted interval (in between nBCen and InCen seismic horizons) is shown inside the three polygons. In the central area, channels are visible along NE-SW orientation). Localization of sections of Figure 6-64 is represented as blue lines.

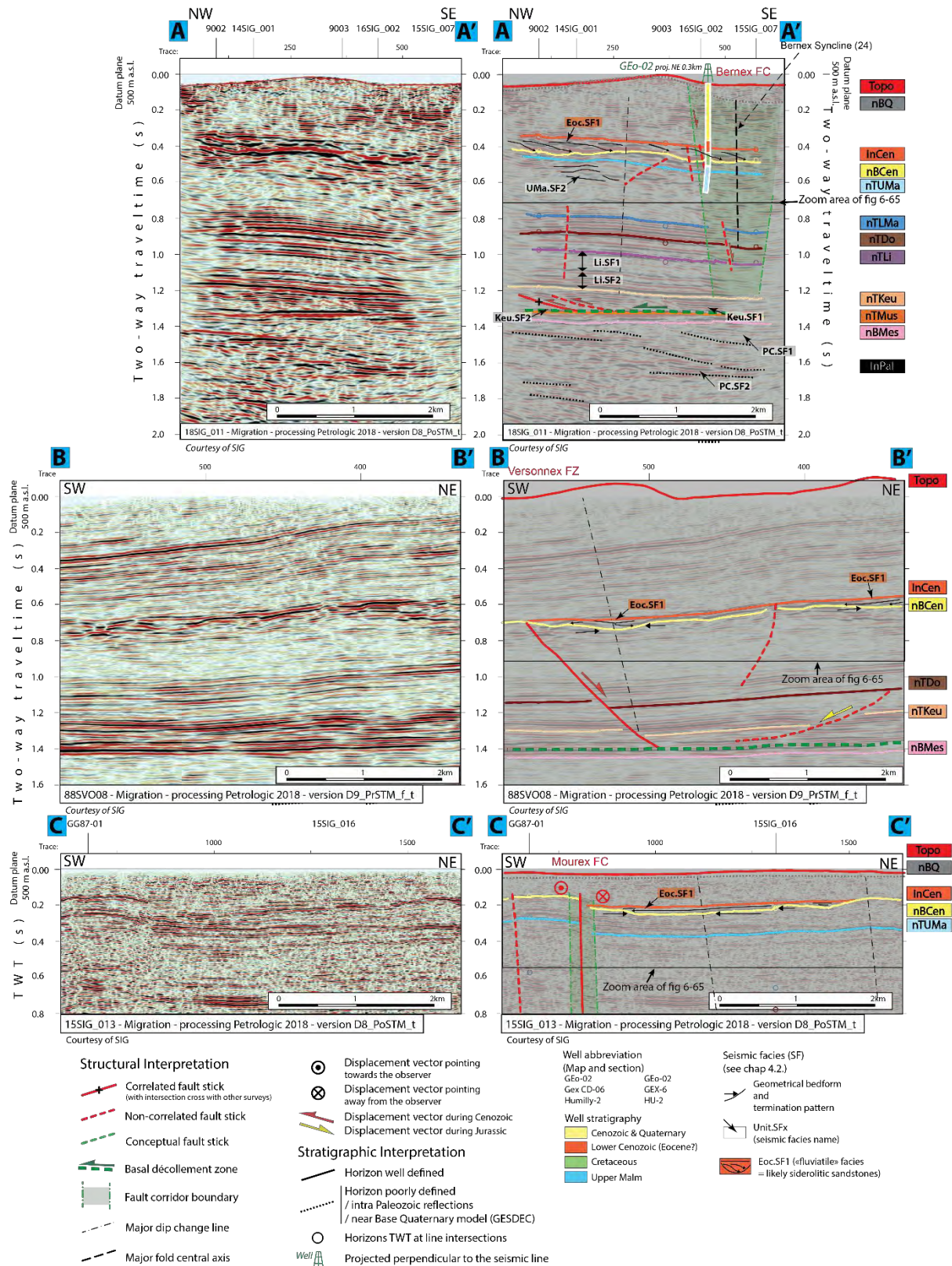


Figure 6-64 : Siderolithic seismic interpretation, with represented seismic facies Eoc.SF1 deposited on top of nBCen seismic horizon. On top is section A in the center of the GVA Molasse Basin. In the middle images is section B located in the Rumilly Molasse Basin. On bottom images is section C in the north part of our study area. Note the termination patterns of the seismic facies that correspond to fluviatile deposits. See respectively Encl 29, Encl 52, and Encl 15 for detailed seismic interpretation of lines 18SIG_011, 88SVO08 and 15SIG_013. See Figure 6-63 for localization of the three sections AA', BB' and CC'. See Figure 6-65, for zoomed interpretation of these sections.

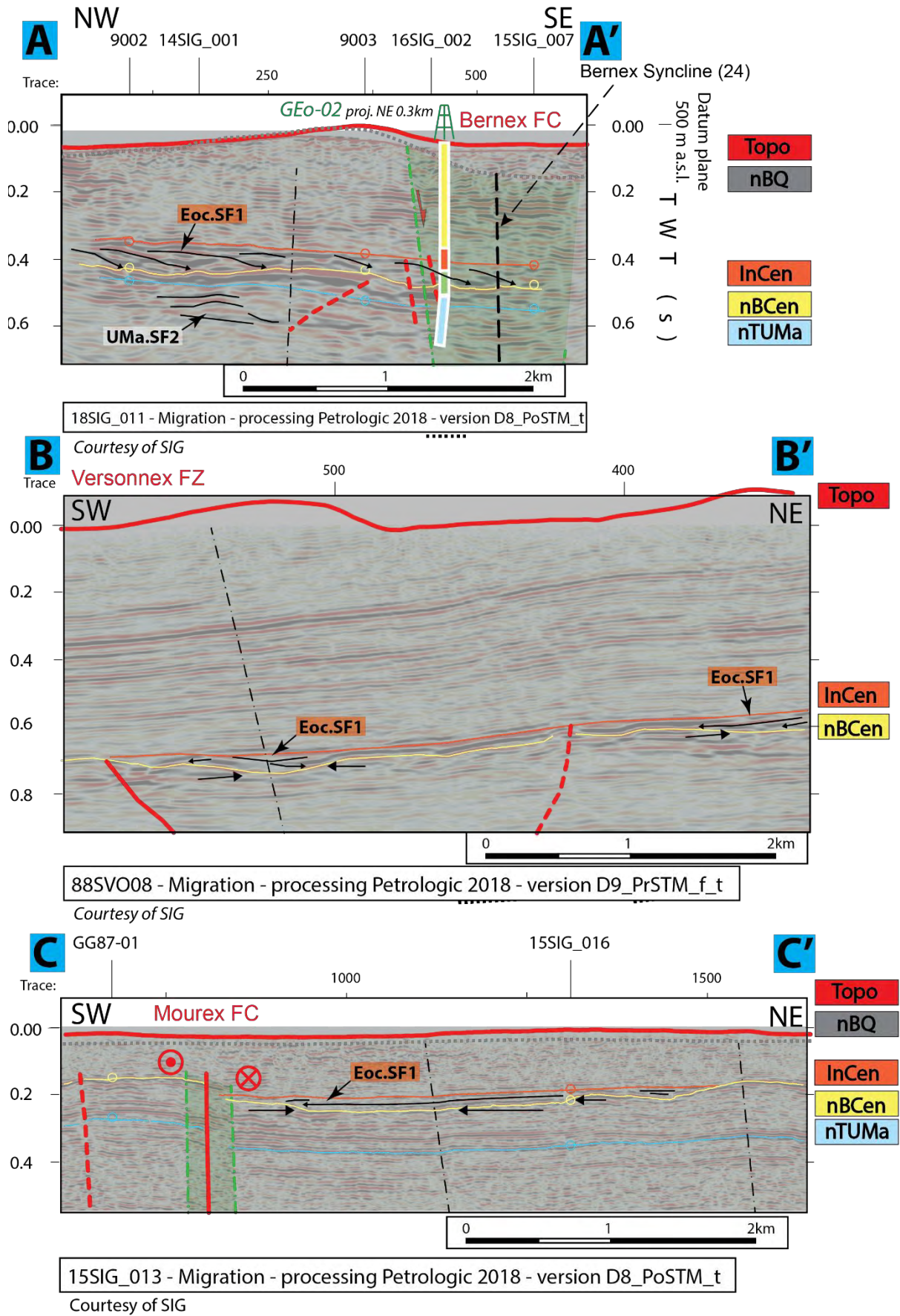


Figure 6-65: Siderolithic seismic interpretation in zoomed areas of lines 18SIG_011, 88SVO08 and 15SIG_013, extracted from Figure 6-64. For legend and annotations, refer to Figure 6-64. See Figure 6-63 for localization of the three sections.

In that sense, the relationship between this seismic facies of this area and the Mourex FC cannot be explained.

The last area of interpreted Eoc.SF1 seismic facies is located in the Rumilly basin south of the Vuache FZ and NW of the Mt d'Âge FT (see section B of Figure 6-64). We see very clearly there, the strongly eroded Cretaceous layer, filled by this Eocene seismic facies units. The top of it the system appears sealed by monoclinical straight Molasse seismic reflections. This infill is developed against the Versonnex FZ striking NE-SW with normal component dipping SE. There is no drilling to confirm this hypothesis, but the image being of high resolution, we can deduce the likely pre-existence of this fault zone in relation to the Eocene deposits. This would date this fault to either Jurassic extensional period or to the flexural bending of the lithosphere during the Eocene times.

These results do not preclude the possibility of finding Siderolithic series outside our areas of specific investigation. It does not insure either a Siderolithic presence, as there is a high uncertainty attached to such seismic facies interpretation. These results should be considered as a first prospective investigation to be expanded and refined.

7. GEOLOGICAL HISTORY

Our study of the subsurface tectonics and stratigraphy made it possible to unravel new information and clarify known information for the pre-Mesozoic, the Mesozoic and the Cenozoic periods of the geological evolution of the area of investigation. Especially five tectonic events/structures (labelled **(1)**; **(2)**; **(3)**; **(4)** and **(5)** hereafter and represented on maps of Figure 7-2, except for **(1)** that cannot be displayed) will be discussed in the following in light of the newly interpreted kinematic setting in the frame of their geological history. Please refer to “the Geodynamic summary of the Greater Geneva Basin” on Figure 2-9 for visual chronology of stratigraphy and tectonic.

7.1 Late Paleozoic

In late Paleozoic times large half grabens, infilled with Permo-Carboniferous clastic sediments, have been known to be present below the Western Molasse Basin and the Jura FTB. They have been locally drilled such as, Chatelblanc-1, La Tailla-1, Essavilly-101, and Treycovagnes-1, (see Schori (2021), and Figure 2-4 for localization) and are well documented from seismic surveys in northern Switzerland (such as the Constance-Frick Trough, see Madritsch et al. (2018); Naef & Madritsch (2014)). Similar grabens are also outcropping in the External Crystalline Massifs such as e.g. in the Rhône valley the Sa Ivan-Dorénaz half-graben (Capuzzo & Wetzel, 2004)). The Permo-Carboniferous terrestrial sediments are also found on the graben shoulders and beyond. In our study area such basins have been revealed by deep wells in such as, Chaleyriat-1, Charmont-1 (more than 500m of P-C sediments drilled), Chatillon-1d, Faucigny-1, Chapery-1, see Figure 2-4, Figure 2-5 and Figure 2-6). However, the directions and locations of the bordering normal faults of these grabens have always remained uncertain (Gorin et al., 1993; Signer & Gorin, 1995). The quality and/or resolution of the seismic data available does not allow to propose a much improved image, but the following observations can nevertheless be ascertained **(1)**: A change of the dipping angle of the near Base Mesozoic horizon is observed from 3.25° SE in the Molasse Basin to 1.7° SE in the internal Jura part alongside the Reculet FT (Figure 6-10); as well as below the first chain of the Meridional Jura FTB part to the SW, at the boundary with the Rumilly Basin in an approximately NE-SW to NNE-SSW strike direction.

This, well documented major dip change of the mechanical basement at the transition of the Geneva Molasse Basin and the Jura FTB is possibly related to the presence of a half graben with P-C sediments infill developed along the NE-SW striking SE-dipping normal basement fault underlying the present backlimb of the Reculet FT (Marro, 2021; Signer & Gorin, 1995), see Figure 6-54. This change in dip appears to occur everywhere at the transition between Jura FTB and Molasse Basin and has locally been interpreted as a step linked to inherited faults (Schori (2021); Marro et al. (2023)).

Concerning the main dip change of the Rumilly Basin – Internal Jura transition, we follow the hypothesis of Guellec et al., (1990) proposing a horst structure in the basement with bordering faults oriented NE-SW to NNE-SSW, between the first chain of the Internal Jura to the SE, and the location of the Oyonnax FBT (Frontal Back Thrust) to the NW (Figure 6-45). The presence of gneiss in the pre-Mesozoic unit found in the well La Chandelière-1D located in the uplifted area (Figure 2-6, Figure 6-52 and Figure 6-53), supports this idea of a major basement horst structure. The western shoulder of the horst may be associated with Permo-Carboniferous sediments, as attested by the well Charmont-1

(more than 500m P-C deposits) (see also Schori, 2021). In this zone, the northwestern shoulder may in fact be associated with a northwestward-vergent inverted half graben as imagined by Philippe (1995).

Even if it is partly attenuated in the depth domain after time-depth conversion (Figure 6-38 and Figure 6-39), another gentle basement high appears to be present below the Gros Foug Mountain, as underscored by a dip change and therefore a possible N-S to NNE-SSW normal basement fault on the eastern side of the structure (Schori, 2021).

Also, the depth of the near top Basement is clearly stepping down from a high position in the Geneva Basin to a lower position in the Rumilly Basin area across a NW-SE line parallel to the Present day Vuache FZ. This vertical offset in the mechanical basement below the Vuache FZ should, however, not be directly related to the overlying Mesozoic structural setting. Indeed, the latter is supposed to have been initiated in the Jurassic period as an extensional, syndepositional fault system (Figure 6-23, Figure 6-26 and Figure 7-1) and has subsequently been transported (and deformed) by some 25 kilometers northwestward during the Miocene compression. Indeed, Schori (2021), based on analogue modelling demonstrates that the thrust geometries to the N-NW of the Vuache FZ (25km distance) are diagnostic of thrusts developed over an oblique basement ramp or step when initially formed, thus making it possible to assess the position of the original basement structure initiating this fault and fold complex (Schori et al. 2021).

Thus, variations of the basement topography suggest the presence of Pre-Mesozoic normal faults, which can be interpreted as post-Variscan tensional half graben and horst structures. However, the suggested basement faults mentioned above, that don't have neighboring wells showing P-C evidence, were not necessarily formed in the Paleozoic times. Indeed, they can also be triggered for example during the Eo-Oligocene down-bending lithospheric flexure, during rift opening of the ECRIS system or during Jurassic syn-rift extension related graben formation/reactivation.

Similar steps in the basement that could have been interpreted from time seismic lines beneath the Mont Salève crest (pull-up effect questioned already by (Guellec et al., 1990)), in fact shows a flat near top basement surface when depth converted with our process (Figure 5-12 and Figure 6-32).

7.2 Triassic

Following the wide spread erosional event at the end of the Paleozoic era which led to the formation of the post-variscan erosional surface and the deposition of lower Triassic marine and near shore marine sandstones, the middle and upper Triassic series are characterized by important evaporite deposits which contain various amounts of pure salt (S.N.P.A, 1969; Schori, 2021). These layers play a key role in the tectonic and mechanical development of the detachment and the deformation of the detached Alpine foreland. Their rheological properties allow them to host the main décollement; especially the pure salt layers which accommodate the main deformation (Sommaruga et al., 2017, and references therein). Although the main décollement should be considered as a broad zone with distributed zones of higher strain and a succession of thrust surfaces (Sommaruga et al., 2017), for reasons of simplicity we position the main décollement surface at the base of the Keuper Group (chapter 6.2 and Figure 6-6). The present thickness of this Keuper Group layer changes across the study area, forming local lens-shape zones. This thickness increase is most likely linked to salt flowage and/or formation of tectonic duplexes during the Miocene compressional evolution of the foreland (Figure

6-8, Figure 6-9 see also Sommaruga (1997)). Locally, thickening of the evaporitic levels can be observed in association with inverted extensional structures related to syndepositional normal faulting in Jurassic times (Figure 6-30). In our area, the highest Triassic thickness observed is located in the Jura Mountains (Figure 2-4, Figure 2-5 and Figure 2-6), where an intense deformation occurred.

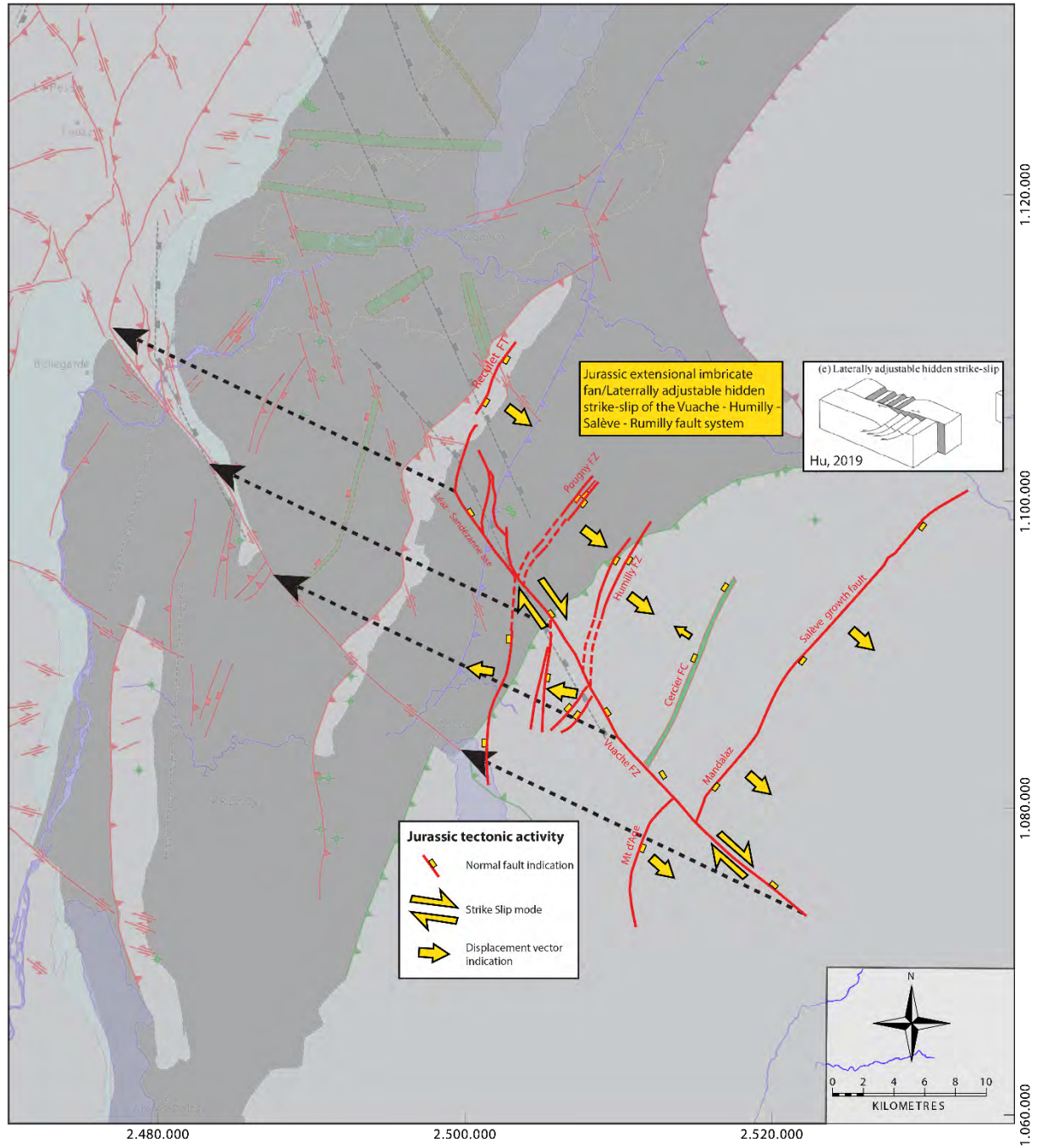
7.3 Jurassic

During the Jurassic period, syn-sedimentary extensional structures developed in the epicontinental depositional environment of our study area. They can be linked to wide-spread extension associated with the opening and rifting of the Alpine Tethys to the S-SE. These normal, listric faults show very steep dips as seen on the seismic surveys (up to 60 degrees in the uppermost part of the faults, Figure 6-30).

A detailed analysis of seismic facies made it possible to propose links with syn-depositional tectonics. The seismic facies analysis helped collecting stratigraphical information. Thus, the Lias layer thickness is varying more than all other Jurassic layers, suggesting a stronger tectonic activity responsible of the lateral thickness changes (see. Part 6.3.2). The NW-SE striking Vuache FZ is likely to have played a major role as a barrier mostly during the Lias period (chapter 6.4.1). Thickness maps derived from seismic interpretation (see Encl_M36 to Encl_M52 and chapters 6.4.1 and 6.4.2), show a depositional trend along an overall NE-SW striking axis during the entire Jurassic period. This is also suggested by 'onlaps' (seismic geometrical features) of Dogger Group layers in northwestward direction and thickness variations indicating an overall trend for a proximal-distal axis in a NW-SE directions.

Following the end of the Alpine Tethys opening phase during the Late Dogger, an overall regression of the Malm unit, and particularly the reef complex unit of the Kimmeridgian can be characterized by seismic facies analysis (chapter 6.4.2). Using a tentative association of seismic facies with depositional environments as proposed by (Paumard et al., 2017), we have interpreted from NW to SE, a classic succession of depositional environments of a reefal carbonate platform with a lagoon-reef-slope transition in the Meyrin area (Figure 6-60). Seismic facies corresponding to a reefal barrier or isolated patch reefs appear in favorable positions along the footwall of normal faults, like in the Humilly FZ (Figure 6-59). The Jurassic-Dogger normal faults thus create a topographic high in the footwall of the fault yielding a suitable elevated position, possibly favoring the development of reefal complexes. The Vuache FZ having also at that period a normal structural component, linked to the Humilly FZ, could thus be an ideal location to host the development of reefal complexes in its footwall, which is in line with outcrops of this formation in the northern part of the Vuache FZ (Meyer, 2000; Rusillon, 2017).

Our study thus, revealed a large-scale (40km long laterally) pull apart extensional fault system in the Humilly-Vuache area (**2**). This structural system possibly stretches the entire foredeep zone (possibly 40km long in NW-SE), along a 15km-20km band along the Vuache FZ. This structural setting is characterized by an extensional imbricated fan (Hu et al., 2019), (see Figure 6-30) associated with a main bounding fault perpendicular to the imbricates. In the Humilly area a NE-SW normal fault dipping SE is very clearly recognized with syn-sedimentary activity/offset mostly during the Liassic and slightly during the Dogger (see Figure 6-30). Higher thicknesses of these layers are observed in the hangingwall of the listric structure, which reaches the base Keuper level. Parallel faults with similar geometry are also present in the Pougny FZ (but without thickening of Lias-Dogger units but slightly during the Malm,



Legend of background Structural Map

Faults in Mechanical Basement
(difficult to confirm on the interpreted data of this study)

- Normal fault from wells and cross-sections (Schori 2021)
- Normal fault from lineament restoration (Schori 2021)

Main Faults at nBCen (near Base Cenozoic)

- Reverse fault
 - Strike-slip fault
 - Normal fault
 - Fault corridor
- FT: Frontal Thrust
FBT: Frontal Back Thrust
FZ: Fault Zone
FC: Fault Corridor

Areas

- Molasse Basin (Quaternary or Molasse outcrops)
- Mesozoic outcrops
- Cretaceous outcrops at the boundary between the Molasse Basin and the Jura fold and Thrust Belt

Other features

- Wells (Geo-01)
- Frontier CH-FR
- Bauges and Subalpines Massifs
- Front Thrust
- Prealpine Units Front Thrust
- Subalpine Molasse Front Thrust

Figure 7-1 : Vuache-Humilly-Salève structural system evolution from its extensional Jurassic origins (foreground) to its actual state after the Miocene deformation (transparent background). The displacement vectors (black dashed arrows) are taken from (Schori, 2021).

see Figure 6-23). These fault zones are interpreted to be all linked to a greater leading NW-SE fault, the Vuache FZ, which shows also synsedimentary activity. The Salève FZ also shows the same synsedimentary tectonic activity/offset during the Liassic-Dogger period (chapter 6.3.3). As a consequence, **(3)** the Salève FZ, like the Humilly FZ and the Pougny FZ are proposed to be an inherited Jurassic extensional faults, that were reactivated as steep reverse fault (thrusts) during the Miocene. An analogue structure (at a different scale) of the Humilly-Vuache-Salève FZ could be the Dead Sea strike slip pull apart basin (Smit et al., 2008). The retrodeformation of the Miocene compression is transposing the Vuache FZ 18-25km to the SE near to the present position of the Le Coin FZ along a potential NW-SE normal pre-Mesozoic basement normal fault that could have played a role in triggering the system (Figure 7-1). This normal fault is difficult to be confirmed it by seismic interpretation (see chapter 6) but we suppose it is likely present. Similar, normal faults are thought to be present in the Rumilly Basin as well with NE-SW strike directions. In that sense, a hypothesis is that the Musiège FZ, the Gros Foug FBT, are in fact part of the large-scale extensional Jurassic Vuache-Humilly-Salève FZ, but dipping NW (opposite dipping orientation than the Humilly FZ) (chapter 6.3.4). In that case, the fault system would then have a configuration of a “laterally adjustable hidden strike-slip” (Hu et al., 2019), around the leading dextral Vuache FZ (Figure 6-44).

7.4 Cretaceous to Eocene

The upper-most part of the Cretaceous series is marked by important thickness variations due to a strong early Tertiary erosion. This remarkable, well-known unconformity is well identified on the seismic sections with a strong amplitude contrast. In our area of study, well drillings have shown in many cases, unforeseen Siderolithic clastic deposits (Eocene) on top of the Lower Cretaceous layers, filling the eroded spaces along near Base Cenozoic horizon. These Eocene Siderolithic subaerial deposits are diagnostic of the Eocene continental erosive conditions. These deposits are frequently found in fracture or karstic systems. It is thus, possible to identify seismic facies geometries corresponding to karst and eroded valleys or base of channels that could correspond to these Eocene deposits, specifically in the Bernex area around G_{Eo}-02 well that met a surprising 140m thickness of that formation ((Chablais & Savoy, 2021), see part 6.4.3). According to our interpretation, this layer may have fluvial origins with deposit in large eroded valleys (Conrad & Ducloz, 1977; Weidmann, 1984). Elsewhere in our study area, and in absence of the Eocene Siderolithic deposits, the Lower freshwater Molasse units overlay the Mesozoic units in an unconformable contact. The preservation of Upper Cretaceous sediments in local spots (Valserine and Bellegarde area) and the reworking of these sediments into early Cenozoic deposits, in the rest of the basin (especially East of the Vuache Mountains (Charollais et al., 2007) indicates a highly probable paleogeomorphology present at the end of the Upper Cretaceous period. This fact supports the idea of a pre-Cenozoic structuration of the foreland basin in the area of study and therefore of the existence of the Jurassic tectonic structures developed around the Vuache FZ, presented in the above paragraph.

7.5 Late Eocene to Oligocene

During Late Eocene to Oligocene, the flexural bending of the European lithosphere induced a NE-SW trending foreland basin with a wedge shape geometry, with depositional onlaps towards the north and deepening towards the south (Homewood & Lateltin, 1988). Normal faulting of the Mesozoic and

Cenozoic units has been recognized in an overall extensional setting due to bending (Gruber, 2017; Schori, 2021 and references therein). These steep faults may form as structures, showing no related thickness variations in the Mesozoic cover, possibly as seen in the case of Pougny FZ (part 6.3.2) or Bellegarde FZ (part 6.3.4). Structures such as the Musiège FZ or Gros Foug FBT (part 6.3.4), which also do not show apparent Jurassic thickness variations, could also be inherited normal faults formed during this extensional period (Late Eocene to Oligocene). Alternatively, this extensional event may have reactivated inherited normal faults formed during syn-depositional extensional tectonics in the Jurassic times (e.g. Humilly FZ, Vuache FZ, Salève FT, (parts 6.3.2, and 6.3.3).

To the SE, tectonic imbrication of the Subalpine Molasse thrusting started during Middle Oligocene (Burkhard, 1990; Bonnet et al., 2007). This incorporation of the Molasse layers into the Alpine wedge has continued during the Miocene and even into Pliocene times (Cederbom et al., 2011). The associated NE-SW oriented frontal thrust (with overall northwestward vergence) is located in our model in front of the Mont-de-Boisy (northeastward) area and in the back of the present-day location of the Salève FZ (southeastward, see part 6.3.3). The décollement level of this structure is present inside the Lower Marine Molasse UMM (clay-rich, Gorin et al. (1993), and see Figure 2-7). Several folds have been described in relation with this Cenozoic structural imbricates, including the Mont-de-Boisy anticline in front of the Prealpine Klippen units, and others in front of the thrust Subalpine Massifs. Its southern termination is positioned near the Vuache FZ. South of Vuache FZ we have the boundary zone between the Bauges Massif (with its frontal Bauges Thrust). In this allochthonous units Molasse sediments are found with piggy-back synclines of the Subalpine Massifs. The northern termination of the Subalpine Molasse imbricates is following the Prealpine Units and continues northeastward along the Penninic and Helvetic nappes frontal thrusts (Ortner et al., 2023). This frontal Subalpine Molasse Thrust is shifted by several NW-SE strike slips faults, particularly by the Arve FZ in the northern termination of the Salève FZ area, probably of Miocene age. It suggests that the formation of the Subalpine Molasse unit is predating the subsequent Miocene deformation (Jura fold-and-thrust belt development).

7.6 Eo-Oligocene rifting of ECRIS

The European Cenozoic Rift System (ECRIS) is a major tectonic event that led to the formation of the Bresse Graben (BG, 50km wide, strike NNE-SSW oriented) just W of the Jura FTB and the Rhine Graben at the edge of the northern Jura FTB (Schori, 2021). It may have started during Eocene but was mainly active during Oligocene period (Madritsch, 2008) and ceased in Chattian (Ring & Gerdes, 2016). The Bresse Graben (Figure 2-1) as the Rhine Graben are rift segments that were formed by reactivation in extension of inherited Variscan and post-Variscan faults. Thus, this rifting event has, as in the case of flexural bending, reactivated numerous inherited faults as normal faults and contributed to create important offsets in the basement and the overlying Mesozoic sedimentary cover prior to the formation of the detachment of the foreland fold-and-thrust belt. During this period, the Alpine compression was generally in a NW direction in relation to the subduction of the Valais Ocean and collision of the Adria with Europe (Bourgeois et al., 2007; Bergerat, 1987; and Radaideh & Mosar, 2021).

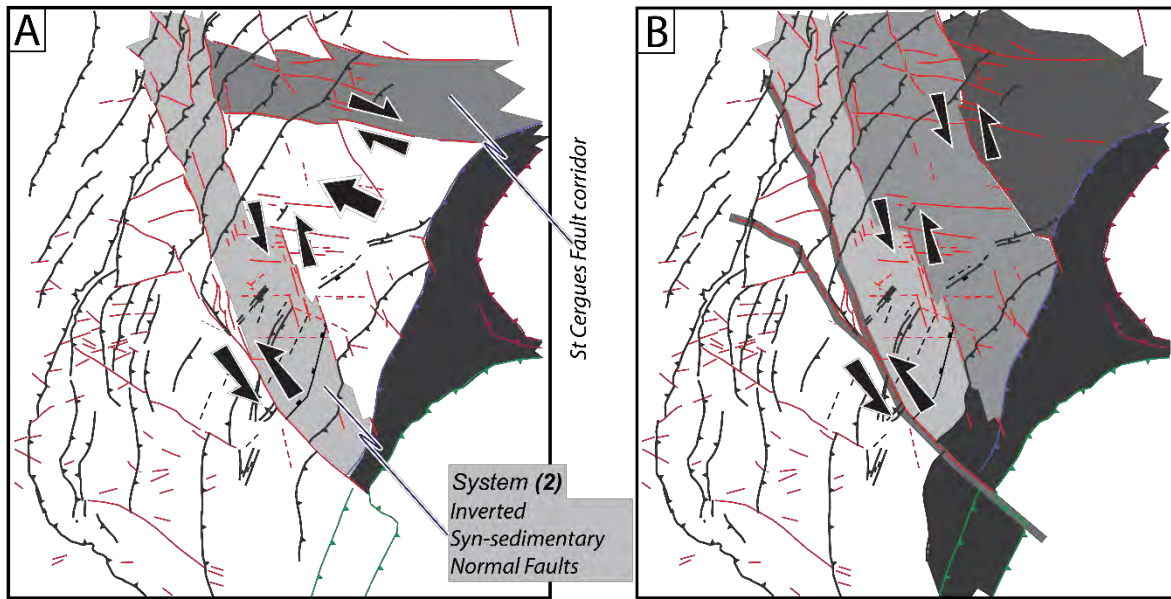
7.7 From Middle Miocene to the present day

During the middle Miocene, the Mesozoic and Cenozoic sedimentary cover was decoupled from the mechanical basement along the main décollement level located at the base of the Keuper Group in the evaporites-salt-rich layers in our area (Figure 6-6). The Alpine compression, specifically the exhumation and emplacement of the External Crystalline Massifs (Bellahsen et al., 2014; Burkhard, 1999; Sommaruga, 1999, and ref therein) and the shortening associated to this, made it possible that the whole cover could be transported by as much as 30 kilometers from its autochthone homeland to its present position (retrodeformation by Affolter & Gratier, (2004) and Schori et al. (2021), and see Figure 7-1). During this major tectonic event the flexural Northern Alpine Foreland Basin developed into a “wedge top” basin (Bonnet et al., 2007; DeCelles & Giles, 1996; Willett & Schlunegger, 2010), which involved the Jura FTB formation (Laubscher, 1961, Figure 6-5). In the Molasse Basin, as well as in the Jura FTB, this deformation phase can be associated, in addition to fold and thrust formation, with the formation of a conjugated strike-slip fault system, but also with the reactivation of inherited normal faults in reverse or in strike-slip mode.

In the Western Alpine Molasse Basin, the impact of the Miocene compression and convergence is well visible with spectacular outcrops such as in the Greater Geneva Molasse Basin, the Salève FT (Frontal Thrust) forming a prominent topographic ridge whose development is linked to a ramp-related fold propagation. In the Rumilly Molasse Basin, the Gros Foug FT and FBT (Frontal Back Thrust) developed during the same deformation event. The orientations of the latter structures along with Jura folding and thrusting indicate the general shortening and transport direction. Two main areas **(4)** and **(5)**, separated by the transpressional, inherited Vuache FZ, can be discriminated by the orientation, not only of the folds and thrusts, but also by the conjugate strike-slip faults (Figure 7-2). As discussed prior the Vuache FZ is part of an inherited, and subsequently transported and inverted normal synsedimentary fault system, with an important alpine tectonic sinistral strike-slip component. Its orientation is thus an inherited orientation, that may be linked to an original feature (fault) in the basement, but which is clearly different from the orientation of the equally sinistral strike-slip fault zones observed in the Molasse Basin and the Jura FTB and which are linked to the tectonic development inside the mechanical wedge of the alpine foreland FTB.

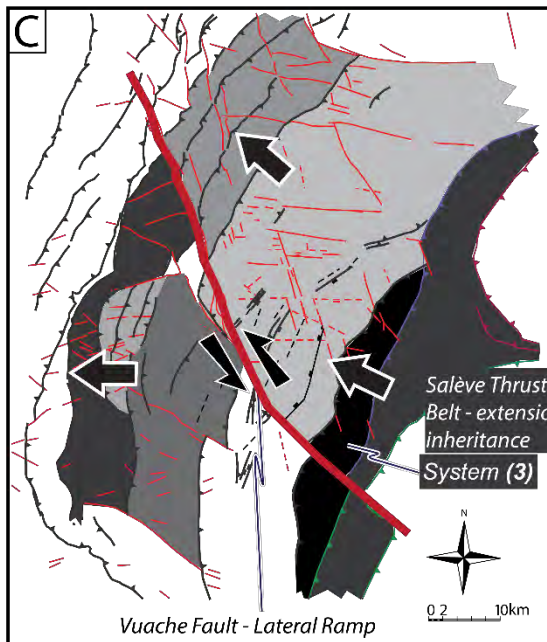
On the eastern side of the Vuache FZ, from the Subalpine Massifs FT to the Jura, a general NW-SE shortening, and a NW-directed transport direction can be deduced based on fold orientation (perpendicular to transport direction), the major thrust orientation and the conjugate strike-slip faults (Figure 7-2). Indeed, it involves an E-W (to ESE-WNW) dextral strike slip system conjugated with a N-S (to NNW-SSE) sinistral system in this area **(4)**. These fault systems are especially prominent in the Jura FTB. Our new interpretation from seismic surveys shows that these structures are also present inside the Molasse Basin. From the seismic signature it was possible to define fault corridors rather than single distinct faults (or narrow fault zones), especially for the E-W oriented zones such as the Aire-la-Ville FC, Meyrin FC, Prévessin FC. The NNW-SSE faults, e.g. Mourex FC, show a more discrete or narrow corridor signature. The Le Coin FC is an exception to this. The corridors of deformation show variable offsets and intensity of faulting inside them, from diffuse small-scale fracturation (Meyrin FC, Prévessin FC) to more pronounced faulting and block segmentation (central fault crossing major part of the Mesozoic cover) surrounded by small scale fracturation (Mourex FC, Divonne FC for instance). Geomorphological lineaments helped identify the orientations of Miocene structures, although these

Strike-slip - deformation "Corridors"



Nappe Tectonics

thrusting - transport direction



Conjugate Fault systems

Strike-slip corridors and Maximum Compression

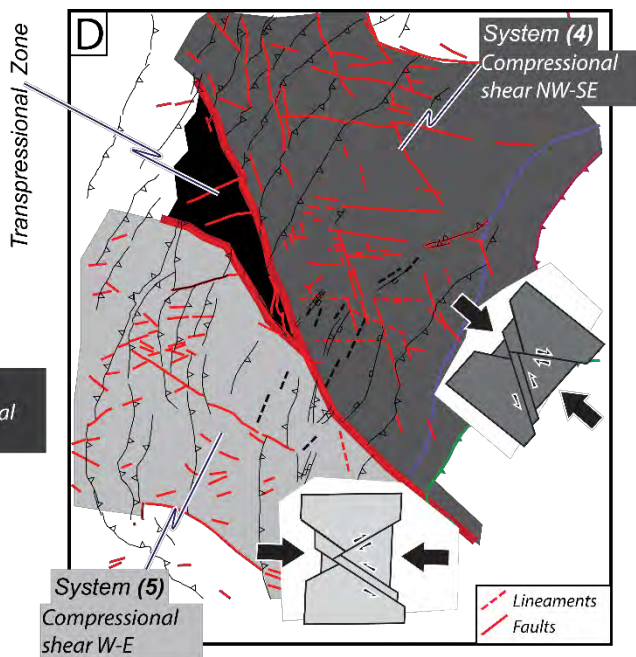


Figure 7-2 : Main blocks and kinematic strains from Middle Miocene compression (blocks delimited by colored polygons). (A) highlights the Humilly-Vuache system. (B) shows various kinematic NW-SE "Corridor" blocks developed in sinistral configuration. (C) presents the main nappe divisions striking N-S to NE-SW. (D) shows the subdivision into two main parts of compressional shear, with the transpositional triangle of the Vuache FZ in the middle.

surface data are often biased by glacial Quaternary erosion and infill. Several prominent surface lineaments brought consistency to our seismic structural interpretation. Especially two major E-W oriented steps in topography of the GGB (Mont de Sion and another one 5km to the N) are important regional geomorphic features that strongly suggest the presence of additional E-W oriented faults. The morphologically different evolution of the river pattern in these two blocks also suggests Quaternary to recent activity.

Thus, from a thrust tectonic perspective, the Geneva Basin and Jura Haute Chaîne form a series of tectonic nappes with a NW transport direction (Figure 7-2). The strike-slip faults form a conjugate system that spans the Jura FTB and the Molasse Basin and shows a NW-SE direction of shortening. In this context, two main regional corridors can be recognized: the St. Cergue FC and the Cruseilles-Allondon FZ.

On the western side of the Vuache FZ from the Bauges FT to the Jura Mountains a rotated strain/stress field can be interpreted **(5)**. In this area an E-W transport direction is deduced from the orientation of the thrusts and associated folds. The conjugated fault system also has a different orientation, with NE-SW oriented dextral strike-slip faults conjugated with a NW-SE (to WNW-ESE) sinistral strike-slip faults. They thus constrain an E-W direction of shortening spanning the Molasse Basin and Jura FTB. The Droisy FZ in this area plays an important role with a clear sinistral component in the Jura part (in line with its orientation) and as a lateral dextral ramp separating the Gros Foug FT with the Gros Foug FBT with opposite thrusting directions. The Musiège FZ may have a normal fault inheritance and reactivation as reverse faulting (pop-up) during the Miocene.

In addition to the displacement and deformation associated with the main décollement level, shallower thrusting along various secondary décollement levels in mechanically weak Mesozoic layers, e.g. in the Lower Malm unit (Effingen marls) or in the Cretaceous levels (“Marnes d’Hauterive”), can be expected. In our study area they correspond to local reverse faulting of rather modest extent, unlike the large regional and more deeply rooted thrusts giving rise to the main tectonic. Indeed, only the main décollement zone in the Triassic series and the Subalpine Molasse décollement in the Rupelian soft layers are proven to be of regional relevance and are thus integrated into the Alpine wedge configuration. Along the main Triassic décollement level, we have observed interesting structures such as intra-Triassic thrusting and duplexes (below low amplitude folds of Ornex and Cercier), or halokinetic activity on the first salt layers of the Keuper (chap 6.2). The latter may have an important role in the development of main thrusts or in the reactivation in compression of former normal listric fault (e.g. rollover structure of the Humilly FZ, see chap 6.3.2).

The most current tectonic activity may be measured using GPS technology (displacement rate), or using the seismicity that gives orientations and type of faulting (Antunes et al., 2020).

8. CONCLUSIONS

In this project, we have investigated the tectonics and lithostratigraphy of the larger Geneva Basin area, including the Haute Chaîne domains of the Jura fold-and-thrust belt, based on surface and subsurface data such as seismic lines (more than 150 seismic 2D profiles, around 2000 km total length) and well data. We have analyzed the structural links between the Geneva Basin with the neighboring region of the Salève to the South, the Vuache fault system and the Rumilly Basin to the West, as well as the Jura Mountains to the North and North-West. The objective was to re-assess the structural setting and kinematics of the westernmost portion of the Western Alpine Molasse Basin in the frame of the detached Alpine foreland. The work combines existing data with new processing and interpretation of seismic data. The seismic interpretation work was combined with surface data e.g. bedding dips, geological maps, DEM, and especially with 66 wells (in the database) and various georeferenced maps from the literature. A proper compilation and preparation of the data was necessary to prepare the work, which led to a complete geodatabase for the area of interest, implemented and dispatched in standard softwares projects: Kingdom Software (IHS Markit), ArcMap (Esri), and in Petrosys software.

This study relied on this large comprehensive dataset to generate the following new geological and geophysical outputs:

- A new **regional** refined positioning of the **near pre-Mesozoic basement surface** (nBMes), for all the neighboring area of the Geneva Basin. It includes the Rumilly Basin, the Subalpine Molasse area and more importantly a part of the Internal Jura. This made it possible, for the first time, to present a coherent depth model with correlations throughout the whole area of investigation and across the major regional tectonic boundaries such as the Salève thrust, the Vuache Fault zone and the Jura - Molasse Basin boundary.

This was achieved using a new more sophisticated **regional velocity modelling** and depth conversion methodology. The velocity model is divided vertically using the four interpreted seismic horizons, near Base Cenozoic (nBCen), near Top Dogger (nTDo), near Top Keuper (nTKeu), near Base Mesozoic (nBMes). Laterally, four regional deep wells with an entire Mesozoic column (LCD-1D, HU-2, CHY-1 and FAY-1) made it possible to produce a velocity distribution of the model into four regional sectors. The main vertical subunits being filled with constant interval velocities varying between the four sectors. One of the main specificities of this modeling is the incorporation of the layer duplications in areas of important thrusting, which was achieved by adapting manually the workflow of the Kingdom software.

The **time-to-depth conversion** allowed us to obtain seismic profiles in depth domain in addition to the classical depth maps. This provides an efficient way of analyzing the present structural depth and geometries of the subsurface seismic horizons with the potentially disturbed geometries in the time domain. The approach assesses and considers artefacts inherent to the time domain, such as pull-up or push-down effects. The technique was especially interesting to constrain the regional morphology and inclinations of the near base Mesozoic seismic horizon. In most of the cases, push down effects were largely compensated and a relatively straight near base Mesozoic surface was obtained. It was thus possible to produce a new regional model of near base Mesozoic (coincident with near top basement). It was also possible to propose uncertainties in depth that range from 100 to 400 m depending

on the depth of the considered seismic reflectors, at depth of 1000 to 4000 m, respectively. As a consequence of our new depth conversion, it was possible to demonstrate that several basement highs or lows that were interpreted in the time domain do not exist anymore in the depth domain of our model. This velocity correction has shown particularly striking results below the Salève Mountain or the Musiège FZ or the Gros Foug FBT, with nearly “flat” near Base Mesozoic horizons (in depth domain). The average dip angle of near base Mesozoic can now be measured to be around 3.25° towards the South-East below the Western Molasse Basin, and some 1.7° below the neighboring Internal Jura.

Remaining highs and lows along the nBMes depth model may be related to underlying tectonic horst and graben structures. Such **fault-related structures** in the **mechanical basement** underlying the detached Mesozoic cover can be recognized but remain difficult to resolve in detail. In agreement with Schori (2021), we suggest the presence of NNE-SSW trending normal basement faults in the Internal Jura part and near its transition to the Molasse Basin associated with steps in the topography of the near basement surface. Another set of basement faults striking NW-SE and crossing the middle of the Geneva Basin, and near the Vuache FZ may be considered. These faults are either inherited pre-Mesozoic faults, linked to post Variscan extension or alternatively be reactivated inherited faults or newly formed faults resulting from the flexural down-bending of the western Northern Alpine Foreland (WNAF) or ECRIS rifting from late Eocene to Oligocene. In addition, these faults may have influenced syn-sedimentary faults in the sedimentary cover (Vuache FZ) during the extensional period of the Jurassic rifting related to the opening of the Alpine Tethys in the far SE.

- A new refined and **high-resolution depth model of the Geneva Basin**. We specifically focused on this area, since one of the main objectives of the study was to obtain new insight into the structural setting, as part of the “GEOthermies” project by SIG in the Geneva Canton. We have thus optimized the seismic interpretation and time-to-depth workflow, according to the available data. We put great attention into accurately interpreting eight Mesozoic seismic horizons, which illustrate the subsurface configuration of the main stratigraphical boundaries inside the Geneva Basin: near Base Cenozoic (nBCen), near Top Upper Malm (nTUMa), near Top Lower Malm (nTLMa), near Top Dogger (nTDo), near Top Lias (nTLi), near Top Keuper (nTKeu), near Top Muschelkalk (nTMu), near Base Mesozoic (nBMes). Subsequently we implemented a more **refined and advanced time-to-depth conversion** method in comparison to the regional velocity model. It consists of a complex polynomial velocity law for the Cenozoic layer and of advanced interpolated interval velocity grids for the other Mesozoic layers. It was possible to elaborate this more refined model, because of the availability of a higher number of well data inside this limited zone. In addition to the refined identification of lithostratigraphic horizons, it was also possible to define major folds, faults and fault zones in depth.
- A **seismic line catalogue**. In addition to the interpretations made in software packages (database accessible in Kingdom Suite format) a series of some 94 interpreted seismic lines were presented in graphical format (PDF files, see Enclosures) showing the raw data, the interpretation and the geological model. In addition, some 20 lines are also presented in depth converted format.
- A new **tectonic map** of the area and **thickness/depth maps** providing a new structural model resulting in a new **kinematic model**. In this approach, we have systematically correlated the seismic interpretation with surface data, e.g. dip data from outcropping Molasse strata to

implement a structural model consistent with the subsurface data. This helped constrain positioning of bedding dip domains and thus locate fold axial surfaces. Known fault zones and geomorphological surface lineaments were also used to define and assess structural trends of major and minor fault zones. Geomorphic lineament mapping helped constrain subsurface interpretation and vice versa. Special attention was given to Quaternary geological deposits and the glacial erosions that could mislead the tectonic interpretation. The resulting **new tectonic map** highlights the geometry and orientations of the main tectonic structures in the detached and deformed sedimentary cover of the area.

Structures identified in the subsurface confirm the locus from the borehole information concerning the main décollement level in the salt rich Keuper Group evaporites. The structures identified were analyzed in relation with the main lithostratigraphic thickness (**thickness maps**) and lateral seismic facies variations. Indeed, the depositional seismic signature of each sub-unit has also been investigated and compiled in a **seismic facies catalog**. The orientations of the structures and geological observations allowed to constrain a new interpretation of the tectonic chronology and geological history of the area. The interpretations and geometric relationships in the maps made it possible to elaborate a new kinematic understanding of the investigated region.

Thus using the main structural and geological findings of our seismic interpretation it was possible to unravel the kinematic and sedimentological-tectonic evolution of the whole area:

- Based on new interpretation of the seismic data it was possible to clearly identify **syn-sedimentary extensional listric normal faults**. The interpretation is based on lateral changes in lithostratigraphic thickness, fault geometry and locally evaporite distribution. Their main syn-depositional activity and growth are interpreted to be during the **Early to Middle Jurassic** period (especially during the Lias). They are arranged in an extensional imbricated fan zone, with a succession of several such syn-depositional normal faults, developed along, and east of the main leading NW-SE strike-slip Vuache Fault Zone. This latter fault zone forms the dominant structure and also act as inherited normal fault. The extensional fan encompasses the NE-SW striking SE-vergent Humilly FZ, and we also included the Pougny FZ and the Cercier FC, despite more tenuous evidence syn-sedimentary activity in the Jurassic layers (alternatively, they may have triggered during the Eo-Oligocene extensional period - down-bending flexure of the lithosphere in the western NAFB and/or ECRIS rifting). All these faults are branching off the main Vuache FZ and have subsequently been modestly inverted during alpine compression. Farther to the S-SE these inherited fault systems, may also include the Salève FZ. Indeed, this structure has been interpreted in the same extensional Jurassic syn-sedimentary activity.

Other NE-SW fault branches may also be associated to the Vuache-Humilly-Salève FZ such as the Musiège FZ or the Gros Foug FBT west of the Vuache FZ. In this scenario a broader syn-sedimentary extensional fault system can be envisaged around one major main, large extensional strike-slip fault (Vuache FZ) creating an important extensional inheritance.

- In combination with the emergence of inherited extensional tectonics, **seismic facies trends** have also been investigated especially in relation to the **Eocene (Siderolithic)** deposits and **Upper Malm facies (reefal complex)**. Concerning the Malm layer, the overall NE-SW striking orientation of the basin with a polarity NW-proximal and SE-distal is confirmed by

progradation sigmoids in this direction identified on seismic lines. The classical lateral succession of depositional environments: lagoon-reef-slope (from NW to SE -carbonate-platform) associated to seismic facies in the Kimmeridgian unit was also tentatively observed. We suspect the role of the previously mentioned extensional imbricated fan in the lateral depositional trend of this reefal units. Indeed, the Vuache-Humilly FZ inherited from Lower-Middle Jurassic times may have influence the reef deposits, with NE-SW or NW-SE paleotopographical highs along the footwalls of the fault systems. Indeed, the the highstanding footwall compartment may provide the necessary relatively elevated topography feature to allow reef complexes to be installed.

Following the same idea, the Siderolithic deposits (Eocene), probably with fluvial origins, following the high erosion in Cretaceous times, may have developed favorably in lows inherited from syndepositional tectonics in Mesozoic times. In that sense, a NE-SW trend (seismic facies) is observed in the middle of the Molasse Basin. Further modeling and drilling evidence are needed to improve this analysis.

- One of the main results in the structural analysis was the identification of **fault corridors**. These corridors measure in the Geneva Molasse Basin, up to 15km length and are around 500m wide, and are made of multiple non-correlated near vertical small-scale fault segments of vertical extent around 100-300ms. They cross the entire Mesozoic cover with higher deformation in brittle intervals such as the Upper Malm or Cretaceous massive limestones layers, leading to segmented fault strings. Broad corridors can be shown to be mostly oriented E-W whereas more narrow fault zones are predominantly oriented more N-S. In addition to lateral movements, vertical shifts or uplifts from one side to another of the corridors are often observed.

From a kinematic perspective these fault systems act as **conjugate strike-slip fault** systems. They are a continuation and extension of the fault systems known from the Jura FTB; and thus are interpreted to extend into the Molasse Basin. The fault corridors root in the main décollement level and are kinematically linked to the thrust (nappe) and fold development inside the orogenic wedge. They locally develop tranpressive/transtensive and pop-up like structures.

Two main distinct conjugate fault settings can be identified east and west of the Vuache Fault Zone:

- East of the Vuache FZ, we observe E-W striking dextral strike-slip faults (e.g Saint-Cergue FC, Divonne FC, Prévessin FC, Meyrin FC, or Aire-la-Ville FC) conjugated with NNW-SSE sinistral strike-slip faults (e.g Le Coin FC, or Mourex FC). This conjugate setting corresponds to a NW-SE oriented shortening direction. This can be correlated with the general NE-SW fold and thrust direction in this area.
- West of the Vuache FZ, ENE-WSW oriented dextral strike-slip faults conjugated with NW-SE sinistral strike-slip faults, suggesting a WNW-ESE shortening direction.

When inspecting the orientations of these faults it can be shown that the Vuache Fault Zone does not correspond to either of these systems since it has a different more NW-SE thus differing from the two conjugate sets. This distinct orientation points to a different kinematic setting and tectonic origin, which is in line with our interpretation that the Vuache Fault Zone as an inherited Mesozoic paleotectonic boundary that has been reactivated during transport towards the foreland in the frame of the formation of the Alpine foreland fold-and-thrust belt.

- The refined, new interpretation of the seismic data has made it possible to acquire a more detailed understanding of the structural evolution and the relevance of inherited structures in the area of investigation between the southern Jura FTB to the Salève ramp-fold and the Châinées Subalpines in the south. The hypothesis of a detached alpine foreland fold-and-thrust belt has been solidified and a refined near top basement interpretation made it possible to confidently locate the main décollement at the base of the Keuper Group evaporites, with an accuracy of 100-400m, as well as change in dip across the transition Jura FTB-Molasses Basin. Borehole data confirm that the décollement is in fact a broad zone with distributed levels with higher strain. Thickness variations in the evaporite layers are shown to be either initial (depositional or linked to syn-sedimentary extensional faulting and salt flowage) and/or due to alpine tectonic deformation during and following detachment of the sedimentary cover (salt pillows, duplexes and flowage). The syn-depositional tectonics have for the first time been clearly demonstrated in the Geneva Basin and show listric normal faults with lithostatigraphic thickness changes across the fault typical of extensional syn-sedimentary half-graben formation rooting in the basal décollement level, of which the Humilly Fault Zone is a typical example. These faults have subsequently been inverted during alpine compression. On a regional scale it was possible to propose a new concept for the structural setting of the Vuache FZ. This unique large-scale strike-slip fault is considered an inherited structure that has been transported some 25km and reactivated in a transpressional mode during alpine compression. Originally this FZ is a synsedimentary steep normal fault zone associated with normal listric, extensional faults at a high angle and forms a regionally large-scale barrier. The formation of this fault system is associated with the extensional tectonic setting due to the opening of the Alpine Tethys to the south. The important fault-induced topography (footwall are standing high) explains e.g. the preferential distribution of reefs on bathymetric highs during the Malm period. This inherited barrier is later also responsible for the difference in sedimentation in the Rumilly and Geneva Basins during the Cenozoic.

Alpine tectonics have strongly reshaped the flexural foreland basin and led to the formation of major ramp-related folds and imbricates, especially well developed in the Salève FT and in the Haute Chaine Jura FTB. More modest gentle folds are recognized in the Molasse Basin of the Geneva area. These structures develop in the frame of a mechanical wedge propagating NW and W-ward towards the Alpine foreland over a very weak décollement in the salt-rich evaporites.

Recent studies on the geometry of the near top mechanical basement and the importance of inherited faults in the substratum make it possible to reframe numerous structures observed in the present detached and deformed cover. As suggested already by Laubscher in the 1960ties and 80ties, basement topography in the form of basement steps may trigger the formation of tectonic structures in the cover. This has been convincingly demonstrated in the compressional domain, but we herein propose that fault systems such as the Vuache inherited normal syn-depositional FZ can be associated with inherited basement faults (steps, of change in basement surface dip). Thus, unfolding the Jura FTB allows us to propose a paleorestitution and locate the possibly basement faults that initiated the synsedimentary faults.

This does not preclude the possibility of formation of other faults, mostly extensional, prior to the fold-and-thrust development during alpine compression. Thus, faults may be linked to

flexural bending and/or to the ECRIS rift development in early Cenozoic times. In addition to the thrust tectonics and the formation of nappe like structures and thrust (ramp) related folds, we also documented the pervasive formation of a vertical fault network forming broad fault corridors, kinematically linked in a conjugate setting and forming locally transpressive and transtensive structures. The fault systems are inside the detached cover, rooting in the basal décollement and affect both the Jura FTB and the Molasse Basin domains. They show the regional shortening in agreement with the fold and thrust orientation changing from a NW-SE orientation east of the Vuache FZ and a more E-W orientation west of it.

Our work made it possible to unravel new structural details and make new structural interpretation and propose a new tectonic map and 3D model of the larger Geneva area. It has helped acquire a new tectonic understanding of the detached foreland fold-and-thrust belt around Geneva and propose a new kinematic model for its development.

REFERENCES

- Affolter, T., & Gratier, J.-P. (2004). Map view retrodeformation of an arcuate fold-and-thrust belt: The Jura case. *Journal of Geophysical Research*, *109*(B03404), 20. <https://doi.org/10.1029/2002JB002270>.
- Allenbach, R. P., & Wetzell, A. (2006). Spatial patterns of Mesozoic facies relationships and the age of the Rhenish Lineament: a compilation. *International Journal of Earth Sciences*, *95*, 803–813. <https://doi.org/10.1007/s00531-006-0071-0>.
- Allenbach, R., Baumberger, R., Kurmann, E., Michael, C. S., & Reynolds, L. (2017). GeoMol: Geologisches 3D-Modell des Schweizer Molassebeckens - Schlussbericht. In *Berichte der Landesgeologie* (Vol. 10). Federal Office of Topography (swisstopo).
- Allenbach, Robin, Andenmatten, N., Atanackov, J., Baumberger, R., Bottig, M., Brenot, A., Brüstle, K., Cagnoni, A., Capar, L., Clerc, N., Couëffé, R., Courrioux, G., Dezayes, C., Diepolder, G. W., Stucki, M. D., Fehn, C., Ferri, F., Gabalda, S., Gietzel, J., ... Kurmann-Matze, E. (n.d.). *GeoMol - Project Report*. 192.
- Altwegg, P. (2015). Gravimetry for geothermal exploration - Methodology, computer programs and two case studies in the Swiss Molasse Basin. *PhD Thesis, Institute of Hydrogeology and Geothermics, University of Neuchâtel*, 240.
- Antunes, V., Planès, T., Zahradník, J., Obermann, A., Alvizuri, C., Carrier, A., & Lupi, M. (2020). Seismotectonics and 1-D velocity model of the Greater Geneva Basin, France–Switzerland. *Geophysical Journal International*, *221*(3), 2026–2047. <https://doi.org/10.1093/gji/ggaa129>.
- Arn R., Conrad, M. A. & W. M. (2005). *Nyon. Atlas géologique de la Suisse 1:25'000. Feuille 12*, explanatory note feuille N° 117: 101p.
- Ashton, C. P., Bacon, B., Mann, A., Moldoveanu, N., Déplanté, C., Aquitaine, E., Ireson, D., Sinclair, T., & Redekop, G. (1994). 3D seismic survey design. *Oilfield Review*, *6*(2), 19–32. <https://doi.org/10.1190/1.9781560801757>.
- Bachmann, G. H., & Müller, M. (1992). Sedimentary and structural evolution of the German Molasse Basin. *Eclogae Geologicae Helvetiae*, *85*(3), 519–530.
- Baize, S., Cushing, M., Lemeille, F., Gelis, C., Texier, D., Nicoud, G., & Schwenninger, J.-L. (2011). Contribution to the seismic hazard assessment of a slow active fault, the Vuache fault in the southern Molasse basin (France). *Bulletin de La Société Géologique de France*, *182*(4), 347–365. <https://doi.org/10.2113/gssgfbull.182.4.347>.
- Ballèvre, M., Manzotti, P., & Dal Piaz, G. V. (2018). Pre-Alpine (Variscan) Inheritance: A Key for the Location of the Future Valaisan Basin (Western Alps). *Tectonics*, *37*(3), 786–817. <https://doi.org/10.1002/2017TC004633>.
- Bashir, Y., Muztaza, N. M., Alashloo, S. Y. M., Ali, S. H., & Ghosh, D. P. (2020). Inspiration for seismic diffraction modelling, separation, and velocity in depth imaging. *Applied Sciences (Switzerland)*, *10*(12). <https://doi.org/10.3390/app10124391>.
- Beck, C., Deville, E., Blanc, E., Philippe, Y., & Tardy, M. (1998). Horizontal shortening control of middle Miocene marine siliciclastic accumulation (Upper Marine Molasse) in the southern termination of the Savoy Molasse Basin (northwestern Alps/southern Jura). *Geological Society of London, Special Publications*, *134*(1), 263–278.

References

- <https://doi.org/https://doi.org/10.1144/GSL.SP.1998.134.01.12>.
- Becker, A. (2000). The Jura Mountains — an active foreland fold-and-thrust belt? *Tectonophysics*, 321(4), 381–406. [https://doi.org/10.1016/S0040-1951\(00\)00089-5](https://doi.org/10.1016/S0040-1951(00)00089-5).
- Beghoul. (2004). *Géométrie des Trous de Forages*. <http://www.begoil-consult.com/begoil/wp-content/uploads/2015/07/wellbore-geometry-interpretation.pdf>.
- Bellahsen, N., Mouthereau, F., Boutoux, A., Bellanger, M., Lacombe, O., Jolivet, L., & Rolland, Y. (2014). Collision kinematics in the western external Alps. *Tectonics*, 33(6), 1055–1088. <https://doi.org/10.1002/2013TC003453>.
- Berger, J.-P., Reichenbacher, B., Becker, D., Grimm, M., Grimm, K., Picot, L., Storni, A., Pirkenseer, C., Derer, C., & Schaefer, A. (2005). Paleogeography of the Upper Rhine Graben (URG) and the Swiss Molasse Basin (SMB) from Eocene to Pliocene. *International Journal of Earth Sciences*, 94, 697–710. <https://doi.org/https://doi.org/10.1007/s00531-005-0475-2>.
- Bergerat, F. (1987). Stress fields in the European platform at the time of Africa-Eurasia collision. *Tectonics*, 6(2), 99–132. <https://doi.org/10.1029/TC006i002p00099>.
- Blondel, Th., Charollais, J., Sambeth, U., & Pavoni, N. (1988). La faille du Vuache (Jura méridional): un exemple de faille à caractère polyphasé. *Bulletin de La Société Vaudoise Des Sciences Naturelles*, 79(2), 65–91.
- Blondel, Th. (1988). La montagne du Vuache (Jura méridional): un exemple de structure géologique d'apparence simple mais de formation complexe. *Le Globe. Revue genevoise de géographie*, 128(1), 16–38. <https://doi.org/10.3406/globe.1988.1252>.
- Bois, C., Cazes, M., Damotte, B., Galdéano, A., Hirn, A., Mascle, A., Matte, Raoult, J. F., & Torreilles, G. (1986). Deep seismic profiling of the crust in northern France: the ECORS project. In M. Barazangi & L. Brown (Eds.), *Reflection seismology: A global perspective* (pp. 21–30).
- Bond, C. E., Gibbs, A. D., Shipton, Z. K., & Jones, S. (2007). What do you think this is? “Conceptual uncertainty” in geoscience interpretation. *GSA Today*, 17(11), 4–10.
- Bonnet, C., Malavieille, J., & Mosar, J. (2007). Interactions between tectonics, erosion, and sedimentation during the recent evolution of the Alpine orogen: Analogue modeling insights. *Tectonics*, 26(6). <https://doi.org/10.1029/2006TC002048>.
- Borderie, S., Mosar, J., Hauvette, L., Marro, A., & Sommaruga, A. (2022). Numerical modelling of current state of stress in the Geneva Basin and adjacent Jura fold-and-thrust belt (Switzerland and France). *EGU General Assembly, Vienna, Austria, 23–27 May 2022, EGU22-8449*. <https://doi.org/https://doi.org/10.5194/egusphere-egu22-8449, 2022>.
- Bordon, J., & Charollais, J. (2009). *Le Vuache, montagne insolite...* SIPCV F-74520.
- Bourgeois, O., Ford, M., Diraison, M., Le Carlier de Veslud, C., Gerbault, M., Pik, R., Ruby, N., & Bonnet, S. (2007). Separation of rifting and lithospheric folding signatures in the NW-Alpine foreland. *International Journal of Earth Sciences*, 96(6), 1003–1031. <https://doi.org/10.1007/s00531-007-0202-2>.
- Bourquin, S., Bercovici, A., Lopez-Gomez, J., Diez, J. B., Broutin, J., Ronchi, A., Durand, M., Arche, A., Linol, B., & Amour, F. (2011). The Permian-Triassic transition and the onset of Mesozoic sedimentation at the northwestern peri-Tethyan domain scale: Palaeogeographic maps and geodynamic implications. *Palaeogeography Palaeoclimatology Palaeoecology*, 299(1–2), 265–

280. <https://doi.org/10.1016/j.palaeo.2010.11.007>.
- Bradley, D. C., & Kidd, W. S. F. (1991). Flexural extension of the upper continental crust in collisional foredeeps. *Geological Society of America Bulletin*, 103(11), 1416. [https://doi.org/10.1130/0016-7606\(1991\)103<1416:FEOTUC>2.3.CO;2](https://doi.org/10.1130/0016-7606(1991)103<1416:FEOTUC>2.3.CO;2).
- Brentini, M. (2018). Impact d'une donnée géologique hétérogène dans la gestion des géo-ressources: analyse intégrée et valorisation de la stratigraphie à travers le bassin genevois (Suisse, France). *PhD Thesis, University of Geneva, CH*, 230. <https://doi.org/ISBN 978-2-940472-41-3>.
- BRGM. (2020). *Infoterre*. <http://infoterre.brgm.fr/viewer/MainTileForward.do>
- Brown, R. J., Stewart, R. R., Gaiser, J. E., & Lawton, D. C. (2000). An acquisition polarity standard for multicomponent seismic data. *Field Polarity Standard for Multicomponent Data*, 12(1).
- Brun, J.-P., & Mauduit, P.-O. (2008). Rollovers in salt tectonics: The inadequacy of the listric fault model. *Tectonophysics*, 457, 1–11.
- Burkhard, M. (1990). Aspects of the large-scale Miocene deformation in the most external part of the Swiss Alps (Subalpine Molasse to Jura fold belt). *Eclogae Geologicae Helvetiae*, 83(3), 559–583. <https://doi.org/10.5169/seals-166602>.
- Burkhard, M. (1999). Strukturgeologie und Tektonik im Bereich AlpTransit. In A. A. Balkema (Ed.), *Tagungsband zum Symposiums Geologie Alptransit* (pp. 45–56).
- Burkhard, M., & Sommaruga, A. (1998). Evolution of the western Swiss Molasse basin: structural relations with the Alps and the Jura belt. *Geological Society Special Publications*, 134, 279–298. <https://doi.org/10.1144/GSL.SP.1998.134.01.13>.
- Buxtorf, A. (1907). Zur Tektonik des Kettenjura. *Bericht Der Versammlung Des Oberrheinischen Geologischen Vereins*, 40, 29–38.
- Buxtorf, A. (1916). Prognosen und Befunde beim Hauensteinbasis- und Grenchenbergtunnel und die Bedeutung der Letzteren für die Geologie des Juragebirges. *Verhandlungen Der Naturforschenden Gesellschaft in Basel*, 27, 184–254.
- Capuzzo, N., & Wetzel, A. (2004). Facies and basin architecture of the Late Carboniferous Salvan-Dorenaz continental basin (Western Alps, Switzerland/France). *Sedimentology*, 51(4), 675–697. <https://doi.org/10.1111/j.1365-3091.2004.00642.x>.
- Cederbom, C. E., van der Beek, P., Schlunegger, F., Sinclair, H. D., & Oncken, O. (2011). Rapid extensive erosion of the North Alpine foreland basin at 5–4 Ma. *Basin Research*, 23, 528–550.
- Chablais, J., & Savoy, L. (2019). Forage de prospection géothermique Géo-01 Rapport de Fin de Sondage. *Report Written by Hydro-Geo Environnement (HGE) Company (Genève) on Behalf of the Services Industriels de Genève (SIG)*, 222.
- Chablais, J., & Savoy, L. (2021). Forage de prospection géothermique Géo-02 Rapport de Fin de Sondage. *Report Written by Hydro-Geo Environnement (HGE) Company (Genève) on Behalf of the Services Industriels de Genève (SIG)*, 175.
- Channell, J. E. T., & Kozur, H. W. (1997). How many oceans? Meliata, Vardar and Pindos oceans in Mesozoic Alpine paleogeography. *Geology*, 25, 183–186.
- Charollais, J., Weidmann, M., Berger, J.-P., Engesser, B., Hotellier, J.-F., Gorin, G. E., Reichenbacher, B., & Schäfer, P. (2007). La Molasse du bassin franco-genevois et son substratum. *Archives Des*

References

- Sciences*, 60, 59–174.
- Charollais, J. (1986). *feuille Annecy-Bonneville No. 678 (XXXIV/30), Carte géologique de la France au 1:50'000, notice*. Bureau des Recherches Géologiques et Minières.
- Charollais, J., Plancherel, R., Montjuvent, G., & Debelmas, J. (1998). *feuille Annemasse No. 654, Carte géologique de la France au 1:50'000, notice* (p. 133). BRGM France.
- Charollais, J., Weidmann, M., Berger, J.-P., Engesser, B., Hotellier, J.-F., Gorin, G., Reichenbacher, B., & Schäfer, P. (2007). La Molasse du bassin franco-genevois. *Archives des Sciences, Genève*, 116.
- Charollais, J., Wernli, R., Du Chene, R. J., Von Salis, K., & Steiner, F. (2006). La Molasse marine supérieure de la Combe d'Évuaz et de la Pesse. *ARCHIVES DES SCIENCES*, 59, 21–46.
- Charollais, J., Wernli, R., Mastrangelo, B., Metzger, J., Busnardo, R., Clavel, B., Conrad, M., Davaud, E., Granier, B., Martin, M. SAINT, & Weidmann, M. (2013). Présentation d'une nouvelle carte géologique du Vuache et du Mont de Musièges (Haute-Savoie, France). *Archives des Sciences, Genève*, 63.
- Chauve, P., Enay, R., Fluck, P., Sittler, C., & Edel, J. B. (1980). France, Introduction à la géologie de l'est: Vosges, Fossé Rhénan, Bresse, Jura. *26th International Geological Congress*, 4(1), 3–80.
- Chauve, P., & Perriaux, J. (1974). Le jura. *Géologie de La France: Les Chaînes Plissées Du Cycle Alpin et Leur Avant-Pays*, 2, 443–464.
- Chopra, S., & Marfurt, K. (2008). Emerging and future trends in seismic attributes. *The Leading Edge*, 27, 298–318. <https://doi.org/10.1190/1.2896620>.
- Chopra, S., & Marfurt, K. J. (2005). Seismic attributes - A historical perspective. *Geophysics*, 70(5). <https://doi.org/10.1190/1.2098670>.
- Clerc, N. (2016). GeoMol-CH project: Interpretation and modeling report of the Geneva area. *Geo-Energy Group, Université de Genève*, 66.
- Clerc, N., & Moscariello, A. (2020). A revised structural framework for the Geneva Basin and the neighboring France region as revealed from 2D seismic data: Implications for geothermal exploration. *Swiss Bulletin for Applied Geology*, 25(1–2), 109–131.
- Conrad, M. A., & Ducloz, C. (1977). Nouvelles observations sur l'Urgonien et le Sidérolithique du Salève. *Eclogae Geologicae Helvetiae (Bâle)*, 70, 127–141.
- Cox, D. R., Newton, A. M. W., & Huuse, M. (2020). An introduction to seismic reflection data: Acquisition, processing and interpretation. In *Regional Geology and Tectonics: Principles of Geologic Analysis Volume 1: Principles of Geologic Analysis*. BV. <https://doi.org/10.1016/B978-0-444-64134-2.00020-1>.
- Cui, T., & Margrave, G. F. (2014). *Comparing Seismic Imaging Methods (Pre & Post Stack) Methods*. <https://www.crewes.org/ForOurSponsors/FridayTalks/2014/CFT201404.pdf>.
- Davis, G. H., Bump, A. P., García, P. E., & Ahlgren, S. G. (2000). Conjugate Riedel deformation band shear zones. *Journal of Structural Geology*, 22, 169–190.
- De la Taille, C. (2018). Évaluation de l'activité tectonique quaternaire des failles du Jura Méridional (France). *PhD Thesis from UNIVERSITÉ GRENOBLE ALPES*, 259. <https://tel.archives-ouvertes.fr/tel-01680848v2>.

- Debrand-Passard, S., Courbouleix, S., & Lienhardt, M.-J. (1984). Synthèse géologique du Sud-Est de la France. *Mémoire BRGM France, N° 125*, 615.
- DeCelles, P. G., & Giles, K. A. (1996). Foreland basin systems. *Basin Research, 8*(2), 105–123. <https://doi.org/10.1046/j.1365-2117.1996.01491.x>.
- Deichmann, N., Baer, M., Braunmiller, J., Husen, S., & Fäh, D. (2000). Earthquakes in Switzerland 1999. *Eclogae Geologicae Helvetiae, 93*(3), 395–408.
- Deichmann, N., Clinton, J., Husen, S., Edwards, B., Haslinger, F., Fäh, D., Giardini, D., Kästli, P., Kradolfer, U., Marschall, I., & Wiemer, S. (2010). Earthquakes in Switzerland and surrounding regions during 2009. *Swiss Journal of Geoscience, 535–549*. <https://doi.org/10.1007/s00015-010-0039-8>.
- Deville, E. (2021). Structure of the Tectonic Front of the Western Alps: Control of Fluid Pressure and Halite Occurrence on the Decollement Processes. *Tectonics, 40*(4), 1–21. <https://doi.org/10.1029/2020TC006591>.
- Deville, E., Blanc, E., Tardy, M., Beck, C., Cousin, M., & Ménard, G. (1994). Thrust Propagation and Syntectonic Sedimentation in the Savoy Tertiary Molasse Basin (Alpine Foreland). In *Hydrocarbon and Petroleum Geology of France* (pp. 269–280). Springer. https://doi.org/10.1007/978-3-642-78849-9_19.
- Dèzes, P., Schmid, S. M., & Ziegler, P. A. (2004). Evolution of the European Cenozoic Rift System: interaction of the Alpine and Pyrenean orogens with their foreland lithosphere. *Tectonophysics, 389*(1–2), 1–33. <https://doi.org/10.1016/j.tecto.2004.06.011>.
- Diebold, P., Naef, H., & Ammann, M. (1991). *NTB 90-04, Zur Tektonik der zentralen Nordschweiz: Interpretation aufgrund regionaler Seismik, Oberflächen-Geologie und Tiefbohrungen*. <http://www.nagra.ch>.
- Diem, B. (1986). Die untere Meeresmolasse zwischen der Saane (Westschweiz) und der Ammer (Oberbayern). *Eclogae Geologicae Helvetiae, 79*(2), 493–559.
- Donath, F. A., & Parker, R. B. (1964). Folds and Folding. *Geological Society of America, Bulletin, 75*, 45–62.
- Donzeau, M., Wernli, M., Charollais, J., & Monjuvent, G. (1997). *Carte géol. France (1/50 000), feuille Saint-Julien-en-Genevois (653)* (p. 144). BRGM France.
- Donzeau, M., Wernli, R., & Charollais, J. (1998). Interprétation nouvelle de la géométrie de l'accident du Vuache dans le Jura méridional: le relais de failles transpressif sénestre Léaz-Champfromier (Ain). *Géologie de La France, 2*, 25–45.
- DT - Département du territoire. (2013). *MNT AGGLO - MODELE NUMERIQUE DE TERRAIN AGGLO 2014 (pixel 0.5 m)*. https://ge.ch/sitg/sitg_catalog/sitg_donnees?keyword=&geodataid=0892&topic=tous&service=tous&datatype=tous&distribution=tous&sort=auto.
- DT de Genève, & SIG. (2022). *Résultats de la campagne sismique 3D: le potentiel géothermique du canton est confirmé*. Communiqués de Presse. <https://www.ge.ch/document/resultats-campagne-sismique-3d-potentiel-geothermique-du-canton-est-confirme>.
- Dupuy, D. (2006). Etude des sédiments quaternaires, de la Molasse et sa tectonique, dans le Grand Lac (Léman) à partir de données sismiques 2D et 3D. *PhD Thesis, Institut de Géophysique, Université de Lausanne, 239*.

References

- Egal, E. (2007). Carte géologique harmonisée du département de l'Ain, rapport final 55512-FR. *BRGM France*, 266.
- Egli, D., Madritsch, H., Mosar, J., & Müller, W. (2017). U/Pb dating of synkinematic calcite fibres from the Randen fault (NE Switzerland): implications for geodynamics of the northwestern Alpine foreland. *NAGRA Report*.
- Favre, S. (2018). *Systèmes d'information pour les données géologiques 2D et 3D: Perspectives et limites pour l'analyse du sous-sol genevois et ses ressources* [Université de Genève, Switzerland]. <https://doi.org/10.13097/archive-ouverte/unige:102945>.
- Fiore, J. (2007). Quaternary subglacial processes in Switzerland: Geomorphology of the Plateau and seismic stratigraphy of Western Lake Geneva. *Terre et Environnement*, 69, DVD.
- Fiore, J., Girardclos, S., Pugin, A., Gorin, G., & Wildi, W. (2011). Würmian deglaciation of western Lake Geneva (Switzerland) based on seismic stratigraphy. *Quaternary Science Reviews*, 30(3–4), 377–393. <https://doi.org/10.1016/j.quascirev.2010.11.018>.
- Fleuty, M. J. (1964). The description of folds. *Proceedings of the Geologists' Association*, 75(4), 461–492. [https://doi.org/10.1016/S0016-7878\(64\)80023-7](https://doi.org/10.1016/S0016-7878(64)80023-7).
- Ford, M., Duchêne, S., Gasquet, D., & Vanderhaeghe, O. (2006). Two-phase orogenic convergence in the external and internal SW Alps. *Journal of the Geological Society*, 163(5), 815–826. <https://doi.org/10.1144/0016-76492005-034>.
- Frei, W. (2019). Hybrid seismic surveying for detailed characterization of the shallow and intermediate depths subsurface. *Modern2020 2nd International Conference about Monitoring in Geological Disposal of Radioactive Waste – Extended Abstract Poster Session 9. – 11. April 2019 – Paris, April, 9*.
- Frey, C., & Lahusen, P. (1994). Rapport final Société Anonyme des Hydrocarbures (SAdH). *Geologische Beratungen Und Studien AG*, 12.
- Ge, J., Zhu, X., Jones, B. G., Zhang, Y., Huang, H., & Shu, Y. (2018). Facies delineation and sandstone prediction using seismic sedimentology and seismic inversion in the Eocene Huizhou Depression, Pearl River Mouth Basin, China. *Interpretation*, 6(2), SD71–SD87. <https://doi.org/10.1190/INT-2017-0155.1>
- GGE. (2018). Petrophysical interpretation RCL of main deep wells around Geneva. *Geneva Geo Energy (GGE) on Behalf of the Services Industriels de Genève (SIG)*, 12.
- Gong, C., Wang, Y., Zhu, W., Li, W., & Xu, Q. (2013). Upper Miocene to Quaternary unidirectionally migrating deep-water channels in the Pearl River Mouth Basin, northern South China Sea. *AAPG Bulletin*, 97(2), 285–308. <https://doi.org/10.1306/07121211159>.
- Gorin, G. (1989). Interprétation géologique de la champagne sismique GG87 dans le Canton de Genève. *Université de Genève on Behalf of the "Département de l'Economie Publique de Geneve"*, Unpublished, 33.
- Gorin, G. E., Racz, L. G., & Walter, M. R. (1982). Late Precambrien-Cambrien sediments of Huqf Group, Sultanate of Oman. *Amer. Ass. Petr. Geol. Bull.*, 66 / 12, 2609–2627.
- Gorin, G., Signer, C., & Amberger, G. (1993). Structural configuration of the western Swiss Molasse Basin as defined by reflection seismic data. *Eclogae Geologicae Helvetiae*, 86(3), 693–716.

- Gruber, M. (2012). Geophysikalische, Geologische und Geomorphologische Untersuchungen an der La Lance Blattverschiebung - Schweiz. In *Departement of Geosciences*. Fribourg.
- Gruber, M. (2017). Structural Investigations of the Western Swiss Molasse Basin - From 2D Seismic Interpretation to a 3D Geological Model. In *GeoFocus* (Vol. 41). PhD Thesis, Département de Géosciences, Sciences de la Terre, Université de Fribourg.
- Guellec, S., Mugnier, J. L., Tardy, M., & Roure, F. (1990). Neogene evolution of the western Alpine foreland in the light of ECORS data and balanced cross sections. In F. Roure, P. Heitzmann, & R. Polino (Eds.), *Deep structures of the Alps* (1st ed., pp. 165–185). Mém. Soc. géol. suisse.
- Guillaume, A., Llac, F., & Meurisse, M. (1972). *Notice explicative de la carte géologique de la France (1/50'000), feuille Saint-Claude (149)*. BRGM France.
- Hauvette, L., Marro, A., Borderie, S., Sommaruga, A., & Mosar, J. (2021). 3D Seismic Model from Salève to Jura. Time to Depth Conversion Explanatory Note. *University of Fribourg, CH, on Behalf of the Services Industriels de Genève (SIG), Unpublished*, 33.
- Hauvette, L. (2017). Traitement de Normalisation Des lignes sismiques Du bassin genevois. *Report Written by Geneva Geo Energy (GGE) Company (Genève) on Behalf of the Services Industriels de Genève (SIG), Unpublished*, 8.
- Hauvette, L. (2020). Malm seismic interpretation of the Geneva Basin using latest 2D seismic 2018 campaign. *PPT Report Written by Geneva Geo Energy (GGE) Company (Genève) on Behalf of the Services Industriels de Genève (SIG), Unpublished*.
- Hauvette, L., Lathion, R., & Fiebig, B. (2018). Analyse Géophysique : Evaluation de la présence D'hydrocarbure (HC) dans la Proche sub-surface du Canton de Genève (« Shallow Gas »). *Geneva Geo Energy (GGE) on Behalf of the Services Industriels de Genève (SIG), Unpublished*, 19.
- Hefny, M., Zappone, A., Makhoulfi, Y., de Haller, A., & Moscariello, A. (2020). A laboratory approach for the calibration of seismic data in the western part of the Swiss Molasse Basin: the case history of well Humilly-2 (France) in the Geneva area. *Swiss Journal of Geosciences*, 113(1), 11. <https://doi.org/10.1186/s00015-020-00364-4>.
- Heuberger, S., Roth, P., Zingg, O., Naef, H., & Meier, B. P. (2016). The St. Gallen Fault Zone: a long-lived, multiphase structure in the North Alpine Foreland Basin revealed by 3D seismic data. *Swiss Journal of Geosciences*, 109(1), 83–102. <https://doi.org/10.1007/s00015-016-0208-5>.
- Homberg, C., Lacombe, O., Angelier, J., & Bergerat, F. (1999). New constraints for indentation mechanisms in arcuate belts from the Jura Mountains, France. *Geology*, 27(9), 827. [https://doi.org/10.1130/0091-7613\(1999\)027<0827:NCFIMI>2.3.CO;2](https://doi.org/10.1130/0091-7613(1999)027<0827:NCFIMI>2.3.CO;2).
- Homewood, P., Allen, P. A., & Williams, G. D. (1986). Dynamics of the Molasse Basin of western Switzerland. In *Foreland basins* (Vol. 8, pp. 199–217). Blackwell Scientific Publications Oxford, UK. <https://doi.org/10.1002/9781444303810.ch10>.
- Homewood, P., & Lateltin, O. (1988). Classic Swiss clastics. Flysch and Molasse. The Alpine connection. *Acta Geodynamica*, 2(1), 1–11.
- Hu, Z., Xu, C., Wang, D., Ren, J., Liu, Y., Xiao, S., & Zhou, X. (2019). Superimposed characteristics and genetic mechanism of strike-slip faults in the Bohai Sea, China. *Shiyou Kantan Yu Kaifa/Petroleum Exploration and Development*, 46(2), 254–267. <https://doi.org/10.11698/PED.2019.02.06>.
- Ibele, T. (2011). Tectonics of the Western Swiss Molasse Basin during Cenozoic Times. *Thesis*,

References

- University of Fribourg, 7--20.
- IGN. (2001). *BD ALTI: Le modèle numérique de terrain (MNT) maillé qui décrit le relief du territoire français à moyenne échelle*. <https://geoservices.ign.fr/bdalti>.
- IHS Markit. (2017). Kingdom Product Summary. *Seismic Interpretation Notice of The Kingdom Software (TKS)*, 1113. <https://query.prod.cms.rt.microsoft.com/cms/api/am/binary/RE4wnyo>.
- Jackson, M. P. A., & Hudec, M. R. (2017a). Contractual Salt-Tectonic Systems. In *Salt Tectonics: Principles and Practice* (pp. 304–335). Cambridge University Press. <https://doi.org/10.1017/9781139003988.015>.
- Jackson, M. P. A., & Hudec, M. R. (2017b). Extensional Salt-Tectonic Systems. In *Salt Tectonics*. <https://doi.org/10.1017/9781139003988.014>.
- Jackson, M. P. A., & Hudec, M. R. (2017c). Extensional Salt-Tectonic Systems. In *Salt-Tectonic Systems* (pp. 256–303). Cambridge University Press. <https://doi.org/DOI: 10.1017/9781139003988.014>.
- Jackson, M. P. A., & Hudec, M. R. (2017d). Strike-Slip Salt-Tectonic Systems. In *Salt Tectonics, Principles and Practice* (pp. 336–362). Cambridge University Press. <https://doi.org/DOI: 10.1017/9781139003988.016>.
- Jenny, J., Burri, J.-P., Muralt, R., Pugin, A., Schegg, R., Ungemach, P., Vuataz, F.-D., & Wernli, R. (1995). Le forage géothermique de Thônex (Canton de Genève): Aspects stratigraphiques, tectoniques, diagénétiques, géophysiques et hydrogéologiques. *Eclogae Geologicae Helveticae*, 88(2), 365–396.
- Jordan, P. (1992). Evidence for large-scale decoupling in the Triassic evaporites of northern Switzerland: an overview. *Eclogae Geologicae Helveticae*, 85(3), 677–693. <https://doi.org/10.5169/seals-167025>.
- Joukowsky, E., & Favre, J. (1913). Monographie géologique et paléontologique du Salève (Haute-Savoie, France). *Mémoires de La Société de Physique et d'Histoire Naturelle de Genève*, 37, 295–523.
- Kalifi, A., Leloup, P. H., Sorrel, P., Galy, A., Demory, F., Spina, V., Huet, B., Quillévéré, F., Ricciardi, F., Michoux, D., Lecacheur, K., Grime, R., Pittet, B., & Rubino, J. L. (2021). Chronology of thrust propagation from an updated tectono-sedimentary framework of the Miocene molasse (western Alps). *Solid Earth*, 12, 2735–2771. <https://doi.org/10.5194/se-12-2735-2021>.
- Koumrouyan, M. (2019). Geomechanical characterisation of geothermal exploration borehole: Implication for the GEO-01 well, in Geneva. *Université de Neuchâtel, Centre d'Hydrogéologie et Géothermie*, 109.
- Lathion, R., & Hauvette, L. (2020). Toit du rocher - Etude du Quaternaire du Bassin de Genève. *Ad Terra (Geneva Geo Energy) on Behalf of GESDEC, Unpublished*, 16.
- Laubscher, H.-P. (1961). Die Fernschubhypothese der Jurafaltung. *Eclogae Geologicae Helveticae*, 54(1), 222–282. <https://doi.org/10.5169/seals-162820>.
- Laubscher, H.-P. (1965). Ein kinematisches Modell der Jurafaltung. *Eclogae Geologicae Helveticae*, 58(1), 232–318. <https://doi.org/10.5169/seals-163266>.
- Laubscher, H. P. (1986). The eastern Jura: Relations between thin-skinned and basement tectonics, local and regional. *Geologische Rundschau*, 75(3), 535–553. <https://doi.org/10.1007/BF01820630>.

- Lemoine, M., Bas, T., Arnaud-Vanneau, A., Arnaud, H., Dumont, T., Gidon, M., Bourbon, M., Graciansky, P. C., Rudkiewicz, J. L., Mégard-Galli, J., & Tricart, P. (1986). The continental margin of the Mesozoic Tethys in the Western Alps. *Marine and Petroleum Geology*, *3*, 179–199.
- Lemoine, M., & Trümpy, R. (1987). Pre-oceanic rifting in the Alps. *Tectonophysics*, *133*, 305–320.
- Leu, W. (2012). Swiss oil/gas exploration and lessons learnt. *Swiss Bulletin Für Angewandte Geologie*, *17*(1), 49–59.
- Li, J., & Mitra, S. (2020). Seismic models of detachment and faulted detachment folds. *Marine and Petroleum Geology*, *117*(December 2019), 104385. <https://doi.org/10.1016/j.marpetgeo.2020.104385>.
- Lofi, J., Pezard, P., Loggia, D., Garel, E., Gautier, S., Merry, C., & Bondabou, K. (2012). Geological discontinuities, main flow path and chemical alteration in a marly hill prone to slope instability: Assessment from petrophysical measurements and borehole image analysis. *Hydrological Processes*, *26*(14), 2071–2084. <https://doi.org/10.1002/hyp.7997>.
- Madritsch, H. (2008). Structural evolution and neotectonics of the Rhine-Bresse transfer zone [Universität Basel, Geologisch-Paläontologisches Institut]. In *PhD Dissertation, University of Basel*. <https://doi.org/10.5451/unibas-004648278>.
- Madritsch, H., Kounov, A., Schmid, S. M., & Fabbri, O. (2009). Multiple fault reactivations within the intra-continental Rhine-Bresse Transfer Zone (La Serre Horst, eastern France). *Tectonophysics*, *471*(3–4), 297–318. <https://doi.org/10.1016/j.tecto.2009.02.044>.
- Madritsch, H., Naef, H., Meier, B., Franzke, H. J., & Schreurs, G. (2018). Architecture and Kinematics of the Constance-Frick Trough (Northern Switzerland): Implications for the Formation of Post-Variscan Basins in the Foreland of the Alps and Scenarios of Their Neogene Reactivation. *Tectonics*, *37*(7), 2197–2220. <https://doi.org/10.1029/2017TC004945>.
- Madritsch, H., Schmid, S. M., & Fabbri, O. (2008). Interactions between thin- and thick-skinned tectonics at the northwestern front of the Jura fold-and-thrust belt (eastern France). *Tectonics*, *27*(5). <https://doi.org/10.1029/2008TC002282>.
- Malzer, H., Hein, G., & Zippelt, K. (1983). Height changes in the Rhenis Massif: determination and analysis. In K. Fuchs (Ed.), *Plateau Uplift* (pp. 164–176). Springer.
- Mann, J., Schleicher, J., & Hertweck, T. (2007). CRS stacking - A simplified explanation. *69th European Association of Geoscientists and Engineers Conference and Exhibition 2007: Securing The Future. Incorporating SPE EUROPEC 2007*, *5*(June), 2696–2700. <https://doi.org/10.3997/2214-4609.201401499>.
- Marchant, R., Ringgenberg, Y., Stampfli, G., Birkhäuser, P., Roth, P., & Meier, B. (2005). Paleotectonic evolution of the Zürcher Weinland based on 2D and 3D seismics in northern Switzerland. *Eclogae Geologicae Helvetiae*, *98*, 345–362.
- Marchant, R. (2016). GeoMol-Vaud final report. *Musée Cantonal de Géologie de Lausanne on Behalf of SWISSTOPO*, 79.
- Marro, A. (2021). Tectonics of the Western Internal Jura Fold-and-Thrust Belt: From the Geneva Basin (Switzerland) to La Biemme Valley (France). *Master Thesis Deposited at UNIFR, University of Fribourg, CH*, 140.
- Marro, A., Hauvette, L., Borderie, S., & Mosar, J. (2023). Kinematics of the Western Internal Jura Fold-

References

- and-Thrust Belt: Forward Modelling. *Swiss Journal of Geosciences*, 116(19), <https://doi.org/10.1186/s00015-023-00435-2>.
- Marsden, D. (1993). Static corrections - a review. *The Leading Edge*, 12(1), 43–49. [https://edisciplinas.usp.br/pluginfile.php/4452519/mod_resource/content/1/static review.pdf](https://edisciplinas.usp.br/pluginfile.php/4452519/mod_resource/content/1/static%20review.pdf).
- Martinuzzi, V., & Sallier, B. (2018). GEo-1 : Rapport d 'acquisitions diagraphiques et Interprétation pétrophysique. *Geneva Geo Energy (GGE) on Behalf of the Services Industriels de Genève (SIG), Unpublished Report*, 48.
- Massironi, M., & Kim, Y.-S. (2015). *Strike-Slip Faults BT - Encyclopedia of Planetary Landforms* (H. Hargitai & Á. Kereszturi (eds.); pp. 2069–2078). Springer New York. https://doi.org/10.1007/978-1-4614-3134-3_548.
- Mastrangelo, B., Charollais, J., Wernli, R., & Metzger, J. (2013). Accidents longitudinaux dans la Molasse rouge auct. et dans son substratum sur le versant oriental du Salève (Haute-Savoie, France). *Swiss Journal of Geosciences*, 106(2), 253–263. <https://doi.org/10.1007/s00015-013-0136-6>.
- Mazurek, M., Hurford, A. J., & Leu, W. (2006). Unravelling the multi-stage burial history of the Swiss Molasse Basin: Integration of apatite fission track, vitrinite reflectance and biomarker isomerisation analysis. *Basin Research*, 18, 27–50.
- McClay, K. R. (1987). *The Mapping of Geological Structures*. Open University Press. https://books.google.ch/books?id=J%5C_NNAQAAIAAJ.
- Medina, P., Bonomo, N., Osella, A., Bernárdez, S., & Limarino, C. (2018). *GPR Prospecting of Fluvial-Eolian Interaction Deposits in the Bermejo Valley, NW Argentina*. <https://doi.org/10.3997/2214-4609.201802474>.
- Medwedeff, D. A. (1992). Geometry and kinematics of an active, laterally propagating wedge thrust, Wheeler Ridge, California. In S Mitra & G. W. Fisher (Eds.), *Structural geology of fold and thrust belts* (pp. 3–28). Johns Hopkins University press.
- Meier, B. (2010). *NAB 10-40, Ergänzende Interpretation reflexionsseismischer Linien zwischen dem östlichen und westlichen Molassebecken: Gebiete Waadtland Nord, Fribourg, Berner Seeland und Jurasüdfuss zwischen Biel und Oensingen (Text und Beilage)*. <http://www.nagra.ch>.
- Meyer, M. (2000). *Le complexe récifal kimméridgien - tithonien du Jura méridional interne (France), évolution multifactorielle, stratigraphique et tectonique*. <https://archive-ouverte.unige.ch/unige:98282>.
- Mitra, S. (1986). Duplex structures and imbricate thrust systems: geometry, structural position and hydrocarbon potential. *American Association of Petroleum Geologists, Bulletin*, 70(9), 1087–1112.
- Mitra, Shankar. (2003). A unified kinematic model for the evolution of detachment folds. *Journal of Structural Geology*, 25(10), 1659–1673. [https://doi.org/10.1016/S0191-8141\(02\)00198-0](https://doi.org/10.1016/S0191-8141(02)00198-0).
- Mock, S., & Herwegh, M. (2017). Tectonics of the central Swiss Molasse Basin: Post-Miocene transition to incipient thick-skinned tectonics? *Tectonics*, 36(9), 1699–1723. <https://doi.org/10.1002/2017TC004584>.
- Mokhtari, M., & Pourhossein, H. (2003). Significance of VSP Data for Surface Seismic Data; South Ghashu Gas Field, South Iran. *Iranian International Journal of Science*, 4(2), 223–240.

- Mooney, W. D., Prodehl, C., & Pavlenkova, N. I. (2002). Seismic velocity structure of the continental lithosphere from controlled source data. *International Geophysics*, 81(PART A), 887–910. [https://doi.org/10.1016/S0074-6142\(02\)80261-3](https://doi.org/10.1016/S0074-6142(02)80261-3).
- Morend, D. (2000). High-resolution seismic facies of alluvial depositional systems in the Lower Freshwater Molasse (Oligocene-early Miocene, western Swiss Molasse Basin). *PhD Thesis, University of Geneva, Terre et E*, 97. <https://doi.org/https://doi.org/10.13097/archive-ouverte/unige:97969>.
- Mosar, J., & Suppe, J. (1992). Role of shear in fault - propagation folding. In K. McClay (Ed.), *Thrust Tectonics* (pp. 123–132). Chapman & Hall.
- Mosar, J. (1999). Present-day and future tectonic underplating in the western Swiss Alps: reconciliation of basement/wrench-faulting and décollement folding of the Jura and Molasse basin in the Alpine foreland. *Earth and Planetary Science Letters*, 173(3), 143–155. [https://doi.org/10.1016/S0012-821X\(99\)00238-1](https://doi.org/10.1016/S0012-821X(99)00238-1).
- Moscardelli, L., Wood, L., & Dunlap, D. (2012). Shelf-edge deltas along structurally complex margins: A case study from eastern offshore Trinidad. *AAPG Bulletin*, 96, 1483–1522. <https://doi.org/10.1306/01241211046>.
- Moscariello, A., Guglielmetti, L., Omodeo-Salé, S., De Haller, A., Eruteya, O. E., Ying Lo, H., Clerc, N., Makloufhi, Y., Do Couto, D., Ferreira de Oliveira, G., Perozzi, L., DeOliveira, F., Hollmuller, P., Quiquerez, L., Nawratil De Bono, C., Martin, F., & Meyer, M. (2020). *Heat production and storage in Western Switzerland: advances and challenges of intense multidisciplinary geothermal exploration activities, an 8 years progress report* (p. 13). Proceedings World Geothermal Congress.
- Nachtmann, W., & Wagner, L. (1987). Mesozoic and Early Tertiary Evolution of the Alpine Foreland in Upper Austria and Salzburg, Austria. *Tectonophysics*, 137(1–4), 61–76. [https://doi.org/Doi10.1016/0040-1951\(87\)90314-3](https://doi.org/Doi10.1016/0040-1951(87)90314-3).
- Naef, H., & Madritsch, H. (2014). Tektonische Karte des Nordschweizer Permokarbondrogs: Aktualisierung basierend auf 2D-Seismik und Schweredaten. In NAGRA (Ed.), *NAGRA Arbeitsbericht 14-17*.
- Nagel, J. L. (2007). *Carte géologique harmonisée du département du Jura, rapport final 55733-FR*. 177. https://www.google.com/url?sa=t&rct=j&q=&src=s&source=web&cd=&ved=2ahUKEwi-w-vA-4X9AhUyi_0HHWBGA-kQFnoECA4QAQ&url=http%3A%2F%2Finfoterre.brgm.fr%2Frapports%2FRP-55733-FR.pdf&usq=AOvVaw2ZnacMiq39DXBH3tyeDwet.
- Nagra. (2014). Tektonische Karte des Nordschweizer Permokarbondrogs: Aktualisierung basierend auf 2D-Seismik und Schweredaten. In *Nagra Arbeitsbericht* (Issue NAB 14-17). Nagra.
- OCEAN. (1994). Forage géothermique de Thônex, Rapport final. *Department of Energy Canton Geneva (OCEAN)*, 112.
- Office fédéral de topographie swisstopo. (2013). *swissALTI3D: Le modèle altimétrique numérique haute précision de la Suisse*. <https://www.swisstopo.admin.ch/fr/geodata/height/alti3d.html>.
- Ortner, H., von Hagke, C., Sommaruga, A., Mock, S., Mosar, J., Hinsch, R. & Beidinger, A. (2023): *The northern Deformation Front of the European Alps*. In: Bellahsen, N. & Rosenberg, C., *Geodynamics of the Alps 3*, ISTE-Wiley, London.

References

- Pace, P., Domenica, A. Di, & Calamita, F. (2014). *the Tectonic Style of Thrust Belts. Figure 1*, 756–785. <https://doi.org/10.1002/2013TC003385>.
- Paolacci, S. (2012). Seismic Facies and Structural Configuration of the Western Alpine Molasse Basin and its Substratum (France and Switzerland). *PhD Thesis from University of Geneva, UNIGE, CH, Unpublished*, 166.
- Paumard, V., Zuckmeyer, E., Boichard, R., Jorry, S. J., Bourget, J., Borgomano, J., Maurin, T., & Ferry, J. N. (2017). Evolution of Late Oligocene - Early Miocene attached and isolated carbonate platforms in a volcanic ridge context (Maldives type), Yadana field, offshore Myanmar. *Marine and Petroleum Geology*, *81*, 361–387. <https://doi.org/10.1016/j.marpetgeo.2016.12.012>.
- Peacock, D. C. P., Nixon, C. W., Rotevatn, A., Sanderson, D. J., & Zuluaga, L. F. (2016). Glossary of fault and other fracture networks. *Journal of Structural Geology*, *92*, 12–29. <https://doi.org/10.1016/j.jsg.2016.09.008>
- Pfiffner, O.-A., Schlunegger, F., & Buitter, S. J. H. (2002). The Swiss Alps and their peripheral foreland basin: Stratigraphic response to deep crustal processes. *Tectonics*, *21*(2), 1–15. <https://doi.org/10.1029/2000TC900039>.
- Philippe, Y., Colletta, B., Deville, E., & Mascle, A. (1996). The Jura fold-and-thrust belt: a kinematic model based on map-balancing. *Mémoires Du Muséum National d'histoire Naturelle (1993)*, *170*, 235–261.
- Philippe, Y. (1995). *Rampes latérales et zones de transfert dans les chaînes plissées: géométrie, conditions de formation et pièges structuraux associés* [Université de Savoie. tel-00755680]. <https://tel.archives-ouvertes.fr/tel-00755680>.
- Rabin, M., Sue, C., Walpersdorf, A., Sakic, P., Albaric, J., & Fores, B. (2018). Present-day deformations of the Jura arc inferred by GPS surveying and earthquake focal mechanisms. *Tectonics*, *37*(10), 3782–3804.
- Rabin, M. (2016). Caractérisation de la déformation récente dans une chaîne orogénique lente : l' arc du Jura . Approches combinées morphotectonique , géodésique et géophysique. *PhD Thesis from l'université de Franche-Comté*, 234. <https://theses.hal.science/tel-01413236>.
- Radaideh, O. M. A., & Mosar, J. (2021). Cenozoic Tectonic Deformation Along the Pontarlier Strike-Slip Fault Zone (Swiss and French Jura Fold-and-Thrust Belt): Insights From Paleostress and Geomorphic Analyses. *Tectonics*, *40*(5), 1–45. <https://doi.org/10.1029/2021TC006758>.
- Ramsayer, G. R. (1979). Seismic stratigraphy, a fundamental exploration tool. *Proceedings of the Annual Offshore Technology Conference, 1979-May(C)*, 1859–1868. <https://doi.org/10.4043/3568-ms>.
- Raynaud, A., & Marmion, D. (1992). *Log fondamentale au 1/500 Charmont 1*, 16-1230.
- Rigassi, D. (1957). *Le Tertiaire de la région genevoise et savoisienne*. <https://doi.org/10.5169/SEALS-189002>.
- Rime, V., Sommaruga, A., Schori, M., & Mosar, J. (2019). Tectonics of the Neuchâtel Jura Mountains: insights from mapping and forward modelling. *Swiss Journal of Geosciences*, *112*(2–3), 563–578. <https://doi.org/10.1007/s00015-019-00349-y>.
- Ring, U., & Gerdes, A. (2016). Kinematics of the Alpenrhein-Bodensee graben system in the Central Alps: Oligocene/Miocene transtension due to formation of the Western Alps arc. *Tectonics*, *35*(6),

- 1367–1391. <https://doi.org/10.1002/2015TC004085>
- Roksandic, M. M. (1978). Seismic facies analysis concepts. *Geophysical Prospecting*, 26(2), 383–398.
- Rusillon, E. (2017). Characterisation and rock typing of deep geothermal reservoirs in the Greater Geneva Basin (Switzerland & France). *PhD Thesis, Université de Genève*, 254. <https://archive-ouverte.unige.ch/unige:105286>.
- Saklani, P.S. (2008). Glossary of Structural Geology and Tectonics. *Department of Geology, University of Dehli, and Netaji Subhas Institute of Technology*, 203. <https://www.google.com/url?sa=t&rct=j&q=&esrc=s&source=web&cd=&ved=2ahUKEwim7ufR-IX9AhWz9rsIHSI3DRoQFnoECA0QAQ&url=https%3A%2F%2Fgsi.ir%2Ffiles%2Fcontent%2FGlossary%2520of%2520Structural%2520Geology.pdf&usg=AOvVaw0hucg7utmPyeitmCqEfUpY>.
- Schaltegger, U. (1997). The age of an Upper Carboniferous Lower Permian sedimentary basin and its hinterland as constrained by U-Pb dating of volcanic and detrital zircons (Northern Switzerland). *Schweizerische Mineralogische Und Petrographische Mitteilungen*, 77(1), 101–111.
- Schardt, H. (1891). Etudes géologiques sur l'extrémité méridionale de la première chaîne du Jura (Chaîne du Reculet-Vuache). *Bull. Soc. Vaud. Sc. Nat.*, XXVII, 69–161.
- Schmid, S. M., & Kissling, E. (2000). The arc of the western Alps in the light of geophysical data on deep crustal structure. *Tectonics*, 19(1), 62–85. <https://doi.org/10.1029/1999TC900057>.
- Schori, M. (2021). The Development of the Jura Fold-and-Thrust Belt: pre-existing Basement Structures and the Formation of Ramps. *GeoFocus*, 50, 200. <https://doi.org/10.51363/unifr.sth.2022.001>.
- Schori, M., Mosar, J., & Schreurs, G. (2015). Multiple detachments during thin-skinned deformation of the Swiss Central Jura: a kinematic model across the Chasseral. *Swiss Journal of Geosciences*, 108, 327–343. <https://doi.org/10.1007/s00015-015-0196-x>.
- Schori, M., Zwaan, F., Schreurs, G., & Mosar, J. (2021). Pre-existing Basement Faults Controlling Deformation in the Jura Mountains Fold-and-Thrust Belt: Insights from Analogue Models. *Tectonophysics*, 814(June), 228980. <https://doi.org/10.1016/j.tecto.2021.228980>.
- Scolari, G. (1956). Nouvelles observations et hypothèses sur la tectonique du Mont Vuache. *Arch. Sci.* 9/1: 553-72, Genève.
- SEG Wiki. (2018). *Seismic Resolution: Vertical and Horizontal*. https://wiki.seg.org/wiki/Seismic_Resolution:_Vertical_and_Horizontal.
- Serneels, V. (1993). Le Sidérolithique du Jura suisse. *Minaria Helvetica*, 13b(Janvier), 74–83.
- Shankar Mitra. (1986). Duplex Structures and Imbricate Thrust Systems: Geometry, Structural Position, and Hydrocarbon Potential. *AAPG Bulletin*, 70(1963). <https://doi.org/10.1306/94886a7e-1704-11d7-8645000102c1865d>.
- Sheriff, R. E. (1975). Factors affecting seismic amplitudes. *Geophysical Prospecting*, 23, 125–138.
- Signer, C. (1992). Interprétation sismique structurale et sismostratigraphique entre Jura et front alpin dans la région genevoise. *PhD Thesis from University of Geneva, UNIGE, CH*, 1–90.
- Signer, C., & Gorin, G. E. (1995). New geological observations between the Jura and the Alps in the Geneva area, as derived from reflection seismic data. *Eclogae Geologicae Helvetiae*, 88(2), 235–265. <https://doi.org/10.5169/SEALS-167674>.

References

- Siletto, G. B., Spalla, M. I., Tunesi, A., Lardeaux, J. M., & Colombo, A. (1993). Pre-Alpine structural and metamorphic histories in the Orobic Southern Alps, Italy. In J. F. von Raumer & F. Neubauer (Eds.), *Pre-Mesozoic geology in the Alps* (pp. 585–598). Springer-Verlag.
- Simm, R., & Bacon, M. (2014). *Seismic Amplitude: An Interpreter's Handbook*. Cambridge University Press. <https://doi.org/10.1017/CBO9780511984501>.
- Sinclair, H. D., Coakley, B. J., Allen, P. A., & Watts, A. B. (1991). Simulation of Foreland Basin Stratigraphy using a diffusion model of mountain belt uplift and erosion: An example from the central Alps, Switzerland. *Tectonics*, *10*(3), 599–620. <https://doi.org/10.1029/90TC02507>.
- Smit, J., Brun, J.-P., Cloething, S., & Ben-Avraham, Z. (2008). Pull-apart basin formation and development in narrow transform zones with application to the Dead Sea Basin. *Tectonics*, *27*, 1–17. <https://doi.org/10.1029/2007TC002119>.
- S.N.P.A. (1969). Rapport de fin de sondage d'Humilly-2. *Société Nationale Pétrologique d'Aquitaine*.
- Sommaruga, A. (1995). Tectonics of the Central Jura and the Molasse Basin. New insight from the interpretation of seismic reflection data. *Bulletin de La Société Neuchâteloise Des Sciences Naturelles*, *118*, 95–108.
- Sommaruga, A. (1997). Geology of the Central Jura and the Molasse Basin: new insight into an evaporite-based foreland fold and thrust belt. *Mémoire de La Société Neuchâteloise Des Sciences Naturelles*, *12*, 1–176.
- Sommaruga, A. (1999). Décollement tectonics in the Jura foreland fold-and-thrust belt. *Marine and Petroleum Geology*, *16*(2), 111–134. [https://doi.org/10.1016/S0264-8172\(98\)00068-3](https://doi.org/10.1016/S0264-8172(98)00068-3).
- Sommaruga, A., Mosar, J., Schori, M., & Gruber, M. (2017). The Role of the Triassic Evaporites Underneath the North Alpine Foreland. In J. I. Soto, J. Flinch, & G. Tari (Eds.), *Permo-Triassic Salt Provinces of Europe, North Africa and the Atlantic Margins* (pp. 447–466). Elsevier. <https://doi.org/10.1016/b978-0-12-809417-4.00021-5>.
- Sommaruga, Anna, Eichenberger, U., & Marillier, F. (2012). Seismic Atlas of the Swiss Molasse Basin. In E. Kissling (Ed.), *Matériaux pour la Géologie de la Suisse - Géophysique* (Vol. 44, p. 90). Federal Office of Topography (swisstopo).
- Stampfli, G. M. (2000). Tethyan oceans. In E. Bozkurt, J. A. Winchester, & J. D. A. Piper (Eds.), *Tectonics and magmatism in Turkey and surrounding area* (Vol. 173, pp. 163–185). Geological Society of London, Special Publication.
- Stampfli, G. M., & Borel, G. (2002). A plate tectonic model for the Paleozoic and the Mesozoic constrained by dynamic plate boundaries and restored synthetic ocean isochrones. *Earth and Planet. Sci. Lett.*, *169*, 17–33.
- Stampfli, G. M., Mosar, J., Favre, P., Pillevuit, A., & Vannay, J.-C. (2001). Permo-Mesozoic evolution of the western Tethys realm: the Neo-Tethys East Mediterranean Basin connection. In Ziegler, W. Cavazza, A. H. F. Robertson, & S. Crasquin-Soleau (Eds.), *Peri-Tethys Memoir 6: Peri-Tethyan Rift/Wrench Basins and Passive Margins* (Vol. 186, Issue January, pp. 51–108). Mémoires du Muséum national d'histoire naturelle.
- Stampfli, G. M., Mosar, J., Marquer, D., Marchant, R., Baudin, T., & Borel, G. (1998). Subduction and obduction processes in the Swiss Alps. *Tectonophysics*, *296*(1–2), 159–204. [https://doi.org/10.1016/S0040-1951\(98\)00142-5](https://doi.org/10.1016/S0040-1951(98)00142-5).

- Strasser, A., Charollais, J., Conrad, M. A., Clavel, B., Pictet, A., & Mastrangelo, B. (2016). The Cretaceous of the Swiss Jura Mountains: an improved lithostratigraphic scheme. *Swiss Journal of Geosciences*, *109*(2), 201–220. <https://doi.org/10.1007/s00015-016-0215-6>.
- Subrahmanyam, D., & Rao, P. H. (2008). Seismic Attributes- A Review. *International Conference & Exposition on Petroleum Geophysics*, 398.
- Suppe, J. (1983). Geometry and kinematics of fault-bend folding. *American Journal of Science*, *283*, 684–721.
- Swiss Committee on Stratigraphy. (2017). *Lithostratigraphic Lexicon of Switzerland*. <http://www.strati.ch>.
- Swisstopo. (2012). *GeoCover geological vector data*. Federal Office of Topography (swisstopo). <http://map.geo.admin.ch>.
- Telford, W. M., Geldart, L. P., & Sheriff, R. E. (1990). Applied Geophysics. In Cambridge University Press (Ed.), *Applied Geophysics*. <https://doi.org/10.1017/cbo9781139167932.007>.
- Thouvenot, F., Fréchet, J., Taponnier, P., Thomas, J.-C., Le Brun, B., Ménard, G., Lacassin, R., Janetton, L., Grasso, J.-R., Coutant, O., Paul, A., & Hatzfeld, D. (1998). The M_L 5.3 Epagny (French Alps) earthquake of 1996 July 15: a long-awaited event on the Vuache fault. *Geophysical Journal International*, *135*, 876–892.
- Ustaszewski, K., & Schmid, S. M. (2006). Control of preexisting faults on geometry and kinematics in the northernmost part of the Jura fold-and-thrust belt. *Tectonics*, *25*(5), 1–26. <https://doi.org/10.1029/2005TC001915>.
- VAIL, P. R., 1987, Seismic stratigraphic interpretation procedure, in Bally, A. W., ed., *Atlas of Seismic Stratigraphy: Tulsa*, American Association of Petroleum Geologists Studies in Geology, *27*, p. 1–10.
- Vermeer, G. J. O. (2003). Acquisition/processing - 3D seismic survey design optimization. *Leading Edge (Tulsa, OK)*, *22*(10), 934–941. <https://doi.org/10.1190/1.1623633>.
- Vernet, J.-P., & Horn, R. (1971). Etudes sédimentologique et structurale de la partie occidentale du lac Léman par la méthode sismique à réflexion continue. *Eclogae Geologicae Helveticae*, *64*(2), 291–317.
- Vernet, J.-P., Horn, R., Badoux, H., & Scolari, G. (1974). Etude structurale du Léman par sismique réflexion continue. *Eclogae Geologicae Helveticae*, *67*(3), 515–529.
- von Raumer, J. F. (1998). The Palaeozoic evolution in the Alps: from Gondwana to Pangea. *Geologische Rundschau*, *87*, 407–435.
- von Raumer, J. F., & Neubauer, F. (1993). *Pre-Mesozoic geology in the Alps* (p. 677). Springer-Verlag.
- Vouillamoz, N., Mosar, J., & Deichmann, N. (2017). Multi-scale imaging of a slow active fault zone: Contribution for improved seismic hazard assessment in the Swiss Alpine foreland. *Swiss Journal of Geosciences*, *110*(2), 547–563.
- Weidmann, M. (1984). Le Sidérolithique et la Molasse basale d'Orbe (Vaud). *Bull. Soc. Vaud. Sc. Nat.*, *366*(77), 135–141.
- Wenning, Q. C., Berthet, T., Ask, M., Zappone, A., Rosberg, J. E., & Almqvist, B. S. G. (2017). Image log analysis of in situ stress orientation, breakout growth, and natural geologic structures to 2.5 km

References

- depth in central Scandinavian Caledonides: Results from the COSC-1 borehole. *Journal of Geophysical Research: Solid Earth*, 122(5), 3999–4019. <https://doi.org/10.1002/2016JB013776>.
- Wetzel, A., Allenbach, R., & Allia, V. (2003). Reactivated basement structures affecting the sedimentary facies in a tectonically “quiescent” epicontinental basin: an example from NW Switzerland. *Sedimentary Geology*, 157(1), 153–172. [https://doi.org/10.1016/S0037-0738\(02\)00230-0](https://doi.org/10.1016/S0037-0738(02)00230-0).
- Wildi, W., Funk, H., Loup, B., Amato, E., & Huggenberger, P. (1989). Mesozoic subsidence history of the European marginal shelves of the alpine Tethys (Helvetic realm, Swiss Plateau and Jura). *Eclogae Geologicae Helveticae*, 82(3), 817–840. <https://doi.org/10.5169/seals-166404>.
- Wildi, W., Blondel, T., Charollais, J., Jaquet, J.-M., & Wernli, R. (1991). Tectonique en rampe latérale à la terminaison occidentale de la Haute-Chaîne du Jura. *Eclogae Geologicae Helveticae*, 84(1), 265–277.
- Wildi, W., & Huggenberger, P. (1993). Reconstitution de la plate-forme européenne anté-orogénique de la Bresse aux Chaînes subalpines; éléments de cinématique alpine (France et Suisse occidentale)x). *Eclogae Geologicae Helveticae*, 86(1), 47–64.
- Willett, S. D., & Schlunegger, F. (2010). The last phase of deposition in the Swiss Molasse Basin: From foredeep to negative-alpha basin. *Basin Research*, 22(5), 623–639. <https://doi.org/10.1111/j.1365-2117.2009.00435.x>
- Yordkayhun, S., Ivanova, A., Giese, R., Juhlin, C., & Cosma, C. (2009). Comparison of surface seismic sources at the CO2SINK site, Ketzin, Germany. *Geophysical Prospecting*, 57, 125–139. <https://doi.org/10.1111/j.1365-2478.2008.00737.x>
- Ziegler, P A. (1990). *Geological Atlas of Western and Central Europe* (2nd ed.). Shell Int. Petroleum Mij.
- Ziegler, P A, & Dèzes, P. (2007). Cenozoic uplift of Variscan Massifs in the Alpine foreland: Timing and controlling mechanisms. *Global and Planetary Change*, 58(1–4), 237–269. <https://doi.org/10.1016/j.gloplacha.2006.12.004>.
- Ziegler, P A, van Wees, J. D., & Cloetingh, S. (1998). Mechanical controls on collision-related compressional intraplate deformation. *Tectonophysics*, 300, 103–129.
- Ziegler, Peter A. (1992). Geological Atlas of Western and Central Europe (2nd Edition). *Geological Society of London*, 2, 256.

CURRICULUM VITAE - LOUIS HAUVETTE

Born on July 26th 1990 - 33 years old - Nationality: French

+33 6 78 51 68 39 / +41 77 412 52 53 / Louis.hauvette@gmail.com / louis.hauvette@hydro-geo.ch

A: Competences

- G&G Interpretation: Experience in seismic interpretation (2D & 3D), from basin evaluation to field development. Integrated G&G approach using seismic facies analysis and depositional environment reconstruction (clastics and carbonates). Exposure on Fluvio-glacial systems in the Quaternary and other near surface geological features.
- Reservoir seismic characterization: post-processing for geostatistical stochastic inversion and attribute analysis. Karst identification, with dip-steered volume computation for supporting seismic attribute analysis.
- Seismic acquisition: Knowledges in Planning and operation support mainly for land 2D lines and VSP acquisitions.
- Seismic Processing: Knowledges in planning, tendering, supervision and QC of 2D/3D processing.
- Seismic to well tie expertise from log preparation to synthetic trace computation and VSP integration.
- Seismic project set-up and QC: 2D seismic lines and 3D seismic cubes with complex misties analysis including also well calibration and 3D QC of all well data imported in the project.
- Good knowledge of various geological styles including carbonate ramps and build-ups, fluvial, deltaic and turbiditic deposits.
- IT skills: Modelling software (*intermediate skills*: Skua-gOcad, Petrel, Move), Geology/ Geophysics software (*strong skills*: Kingdom, Petrosys, Seisearch, OpendTect, Arcmap/Arcgis, Seismic Unix, Madagascar, Surfer), Programming /Computation software (*intermediate skills*: MATLAB, CodeBlocks (C++), Python, Mathematica).

B: Career

Geophysicist at HydroGeo Environnement SA (HGE), Geneva, Switzerland (2022-onward):

- Project leader for geothermal exploration in Switzerland:
 - Seismic interpretation 2D/3D
 - Seismic acquisition planning and supervision
 - 3D modelling and geothermal prospect portfolio

Geophysicist at Ad Terra Energy (ATE), Geneva, Switzerland (2014 - 2022):

- **SIG** geothermal project participation as a geophysicist from Quaternary Geology to deep Geology:
 - Seismic interpretation of all 2D seismic lines in the Geneva Canton, including all regional wells. Each intervals of the Mesozoic cover were investigated, from horizon picking, fault identification, to facies or special seismic features analysis.
 - Special focus on structural interpretation, especially with a part time academic work (PhD student) at the University of Fribourg, integrating geodynamic knowledge.
 - Participation in many seismic acquisition programs (2D and coming 3D) in the Geneva Canton; planning, QC and field work.
 - Well/ targets portfolio elaboration with special implications in the first Geo-01&02 wells drilled for the project
- **NAGRA** projects participation: Seismic interpretation using seismic attributes and special processing from Quaternary Geology to deep Geology:
 - Karst Identification and Seismic Facies Analysis within the Upper Malm based on the OPA-97 3D Seismic Data (2016).

- Quaternary study in NL and ZNO areas using PostSDM processing (2017).
- Seismo-Facies Reconnaissance study Middle-Upper Dogger/ Jura Ost area (2017).
- 3D seismic interpretation review (2018-2020).
- 3D seismic processing review (2018).
- Neotectonic study on shallow high resolution 2D seismic lines (2018).
- o Participation in many projects in Geophysics/Geomodelling/Geology for different clients including:
 - Several geophysical projects in Switzerland, Germany, France, Iraq, Oman, Nigeria, Gabon, Congo.

Geophysics for Geomodelling (G4G) at TOTAL, Pau, France, (March-Aug 2014):

- o Use of both 3D and 4D seismic constraints in the infill of reservoir models on SISMAGE.

Reservoir Seismic Characterization (CSR) at TOTAL, Pau, France, (July-Aug 2013):

- o Participation in the development of a prototype program (MATLAB) of post-processing for geostatistical stochastic Inversion.

C: Qualifications

2019-2024 University of Fribourg (UNIFR, Switzerland)

- o PhD candidate in structural geology (supervisors Prof. Jon Mosar and PD Dr. Anna Sommaruga). Title of the study: Tectonics of the Western Alpine Foreland based on Seismic interpretation of the Greater Geneva Basin.

2011-2014 Ecole Nationale Supérieure de Géologie (ENSG) (Nancy, France)

- o French engineering school specialized in geosciences (MSc)

2008-2011 Lycée Pasteur / Maths Sup-Maths Spé-option PSI (Neuilly sur Seine, France).

- o Intensive undergraduate studies in mathematics, physics, chemistry and engineering sciences in preparation for Nationwide competitive examinations for admission to French engineering school

D: Scientific Publications

Marro, Adeline & Sommaruga, Anna & Hauvette, Louis & Borderie, Sandra & Schori, Marc & Mosar, Jon. (2022). Tectonics of the Western Jura Fold-and-Thrust Belt: from the Geneva Basin to the Bienne Valley (France). Mapping and forward modelling. 10.5194/egusphere-egu22-4607.

Marro, A., Hauvette, L., Borderie, S., & Mosar, J. (2023). Kinematics of the Western Internal Jura Fold-and-Thrust Belt: Forward Modelling. Swiss Journal of Geosciences, 116(19), <https://doi.org/10.1186/s00015-023-00435-2>.

Borderie, S. & Mosar, J. & Hauvette, L. & Marro, A. & Sommaruga, A. & Meyer, M.: Numerical modelling of current state of stress in the Geneva Basin and adjacent Jura fold-and-thrust belt (Switzerland and France)., EGU General Assembly 2022, Vienna, Austria, 23–27 May 2022, EGU22-8449, <https://doi.org/10.5194/egusphere-egu22-8449>, 2022.

Haddad, Antoine & Lathion, Rodolphe & Courgeon, Simon & Fabre, Gilles & Martinuzzi, Vincent & Pedraza, Sergio & Hauvette, Louis & Games, Federico. (2022). Multi-Scale Karstic Reservoir Characterization: An Innovative Approach to Improve Reservoir Model Predictions and Decision Making. 10.2523/IPTC-22253-MS.

Madritsch, Herfried & Hammer, Paul & Hauvette, Louis & Fiebig, Bernd & Hölker, Andreas & Spillmann, Thomas. (2020). Tracking low rate Quaternary tectonic activity via high resolution topographic and subsurface imaging in the northern foreland of the European Alps (Switzerland).

Spillmann, Thomas & Madritsch, Herfried & Deplazes, G. & Hauvette, Louis & Fiebig, Bernd & Keller, Lorenz & Hölker, Andreas. (2019). Seismic analysis of overdeepened Quaternary deposits, northern Switzerland.

Already published:

- Vol. 1 **HILLGÄRTNER, Heiko** (1999) The evolution of the French Jura platform during the Late Berriasian to Early Valanginian: controlling factors and timing (203 pp.).
- Vol. 2 **DUPRAZ, Christophe** (1999) Paléontologie, paléoécologie et évolution des faciès récifaux de l'Oxfordien Moyen-Supérieur (Jura suisse et français) (247 pp.).
- Vol. 3 **BASSANT, Philip** (1999) The high-resolution stratigraphic architecture and evolution of the Burdigalian carbonate-siliciclastic sedimentary systems of the Mut Basin, Turkey (278 pp.).
- Vol. 4 **COLOMBIÉ, Claude** (2002) Sédimentologie, stratigraphie séquentielle et cyclostratigraphie du Kimméridgien du Jura suisse et du Bassin vocontien (France): relations plate-forme - bassin et facteurs déterminants (198 pp.).
- Vol. 5 **PICOT, Laurent** (2002) Le Paléogène des synclinaux du Jura et de la bordure sud-rhénone: paléontologie (Ostracodes), paléoécologie, biostratigraphie et paléogéographie (240 pp.).
- Vol. 6 **DAPPLES, Florence** (2002) Instabilités de terrain dans les Préalpes fribourgeoises (Suisse) au cours du Tardiglaciaire et de l'Holocène: influence des changements climatiques, des fluctuations de la végétation et de l'activité humaine (158 pp.).
- Vol. 7 **HUG, Wolfgang Alexander** (2003) Sequenzielle Faziesentwicklung der Karbonatplattform des Schweizer Jura im Späten Oxford und frühesten Kimmeridge (156 pp.).
- Vol. 8 **OSWALD, Daniel** (2003) Analyse de l'activité de glissements de terrain et relation avec les conditions climatiques: Exemples dans les Préalpes fribourgeoises (Suisse) (147 pp.).
- Vol. 9 **BECKER, Damien** (2003) Paléoécologie et paléoclimats de la Molasse du Jura (Oligo-Miocène): apport des Rhinocérotoidea (Mammalia) et des minéraux argileux (327 pp.).
- Vol. 10 **DELALOYE, Reynald** (2005) Contribution à l'étude du pergélisol de montagne en zone marginale (240 pp.).
- Vol. 11 **FREUDIGER-BONZON, Jeanne** (2005) Archaeometrical study (petrography, mineralogy and chemistry) of Neolithic Ceramics from Arbon Bleiche 3 (Canton of Thurgau, Switzerland) (187 pp.).
- Vol. 12 **STOFFEL, Markus** (2005) Spatio-temporal variations of rockfall activity into forests - results from tree-ring and tree analysis (188 pp.).
- Vol. 13 **RAMEIL, Niels** (2005) Carbonate sedimentology, sequence stratigraphy, and cyclostratigraphy of the Tithonian in the Swiss and French Jura Mountains - a high-resolution record of changes in sea level and climate (246 pp.).
- Vol. 14 **BRAILLARD, Luc** (2006) Morphogenèse des vallées sèches du Jura tabulaire d'Ajoie (Suisse): rôle de la fracturation et étude des remplissages quaternaires (224 pp.).
- Vol. 15 **GOYETTE-PERNOT, Joëlle** (2006) L'Ambroisie: analyse statistique et modélisation numérique de sa trajectoire aérobiologique (274 pp.).
- Vol. 16 **TRESCH, Jonas** (2007) History of a Middle Berriasian transgression (Switzerland, France, and southern England) (271 pp.).
- Vol. 17 **BONNET, Cécile** (2007) Interactions between tectonics and surface processes in the Alpine foreland: Insights from analogue model and analysis of recent faulting (189 pp.).

Already published:

- Vol. 18 **VONLANTHEN, Pierre** (2007) EBSD-based investigations of upper mantle xenoliths, snowball garnets and advanced ceramics (114 pp.).
- Vol. 19 **VÉDRINE, Stéphanie** (2007) High-frequency palaeoenvironmental changes in mixed carbonate-siliciclastic sedimentary systems (Late Oxfordian, Switzerland, France, and southern Germany) (216 pp.).
- Vol. 20 **BOLLSCHWEILER, Michelle** (2008) Spatial and temporal occurrence of past debris flows in the Valais Alps - results from tree-ring analysis (182 pp.).
- Vol. 21 **MARTY, Daniel** (2008) Sedimentology, taphonomy, and ichnology of Late Jurassic dinosaur tracks from the Jura carbonate platform (Chevenez-Combe Ronde tracksite, NW Switzerland): insights into the tidal-flat palaeoenvironment and dinosaur diversity, locomotion, and palaeoecology (278 pp.).
- Vol. 22 **STIENNE, Noémie** (2010) Paléoécologie et taphonomie comparative en milieux carbonatés peu profonds (Oxfordien du Jura Suisse et Holocène du Belize) (248 pp.).
- Vol. 23 **WAITE, Richard** (2010) The palaeoecology of high-spired gastropods and the lost palaeosols: depositional reconstructions on a shallow carbonate platform (Late Kimmeridgian, Swiss Jura Mountains) (149 pp.).
- Vol. 24 **MARGRET, Stephan** (2010) Benthic foraminifera associated to cold-water coral ecosystems (248 pp.).
- Vol. 25 **VON ALLMEN, Katja** (2010) Variations of calcium and barium isotopes and elemental contents in biogenic and abiogenic geological archives (97 pp.).
- Vol. 26 **VOUILLAMOZ, Naomi / SAUDAN, Corinne / MOSAR, Jon** (2010) Microzonage sismique du canton de Fribourg - Cartographie au 1:25'000 des sols de fondation selon la norme SIA 261 (57 pp.).
- Vol. 27 **IBELE, Tobias** (2011) Tectonics of the Western Swiss Molasse Basin during Cenozoic Time (166 pp.).
- Vol. 28 **GENNARI, Giordana** (2011) The Mediterranean - Black Sea connections: The fundamental role of foraminifera as a multifaceted tool for the geological reconstruction of the last 10 ky (171 pp.).
- Vol. 29 **MORARD, Sébastien** (2011) Effets de la circulation d'air par effet de cheminée dans l'évolution du régime thermique des éboulis froids de basse et moyenne altitude (220 pp.).
- Vol. 30 **BOCHUD, Martin** (2011) Tectonics of the Eastern Greater Caucasus in Azerbaijan (201 pp.).
- Vol. 31 **MATZENAUER, Eva** (2012) Tectonics of the Préalpes Klippen and the Subalpine Molasse (Canton Fribourg, Switzerland) (207 pp.).
- Vol. 32 **MENNECART, Bastien** (2012) The Ruminantia (Mammalia, Cetartiodactyla) from the Oligocene to the Early Miocene of Western Europe: systematics, palaeoecology and palaeobiogeography (263 pp.).
- Vol. 33 **JARAMILLO-VOGEL, David** (2013) Shallow-marine sedimentary records of the Eocene-Oligocene greenhouse-icehouse transition (Italy, Switzerland and France) (182 pp.).
- Vol. 34 **TRITTSCHACK, Roy** (2013) Dehydroxylation kinetics of the serpentine group minerals (132 pp.).
- Vol. 35 **LAVOYER, Thibault** (2013) Paléontologie et stratigraphie de la partie nord du fossé rhénan supérieur moyen au cours du Paléogène : relations entre le système du rift, les transgressions marines et le paléoclimat (204 pp.).
- Vol. 36 **KÖNIG, Daniela Kati** (2014) Roman metallurgical ceramics : an archaeometrical approach (155 pp.).
- Vol. 37 **RAUSCH, Juanita** (2014) Eifel Maars : external water vs. magmatic volatiles (Eifel Volcanic Field, Germany) (194 pp.).
- Vol. 38 **VOUILLAMOZ, Naomi** (2015) Microseismic characterization of Fribourg area (Switzerland) by Nanoseismic Monitoring (278 pp.).
- Vol. 39 **SOMMARUGA, Anna / GRUBER, Marius / MOSAR, Jon** (2016) Synthèse des données géologiques utiles pour la construction d'un modèle du sous-sol du Canton de Fribourg (103 pp.).
- Vol. 40 **ABEDNEGO, Martinus** (2015) Microseismic Tomography Analysis of the larger Fribourg area (western Swiss Molasse Basin) (162 pp.).
- Vol. 41 **GRUBER, Marius** (2017) Structural Investigations of the Western Swiss Molasse Basin - From 2D Seismic Interpretation to a 3D Geological Model (190 pp.).
- Vol. 42 **CONSTANTDACHE, Monica** (2017) Morphometric study of porosity and morphology of fossil Globigerinoides, during the Late Oligocene and Early Pliocene - Implications for the construction of a climatic and environmental paleoproxy (163 pp.).
- Vol. 43 **BLOUET, Jean-Philippe** (2017) Tracking Hydrocarbon: From Seep Carbonates Down to Petroleum Systems (159 pp.).
- Vol. 44 **EL KATEB, Akram** (2018) Lesser Syrtis (South of Tunisia): Phosphate industry contamination assessment using a multidisciplinary approach (274 pp.).
- Vol. 45 **FEENSTRA, Eline** (2020) Carbonate preservation pathways in cold-water coral mounds (133 pp.).
- Vol. 46 **SCHEIDT, Nicole** (2020) Fault anatomy, porosity and pore connectivity: The La Sarraz-Mormont Fault System (191 pp.).
- Vol. 47 **FENTIMEN, Robin** (2020) Past and present development of cold-water coral mounds in the Western Mediterranean and Northeast Atlantic (504 pp.).
- Vol. 48 **RADAIDEH, Omar M. A.** (2020) Tectonic paleostress and tectonic geomorphology in the close vicinity of the pontarlier strike-slip fault system (Swiss and French Jura Fold-and-Thrust-Belt) (143 pp.).
- Vol. 49 **LAUPER, Bruno** (2021) Characterisation of lithological heterogeneity within the Opalinus Clay and at its upper lithostratigraphic boundary (N Switzerland) (168 pp.).
- Vol. 50 **SCHORI, Marc** (2021) The Development of the Jura Fold-and-Thrust Belt: pre-existing Basement Structures and the Formation of Ramps (200 pp.).
- Vol. 51 **RIME, Valentin** (2023) Multi-scale basin dynamic study of the Danakil Depression (Afar) (290 pp.)